# CORE AND WIRELINE LOG BASED, SHELF TO BASIN STRATIGRAPHIC FRAMEWORK OF MISSISSIPPIAN STRATA, EAST-CENTRAL OKLAHOMA

By

ETHAN D. HILL

Bachelor of Science in Geology

Oklahoma State University

Stillwater, Oklahoma

2014

Submitted to the Faculty of the
Graduate College of the
Oklahoma State University
in partial fulfillment of
the requirements for
the Degree of
MASTER OF SCIENCE
December, 2017

CORE AND WIRELINE LOG BASED, SHELF TO BASIN STRATIGRAPHIC FRAMEWORK OF MISSISSIPPIAN STRATA, EAST-CENTRAL OKLAHOMA

Thesis Approved:

Dr. James Puckette

Thesis Adviser

Dr. Michael Grammer

Dr. William Coffey

## ACKNOWLEDGEMENTS

First I would like to thank my advisor Dr. Puckette, for taking a chance on me, and for his oversight and guidance throughout this study. Dr. Puckette has been there for me since day one, when I set foot in the NRC. Without his enthusiasm and passion for teaching geology, none of this would have been possible. I would also like to thank my committee members, Dr. Grammer for his endless carbonate knowledge and always pushing to find out "so what?", and Dr. Coffey for affording me the opportunity to do this research. A big thank you goes to Devon Energy for making this research possible and for supporting my education. Thank you to Boone Pickens School of Geology for all the assistance along the way.

I would also like to give a huge thank you to my mother, Nita Hill, who has always supported and believed in me. No amount of thanks can express how grateful I am to have her in my life. There were several times throughout this journey where I felt defeated, but she always encouraged me to pursue on. Without her support, I would not be where I am today or the person I have become. I would also like to thank my uncle Walter Lamle, who was the one that inspired me to pursue geology and has been by my side, offering his advice from the start. His influence and impact on me is what generated my passion for geology and I will be forever grateful of that. I would not be in the position I am today without his help and guidance throughout this process. I would also like to thank my sister, Katelyn Hill, for always being there for me and for putting up with me through all of this.

I would also like to thank my colleagues CJ Appleseth, Connor Cain, Garrett Powell, John Hunt, and Scott Shelley. Their insight and assistance with my study is greatly appreciated. They made my grad school experience very fun and memorable. I am very thankful to have had/made such good friends at the Boone Pickens School of Geology. I also give thanks to Dr. Mohamed Abdel Salam for his guidance throughout the graduate school process. I would be remiss if I did not thank the big man upstairs, God, for continually blessing me and guiding me through life.

Lastly, nothing is more important than family, so a huge thank you to all the family members who believed in me, encouraged, and inspired me along the way. This work and my education was accomplished in hopes to make my family members proud to call me their son, brother or nephew. Thank you to everyone who stuck by my side through this journey, even though I wasn't the most enjoyable person to be around, you guys are the real MVPs.



Acknowledgements reflect the views of the author and are not endorsed by committee members or Oklahoma State University.

Name: ETHAN D. HILL

Date of Degree: DECEMBER, 2017

Title of Study: CORE AND WIRELINE LOG BASED, SHELF TO BASIN STRATIGRAPHIC FRAMEWORK OF MISSISSIPPIAN STRATA, EAST-CENTRAL OKLAHOMA

Major Field: GEOLOGY

Abstract:

The “Mississippian Limestone” of the Mid-Continent contains a geologically complex organization of facies and is an areally extensive mixed carbonate-siliciclastic system. Lateral and vertical heterogeneity commonly occurs within carbonates and has been illustrated within the Mississippian Subsystem of the Mid-Continent. These facies shoal upwards from siliciclastic dominated facies (argillaceous siltstones/sandstones and silty shale) into progressively more carbonate-dominated facies (burrowed mudstones-wackestones), and conclude in mud-lean packstones-grainstones. Facies and sedimentary structures from core and thin section analysis, along with bed geometries (observed within the study area) suggest deposition within the distal mid-ramp to outer ramp region of a distally-steepened ramp during fluctuations in sea level with occasional influence from storms.

Previous studies on the “Mississippian Limestone” have focused on larger scale variations in lithofacies. More recent work has identified a sequence stratigraphic hierarchy of facies changes due to variations in sea level. While recent studies have focused on proximal locations of the ramp, little work had been done within the more distal portions of the ramp. This study shows the stratigraphic relationship between more distal facies and the proximal facies in the Mississippian section within the study area. This work is important, as it builds upon previous work (LeBlanc, 2014; Bertalott, 2014) and demonstrates the stratigraphic relationship between proximal carbonate-rich facies and distal siliciclastic-rich, argillaceous facies. Bertalott (2014) demonstrated that prograding carbonate wedges in a ramp setting were a logical interpretation of Mississippian depositional packages within the northern part of the study area. This study tested the hypothesis that prograding carbonate wedge geometries extend into a more basinal depositional setting by expanding upon previous studies with subsurface data from Creek and Lincoln Counties, Oklahoma and employing a sequence stratigraphic framework, this study extended the ramp model basinward and identified associated siliciclastic dominated depositional facies.

**TABLE OF CONTENTS**


Chapter Page

I. INTRODUCTION ..... 1

Problem Statement ..... 1
Hypothesis and Fundamental Questions ..... 3
Purpose and Objectives of Study ..... 4

II. GEOLOGIC BACKGROUND ..... 6

Structural and Tectonic History ..... 6
The Nemaha Ridge ..... 9
Paleogeography and Climate ..... 12
Sea Level and Cycle Hierarchy ..... 16
Mississippian Sea Level ..... 20
Problems in Expounding High Frequency Cyclicity ..... 22
Problems with Classifying Facies ..... 22
Problems with Subsurface Correlation ..... 25
Regional Stratigraphy ..... 25
Kinderhookian Strata ..... 26
Osagean Strata ..... 27
Meramecian Strata ..... 27
Chesterian Strata ..... 28

III. DATA AND METHODS ..... 29

Core Descriptions ..... 30
Petrographic Analysis ..... 31
X-Ray Diffraction (XRD) ..... 34
Sequence Stratigraphic Analysis ..... 34
Subsurface Correlation/ Wireline Logs ..... 35
Geologic Mapping ..... 36
Dataset Limitations ..... 36

Chapter Page

IV. RESULTS & DISCUSSION ..... 39

Facies Associations ..... 39
DOBERMAN FACIES ..... 42
Doberman Facies 1: Glauconitic Sandstone ..... 42
Doberman Facies 2: Clay-Rich Siltstone ..... 44
Doberman Facies 3: Slightly Sandy Argillaceous Siltstone ..... 46
Doberman Facies 4: Silty Argillaceous Sandstone ..... 48
Doberman Facies 5: Silty Burrowed Mudstone-Wackestone ..... 50
Doberman Facies 6: Silty Peloidal Packstone-Grainstone ..... 52
IHLE FACIES ..... 56
Ihle Facies 1: Glauconitic Sandstone ..... 56
Ihle Facies 2: Silty Shale ..... 58
Ihle Facies 3: Phosphatic Dolomitic Shale ..... 60
Ihle Facies 4: Clay-Rich Siltstone ..... 62
Ihle Facies 5: Slightly Sandy Calcareous Siltstone ..... 64
Ihle Facies 6: Silty Argillaceous Sandstone ..... 66
Ihle Facies 7: Argillaceous Mudstone-Wackestone ..... 68
Ihle Facies 8: Silty Burrowed Mudstone-Wackestone ..... 70
Ihle Facies 9: Silty Argillaceous Dolomitic Packstone ..... 72
Ihle Facies 10: Packstone-Grainstone ..... 74
Ihle Facies 11: Silty Peloidal Packstone-Grainstone ..... 76
Sequence Stratigraphic Framework ..... 80
Idealized Facies Successions ..... 80
Sequence Stratigraphic Hierarchy ..... 83
Wireline Log Correlation ..... 88
Sequence Stratigraphic Architecture ..... 92
Subsurface Cross Sections ..... 92
Thickness Maps ..... 99
Comparison of Results to Previous Studies ..... 108

V. SUMMARY AND CONCLUSIONS ..... 110

REFERENCES ..... 112
APPENDICES ..... 124
Appendix A: Doberman #1-25 SWD ..... 125

Chapter Page

Whole Core Photographs ..... 126
Core Description ..... 152
Thin Section Photomicrographs ..... 161
Appendix B: Ihle #1-26 ..... 185
Whole Core Photographs ..... 186
Core Description ..... 231
Thin Section Photomicrographs ..... 243
Appendix C: Architecture of Mississippian Strata/Subsurface Mapping ..... 283
Subsurface Cross Sections and Correlations ..... 284
Thickness Maps ..... 288

## LIST OF TABLES

Table Page


1. List of Cored Wells Utilized in This Study ..... 4
2. Cycle Hierarchy ..... 17
3. List of Cored Wells Utilized in This Study ..... 30
4. Doberman #1-25 Depositional Facies ..... 40
5. Ihle #1-26 Depositional Facies ..... 41
6. Doberman #1-25 Core Image Labels ..... 124
7. Doberman #1-25 Rock Color Chart ..... 150
8. Bioturbation Index ..... 151
9. Fracture Density ..... 152
10. Doberman #1-25 Thin Section Image Labels ..... 159
11. Ihle #1-26 Core Image Labels ..... 184
12. Ihle #1-26 Rock Color Chart ..... 229
13. Fracture Density ..... 230
14. Ihle #1-26 Thin Section Image Labels ..... 241

## LIST OF FIGURES

Figure Page


1. "Mississippian Limestone" Play Map .....2
2. Tectonic features of Oklahoma with Study Area and Core Locations .....6
3. Generalized Paleodepositional Model of the Mid-Continent during the Early Mississippian .....8
4. Fault Map of Oklahoma and Study Area .....11
5. Paleogeographic Map during the Early Mississippian .....13
6. Paleogeographic Map during the Late Mississippian .....14
7. Greenhouse and Icehouse Conditions Throughout the Phanerozioc.....15
8. Milankovitch Orbital Patterns .....18
9. Sea Level Curves Associated with Milankovitch Cycles .....19
10. Mississippian Sea Level Curve .....21
11. Distribution of Depositional Environments in Arkansas during the Chesterian .....24
12. Mississippian Stratigraphic Column for Ozark Region.....26
13. Dunham Classification of Carbonate Rocks.....31
14. Measured Core Sections and Sample Locations.....33
15. Environments of Deposition on a Ramp Setting .....42
16. Core Photo and Thin Section Photomicrographs of Doberman Facies 1 .....43
17. Core Photo and Thin Section Photomicrographs of Doberman Facies 2 .....45
18. Core Photo and Thin Section Photomicrographs of Doberman Facies 3 .....47
19. Core Photo and Thin Section Photomicrographs of Doberman Facies 4 .....49
20. Core Photo and Thin Section Photomicrographs of Doberman Facies 5 .....51
21. Core Photo and Thin Section Photomicrographs of Doberman Facies 6 .....53

Figure Page

22. Core Photo and Thin Section Photomicrographs of Ihle Facies 1.....56
23. Core Photo and Thin Section Photomicrographs of Ihle Facies 2.....58
24. Core Photo and Thin Section Photomicrographs of Ihle Facies 3.....60
25. Core Photo and Thin Section Photomicrographs of Ihle Facies 4.....62
26. Core Photo and Thin Section Photomicrographs of Ihle Facies 5.....64
27. Core Photo and Thin Section Photomicrographs of Ihle Facies 6.....66
28. Core Photo and Thin Section Photomicrographs of Ihle Facies 7.....68
29. Core Photo and Thin Section Photomicrographs of Ihle Facies 8.....70
30. Core Photo and Thin Section Photomicrographs of Ihle Facies 9.....72
31. Core Photo and Thin Section Photomicrographs of Ihle Facies 10.....74
32. Core Photo and Thin Section Photomicrographs of Ihle Facies 11.....76
33. Doberman #1-25 Idealized Facies Succession .....79
34. Ihle #1-26 Idealized Facies Succession .....80
35. Sequence Stratigraphic Hierarchy of Both Cores .....82
36. Sequence Stratigraphic Hierarchy of Both Cores with 4$^{th}$ Order Correlations .....85
37. Core-Calibrated Sequences on Wireline Logs .....88
38. Sequence Stratigraphic Hierarchy and Cored Wireline Logs.....89
39. Subsurface Cross Section (A to A') with Both Cores.....92
40. Strike-Oriented Cross Section B to B' .....93
41. Dip-Oriented Cross Section C to C' .....95
42. Dip-Oriented Cross Section D to D' .....96
43. "Mississippian Limestone" Thickness Map.....98
44. Sequence 1 – Sequence 3 Thickness Maps .....101
45. Sequence 4 – Sequence 6 Thickness Maps .....105
46. Conodont Biostratigraphy Results from Hunt (2017).....107

# CHAPTER I

## INTRODUCTION

### Problem Statement

The "Mississippian Limestone" is a comprehensive mixed carbonate/siliciclastic unconventional play throughout much of Oklahoma and southern Kansas. This unconventional play is characterized by low porosity and/or permeability that impedes the migration of hydrocarbons, and well completions require hydraulic stimulation in order to produce economic volumes of oil and gas. The Mississippian Subsystem of Oklahoma, despite being lithologically heterogeneous and poorly age-constrained, is economically due to its long history as a hydrocarbon-producing play (Figure 1). Though the Mississippian section has a long history of producing, there are limited studies of the distal or more basinal sections of the "Mississippian Limestone" resulting in poor resolution of the stratigraphy and confusion concerning subsurface correlations. This is largely due to the changes in facies from the outcrop to the subsurface, a lack of biostratigraphic control, and absence of core that is necessary to develop facies models (Mazzullo et al., 2011). Understanding the depositional processes is essential to resolving Mississippian stratigraphy. This study is designed to expand the correlation of Mississippian subunits in the subsurface of east-central Oklahoma, which has not previously been accomplished. Lithostratigraphic nomenclature applied to the Mississippian strata in the Mid-Continent region is inconsistent and poorly constrained biostratigraphically and temporally (Mazzullo et al., 2013).

An important factor for the success of this study was a concurrent conodont biostratigraphic study (Hunt, 2017) on the Doberman #1-25 SWD core, which was also examined in this study (Table 1). The combined efforts of these two studies have resulted in a better understanding of the depositional processes and age of the Mississippian section. Conodont biostratigraphy, with its ability to yield high-resolution age constraints (one million years maximum resolution), has produced the most accurate dataset for correlating within the Mississippian (Boardman et al., 2013). Establishing a temporal and spatial relationship between the more limestone-rich facies of the outcrop and subsurface in northern Oklahoma, to the deeper water, more silty and argillaceous facies, provides a major step in resolving facies relationships within ramp settings, thereby making a significant contribution to the science of stratigraphy. Both cores utilized in this study appear to be unique in that they contain examples of both the limestone-rich facies and the siltier, quartz- and clay-rich facies.

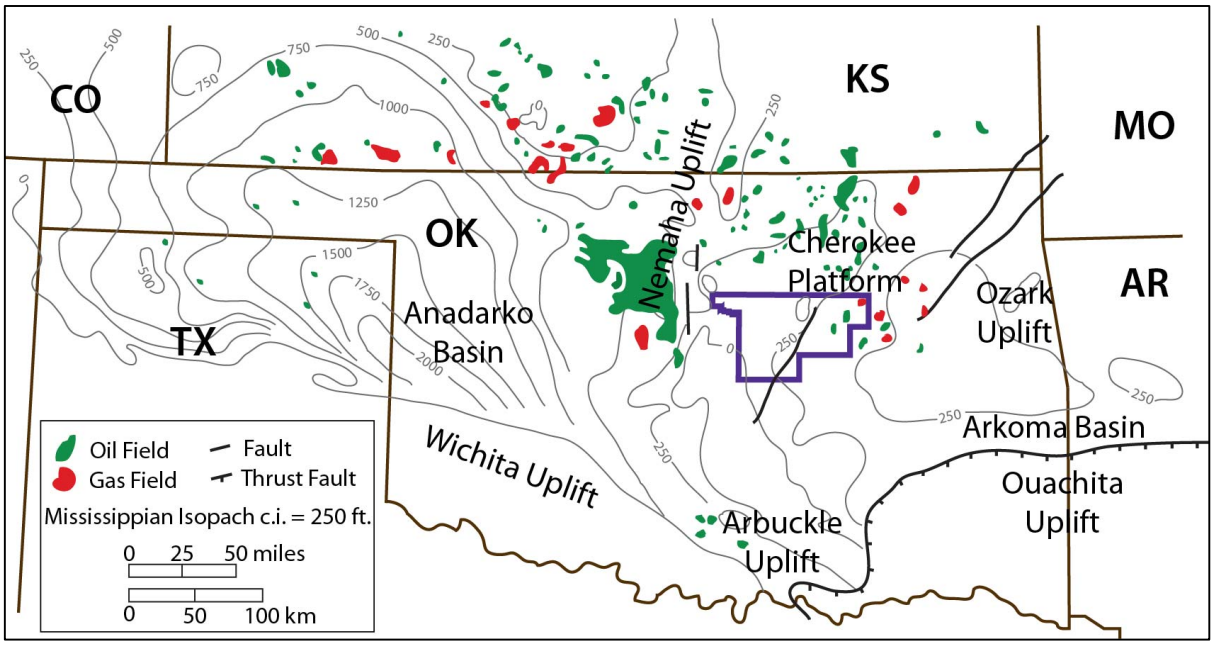


Figure 1. Historical map of the "Mississippian Limestone" play (vertical production) with the study area outlined in purple. The map shows production of oil (green) and gas (red) from "Mississippian Limestone" vertical wells across Oklahoma and Kansas. The thickness of the Mississippian section is indicated by grey contour lines with a contour interval of 250ft (62.5m). The thickness trend of the Mississippian shows thickening to the west and thinning to the east. The largest producing field in Oklahoma is the Sooner Trend on the western flank of the Nemaha Ridge. Modified from Harris (1987).

## Hypotheses and Fundamental Questions

In order to ascertain the impact of high-frequency eustatic sea level changes and their influence on the stratigraphy of the "Mississippian Limestone", this study utilized two "Mississippian Limestone" cores (Table 1) (Figure 1). These cores were chosen because they have a complete or near complete section of the "Mississippian Limestone", a suite of conventional wireline logs, and differing thicknesses of the "Mississippian Limestone" section. These cores offer sedimentological evidence of changes in sea level, and depositional energy, and the resulting depositional facies and their stacking patterns that were used to establish a hierarchy of sea level cyclicity. Two overarching hypotheses were formulated for this study:

1. The Doberman #1-25 and Ihle #1-26 cores, in the southern and southeastern part of the study area, contain a cleaner carbonate section toward the base of the cores that is a thinner more distal equivalent to the same section in the Payne County cores previously studied by LeBlanc (2014).
2. Probable 3$^{rd}$ order, sequences and higher frequency depositional cycles observed within the Doberman and Ihle cores are part of prograding carbonate packages, whose deposition was likely influenced by eustatic sea level changes associated with Milankovitch cyclicity.

The fundamental questions addressed by this research are in regard to the "Mississippian Limestone" section in Creek, Lincoln, and southern Payne Counties in east-central Oklahoma (Figure 2). These fundamental questions are as follows:

1. Is there a stratigraphic hierarchy of depositional sequences and cycles that exist within the Mississippian section of the examined cores?
2. If a stratigraphic hierarchy exists within the cores, can it be tied to their respective wireline log signatures, and then correlated to adjacent wells in the study area?

3. Do prograding carbonate wedge geometries, demonstrated in the northern part of the study area by Bertalott (2014), extend into a more distal (basinal) depositional setting?

| Core # | Lease Name | Well No. | "Mississippian Limestone" Interval (ft) | Operator | County |
|---|---|---|---|---|---|
| 1 | Doberman | 1-25 | 4964.75′ - 5199.20′ | Devon Energy | Payne |
| 2 | Ihle | 1-26 | 2783.00′ - 3206.55′ | Devon Energy | Creek |

Table 1. List of cored wells utilized within this study including lease name, well number, depths through the Mississippian section in feet, operator, and county. Well information was obtained from the well logs and log headers.

## Purpose and Objectives of Study

The primary purpose of this study was to establish a core and wireline log based stratigraphic framework for the "Mississippian Limestone" in portions of east-central Oklahoma. The primary objectives were:

1) Examine cores to identify significant stratigraphic surfaces that can be attributed to changes in relative sea level, such as flooding surfaces or subaerial exposure surfaces.
    a. Establish a set of depositional facies based on core descriptions and thin sections
    b. Document depositional cycles based on facies stacking patterns and compare them to the hierarchy of cycles established for the "Mississippian Limestone" section in previous studies.
2) Correlate these stratigraphic surfaces and facies assemblages observed in the cores to their signatures on wireline logs and establish electrofacies.

3) Establish a regional stratigraphic framework using the electrofacies interpreted from patterns on wireline logs and stratigraphic surfaces observed within the cores.

The major research tasks included in this study were core and thin section descriptions, correlating cores to wireline logs, and correlating the stratigraphic hierarchy away from the cored wells. The anticipated results expected to show the stratigraphic relationship between more distal (basinal) facies and the proximal (landward) facies in the Mississippian section within the study area. This work is important, as it built upon previous work (LeBlanc, 2014; Bertalott, 2014) and demonstrated the stratigraphic relationship between proximal limestone rich facies and distal siliciclastic-rich, argillaceous facies. Bertalott (2014) demonstrated that prograding carbonate wedges in a ramp setting were a logical interpretation of Mississippian depositional packages within the northern part of the study area. This study tested the hypothesis that prograding carbonate wedge geometries extend into a more basinal depositional setting.

# CHAPTER II

## GEOLOGIC BACKGROUND

### Structural and Tectonic History

The study area is located in east-central/northeast Oklahoma on the Cherokee Platform in Lincoln, Creek, and southern Payne counties. Bordering the study area are tectonic features including the Nemaha Uplift, also referred to as the Nemaha Ridge, to the west, the Anadarko Basin to the west and southwest, the Ozark Uplift to the east, the Arkoma Basin to the southeast, and the Arbuckle Uplift to the south (Northcutt and Campbell, 1996). The orientations of the previously mentioned tectonic features are illustrated by figure 2.

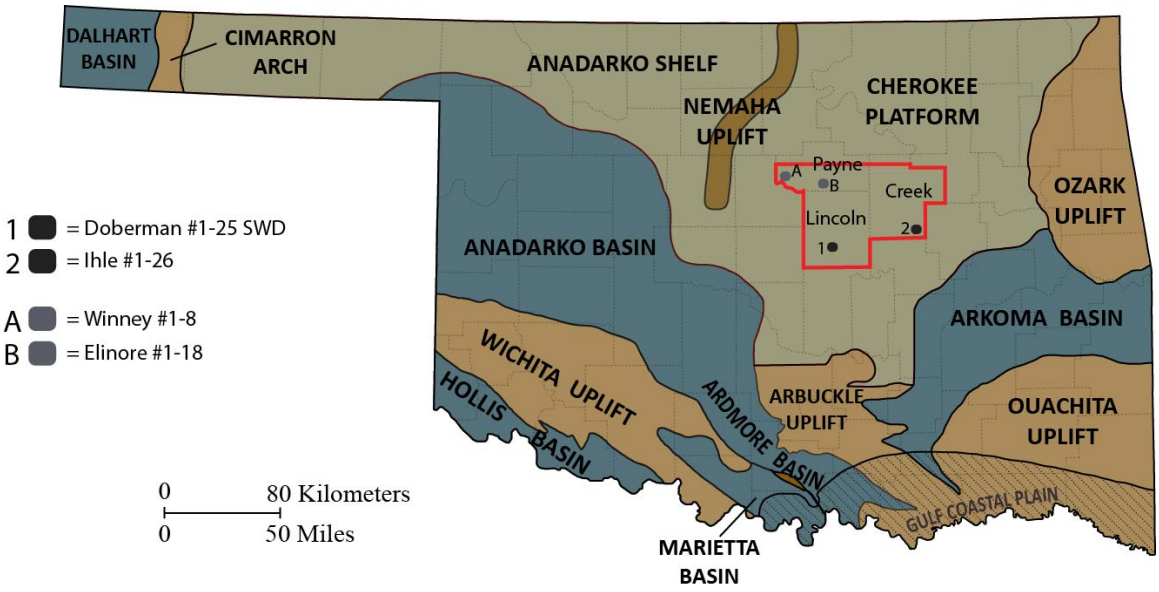

Figure 2. Map of Oklahoma showing major tectonic features in reference to the study area (shown by red outline). Cores utilized in this study are shown by black dots (1 and 2), the gray dots (A and B) are cores described by LeBlanc, 2014 that were integrated into this study for subsurface correlation purposes. Uplifted regions are shown in brown, while basins are shown in blue. Green shaded areas represent platform and shelf regions. Modified from Northcutt and Campbell (1996).

Understanding the location and timing of these tectonic features is important because of the role they played in influencing depositional settings, environments and the amount of accommodation during deposition, all of which directly affect the type of facies and reservoir distribution. Accommodation and environment directly influence facies stacking patterns and reservoir distribution (Drummond and Wilkinson, 1993). In addition, tectonism and erosion associated with uplift modified the Mississippian section prior to Pennsylvanian deposition and it is important to consider erosion during correlation and facies analysis.

With respect to tectonic activity or structural deformation, the Early (~360 Ma) and Middle (~347 Ma) Mississippian was relatively quiet or inactive within the Mid-continent (Gutschick and Sandberg, 1983). During this time, a large percentage of the southern United States was immersed under a shallow, warm, epeiric sea where temperate to subtropical climates existed. As a result, Mississippian carbonates were deposited on the Burlington Shelf across portions of Arkansas, Colorado, Illinois, Iowa, Kansas, Nebraska, New Mexico, Oklahoma, and Texas (Figure 3; Curtis and Champlin, 1959; Gutschick and Sandberg, 1983). Depositional dip was towards the south southeast and the depositional strike was roughly east to west, with shallower waters occurring to the north and deeper water settings to the south. Bounding the Mid-Continent ramp/shelf system was the Transcontinental Arch to the north. The Burlington Shelf was also bounded to the east by the Ozark Uplift and Illinois basin and by the Oklahoma Basin and Ouachita Trough to the south (Figure 3; Lane and De Keyser, 1980).

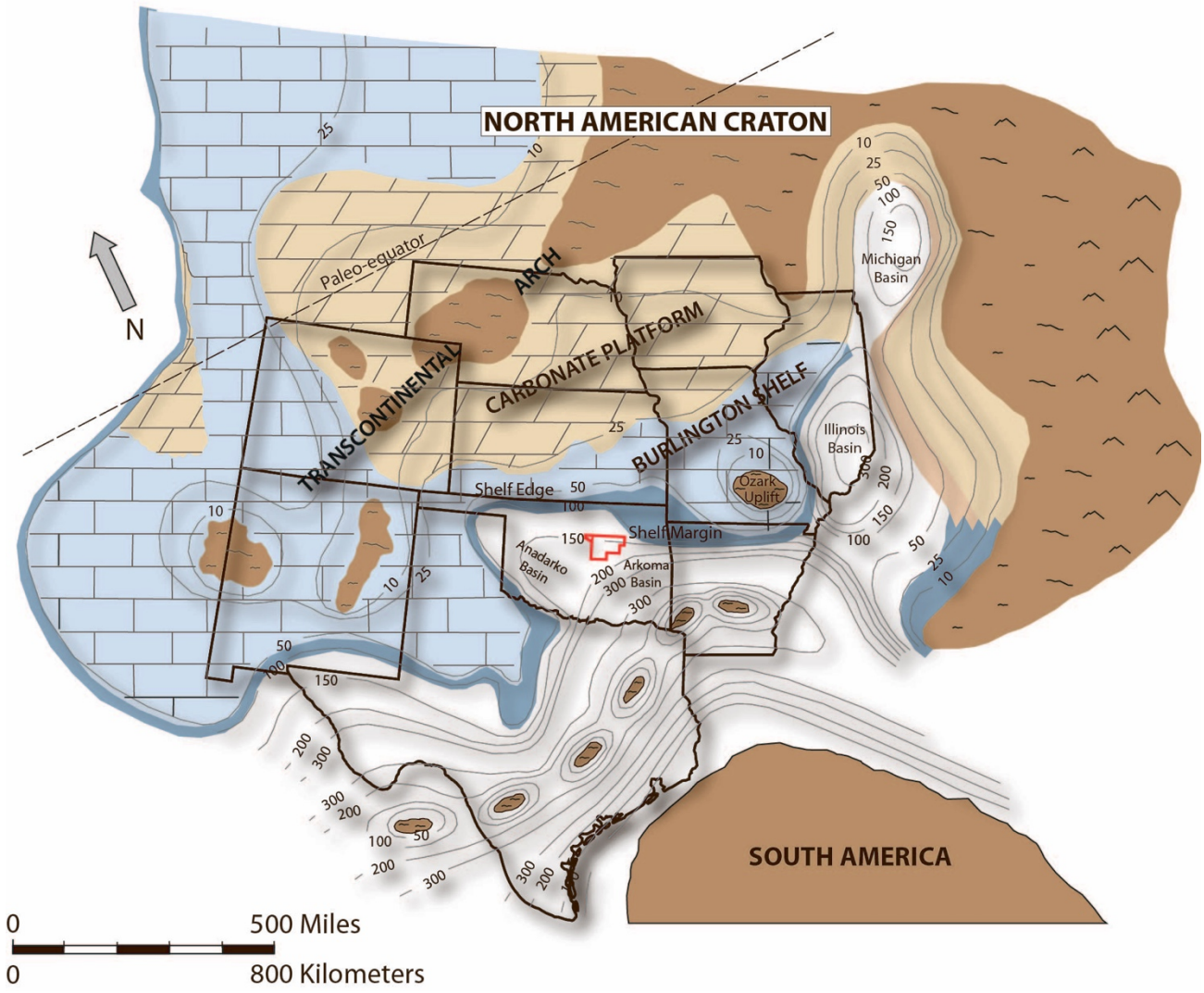


Figure 3. Regional paleo-depositional time-slice map of the Mid-continent representative of deposition during Late Tournaisian, or Early to Middle Osagean. Approximate water depths (in meters) are illustrated by gray contour lines with a contour interval of 50m (164ft). Shallower waters were to the north while deeper waters persisted to the south. The carbonate system was bounded to the north northwest by the Transcontinental Arch, to the east by the Ozark Uplift, and the Oklahoma Basin to the south, a position occupied by the present day Anadarko and Arkoma basins. The study area is denoted by the red outline and had an estimated water depth of 150 to 175 meters. Note that this figure only represents a generalized time slice of a dynamic mixed carbonate-siliciclastic system and that it represents a carbonate shelf/platform rather than a carbonate ramp. Modified from LeBlanc (2014), originally re-drafted by Bertalott (2014) after Gutschick and Sandberg (1983) and Lane and De Keyser (1980).

The Ozark Uplift, which formed during the Paleozoic and is thought to have been paleogeographically positive during the deposition of Mississippian sediments, was reactivated during the Pennsylvanian, generating folds and faults around the area (Huffman, 1958). As previously stated, the Early and Middle Mississippian were tectonically quiet. However, during the Late Mississippian (~331 Ma) and Early Pennsylvanian (~320 Ma), tectonic activity increased. Tectonism accompanying the Pennsylvanian Orogeny directed the growth of structural and geologic features within the southern Mid-Continent and study area, influencing available accommodation and deposition of carbonates during Late Mississippian time.

**Nemaha Ridge**

The Nemaha Ridge is a large north-south trending structural uplift extending south-southwest from Nebraska and northeastern Kansas, through Kansas and southward into central Oklahoma where it terminates (McBee, 2003). The uplift structurally divides the Cherokee Platform in north-central Oklahoma from the Anadarko Basin in west-central Oklahoma. The Nemaha Ridge is relatively narrow, extending roughly 80 miles (129 km) across at its widest in the north and outspreading to approximately 500 miles (805 km) in length (Gay, 2003). In north-central Oklahoma, it is roughly 30 miles (48 km) wide and narrows towards the southwest, where it is less than 6 miles (10 km) across (McBee, 2003; Gay, 2003). The complex history of the Nemaha Ridge played a role in determining the thickness and distribution of the "Mississippian Limestone" in north-central and east-central Oklahoma (Bertalott, 2014). Dolton and Finn (1989) indicate that the Nemaha Ridge is an intricate structural feature where associated folding and faulting control the distribution of oil and gas. Faulting (Figure 4) affected the thickness of subunits within the Middle to Late Mississippian (Bertalott, 2014). The timing of the structural events accompanying the Nemaha Ridge are still uncertain for the older Paleozoic. Although, it is known and understood that the uplift was a prominent structural feature by the Late Mississippian that affected Carboniferous deposition and sediment distribution, Gay (1999) suggests the

Nemaha Ridge initially moved, as early as, the Middle Ordovician (Taconic), with the main uplift taking place through Late Mississippian into Early Pennsylvanian (Alleghanian). According to Steen (in progress) uplift occurred pre-, during, and post-Mississippian time based upon synsedimentary uplift and accelerated erosion of the unit. Steen (in progress) also states a thicker sedimentary section occurs along the flanks of the structure compared to the apex. Recent studies of outcrops and subsurface sections suggest that the Ouachita orogeny initiated syndepositional tectonism (Mazzullo et al., 2011; Wilhite et al., 2011).

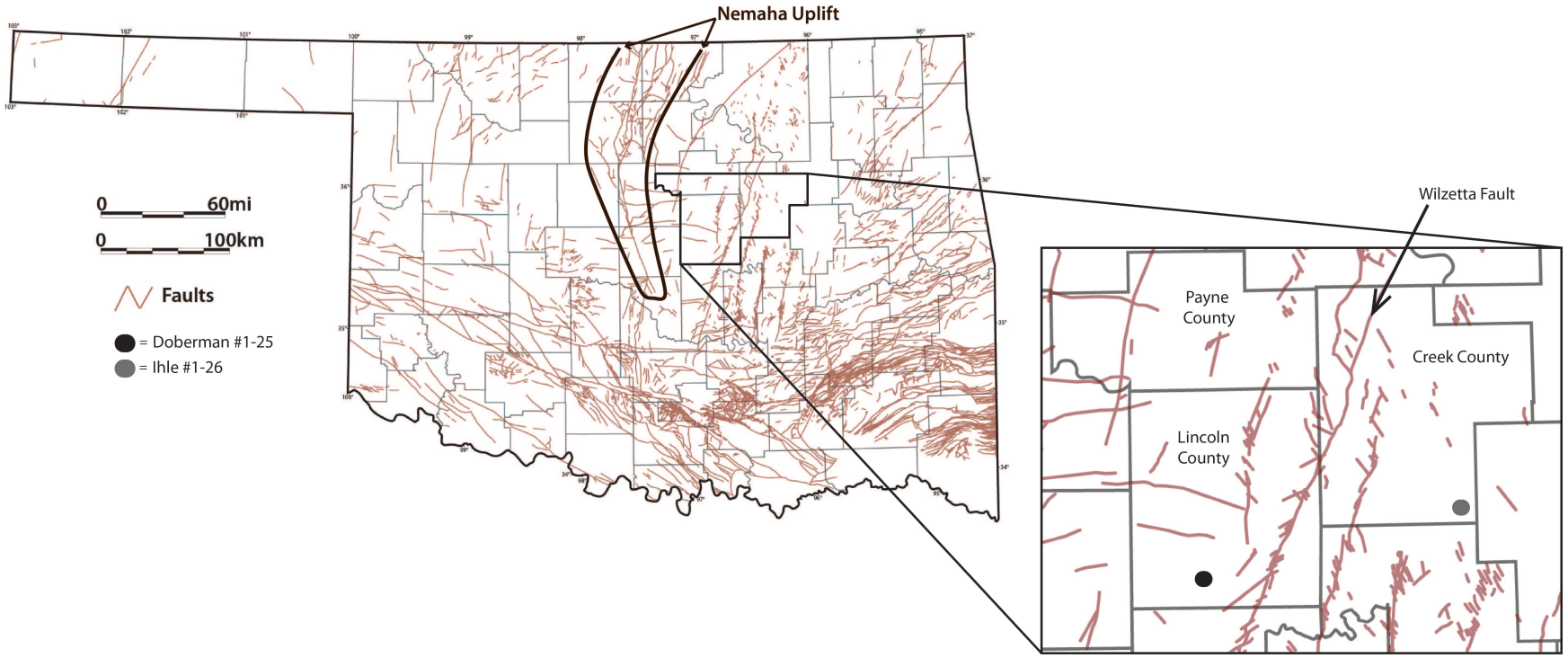


Figure 4. Map illustrating the faulting within Oklahoma and in the study area. Faults within the study area are likely associated with the Pennsylvanian Orogeny. The two cores utilized in this study are shown by the black and gray dots. Note that the Doberman #1-25 is located closer to the Nemaha Ridge and its associated faults. Modified from Mohammadi (2016), after Darold and Holland (2015).

## Paleogeography and Climate

During the Mississippian, a large portion of the southern North American craton was immersed under a shallow, warm, epeiric sea in temperate to subtropical climates. The result was deposition of Mississippian carbonates across the Burlington Shelf (Figures 3 and 5; Curtis and Champlin, 1959; Gutschick and Sandberg, 1983). The combination of climate and water conditions provided a relatively large area suitable for carbonate production (Figure 5). Following deposition of Woodford sediments (Late Devonian, Early Mississippian), sea level declined resulting in a shallow, relatively well-oxygenated environment in Early Mississippian (Tournaisian) time (Frezon and Jordan, 1979).

Northern Oklahoma (including the study area) was located approximately 20°-30° south of the paleoequator (Figures 5 and 6). During the Middle to Late Mississippian, global sea level continued to fall, which resulted in significantly more land mass being exposed across the Mid-Continent (Figure 6). In the oxygenated, shallow water north and northwest of the Ouachita Trough, an ample amount of invertebrate fauna was capable of growing (Huffman, 1958). Due to heavy siliciclastic input during Late Mississippian within the study area, carbonate production was likely hindered and prevented extensive growth of normal marine faunas in what was an otherwise favorable environment (Frezon and Jordan, 1979).

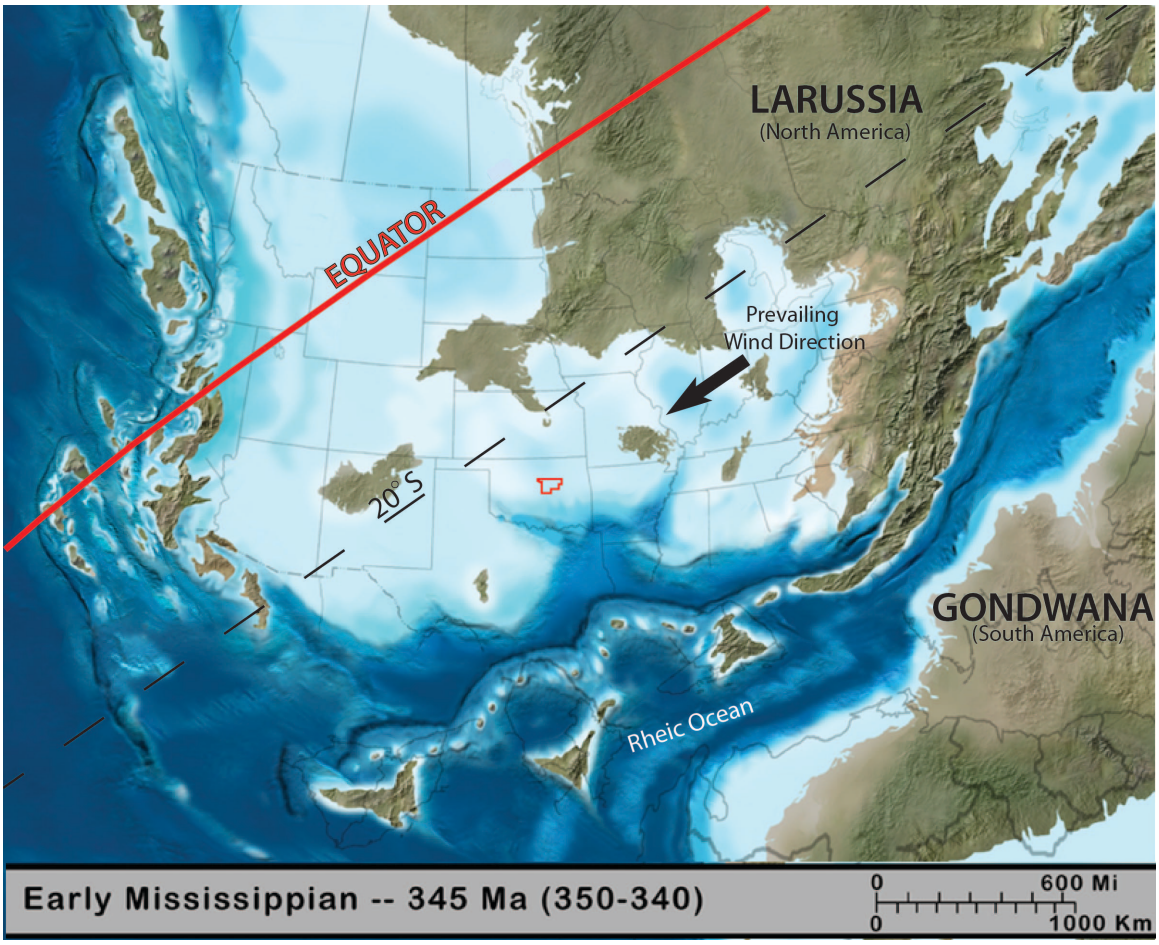


Figure 5. Early Mississippian (~345 Ma) paleogeography. The red outline indicates the study area, which is located roughly 25-30 degrees south of the paleoequator. Water depths are indicated by contrasts in color, with deeper water being darker blue and shallower waters being lighter blue. Exposed land masses are indicated by browns and green. During this time the study area was characterized by shallow water marine conditions, while deeper water conditions existed to the south. The dominant paleo wind direction is interpreted to have been from the northeast. Modified from Blakey (2015).

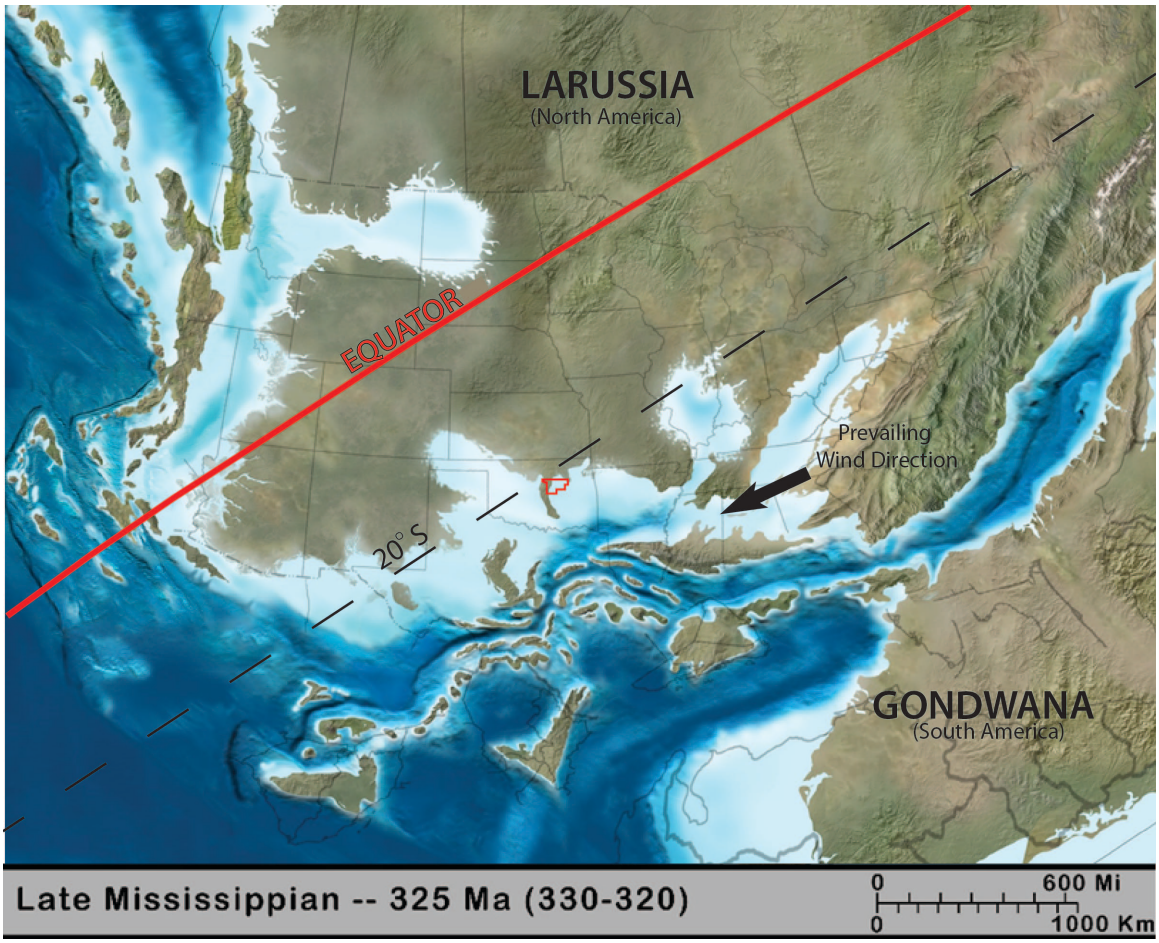


Figure 6. Late Mississippian (~325 Ma) paleogeography. The red outline indicates the study area, which is located roughly 20-25 degrees south of the paleoequator. Water depths are indicated by contrasts in color, with deeper water being darker blue and shallower waters being lighter blue. Exposed land masses are indicated by browns and green. During this time the study area was characterized by shallow water marine conditions, while deeper water conditions existed to the south. The dominant paleo wind direction is interpreted to have been from the northeast. Unlike the Early Mississippian, during Late Mississippian time there was significantly more land mass exposed, which could have affected sediment supply and the distribution of facies throughout the study area. Modified from Blakey (2015).

The Mississippian represents a transitional period between the greenhouse climate of the Devonian to icehouse climatic conditions during the Pennsylvanian (Buggisch et al., 2008; Read, 1995). Coinciding with this transitional period from greenhouse conditions to icehouse conditions

was a time of low carbon dioxide concentrations, globally (Figure 7; Read, 1995). According to Haq and Schutter (2008), surface temperatures within the ocean were also transitional through Mississippian time. The first major glaciation event within the Mississippian occurred during Tournaisian and continued through the Visean (Middle Mississippian), another glaciation event occurred within the Serpukhovian (Late Mississippian), but between the two glaciation events warm conditions existed (Buggisch et al., 2008; Pfefferkorn et al., 2014).

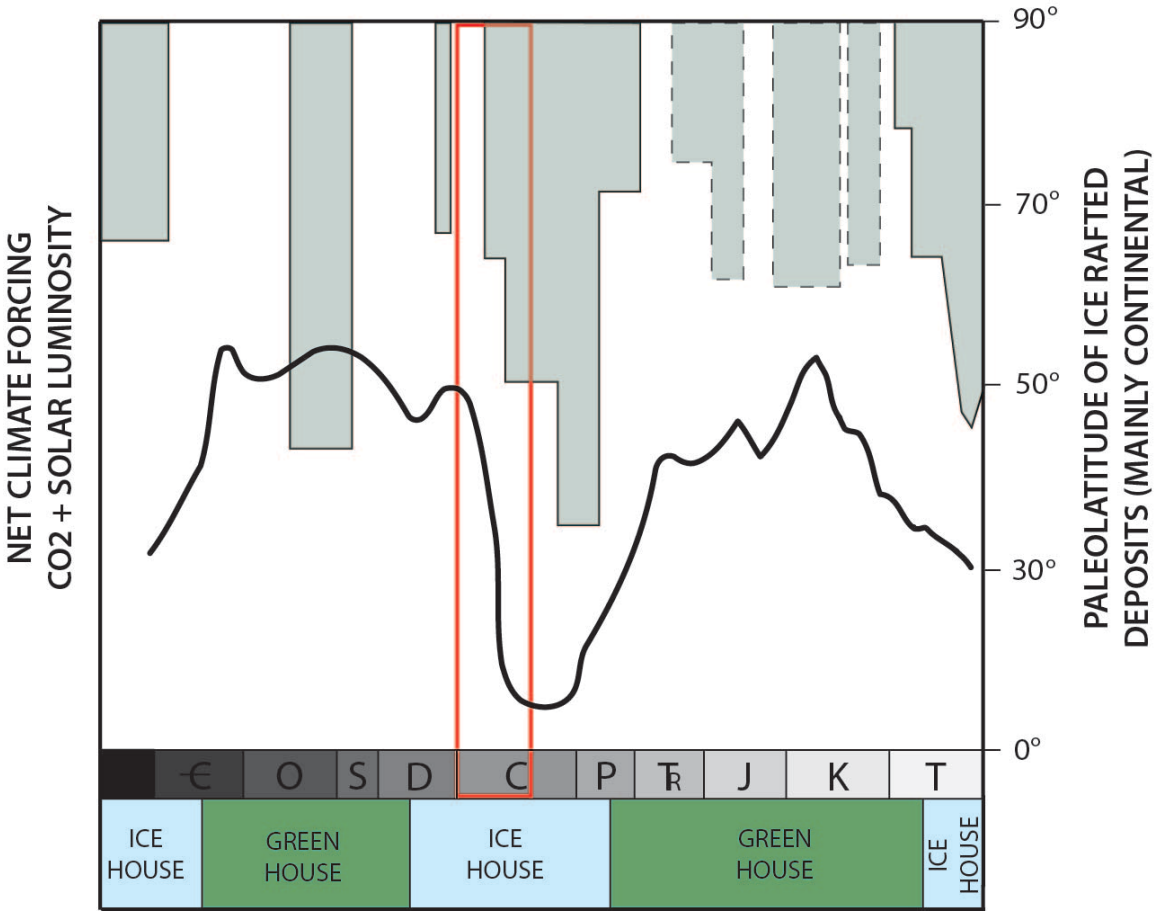


Figure 7. Illustration of greenhouse and icehouse conditions existing through the Phanerozoic. Paleo-latitudes of ice-rafted deposits (shown by gray boxes with solid black outline) and marine ice-rafted deposits (shown by gray boxes with dashed black line) combined with the change in climate due to deviations in carbon dioxide and solar intensity (solid black curve) demonstrate the transitional state that existed during the Mississippian. The Mississippian is outlined by the red rectangle, noting the increase in ice-rafted deposits during this time. Modified from Read (1995), who redrafted it from Fischer (1982).

## Sea Level and Cycle Hierarchy

Eustatic sea level change is controlled by two main influences: (1) variations in global ice capacity and (2) fluctuations in ocean basin volume from the flow of heat through mid-ocean ridges. A hierarchy of sea level fluctuations, denoted as cycles and sequences, is created from the amalgamation of the two mechanisms mentioned above. Characteristics such as magnitude, length of time, and processes controlling sea level change differentiate sea level cycles and/or sequences (Table 2; Read, 1995). First order supersequences are more than 100 million years (m.y.) in length (typically 200-300 m.y. long) and are related to plate tectonics and the opening and closing of ocean basins (Read, 1995). Second order supersequences typically range from 10 to 50 million years in length and are caused by changes in ocean basin volumes, plate tectonics, and to a lesser extent fluctuations in global ice capacity (Read, 1995). Superimposed on second order supersequences are third order sequences of 1 to 10 million years in length, but typically less than 3 million years (Plint et al., 1992). The controlling mechanisms of third order sequences are controversial and challenging. However, most researchers believe that third order sequences are likely controlled by ocean floor spreading and plate tectonics (Haq and Schutter, 2008; Plint et al., 1992; Kerans and Tinker, 1997), while (Read, 1995) attributes them to waxing and waning of continental ice sheets.

| Cycle Hierarchy | | | | |
|---|---|---|---|---|
| Tectono-Eustatic Cycle Order | Sequence Stratigraphic Unit | Duration (n = my) | Relative Sea Level Amplitude (m) | Relative Sea Level Rise/Fall Rate (cm/1000 yrs) |
| First | Supersequence | > 100 | | < 1 |
| Second | Supersequence | 10 - 100 | 50 - 100 | 1 - 3 |
| Third | Depositional Sequence Composite Sequence | 1 - 10 | 50 - 100 | 1 - 10 |
| Fourth | High-Frequency Sequence, Parasequence and Cycle Set | 0.1 - 1 | 1 - 150 | 40 - 500 |
| Fifth | Parasequence, and High-Frequency Cycle | 0.01 - 0.1 | 1 - 150 | 60 - 700 |

Table 2. Chart illustrating cycle hierarchy and showing characteristics among first through fifth order sea level cycles and sequences. 4th order sequences and 5th order cycles have relatively high sea level amplitudes and sea level rise/fall rates. This study concentrates on 3rd and 4th order sequences, and to a lesser degree 5th order cycles. Modified from Kerans and Tinker (1997).

High frequency 4th order sequences (HFS) and high frequency 5th order cycles (HFC) are superimposed on 3rd order sequences and are likely driven by Milankovitch-band glacio-eustacy (Kerans and Tinker, 1997; Read, 1995). Cyclical changes in the orbital variability of earth along with the tilt and wobble of the earth's axis are known as Milankovitch cycles. The functions associated with Milankovitch cycles (listed above) are responsible for change in climate, which then causes changes in the ice budget and eustatic sea level (Read, 1995). These fluctuations in eustatic sea level occur on the order of less than 20 to 400 thousand years (k.y.) and can cause rapid flooding of platforms (Kerans and Tinker, 1997; Read, 1995). There are three Milankovitch-band frequencies: eccentricity, obliquity, and precession (Figures 8 and 9; Read, 1995). Eccentricity is the variation in the shape of earth's orbit around the sun and occurs on a 4th

order scale every 100 to 400 k.y. Obliquity is the change in the tilt of the earth's axis that occurs on a 5th order scale every 40 k.y. Precession is the wobble of the axis of the earth and occurs on a 5th order scale every 19 to 23 k.y. (Kerans and Tinker, 1997; Read, 1995). Sub-Milankovitch cycles, likely on the order of 10 k.y. or less, have been identified within the stratigraphic record (Grammer et al., 1996; Read, 1995).

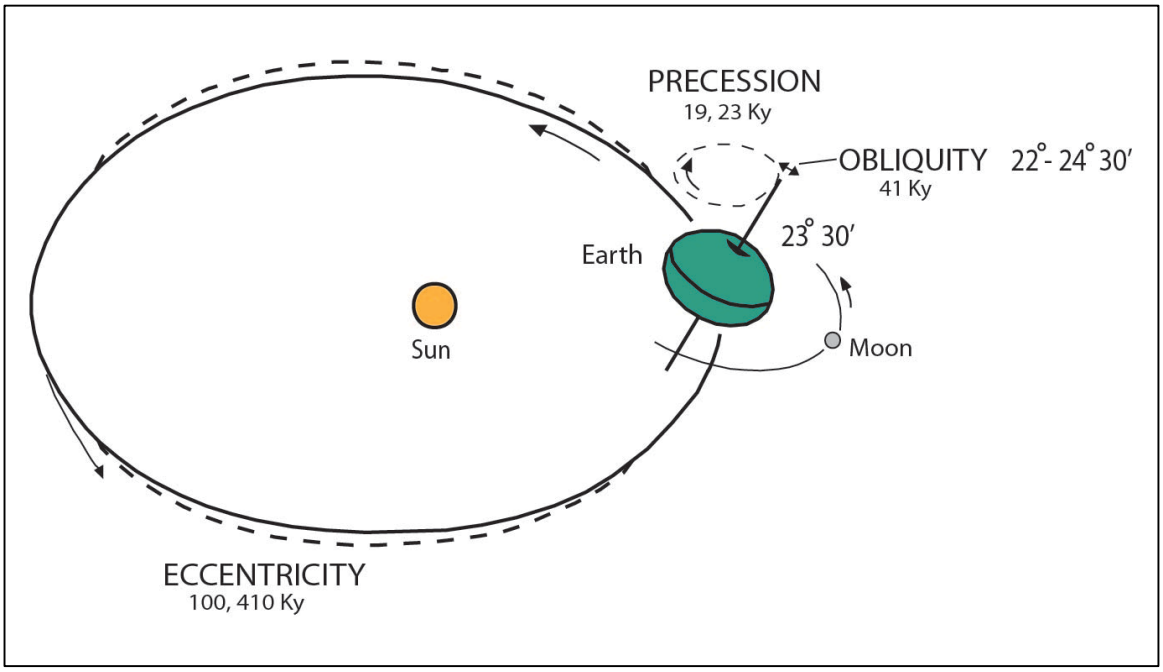


Figure 8. Illustration of the relationship between Milankovitch orbital patterns of eccentricity, obliquity (tilt), and precession (wobble) from Read, 1995. Eccentricity (change in the shape of earth's orbit) occurs approximately every 100,000 to 400,000 years. Obliquity (tilt of the earth's axis) occurs approximately every 40,000 years. Precession (wobble of the earth's axis) occurs approximately every 19,000 to 23,000 years. Modified from Read (1995) who obtained the figure from Einsele and Ricken (1994).

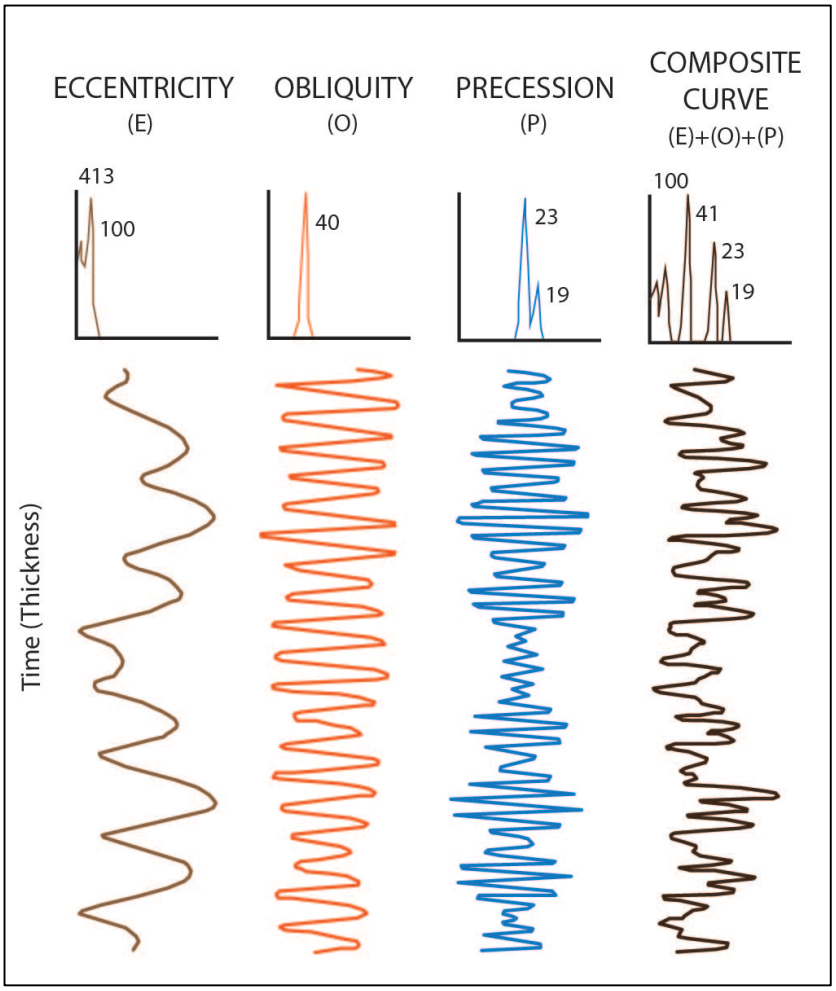


Figure 9. Diagram showing Milankovitch-band frequencies accountable for fluctuations in sea level. The composite curve shows how eccentricity, obliquity, and precession interact to cultivate the climate change signal, or sea level change. Modified from Read (1995) who obtained the figure from Einsele and Ricken (1994).

Sea level fluctuations are primarily related to the amount of continental ice existing during a particular sequence or cycle; this is correlative to the variation in greenhouse and icehouse environments through geologic time (Read, 1995). During greenhouse times, changes in sea level are typically small (less than 10m (33ft)) and can be controlled by precessional cycles and low amplitude 40, 100 and 400 k.y. cycles (Kerans and Tinker, 1997; Read, 1995). During icehouse times, sea level gradually falls during times of high glaciation and rapidly rises during times of deglaciation. This results in rapid transgressions that are usually higher than most rates

of sedimentation (Read, 1995). In global icehouse conditions, Milankovitch sea level fluctuations were typically large (up to 100m (328ft) or more) and were likely controlled by 100 and 400 k.y. eccentricity cycles (Kerans and Tinker, 1997; Read, 1995). According to Read (1995), obliquity cycles may be more important during transitional times (from greenhouse to icehouse) and icehouse times. This is important as the Mississippian was a transitional period from greenhouse conditions to icehouse conditions.

**Mississippian Sea Level**

The Mississippian represents a transitional period from greenhouse conditions that occurred throughout the Devonian to icehouse conditions that occurred throughout the Pennsylvanian and Permian (Read, 1995). During the Mississippian, Milankovitch sea level oscillations were usually large, being up to 100m (328ft) or more (Read and Horbury, 1993). Long term, 1$^{st}$ order, global sea level was some 50-100m (164-328ft) above the present day sea level (Haq and Schutter, 2008). Ross and Ross (1988) acknowledged 14-15 transgressive-regressive cycles (3$^{rd}$ order sequences) within the Mississippian that range from 1-3 million years in length. Haq and Schutter (2008) recognized 21 transgressive-regressive cycles within the same time period (Tournaisian through Serpukhovian) and noted temporally long 3$^{rd}$ order sequences (1-6 million years) can likely be correlated worldwide (Figure 10).

Overall, the Mississippian was a time of overall eustatic regression between submergence during Devonian and emergence during the Carboniferous (Buggish et al., 2008). During transitional periods from greenhouse to icehouse, the stratigraphic record shows that sea level changes illustrate minor evidence of precessional (19 to 23 k.y.) cycles and are more likely to be controlled by eccentricity (100 to 400 k.y.) and obliquity (40 k.y.) cycles (Read, 1995). According to Kerans and Tinker (1997), during transitional periods the stratigraphic record is characterized by high-frequency cyclicity that has well-defined stacked rock fabric units. Through the mid-Visean (Late Osagean/Meramecian) sea level began to decline considerably relative to sea level during the Tournaisian (Kinderhookian & Early Osagean), reaching a low in the

Serpukhovian (Chesterian) (Figure 10; Haq and Schutter, 2008).

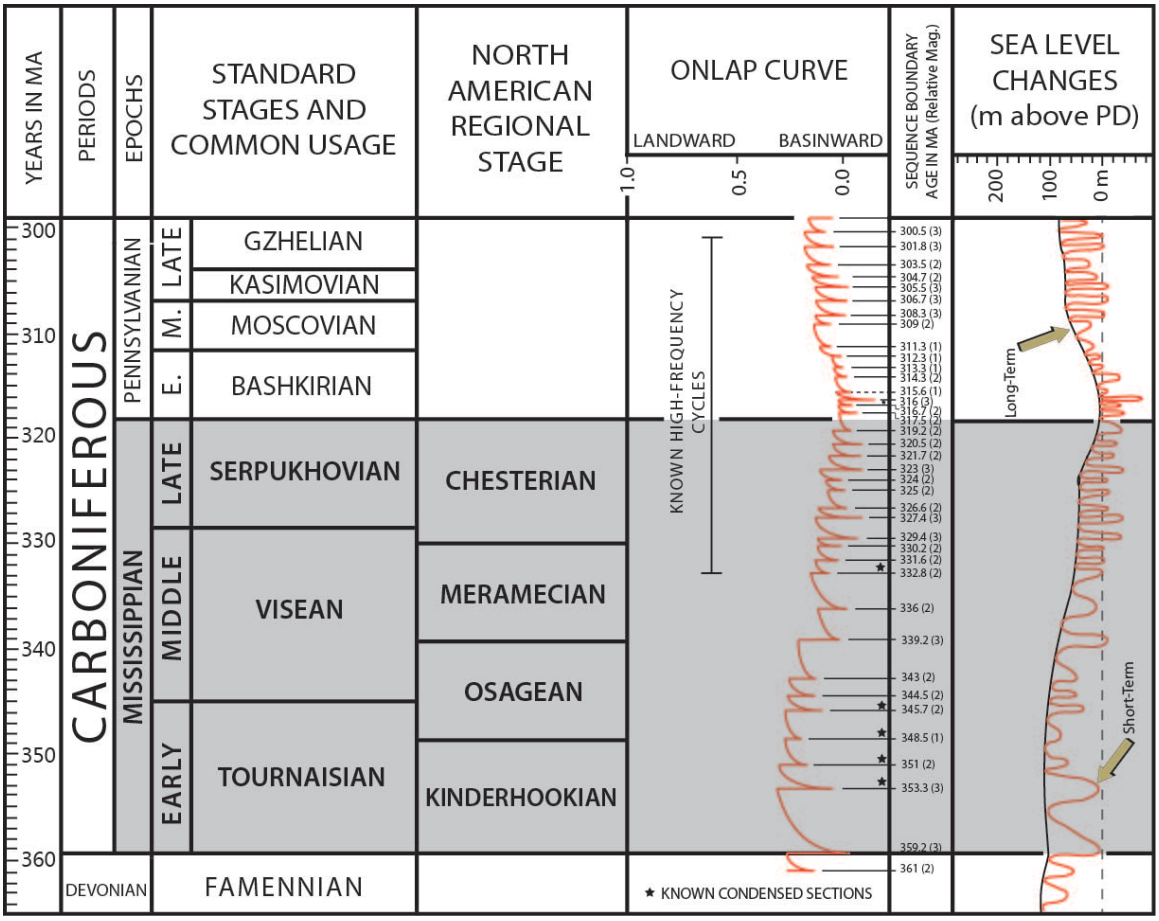


Figure 10. Diagram illustrating global sea level fluctuations throughout the Carboniferous Period. Stages of the Mississippian Epoch are bolded and highlighted in gray. The North American regional stage names are typically used in literature. Kinderhookian and Osagean strata link to the Tournaisian and Middle Visean Stages, while Meramecian and Chesterian strata link to the Middle Visean and Serpukhovian Stages. The decrease in the temporal span of 3rd order composite sequences during the Middle and Upper Mississippian is believed to be the result of the dominance of icehouse conditions. Modified from Haq and Schutter (2008).

## Problems in Expounding High Frequency Cyclicity

Regardless of the association between sea level oscillations and the subsequent changes in carbonate sedimentary systems, there are several other variables that can constrain high frequency cyclicity. Sedimentation rate, subsidence, and sediment body migration are acknowledged to develop meter scale packages of strata similar to those accredited to the higher frequency eustatic cycles ($4^{th}$ and $5^{th}$ order) (Cowan and James, 1996; Drummond and Wilkinson, 1993). Understanding the processes responsible for the formation of these cycles is necessary to avoid misconstruing facies patterns. Allocyclic and autocyclic processes can muddle the signal of sea level oscillation. Understanding how facies, attributed to these processes, migrate and are distributed within a system, as well as how subsidence rates along with tectonic activity affect facies distributions, are essential to discriminating allocyclic cycles, including eustatic cycles from autocyclic cycles (Drummond and Wilkinson, 1993).

Extracting high-frequency sea level cyclicity from the sequence stratigraphic hierarchy can prove to be problematic for various reasons. Some problems are external to the high-frequency cyclic nature of the system (as mentioned above), while other problems arise from the previously mentioned Milankovitch cycles. Likewise, correctly classifying the primary rock fabric and facies, in order to positively interpret the depositional environment, can be difficult in units having mixed siliciclastic-carbonate sediments and diagenetic changes. Finally, correlating high-frequency cycles within the subsurface can be difficult due to misinterpretation and the observation that high-frequency cycles are often below the resolution of wireline logs. Identifying these potential problems and their effects is fundamental to correctly determining the role of high-frequency sea level cycles within the complex sequence stratigraphic hierarchy.

### Problems in Classifying Facies

Correctly characterizing and classifying rock fabrics in both core and thin section is essential to interpreting depositional environments, because the rock fabric or facies reflect depositional energy related to high-frequency sea level oscillations. Input of siliciclastic sediment

can disturb the production of carbonates and successive diagenetic events can mask the primary rock fabric. These potential problems can lead to difficulties classifying lithofacies, and directly affect the interpretation of vertical stacking patterns and depositional processes.

**Mixed Carbonate-Siliciclastic System**

The name "Mississippian Limestone" is somewhat misleading. Thin section petrography demonstrates that throughout much of subsurface Oklahoma and the outcrop belt in the Ozark region and southern Oklahoma, the Mississippian section contains a significant amount of detrital quartz and clay minerals – mainly illite (Childress, 2015; LeBlanc, 2015; Flinton, 2016; Jaeckel, 2016; Price, 2014; Shelley, 2016). Sedimentation can alternate between carbonates and siliciclastics laterally and vertically, and may be separated temporally or can be deposited within the same period of time (McNeill et al., 2004). There are several hypotheses as to the origin of siliciclastic sediments within the study area, but the exact source(s) have yet to be determined. The occurrence of siliciclastic sediments is important to note due to its capability of disturbing and disrupting the fragile nature of carbonate environments (McNeill et al., 2004; Yancey, 1991). The Ozark Uplift is thought to have been a paleogeographic high during the Mississippian and could have been a regional source of siliciclastics for the mixed lithology system (Huffman, 1958). Another possible source is eolian as wind-blown silt is proposed for the underlying Woodford Shale. The Batesville Delta in northeast Arkansas is proposed as a fluvial-deltaic source of siliciclastic sediments in the Late Mississippian, and during the Chesterian. The Batesville Delta (Figure 11) was actively transporting sediment (Glick, 1979). With the dominant paleo wind and ocean current direction from the east northeast, it is probable that fine grained siliciclastic sediments were transported into the study area from the Batesville Delta. Siltstones dominate the upper intervals of both cores examined in this study. Moura et al. (2016) illustrates that a plume, hundreds of kilometers in size, created by the dumping of sediment from the Amazon River into the Atlantic ocean alters the photic and oxic zones, which hinders reef and carbonate production. A similar effect could have taken place from the Batesville Delta during

Chesterian time. Abundant siliciclastics hindered carbonate production and resulted in the dominance of siliciclastic sediments within the upper Chesterian (Hunt, 2017) intervals of the studied cores.

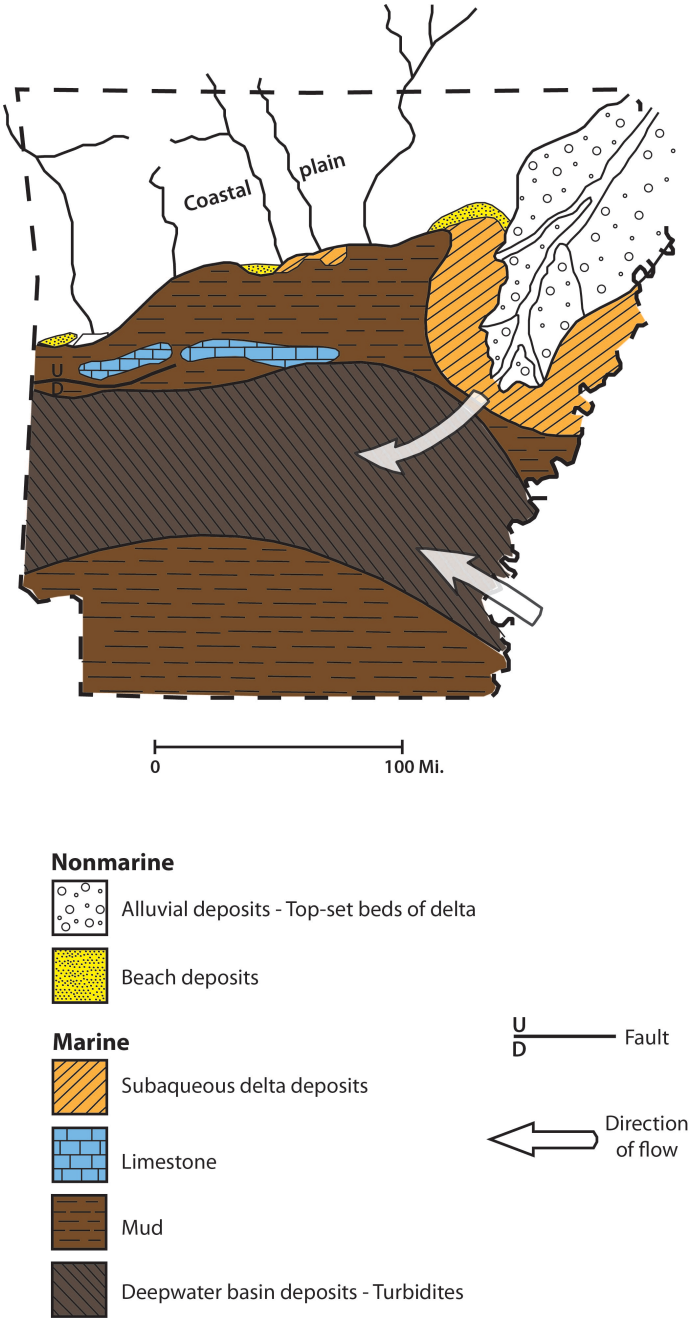


Figure 11. Distribution of environments, sediment types and direction of ocean current flow during Chesterian time. Modified from Glick (1979).

**Problems with Subsurface Correlation**

Correlations based on lithology alone can and will lead to erroneous chronostratigraphic correlations, especially when correlating carbonate packages. High-frequency sequences and cycles recognized in cores may not be resolved by wireline logs and in turn would not be recognized in correlations based on log data. Impending problems associated with delineating high-frequency cyclicity were anticipated with this study because facies stacking patterns likely do not represent the individual 20, 40, 100 and 400 k.y. Milankovitch cycles, but are composite cycles affected by additional variables including other allo- and autocyclic processes and siliciclastic input. These all contribute to making the "Mississippian Limestone" a complex system that is difficult to interpret.

## Regional Stratigraphy

"Mississippian Limestone" is an informal term that is used predominately within industry to label Mississippian-aged carbonate-dominated strata in the Mid-Continent. However, the Mississippian section can more precisely be defined as a mix of carbonate and siliciclastic sediments. The term "Mississippian Limestone" is a "catch all" term applied to carbonates of all ages in the subsurface of Oklahoma and Kansas. The stratigraphy of these Mississippian aged rocks is not clear-cut and is also convoluted by variations in nomenclature spanning short distances (Mazzullo et al., 2013). Relatively recent studies of outcrops by Mazzullo et al. (2013) have resulted in more useful nomenclature for correlating strata in the Ozark region (Figure 12). These proposed changes to the nomenclature by Mazzullo et al. (2013) have yet to be accepted or approved by the Stratigraphic Commission of North America and the USGS.

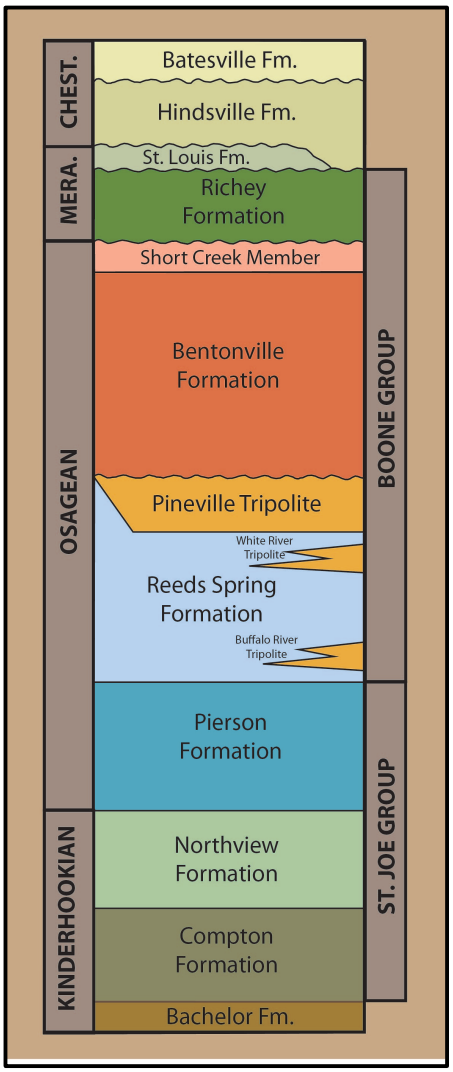


Figure 12. Stratigraphic column with newly proposed nomenclature of the Mississippian Subsystem. Modified from Mazzullo et al. (2013).

## Kinderhookian Strata

Kinderhookian-aged strata are commonly characterized by greenish-gray to gray silty calcareous shales and greenish-gray, finely crystalline limestone that may contain silt and dolomite (Jordan and Rowland, 1959). According to Frezon and Jordan (1979), Kinderhookian-aged strata are largely limestones and argillaceous limestones with minor amounts of calcareous mudstones. In some areas, sand and silt occur in basal beds. The silt or sand, where present, typically consists of sandy or silty limestone and muddy limestone. These sand-rich packages are

usually not prevalent enough to be replicated within the lithofacies pattern (Frezon and Jordan, 1979). Kinderhookian strata typically contain less chert than overlying Osagean-aged strata and are believed to represent deposition on a carbonate ramp or distally steepened carbonate ramp (Wilhite et al., 2011). Kinderhookian strata are thickest (150ft; 45.7m) in the Panhandle of Oklahoma, thin towards the east, and likely absent in the majority of eastern Oklahoma (Curtis and Champlin, 1959).

**Osagean Strata**

Regionally, strata labeled Osagean are characterized by brownish gray to dark gray, finely crystalline limestone that contains fluctuating amounts of dolomite, chert, and silt that is interbedded with gray to brownish gray, slightly calcareous shale (Curtis and Champlin, 1959; Heinzelmann, 1957). Osagean strata are characteristically cherty, with the chert being a product of replacement of the carbonates by silica (Frezon and Jordan, 1979). It is inferred that during the Osagean, from Kansas southward, the deposition occurred on a southerly dipping ramp containing low inclination (Wilhite et al., 2011). During this time, variations in sea level led to progradation of strata in a basinward direction (Childress and Grammer, 2015; Mazzullo et al., 2011). Oagean strata are thickest (700ft; 213m) in western Oklahoma and thin towards the south southeast, demonstrating that depositional strike paralleled the Transcontinental Arch (Curtis and Champlin, 1959; Lane and DeKeyser, 1980).

**Meramecian Strata**

According to Frezon and Jordan (1979) Meramecian rocks are comprised of muddy limestones and calcareous mudstones, with muddy limestones being the most widespread lithology across the northern third of Oklahoma. However, regionally within the study area, Meramecian strata are characterized by calcareous siltstones and silty argillaceous limestones that are interbedded with silty shales and argillaceous siltstones that contain irregular amounts of glauconite, dolomite, and chert (Curtis and Champlin, 1959; Heinzelmann, 1957; Jordan and Rowland, 1959). Lithologies labeled Meramecian are similar to the east and west of the Nemaha

Ridge (Flinton, 2016; Hunt, 2017; LeBlanc, 2014). In eastern Oklahoma, the Meramecian section is generally less than 100ft (30.5m) thick and thins toward the north (Curtis and Champlin, 1959).

**Chesterian Strata**

Regionally, Chesterian-aged strata are characterized by gray to black, silty and calcareous shales interbedded with gray to grayish brown, crystalline, fossiliferous limestones (Curtis and Champlin, 1959; Jordan and Rowland, 1959; Rowland, 1964). In the northwestern part of Oklahoma, fine-grained sandstone or siltstones occur towards the base of the section (Jordan and Rowland, 1959). Heinzelmann (1957) proposed that within the study area, Chesterian strata contains both the Fayetteville and Hindsville formations with the Fayetteville being present in the easternmost part. Chesterian rocks are thickest in southern Oklahoma and thin toward the north-northeast or shoreward, a similar depositional pattern as shown by underlying Meramecian strata (Curtis and Champlin, 1959; Rowland, 1964). During deposition of Chesterian sediments, subsidence rates increased and an incursion of siliciclastic sediments spread across portions of Oklahoma (Curtis and Champlin, 1959).

# CHAPTER III

## DATA AND METHODS

The primary objective of this research is to construct a sequence stratigraphic framework based on facies and stratal associations that can be used to characterize the relationship between shelfal (proximal) packages and basinal (distal) packages within the Mississippian section in east-central Oklahoma. The stratigraphic framework was established employing a sequence stratigraphic approach rather than a lithostratigraphic approach. Sequence stratigraphy is defined as the branch of stratigraphy that uses unconformities and their correlative conformities to compile successions of depositional packages into temporally and spatially confined sequences (Sloss, 1963). As a result, predicting the distribution of depositional facies becomes more apparent. The major strength of sequence stratigraphy is its potential to predict the lateral and vertical distribution or continuity of facies within a sedimentary basin, whereas a lithostratigraphic approach fails to accomplish this (Handford and Loucks, 1993). The sequence stratigraphic framework for the Mississippian section in east-central Oklahoma was established using core, thin section, and wireline log data.

Two cores through the "Mississippian Limestone" interval, ranging in thickness from 235-425 ft. (71.6-129.5m), were studied (Table 3). A total of ninety-seven thin sections were obtained from both cores across the Mississippian section. A sequence hierarchy was identified during core analysis (centimeter to meter-scale), and developed and quantified through the

analysis of thin sections (micrometer to centimeter-scale). X-ray diffraction was supplied and used to establish bulk mineralogy in intervals where mineralogy was not evident based on core and petrographic analyses. Significant surfaces of the stratigraphic hierarchy (noted in core) were correlated to their respective subsurface wireline log signatures and then extrapolated throughout the study area (kilometer-scale), which established the sequence stratigraphic architecture of the Mississippian section.

| Core # | Lease Name | Well No. | "Mississippian Limestone" Interval (ft) | Operator | County |
|---|---|---|---|---|---|
| 1 | Doberman | 1-25 | 4964.75′ - 5199.20′ | Devon Energy | Payne |
| 2 | Ihle | 1-26 | 2783.00′ - 3206.55′ | Devon Energy | Creek |

Table 3. List of cored wells utilized in this study including lease name, well number, depths through the Mississippian section in feet, operator, and county. Well information was obtained from the well logs and log headers.

## Core Descriptions

Examining and describing core is essential for understanding the characteristics of the rocks within the subsurface, specifically within the "Mississippian Limestone". Two cores (658 total feet, 200.5m) provided by Devon Energy were evaluated for detailed facies descriptions as well as detailed observations regarding fossil content, significant stratigraphic surfaces, and sedimentary structures. Depositionally significant surfaces (i.e. – flooding surfaces) were noted to delineate vertical stacking patterns and to help aid in the development of cycle hierarchy, as these surfaces often represent cycle boundaries. For the more carbonate-rich lithofacies, the Dunham (1962) classification scheme (Figure 13) was utilized. Siliciclastic-rich lithofacies were grouped/named based upon grain type, percentages of dominate grain types, texture, sedimentary structures, and the degree of bioturbation. The degree of bioturbation was determined using a bioturbation index chart from Bann et. al. (2008) (refer to appendices A&B for figure). A detailed

core description was completed to identify the depositional facies, interpret their respective depositional environments, and demonstrate the effects of high frequency cyclicity on facies stacking patterns. The distance between the two cored wells is approximately 54 miles (86.9km), resulting in both similarities and distinct differences in facies.

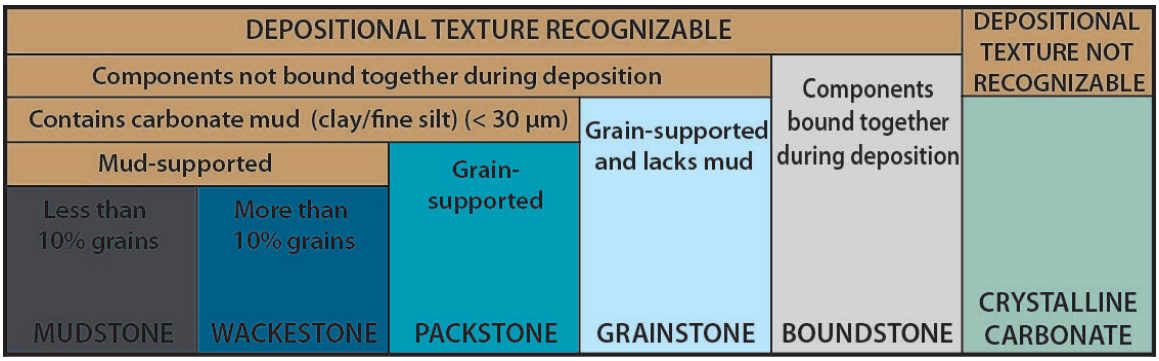


Figure 13. Illustration showing the Dunham (1962) classification of carbonate rocks according to depositional textures. This classification scheme was used in this study for the carbonate rich lithofacies. Modified from Scholle and Ulmer-Scholle (2003).

## Thin Section Analysis

A total of 97 thin sections were prepared for samples collected from the Mississippian section in both cores (Figure 14). Seventy-one of these thin sections were provided by Devon Energy. The additional twenty-six thin sections were prepared by Tulsa Thin Sections from samples collected from the butt end of the core. All 97 thin sections were stained with alizarin red to easily identify calcite; thin sections provided by Devon Energy were also stained with potassium ferrocyanide to identify dolomite. All thin sections were blue epoxy impregnated to facilitate the identification of open pores. The Mississippian section in both cores is so fine grained that thin section petrography is crucial to determining and describing variations within the facies that are not apparent in hand sample. Thin sections provided essential information for quantifying grain size, allochem or fossil content, textural classification, and various pore types.

As with hand sample core descriptions, the thin section descriptions employed the Dunham (1962) classification scheme (Figure 13) to define observed textures. Allochem content along with grain size were estimated using standard visual estimation charts. Grain size and morphology can be critical indicators of depositional energy, which is critical to evaluating depositional processes and settings. Thin section data were fundamental in constructing interpretations of depositional environment, conditions during deposition, facies, and facies stacking patterns.

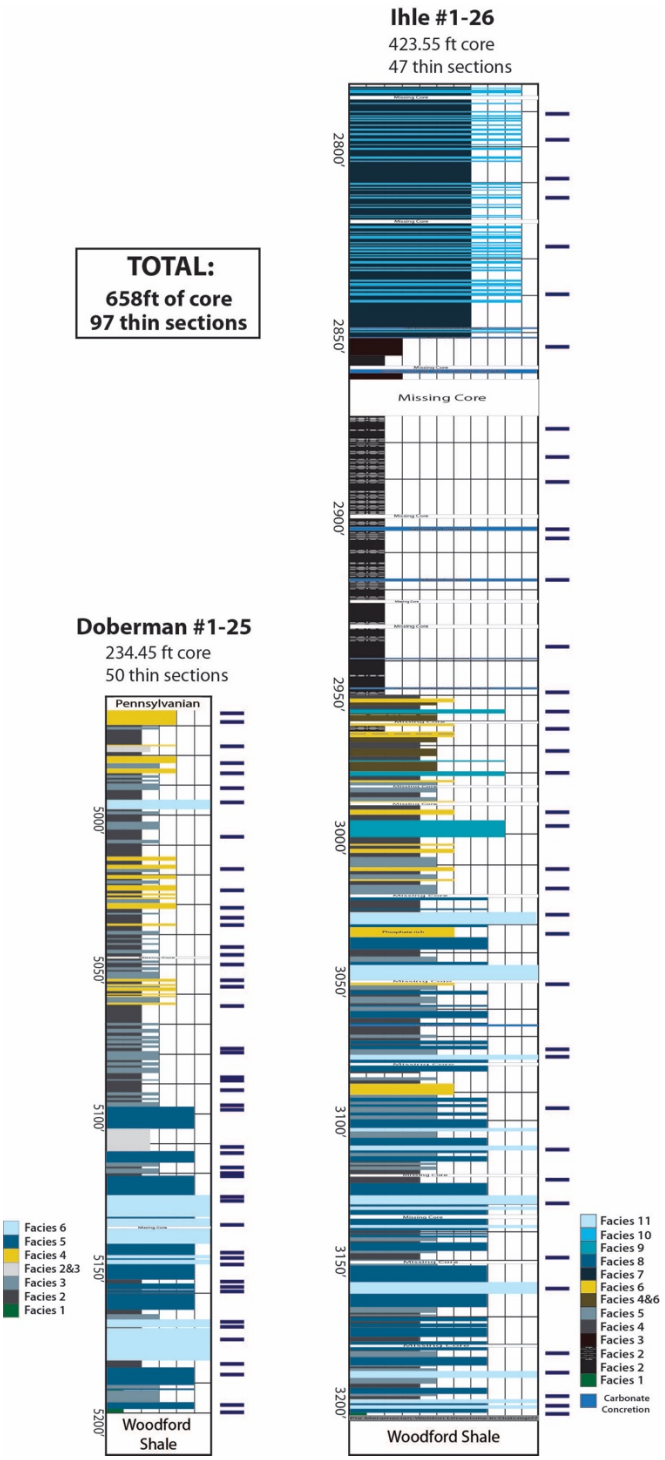


Figure 14. Measured sections for both cores showing their total footage, facies variability, and locations of thin sections (purple rectangles next to facies column) throughout the Mississippian section. Thin section sample locations were selected based on changes in composition and apparent sharp contacts. The frequency of samples within the Doberman #1-25 reflects the rapid changes in facies compared to the Ihle #1-26.

## X-Ray Diffraction (XRD)

X-ray diffraction (XRD) is diagnostic for identifying crystalline materials in rocks and provides quantitative estimates of bulk and clay mineralogy. Devon Energy sampled the butt section of the core and x-rayed samples that correspond to the 71 thin section depths. These samples were evaluated using whole rock bulk mineralogy to identify and quantify the abundances of common framework grains and cements including calcite, dolomite, quartz, and feldspars. Clay mineral types and abundances were also determined using bulk XRD data. For the purpose of this study, XRD composition augmented mineral composition determined using thin section petrography and were used to classify facies trends and interpret depositional processes, depositional setting, and cyclic boundaries. Abundances of clay and calcite change over short lengths of the cores (centimeter to meter scale). XRD data proved useful for detecting these changes, providing more accurate mineralogy than was apparent in hand sample and thin section, and helped to more accurately classify facies.

## Sequence Stratigraphic Analysis

A sequence stratigraphic hierarchy in this study was defined using the principles of sequence stratigraphy and associated Milankovitch bound high-frequency cycles. Probable 3$^{rd}$ order sequences and 4$^{th}$ order high-frequency sequences, containing transgressive and regressive segments, were interpreted from facies stacking patterns and correlated to their respective wireline log signatures. These sequences were first correlated to gamma-ray log curves. Secondly, they were correlated to resistivity curves (which proved very useful for identifying sequences on adjacent well logs within the study area), and finally to the neutron and density porosity logs. Correlating facies stacking patterns to log signatures allowed correlation of facies/sequences away from cored wells and mapping of sequence distribution.

## Subsurface Correlation/ Wireline Logs

Devon Energy provided a suite of well logs including: caliper, gamma-ray, spontaneous potential, shallow medium and deep resistivity, density porosity, neutron porosity, and P.E. for the two cored wells as well as a data set of additional wells within the study area. Wireline logs measure properties of the rock and the fluid within, and are used to correlate zones of interest and evaluate reservoir properties. Caliper log measurements represent the diameter of the borehole and therefore indicate zones that are washed out (increased caliper reading) or zones that are permeable (decreased caliper reading). The caliper log proved useful for determining the boundary between Mississippian and Pennsylvanian strata, as less indurated Pennsylvanian strata wash out, whereas better cemented Mississippian strata are more competent and resist erosion during drilling. Gamma-ray (GR) logs measure the natural radioactivity from radiogenic potassium, thorium, and uranium that frequently occur in clay-mineral rich shales and mudrocks. The GR is largely used to distinguish between clay-rich and less-clay-rich (cleaner) lithologies and is a useful correlation tool to distinguish between mudrock and non-mudrock lithofacies. Spontaneous potential or SP, which measures the electric potential between the drilling fluid and the drilled rock and its natural fluids, is used to determine the variation of ionic concentrations in pore fluids within the rock. Resistivity logs use electrical conductivity of strata and the fluids therein to identify permeable strata and differentiate between water-saturated rocks and hydrocarbon saturated zones. The density tool measures porosity via measuring electron density for specific minerals, whereas the neutron log measures porosity by determining hydrogen concentrations. Together these tools provide an estimation of mineralogy dependent porosity and the presence of gas, petroleum or water-bearing zones. Asquith and Krygowski (2004) provide in depth information concerning logging tools including the basics of how they work and are used to interpret subsurface strata and fluids.

Core spectral gamma-ray and borehole gamma-ray were both used to interpret lithology and trends in clay content. The core spectral gamma-ray curve was compared to core lithology and the borehole gamma-ray for both wells. Core lithology, thin sections, core gamma-ray curve and open-hole wireline log signatures were correlated to establish the characteristic log signatures for specific facies and facies stacking patterns. Tying these facies and the derived sequences to their respective wireline log signatures resulted in more accurate correlation of wireline logs and subsurface mapping, and facilitated constructing the sequence stratigraphic architecture of the "Mississippian Limestone" within the study area. Using mostly gamma-ray and resistivity curves, wells adjacent to the cored wells were correlated to the cored wells and became the basis for cross-section construction and mapping.

## Geologic Mapping

Through geologic mapping, the lateral continuity and distribution of depositional sequences were revealed. Mapping showed that sequences have consistent thickness and are laterally continuous moving subparallel-parallel to depositional strike, but exhibit variable thicknesses parallel to depositional dip and can be discontinuous. 3$^{rd}$ Order sequences were mapped to determine their distribution patterns and thicknesses. Along with the thickness maps, structure maps were constructed to gain insight into the present structural attitude of these packages and determine if tectonics, especially faulting, affected the thickness of the depositional sequences and the Mississippian section as a whole.

## Dataset Limitations

For this study, two cores were used to define a sequence stratigraphic framework that enhanced and expanded upon previous models of sequence stratigraphy within the "Mississippian Limestone". Both of the cores utilized in this study contain the contact between the Mississippian section and the underlying Woodford Shale. However, only one of the cores (Doberman #1-25)

contains the contact between the Mississippian section and the overlying Pennsylvanian strata. The Ihle #1-26 core did not capture the contact between Pennsylvanian and Mississippian strata. The Mississippian-Pennsylvanian contact was determined from well log responses and specifically, similar signatures from the Doberman #1-25 core and adjacent wells in close proximity within the study area. The distance between the cored wells is a little over 54 miles (86.9km), which is different from other recent studies (Flinton, 2016; Jaeckel, 2016; LeBlanc, 2014) that utilized cores where spacing between the cored wells was smaller. Eleven depositional facies were identified in the Ihle core, whereas the Doberman core contains only six. However, all six facies observed within the Doberman occur in the Ihle. Based on the previous work of LeBlanc (2014) and Flinton (2016) and the facies relationships in the Ihle and Doberman cores, it is apparent that the vertical changes in facies occur quickly, but that facies patterns are predictable. It is important to consider that the two cores in this study, while demonstrating distribution of facies within the study area, might not be representative of Mississippian depositional facies at locations outside of the study area.

The age of the cores is acknowledged to be Mississippian, but without biostratigraphic data, the exact age of the cores was unknown. Another study (Hunt, 2017) concurrent with this one, established conodont biostratigraphy of Mississippian strata, including the Doberman #1-25. Unfortunately due to poor recovery of conodont samples (whether the result of conodonts not being present or samples being incomplete or unidentifiable) absolute dating across much of the core was inconclusive. However, of the conodont samples that were identifiable, the Doberman #1-25 core appears to be Meramecian and Chesterian in age, with the majority of the core being Chesterian. Conodont biostratigraphic analysis provides relatively high-resolution age constraint (maximum resolution of one million years) and it is the most accurate dataset for correlation within the Mississippian (Boardman et al., 2013). With a maximum resolution of one million years, conodont biostratigraphy is useful for pinpointing 3$^{rd}$ order sequences, but is not useful in

defining higher-frequency 4th and 5th order cyclicity that falls below its resolution. Recognizing these limitations, the hierarchy of cyclicity evident in these cores will follow the findings of previous studies (Flinton, 2016; Jaeckel, 2016; LeBlanc, 2014) and be labeled as 3rd, 4th, and 5th order. For this study, as with previous ones, high-frequency cyclicity was determined based on repetitive facies stacking patterns and significant stratigraphic surfaces (i.e. – flooding surfaces or exposure surfaces) that were observed in core and recognized on wireline log signatures (electrofacies), without a direct reference to a certain length of time. In carbonate systems, the high-frequency sequences and cycles commonly act as individual flow or reservoir units; (Grammer et al., 2004) therefore, identifying these units is critical.

# CHAPTER IV

## RESULTS AND DISCUSSION

### Facies Associations

Eleven total depositional facies were identified through the examination of both cores (658ft total; 200m). These facies associations were established based upon texture, grain/ bioclast type, grain size, sedimentary structures, color, and interpreted depositional environment. Interpretations from the core examination were augmented through the use of thin sections (97 total) taken from both cores. The input of siliciclastic sediments and gradational/rapid changes in sediment type and composition made delineating facies problematic. To combat these changes, facies were determined using average grain size, as well as percentages of the grain sizes observed. This was done through petrographic analysis, point counting, and inspection of core slabs under a microscope. Devon Energy provided XRD analysis for both cores, which allowed for the quantifying of mineralogical composition of each facies. The Ihle 1-26 (core #2) contains all eleven depositional facies within the "Mississippian Limestone" interval. However, the Doberman 1-25 (core #1) "Mississippian Limestone" interval contains only six of the depositional facies. This is likely due to either non-deposition or post depositional erosion. Facies composition falls into two general categories: carbonate-dominated and siliciclastic-dominated. The carbonate-dominated facies types range from mudstones-wackestones to higher-energy packstones-grainstones indicated by an increase of faunal assemblages (peloids, crinoids, and brachiopods). The siliciclastic-dominated facies

types range from silty shales/mudstones to siltstones and sandstones. Tables 4 and 5 provide detailed summaries of each facies and their characteristics for both cored wells. Colors were determined using GSA's Rock-Color-Chart that was prepared by the Rock-Color Chart Committee. Supplementary core photos with corresponding facies, as well as thin section photomicrographs of each facies for core #1 and core #2 are located in Appendices A and B.

| Doberman Facies | | Color | Mineralogy (Avg. %) | | | Sedimentological Character | Primary Grain Constituents |
|---|---|---|---|---|---|---|---|
| | | | Quartz | Carbonate | Clays | | |
| 6 | Silty Peoloidal Packstone-Grainstone | Very Light Gray to Medium Gray & Moderate Yellowish Brown (in areas) | 29.4 | 56.6 | 4.4 | Massive Bedded, Mineralized Fractures | Peloids, Crinoids, Brachiopods, and Minor Bryozoan Fragments |
| 5 | Silty Burrowed Mudstone-Wackestone | Light Olive Gray & Greenish Black to Grayish Black | 30.5 | 46.2 | 15.0 | Burrowed, Mineralized Fractures | Brachiopods, Crinoid Fragments, Indistinguishable Skeletal Debris |
| 4 | Silty Argillaceous Sandstone | Dark Greenish Gray to Dusky Yellow Green & Moderate Olive Brown | 56.0 | 8.4 | 18.8 | Burrowed and Bioturbated to Laminated parallel to bedding | Brachiopods, Very Fine Sand and some Silt Sized Quartz Grains |
| 3 | Slightly Sandy Calcareous Siltstone | Olive Gray to Dark Gray | 47.0 | 19.3 | 15.7 | Bioturbated and Burrowed, Mineralized Fractures | Brachiopods, Silt and some Very Fine Sized Quartz Grains |
| 2 | Clay-rich Siltstone | Dusky Green Greenish Black & Grayish Black | 43.5 | 11.8 | 24.6 | Planar Laminae, Locally-Thinly Bedded | Brachiopods, Silt Sized Quartz Grains |
| 1 | Glauconitic Sandstone | Dusky Yellowish Green to Dark Grayish Green | 45.0 | 3.0 | 37 | Massive Bedded, Burrowed | Conodonts, Brachiopod Fragments, Glauconitic Quartz Grains |

Table 4. Mississippian depositional facies observed in the Doberman #1-25 core. The table includes the color, average bulk mineralogy from XRD, primary grain constituents, and sedimentological character for each facies.

| Ihle Facies | | Color | Mineralogy (Avg. %) | | | | Sedimentological Character | Primary Grain Constituents |
|---|---|---|---|---|---|---|---|---|
| | | | Quartz | Calcite | Dolo. | Clays | | |
| 11 | Silty Peoloidal Packstone-Grainstone | Light Gray to Medium Dark Gray | 19.1 | 65.3 | 2.1 | 6.0 | Massive Bedded, Mineralized Fractures, mm Scale Burrows | Peloids, Crinoids, Brachiopods, and Minor Bryozoan Fragments |
| 10 | Recrystallized Packstone-Grainstone | White to Very Light Gray | 2.0 | 87.7 | 3.0 | 6.7 | Indistinguishable Fossils due to Heavy Recrystallization, Locally Thin-Bedded & Innerbedded with Facies 7 | Recrystallized Calcite, Indistinguishable Skeletal Debris |
| 9 | Silty Argillaceous Dolo Packstone | Very Light Gray to Medium Gray & Light Bluish Gray | 30.0 | 7.0 | 28.7 | 25.0 | Massive Bedded, Mineralized Fractures, Fluid Escape Pathways | Brachiopod Fragments, Euhedral Dolomite, Clay Clasts |
| 8 | Silty Burrowed Mudstone-Wackestone | Greenish Black to Brownish Black & Grayish Black | 27.0 | 45.0 | 1.0 | 14.0 | mm to cm Burrows, Mineralized Fractures, Fossiliferous | Brachiopods, Crinoid Fragments, Indistinguishable Skeletal Debris |
| 7 | Argillaceous Mudstone-Wackestone | Grayish Black to Black | 11.0 | 46.3 | 2.7 | 43.0 | Planar Laminae, Locally Thin-Bedded and Innerbedded with Facies 10 | Brachiopods, Carbonate Mud, Indistinguishable Skeletal Debris |
| 6 | Silty Argillaceous Sandstone | Medium Light Gray to Greenish Gray & Dusky Yellow Green | 53.0 | 6.6 | 2.6 | 21.4 | Burrowed to Bioturbated & Laminated parallel to bedding | Brachiopods, Very Fine Sand and some Silt Sized Quartz Grains |
| 5 | Slightly Sandy Calcareous Siltstone | Greenish Gray to Medium Gray | 44.0 | 20.0 | 4.7 | 16.7 | Bioturbated and Burrowed, Mineralized Fractures | Brachiopods, Silt and some Very Fine Sized Quartz Grains |
| 4 | Clay-rich Siltstone | Medium Dark Gray to Grayish Black & Dusky Brown | 47.3 | 7.3 | 3.0 | 25.7 | Planar Laminae, Locally Thin-Bedded | Brachiopods, Silt Sized Quartz Grains |
| 3 | Phosphatic Dolomitic Shale | Brownish Black to Dusky Brown and Dusky Blue Green | 29.0 | 1.0 | 24.0 | 29.0 | Laminated to Massive Bedded, Abundant Phosphate Nodules Seen in Thin Section | Silt to Sand Sized Phosphate Clasts, Euhedral Dolomite |
| 2 | Silty Shale | Brownish Black to Black | 25.9 | 3.5 | 0.6 | 56.9 | Irregular Beds of High Fissility, Pyrite and Calcite Laminae, Pyrite Burrows (in areas) | Illite and or Smectite Clays, Silt Sized Quatrz Grains |
| 1 | Glauconitic Sandstone | Greenish Gray to Greenish Black | 39.0 | 2.0 | 5.0 | 45.0 | Massive Bedded, Heavily Burrowed | Conodonts, Dolomite, Brachiopod Fragments, Glauconitic Quartz Grains |

Table 5. Mississippian depositional facies observed in the Ihle #1-26 core. The table includes the color, average bulk mineralogy from XRD analysis, primary grain constituents, and sedimentological character of each facies.

The facies identified in both cores were ordered and presented in a shallowing or shoaling-upward sequence that is based on the findings of previous studies (Flinton, 2016; LeBlanc, 2014). The numeration begins with the facies determined to represent the most distal depositional environment and concludes with facies determined to represent the most proximal depositional environment. Based on the occurrence of the facies presented in tables 4 and 5, as well as previous work (LeBlanc, 2014; Childress, 2015), it is interpreted that deposition occurred on a gently sloping ramp-like setting, such as a distally steepened carbonate ramp (Figure 15).

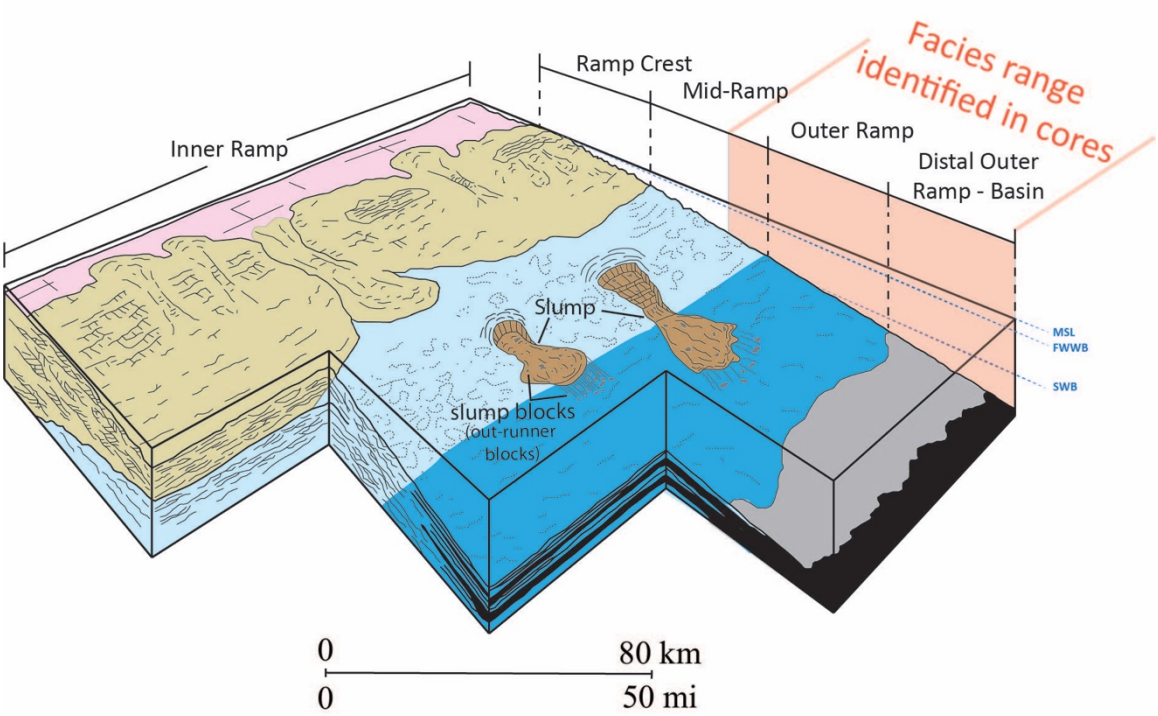


Figure 15. Diagrammatic representation of a distally steepened carbonate ramp environment showing the key environmental subdivisions. The facies observed from both cores in the Mississippian section are characteristic of depositional lithofacies within a mixed carbonate-siliciclastic ramp-like setting. The area highlighted in red represents the range of depositional facies observed in this study. The range of facies varies from shales and mudstones-wackestones in the distal outer ramp to packstones-grainstones in the distal portion of the mid-ramp. Modified from Childress (2015), originally re-drafted by LeBlanc (2014) after

## DOBERMAN #1-25 SWD FACIES

### Doberman Facies 1: Glauconitic Sandstone

The glauconitic sandstone facies is dusky yellowish green to dark grayish green color, grain dominated, and burrowed (Figure 16). Based on thin section petrography and XRD analysis, Facies 1 is composed primarily of fine to medium sand-sized glauconite grains (50-60%) that are sub- to well-rounded and moderately sorted, silt to very fine sand-sized quartz grains (35-45%) that are sub-rounded to well-rounded and well sorted, clay minerals – mainly illite (20-45%), and dolomite (3-10%). The glauconitic sandstone facies also contains pyrite (5-6%) and phosphate

grains (2-3%). To a lesser degree, skeletal debris occurs in the form of thin-shelled brachiopod fragments, as well as phosphatic bone fragments. This facies is only present in the lowermost 10ft (3m) of the Doberman core (core #1) and ranges in thickness from 0.1ft (0.03m) to 1ft (0.3m).

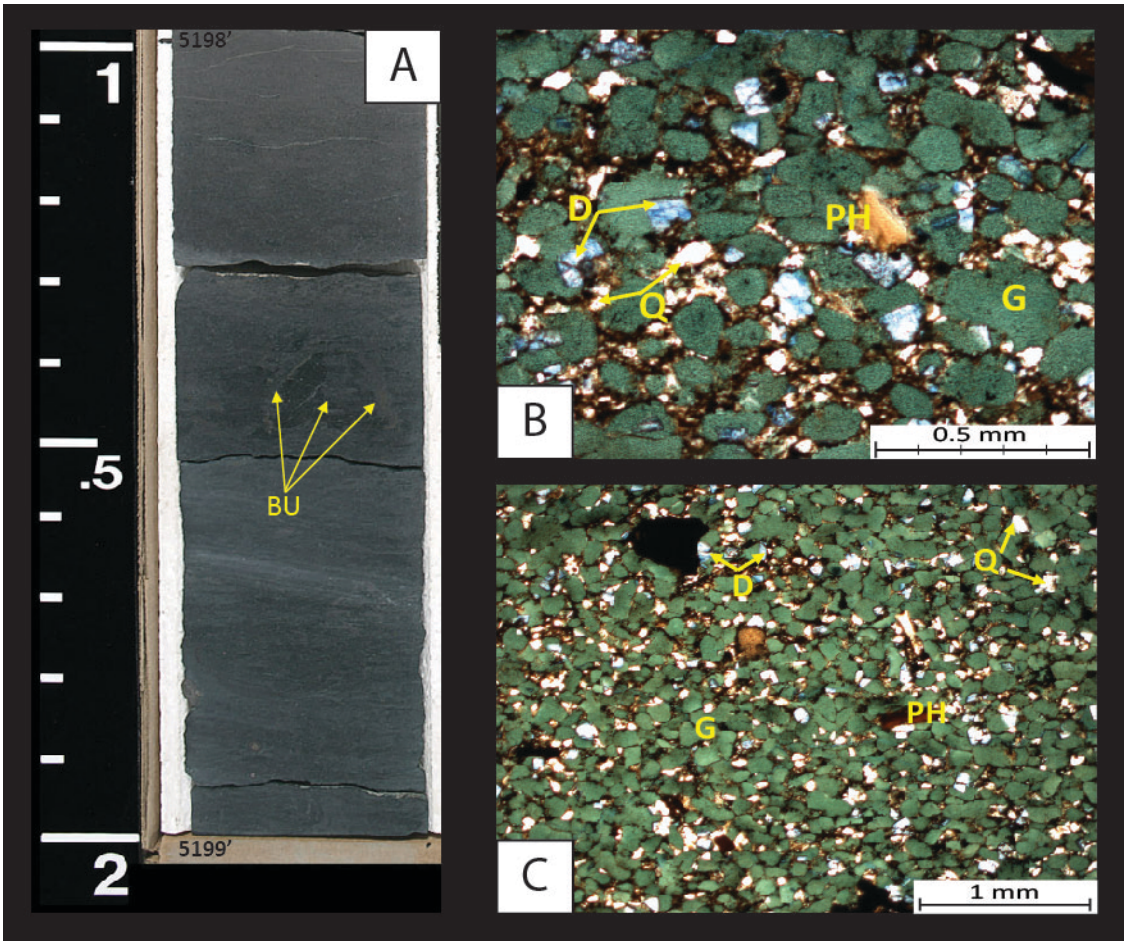


Figure 16. Doberman Facies 1: Glauconitic Sandstone Facies. **A)** Core photograph of Doberman Facies 1 in white light. The scale to the left of the core is in tenths of feet. Doberman Facies 1 is dusky yellowish green to dark grayish green in color and commonly displays burrowing (BU). **B-C)** Thin section photomicrograph of the glauconitic sandstone facies within the Doberman core at 5198.30'. Images are in PPL. The sample is blue epoxy impregnated. This sample shows the sand-sized glauconite (G) grains, silt to fine sand-sized quartz (Q) grains, dolomite (D) grains and phosphate (PH) grains. XRD analysis: 45% quartz, 3% carbonates (3% dolomite), 37% clay minerals (28% illite/mica, 9% mixed layer illite/smectite), and 15% other minerals (5% plagioclase feldspar, 4% potassium feldspar, 5% pyrite, and 1% marcasite).

The glauconitic sandstone facies often occurs in the lowermost portion of the "Mississippian Limestone" interval in subsurface cores and is commonly reported in bit cuttings immediately above the Woodford Shale across northern Oklahoma. As a result of its widespread distribution, Facies 1 is interpreted to represent regional-scale deposition in a low-energy environment, where circulation was limited, during the initial stages of a transgressive event or flooding of the post-Woodford surface. Low-energy conditions along with little to no sediment supply, within a submarine environment, are idealized conditions for the formation of glauconite (Amorosi, 1997; Middleton et al., 2003). The occurrence of thin-shelled brachiopod fragments also supports the interpretation of deposition occurring in a relatively low-energy environment, probably below storm wave base (SWB). It is interpreted that this facies represents the onset of a widespread transgression across the area of study.

**Doberman Facies 2: Clay-Rich Siltstone**

The clay-rich siltstone facies is dusky green to greenish black and grayish black in color and commonly has visible, intact laminae (Figure 17). This facies contains abundant silt-sized quartz grains (40-50%) that are sub-angular to sub-rounded and are moderately to well sorted, abundance of clay minerals (highest percentage of all Doberman facies) – largely illite (20-30%), and in areas, phosphate nodules can be seen in hand sample and thin section. The clay-rich siltstone facies also contains carbonate – mainly calcite (10-17%). To lesser degree, it contains sparse skeletal debris, mainly brachiopod fragments. In core, this facies is generally thin-bedded, darker colored, and has intact laminae that contrasts disrupted/bioturbated laminae in the calcareous siltstone facies. The contacts between overlying and underlying facies are commonly sharp.

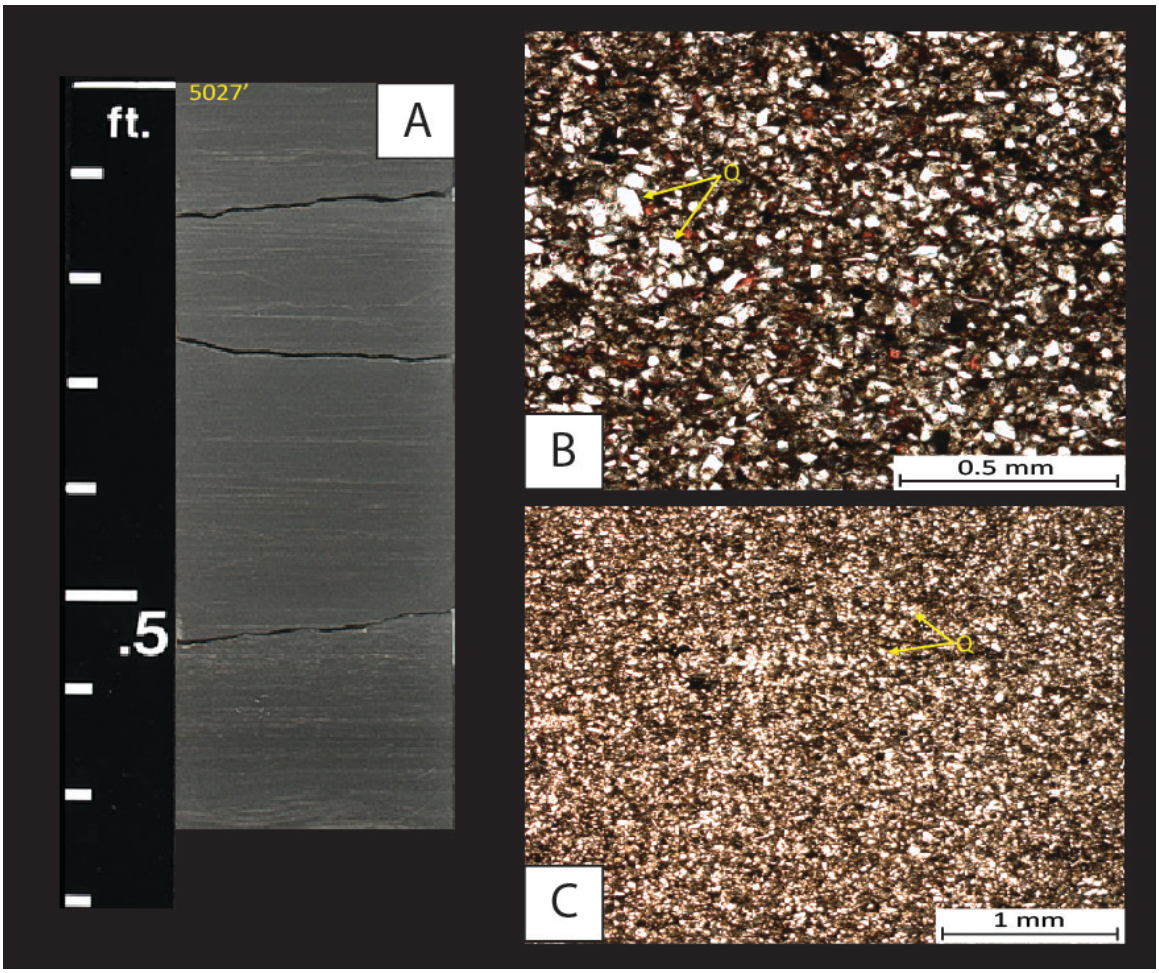


Figure 17. Doberman Facies 2: Clay-Rich Siltstone. **A)** Core photograph under white light showing the dusky green to greenish black and grayish black color and intact laminae. This facies is generally thinly bedded and contacts with other facies are generally sharp. The scale on the left of the core photo is in tenths of feet. **B-C)** Thin section photomicrographs of the clay-rich siltstone facies in the Doberman core at 5027.10'. Images are in PPL. The sample is dominated by quartz silt (Q) to very fine sand-sized quartz grains in areas and contains an abundance of clays (20-30%) and organic matter. This facies contains sparse amounts of carbonates (~11%) – calcite grains (pink). The calcite grains are indistinguishable bioclasts/fossils. XRD analysis: 44% quartz, 11% carbonates (10% calcite, and 1% dolomite), 26% clay minerals (19% illite, 4% illite/smectite, and 3% chlorite), 19% other minerals (11% plagioclase feldspar, 4% potassium feldspar, 3% pyrite, and 1% apatite). The average porosity for this facies based on 3 samples was 5%, and average permeability was 0.066 millidarcies (mD) (air) and 0.039 mD (Klinkenberg).

The clay-rich siltstone facies is interpreted to represent continued transgression following Facies 1. The angular silt-sized quartz grains could be eolian in origin, however, the presence of sub-rounded grains suggest that some were transported via water current. Preserved laminations along with a relative abundance of clays support the interpretation that during deposition, the environment was restricted, calm and fairly low-energy. The low abundance and assortment of organisms (crinoids and brachiopods) suggests an environment that periodically alternated from dysoxic to slightly oxygenated water conditions (Ekdale et al., 1984). Due to minimal abundance and diversity of organisms, Facies 2 is interpreted to be part of the outer to distal outer ramp (Figure 15) with deposition below FWWB – fair weather wave base and likely below SWB – storm wave base (Ekdale et al., 1984).

**Doberman Facies 3: Slightly Sandy Calcareous Siltstone**

The slightly sandy calcareous siltstone facies (Figure 18) is commonly bioturbated and olive gray to dark gray in color. This facies is dominated by silt- to very fine sand-sized quartz grains (37-49%) that are sub-angular to sub-rounded and moderately sorted, an abundance of carbonate (calcite) content (24-35%), and clay minerals (12-18%). The difference between this Facies 3 and the clay-rich siltstone (Facies 2) is that Facies 3 is characterized by an increase in biogenic structures (burrows) over physical sedimentary structures (compared to that of Facies 2). These burrows and beds range from completely burrowed to slightly laminated beds. This calcareous siltstone facies generally has higher carbonate content and lower clay content compared to the clay-rich siltstone facies. This facies is commonly bioturbated or burrowed whereas the clay-rich siltstone facies is generally laminated and thinly bedded. However, some intervals within the Doberman Facies 3 have remnant parallel laminations surrounded by beds of the same facies that are heavily burrowed. The contacts between the two siltstone facies are generally sharp and easily recognizable.

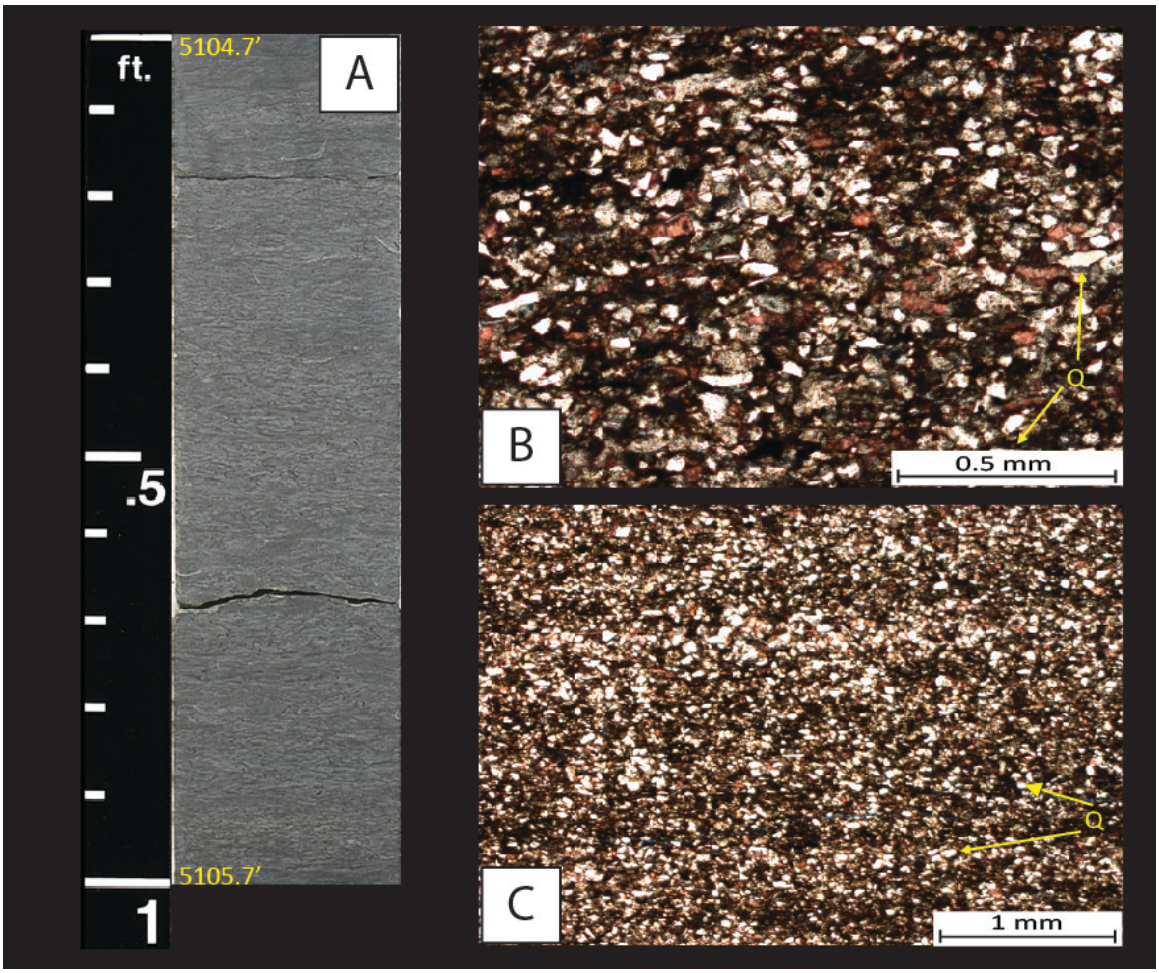


Figure 18. Doberman Facies 3: Slightly Sandy Calcareous Siltstone. **A)** Core photograph of the Doberman facies 3 under white light. The scale to the left of the core is in tenths of feet. This facies is commonly bioturbated dark gray to olive gray in color. Doberman Facies 3 commonly contains small (mm scale) burrows that likely represent the *Phycosiphan* Ichnofacies. **B-C)** Thin section photomicrographs of the slightly sandy calcareous siltstone facies within the Doberman core at 5107.25'. Images are in PPL. The sample is dominated by silt- to very fine sand-sized quartz (Q) grains, carbonate – mainly calcite (pink) grains, occasional clays – mainly illite, and a muddy organic-rich matrix. Usually the calcite grains in this facies are indistinguishable bioclasts or micritized grains; when the grains are recognizable, they are generally brachiopod and crinoid fragments. XRD analysis: 42% quartz, 25% carbonates (22% calcite and 3% dolomite), 18% clay minerals (12% illite, 5% illite/smectite, and 1% chlorite), and 15% other minerals (9% plagioclase feldspar, 4% potassium feldspar, and 2% pyrite). The average porosity for this facies based on 3 samples was 5%, and average permeability was 0.038 mD (air) and 0.021mD (Klinkenberg).

During deposition of Doberman Facies 3, there appears to have been an increase in water energy (moderate), increase of oxygen levels, and increased circulation of water compared to that of Facies 2. Evidence for an increase in the oxygen levels and circulation of water is increased fauna activity, particularly small (mm) horizontal burrows likely due to *Phycosiphan* and/or *Teichichnus* (MacEachern et al., 2009). Another line of evidence for an increase in the quality of the water during deposition is an increase in the appearance of fossils (i.e. thin-shelled brachiopods). An increase of carbonate (calcite) grains, although indistinguishable bioclasts, from that of Facies 2 supports intensification in water energy along the ramp (Tucker and Wright, 1990). Doberman Facies 3 is interpreted to have been deposited in relatively oxygenated water environment in the distal mid-ramp to proximal outer ramp setting, below FWWB and near SWB (Figure 15).

**Doberman Facies 4: Silty Argillaceous Sandstone**

The silty argillaceous sandstone facies (Figure 19) within the Doberman occurs in the upper 98ft (29.9m) of the core and is dark greenish gray to dusky yellow green and moderate olive brown. This facies is dominated by sub-angular to sub-rounded, moderately sorted to well sorted very fine to fine sand-size quartz grains (50-61%), clay minerals – mainly illite (15-27%), and carbonate (calcite) grains (7-21%). The silty argillaceous sandstone contains small amounts of skeletal debris that is dominantly brachiopod fragments, and has a dark organic matter (?) and muddy matrix. Bioturbation is the dominant biogenic structure within this facies. Parallel laminations, and to a lesser degree cross-bedding, are the only physical sedimentary structures identified.

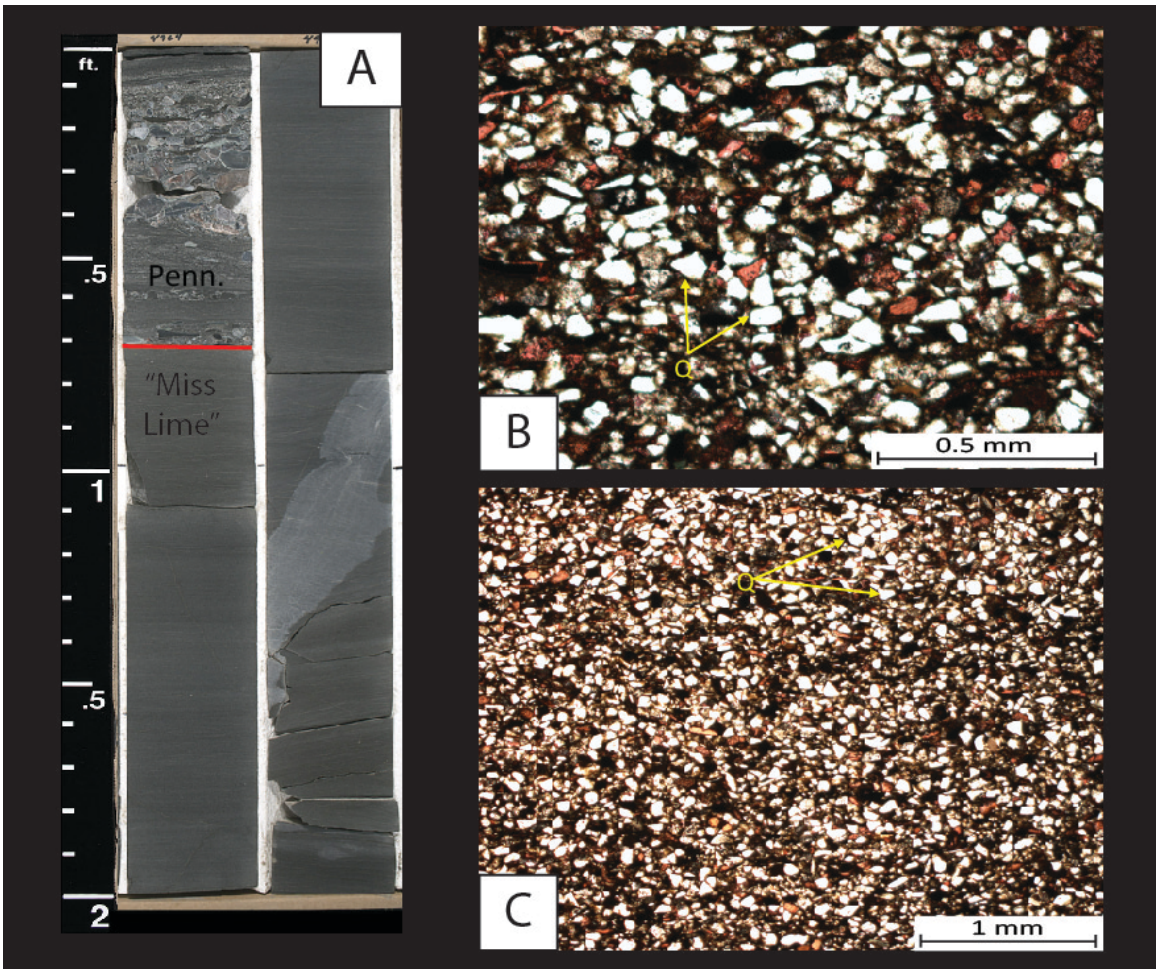


Figure 19. Doberman Facies 4: Silty Argillaceous Sandstone. The scale to the left of the core photo is in tenths of feet. **A)** Core photograph of Doberman Facies 4 under white light, it is dark greenish gray to dusky yellow green and moderate olive brown colored and is present in the upper 98 feet of the core. The structures within this facies are biogenic and to a lesser degree physical, in the way of laminated to bioturbated/burrowed beds. The red line represents the boundary between the Pennsylvanian (above) and Mississippian (below) strata. **B-C)** Thin section photomicrographs of the silty argillaceous sandstone facies within the Doberman core at 4966.75'. Images are in PPL. The sample is dominated by very fine to fine sand-sized quartz (Q) grains as well as silt-sized quartz grains in areas, carbonate – mainly calcite (pink) grains, and some clays. Calcite grains are commonly brachiopod fragments and indistinguishable bioclasts. XRD analysis: 61% quartz, 12% carbonates (10% calcite and 2% dolomite), 12% clay minerals (9% illite, 2% illite/smectite, and 1% chlorite), and 15% other minerals (9% plagioclase feldspar, 4% potassium feldspar, 2% pyrite, and trace amounts of apatite). The average porosity for this facies based on 4 samples was 8%, and average permeability was 0.037 mD (air) and 0.020 mD (Klinkenberg).

Facies 4 represents increased water oxygenation (compared to Doberman Facies 3), as expressed by the increase in bioturbation. Physical sedimentary structures (laminated beds) within this facies are still recognizable. However, it is apparent that sediment was reworked by fauna (burrowed beds). The occurrence of laminated sand/silty sand beds along with bioturbated beds suggests that occasionally the influence of current reworking is an essential process while at other times biogenic activity is the dominate influence, a sign that interplay between fair weather and storm conditions occurred (Howard and Reineck, 1980). The amount of siliciclastics, and size of quartz, increased during deposition of Facies 4. The reason for this increase is unknown, but could be due to flooding of the siliciclastic source (due to high frequency changes in sea level) or an increase in siliciclastic sediment supply. The more dominant ichnofacies (in decreasing order) within the silty argillaceous sandstone facies are *Phycosiphon, Zoophycos*, and *Teichichnus* (MacEachern et al., 2009). The silty argillaceous sandstone facies is likely to represent deposition between the distal mid-ramp to proximal outer ramp environment, (Figure 15) below FWWB and near SWB.

**Doberman Facies 5: Silty Burrowed Mudstone-Wackestone**

The silty burrowed mudstone – wackestone facies (Figure 20) is commonly bioturbated as well as laminated to massive or blocky and is light olive gray and greenish black to grayish black. Burrows are vertical, horizontal, and millimeter to centimeter in scale. This facies contains sub-angular to sub-rounded, moderately to well sorted silt to very fine-sand-sized quartz grains (20-35%), silt-sized carbonate grains (35-48%), and clay minerals (15%). Doberman Facies 5 is similar to the slightly sandy calcareous facies, but contains less carbonate and quartz. Skeletal debris in Facies 5 includes brachiopods, crinoids and some indistinguishable bioclasts. Generally, Facies 5 contains abundant silt sized quartz and calcareous grains dispersed throughout a muddy organic-rich matrix.

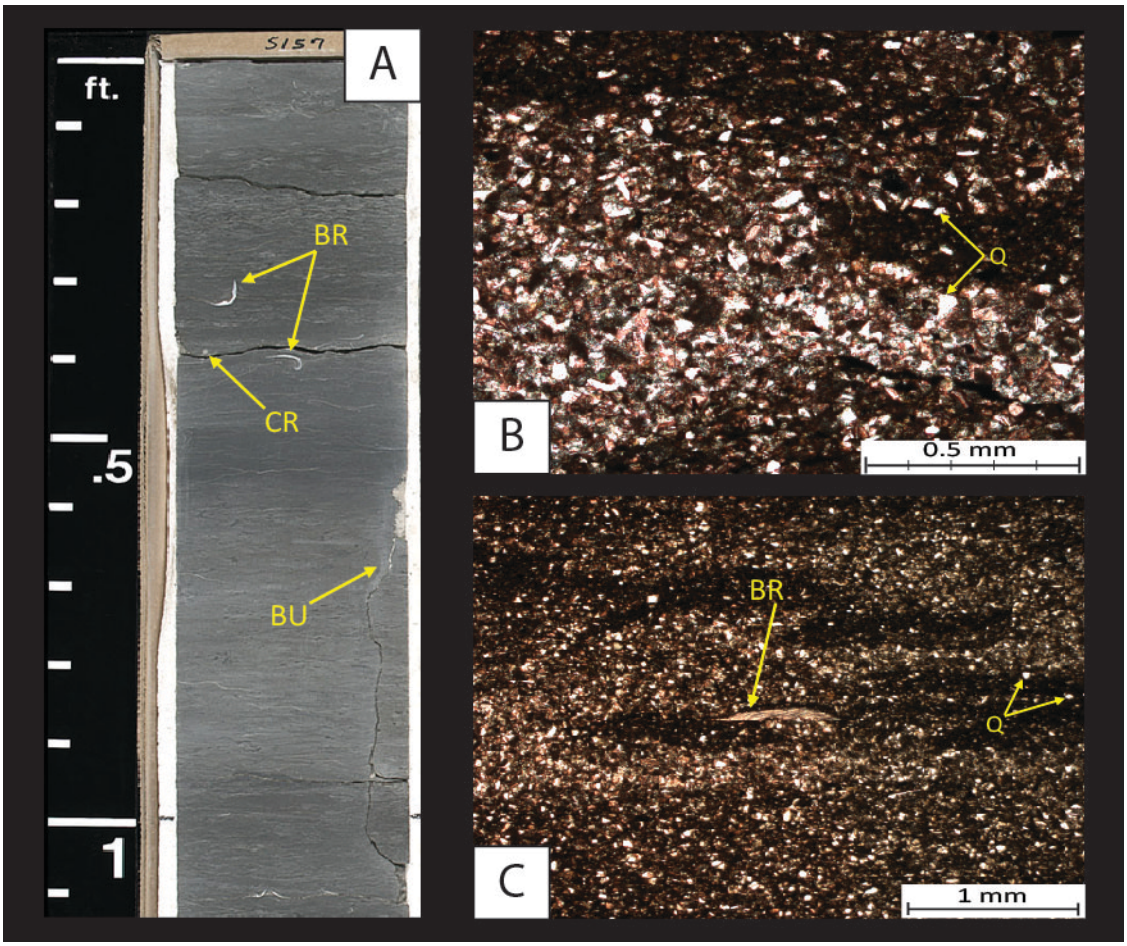


Figure 20. Doberman Facies 5: Silty Burrowed Mudstone-Wackestone. The scale to the left of the core image is in tenths of feet. **A)** Core photograph of the silty burrowed mudstone-wackestone facies under white light. It is commonly bioturbated or burrowed (BU) as well as laminated to blocky or massively bedded in areas, and light olive gray and greenish black to grayish black in color. This facies commonly contains brachiopods (BR) and crinoids (CR). **B-C)** Thin section photomicrographs of the silty burrowed mudstone – wackestone facies within the Doberman core at 5158.20'. The images are in PPL. The sample contains abundant silt- to very fine sand-sized quartz (Q) grains, carbonate – calcite (pink) grains, brachiopods (BR), as well as clays (illite) in a muddy organic-rich matrix. XRD analysis: 31% quartz, 46% carbonates (40% calcite, 6% dolomite), 15% clay minerals (9% illite, 4% illite/smectite, 2% chlorite), and 8% other minerals (5% plagioclase feldspar, 2% potassium feldspar, 1% pyrite). The average porosity for this facies based on 2 samples was 3%, and average permeability was 0.007 mD (air) and 0.002 mD (Klinkenberg).

Doberman Facies 5 was likely deposited within moderately deep water and under low to moderate energy water conditions based upon the increase in carbonate mud composition and extensive burrowing/bioturbation. This facies has alternating intervals of preserved laminated beds with small scale (millimeter) burrowed beds, an indication of changing environmental conditions between oxygen restricted and oxygen enriched water (Ekdale et al., 1984). The relative abundance of carbonates increased during deposition of Doberman Facies 5, reflecting a slowdown in siliciclastic sediment input to a point, as not to impede the carbonate system via siliciclastic poisoning. The dominant burrowing organisms observed within this facies include *Phycosiphon, Planolites*, and *Zoophycos*. Doberman Facies 5 is interpreted to represent deposition between the distal mid-ramp to outer ramp environment, below FWWB and near SWB (Figure 15). Well preserved bedding supports the interpretation that most deposition took place within the outer ramp, near SWB.

**Doberman Facies 6: Silty Peloidal Packstone-Grainstone**

The silty peloidal packstone – grainstone facies is the "cleanest" carbonate facies within the Doberman core and is light gray to medium gray and moderate yellowish brown (in some areas) color, and massively bedded (Figure 21). This facies is dominated by silt to fine sand-sized peloids (>50%), carbonate grains (45-71%), and silt-sized quartz grains (22-35%) that are sub-angular to sub-rounded and moderately sorted to well-sorted. Micritized grains are also commonly observed in thin section and appear to be distributed throughout this facies. Facies 6 also contains skeletal debris (in decreasing order of abundance) such as: brachiopods, crinoids, and in rare occasions, sponge spicules. Chert is observed in certain sections of Doberman Facies 6, but overall it is not abundant in this facies or the core as a whole. Contacts in the Doberman core between Facies 6 and other facies are commonly sharp.

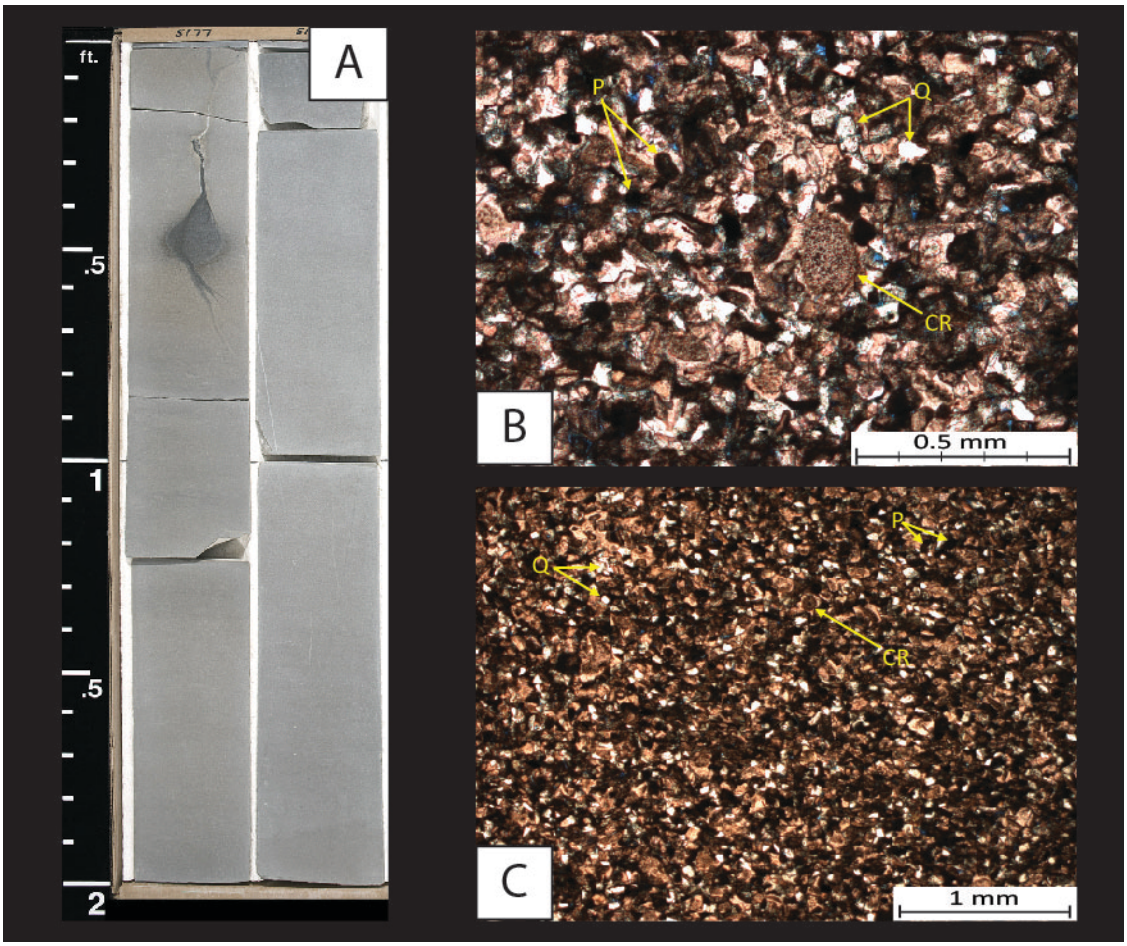


Figure 21. Doberman Facies 6: Silty Peloidal Packstone – Grainstone Facies. **A)** Core photograph of Doberman facies 6, the scale to the left of the image is in tenths of feet. This facies is the only "clean" carbonate facies within the Doberman core. The silty peloidal packstone – grainstone facies is predominantly very light gray to medium gray in color, but in some intervals it is a moderate yellowish brown color and is commonly massively bedded. **B-C)** Thin section photomicrographs of Doberman facies 6 at 5178.25'. Images are in PPL. The sample is composed of silt to mostly sand-sized peloid (P) grains, carbonate – mainly calcite (pink) grains, and silt- to very fine sand-sized quartz (Q) grains. Skeletal debris includes crinoids (CR) and brachiopods. XRD analysis: 22% quartz, 71% carbonates (65% calcite, 6% dolomite), 1% clay minerals – illite, 6% other minerals (3% plagioclase feldspar, 1% potassium feldspar, 1% pyrite, 1% apatite). The average porosity for this facies based on 5 samples was 3.9%, and average permeability was 0.004 mD (air) and 0.001 mD (Klinkenberg).

The increase in abundance of skeletal grains, (mainly brachiopods, crinoids, and the occasional sponge spicule) suggests an increase in depositional energy and also indicates conditions were more suitable for marine fauna, in respect to Doberman Facies 5 (Flügel, 2010). The abundance of peloids implies a somewhat restricted and/or quiet environment of deposition, however, this was likely not the case given the other environmental indicators (increase in fauna and relative lack of sedimentary structures). In areas subject to occasional storms or events, peloids can be moved into shallower or deeper environments, and peloid packstones to grainstones can be components of slope and basin sequences formed by mass transport deposits (Flügel, 2010; Scholle and Scholle, 2003). In comparison with the previously mentioned facies, the peloidal packstone-grainstone facies is interpreted to be a shallower water facies that was periodically affected by storm events. The silty peloidal packstone to grainstone facies is interpreted to represent deposition within the middle ramp environment (conceivably a more distal portion of the mid-ramp), likely below FWWB and above SWB (Figure 15).

## IHLE #1-26 FACIES

### Ihle Facies 1: Glauconitic Sandstone

The Ihle glauconitic sandstone facies is greenish gray to greenish black in color, grain dominated, and heavily burrowed (Figure 22). It is composed primarily of fine sand sized, to sparse medium sand sized, glauconite grains (40-55%) that are sub to well-rounded and poorly to moderately sorted, silt- to very fine sand-sized quartz grains (35-45%) that are sub to well-rounded and well sorted, clay minerals – mainly illite (20-40%), and carbonates (~7%) – 5% dolomite and 2% calcite. Ihle Facies 1 also contains pyrite (5-7%) and phosphate grains (3-4%). Skeletal debris occurs in the form of thin-shelled brachiopod fragments, as well as phosphatic bone fragments and occasional conodonts. This facies is only present in the lowermost 3ft (~1m) of the "Mississippian Limestone" interval in the Ihle 1-26 core (core #2) and is 1ft (0.3m) thick. Ihle Facies 1 does not directly overlie the Woodford Shale like the Doberman Facies 1 does. Instead, Ihle Facies 1 directly overlies a limestone (appears to be packstone to grainstone) unit (Weldon Limestone?), which overlies the Woodford Shale.

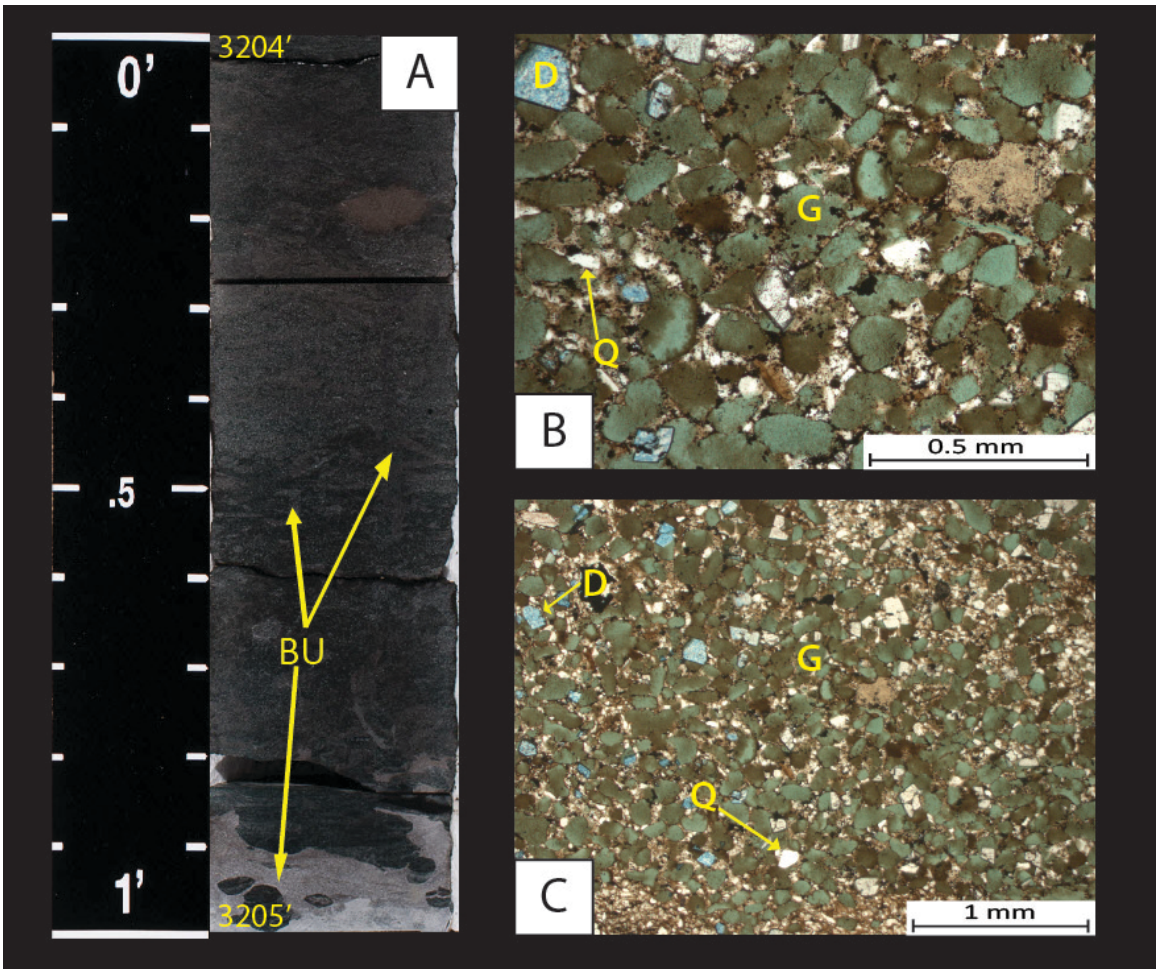


Figure 22. Ihle Facies 1: Glauconitic Sandstone Facies. **A)** Core photograph of Ihle Facies 1 in white light. The scale on the left of the image is in tenths of feet. Ihle Facies 1 is greenish gray to greenish black in color and is heavily burrowed (BU). **B-C)** Thin section photomicrographs of the Ihle glauconitic sandstone facies at 3204.25'. Images are in PPL. The sample is blue epoxy impregnated. This sample shows the sand-sized glauconite (G) grains, silt- to fine sand-sized quartz (Q) grains, dolomite (D) grains and some phosphate grains. XRD analysis: 39% quartz, 7% carbonates (5% dolomite, and 2% calcite), 45% clay minerals (inconclusive results on breakdown of clay types with XRD), and 9% other minerals (1% plagioclase feldspar, 2% potassium feldspar, and 6% pyrite). The measured porosity for this facies based on 1 sample was 12%, and average permeability was 0.010 mD (air) and 0.0047 mD (Klinkenberg).

Ihle Facies 1 is interpreted to represent deposition during the early stages of a transgression or flooding event of regional scale. The glauconitic sandstone facies frequently occurs in the lowermost portion of the "Mississippian Limestone" interval in subsurface cores throughout Oklahoma. Idealized conditions for the formation of glauconite require deposition in a low-energy shallow marine environment where circulation is limited, and sedimentation rates (Amorosi, 1997; Bentor and Kastner, 1965). The occurrence of thin-shelled brachiopod fragments also supports the interpretation of deposition occurring in a relatively low-energy environment, probably below SWB – storm wave base (Figure 15). The abundance of burrows, likely from *Zoophycos* ichnofacies, indicates a relatively dysaerobic depositional environment (Middleton et al., 2003).

**Ihle Facies 2: Silty Shale/Mudstone**

The silty shale/mudstone facies in the Ihle #1-26 does not occur in the Doberman core (core #1); this is likely due to non-deposition or erosion. The silty shale/mudstone facies within the Ihle is brownish black to black in color, occurs in the uppermost 166ft (50.6m) of the core, and ranges from 2.5ft (0.76m) to 76ft (23.2m) in thickness. This facies is composed of silt- to very fine sand-sized quartz (18-32%) grains, clay minerals (46-66%) – illite and mixed layer illite/smectite, and rare carbonate (0-9%) and 2-10% phosphate (Figure 23). Ihle Facies 2 also contains occasional fossils (mainly thin-shelled brachiopods) and pyritized burrows. Where brachiopods are present, they are concentrated in thin layers that resemble storm events (tempestites). This facies displays alternating intervals of competent beds, and friable/fissile beds. The alternation of competent and less-competent (crumbly) intervals is attributed to clay mineral type within the facies as well as available quartz. Mixed layer illite/smectite is more abundant in the less-competent bedded intervals, while illite-dominated intervals are less-crumbled/broken (along with an increase in quartz) relatively massive-bedded units. Ihle Facies 2 also has visible laminations (3-10mm in width) that are primarily calcareous.

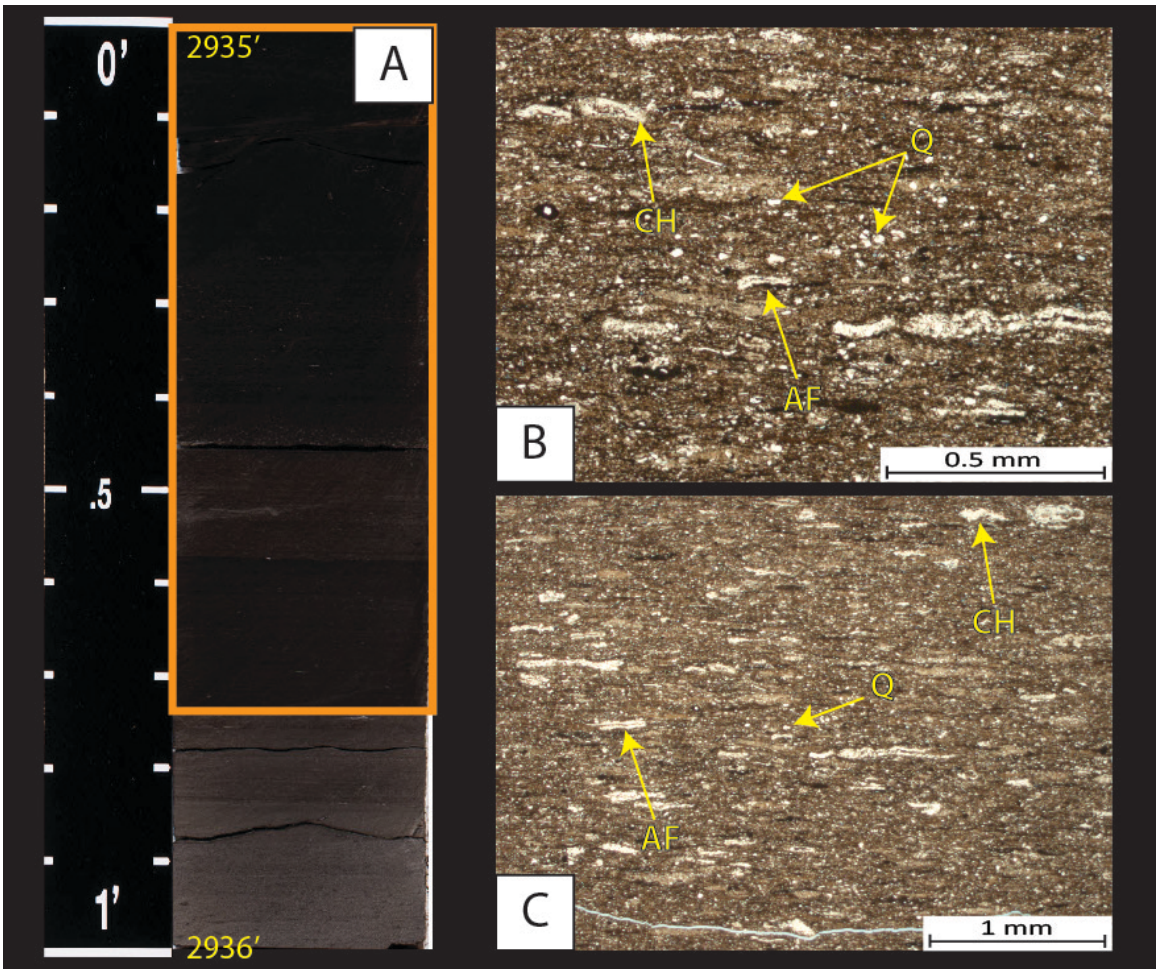


Figure 23. Ihle Facies 2: Silty Shale/Mudstone Facies. **A)** Core photograph of Ihle Facies 2 in white light. The scale to the left of the image is in tenths of feet. Ihle Facies 2 is brownish black to black in hand sample. This facies contains intervals of alternating beds of, crumbly/fissile shale and competent relatively massively bedded ones. Occasional thin-shelled brachiopods are present and tend to occur in concentrations, possibly derived from storm events. **B-C)** Thin section photomicrographs of the Ihle silty shale/mudstone facies at 2935.15'. Images are in PPL. The sample is blue epoxy impregnated. This sample shows silt- to very fine sand-sized quartz (Q) grains, clayey/muddy matrix, clusters of chert (CH), flattened (evidence of compaction) agglutinated foraminifera enclosed with microcrystalline quartz (AF). XRD analysis: 22% quartz, 9% carbonates (9% calcite with trace amounts of dolomite), 58% clay minerals (43% illite, 10% mixed layer illite/smectite, 3% kaolinite, and 2% chlorite), and 11% other minerals (3% plagioclase feldspar, 2% potassium feldspar, 4% pyrite, 1% marcasite, and 1% apatite).

Ihle Facies 2 is interpreted to represent a continuing transgression following deposition of Facies 1 (Figure 15). The lack of normal marine fauna, but the occasional presence of thin shelled brachiopods, suggests an environment alternating from dysoxic to anoxic conditions (Ekdale et al., 1984). Within Ihle Facies 2, occasional and rare beds of fossils (mainly thin shelled brachiopods and crinoids) occur. These fossil beds are interpreted to be infrequent storm deposits brought in periodically within the outer ramp to basin environment (Handford, 1986). The silty shale/mudstone facies is dominated by clay minerals of illite and mixed layer illite/smectite composition. Due to the abundance of clays and silt sized quartz grains, Ihle Facies 2 is understood to have been deposited in a relatively calm low-energy environment that was influenced by occasional storm events (Harms et al., 1982). The silty shale/mudstone facies likely represents deposition within the outer ramp setting, below FWWB and SWB.

**Ihle Facies 3: Phosphatic Dolomitic Shale:**

The phosphatic dolomitic shale facies within the Ihle #1-26 core is not present within the Doberman #1-25 core. In hand sample, Ihle Facies 3 is brownish black to dusky brown and dusky blue green (Figure 24). This facies only occurs in the uppermost portion of the silty shale/mudstone facies and is represented by approximately six total feet. Facies 3 is composed mainly of silt-sized quartz grains (29%), carbonates – dolomite (24%), and calcite grains that are primarily brachiopod fragments (1%), clay minerals – mainly illite (29%), and organic matter along with an abundance of sand sized phosphate grains observed mostly in thin section and occasionally in hand sample. Phosphate present in hand sample is typically concentrated along bedding planes or forms lenses and nodules. Pyrite tends to be associated with the phosphate. Ihle Facies 3 contains fossil debris, mainly brachiopod fragments. Laminated to massively bedded beds are observed within the core, and laminations that are present tend to be composed of the phosphate grains or nodules along with minor amounts of calcareous debris.

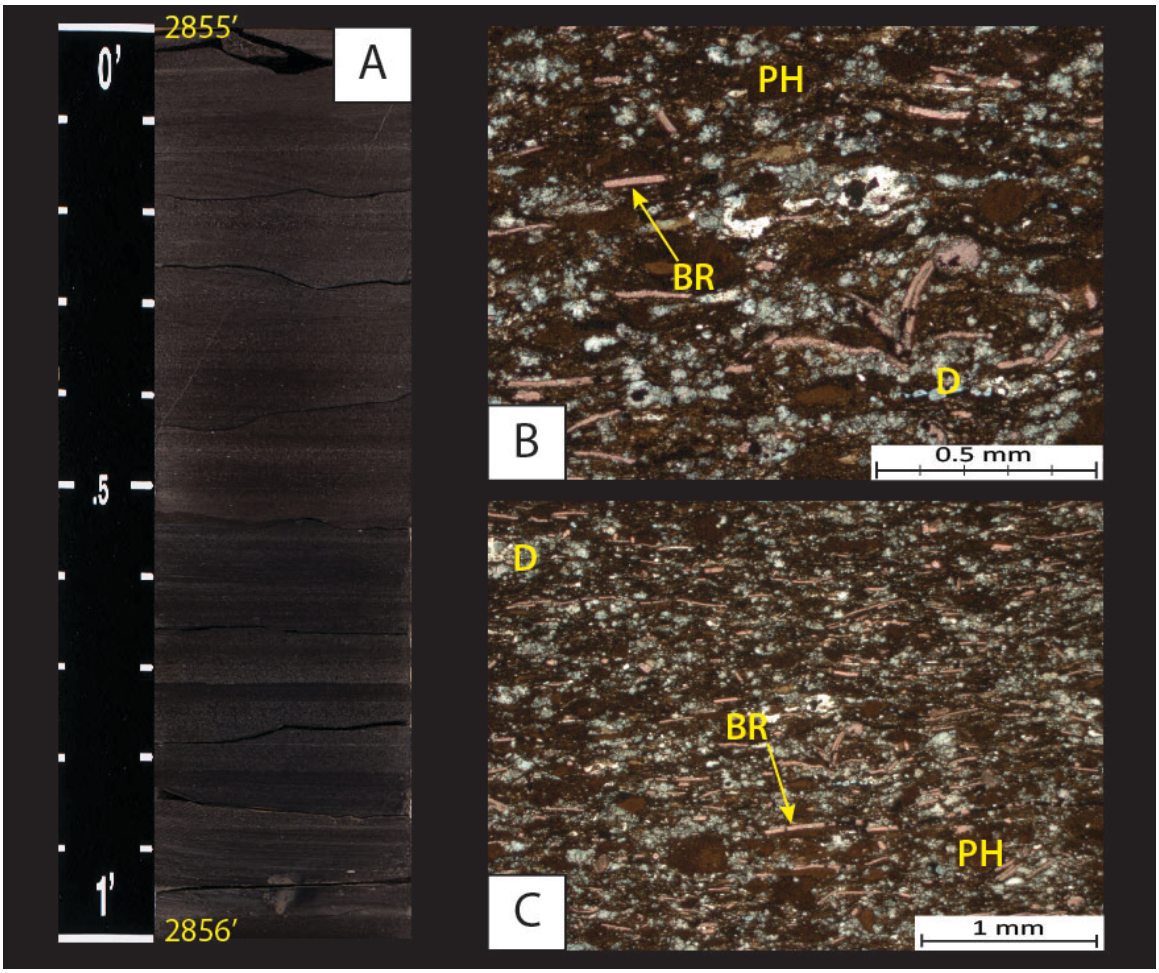


Figure 24. Ihle Facies 3: Phosphatic Dolomitic Shale Facies. **A)** Core photograph of Ihle Facies 3 in white light. The scale to the left of the image is in tenths of feet. Ihle Facies 3 is brownish black to dusky brown and dusky blue green in hand sample. Phosphate grains observed in hand sample are millimeter scale and are nodular to laminated. **B-C)** Thin section photomicrographs of the phosphatic dolomitic shale facies within the Ihle core at 2855.50'. Images are in PPL. The sample is blue epoxy impregnated. This sample shows silt-sized quartz grains, an abundance of sand-sized phosphate grains (PH), dolomite (D), and brachiopod fragments (BR). XRD analysis: 29% silt sized quartz grains, 29% clay minerals (18% illite, 7% mixed layer illite/smectite, 2% kaolinite, and 2% chlorite), 25% carbonates (24% dolomite, 1% calcite – occurring as brachiopod fragments), and 17% other minerals (9% apatite, 4% plagioclase feldspar, 2% potassium feldspar, and 2% pyrite).

During deposition of Ihle Facies 3 dysoxic and intermittent oxic conditions likely existed near the sea floor that allowed colonization by thin-shelled brachiopods. A stratified water column influenced by marine upwelling and slow deposition over a relatively long time span, supported accumulations of phosphates and organic matter (Kidder, 1985). The majority of dolomite within the phosphatic dolomitic shale facies appears to be ferroan, which typically implies formation during deeper burial. Due to Ihle Facies 3 only comprising six total feet of the core, it is a volumetrically less-significant facies. Ihle Facies 3 is interpreted to represent deposition within the outer ramp, below FWWB and SWB under relatively low to moderate energy settings (Figure 15).

**Ihle Facies 4: Clay-Rich Siltstone**

The clay-rich siltstone facies occurs in both the Ihle and Doberman cores, and are compositionally similar. This facies within the Ihle contains a slightly higher percentage of silt-sized quartz grains (46-49%) that are sub angular to sub-rounded and clay minerals – mainly illite (20-31%) than the same facies in the Doberman core. However, in the Ihle core the carbonate content is marginally lower (7-18%). The carbonate is primarily calcite and in hand sample Facies 4 is medium dark gray to grayish black and dusky brown (Figure 25). As it was in the Doberman, the clay-rich siltstone facies in the Ihle is generally thin-bedded and laminated. In the Ihle, this facies is commonly interbedded with the silty argillaceous sandstone facies, and to a lesser degree, the calcareous siltstone facies. Intervals of clay-rich siltstone within the Ihle are not as thick as intervals of this same facies within the Doberman core. Occasional small scale cross-bedding is observed in this facies.

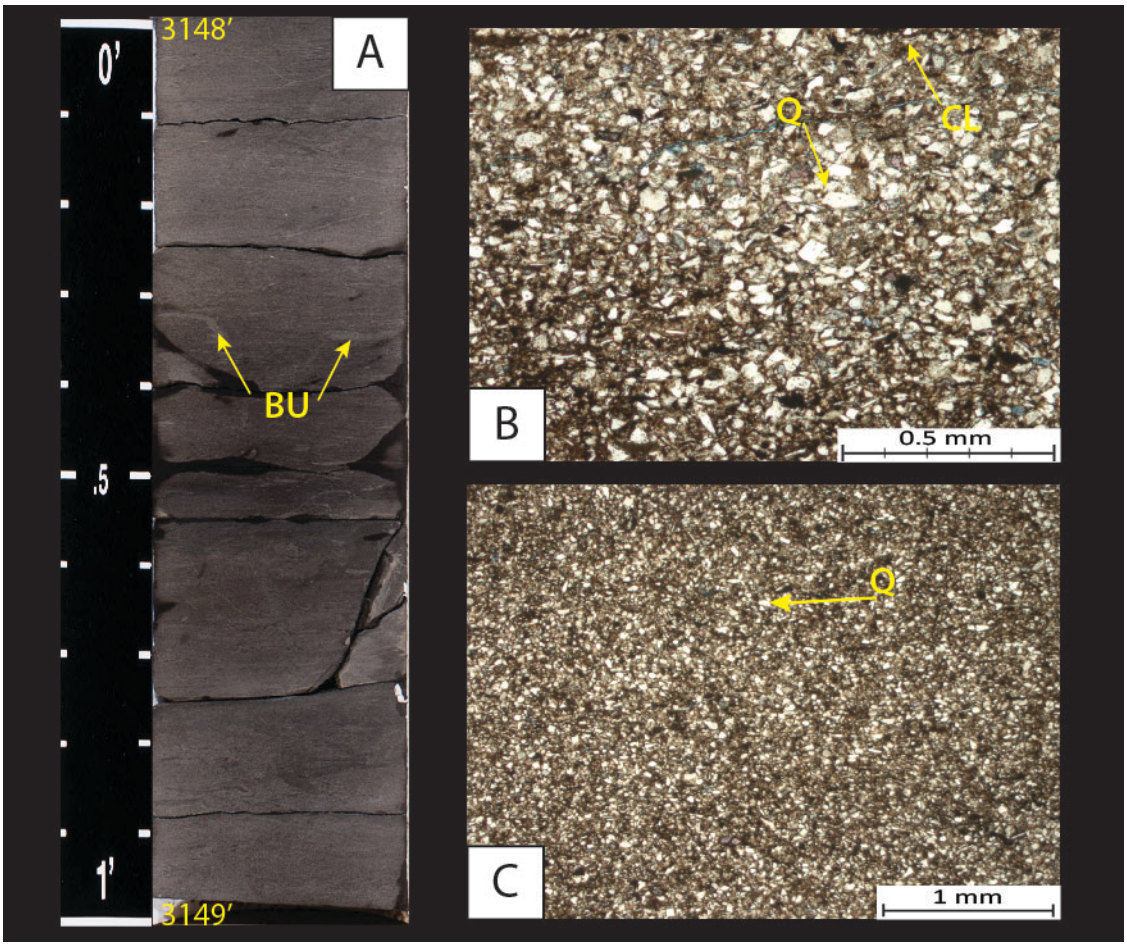


Figure 25. Ihle Facies 4: Clay-Rich Siltstone. **A)** Core photograph under white light. The scale on the left of the core photo is in tenths of feet. This facies is medium dark gray to grayish black and dusky brown in color and contains burrowed to laminated beds. This facies is generally thinly bedded and contacts with other facies are more gradational than contacts in the Doberman core. **B-C)** Thin section photomicrographs of the clay-rich siltstone facies in the Ihle core at 3148.25'. Images are in PPL. The sample is dominated by silt-sized quartz (Q) to very fine sand-sized quartz grains in some areas, and contains an abundance of clays along with some organic matter. This facies also contains sparse amounts of carbonates – mainly calcite grains (pink). The calcite grains are primarily indistinguishable bioclasts/fossils. XRD analysis: 46% quartz, 6% carbonates (4% calcite, and 2% dolomite), 31% clay minerals (18% illite, 10% mixed layer illite/smectite, and 3% chlorite), and 17% other minerals (9% plagioclase feldspar, 5% potassium feldspar, 2% pyrite, and 1% apatite).

In the Doberman core, the clay-rich siltstone facies is predominantly laminated and lacks an abundance/diversity of organisms. However, in the Ihle, this facies contains a greater density of burrows and an increased abundance of fossils (brachiopods and crinoids). Due to the factors above, the clay-rich siltstone within the Ihle is interpreted to have been deposited in the outer ramp environment (conceivably a more proximal portion of the outer ramp) likely below SWB (Figure 15). Based on the presence of brachiopods and crinoids, the environment was at times oxygenated (Ekdale et al., 1984). Preserved laminations reflect a relatively low-energy depositional environment that was occasionally affected by storms. Facies 4 in the Ihle core, represents a slightly more proximal location on the ramp compared to the same facies in the Doberman core that has a lower abundance and diversity of organisms and less bioturbation/burrowing.

**Ihle Facies 5: Slightly Sandy Calcareous Siltstone**

The slightly sandy calcareous siltstone is observed in both cores and is greenish gray to medium gray in color in the Ihle core (Figure 26). In the Doberman core, bioturbation is extensive and common throughout this facies. While the Ihle contains bioturbated bedding, preserved laminations occur more frequently compared to the same facies in the Doberman core. In the Ihle, this facies is dominated by silt- to very fine sand-sized quartz grains (36-51%) that are sub angular to sub-rounded, carbonate – primarily calcite (16-37%), and a lesser amount of clay minerals (14-20%). Clay mineral percentages for Facies 5 in the Ihle are slightly higher than in the same facies in the Doberman. Brachiopods and small scale cross-bedding are commonly observed in hand sample within both the Ihle and Doberman. In thin section, peloids are frequently noted within the Ihle, while they are not as common in the Doberman.

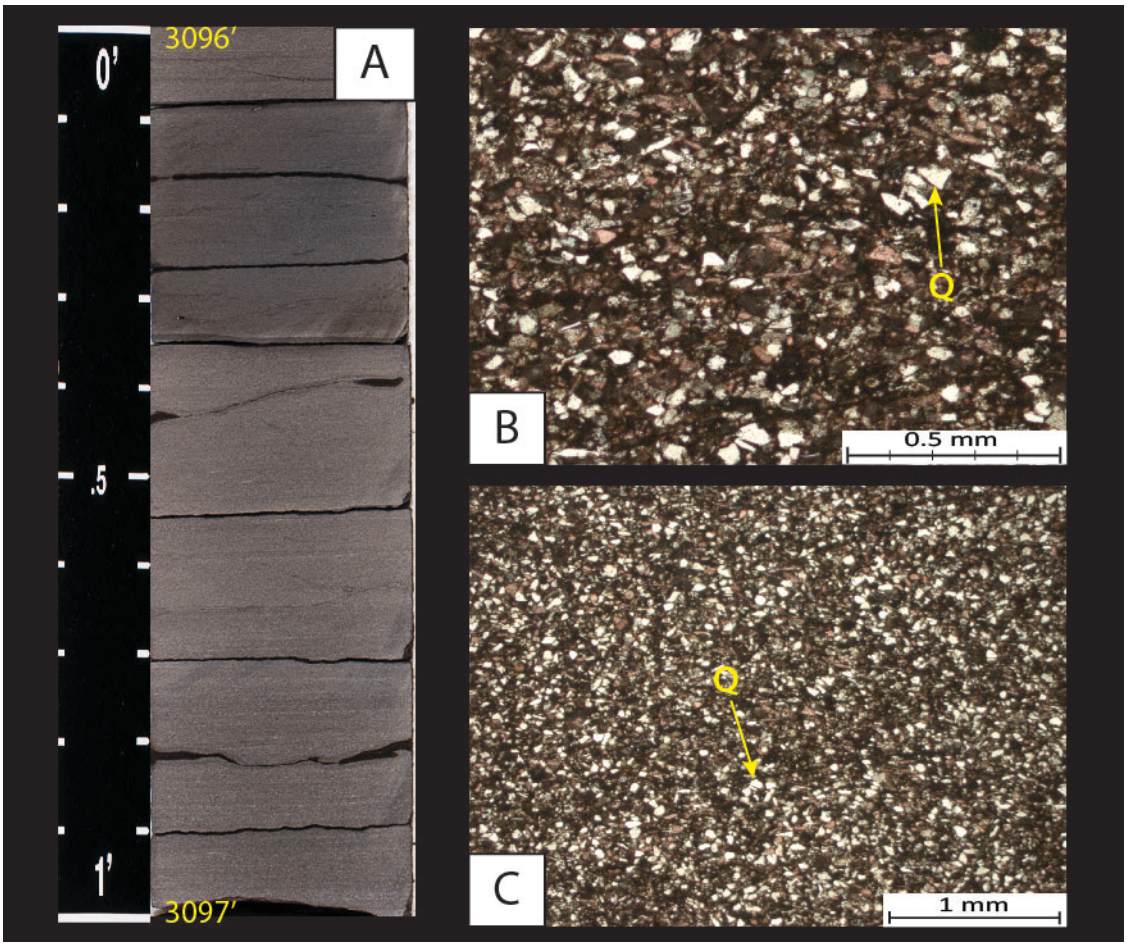


Figure 26. Ihle Facies 5: Slightly Sandy Calcareous Siltstone. **A)** Core photograph of Ihle facies 3 under white light, the scale to the left of the core is in tenths of feet. Bioturbation is common and seen in the sample, there are also frequent sections containing preserved laminations. In hand sample, this facies is greenish gray to medium gray. Bioturbation in Ihle facies 3 commonly occurs as small (mm scale) burrows. **B-C)** Thin section photomicrographs of the slightly sandy calcareous siltstone facies, Ihle core at 3096.10'. Images are in PPL. The sample is dominated by silt- to very fine sand-sized quartz (Q) grains that are sub-angular to sub-rounded and moderately sorted, carbonate – mainly calcite (pink) grains, sparse clays, and a muddy organic-rich matrix. Most calcite grains in this facies are unidentified bioclasts or micritized grains. When the grains are recognizable, they are mostly brachiopod and crinoid fragments. XRD analysis: 38% quartz, 37% carbonates (33% calcite, and 4% dolomite), 16% clay minerals (9% illite, 6% mixed layer illite/smectite, and 1% chlorite), and 9% other minerals (5% plagioclase feldspar, 2% potassium feldspar, and 2% pyrite).

The increased number of brachiopods and crinoids, in comparison with the clay-rich siltstone facies, and the increase in non-identified carbonate grains, indicate the slightly sandy calcareous siltstone facies likely formed slightly higher on the ramp and in a marginally intensified water energy environment compared to the clay-rich siltstone facies (Flügel, 2010; Tucker and Wright, 1990). The slightly sandy calcareous siltstone contains coarser-grained quartz (compared to clay-rich siltstone facies), possibly a result of this facies being in a more proximal location to the siliciclastic source. The increase in abundance of brachiopods and crinoids, presence of peloids, and the increase in size of quartz grains support a higher-energy environment with respect to the clay-rich siltstone facies (Flügel, 2010). Ihle Facies 5 is interpreted to represent deposition on a distal mid-ramp to outer ramp setting, below FWWB and close to SWB (Figure 15).

**Ihle Facies 6: Silty Argillaceous Sandstone**

The silty argillaceous sandstone facies is a facies that occurs in both cores. In the Ihle core, this facies is medium light gray to greenish gray and dusky yellow green in hand sample (Figure 27). It is dominated by sub-angular to sub-rounded and moderately to well-sorted very fine to fine sand-sized quartz grains (40-70%), clay minerals – mainly illite (16-37%), and rare carbonate grains (2-19%). Burrows are prominent in Facies 6, and sedimentary structures include parallel laminations, and to a lesser degree, small scale cross-bedding. The amount of small scale cross-bedding in Facies 6 has increased compared to the calcareous siltstone facies. In hand sample, small (mm scale) phosphate nodules and clay clasts are observed.

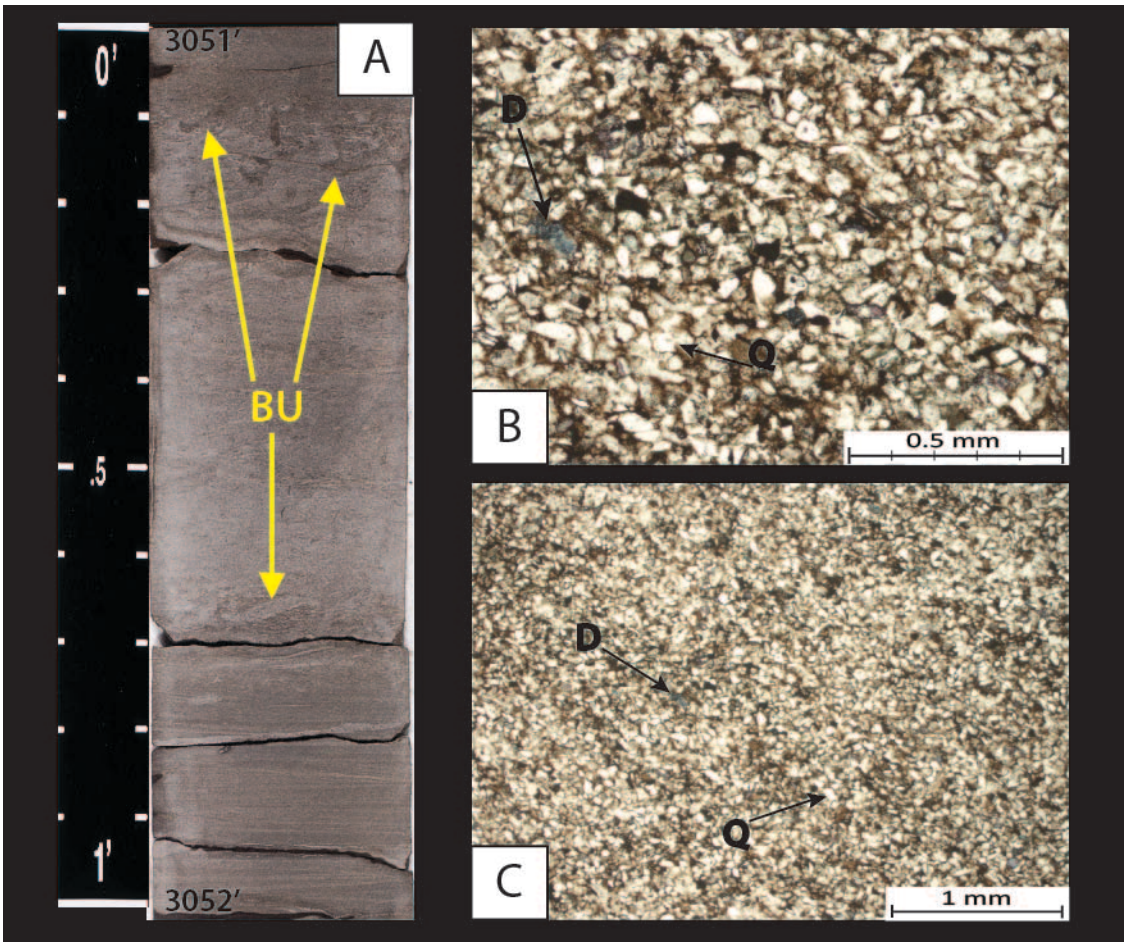


Figure 27. Ihle Facies 6: Silty Argillaceous Sandstone. The scale to the left of the core image is in tenths of feet. **A)** Core photograph of Ihle facies 6 under white light; it is medium light gray to greenish gray and dusky yellow green color in hand sample. Structures in this facies are biogenic and physical, and include laminated to bioturbated/burrowed beds. **B-C)** Thin section photomicrographs of the silty argillaceous sandstone facies within the Ihle core at 3051.15'. Images are in PPL. The sample is dominated by very fine to fine sand-sized quartz (Q) grains as well as silt-sized quartz grains, carbonates – mainly calcite (pink) grains, and occasional clays – primarily illite. Calcite grains are commonly brachiopod and crinoid fragments along with indistinguishable bioclasts. XRD analysis: 61% quartz, 12% carbonates (10% calcite and 2% dolomite), 12% clay minerals (9% illite, 2% mixed layer illite/smectite, and 1% chlorite), and 15% other minerals (9% plagioclase feldspar, 4% potassium feldspar, and 2% pyrite). The measured porosity for this facies based on 1 sample was 9.4%, and average permeability was 0.0063 mD (air) and 0.0026 mD (Klinkenberg).

The increase in bioturbated and burrowed beds in the silty argillaceous sandstone facies, compared to the slightly sandy calcareous siltstone facies, suggests more oxygenated water conditions during deposition. The occurrence of laminated sand/silty sand beds along with bioturbated/burrowed beds suggests that occasionally, the influence of wave reworking is an essential process while at other times biogenic activity is the dominate influence, a sign that interplay between fair weather and storm conditions occurred (Howard and Reineck, 1980). The increase in small scale cross-bedding and size of the quartz grains, along with the presence of laminated sections suggests a higher-energy environment during deposition compared to the calcareous siltstone facies (Flügel, 2010). Based on the increase in abundance and size of the quartz grains, this facies was deposited more proximal to the siliciclastic sediment source than the calcareous facies. Ihle Facies 6 likely represents deposition from the distal mid-ramp to outer ramp environments, below FWWB, while immediately above or below SWB (Figure 15).

**Ihle Facies 7: Argillaceous Mudstone-Wackestone**

The argillaceous mudstone-wackestone facies occurs within the upper 68ft (28.7m) of the Ihle core and is not present within the Doberman. In hand sample, it is grayish black to black (Figure 28) and interbedded with Ihle Facies 10, which is a packstone to grainstone that has been heavily recrystallized. Ihle Facies 7 is thinly bedded and dominated by carbonate mud and bioclasts (30-53%), clay minerals – mainly mixed layer illite/smectite (36-50%), and minor amounts of silt-sized quartz grains (8-15%). The argillaceous mudstone-wackestone facies is highly fossiliferous, containing primarily brachiopods and crinoids. Similar to Ihle Facies 2, this facies also contains concentrations of fossils that resemble storm events/beds. However, within the argillaceous mudstone-wackestone facies, these concentrations of fossils occur more frequently compared to Ihle Facies 2. Planar laminations along with minor areas of bioturbation/burrowing are the dominant types of sedimentary and biogenic structures observed within this facies.

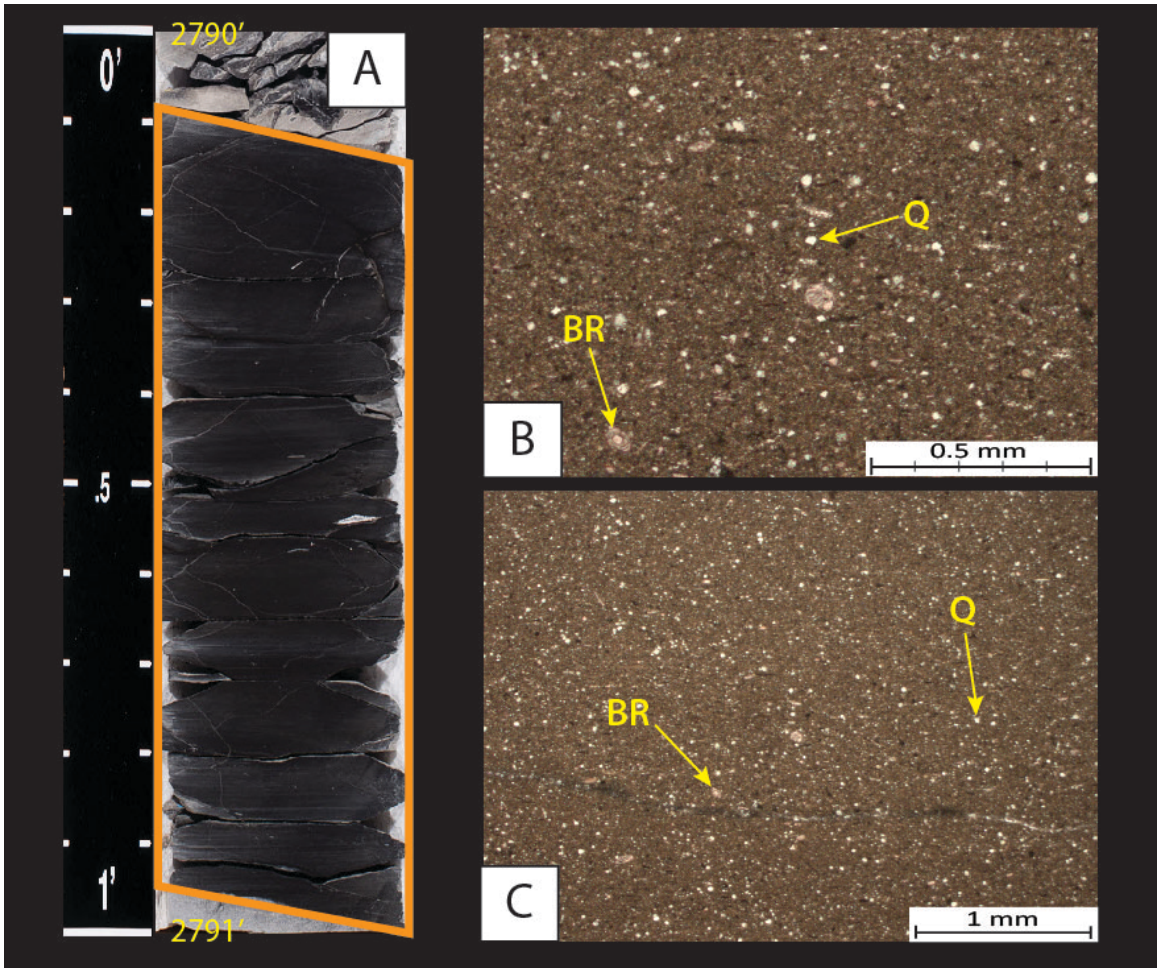


Figure 28. Ihle Facies 7: Argillaceous Mudstone – Wackestone. The scale to the left of the core image is in tenths of feet. **A)** Core photograph of Ihle facies 7 was taken using white light, and illustrates the grayish black to black color. The sedimentary and biogenic structures within this facies are planar laminated beds and to a lesser degree, bioturbated/burrowed beds. Ihle facies 7 is interbedded with Ihle facies 10 and only occurs within the upper 68ft (20.7m) of the core. **B-C)** Thin section photomicrographs of the argillaceous mudstone-wackestone facies within the Ihle core at 2790.40'. Images are in PPL. The sample is dominated by carbonate mud and carbonate grains – mainly calcite (pink) grains, clays – mainly mixed layer illite/smectite, and minor silt-sized quartz grains (Q). Calcite grains are commonly brachiopod (BR) and crinoid fragments and to a lesser degree indistinguishable bioclasts. XRD analysis: 8% quartz, 53% carbonates (49% calcite and 4% dolomite), 36% clay minerals (3% illite, 23% mixed layer illite/smectite, 6% kaolinite, and 4% chlorite), and 3% other minerals (trace amounts of plagioclase feldspar, 1% potassium feldspar, and 2% pyrite).

The carbonate mud could have been delivered into the system from carbonate sources higher up on the ramp, but it likely originated at the site of deposition. It is apparent from accumulations of condensed brachiopod sections and interbedded packstones to grainstones, that during deposition, storm events were highly active within the area and transported bioclastic debris basinward (Handford, 1986). The common occurrence of fossils (brachiopods and crinoids) suggests that either the depositional environment was oxygenated enough to be favorable for their accumulation or that they were brought into this area via storm processes. The condensed fossil accumulations tend to form in laminations parallel to bedding. It is possible that these were formed by typical low energy marine currents moving across the ramp (Flügel, 2010). In some instances the brachiopod fragments are convex side down, which implies that suspension settling took place. The argillaceous mudstone-wackestone facies in the Ihle core is interpreted to represent deposition on the outer ramp, below FWWB and SWB (Figure 15).

**Ihle Facies 8: Silty Burrowed Mudstone-Wackestone**

The silty burrowed mudstone-wackestone facies occurs in both the Ihle and Doberman cores. This facies is commonly burrowed and/or bioturbated and to a lesser degree, laminated. This facies is greenish black to brownish black and grayish black in hand sample (Figure 29). The silty burrowed mudstone-wackestone facies contains sub-angular to sub-rounded, moderately to well sorted silt- to very fine sand-sized quartz grains (24-32%), silt- to very fine sand-sized calcite grains and carbonate mud (38-46%), sparse clay minerals – primarily illite (10-14%), with the various grains dispersed throughout a muddy organic-rich matrix. This facies is commonly fossiliferous containing primarily brachiopods along with occasional crinoids. The calcareous siltstone facies is similar to this facies, the notable difference being the relative abundance and percentages of quartz and carbonate grains.

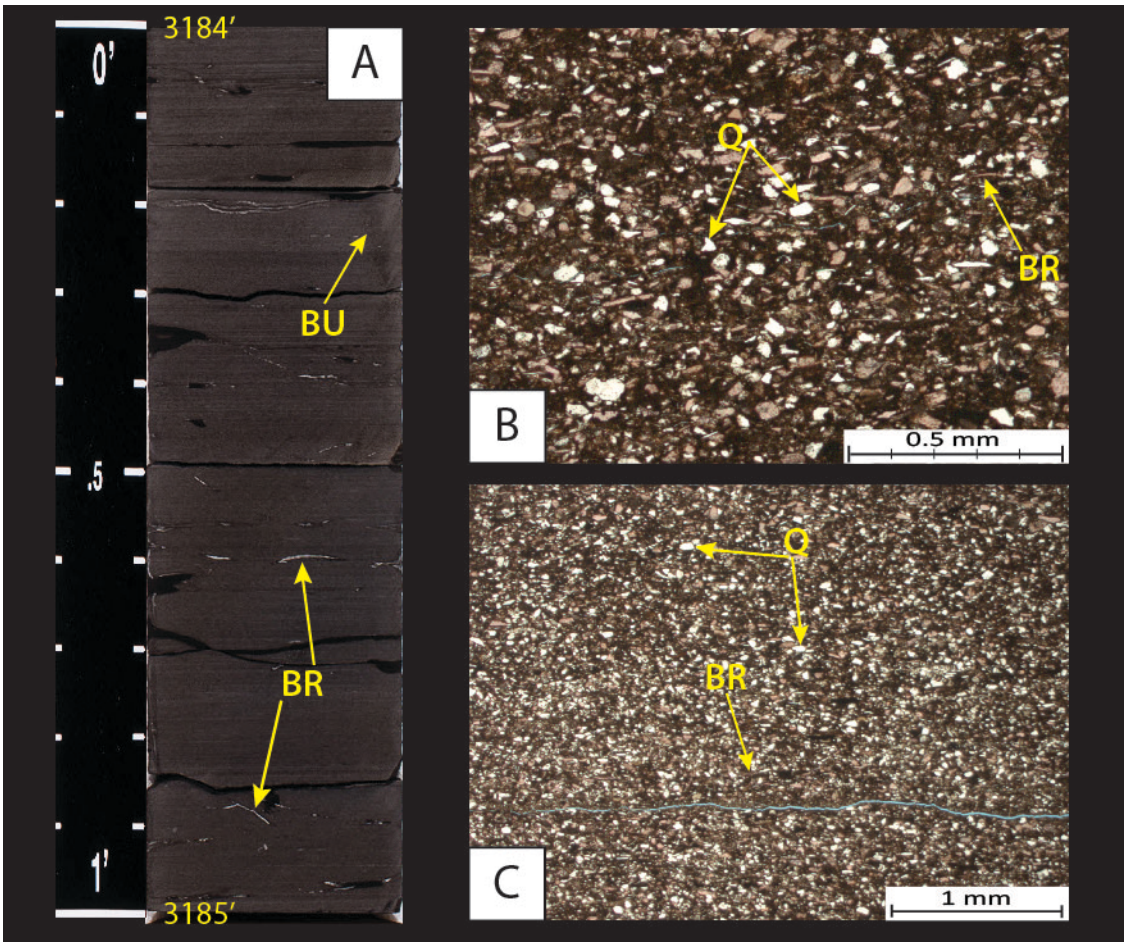


Figure 29. Ihle Facies 8: Silty Burrowed Mudstone-Wackestone. The scale to the left of the core image is in tenths of feet. **A)** Core photograph of the silty burrowed mudstone-wackestone facies (Ihle, 3184-85') under white light. Facies 8 is commonly bioturbated or burrowed (BU) as well as laminated to massively bedded in areas, and greenish black to brownish black and grayish black in hand sample. This facies is fossiliferous and contains brachiopods (BR) and crinoids. **B-C)** Thin section photomicrographs of the silty burrowed mudstone – wackestone facies from the Ihle core at 3184.20'. Both images are in PPL and contain abundant silt- to very fine sand-sized quartz (Q) grains, carbonate – calcite (pink) grains, brachiopods (BR), as well as clays (illite) in a muddy organic-rich matrix. XRD analysis: 27% quartz, 46% carbonates (45% calcite and 1% dolomite), 14% clay minerals (11% illite, 1% mixed layer illite/smectite, 1% kaolinite, and 1% chlorite), and 13% other minerals (5% plagioclase feldspar, 4% potassium feldspar, 2% pyrite, and 2% apatite).

Similar to Ihle Facies 7, the silty burrowed mudstone-wackestone facies contains carbonate mud that could have been delivered into the system from carbonate sources higher up the ramp in a more proximal location or originated at the site of deposition. Ihle Facies 8 has alternating layers of preserved laminated beds with small scale (millimeter) burrowed beds, perhaps an indication of alternating conditions during deposition between oxygen-restricted and oxygen-enriched (Ekdale et al., 1984). During oxygen enriched water conditions, the environment was favorable for accumulations of local benthic organisms in addition to those that may have been transported into the system. Like Ihle Facies 7, the silty burrowed mudstone-wackestone facies contains brachiopods deposited convex side down, which suggests that suspension settling (Dr. Grammer, personal communication). The silty burrowed mudstone-wackestone facies is interpreted to have been deposited below FWWB, and at or below SWB within the proximal outer ramp environment (Figure 15).

**Ihle Facies 9: Silty Argillaceous Dolomitic Packstone**

The silty argillaceous dolomitic packstone facies occurs in the Ihle #1-26 core, but is not present within the Doberman #1-25 core. This facies occurs near the middle of the Mississippian section and ranges in thickness from 0.5ft (0.15m) to 5.5ft (1.7m) at its thickest and combines for 9.3 total feet (2.8m) within the Ihle core. In hand sample, Ihle Facies 9 is very light gray to medium gray and light bluish gray in color (Figure 30). Ihle Facies 9 is composed of sub-angular to sub-rounded silt-sized quartz grains (25-35%), carbonates (34-37%) – mainly dolomite (27-30%), clay minerals (22-29%), and silt- to sand-sized peloids. This facies contains burrows (mm to cm scale), mineralized fractures, and abundant bioclasts based on thin section petrography. Fossils observed in Facies 9 are dominantly brachiopods.

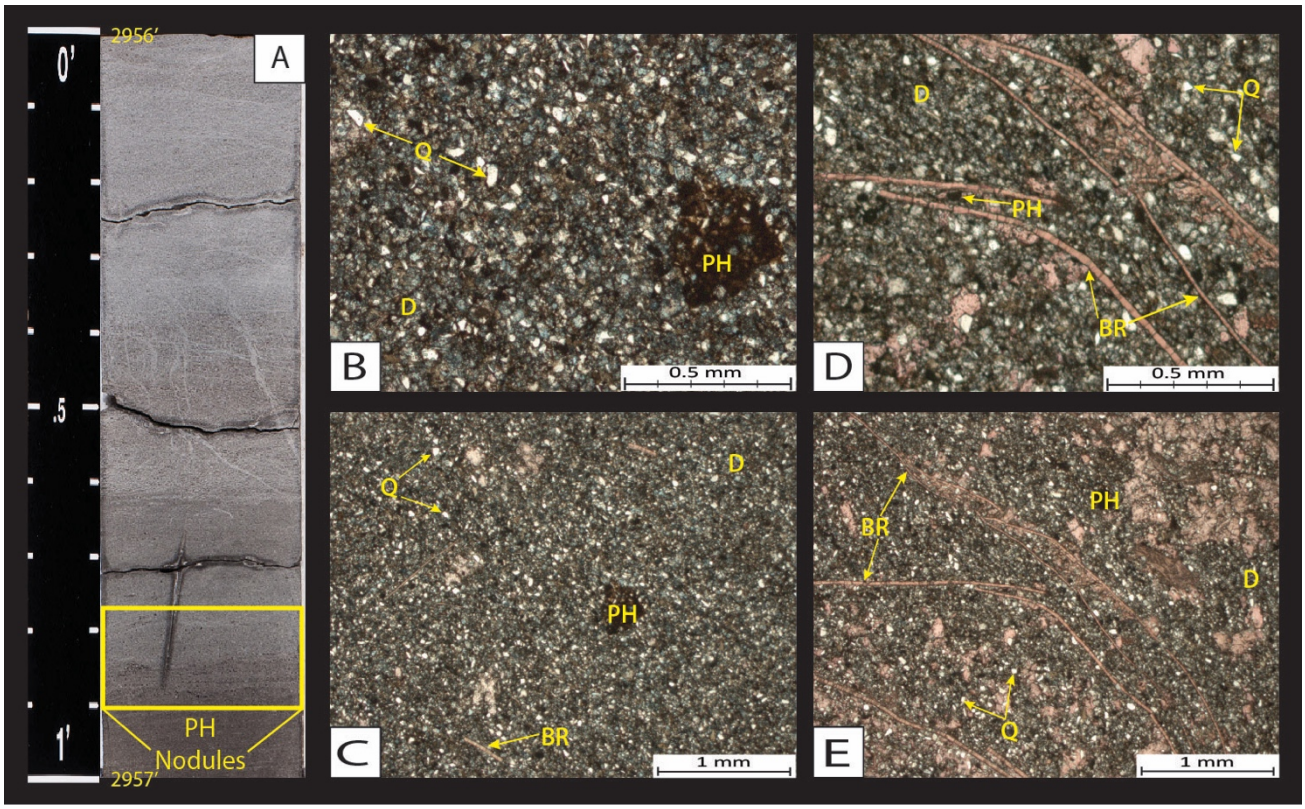


Figure 30. Ihle Facies 9: Silty Argillaceous Dolomitic Packstone. The scale to the left of the core image is in tenths of feet. **A)** Core photograph of the silty argillaceous dolomitic packstone facies under white light, showing burrows (BU) as well as preserved laminations, and the light gray to medium gray and light bluish gray color. This facies is fossiliferous and contains abundant thin-shelled brachiopods (BR). **B-C)** Thin section photomicrographs of the silty argillaceous dolomitic packstone facies from the Ihle core at 2956.70'. Both images are PPL. The sample contains abundant silt sized quartz (Q) grains, carbonates – dolomite (D), and brachiopods (BR), as well as clay minerals. XRD analysis: 25% quartz, 37% carbonates (30% dolomite and 7% calcite), 29% clay minerals (inconclusive results on breakdown of clay types with x-ray diffraction), and 9% other minerals (4% plagioclase feldspar, 2% potassium feldspar, and 3% pyrite). The average porosity for this facies based on 2 samples was 4.5%, and average permeability was 0.0036 mD (air) and 0.0013 mD (Klinkenberg).

Oxic water conditions during deposition are indicated by the abundance of brachiopods (Ekdale et al., 1984). This facies contains sections that are burrowed along with other sections that contain laminated bedding. The occurrence of laminated sand/silty sand beds along with bioturbated beds suggests that occasionally currents dominate while at other times biogenic activity is the dominate influence, evidence of interplay between fair weather and storm conditions (Howard and Reineck, 1980). The dolomite appears to be ferroan, which implies formation during burial. Like Ihle Facies 3, this facies appears volumetrically insignificant as it is only nine total feet (2%) of the Mississippian section. Ihle Facies 9 is interpreted to represent deposition within the mid-ramp to distal mid-ramp environment below FWWB and above SWB (Figure 15).

**Ihle Facies 10: Recrystallized Packstone-Grainstone**

The recrystallized packstone-grainstone facies is observed within the upper 68ft (28.7m) in the Ihle core and is absent in the Doberman core. This facies is interbedded with Ihle Facies 7 and is white to very light gray in color (Figure 31). Ihle Facies 10 is thinly bedded and dominated by calcite grains (88-92%) that are recrystallized, making the original grains unrecognizable. Facies 10 also contains minor amounts of clay minerals (6-8%) that are mainly mixed layer illite/smectite, and to a lesser extent, silt-sized quartz (1-3%) grains. Ihle Facies 10 is heavily cemented and microbioclastic debris is observed in thin section. The original depositional framework or composition cannot be identified due to the apparent total recrystallization. Contacts between this facies and Ihle Facies 7 are both gradational and sharp, with no apparent preference toward one or the other.

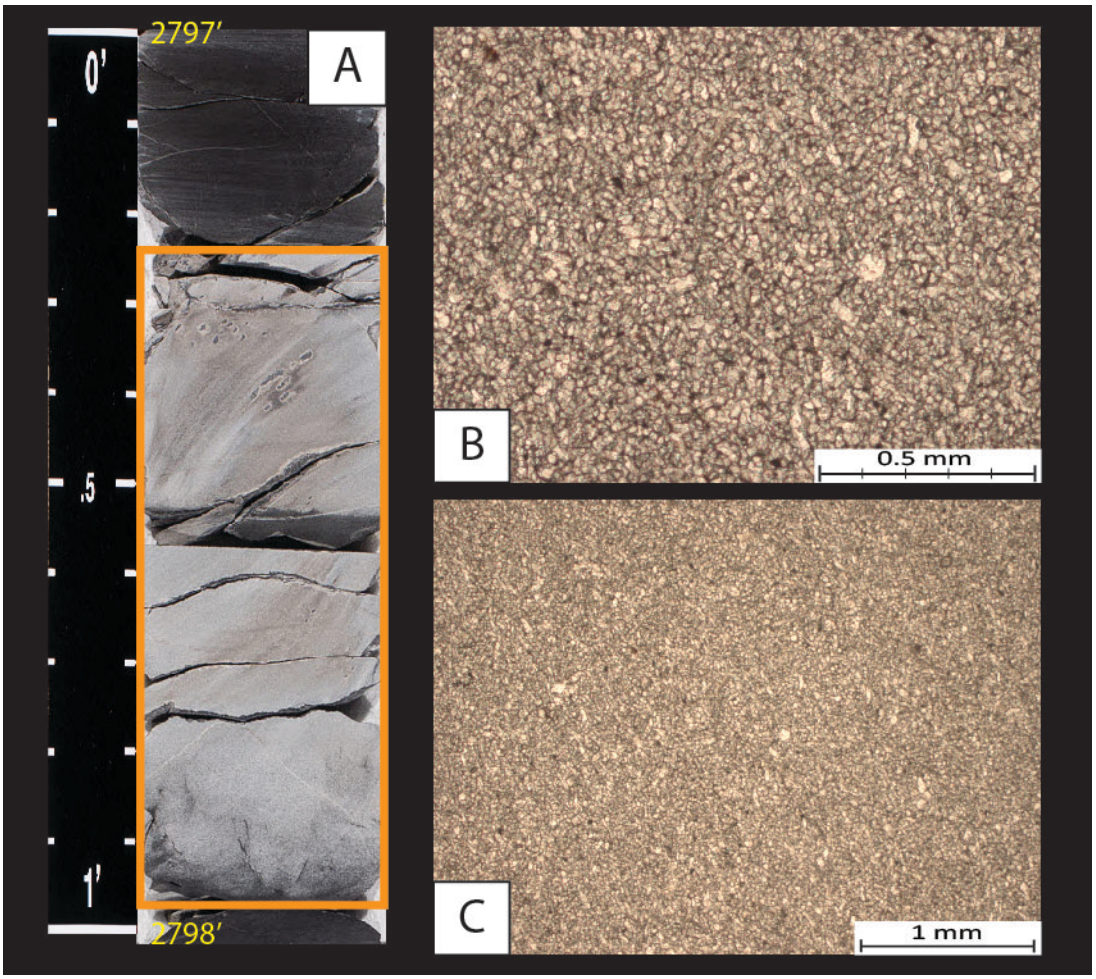


Figure 31. Ihle Facies 10: Recrystallized Packstone-Grainstone. The scale to the left of the core image is in tenths of feet. **A)** Core photograph of the recrystallized packstone-grainstone facies under white light, displaying massive bedding and its white to very light gray color. This facies is highly fossiliferous as observed in thin section, but identity of the skeletal debris is obscured by recrystallization. **B-C)** Thin section photomicrographs of the recrystallized packstone-grainstone facies within the Ihle core at 2797.30'. The images are in PPL. The sample is dominated by unidentifiable calcite grains and contains minor amounts of clays and silt sized quartz grains. XRD analysis: 1% quartz, 92% carbonates (91% calcite and 1% dolomite), 6% clay minerals (3% mixed layer illite/smectite, 1% illite, 1% kaolinite, and 1% chlorite), and 1% other minerals (1% pyrite).

The recrystallized packstone-grainstone facies within the Ihle is interbedded with Ihle Facies 7, which was deposited in the outer ramp to basin below SWB. As a result, the juxtaposition of Facies 10 and Facies 7 requires explanation. It is possible that a proximal carbonate facies 10 was transported into this area of the ramp by storms. This interpretation of Ihle Facies 10 is supported by its irregular thickness and marked difference in composition compared to the adjacent Ihle Facies 7 (Handford, 1986). As a result of the relative thicknesses of Facies 10, it is volumetrically insignificant from a reservoir perspective.

**Ihle Facies 11: Silty Peloidal Packstone-Grainstone**

The silty peloidal packstone-grainstone facies is observed in both, the Ihle and Doberman cores. In hand samples from the Ihle core, Facies 11 is light to medium dark gray and commonly massively bedded (Figure 32). Ihle Facies 11 is composed of silt- to sand-sized peloids (>50%), carbonate grains (59-81%) – mainly calcite, silt-sized quartz grains (11-26%) that are sub-angular to sub-rounded, and minor amounts of clay minerals (4-9%). Micritized grains/peloids are common in thin sections. Skeletal debris include (in decreasing order of abundance) brachiopods, crinoids, and in rare occasions, sponge spicules. Contacts between this facies within the Doberman were primarily sharp; however, the contacts between this facies and overlying/underlying facies within the Ihle are both sharp and gradational.

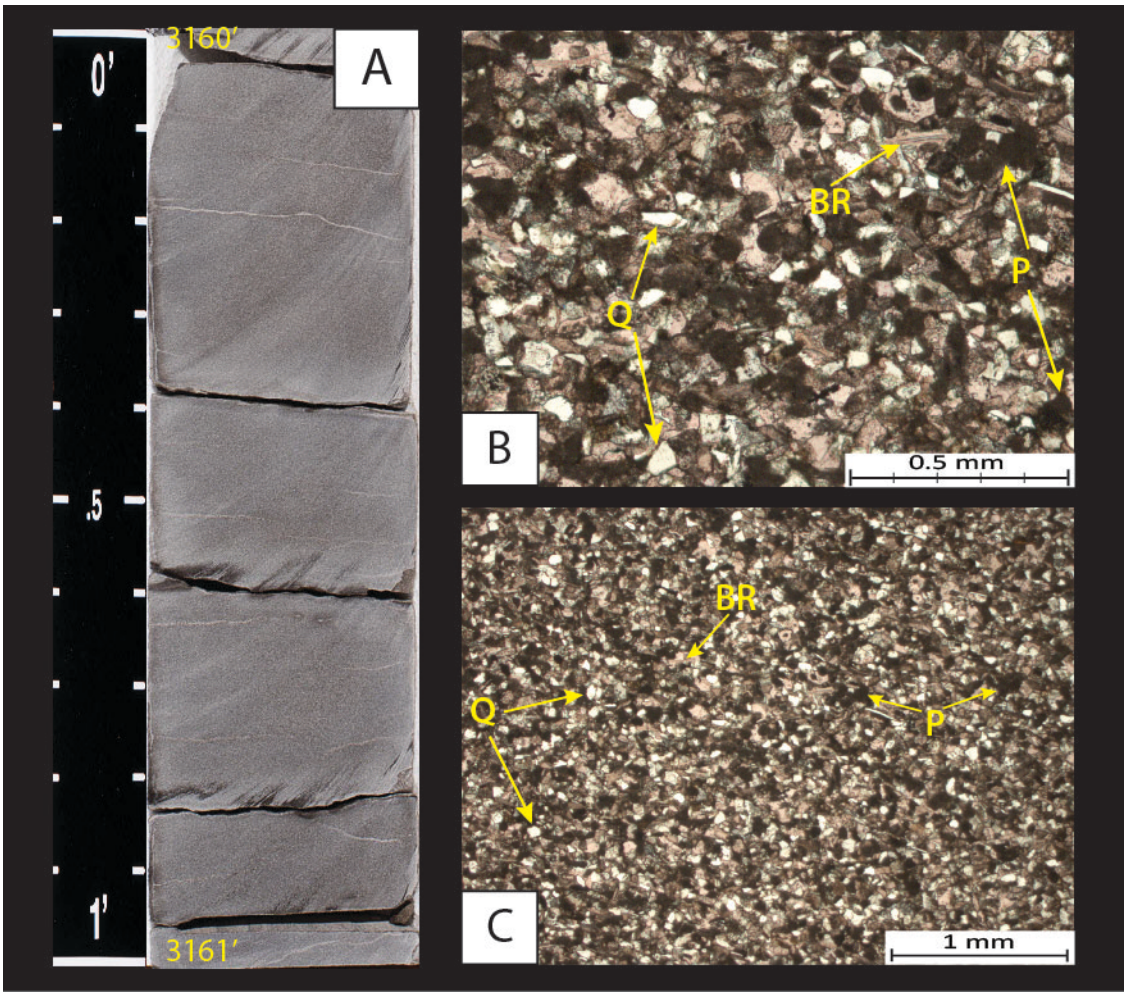


Figure 32. Ihle Facies 11: Silty Peloidal Packstone – Grainstone. **A)** Core photograph of Ihle facies 11, the scale to the left of the image is in tenths of feet. This facies is the only "clean" carbonate facies within the Doberman core. The silty peloidal packstone – grainstone facies is predominantly light to medium dark gray color, commonly massively bedded, and contains mineralized fractures. **B-C)** Thin section photomicrographs of Ihle facies 11 at 3160.20'. Images are in PPL. The sample is composed of silt- to mostly sand-sized peloid (P) grains, carbonate – mainly calcite (pink) grains, and silt- to very fine sand-sized quartz (Q) grains. It also contains skeletal debris such as crinoids (CR) and brachiopods (BR). XRD analysis: 24% quartz, 65% carbonates (61% calcite, 4% dolomite), 4% clay minerals (inconclusive results on breakdown of clay types with x-ray diffraction), 7% other minerals (4% plagioclase feldspar, 2% potassium feldspar, 1% pyrite). The average porosity for this facies based on 6 samples was 2.5%, and average permeability was 0.05 mD (air) and 0.037 mD (Klinkenberg).

Ihle Facies 11, along with Ihle Facies 9, are likely the shallowest water facies within the succession based on their abundant carbonate composition and high concentrations of skeletal debris. An abundance of peloids implies a somewhat restricted and/or quiet environment of deposition, however, this was likely not the case given the other environmental indicators (increase in fauna and relative lack of sedimentary structures). Evidence from other Ihle facies (and some Doberman facies) place the location of the Ihle core in an area that was influenced by storm events. In areas subjected to recurrent storms, peloids can be moved into shallower or deeper water environments, and peloid packstones to grainstones can be important components of slope and basin sequences formed by MTDs – mass transport deposits (Flügel, 2010; Scholle and Scholle, 2003). Like the silty peloidal packstone-grainstone facies within the Doberman, it is thought that these peloids were transported into this area of the ramp from another area of active peloid formation. Ihle Facies 11 is interpreted to represent deposition within the mid-ramp environment, below FWWB and above SWB (Figure 15).

## Sequence Stratigraphic Framework

### Idealized Facies Successions

The sequence stratigraphic framework for the Mississippian section in east-central Oklahoma was established using an idealized vertical stacking pattern of facies identified from the Doberman #1-25 and Ihle #1-26 subsurface cores as described in the preceding section. To better explain observed facies stacking patterns, facies were separated into a siliciclastic-dominated facies stacking pattern and a carbonate-dominated facies stacking pattern. The siliciclastic- and carbonate-dominated idealized facies successions for both cores demonstrate a shoaling- or shallowing-upwards profile that consists of a transgressive and regressive phase of one complete rise and fall in relative sea level (Figures 33 and 34). To better represent

components of a sequence/cycle, transgressions are shown by blue triangles pointing upward and regressions are shown by red triangles pointing downward. These idealized facies successions were used to better understand variability of facies, delineate sequences within the cored intervals, and outline the hierarchy of these sequences and cycles. After vertically constraining the hierarchy of depositional sequences and cycles for both cores, their respective boundaries were correlated laterally between the cored wells and then where possible, laterally to other wells. All six facies present within the Doberman #1-25 were correlated to the Ihle #1-26 core. However the Ihle #1-26 core has eleven facies in total and roughly an additional 190ft (58m) of core (mostly silty shales and mudstones) not seen in the Doberman #1-25. Flooding surfaces within both cores were noted by a sharp or abrupt change in lithology from shallow water to deeper water facies. Identifying flooding surfaces within both cores helped define stacking patterns and hierarchical levels of cyclicity. In the Doberman core, carbonate-dominated facies begin at the bottom and extend upward approximately 100ft (31m). The remaining 135ft (41m) is dominated by siliciclastic facies. It is important to point out that occasional carbonate facies occur in the siliciclastic-dominated interval and vice-versa. However, these isolated occurrences are not repetitive and therefore are not included in the idealized stacking patterns. In the Ihle core, carbonate-dominated facies begin at the contact with the Woodford Shale and extend upward approximately 180ft (55m). Continuing upward, siliciclastic-dominated facies comprise the next ~175ft (53m), then the remaining 70ft (21m) of uppermost core switches back to carbonate-dominated facies.

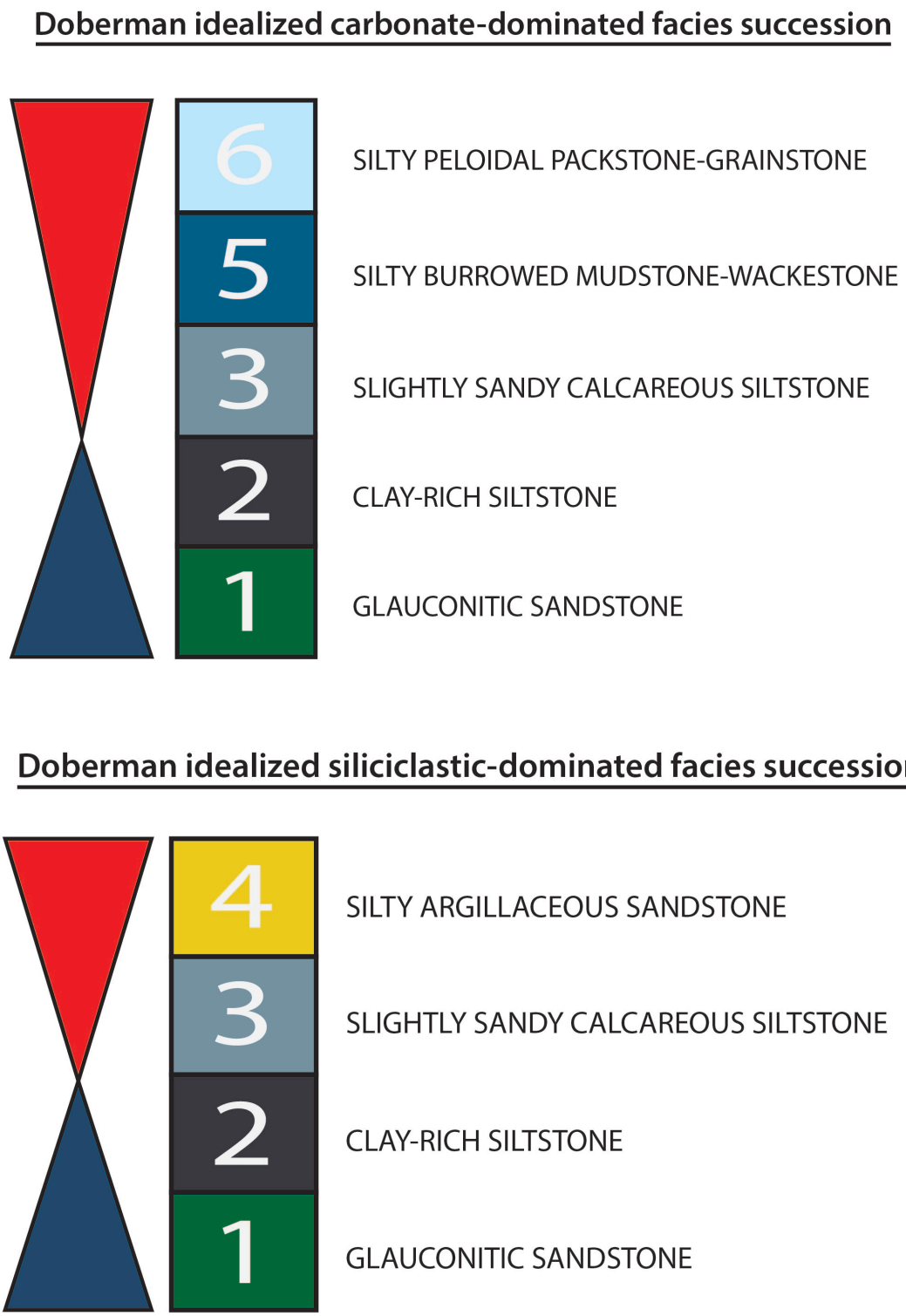


Figure 33. Top: Idealized carbonate-dominated facies succession for the Mississippian section within the Doberman #1-25. Bottom: Idealized siliciclastic-dominated facies succession for Doberman #1-25. This succession is representative of the preserved depositional facies during a complete rise and fall of sea level. The blue triangle illustrates the transgressive phase of the system while the red triangle illustrates the regressive phase.

## Ihle idealized carbonate-dominated facies succession

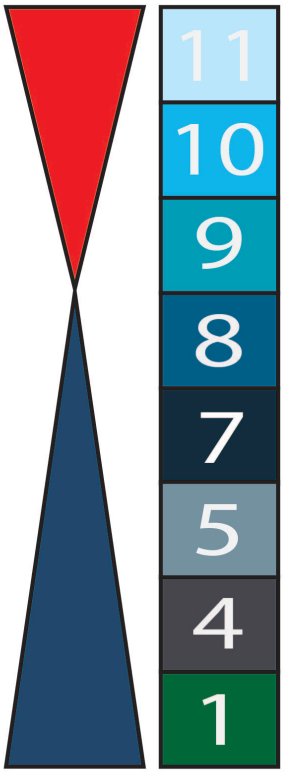


SILTY PELOIDAL PACKSTONE-GRAINSTONE

RECRYSTALLIZED PACKSTONE-GRAINSTONE (rare - upper core)

SILTY ARGILLACEOUS DOLO PACKSTONE (rare - upper core)

SILTY BURROWED MUDSTONE-WACKESTONE

ARGILLACEOUS MUDSTONE-WACKESTONE (rare - upper core)

SLIGHTLY SANDY CALCAREOUS SILTSTONE

CLAY-RICH SILTSTONE

GLAUCONITIC SANDSTONE

## Ihle idealized siliciclastic-dominated facies succession

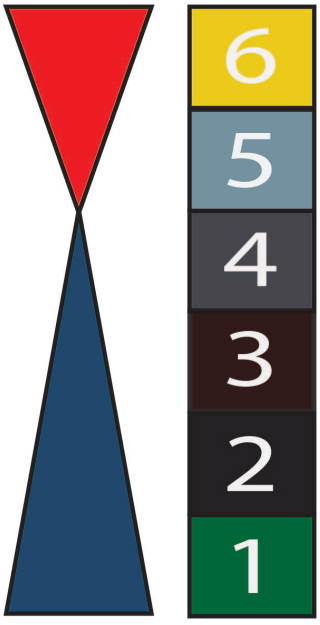


SILTY ARGILLACEOUS SANDSTONE

SLIGHTLY SANDY CALCAREOUS SILTSTONE

CLAY-RICH SILTSTONE

PHOSPHATIC DOLOMITIC SHALE (rare - upper core)

SILTY SHALE

GLAUCONITIC SANDSTONE

Figure 34. Top: Carbonate –dominated idealized facies succession for the Mississippian section based on the Ihle #1-26 core. Bottom: Siliciclastic-dominated idealized facies succession for the Ihle #1-26 core. The succession represents depositional facies preserved in the Ihle core. The blue triangle illustrates the transgressive phase of the system while the red triangle illustrates the regressive phase.

## Sequence Stratigraphic Hierarchy

The vertical stacking patterns of facies identified in the Doberman and Ihle cores yielded a hierarchy containing three levels of cyclicity, which is similar to the results of other Mississippian studies (LeBlanc, 2015; Flinton, 2016; Jaeckel, 2016). Though a conodont biostratigraphy study (Hunt, 2017) was conducted on the Doberman #1-25 core, it is important to note that the temporal resolution of these cycles is still unresolved due to the maximum 1-3 million year temporal resolution of conodont biostratigraphy (Boardman et al., 2013). Conodont biostratigraphy, while useful in constraining 3$^{rd}$ order sequences at best, still provided valuable stage resolution (Hunt, 2017). As conodont biostratigraphy does not provide the required resolution to define the higher-frequency 4$^{th}$- and 5$^{th}$-order cycles, the proposed "3$^{rd}$-, 4$^{th}$-, and 5$^{th}$-order" cycles in this study are not assigned specific intervals of time.

Within the Doberman #1-25 core there are four probable 3$^{rd}$ –order sequences encompassing ~236ft (72m) of Mississippian section. Within the Ihle #1-26 core there are six probable 3$^{rd}$ –order sequences comprising the ~424ft (129m) of Mississippian section, with the first four 3$^{rd}$ –order sequences correlating to the four 3$^{rd}$ –order sequences within the Doberman #1-25 core (Figure 35). The higher-frequency (4$^{th}$-order high-frequency sequences (HFSs) and 5$^{th}$-order high-frequency cycles (HFCs)) packages are interpreted as being the result of either Milankovitch band sea level cyclicity or other auto-/allocyclic processes. While their origins may not be resolved, these packages can control the evolution of reservoir flow units within carbonate reservoirs (Grammer et al., 2004).

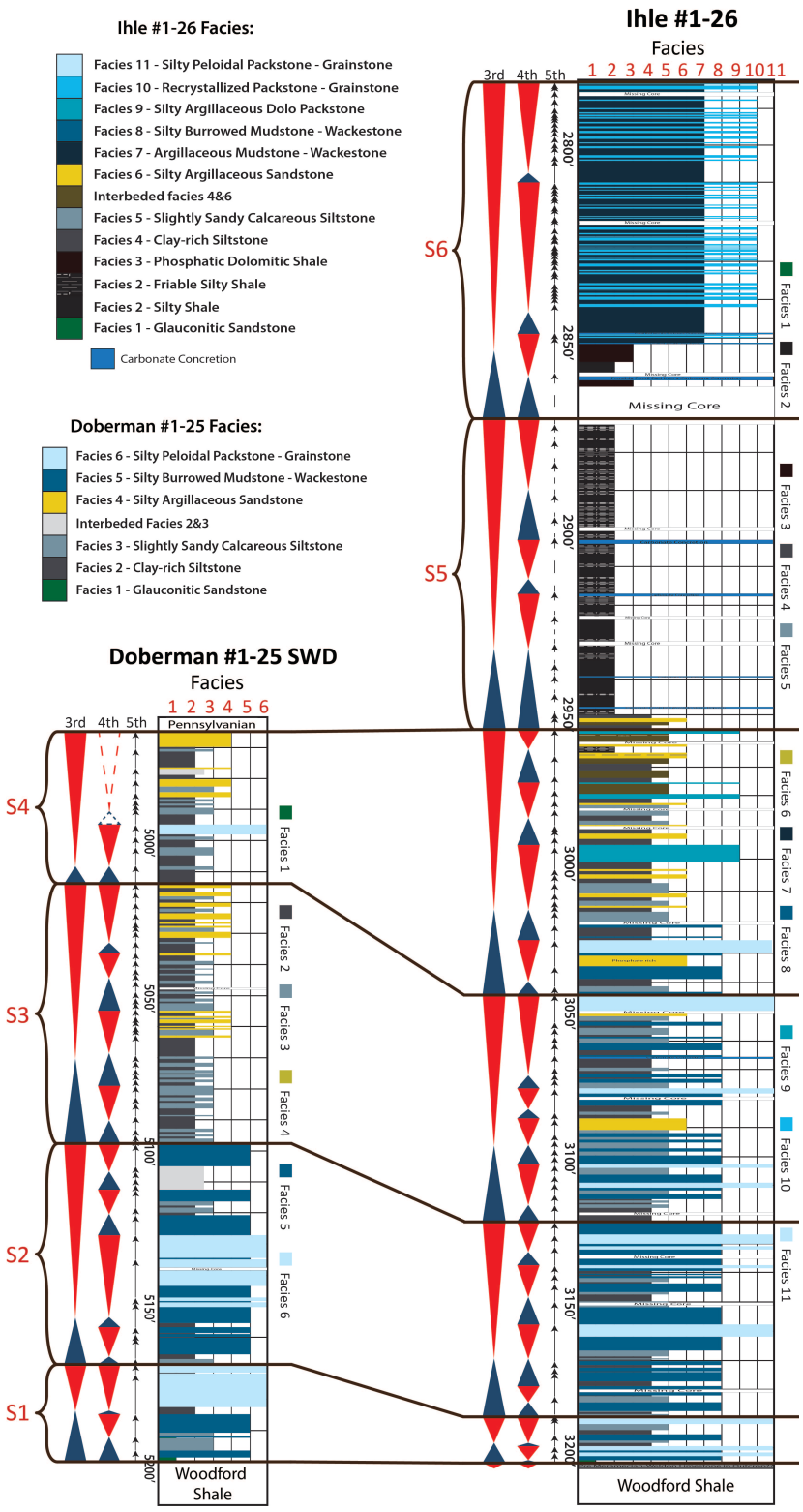


Figure 35. Sequence Stratigraphic Hierarchy of both cores in this study. Dark brown correlation lines represent the probable 3rd –order sequences common to the two cored wells. These probable 3rd –order sequences display a shallowing upward pattern (refer to figures 35 and 36) and contain various 4th –order HFSs. 5th –order HFCs (represented by the black arrows) were observed and are inferred to be the result of high-frequency Milankovitch sea level cyclicity (20-40 k.y.)

**"Third" Order Sequences**

In the Doberman #1-25 core, four probable 3rd order sequences (S1 – S4) were recognized and correlated to similar sequences in the Ihle # 1-26 core. The Ihle core contains an additional ~190ft (58m) more Mississippian section than the Doberman, and within this section, two additional probable 3rd order sequences (S5 and S6) were identified (Figure 35). The 3rd order sequences identified in the Doberman core range in thickness from 31ft (9.5m) to 84ft (25.6m) with S3 being the thickest, and the base of each sequence is indicated by a noticeable shift to deeper-water facies (Facies 1, 2, and 3) relative to the underlying shallower-water facies (Facies 4&6). Within the Ihle core, the 3rd order sequences range in thickness from 16ft (5m) to 89ft (27m) with S4 being the thickest, and like the Doberman, the base of the sequences are marked by a distinct deepening as facies change from shallow water Facies (9&11) to deeper-water Facies (1, 2, and 3). This relationship is indicative of a landward shift in facies belts resulting from a rise in relative sea level (LeBlanc, 2014; Price, 2014; Childress and Grammer, 2015). In both cores, it was observed that these 3rd order sequences have a common shallowing upward pattern from deeper-water facies at the base, to shallower-water facies at the top, which is demonstrative of a steady decrease in relative sea level. Each 3rd order sequence, within both cores, consists of two to four ingrained 4th order high-frequency sequences (Figure 36).

**"Fourth" Order High-Frequency Sequences**

Both the Doberman and Ihle cores display probable 4th order high-frequency sequences (HFSs) that, like the 3rd order sequences, illustrate a shoaling upwards succession of depositional facies. Within both cores, S1 contains two 4th order HFSs, while S2 and S3 contain four (Figure 36). The Doberman core contains two nested 4th order HFSs within S4 and in the Ihle core S4 contains four HFSs. In this case, the additional 4th order HFSs in the Ihle core are attributed to the additional Mississippian section as the Doberman S4 sequence is truncated by the pre-

Pennsylvanian unconformity. As previously mentioned, the Ihle has two more probable 3rd order sequences (S5 and S6) than the Doberman. S5 and S6 in the Ihle each contain three 4th order HFSs (Figure 36). Thicknesses of the HFSs within the Doberman range from 11ft (3.4m) to 30 ft (9m), and within the Ihle the thicknesses range from 6 ft (2m) to 40 ft (12m). 4th order high frequency sequences typically display the same or similar facies stacking patterns and depositional successions as their host 3rd order sequences.

**"Fifth" Order High-Frequency Cycles**

Probable 5th order high-frequency cycles (HFCs) were identified in both cores and range from 1ft (0.3m) to 10ft (3m) in thickness (Figures 35 and 36, black arrows). These highest frequency packages are cyclic and were recognized by the repetition of facies within the complete facies stacking pattern. It is likely that autocyclic and other allocyclic processes were occurring, simultaneously with eustatic ones, complicating the interpretation of these small scale packages. As a result of depositional processes being influenced by occasional to frequent storms, it is difficult to interpret if these high-frequency 5th order cycles are the result of autocyclic and/or tectonic processes or the result of Milankovitch band sea level cyclicity. If Milankovitch band sea level cyclicity is the controlling factor, these cycles are likely related to precession (19 to 23 k.y.) and/or obliquity (40 k.y.). If these HFCs are the result of autocyclic or other allocyclic processes, storms and/or tides could cause fluctuations in FWWB leading to unforeseen discrepancies and disruptions in stacking patterns that are not related to eustatic changes in sea level.

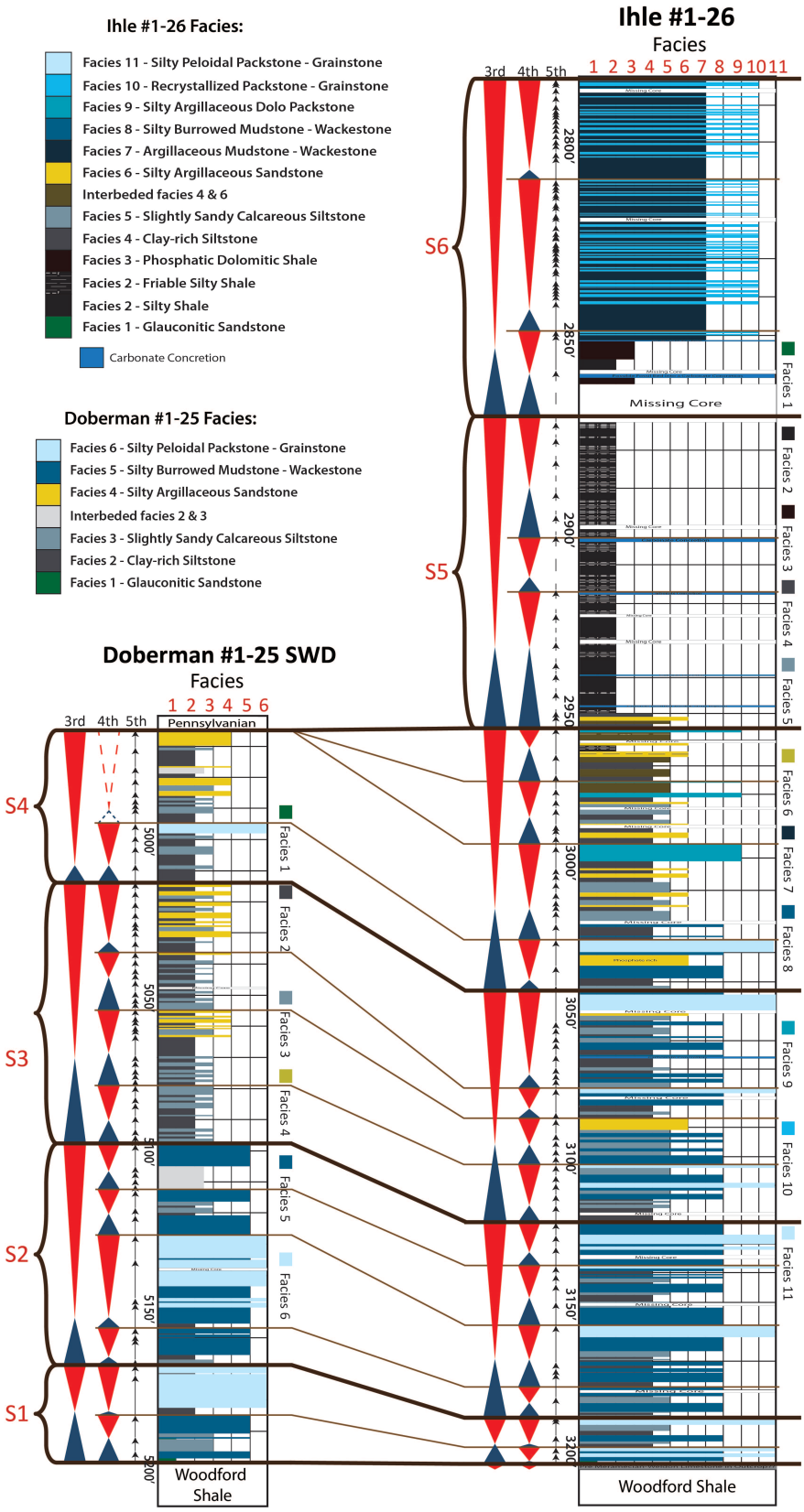


Figure 36. Complete Sequence Stratigraphic Hierarchy of both cores in this study, from west to east. Dark brown correlation lines represent the probable 3rd –order sequences, while the thinner light brown lines represent the probable 4th –order high-frequency sequences (HFSs). 5th –order HFCs (represented by the black arrows) were observed. Note the thinning of S1 and S2 in the Ihle core.

## Wireline Log Correlation

Correlating and mapping sequences across the study area incorporated multiple data sets, including wireline logs. Stratigraphic surfaces associated with 3rd order sequences identified in cores were tied to their respective wireline log signatures to establish facies trends on wireline logs and correlate trend signatures between wells. Boundaries for the probable 3rd order sequences were selected based on regressive facies (shallower-water facies) being succeeded by transgressive facies (deeper-water facies). Correlating these boundaries from the "ground truthed" sequence stratigraphic framework identified in the cores, produced wireline log markers that could be correlated with confidence.

### Gamma-ray

Spectral gamma-ray and borehole measured gamma-ray data were both utilized in this study to help correlate the sequences identified on core-truthed wireline logs. Gamma-ray signatures consistently correlated to the boundaries of the 3rd order sequences, typically displaying an increase in the overall value of greater than 80 API units. These higher API values correspond with the onset of the transgressive phase within the 3rd order sequences, and there is a general trend of the gamma-ray values decreasing as the sequence transitions into the regressive phase (Figures 37 and 38). However, not every increase in gamma-ray value marks a 3rd order sequence boundary, as seen within the sequence stratigraphic hierarchy of facies correlated to wireline log signatures (Figure 38). The 3rd order sequences can be regionally correlated within the subsurface using the gamma-ray log. Although the 4th order HFSs were correlatable in some areas, these correlations were not as predictable as those tied to 3rd order sequence boundaries. Overall, the gamma-ray curve was not a reliable tool to identify and correlate the higher-frequency 4th order HFSs and 5th order HFCs.

**Resistivity**

The resistivity curves for both cores were evaluated to gauge their capability as a correlation tool for 3rd order sequence boundaries and to see if they had further value in correlating 4th order HFSs. The resistivity curve signatures proved useful for correlating and extrapolating 3rd order sequences, away from the cored wells. Typically, resistivity values were higher in the carbonate-rich facies (800 – 1100 ohm-m) compared to the silt- and clay-rich facies (50 – 200 ohm-m). The resistivity curve for the Ihle is more erratic and less smooth than the Doberman resistivity curve, a characteristic attributed to the higher percentage of siliciclastics in the Ihle. In the Doberman core, the resistivity curve was useful in differentiating between silt-rich zones and calcite-rich zones with the silt-rich zones having lower values (Figures 37 and 38). While the resistivity curve proved valuable for correlating 3rd order sequences between wells, it added little value (if any) in terms of correlating 4th order HFSs. No consistent signatures were observed that were deemed useful for correlating the boundaries of the 4th order HFSs. Overall, the resistivity curve, when paired with the gamma-ray curve, proved to be more useful for correlating than the density and neutron porosity curves. The density and neutron porosity curves were useful in identifying the boundary between Mississippian strata and Pennsylvanian strata. At this boundary, the density and neutron porosity curves tracked each other and typically went off scale to the left, or to the positive side (Figure 38). Meaning, at the Pennsylvanian-Mississippian boundary the density and neutron porosity curves displayed a characteristic increase in porosity, which in some cases was attributed to poor tool pad contact to the rock because of hole washout.

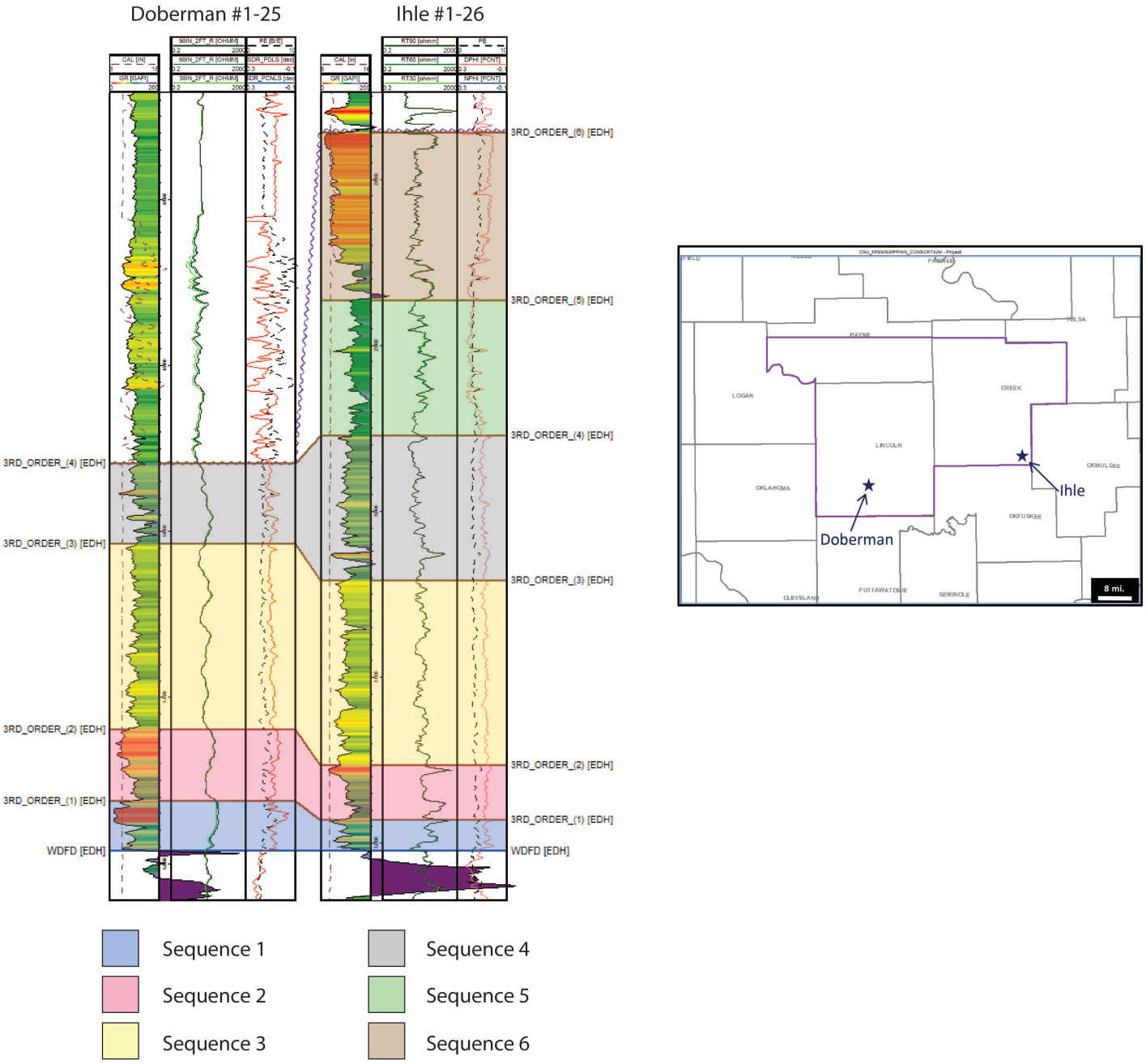


Figure 37. Left: Illustration showing the wireline log signatures of the probable 3rd order sequences. Right: Location (within Oklahoma) of cored wells within the study area (outlined in purple).

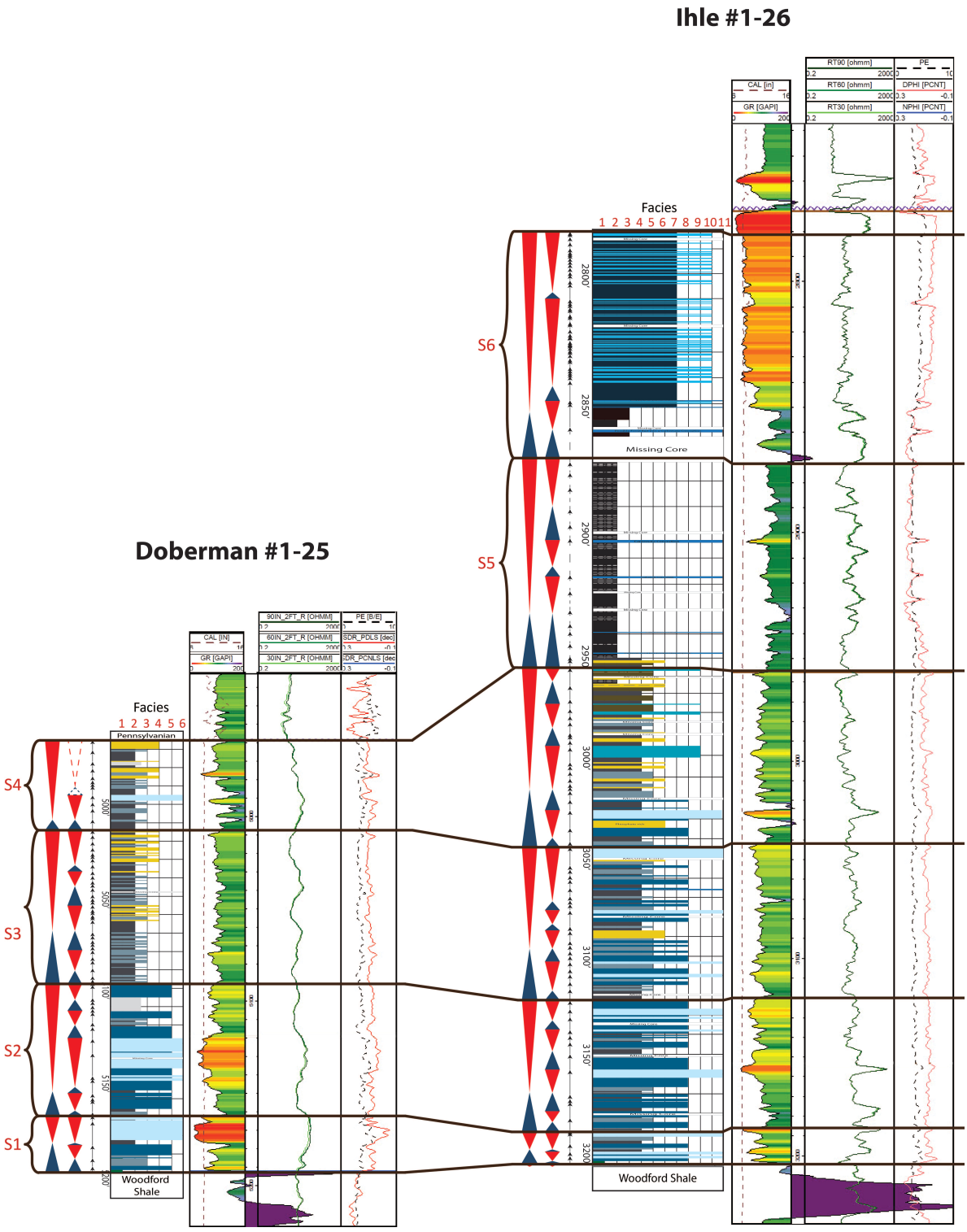


Figure 38. Wireline log signatures and associated facies of both cores. Tracts from left to right for each core: 3rd, 4th, and 5th order sequences and cycles, depositional facies and wireline logs (gamma-ray, resistivity (green curves), PE curve (black dashed line) and density neutron porosity (red curves)). Refer to Figures 35 & 36 for facies names and color associations. Note the correlation between facies and gamma-ray signatures. 3rd order sequences correlate better, whereas the higher-frequency 4th and 5th order sequences and cycles are inconsistent and correlated with less confidence.

## Sequence Stratigraphic Architecture

The recognized sequence stratigraphic architecture of the "Mississippian Limestone" within the study area exhibits strike-elongate geometries that are characteristic of a carbonate ramp environment (Ahr, 1973; Tucker and Wright, 1990). Progradation of the probable 3rd order sequences was observed in both subsurface cross sections (Figures 41 and 42) and thickness maps (Figures 44 and 45) and is likely the result of a global decline in sea level (2nd order) throughout Mississippian time (Haq and Schutter, 2008). Although 4th order HFSs and 5th order HFCs were observed, they were unable to be correlated confidently to well logs in the study area.

### Subsurface Cross Sections

Subsurface stratigraphic cross sections were constructed to extrapolate correlations from cored wells and evaluate thickness trends. Mississippian strata were correlated between wells using gamma-ray, resistivity, and to a lesser extent density and neutron porosity logs tied to the sequence stratigraphic framework established for the Doberman and Ihle cores. Correlating the sequence stratigraphic framework from the cores to the gamma-ray log signatures was critical to constructing cross sections and correlating wireline log signatures. Sequences designated based on shoaling-upwards or shallowing-upwards packages on wireline logs of the cored wells, were recognized in non-cored wells. Correlations within the cross sections are referenced to a flat datum on the top of the Devonian Woodford Shale. Cross sections were constructed along depositional strike and depositional dip directions to reveal thickness trends and geometries associated with depositional processes. Cross-sections transect all counties within the study area and provide evidence to support inferences concerning the stratigraphic architecture and depositional environments. Gamma-ray and resistivity curves were the most useful well log signatures for correlating and logs containing these curves were preferred for inclusion in cross sections.

**Strike-Oriented Cross Sections**

Two west-east transects were constructed in a depositional strike direction (Figures 39 and 40) to illustrate the geometry of sequences and their correlation across the study area. Each cross section contains two core-calibrated wireline logs, either from this study or from LeBlanc (2014). Flooding surfaces and shoaling-upwards packages identified in cores correlated to wireline log signatures and were used to delineate sequence boundaries. Cross section A to A' (Figure 39) represents correlations subparallel to depositional strike (WSW to ENE), spans roughly 55 miles (88.5 km), contains 19 wells, and includes both core calibrated logs examined within this study. Figure 39 illustrates the lateral continuity of these 3$^{rd}$ order sequences along inferred depositional strike, as previously shown. The absence of S5 and S6 to the west was likely influenced by the prominent Wilzetta Fault trend, where on the downthrown side an additional ~200ft (61m) of section occurs at the top of the Mississippian interval (Figure 39). Subsurface cross section A-A' displays the six depositional sequences identified within the cores and are color coated by sequence throughout the cross section.

Subsurface cross section B to B' (Figure 40) is an west to east trending strike-oriented cross section through the northern part of the study area. Cross-section B to B' spans ~68mi (109km), contains 29 wells, and includes the Elinore #1-18 and Winney#1-8 cored wells from LeBlanc (2014). This cross section displays relatively laterally continuous sequences of uniform thickness (similar to A to A') from west to east until the Wilzetta Fault trend, where extra section is evident on the downthrown side. Based on wireline log correlations, cross-section B to B' may contain as many as nine sequences.

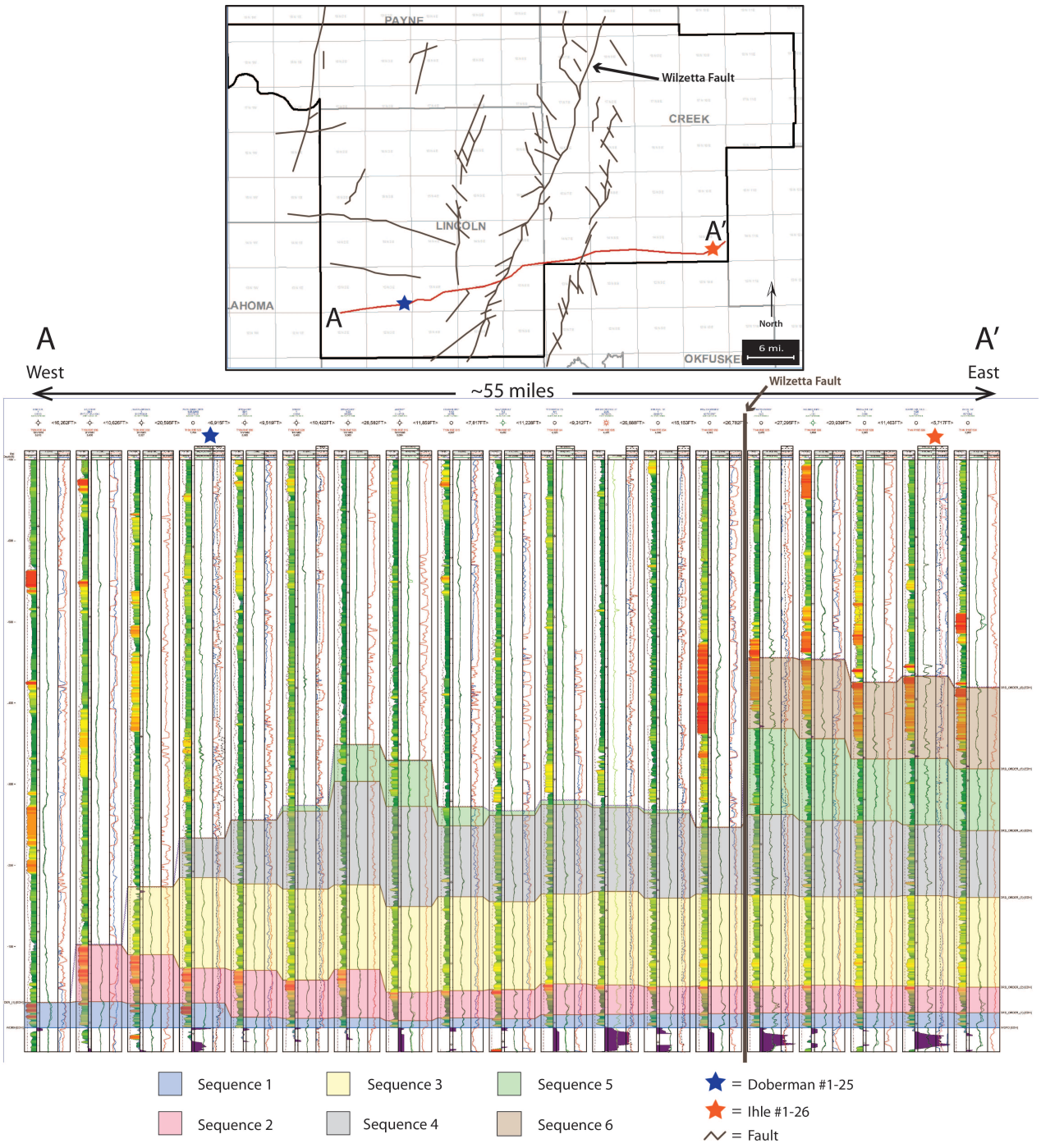


Figure 39. Top: Map of study area (outlined in black) showing the location of cross-section A to A' (red line). From west to east, the Doberman #1-25 well is indicated by the blue star and the Ihle #1-26 well is indicated by the orange star. Faults in the study area are illustrated by gray lines. Bottom: Strike oriented subsurface cross section shown by red line on map. Cross-section A to A' shows six probable 3rd order sequences. Wilzetta Fault indicated by dark gray line. Vertical scale exaggerated aprroximately16x.

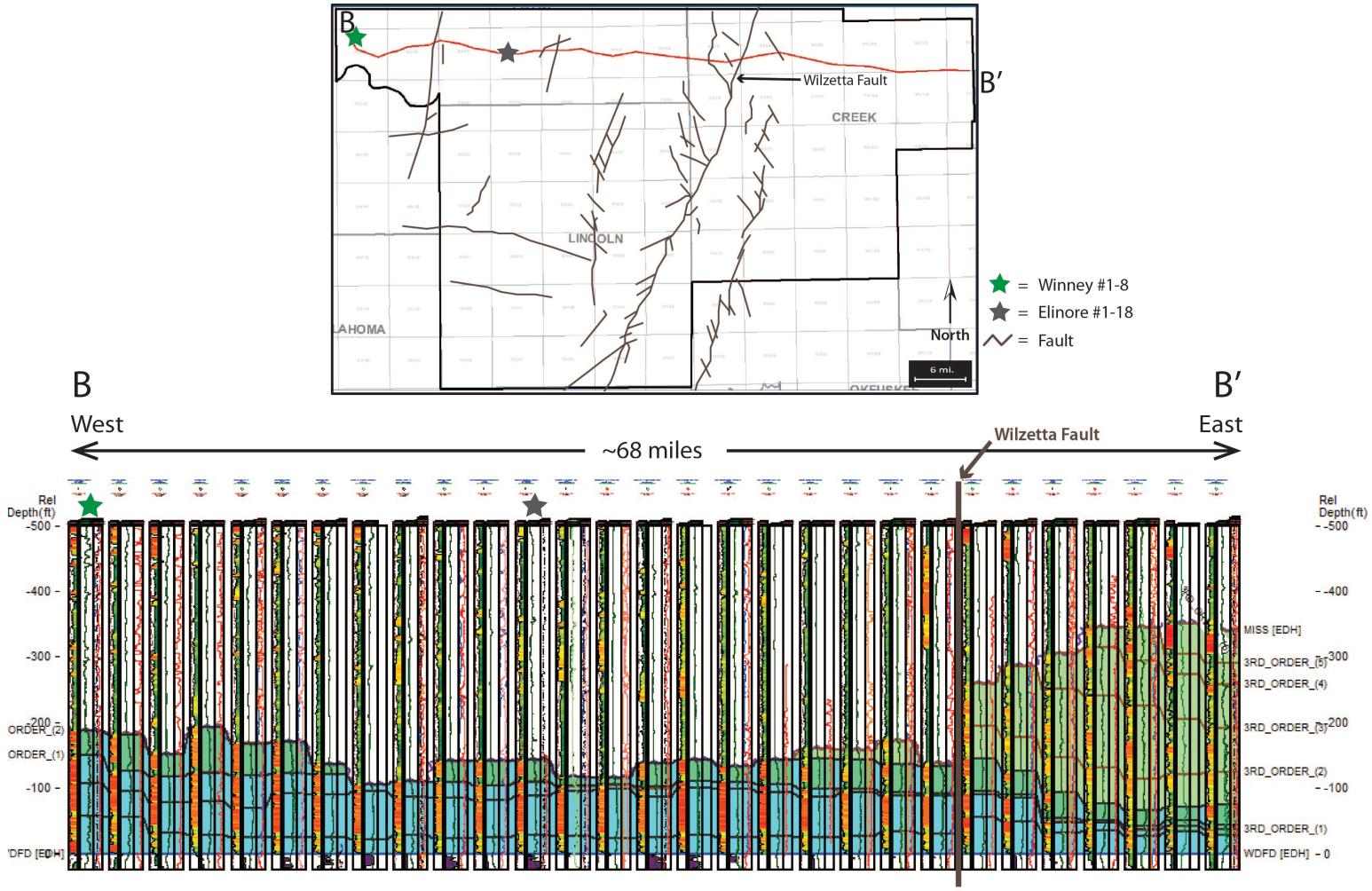


Figure 40. Top: Map of study area (outlined in black) showing the location of cross-section B to B' (red line). From west to east, the Winney #1-8 well is indicated by the green star and the Elinore #1-18 well is the gray star. Faults in the study area are illustrated by gray lines. Bottom: Strike oriented subsurface cross-section B to B'. Cross section displays the lateral continuity of these sequences moving along depositional strike. Wilzetta Fault indicated by dark gray line. Vertical scale exaggerated approximately 8x.

### Dip-Oriented Cross Sections

Two cross sections were constructed in the expected depositional dip direction (Figures 41 and 42) to demonstrate the distribution of depositional sequences and their geometries. Both cross sections contain the Elinore #1-18 from LeBlanc (2014) and extend to each of the cores used in this study. As with the strike-oriented cross sections, flooding surfaces and shoaling-upwards patterns identified in cores were correlated to wireline log signatures and used to delineate sequence boundaries. Cross-section C - C' (Figure 41) spans roughly 45 miles (72 km) with 21 wells and includes the Doberman #1-25 near the south end area and the Elinore #1-18 at the north end. Cross-section C - C' displays eight probable sequences, whose geometries suggest progradation in a southerly direction. Some sequences (2 & 3 from this study) exhibit relatively uniform thickness (Figure 41).

Subsurface cross section D to D' (Figure 42) starts at the Elinore #1-18 in the northwest part of the study area and extends in a dip direction, roughly 42 mi (67 km) to the Ihle #1-26 in the southeast corner of the study area. Cross section D to D' (like C to C') contains core calibrated sequences from LeBlanc (2014) and this study that provide the facies basis for nine possible depositional sequences. These sequences display a progradational stacking pattern moving basinward. Cross section D to D' crosses the Wilzetta Fault zone, evident by the significant increase in thickness of Mississippian strata on the downthrown side (Figure 42). The thinning of the Mississippian section on the upthrown (west) side of the Wilzetta Fault is likely related to uplift associated with the subsequent erosion of the uplifted block to the west.

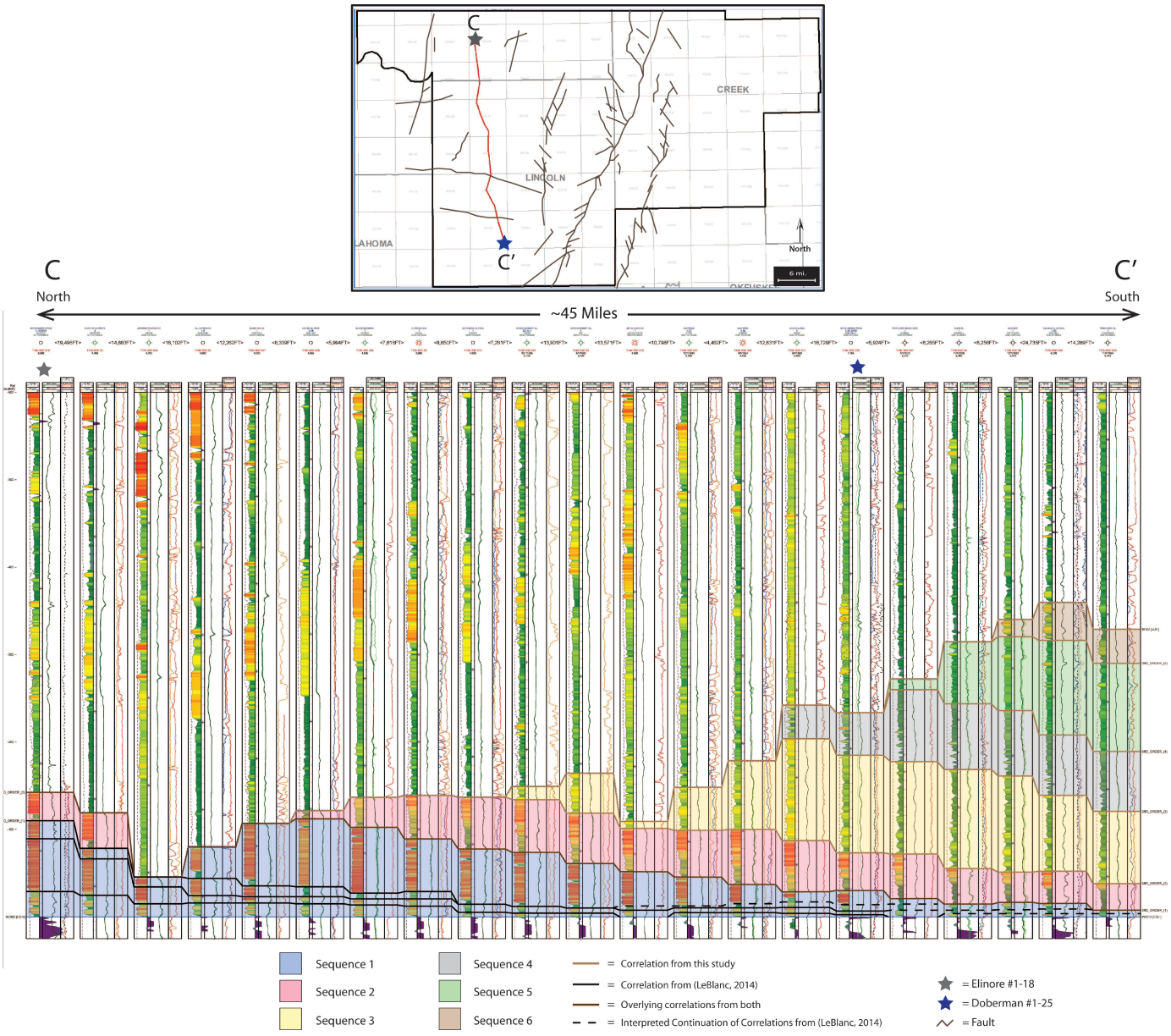


Figure 41. Top: Map of study area (outlined in black) showing the location of cross-section C – C′ (red line). From north to south, the Elinore #1-18 well is indicated by the gray star and the Doberman #1-25 well is indicated by the blue star. Faults in the study area are illustrated by gray lines. Bottom: Dip oriented subsurface cross section of the red line in the above photo. Cross-section C – C′ displays the geometry of these sequences moving along depositional dip. These correlations show these packages prograding in the dip direction. Correlations also reveal that prograding carbonate clinoforms are a logical interpretation for this system. Vertical scale exaggerated approximately 16x.

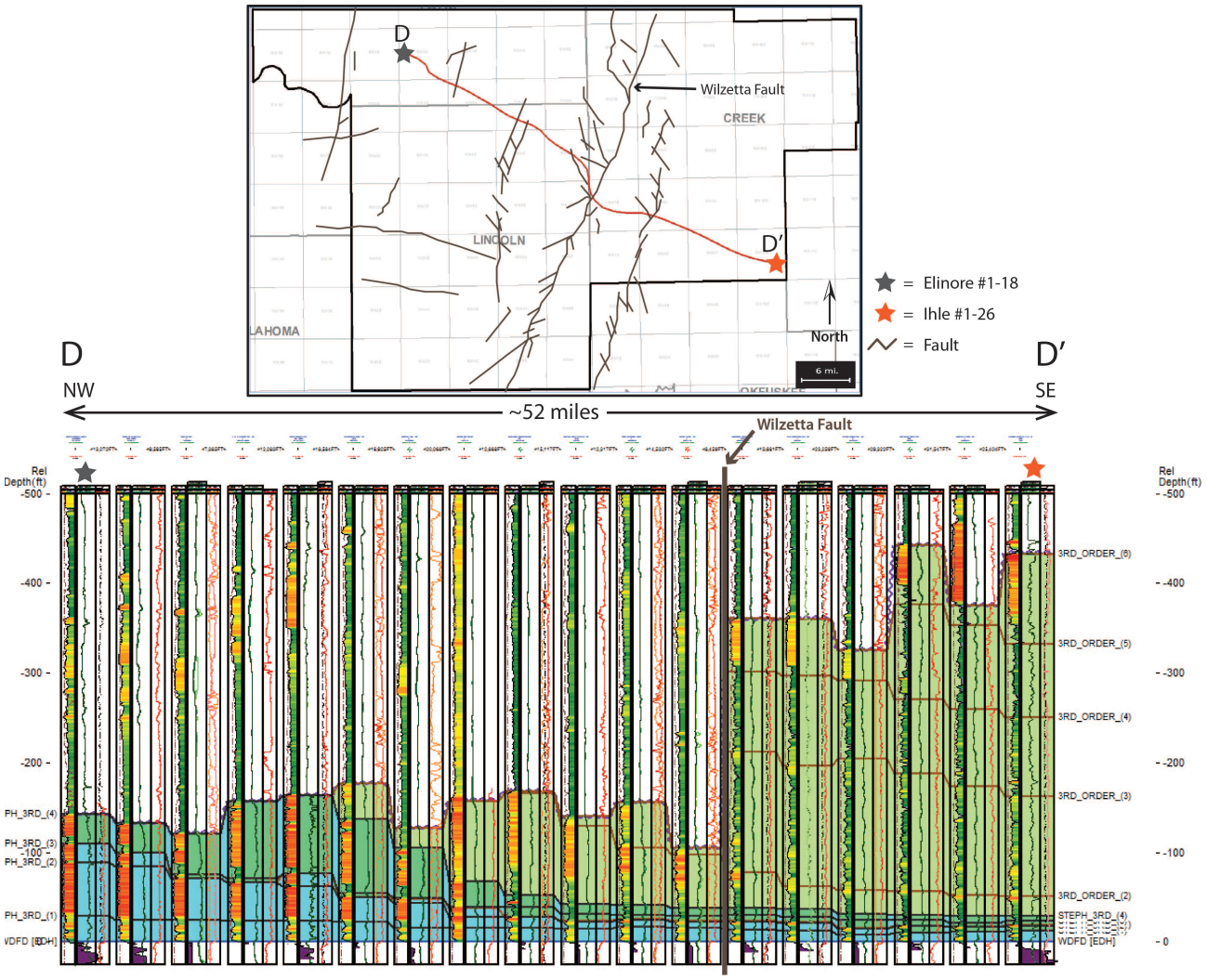


Figure 42. Top: Map of study area (outlined in black) showing cross-section D to D' (red line). From northwest to southeast, the Elinore #1-18 well is indicated by the gray star and the Ihle #1-26 by the orange star. Faults in the study area are illustrated by gray lines. Bottom: Cross -section D to D' in the expected dip direction. Cross-section D to D' displays the geometry of these sequences moving along expected depositional dip. Correlations show these packages prograding towards the southeast. Correlations also reveal that prograding carbonate clinoforms are a logical interpretation for this system. Note the significant increase in the thickness of strata starting in the sixth well from the right to the end of the cross section. This thickness increase occurs on the downthrown side of the Wilzetta Fault (dark gray line). Vertical scale exaggerated approximately 8x.

**Thickness Maps**

The thickness trends of the "Mississippian Limestone" along with 3rd order sequences 1 – 6 (S1-S6) were mapped. The thickness map of the Mississippian interval (Figure 43) displays regional distribution patterns. The Mississippian interval is marked at the top by the pre-Pennsylvanian unconformity and the Woodford Shale at the base. These are recognized by characteristic wireline log signatures and are relatively easy to identify. Mississippian strata, in east-central Oklahoma, thicken towards the south-southeast and thin towards the north-northwest (Figure 43). The thickness maps of individual 3rd order sequences disclose trends that support specific types of depositional geometries. Each younger sequence appears to shift basinward compared to its predecessor and thickens towards the south-southeast or in a basinward direction (Figures 44 and 45).

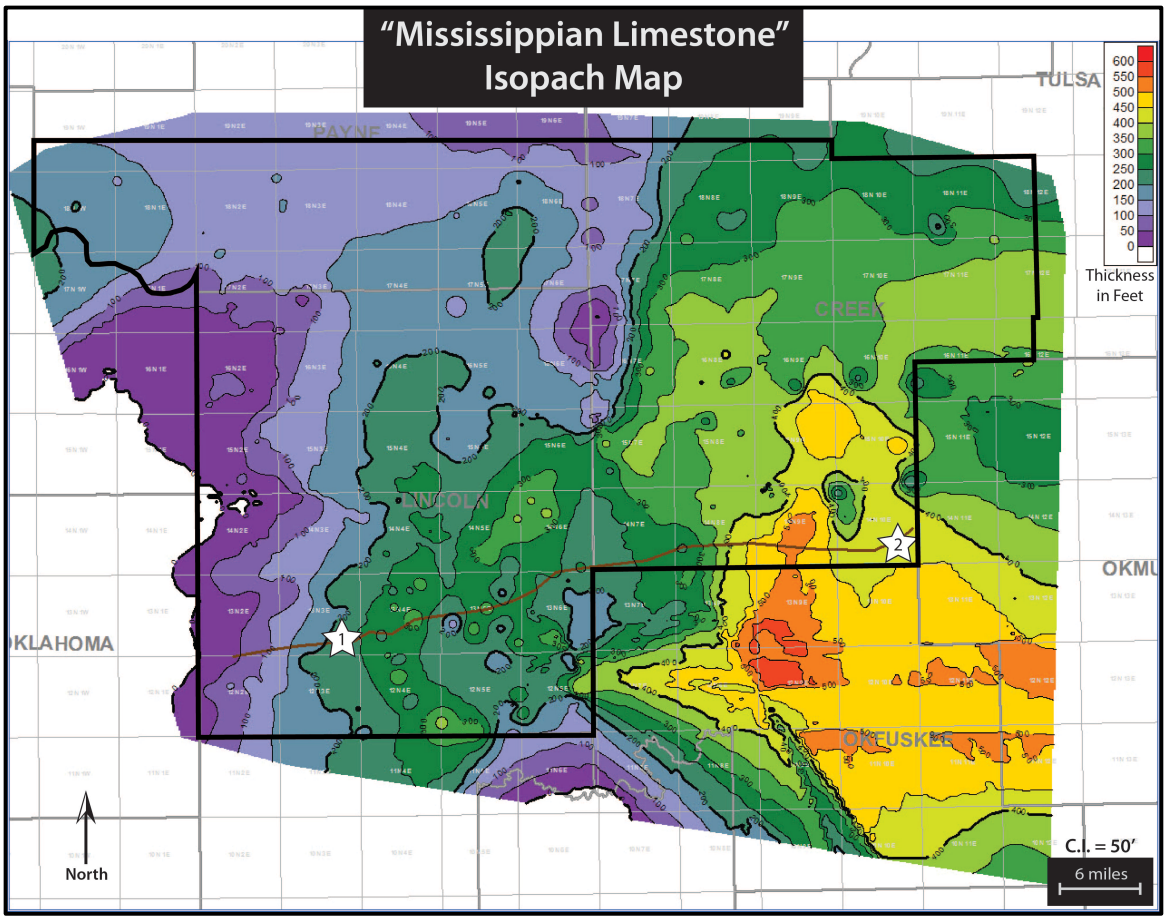


Figure 43. Thickness map of the "Mississippian Limestone". Boundaries were defined by the strata between the Woodford Shale and pre-Pennsylvanian unconformity. The thickness of the interval generally thickens towards the south-southeast towards the present day Arkoma basin, which occupies the position of the Oklahoma basin during the Mississippian. Star #1 and star #2 indicate locations of Doberman and Ihle cores, respectively. Contour interval is fifty feet and the color bar in the top right corner indicates the thickness values, which range from 0 feet (white and dark purple) to 500 feet (orange).

**Sequence 1**

Sequence 1 (S1) is bound at its base by the underlying Woodford Shale and overlying siltstone facies (Facies 2 & 3 and Facies 4 &5 in the Doberman and Ihle, respectively). On wireline logs, S1 is characterized by an abrupt decrease in gamma-ray values from 200+ API Units to ~80-90 API units (Figures 37 and 38). Overall, S1 displays a shallowing-upward

signature to Facies 6 and Facies 11 for the Doberman and Ihle, respectively. Sequence 1 contains two embedded 4th order HFSs. In the Doberman, S1 is 31ft (9m) thick and thins down to 16ft (5m) within the Ihle. Sequence 1 is thickest (~140ft; 43m) in the northern and northwestern part of the study area and is at its thinnest (0-10ft; 0-3m) in the southern and southeastern part of the study area (Figure 44). Along the western border of Lincoln County, S1 thins to <5 ft. (1.5m) and appears to be absent.

**Sequence 2**

Sequence 2 (S2) is bound by a calcareous siltstone facies (Facies 3 & 5 for the Doberman and Ihle, respectively) at the base and demonstrates a shallowing-upward signature into the more carbonate-rich facies and is capped by the silty burrowed mudstone-wackestone facies (Facies 5 & 8 for the Doberman and Ihle, respectively). The boundary of S2 can be identified on wireline log signatures by an increase in the gamma-ray value from 40-50 API units to 120-125 API units and an overall decrease in resistivity values (Figures 37 and 38). Within S2, there are four 4th order HFSs that were observed in both cores. Sequence 2 is 70ft (21m) thick in the Doberman core and 68ft (20.7m) in the Ihle core. Like S1, the maximum thickness (~150ft; 46m) of S2 is in the northern part of the study area, but has shifted farther to the south-southeast compared to S1 (Figure 44). Sequence 2 thins to ~10-20ft (3-6m) towards the southeast and northwest.

**Sequence 3**

In both cores, sequence 2 contains carbonate-dominated facies, whereas sequence 3 (S3) transitions to siliciclastic-dominated facies. However, the Ihle core has thin beds of carbonate-dominated facies in S3, whereas the Doberman core displays only siliciclastic-dominated facies within the same sequence. Sequence 3 (S3) is bound by the silty burrowed mudstone-wackestone facies (Facies 5 & 8 for the Doberman and Ihle, respectively) at the base and displays a shallowing-upward pattern into Doberman Facies 4 and Ihle Facies 11. In the Doberman core, the

uppermost 5-10ft (1.5-3m) of S3 is identified as a slightly calcareous (avg. 9-12%) expression of facies 4. On wireline logs, S3 is recognized by an increase in gamma-ray values from 60-65 API units to 100-110 API units and a slight decrease (90-100 ohm-m to 70-80 ohm-m) in resistivity values (Figures 37 and 38). Sequence 3 contains four nested 4$^{th}$ order HFSs that were observed and correlated in both cored wells (Figure 38). Out of the four recognized 3$^{rd}$-order sequences, S3 is the thickest and is 85ft (26m) thick in the Doberman and displays relatively consistent thicknesses, moving subparallel to strike (east), towards the Ihle (78ft; 24m). The thickest area of S3 (~130-160ft; 40-49m) is located in the central to east-central part of the study area, indicating continued progradation in a basinward direction, to the southeast (Figure 44). Sequence 3 thins (~0-10ft; 0-3m) slightly toward the south-southeast, but thins rapidly to the northwest, and is absent in the upper (northwestern) part of the study area. Thickness trends for S1 to S3 appear to develop in a northeast to southwest linear pattern.

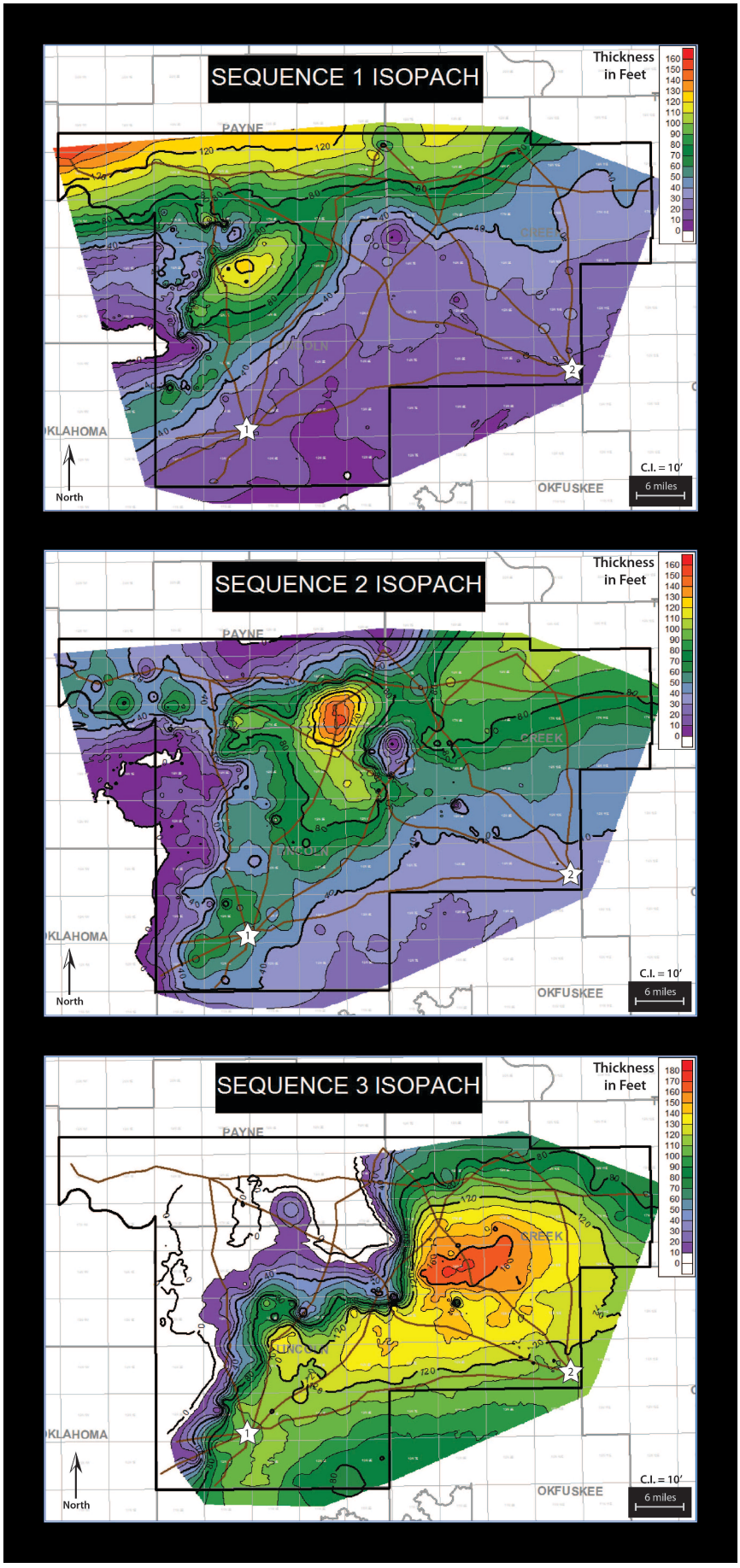
SEQUENCE 1 ISOPACH
Thickness in Feet
160
150
140
130
120
110
100
90
80
70
60
50
40
30
20
10
0
PAYNE
120
120
80
40
40
40
80
40
40
40
40
40
80
80
80

**Sequence 4**

In the Ihle core, the base of sequence 4 (S4) is bound by a calcareous siltstone (Ihle Facies 5) overlying Ihle Facies 11, which would indicate a landward shift in facies if Ihle Facies 11 was deposited in place and not transported to its present position via storm processes. The top of S4 within the Ihle is bound by a silty argillaceous dolomitic packstone (Facies 9). Sequence 4 in the Doberman core is not a complete representation of the sequence due to its truncation by the Pennsylvanian-Mississippian unconformity at the top of the Mississippian section. In the Doberman core, sequence 4 is bound at the base by argillaceous siltstones (Doberman Facies 2) and sandstones (Doberman Facies 4).

The boundary of S4 is recognized on wireline logs as an increase in gamma-ray values from 50-55 API units to 110-115 API units and a slight decrease in resistivity values of approximately 100 ohm-m to 70-80 ohm-m (Figures 37 and 38). Sequence 4 contains four nested $4^{th}$ order HFSs that were observed in the Ihle core. However, in the Doberman core there are only two observed $4^{th}$ order HFSs, due to the truncation by the Pennsylvanian unconformity. The incomplete sequence 4 within the Doberman is only 49ft (15m) thick, but in the Ihle it is 89ft (27m) thick. The maximum thickness of S4 is ~100-120ft (30-37m) in the south-southeast part of the study area (Figure 45). Sequence 4 thins (0-10ft; 0-3m) quickly to the northwest (similar to S3) and is absent in the northwestern study area (Figure 45).

**Sequence 5**

The Ihle core has an additional ~190ft (58m) of upper Mississippian section compared to the Doberman. Therefore, sequence 5 (S5) is observed within the Ihle core, but not in the Doberman. This additional upper Mississippian section seen in the Ihle, compared to the Doberman, could be the result of increased accommodation due to the Ihle being closer to the axis of the Oklahoma Basin, non-deposition of the extra Mississippian section in the Doberman,

or uplift and erosion of the section from the Doberman as a result of its closer proximity to the Nemaha Ridge. Sequence 5 is bound at its base by clay-rich siltstones (Ihle Facies 4) overlying a silty dolomitic packstone (Ihle Facies 9) and can be recognized on wireline logs by an increase in gamma-ray value from 65-70API units to 120-125API units and a general decrease on the resistivity log from 200 ohm-m to 90-100 ohm-m (Figures 37 and 38).

Overall, S5 is largely comprised of clay-rich siltstone (Ihle Facies 4) and silty shale (Ihle Facies 2) with sparse carbonate beds (storm deposits or concretions) in the Ihle core sequence 5 is ~83ft (25m) thick and consists of three probable 4$^{th}$ order HFSs. Accurate determination of HFSs and HFCs within S5 proved difficult due to similar lithology throughout the sequence, and the sparse carbonate beds may represent transported material. The thickness of S5 trends SW to NE, similar to the previously described sequences. The maximum thickness (~100-110ft; 30-34m) of S5 is to the southeast of S4 and is located in the southeastern part of the study area (Figure 45). S5 thins gradually to the northwest (compared to S3 and S4) and is absent in the northwestern study area.

**Sequence 6**

Sequence 6 (S6) is bound at the base by the contact with the underlying S5. However, the basal ten (10) feet of S6 is missing from the Ihle core and the sequence is not present in the Doberman core. The base of sequence 6 is interpreted from the wireline log signatures of the Ihle borehole and is marked by a sharp increase in the gamma-ray signature from 115-120API units to 270-275 API units along with a sharp increase in resistivity of 90-100 ohm-m to 300-400 ohm-m (Figures 37 and 38). S6 displays a prominent shallowing-upward signature to the top of the core where the section is alternating beds of carbonate mudstones and recrystallized packstones-grainstones (Ihle Facies 7 & 10 respectively). Sequence 6 is 89ft (27m) thick and contains three probable 4$^{th}$ order HFSs. Inferred sequence and cycle boundaries in this section of the core are

picked with less confidence as it may represent a storm dominated interval (refer to pgs. 70 & 76). S6 is similar to S5 in that the maximum thickness of S6 (~120ft; 37m) occurs in the southeastern part of the study area (Figure 45). Sequence 6 thins somewhat rapidly to the northwest and is absent in the northern and northwestern parts of the study area.

Based on thickness maps of the individual sequences, these sequences (S1 – S6) appear to prograde from the northwest to the southeast (Figures 44 and 45) and display geometries indicative of prograding "carbonate" clinoforms (Bertalott, 2014; Flinton, 2016; Jaeckel, 2016; LeBlanc, 2014). As a result of their shape and orientation to depositional strike, these clinoforms are interpreted to be strike-elongate sigmoidal clinoforms (Patruno et al., 2015).

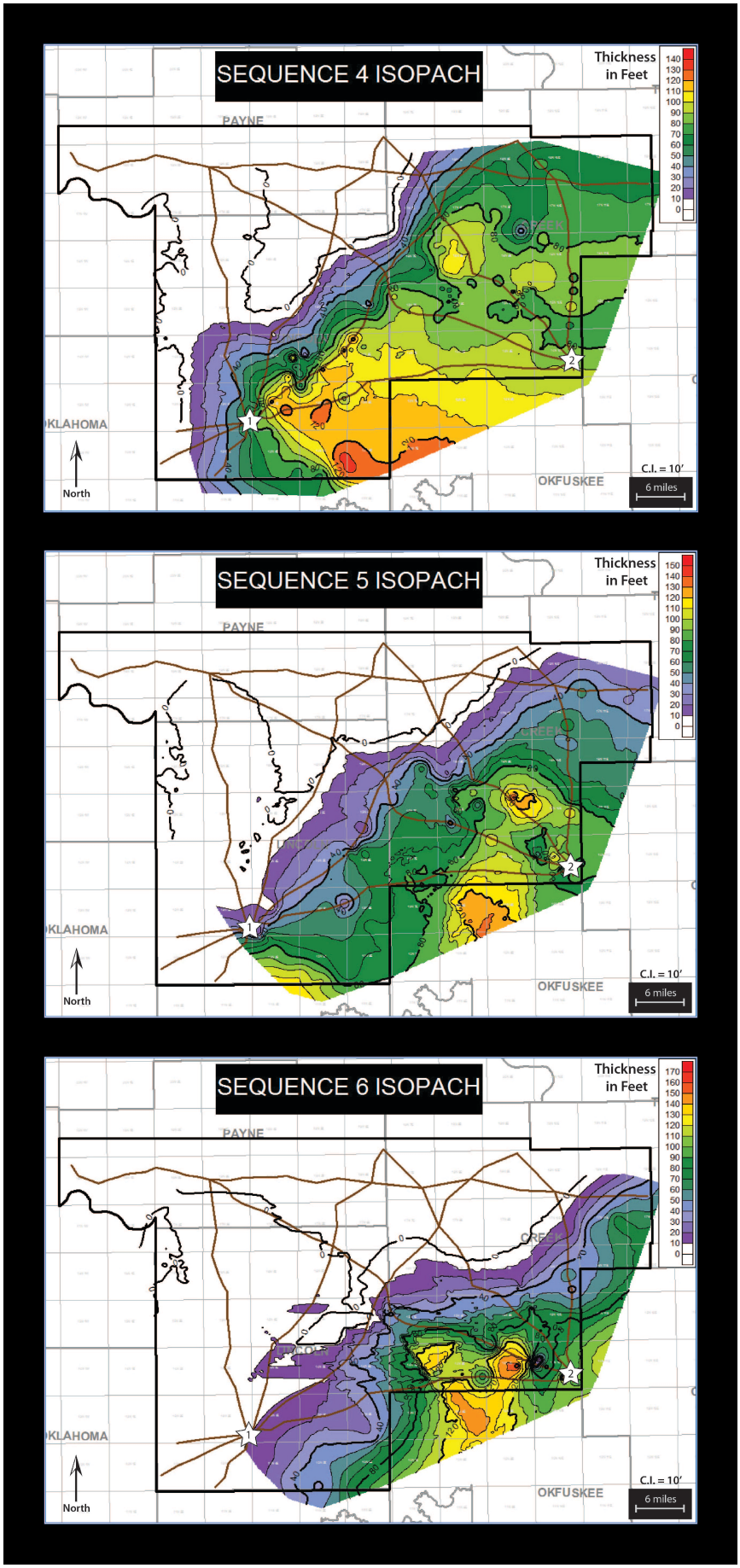


Figure 45. Thickness maps of sequence 4 through sequence 6. Contour interval for all three maps is 10ft. (3m), brown lines crossing through the study area represent dip- and strike-oriented subsurface cross section lines, color bars in the top right corner of maps indicate thickness values with warmer colors (red, orange, yellow) being thickest and cooler colors (purple and white) being thinner. Location of Doberman and Ihle cores are indicated by white star #1 and white star #2 respectively. Compared to sequence 3 (Figure 42), Sequence 4 has prograded farther to the southeast, a pattern followed by S5-S6. S1 – S6 display prograding geometries indicative of clinoforms that are strike elongate and sigmoidal in shape. All mapped clinforms are prograding from the northwest (landward) to the southeast (basinward).

## Comparison of Results to Previous Studies

These results suggest the Doberman #1-25 and Ihle #1-26 Mississippian sections represent deposition in deeper water settings than the Mississippian sections detailed in LeBlanc (2014). The Doberman #1-25 contains roughly 30ft (9m) of "clean" carbonates compared to the roughly 95ft (29m) of "clean" carbonates within the Elinore #1-18 from LeBlanc (2014). Hunt (2017) established that the lower cleaner carbonate in the Doberman #1-25, and perhaps the lower 15ft (4m) of Mississippian section within the Ihle #1-26, are Meramecian and correlate to carbonate section in the Elinore #1-18. In contrast, the silty/sandy generally more argillaceous upper section in the Doberman #1-25 core and perhaps essentially the complete preserved Mississippian section in the Ihle #1-26 are both Chesterian age (Figure 46).

A similar relationship exists between the cleaner carbonate sections in the Adkisson #1-33 and Winney #1-8 cores detailed in LeBlanc (2014). The lower cleaner limestone that correlates to the similar interval in the Doberman #1-25 is Meramecian, whereas the more argillaceous carbonates are Chesterian. If these correlations are correct, the upper sequence in the Adkisson #1-33, Winney #1-8, and Elinore #1-18 cores correlate to and represent a more proximal facies of sequence 2 (S2) within the Doberman #1-25.

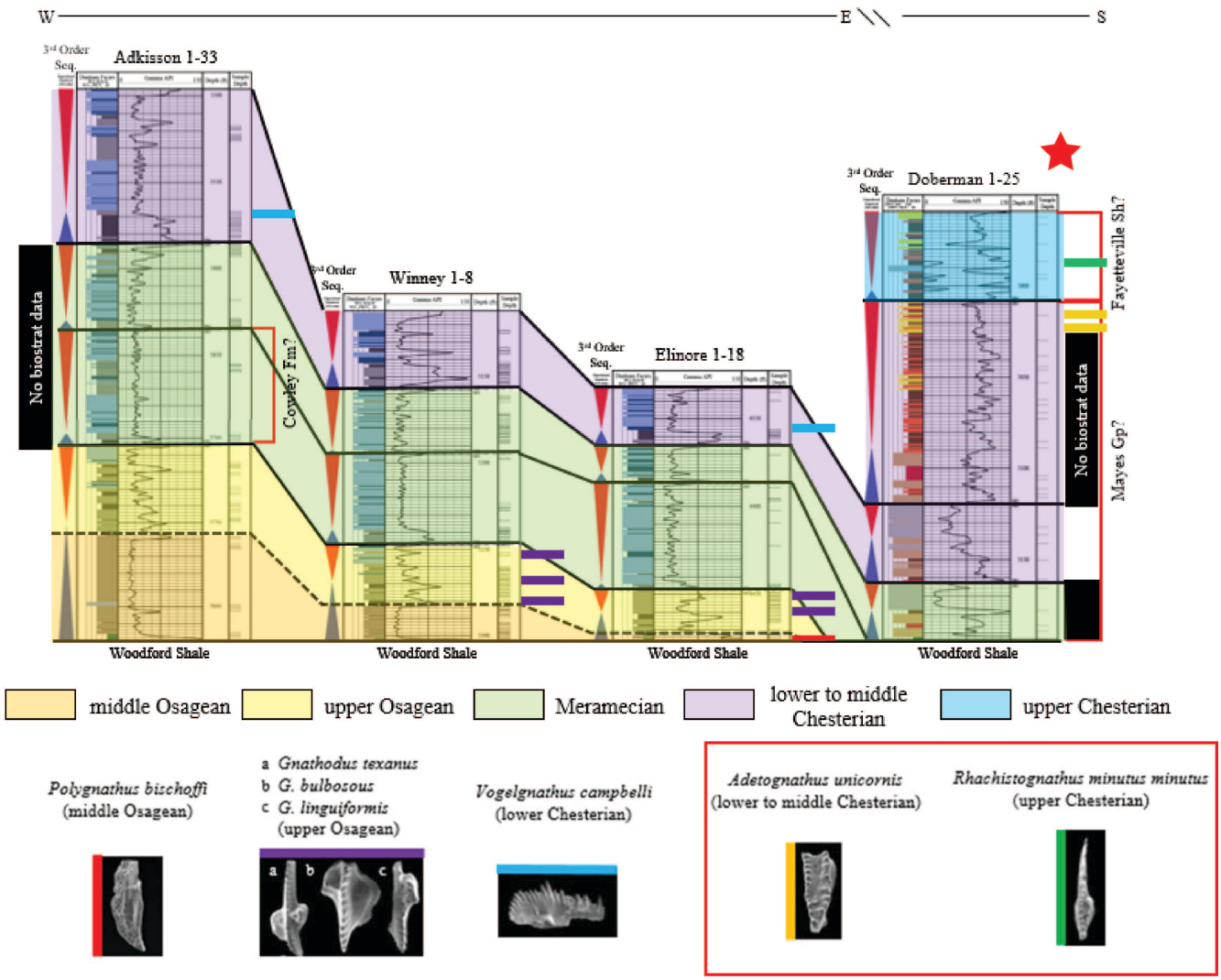


Figure 46. Conodonts recovered from the Adkisson #1-33, Winney #1-8, Elinore #1-18, and Doberman #1-25 (red star) cores are illustrated by colored rectangles. Conodonts recovered from the Doberman #1-25 core (described in this study) are outlined by red box. The results correlate the lower cleaner carbonate (sequence 1) within the Doberman #1-25 core to sequences 2 and 3 within the other cores. Conodonts recovered within the upper, argillaceous and siliciclastic dominated section of the Doberman #1-25 core suggests it is Chesterian in age. Modified from Hunt (2017).

# CHAPTER V

## SUMMARY AND CONCLUSIONS

This study utilized an integrated approach to characterize Mississippian-aged deposits to the east of the Nemaha Ridge using cores located in Creek, Lincoln, and Payne counties, east-central Oklahoma. Through detailed core and thin section analysis a sequence stratigraphic framework was established providing insight and understanding into the depositional processes and environments during Mississippian time. The construction of wireline log cross sections allowed for a regional sequence stratigraphic analysis of the "Mississippian Limestone" in east-central Oklahoma and provided insight into the architecture and spatial distribution of the recognized depositional sequences. Where present, core calibrated sequences were correlated in the study area using wireline logs. The key findings of this core- and wireline log-based study are:

1. Eleven total depositional facies were identified in the Ihle #1-26 core using core and thin sections. Six of these facies were identified in the Doberman #1-25 core. The facies identified were consistent with facies identified in other regional studies of the Mississippian section and support the hypothesis that deposition occurred on a distally-steepened ramp.
2. Idealized vertical stacking patterns were established for depositional facies in both cores (eleven facies in Ihle #1-26 and six facies in Doberman #1-25). The transgressive phase

of a sequence contains siliciclastic dominated facies (argillaceous siltstones/sandstones and silty shale) that transitions into more carbonate-rich facies (silty mudstones-wackestones and silty packstones-grainstones) within the regressive phase.

3. The idealized stacking patterns for both cores revealed a three-fold sequence stratigraphic hierarchy that consists of probable 3rd order sequences that contain ingrained 4th order high-frequency sequences and 5th order high-frequency cycles.
4. The facies stacking patterns and bounding stratigraphic surfaces for 3rd order sequences were correlated to wireline log signatures, especially gamma-ray and resistivity curves. 3rd order sequences typically display an upward decrease in gamma-ray values, while displaying an upward increase in resistivity values. The 3rd order sequences bounded by flooding surfaces were correlative throughout the study area, whereas 4th order sequences and 5th order cycles could not be correlated with confidence.
5. Wireline log cross sections illustrate that lower to middle Mississippian sequences are relatively consistent in thickness in a strike-oriented direction (largely W to E), whereas dip-oriented cross sections reveal that probable 3rd order Mississippian sequences are a series of prograding clinoforms that mainly prograde in a basinward direction (NNW to SSE).
6. The geometry and distribution of these probable 3rd order sequences are consistent with previous regional studies and support the interpretation that Mississippian deposition occurred on a distally-steepened ramp.
7. The strike-elongate prograding clinoform geometries evident in this study support the hypothesis that clinoforms demonstrated in the northern part of the study area by Bertalott (2014) and LeBlanc (2014) extend into a more distal (basinal) depositional setting.

# REFERENCES


Ahr, W.M., 1973, The Carbonate Ramp: An Alternative to the Shelf Model, in S. Chuber, ed., Gulf Coast Association of Geological Societies Transactions, V. 23, p. 221-225.

Amorosi, A., 1997, Detecting compositional, spatial, and temporal attributes of glaucony: a tool for provenance research: Sedimentary Geology, v. 109, p. 135-153.

Archie, G.E., 1950, Introduction to Petrophysics of Reservoir Rocks, AAPG Bulletin, V. 34, No. 5, p. 943-961.

Asquith, G., and Krygowski, D., 2004, Basic Well Log Analysis, 2nd Edition, AAPG Methods in Exploration Series, No. 18, 244 p.

Bentor, Y.K., and Kastner, M., 1965, Notes on the Mineralogy and Origin of Glauconite, Journal of Sedimentary Petrology, V. 35, No. 1, p. 155-166.

Bertalott, J., 2014, Core and log based stratigraphic framework of the Mississippian limestone in portions of north-central Oklahoma: unpublished M.S. thesis, Oklahoma State University, 132 p.

Blakey, R., 2016, Global Paleogeography and Tectonics in Deep Time Series, <https://deeptimemaps.com/map-room-individual/> Accessed April, 2017.

Boardman, D.R., Thompson, T.L., Godwin, C., Mazzullo, S.J., Wilhite, B.W., and Morris, B.T., 2013, High-Resolution Conodont Zonation for Kinderhookian (Middle Tournaisian) and

Osagean (Upper Tournaisian-Lower Visean) Strata of the Western Edge of the Ozark Plateau, North America, Oklahoma City Geological Society, The Shale Shaker Digest, V. 64, p. 98-151.

Buggisch, Werner, Joachimski, Michael M., Sevastopulo, George, and Morrow, Jared R., 2008, Mississippian $\delta^{13}$ $C_{carb}$ and Conodont Apatite $\delta^{18}O$ Records – Their Relation to the Late Palaeozoic Glaciation, Palaeogeography, Palaeoclimatology, Palaeoecology 268, p. 273-292.

Burchette, T. P., and Wright, V. P., 1992, Carbonate ramp depositional systems, Sedimentary Geology, V. 79, p. 3-57.

Burst, J.F., 1958, "Glauconite" Pellets: Their Mineral Nature and Applications to Stratigraphic Interpretations, AAPG Bulletin, V. 42, No. 2, p. 310-327.

Childress, M., 2015, High Resolution Sequence Stratigraphic Architecture of a Mid-Continent Mississippian Outcrop in Southwest Missouri, M.S. Thesis, Oklahoma State University, Stillwater, Oklahoma, 272 p.

Childress, M. and Grammer, G.M., 2015, High Resolution Sequence Stratigraphic Architecture of a Mid-Continent Mississippian Outcrop in Southwest Missouri, Oklahoma City Geological Society, The Shale Shaker Digest, V. 66, No. 1, p. 206-234.

Choquette, P.W., and Pray, L.C., 1970, Geologic Nomenclature and Classification of Porosity in Sedimentary Carbonates, AAPG Bulletin, V. 54, No. 2, p. 207-250.

Cowan, C.A., and James, N. P., 1996, Autogenic Dynamics in Carbonate Sedimentation: Meter-Scale Shallowing Upward Cycles, Upper Cambrian, Western Newfoundland, Canada, American Journal of Science, v. 296, p. 1175-1207.

Curtis, D.M., and Champlin, S.C., 1959, Depositional Environments of Mississippian Limestones of Oklahoma, Tulsa Geological Society Digest, V. 27, No. 1, p. 90-103.

Darold, A. P., and A. A. Holland, 2015, Preliminary Oklahoma optimal fault orientations: Oklahoma Geological Survey Open-File Report, OF4-2015.

Dehcheshmehi, S. M., Gregg, J. M., Shelton, K. L., and Appold, M.S., 2015, Influence of Diagenetic Fluids on Mississippian Carbonate Rock Properties in the Southern Midcontinent, AAPG Search and Discovery Article #51165. 25 p.

Dolton, G.L., and Finn, T.M., 1989, Petroleum geology of the Nemaha Uplift, central mid-continent: United States Geological Survey Open-File Report 88-450-D.

Doveton, J. H., 1994, Geologic Log Interpretation: reading the rocks from wireline logs, SEPM Short Course 29, 169 p.

Drummond, C.N., and Wilkinson, B.H., 1993, Carbonate Cycle Stacking Patterns and Hierarchies of Orbitally-Forced Eustatic Sea Level Change, Journal of Sedimentary Petrology, V. 63, p. 369-377.

Dunham, R.J., 1962, Classification of Carbonate Rocks According to Depositional Texture, in W.E. Ham, ed., Classification of Carbonate Rocks, AAPG Memoir 1, p. 108-121.

Ekdale, A.A., Bromley, R.G., and Pemberton, S.G., 1984, Ichnology – Trace Fossils in Sedimentology and Stratigraphy, SEPM Short Course No. 15, 317 p.

Elrick, M. and Read, J.F., 1991, Cyclic ramp-to-basin carbonate deposits, Lower Mississippian, Wyoming and Montana: A combined field and computer modeling study: Journal of Sedimentary Petrology, v. 61, p. 1194-1224.

Estaban, M., and Klappa, C.F., 1983, Subaerial Exposure Environment, in P.A Scholle, D.G. Bebout, and C.H., Moore, eds., Carbonate Depositional Environments, AAPG Memoir 33, p. 1-92.

Flinton, K, 2016, The effects of high-frequency cyclicity on reservoir characteristics of the "Mississippian Limestone", Anadarko basin, Kingfisher County, Oklahoma: Oklahoma State University, 175p.

Flügel, Erik, 2010, Microfacies of Carbonate Rocks: Anaylsis, Interpretation, and Application, 2nd Ed., Springer-Verlag, Berlin, Heidelberg, New York, 1007 p.

Friesenhahn, T.C., 2012, Reservoir Characterization and Outcrop Analog: The Osagean Reeds Spring Formation (Lower Boone), Western Osage and Eastern Kay County, Oklahoma, M.S. Thesis, University of Arkansas, Fayetteville, Arkansas, 86 p.

Frezon, S.E., and Jordan, L., 1979, Oklahoma, in L.C. Craig and C.W. Connor, eds., Paleotectonic Investigations of the Mississippian System in the United States: U.S. Geological Survey Professional Paper 1010, p. 146-159.

Friedman, G.M., and Sanders, J.E., 1978, Principles of Sedimentology, New York, John Wiley & Sons, 792 p.

Gary, M., McAfee, R. Jr., and Wolf, C.L., eds., 1974, GI's Glossary of Geology, American Geological Institute, Falls Church, Virginia, 805 p. +52 page appendix A.

Gay, Parker S. Jr., 1999, Strike-Slip, Compressional Thrust-Fold Nature of the Nemaha System in Eastern Kansas and Oklahoma, Kansas Geological Society, Transactions of the 1999 American Association of Petroleum Geologists Midcontinent Section Meeting (Geoscience for the 21st Century), p. 39-50.

Gay, P.S. Jr., 2003, The Nemaha Trend – A System of Compressional Thrust-Fold, Strike-Slip Structural Features in Kansas and Oklahoma, Parts 1 & 2, Oklahoma City Geological Society, The Shale Shaker Digest, V. 54, Nos. 1 & 2, p. 9-49.

Glick, E. E., 1979, Arkansas: in Paleotectonic Investigations of the Mississippian System in the U.S.: Part I, Introduction and Regional Analysis of the Mississippian System: Geological Surv. Prof. Paper 1010, pp. 125-145.

Goddard, E.N., Trask, P.D., De Ford, R.K., Rove, O.N., Singewald, J.T., and Overbeck, R.M., 1951, Rock Color Chart, Geological Society of America, Boulder, Colorado.

Grammer, G.M., Eberli, G.P., Van Buchem, F.S.P., Stevenson, G.M., and Homewood, P., 1996, Application of High-Resolution Sequence Stratigraphy to Evaluate Lateral Variability in Outcrop and Subsurface—Desert Creek and Ismay Intervals, Paradox Basin, in M.W. Longman and M.D. Sonnenfeld, eds., Paleozoic Systems of the Rocky Mountain Region, Rocky Mountain Section, SEPM, p. 235-266.

Grammer, G.M., Harris, P.M., and Eberli, G.P., 2004, Integration of Outcrop and Modern Analogs in Reservoir Modeling: Overview with Examples from the Bahamas, in G. M. Grammer, P.M. Harris, and G.P. Eberli, eds., Integration of Outcrop and Modern Analogs in Reservoir Modeling: AAPG Memoir 80, p. 1-22.

Gutschick, R.C., and Sandberg, C.A., 1983, Mississippian Continental Margins of the Conterminous United States, in D.J. Stanley and G.T. Moore, The Shelfbreak: Critical Interface on Continental Margins, SEPM Special Publication 33, p. 79-96.

Halley, R.B., 1983. An outline of carbonate sedimentation and diagenesis, the Rocky Mountain Section SEPM, p. 1 -133.

Handford, C.R., 1986, Facies and Bedding Sequences in Shelf-Storm-Deposited Carbonates – Fayetteville Shale and Pitkin Limestone (Mississippian), Arkansas, Journal of Sedimentary Petrology, V. 56, No. 1, p 123-137.

Handford, C.R., 1988, Review of Carbonate Sand-Belt Deposition of Ooid Grainstones and Application to Mississippian Reservoir, Damme Field, Southwestern Kansas, AAPG Bulletin, V. 72, No. 10, p. 118-1199.

Handford, C.R., and Loucks, R.G., 1993, Carbonate Depositional Sequences and Systems Tracts – Responses of Carbonate Platforms to Relative Sea-Level Changes, in R.G. Loucks, and F. Sarg, eds., Carbonate Sequence Stratigraphy: Recent Developments and Applications, AAPG Memoir 57, p. 3-42.

Harms, J.C., Southard, J.B., and Walker, R.G., 1982, Structure and Sequence in Clastic Rocks, SEPM Short Course Notes, V. 9, 51 p.

Harris, S.A., 1987, Hydrocarbon Accumulation in "Meramec-Osage" (Mississippian) Rocks, Sooner Trend, Northwest-Central Oklahoma, in B. Rascoe, Jr., N.J. Hyne, eds., Tulsa Geological Society, Special Publication No. 3: Petroleum Geology of the Mid-Continent. P. 74-81

Haq, B.U., and Schutter, S.R., 2008, A Chronology of Paleozoic Sea-Level Changes, Science, V. 322, p. 64-68.

Heinzelmann, Gerald Mathias, 1964, Mississippian Rocks in the Stillwater-Chandler Area, Oklahoma City Geological Society, The Shale Shaker Digest V, v. XV-XVII, p. 195-207.

Howard, J.D., and Reineck, H-E., 1980, Depositional Facies of High-Energy Beach-to-Offshore Sequence: Comparison with low-energy sequence, AAPG Bulletin, V. 65, p. 807-830.

Huffman, George G., 1958, Geology of the Ozark Uplift, Northeastern Oklahoma, Oklahoma City Geological Society, The Shale Shaker Digest I, v. I-V, p. 36-42.

Hunt, J.E., 2017, Conodont biostratigraphy in middle Osagean to upper Chesterian strata, north-central Oklahoma, USA, M.S. Thesis, Oklahoma State University, Stillwater, 167 p.

Jaeckel, J., 2016, High Resolution Sequence Stratigraphy and Reservoir Characterization of Mid-Continent Mississippian Carbonates in North-Central Oklahoma and South Central Kansas, M.S. Thesis, Oklahoma State University, Stillwater, Oklahoma, 357 p.

James, N.P., and Clarke, J.A.D., eds., 1997, Cool-water Carbonates, SEPM Special Publication 56, p. 1-20.

Jordan, L., and Rowland, T.L., 1959, Mississippian Rocks in Northern Oklahoma, Tulsa Geological Society Digest, V. 27, p. 124-136.

Kerans, C., and Tinker, S.W., 1997, Sequence Stratigraphy and Characterization of Carbonate Reservoirs, SEPM Short Course No. 40, 130 p.

Kerans, C., Lucia, F.J., and Senger, R.K., 1994, Integrated Characterization of Carbonate Ramp Reservoirs Using Permian San Andres Formation Outcrop Analogs, AAPG Bulletin, V. 78, No. 2, p. 181-216.

Kreisa, R.D., 1981, Storm-Generated Sedimentary Structures in Subtidal Marine Facies with Examples from the Middle and Upper Ordovician of Southwestern Virginia, Journal of Sedimentary Petrology, V. 51, No. 3, p. 823-848.

Krueger, Robert Carl, 1965, Subsurface Study of Mississippian Rocks in the Tulsa Area, Oklahoma City Geological Society, The Shale Shaker Digest V, v. XV-XVII, p. 217-239.

Lane, H.R., and De Keyser, T.L., 1980, Paleogeography of the Late Early Mississippian (Tournaisian 3) in the Central and Southwestern United States, SEPM, Rocky Mountain Symposium 1, p. 149-162.

Law, B.E., and Curtis, J.B., 2002, Introduction to Unconventional Petroleum Systems, AAPG Bulletin, V. 86, No. 11, p. 1851-1852.

LeBlanc, S.E., 2014, High Resolution Sequence Stratigraphy and Reservoir Characterization of the "Mississippian Limestone" in North-Central Oklahoma, M.S. Thesis, Oklahoma State University, Stillwater, Oklahoma, 443 p.

MacEachern, James A., Bann, Kerrie L., Gingras, Murray K., and Pemberton, S. George, 2009, Applied Ichnology, SEPM Short Course Notes 52: Revised Edition, Society for Sedimentary Geology (SEPM), Tulsa, OK, 145 p.

Mazzullo, S.J., Boardman, D.R., Wilhite, B.W., Godwin, C., and Morris, B.T., 2013, Revisions of Outcrop Lithostratigraphic Nomenclature in the Lower to Middle Mississippian Subsystem (Kinderhookian to Basal Meramecian Series) Along the Shelf-Edge in Southwest Missouri, Northwest Arkansas, and Northeast Oklahoma, Oklahoma City Geological Society, The Shale Shaker Digest, V. 63, No. 6, p. 414-454.

Mazzullo, S.J., Wilhite, B.W., and Boardman, D.R., 2011a, Lithostratigraphic Architecture of the Mississippian Reeds Spring Formation (Middle Osagean) in Southwest Missouri, Northwest Arkansas, and Northeast Oklahoma: Outcrop analog of subsurface petroleum reservoirs, Oklahoma City Geological Society, The Shale Shaker Digest, V. 61, No. 5, p. 254-269.

Mazzullo, S.J., Wilhite, B.W., and Morris, B.T., 2011b, Mississippian Oil Reservoirs in the Southern Midcontinent: New exploration concepts for a mature reservoir objective,

AAPG Search and Discovery Article #10373, 34 p.

Mazzullo, S.J., Wilhite, B.W., Morris, B.T., and Boardman, D.R., 2011c, Syndepositional Tectonism and its Effects on Mississippian (Kinderhookian to Osagean) Lithostratigraphic Architecture: Part 2 – Subsurface Occurrences in the Midcontinent USA, AAPG Search and Discovery Article #30208, Tulsa, Oklahoma, 32 p.

Mazzullo, S.J., Wilhite, B.W., and Woolsey, I.W., 2009a, Petroleum Reservoirs Within a Spiculite-Dominated Depositional Sequence: Cowley formation (Mississippian: Lower Carboniferous), south-central Kansas, AAPG Bulletin, V. 93, No. 12, p. 1649-1689.

Mazzullo, S.J., Wilhite, B.W., and Woolsey, I.W., 2009b, Rhythmic Carbonate Versus Spiculite Deposition in Mississippian Hydrocarbon Reservoirs in the Midcontinent USA: Causative factors and resulting reservoir petrophysical attributes, AAPG Search and Discovery Article #10209, 6 p.

McBee, William J., 2003, Nemaha Strike-slip Fault Zone: AAPG, Search & Discovery Article #10055.

McNeill, D.F., Cunningham, K.J., Guertin, L.A., and Anselmetti, F.S., 2004, Depositional Themes of Mixed-Carbonate-Siliciclastics in the South Florida Neogene: Application to ancient deposits, in G.M. Grammer, P.M. Harris, and G.P. Eberli, eds., Integration of Outcrop and Modern Analogs in Reservoir Modeling: AAPG Memoir 80, p. 23-43.

Middleton, G.V., 1973, Johannes Walther's Law of Correlation of Facies: Geological Society of America Bulletin, V. 38, p. 979-988.

Middleton, G.V., Church, M.J., Coniglio, M., Hardie, L.A., and Longstaffe, F.J., 2003, Encyclopedia of Sediments and Sedimentary Rocks, The Netherlands, Kluwer Academic Publishers, 821 p.

Mohammadi Dehcheshmehi, S., 2016, "Regional diagenesis of Mississippian strata of the Southern Midcontinent, USA": PhD Dissertation, Oklahoma State University, 133 p.

Moura RL, Amado-Filho GM, Moraes FC, Brasileiro PS, Salomon PS, Mahiques MM et al., 2016, An extensive reef system at the Amazon River mouth. Sci Adv 2:e1501252

Northcutt, R.A., and Campbell, J.A., 1996, Geologic Provinces of Oklahoma, Transactions of the 1995 AAPG Mid-Continent Section Meeting, 1996, p. 128-134.

Patruno, S., Hampson, G., Jackson, C., 2015, Quantitative Characterisation of Deltaic and Subaqueous Clinoforms, Earth-Science Reviews, Vol. 142, p. 79-119.

Pfefferkorn, H.W., Alleman, V, and Iannuzzi, R., 2014, A Greenhouse Interval Between Icehouse Times: climate change, long-distance plant dispersal, and plate motion in the Mississippian (late Visean-earliest Serpukhovian) of Gondwana, Gondwana Research V. 25, No. 4, p. 1338-1347.

Pirson, S.J., 1963, Handbook of Well Log Analysis: Modern well log interpretation techniques for oil and gas formation evaluation, Englewood Cliffs, New Jersey, Prentice Hall, 326 p.

Plint, A.G., et al., 1992, Control of sea level change, in R.G. Walker and N.P. James, eds., Facies Models, Response to Sea Level Change, Chapter 2, p. 15-25.

Price, B., 2014, Sequence Stratigraphic Control on Distribution and Porosity Evolution in Cherts in the Mississippian of the Mid-Continent, M.S. Thesis, Oklahoma State University, Stillwater, Oklahoma, 144 p.

Read, J.F., 1995, Overview of Carbonate Platform Sequences, Cycle Stratigraphy and Reservoirs in Greenhouse and Icehouse Worlds, in J.F. Read, C. Kerans, L.J. Weber, J.F. Sarg, and F.M. Wright, eds., Milankovitch Sea Level Changes, Cycles, and Reservoirs on

Carbonate Platforms in Greenhouse and Ice-House Worlds: SEPM Short Course 35, p. 1-102.

Read, J.F., and Horbury, A.D., 1993, Eustatic and Tectonic Controls on Porosity Evolution Beneath Sequence-Bounding Unconformities and Parasequence Disconformities on Carbonate Platforms, in A.D. Horbury and A.G. Robinson, eds., Diagenesis and Basin Development: AAPG Studies in Geology 36, p. 155-197.

Ross, C. A., and Ross, J. R., 1988, Late Paleozoic Transgressive-Regressive Deposits, in Wilgus, Cheryl K., Hastings, Bruce S., Posamentier, Henry, Wan Wagoner, John, Ross, Charles A., and Kendall, Christopher G. St. C., eds., Sea-Level Changes - An Integrated Approach, SEPM Special Publication No. 42, p. 227-247.

Rowland, T.L., 1964, Mississippian Rocks in the Subsurface of the Kingfisher-Guthrie Area, Oklahoma, Oklahoma City Geological Society, The Shale Shaker Digest IV, V. 12-14, p. 145-162.

Scholle, P.A., and Ulmer-Scholle, D.S., 2003, A Color Guide to the Petrography of Carbonate Rocks: Grains, textures, porosity, diagenesis, AAPG Memoir 77, 474 p.

Scholle, P.A., Bebout, D.G. and Moore, C.H., 1983, Carbonate Depositional Environments, AAPG Memoir 33. AAPG, Tulsa, Oklahoma, 691 pp.

Shoeia, O.K., 2012, High Resolution Stratigraphy of Lower Mississippian Strata Near Jane, Missouri, M.S. Thesis, Oklahoma State University, Stillwater, Oklahoma, 262 p.

Sloss, L.L., 1963, Sequences in the Cratonic Interior of North America, Geological Society of America Bulletin, V. 74, No. 2, p 93-114.

Thompson, T.L., 1986, Paleozoic Succession in Missouri, Part 4, Mississippian System: Missouri Department of Natural Resources Report of Investigations, No. 70, 182 p.

Thompson, T.L., and Fellows, L.D., 1970, Stratigraphy and Conodont Biostratigraphy of Kinderhookian and Osagean (Lower Mississippian) Rocks of Southwestern Missouri and Adjacent Areas, Missouri Geological Survey and Water Resources Report of Investigations 45, 263 p.

Thornton, Wayne D., 1961-1964, Mississippian Rocks in the Subsurface of Alfalfa and Parts of Woods and Grant Counties, Northwestern Oklahoma, Oklahoma City Geological Society, The Shale Shaker Digest IV, v. XII-XIV, p. 117-128.

Tucker, M.E., and Wright, V.P, 1990, Carbonate Sedimentology, Blackwell Science Ltd., London, Ch. 2.6: Carbonate Ramps, p. 47-52.

Wehner, M., Gardner, P., Tice, M.M., Pope, M.C., Donovan, A.D., and Staerker, T.S., 2015, Anoxic, Storm Dominated Inner Carbonate Ramp Deposition of Lower Eagle Ford Formation, West Texas, URTeC, 16 p.

Wilhite, B.W., Mazzullo, S.J., Morris, B.T., and Boardman, D.R. II, 2011, Syndepositional Tectonism and its Effects on Mississippian (Kinderhookian to Osagean) Lithostratigraphic Architecture: Part 1–Based on Exposures in the Midcontinent USA, AAPG Search and Discovery Article #30207.

Yancey, T.E., 1991, Controls on Carbonate and Siliciclastic Sediment Deposition on a Mixed Carbonate-Siliciclastic Shelf (Pennsylvanian Eastern Shelf of north Texas), in Sedimentary Modeling: Computer simulations and methods for improved parameter definition, Kansas Geological Survey, Bulletin 233, p. 263-272.

# APPENDICES

**Appendix A: Doberman #1-25 SWD**

I. Whole Core Photographs
II. Core Descriptions
III. Thin Section Photomicrographs

**Appendix B: Ihle #1-26**

I. Whole Core Photographs
II. Core Descriptions
III. Thin Section Photomicrographs

**Appendix C: Architecture of Mississippian Strata/Subsurface Mapping**

I. Subsurface Cross Sections and Correlations
II. Sequence Isopach Maps

# APPENDIX A:

Doberman #1-25 SWD

## I. Doberman #1-25 SWD Whole Core Photographs

Core Photographs are shown under white light and are labeled with the abbreviations in the table shown below. The core is in boxes containing 10 feet of core (when full) and within each box, cores are split into 2 foot intervals. The shallowest depths are located in the top left corner of the boxes, while the deepest depths are in the bottom right corner. The scales next to the core boxes are in tenths of feet. The contacts between the "Mississippian Limestone" and differing strata are marked where present. Next to the cores are colored rectangles that correspond to the facies stacking pattern colors.

| Doberman Core Image Labels | |
|---|---|
| BR | brachiopod |
| BU | burrow |
| CH | chert |
| CR | crinoid |
| FR | fracture |
| G | glauconite |
| PH | phosphate |
| PY | pyrite |
| XB | cross-bedding |

Table 6. Abbreviations and their meanings used in labeling the whole box core photos for the Doberman #1-25 SWD core.

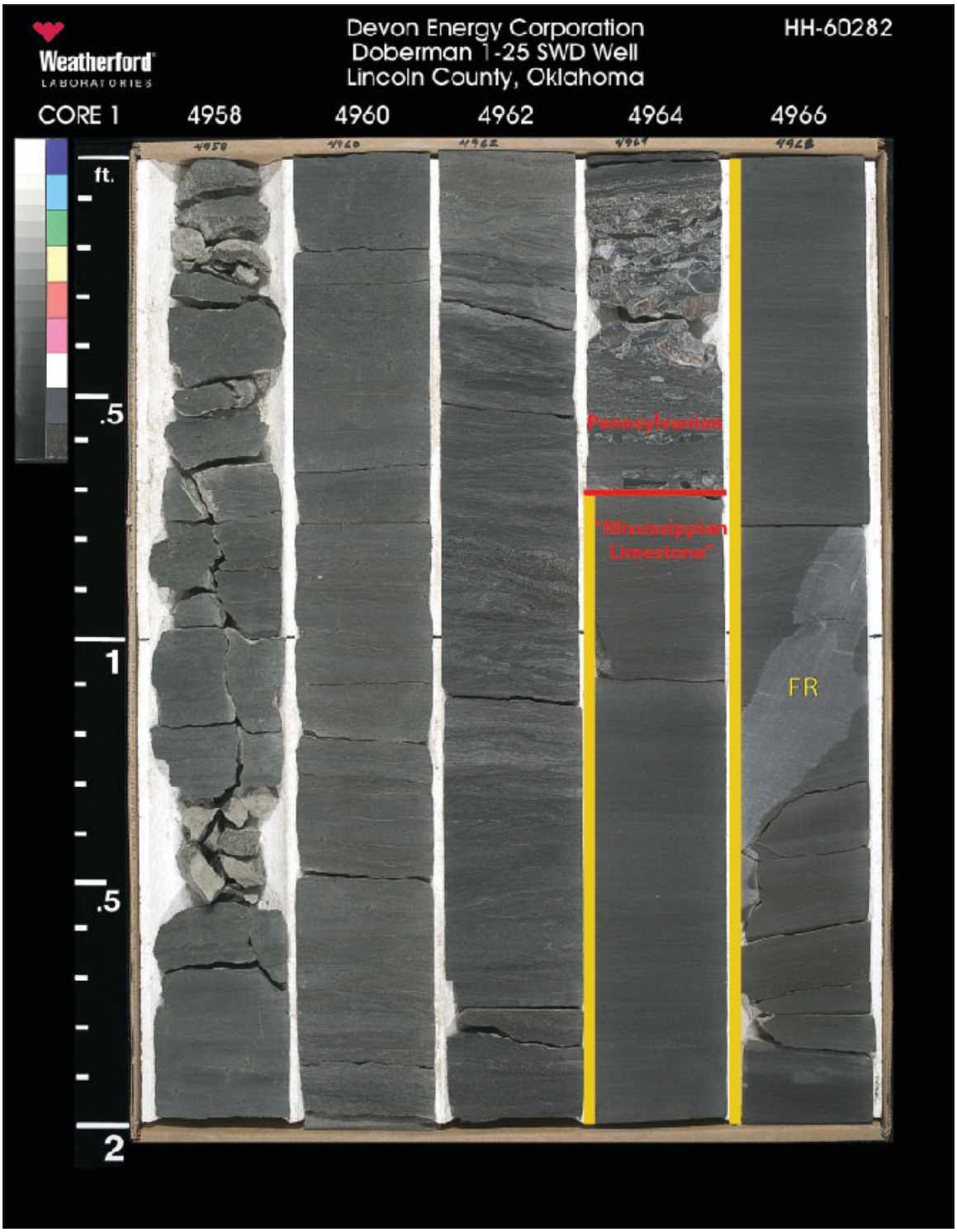
Weatherford
LABORATORIES
Devon Energy Corporation
Doberman 1-25 SWD Well
Lincoln County, Oklahoma
HH-60282
CORE 1
4958
4960
4962
4964
4966
ft.
.5
1
.5
2
Pennsylvanian
"Mississippian Limestone"
FR

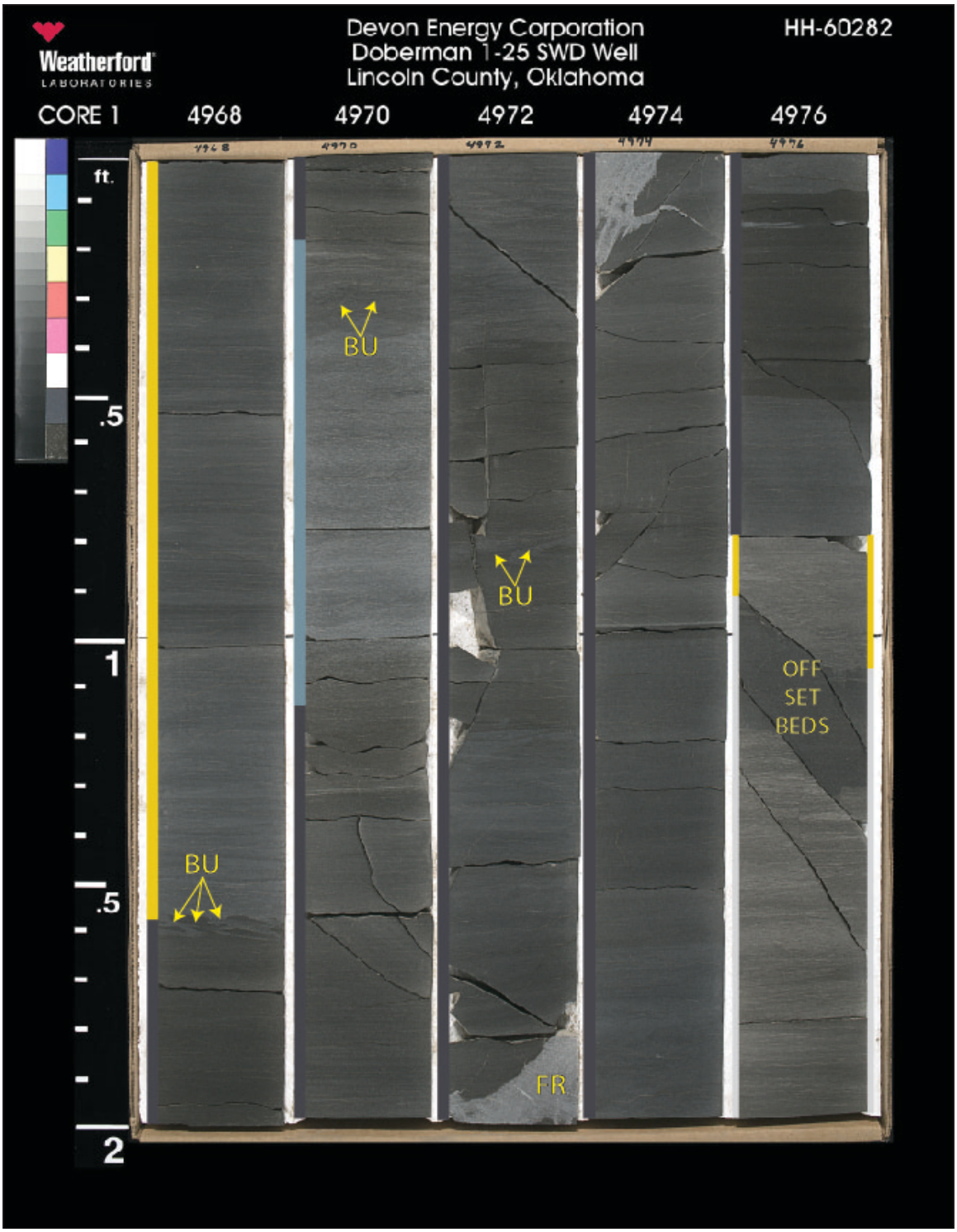
Weatherford
LABORATORIES
Devon Energy Corporation
Doberman 1-25 SWD Well
Lincoln County, Oklahoma
HH-60282
CORE 1
4968
4970
4972
4974
4976
ft.
.5
1
.5
2
BU
BU
BU
OFF
SET
BEDS
FR

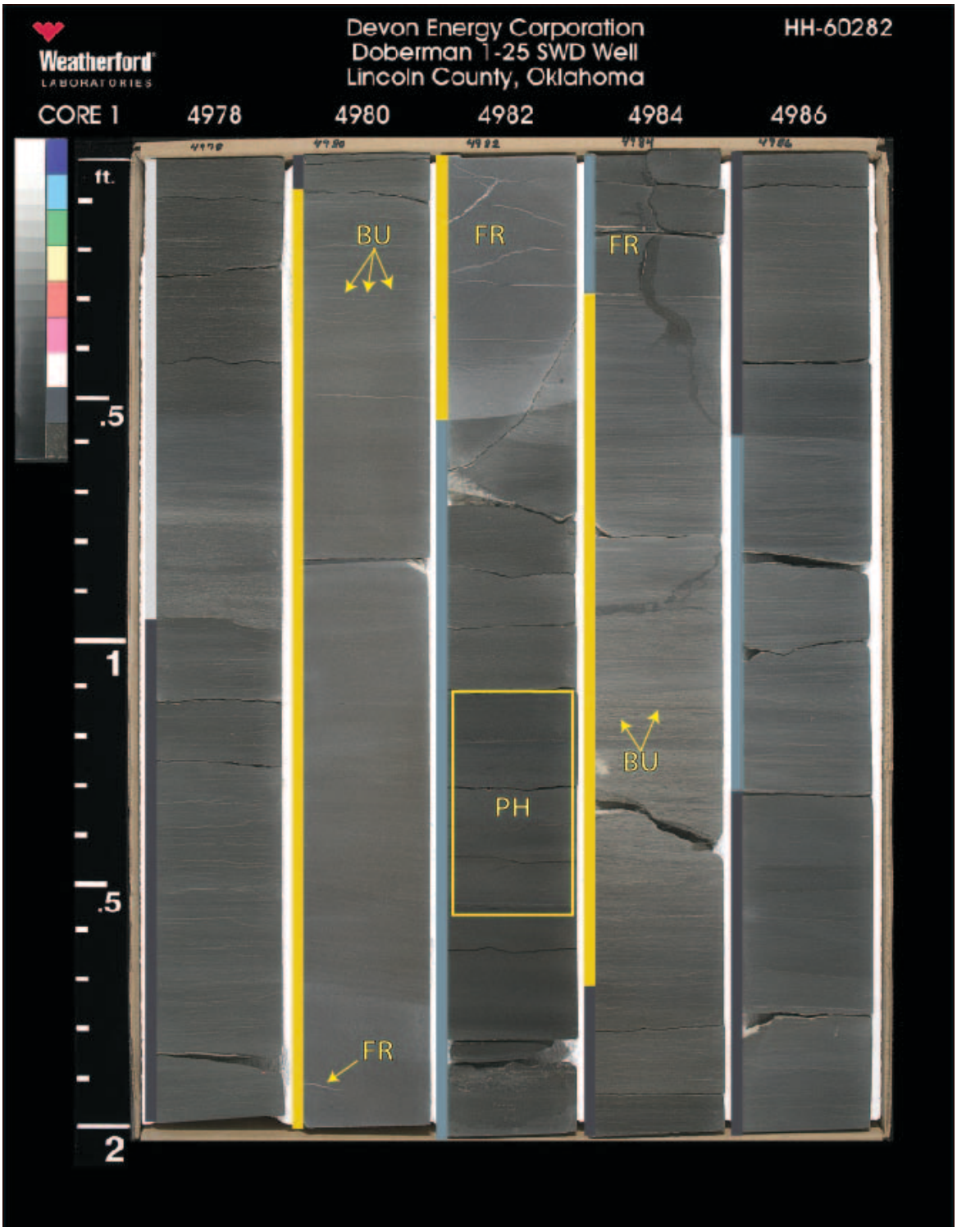
Weatherford
LABORATORIES
Devon Energy Corporation
Doberman 1-25 SWD Well
Lincoln County, Oklahoma
HH-60282
CORE 1
4978
4980
4982
4984
4986
ft.
.5
1
.5
2
BU
FR
FR
BU
PH
FR

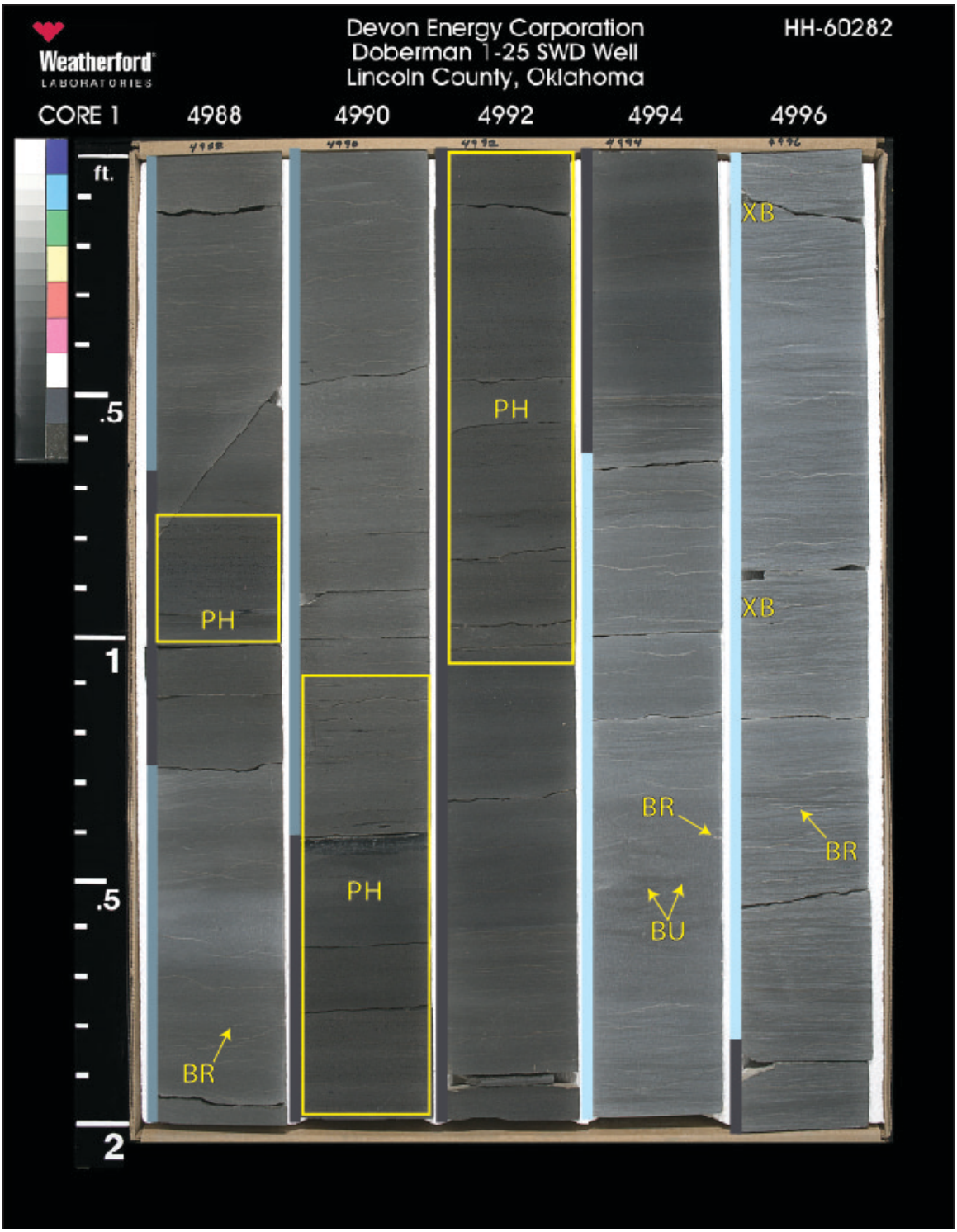
Weatherford
LABORATORIES
Devon Energy Corporation
Doberman 1-25 SWD Well
Lincoln County, Oklahoma
HH-60282
CORE 1
4988
4990
4992
4994
4996
ft.
.5
1
.5
2
PH
PH
PH
XB
XB
BR
BR
BR
BU

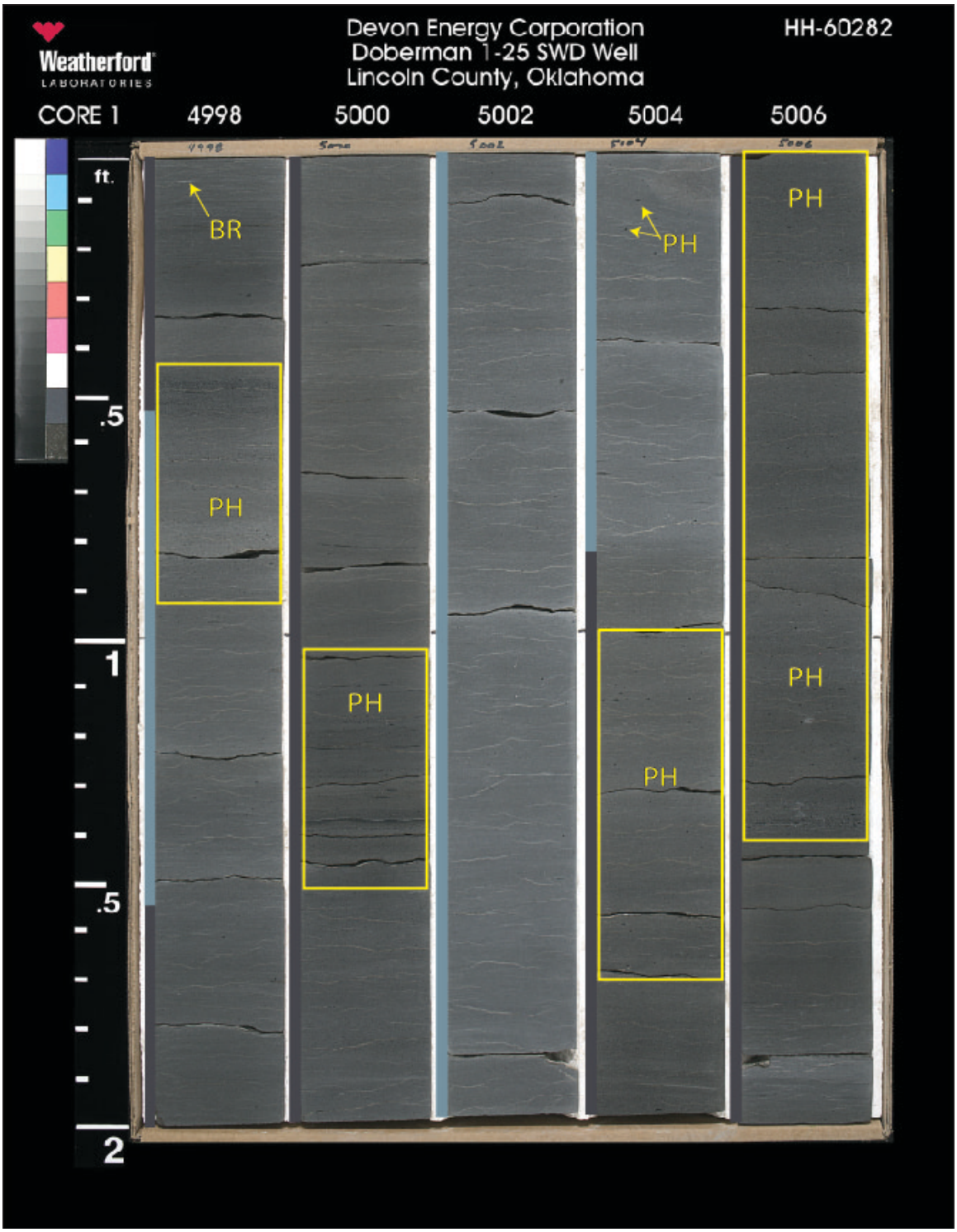
Weatherford
LABORATORIES
Devon Energy Corporation
Doberman 1-25 SWD Well
Lincoln County, Oklahoma
HH-60282
CORE 1
4998
5000
5002
5004
5006
ft.
.5
1
.5
2
BR
PH
PH
PH
PH
PH

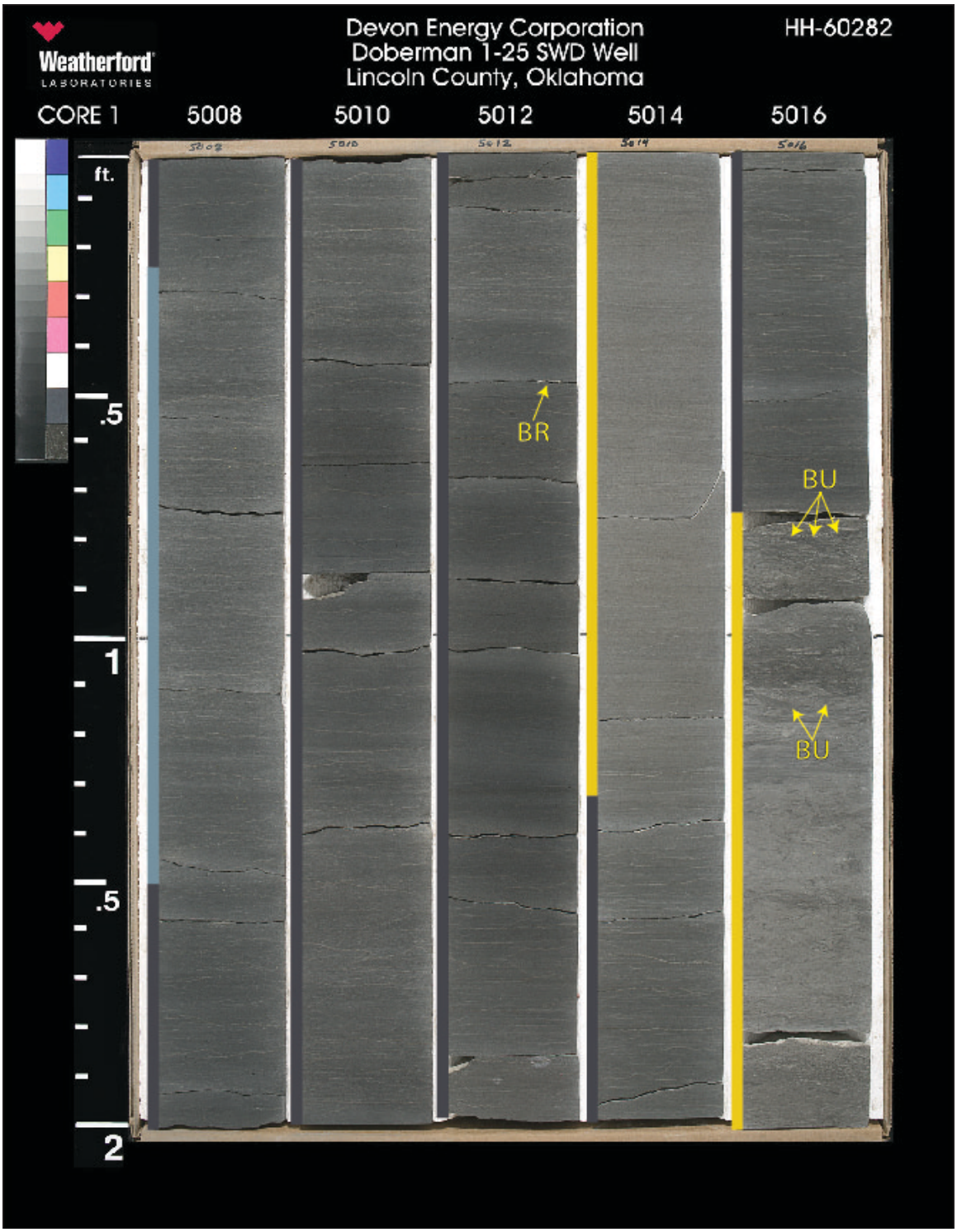
Weatherford
LABORATORIES
Devon Energy Corporation
Doberman 1-25 SWD Well
Lincoln County, Oklahoma
HH-60282
CORE 1
5008
5010
5012
5014
5016
ft.
.5
1
.5
2
BR
BU
BU

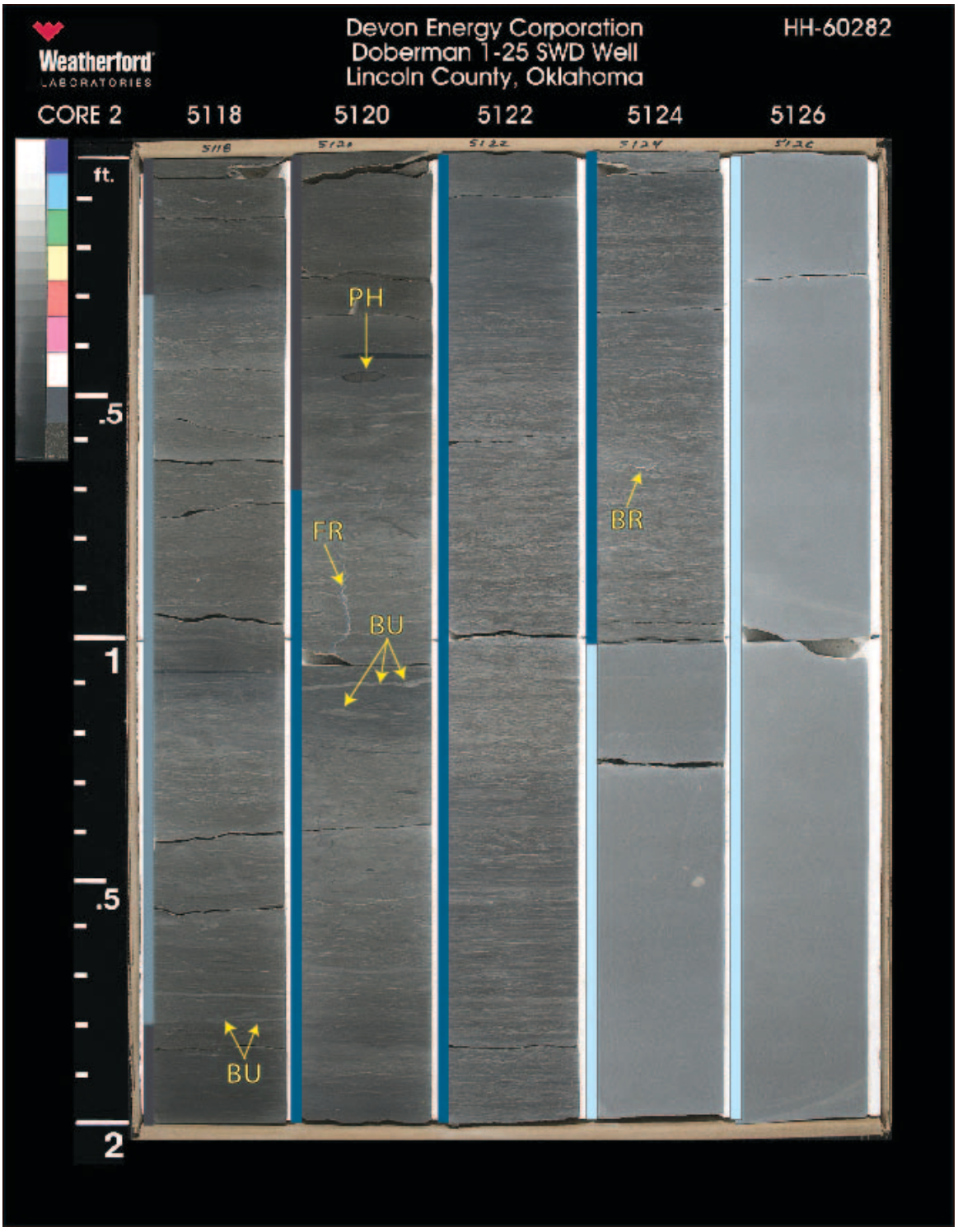
Weatherford
LABORATORIES
Devon Energy Corporation
Doberman 1-25 SWD Well
Lincoln County, Oklahoma
HH-60282
CORE 2
5118
5120
5122
5124
5126
ft.
.5
1
.5
2
PH
FR
BU
BR
BU

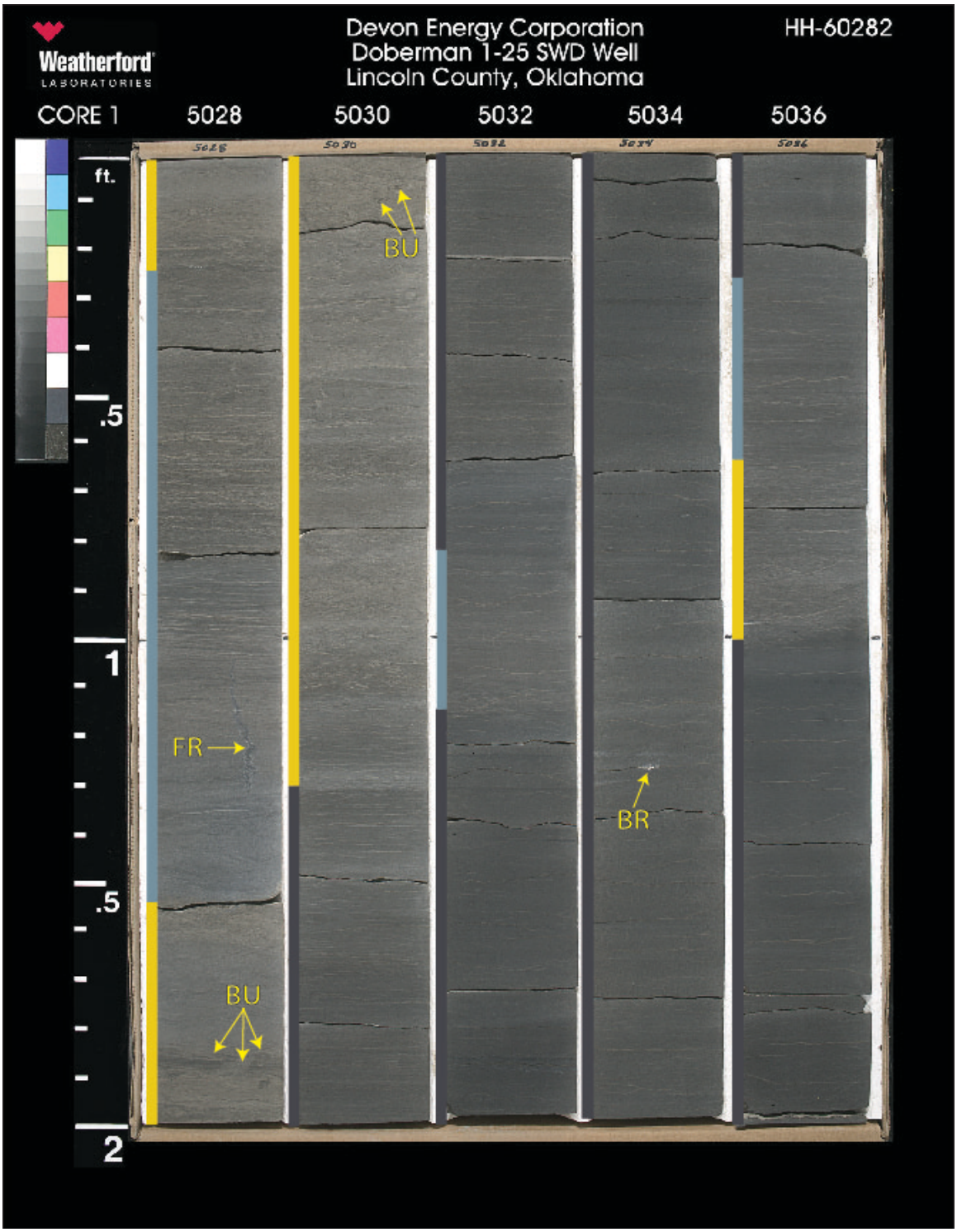
Weatherford
LABORATORIES
Devon Energy Corporation
Doberman 1-25 SWD Well
Lincoln County, Oklahoma
HH-60282
CORE 1
5028
5030
5032
5034
5036
ft.
.5
1
.5
2
BU
FR
BU
BR

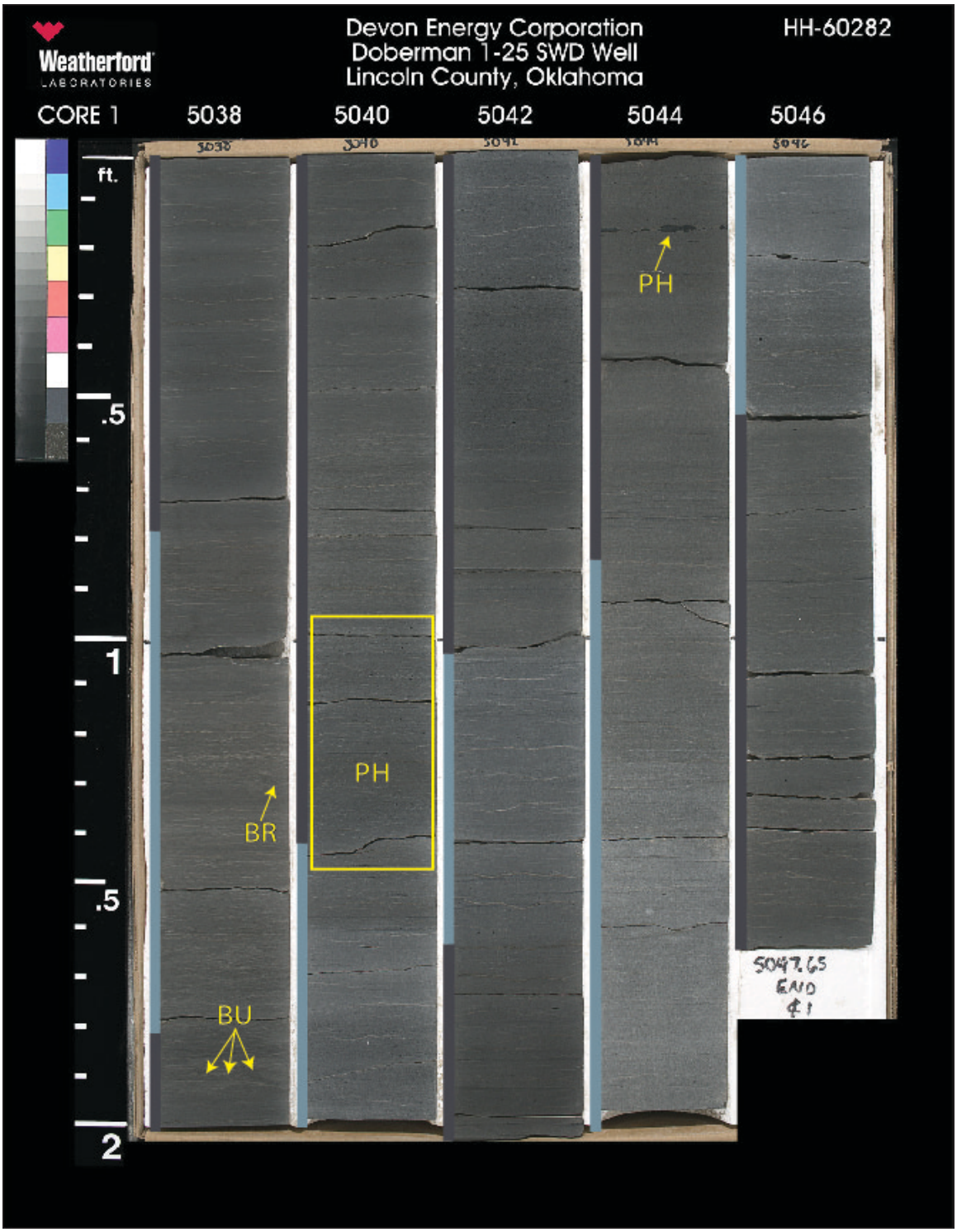
Weatherford
LABORATORIES
Devon Energy Corporation
Doberman 1-25 SWD Well
Lincoln County, Oklahoma
HH-60282
CORE 1
5038
5040
5042
5044
5046
ft.
.5
1
.5
2
PH
PH
BR
BU
5047.65
END
CI

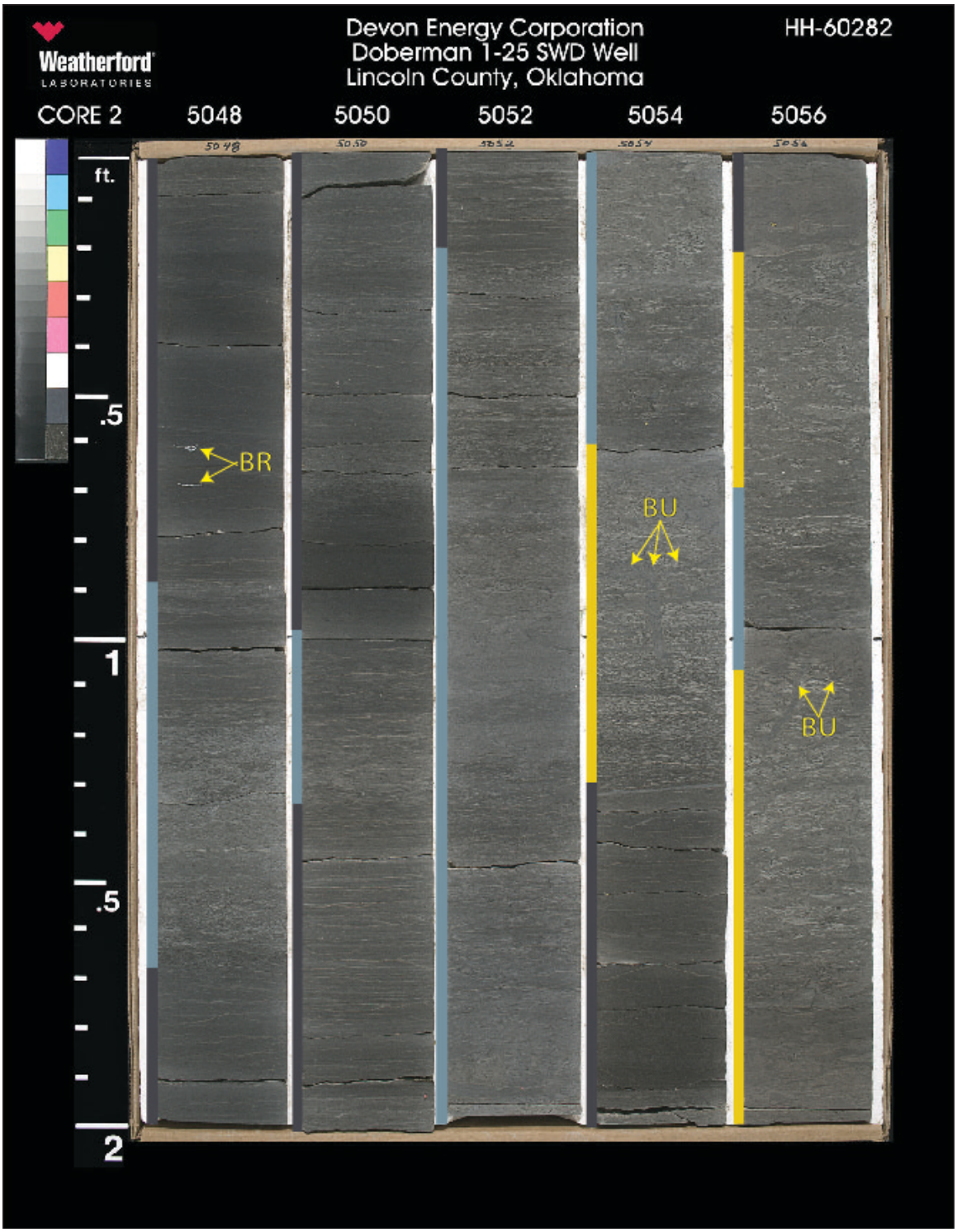
Weatherford
LABORATORIES
Devon Energy Corporation
Doberman 1-25 SWD Well
Lincoln County, Oklahoma
HH-60282
CORE 2
5048
5050
5052
5054
5056
ft.
.5
1
.5
2
BR
BU
BU

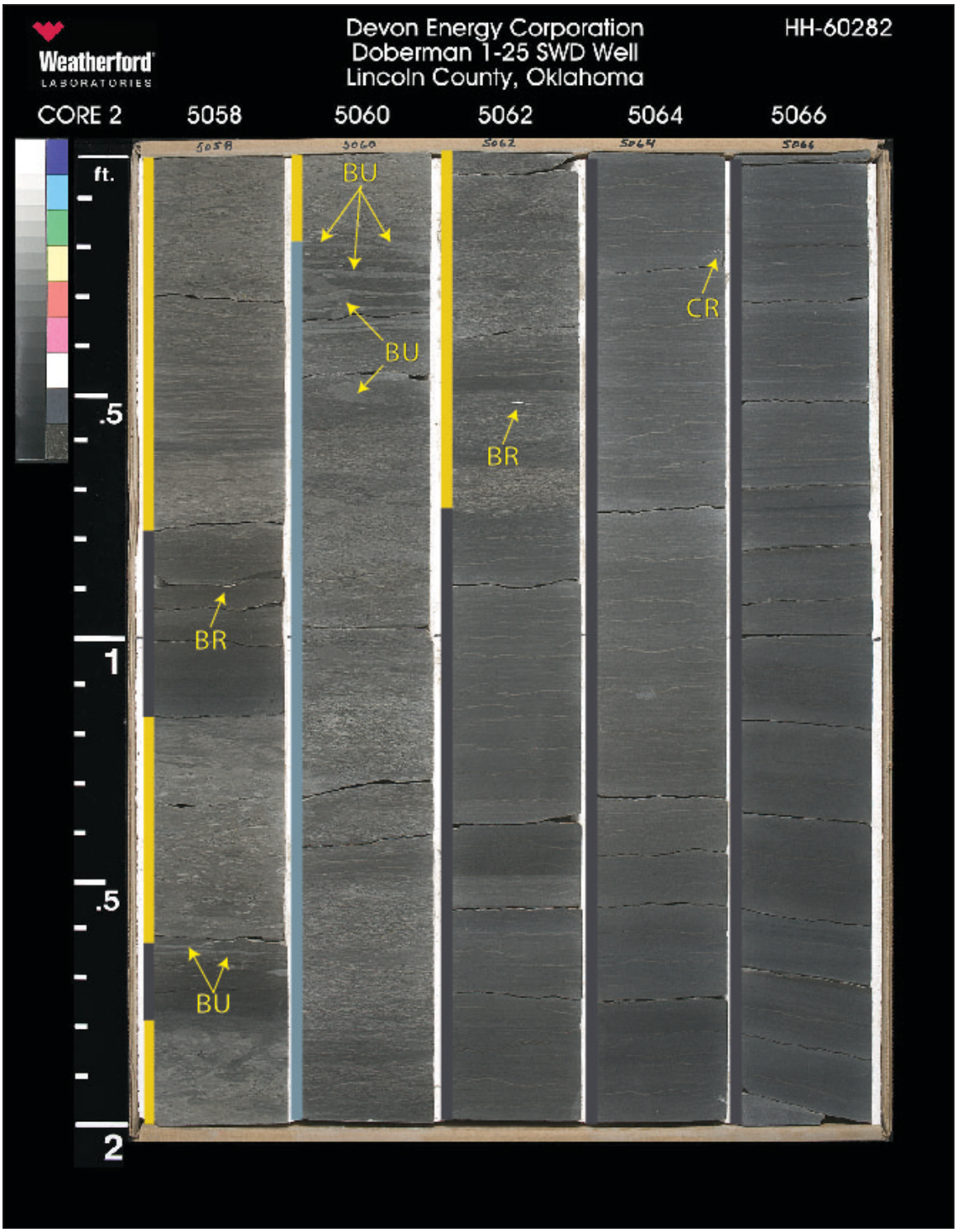
Weatherford
LABORATORIES
Devon Energy Corporation
Doberman 1-25 SWD Well
Lincoln County, Oklahoma
HH-60282
CORE 2
5058
5060
5062
5064
5066
ft.
.5
1
.5
2
BU
BU
BR
CR
BR
BU

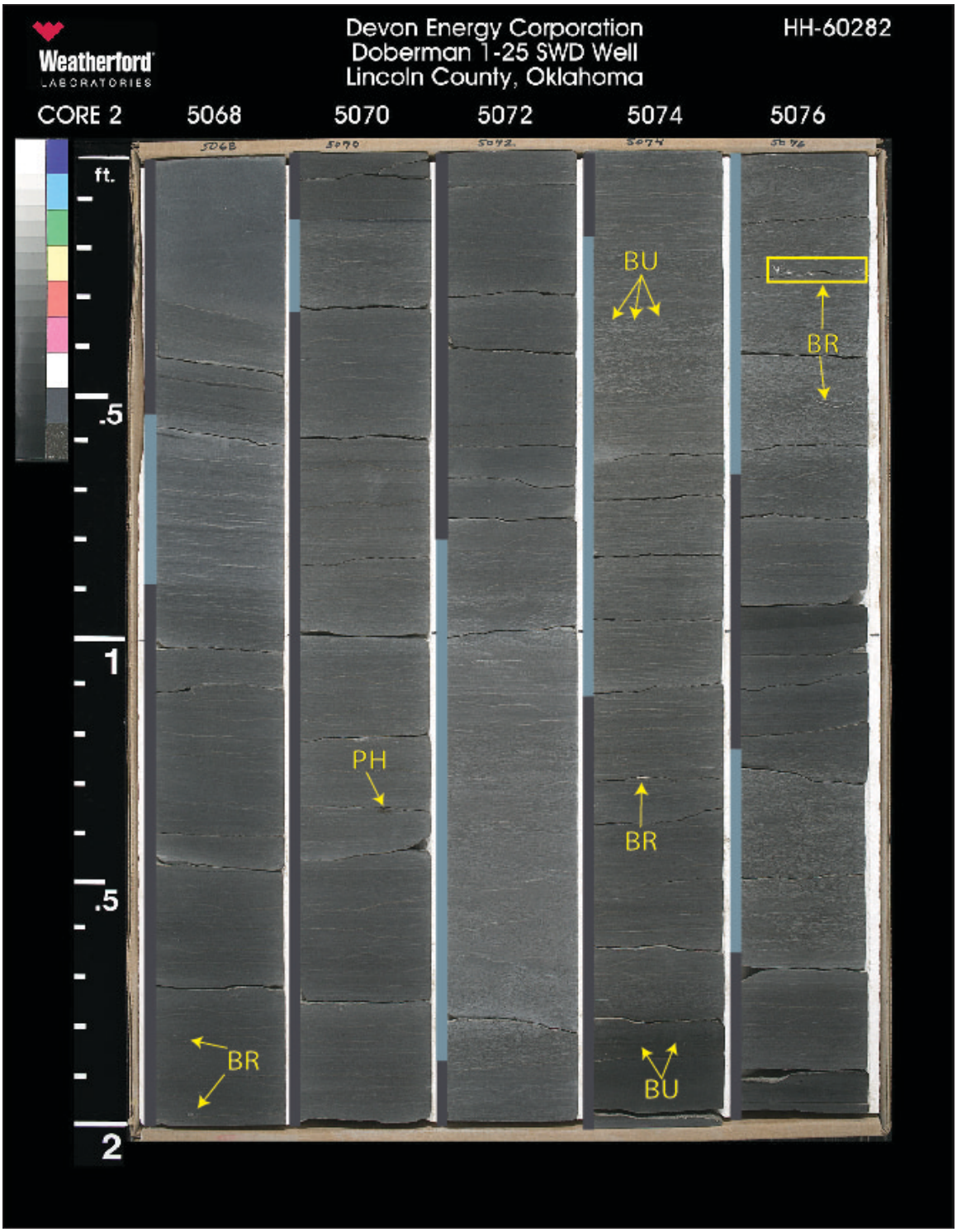
Weatherford
LABORATORIES
Devon Energy Corporation
Doberman 1-25 SWD Well
Lincoln County, Oklahoma
HH-60282
CORE 2
5068
5070
5072
5074
5076
ft.
.5
1
.5
2
BU
BR
PH
BR
BR
BU

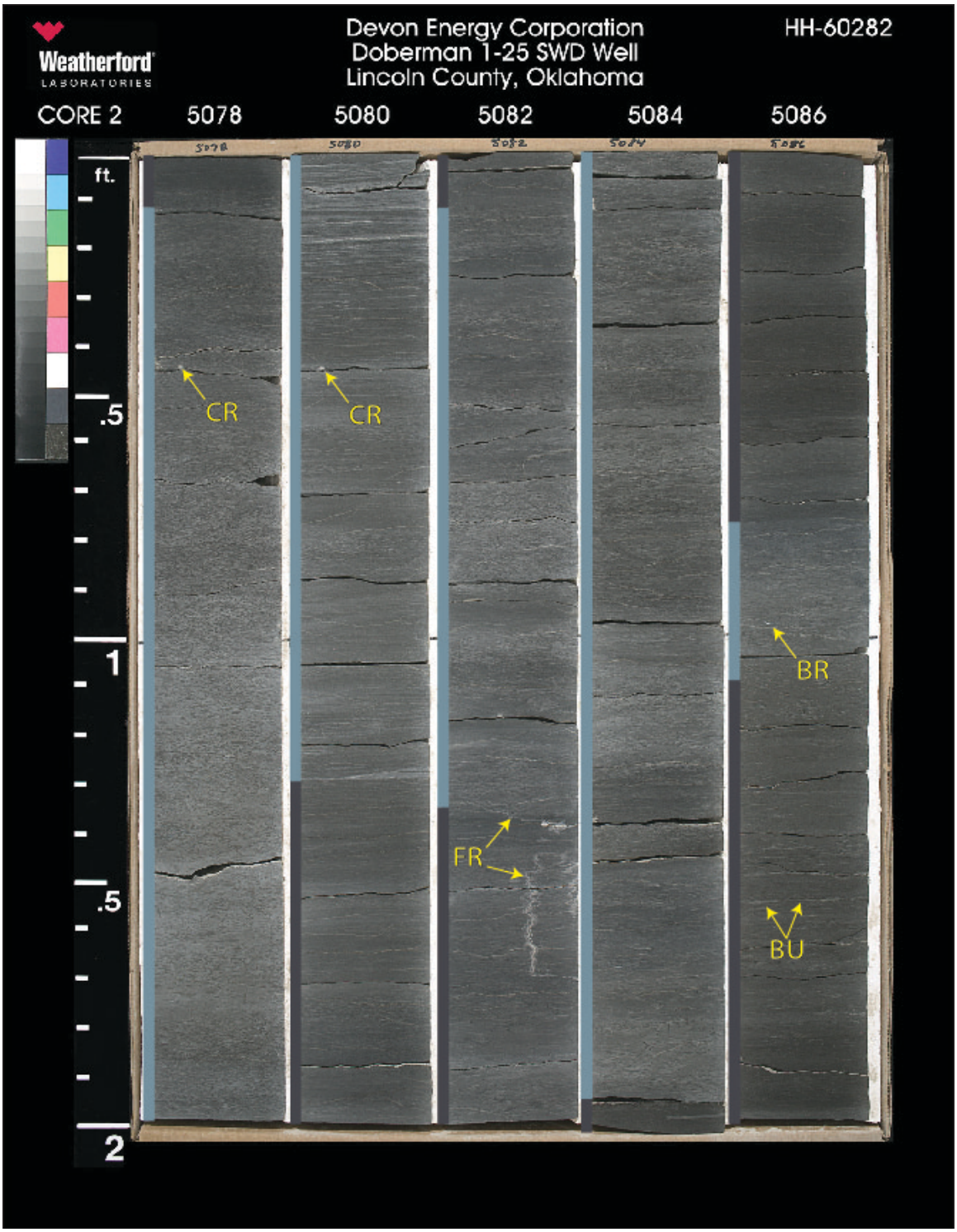
Weatherford
LABORATORIES
Devon Energy Corporation
Doberman 1-25 SWD Well
Lincoln County, Oklahoma
HH-60282
CORE 2
5078
5080
5082
5084
5086
ft.
.5
1
.5
2
CR
CR
FR
BR
BU

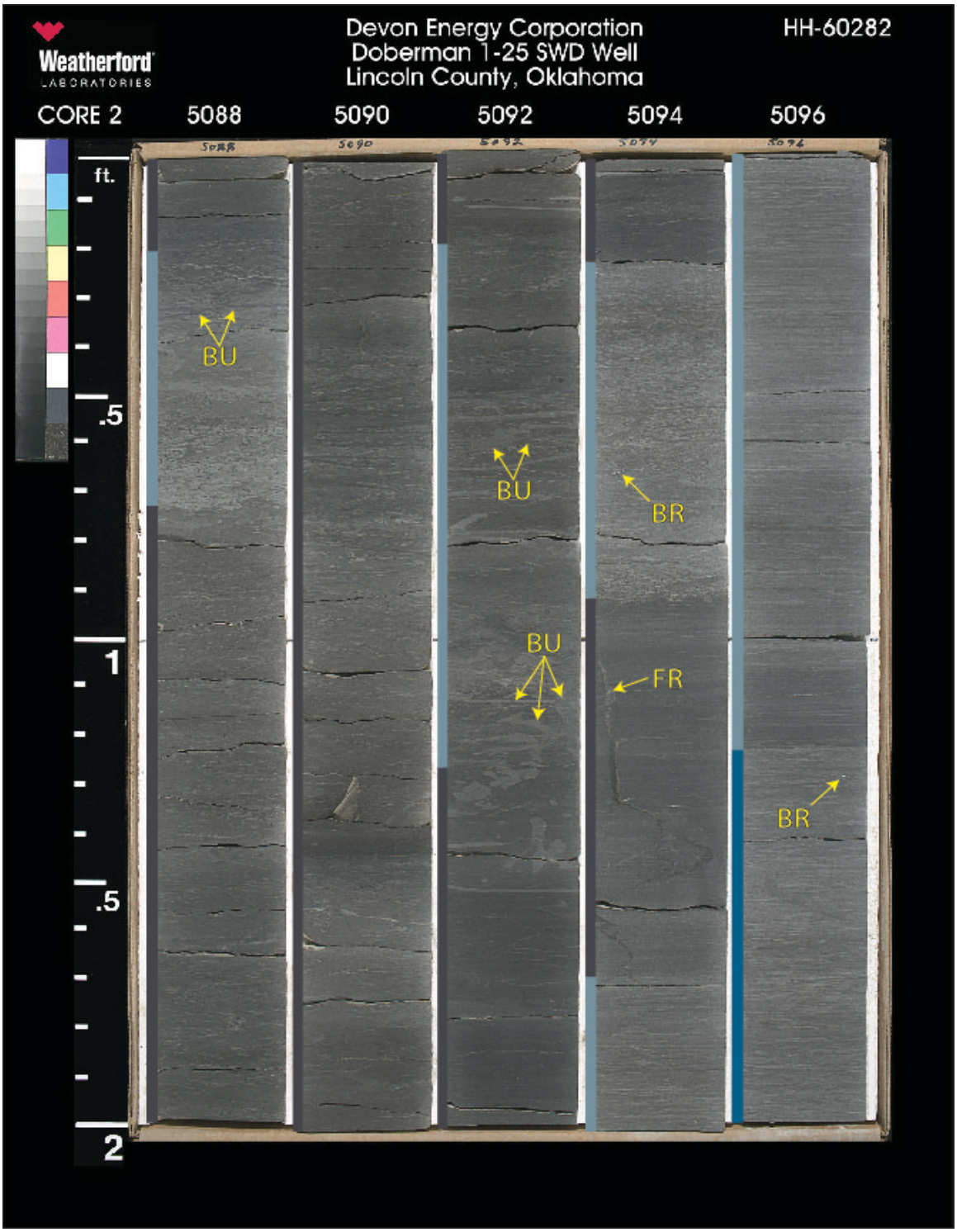
Weatherford
LABORATORIES
Devon Energy Corporation
Doberman 1-25 SWD Well
Lincoln County, Oklahoma
HH-60282
CORE 2
5088
5090
5092
5094
5096
ft.
.5
1
.5
2
BU
BU
BU
BR
FR
BR

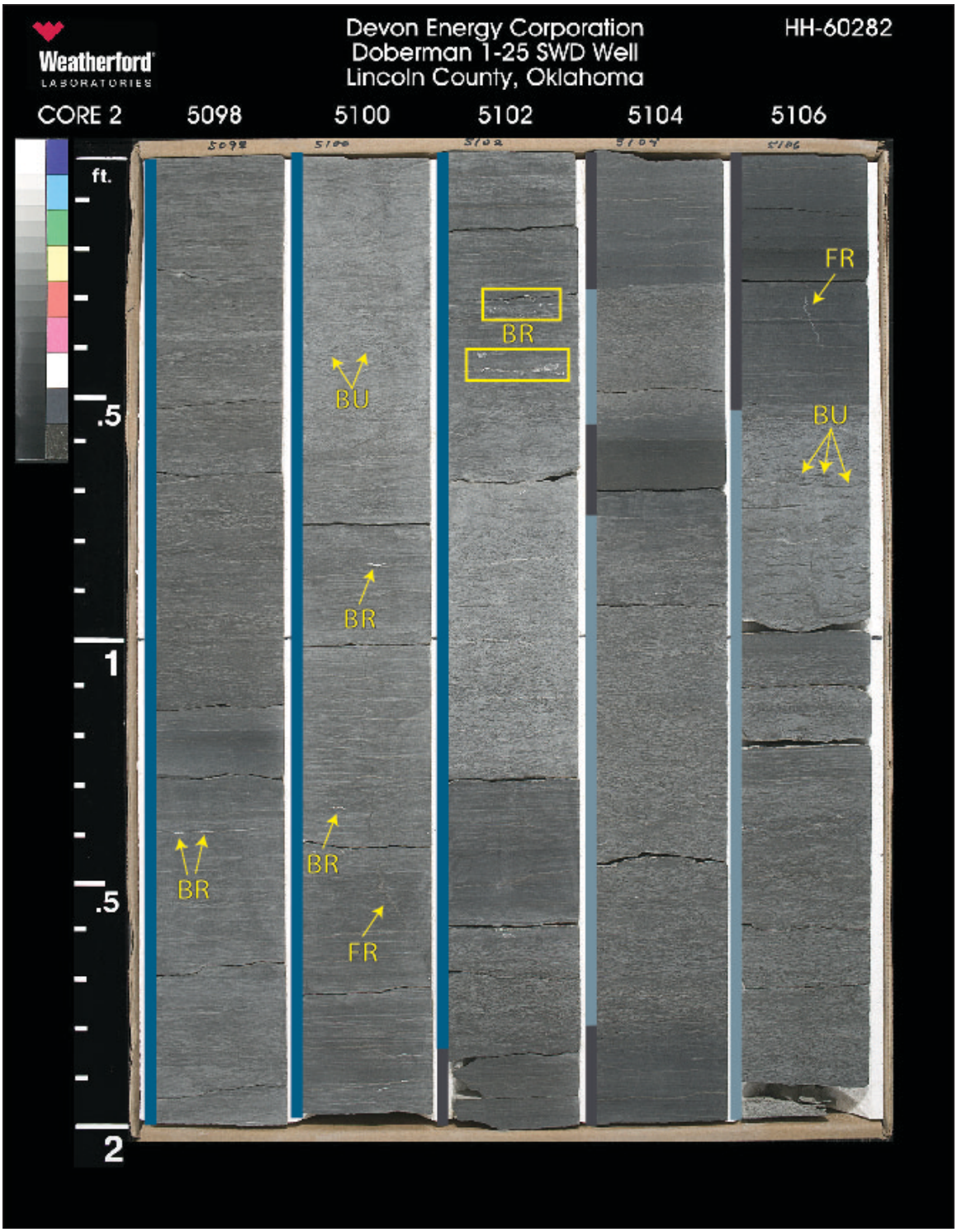
Weatherford
LABORATORIES
Devon Energy Corporation
Doberman 1-25 SWD Well
Lincoln County, Oklahoma
HH-60282
CORE 2
5098
5100
5102
5104
5106
ft.
.5
1
.5
2
BR
BU
BR
BR
FR
BR
FR
BU

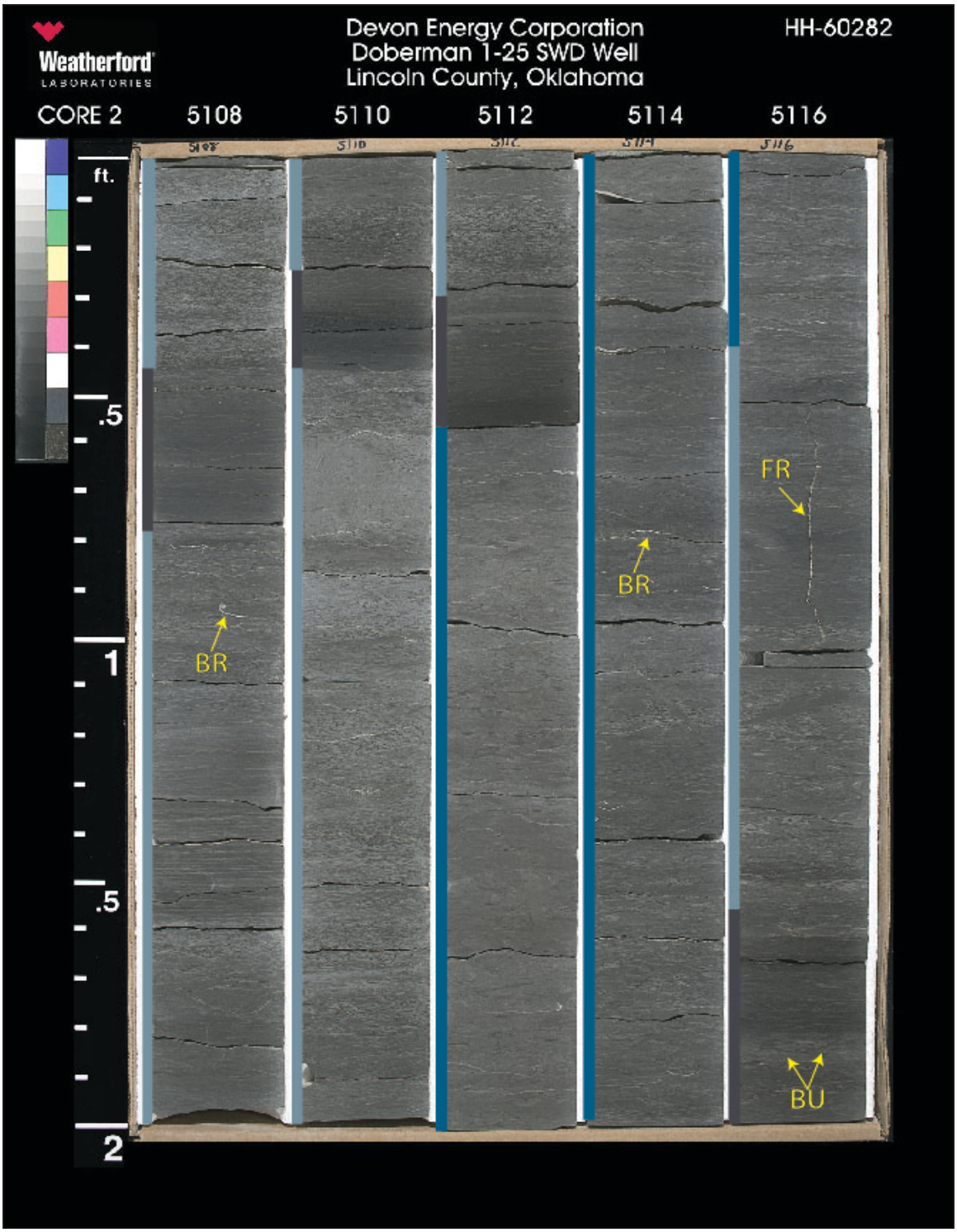
Weatherford
LABORATORIES
Devon Energy Corporation
Doberman 1-25 SWD Well
Lincoln County, Oklahoma
HH-60282
CORE 2
5108
5110
5112
5114
5116
ft.
.5
1
.5
2
BR
BR
FR
BU

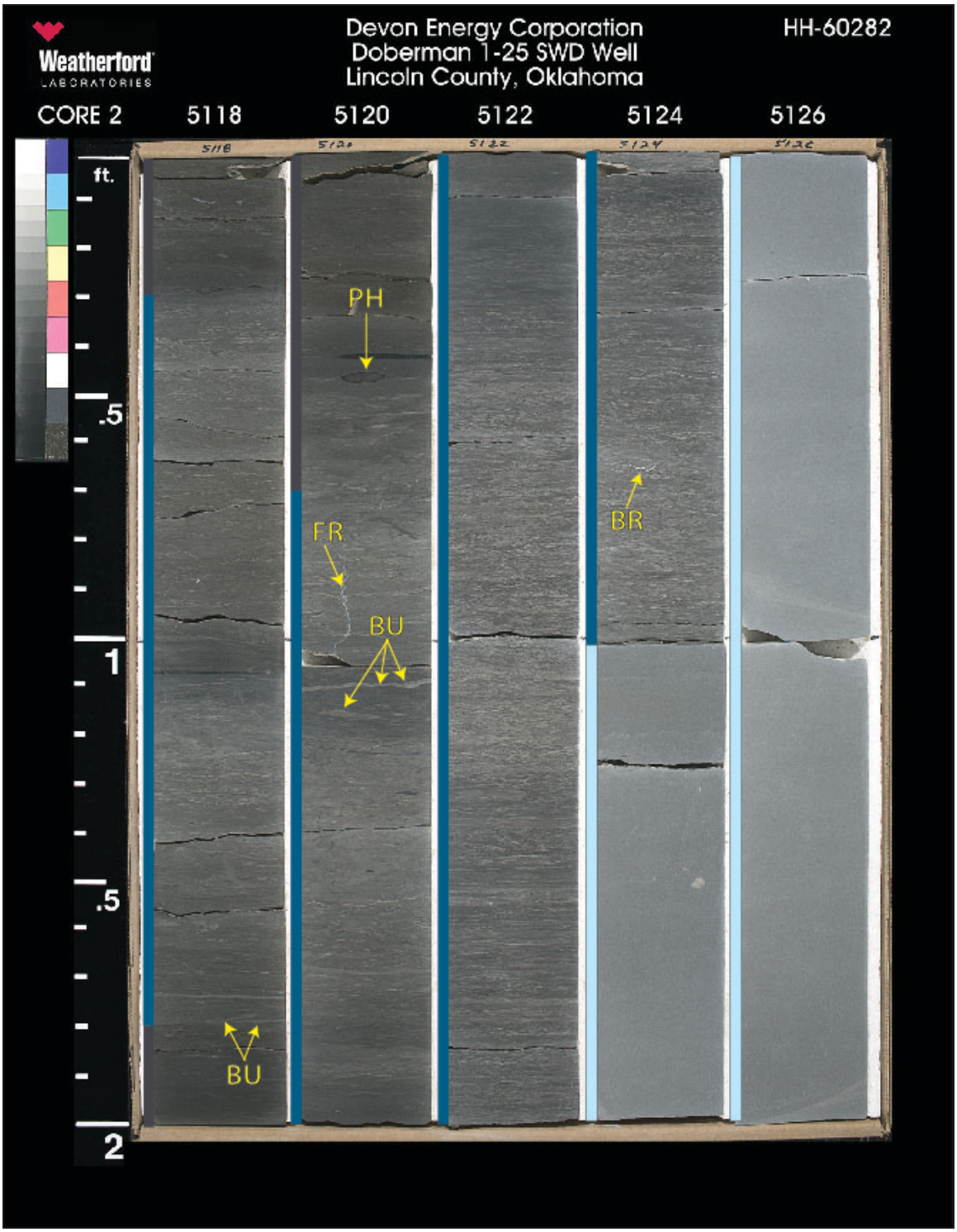
Weatherford
LABORATORIES
Devon Energy Corporation
Doberman 1-25 SWD Well
Lincoln County, Oklahoma
HH-60282
CORE 2
5118
5120
5122
5124
5126
ft.
.5
1
.5
2
PH
FR
BU
BR
BU

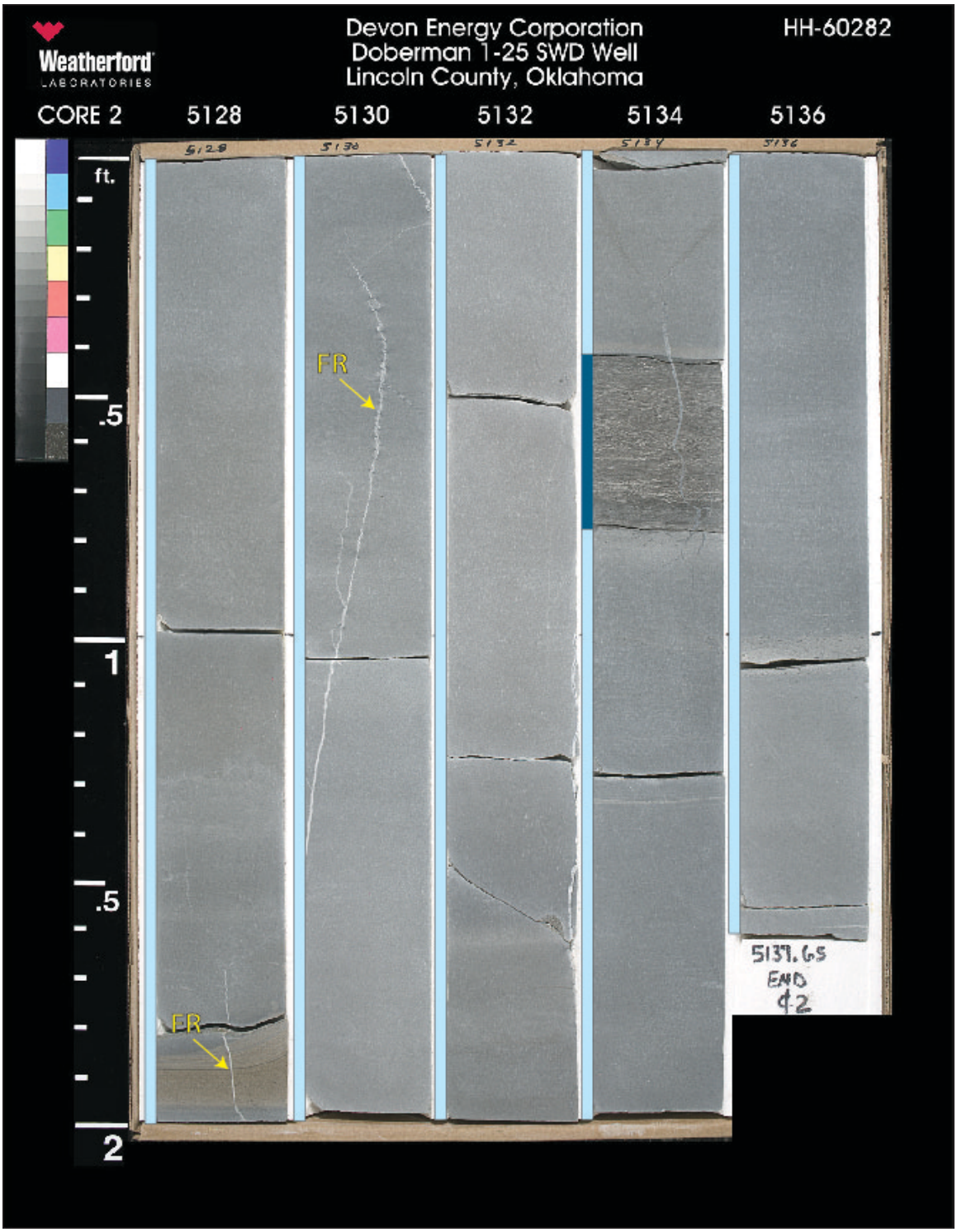
Weatherford
LABORATORIES
Devon Energy Corporation
Doberman 1-25 SWD Well
Lincoln County, Oklahoma
HH-60282
CORE 2
5128
5130
5132
5134
5136
ft.
.5
1
.5
2
FR
FR
5137.65
END
#2

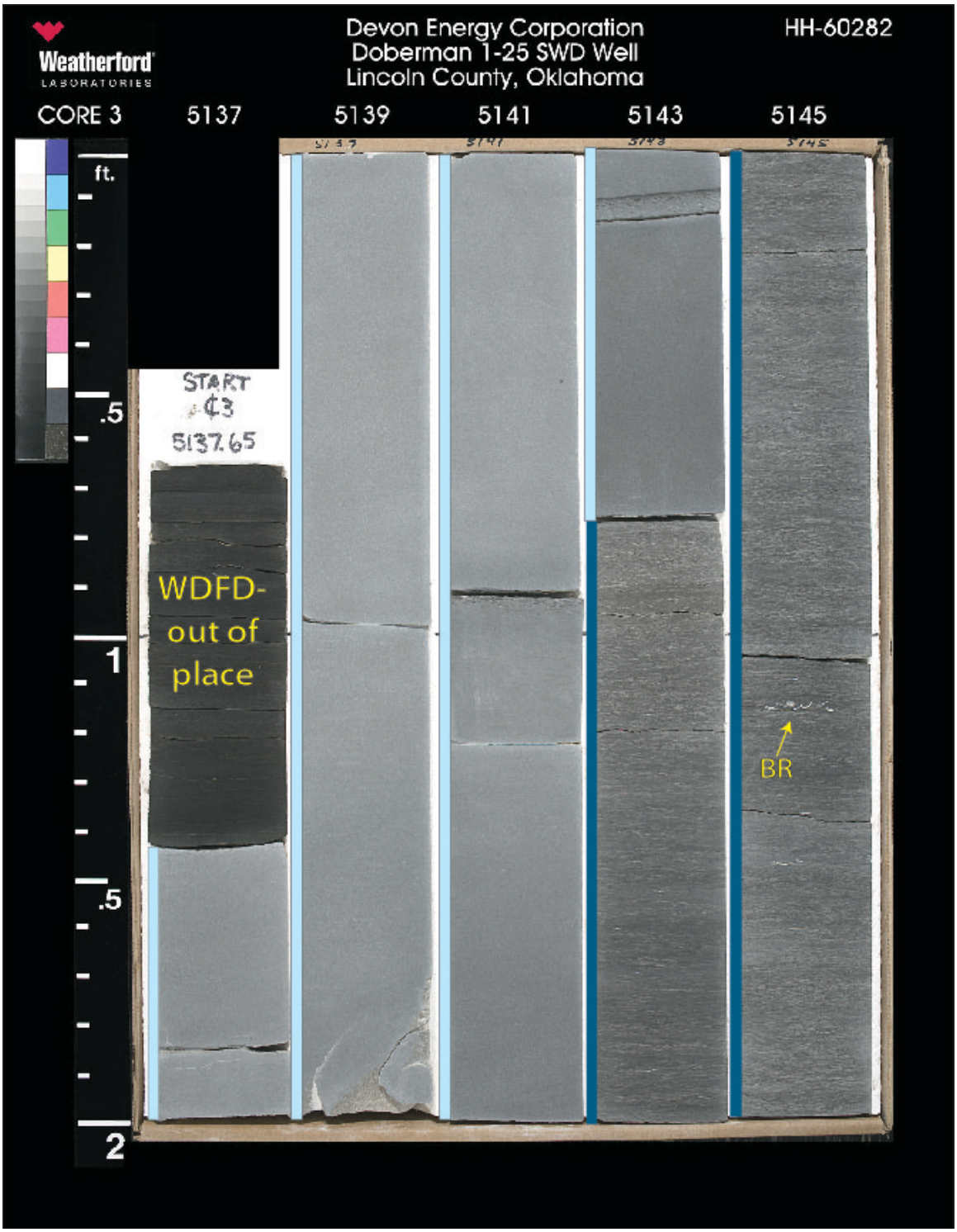
Weatherford
LABORATORIES
Devon Energy Corporation
Doberman 1-25 SWD Well
Lincoln County, Oklahoma
HH-60282
CORE 3
5137
5139
5141
5143
5145
ft.
.5
1
.5
2
START
¢3
5137.65
WDFD-
out of
place
BR

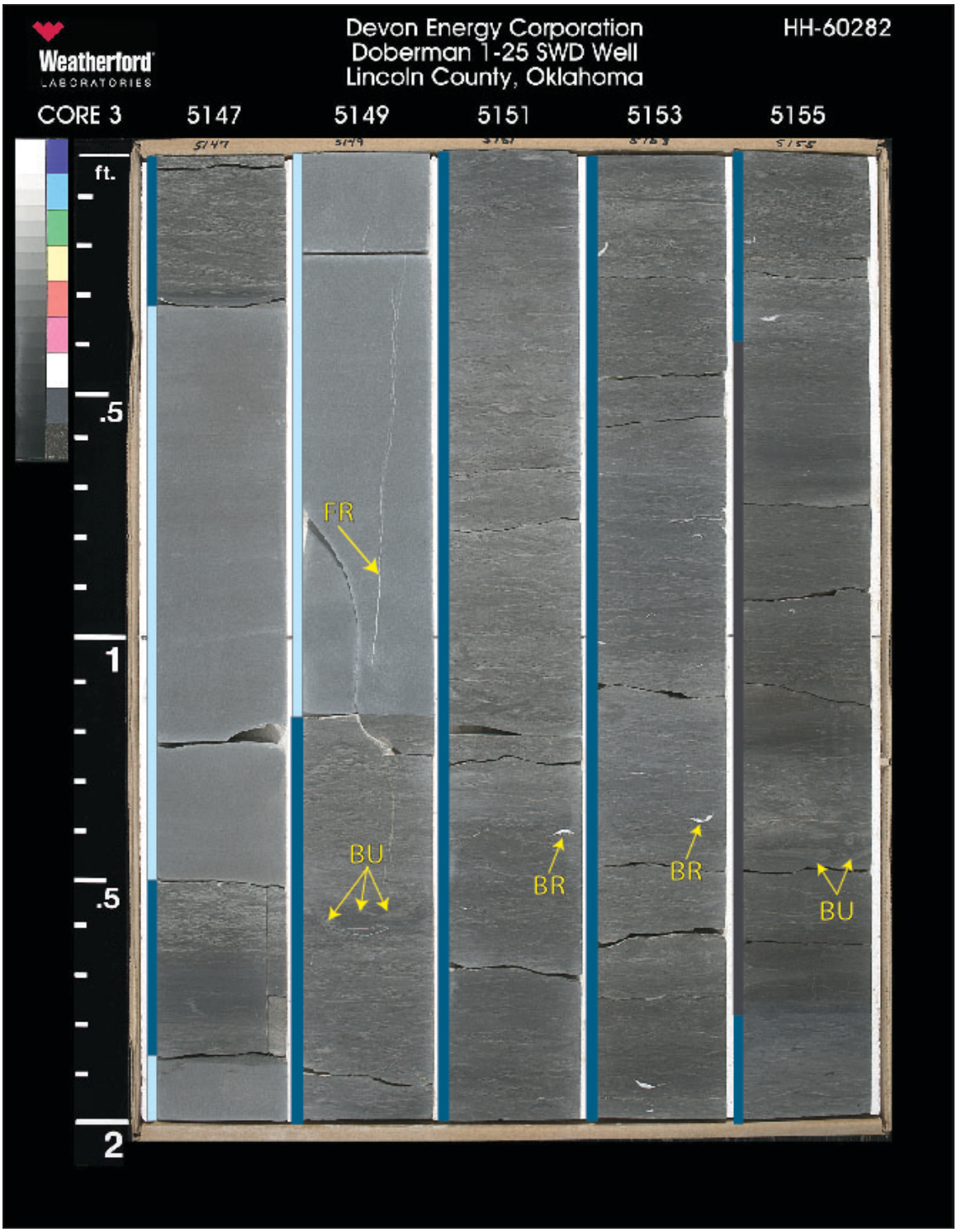
Weatherford
LABORATORIES
Devon Energy Corporation
Doberman 1-25 SWD Well
Lincoln County, Oklahoma
HH-60282
CORE 3
5147
5149
5151
5153
5155
ft.
.5
1
.5
2
FR
BU
BR
BR
BU

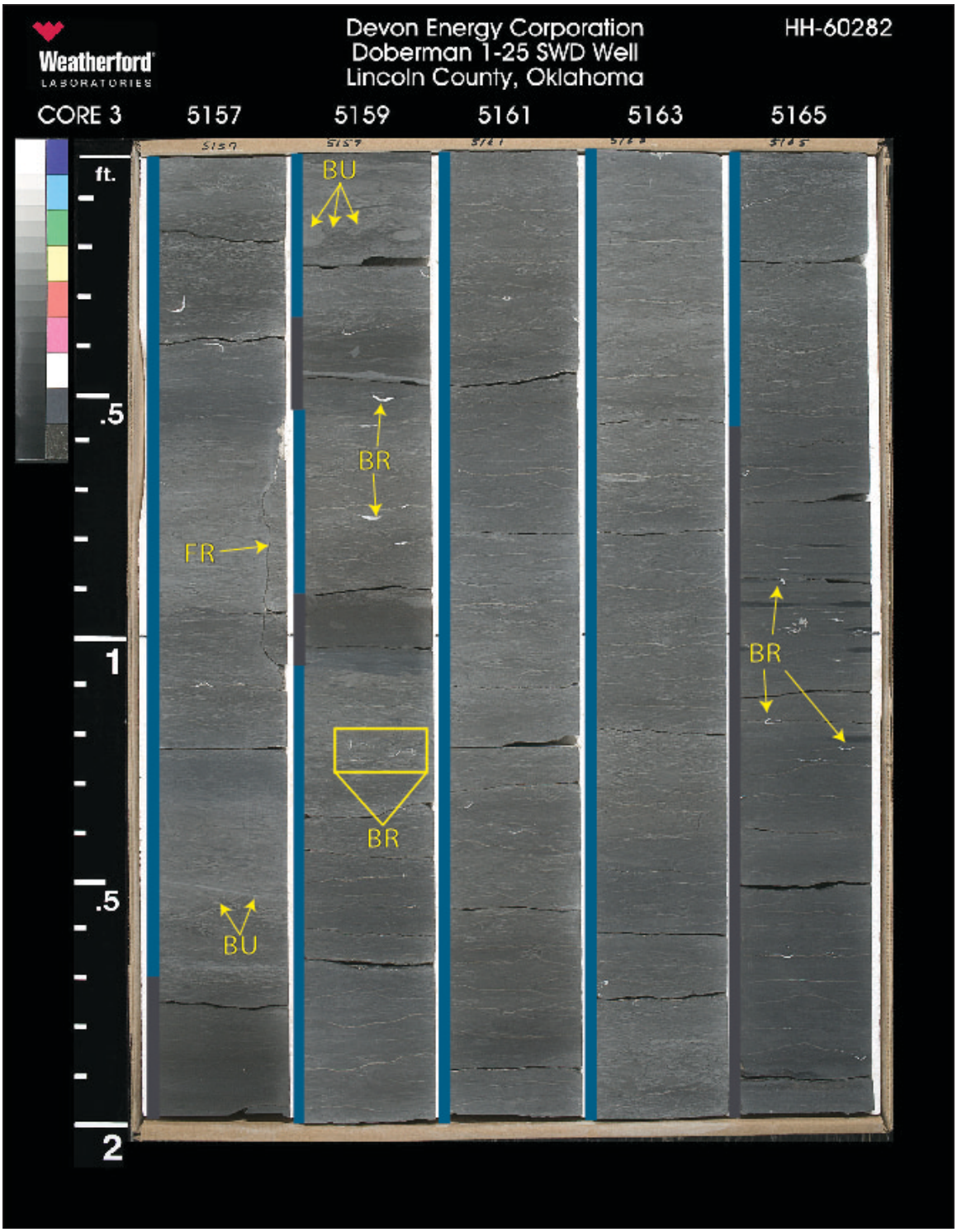
Weatherford
LABORATORIES
Devon Energy Corporation
Doberman 1-25 SWD Well
Lincoln County, Oklahoma
HH-60282
CORE 3
5157
5159
5161
5163
5165
ft.
.5
1
.5
2
BU
BR
FR
BR
BR
BU

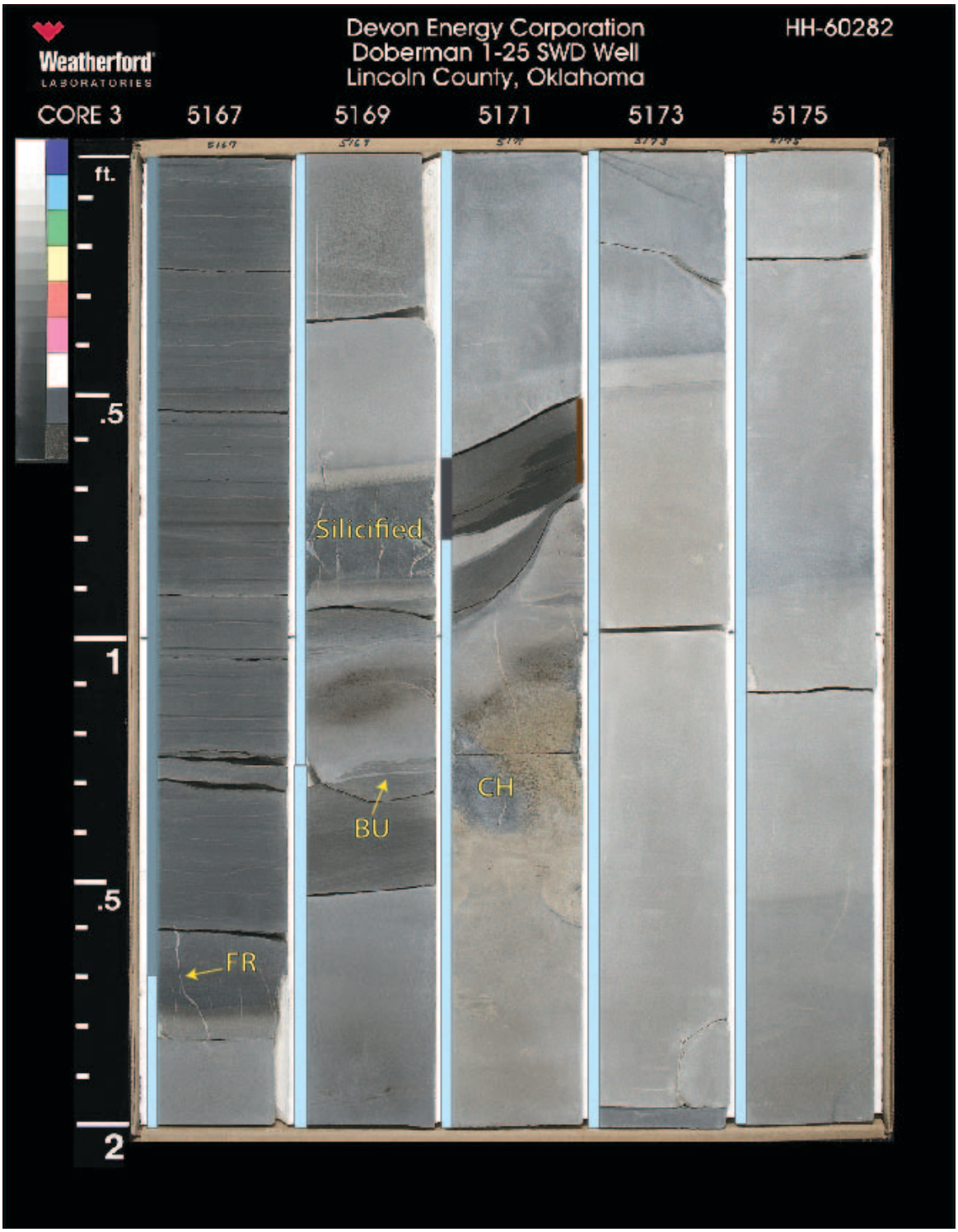
Weatherford
LABORATORIES
Devon Energy Corporation
Doberman 1-25 SWD Well
Lincoln County, Oklahoma
HH-60282
CORE 3
5167
5169
5171
5173
5175
ft.
.5
1
.5
2
Silicified
BU
CH
FR

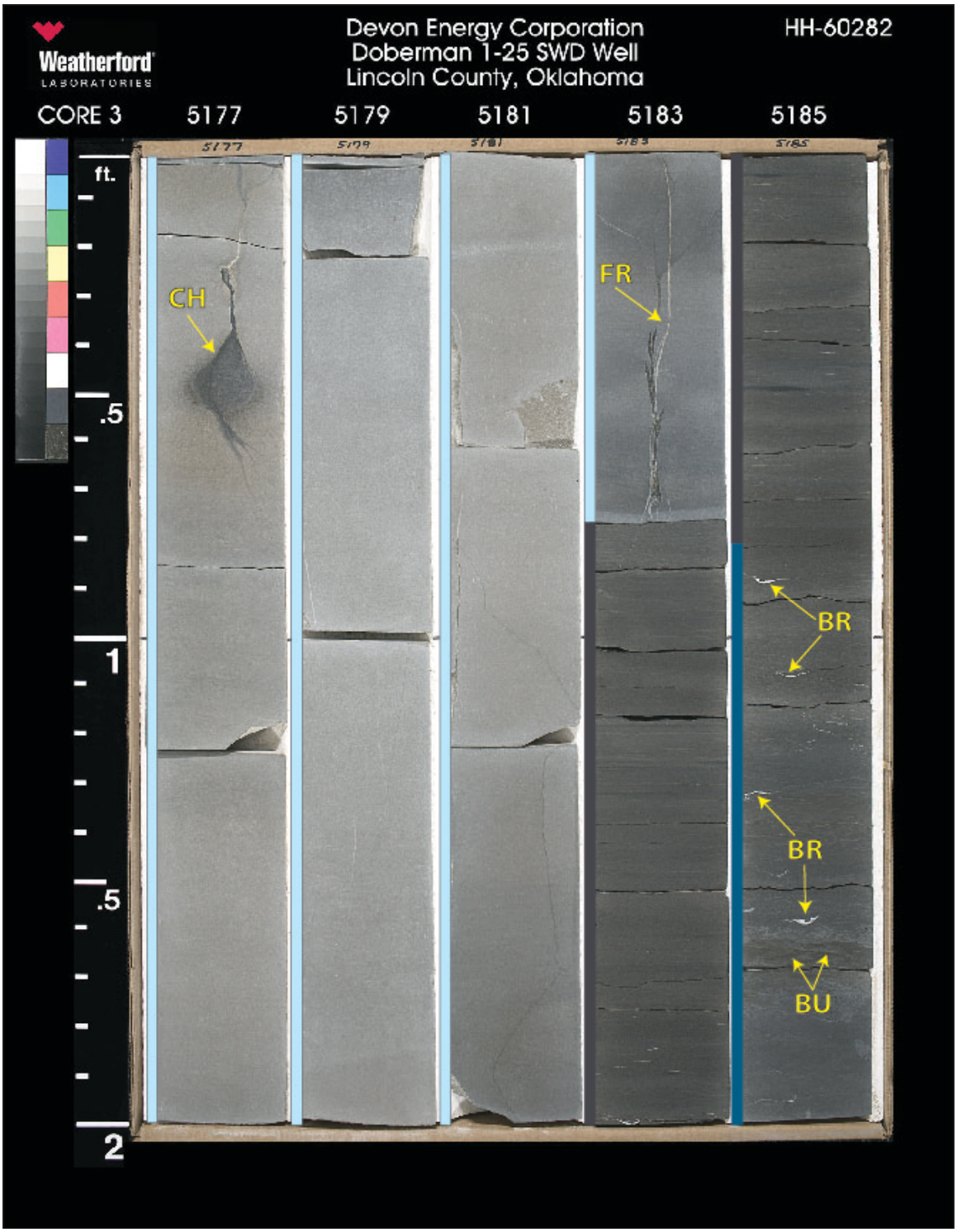
Weatherford
LABORATORIES
Devon Energy Corporation
Doberman 1-25 SWD Well
Lincoln County, Oklahoma
HH-60282
CORE 3
5177
5179
5181
5183
5185
ft.
.5
1
.5
2
CH
FR
BR
BR
BU

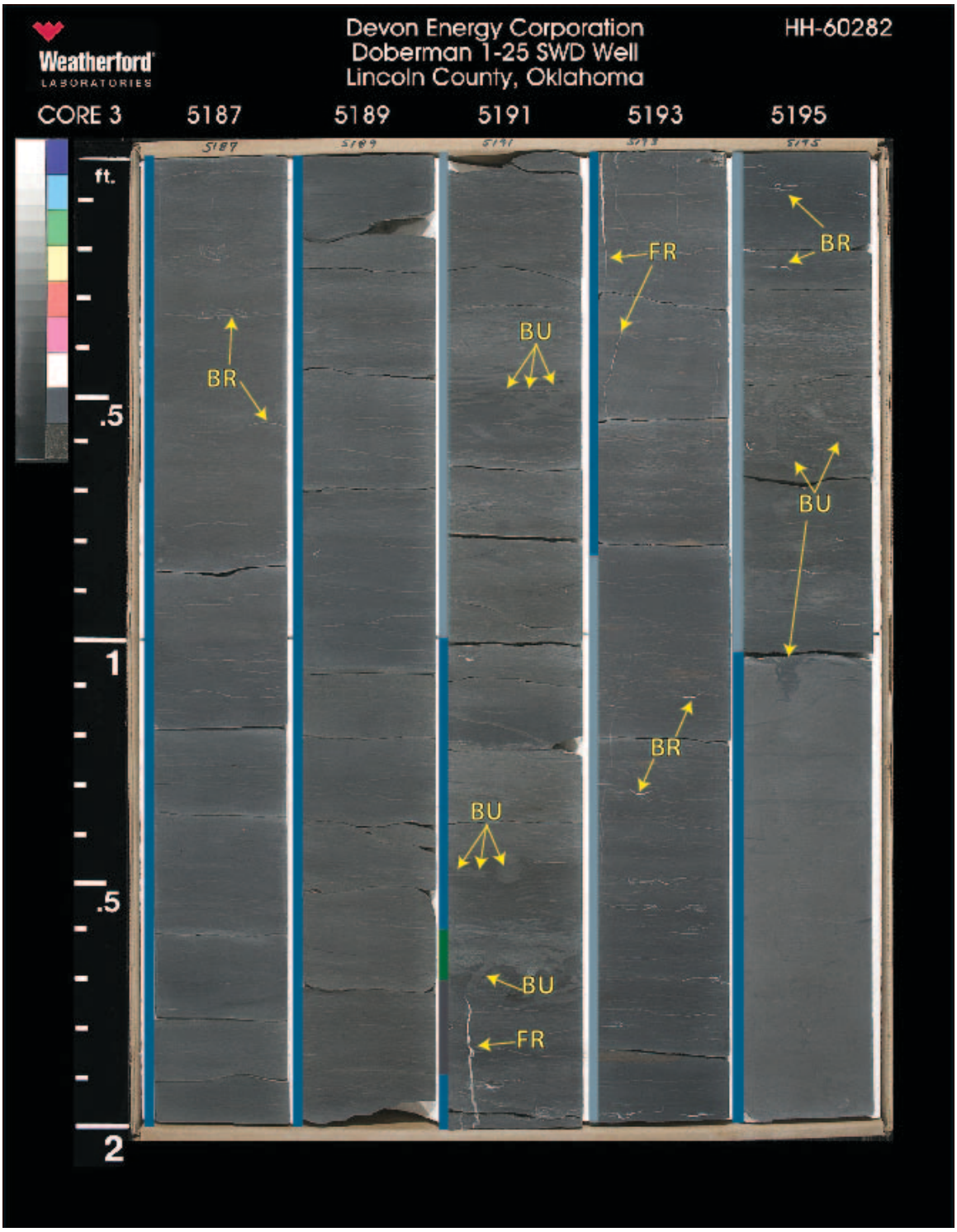
Weatherford
LABORATORIES
Devon Energy Corporation
Doberman 1-25 SWD Well
Lincoln County, Oklahoma
HH-60282
CORE 3
5187
5189
5191
5193
5195
ft.
.5
1
.5
2
BR
BU
FR
BR
BU
BR
BU
BU
FR

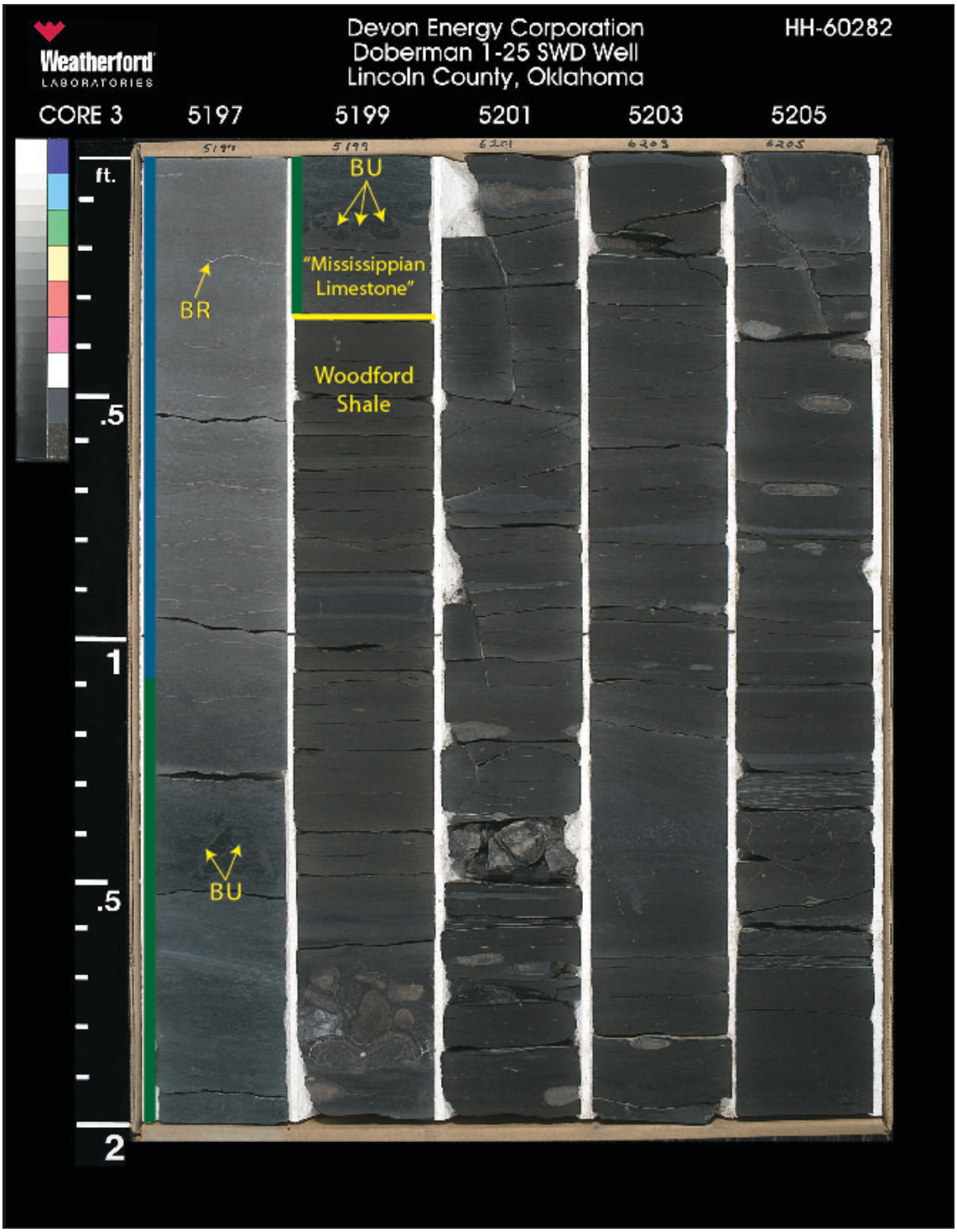
Weatherford
LABORATORIES
Devon Energy Corporation
Doberman 1-25 SWD Well
Lincoln County, Oklahoma
HH-60282
CORE 3
5197
5199
5201
5203
5205
ft.
.5
1
.5
2
BU
"Mississippian
Limestone"
BR
Woodford
Shale
BU

## II. Doberman #1-25 SWD Core Descriptions

The Doberman core was described using the Dunham (1962) classification scheme where applicable (i.e. – carbonate-rich intervals), while siliciclastic-rich intervals were classified based on abundant grain type and composition. The colors described from the core relate to the standardized color chart key (Table 7), which has been adapted from the revised rock-color chart developed by the rock-color chart committee (2009). The descriptions of bioturbation uses a bioturbation index implemented from Bann et al., 2008 (Table 8).

| Rock-Color Chart - Doberman #1-25 SWD | | | |
|---|---|---|---|
| **Color Name** | **Numerical Designation** | **Color Name** | **Numerical Designation** |
| Dark Gray | N3 | Olive Gray | 5Y 3/2 |
| Dark Greenish Gray | 5G 4/1 | Very Light Gray | N8 |
| Dusky Green | 5G 3/2 | | |
| Dusky Yellow Green | 5GY 5/2 | | |
| Dusky Yellowish Green | 10GY 3/2 | | |
| Grayish Black | N2 | | |
| Grayish Green | 10G 4/2 | | |
| Greenish Black | 5GY 2/1 | | |
| Light Olive Gray | 5Y 6/1 | | |
| Medium Gray | N5 | | |
| Moderate Olive Brown | 5Y 4/4 | | |
| Moderate Yellowish Brown | 10YR 5/4 | | |

Table 7. Modified from the Rock-Color Chart prepared by the Rock-Color Chart Committee (representing the U.S.G.S., GSA, AAPG, SEG, and AASG) and distributed by The Geological Society of America. Revised and reprinted in 2009.

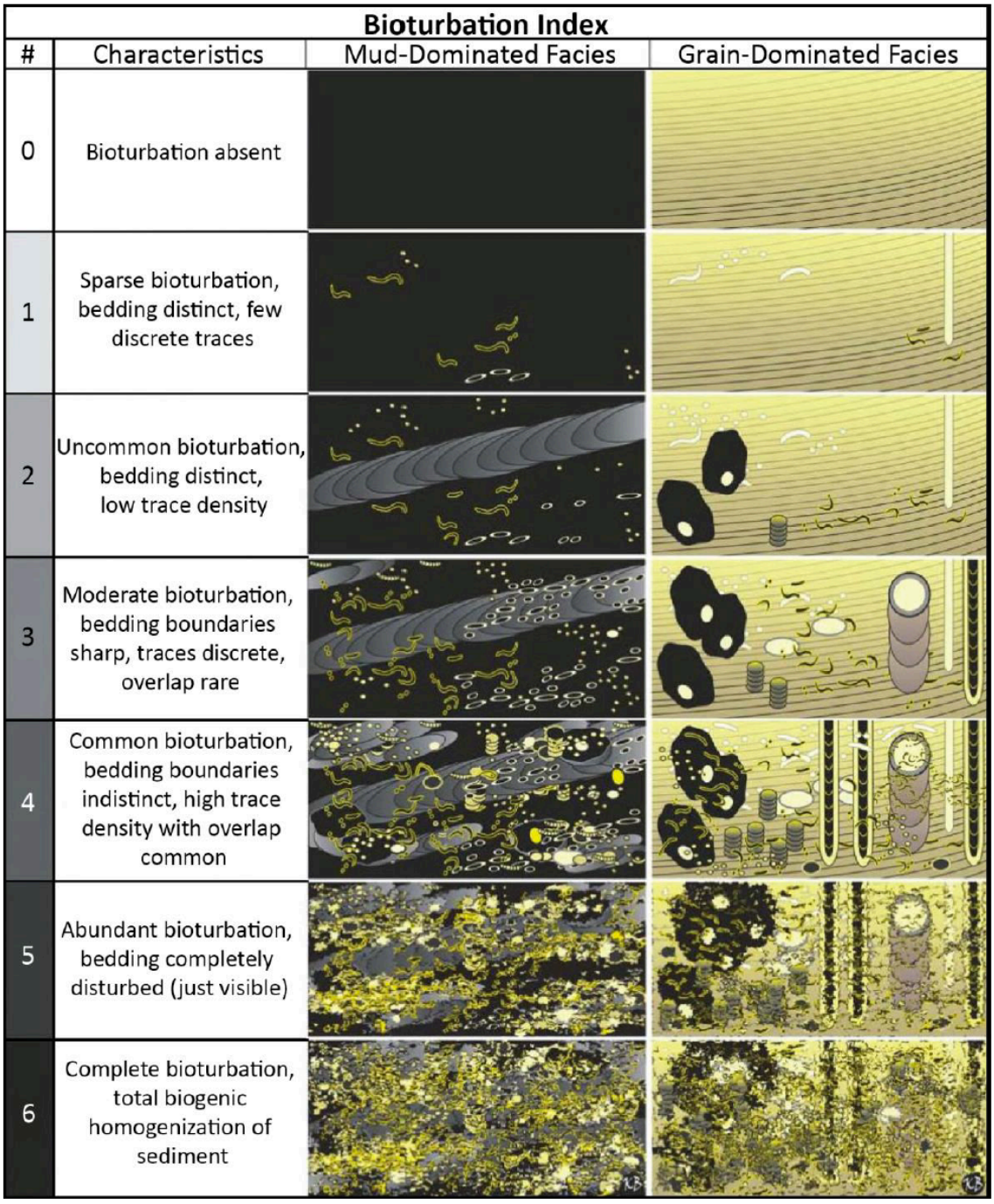


Table 8. Bioturbation index utilized for core descriptions. Modified from Bann et al (2008).

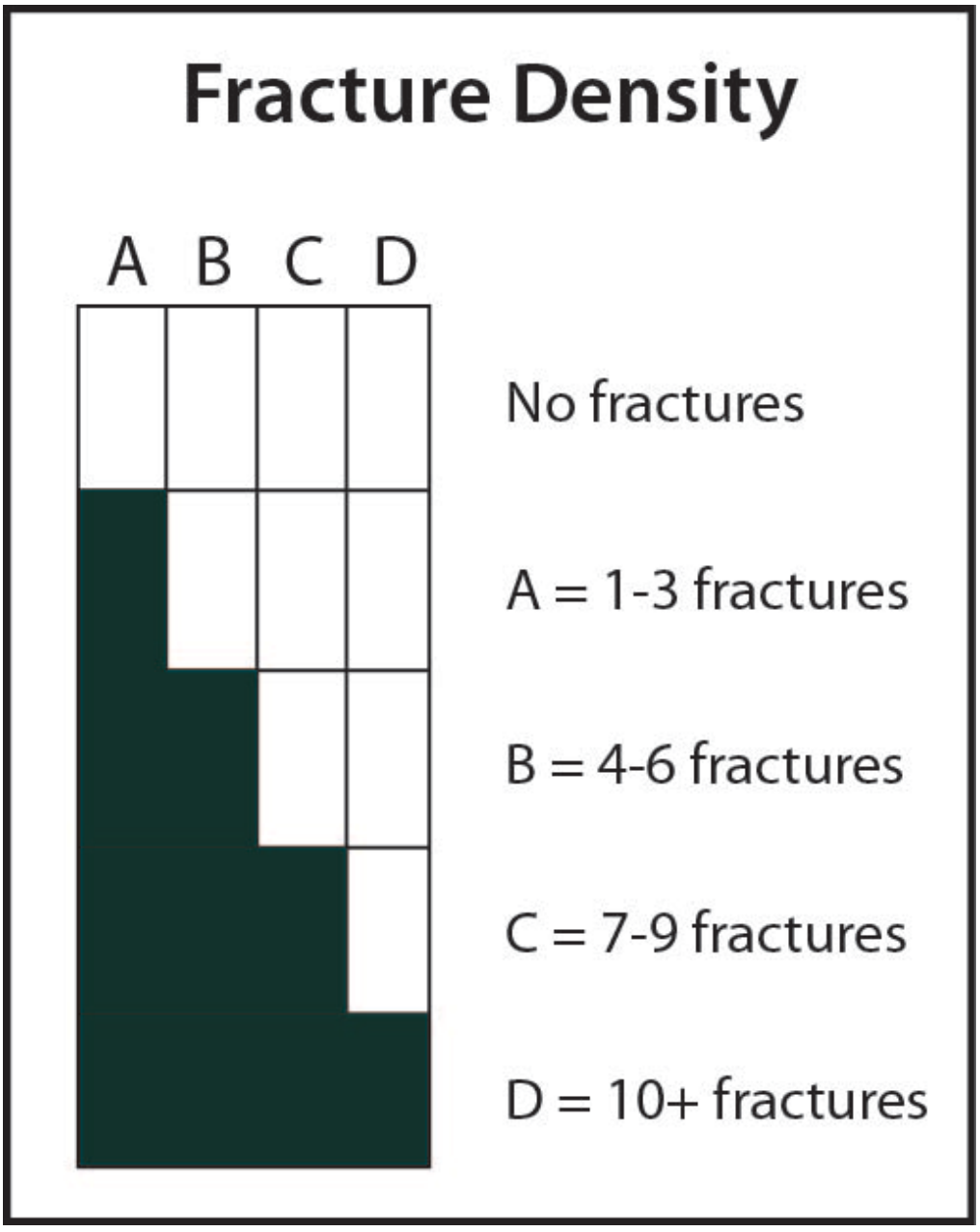


Table 9. Chart used for illustrating the fracture density within the core descriptions. The letters A through D relate to the number of fractures in one foot of core.

## LITHOLOGIC SYMBOLS

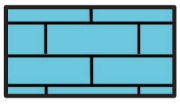
Limestone

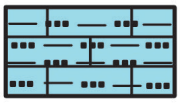
Silty Limestone

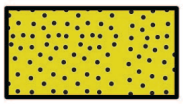
Sandstone

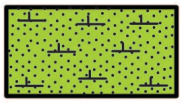
Calcareous Sandstone

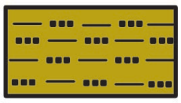
Siltstone

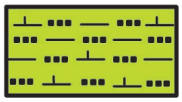
Calcareous Siltstone

## GRAIN TYPES, SEDIMENTARY STRUCTURES, & DIAGENETIC FEATURES

Bioturbated

Horizontal Burrow

Vertical Burrow

Brachiopod

Crinoid

Cross-Bedded

Unrecognizable Fossils

Fracture

Undulate Stratification

Horizontal Laminae

Argillaceous

Peloids

Glauconite

Pyrite

Nodule

## TRACE FOSSILS

Ph - Phycosiphon

Te - Teichichnus

Pl - Planolites

Zo - Zoophycos

# Devon Energy - Doberman #1-25 SWD, Lincoln County, OK

Formation: "Mississippian Limestone"

Depth Interval: 4964' - 5044'

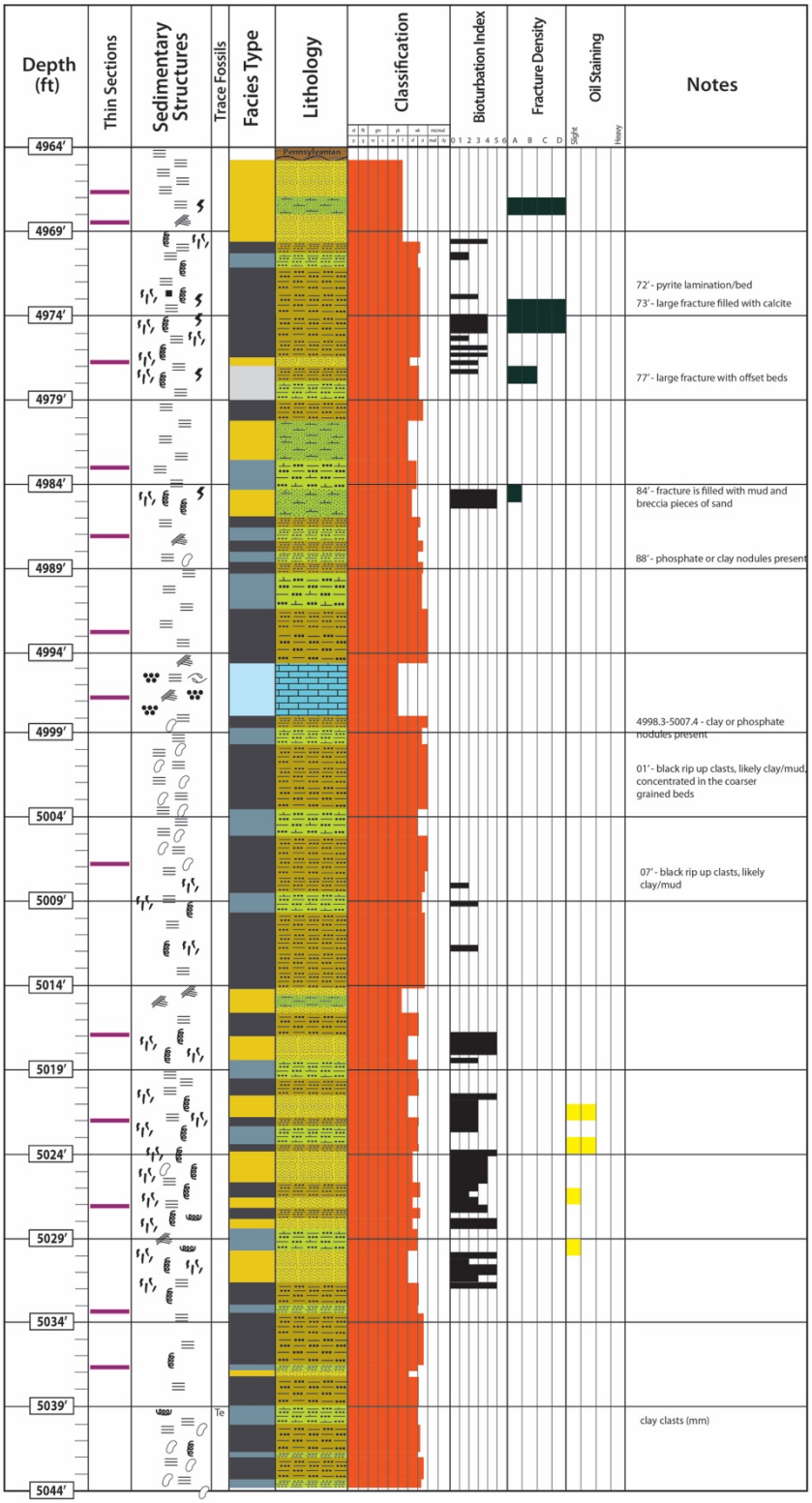

# Devon Energy - Doberman #1-25 SWD, Lincoln County, OK

Formation: "Mississippian Limestone"

Depth Interval: 5044' - 5124'

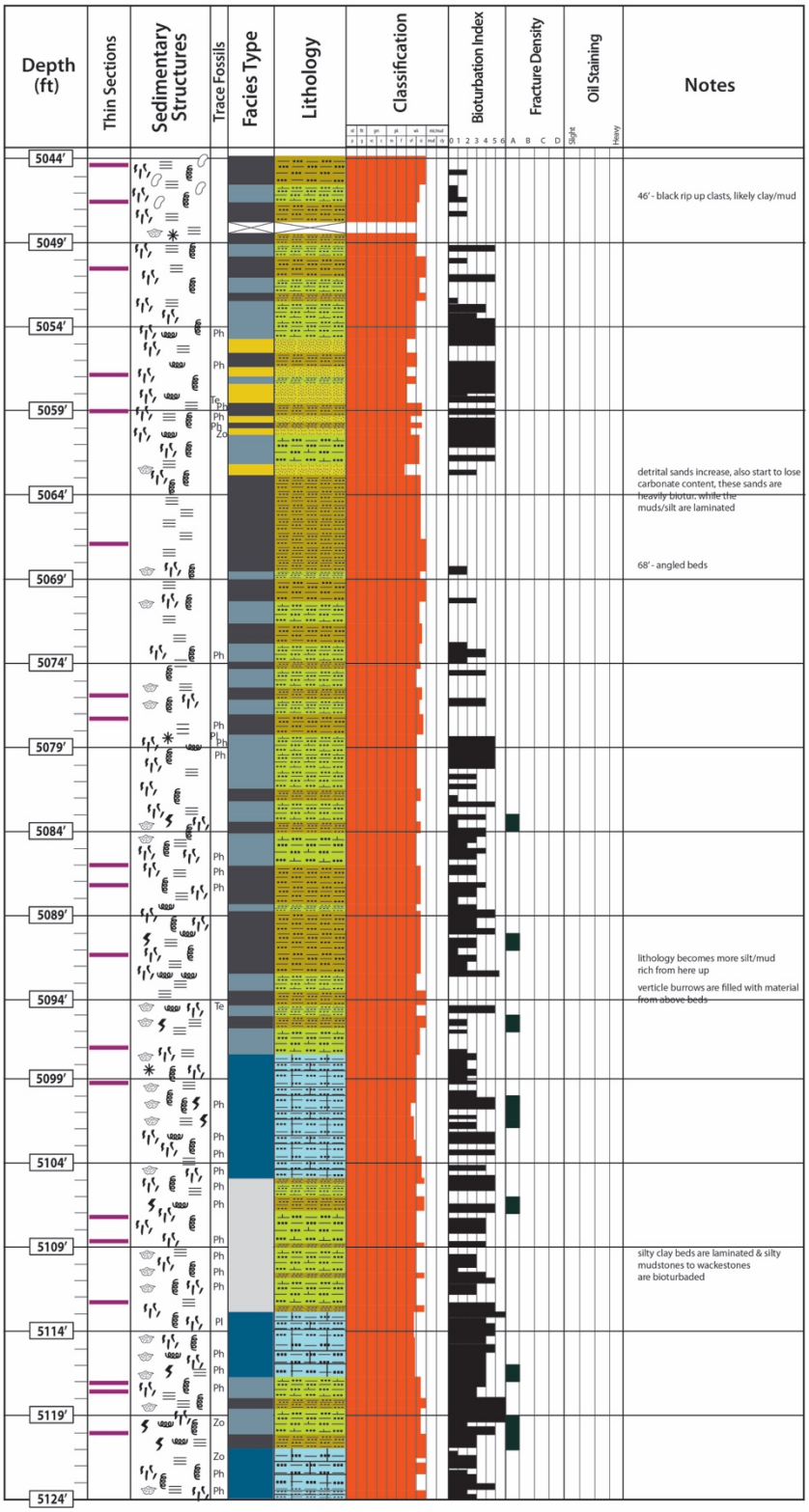

# Devon Energy - Doberman #1-25 SWD, Lincoln County, OK

Formation: "Mississippian Limestone"

Depth Interval: 5124' - 5204'

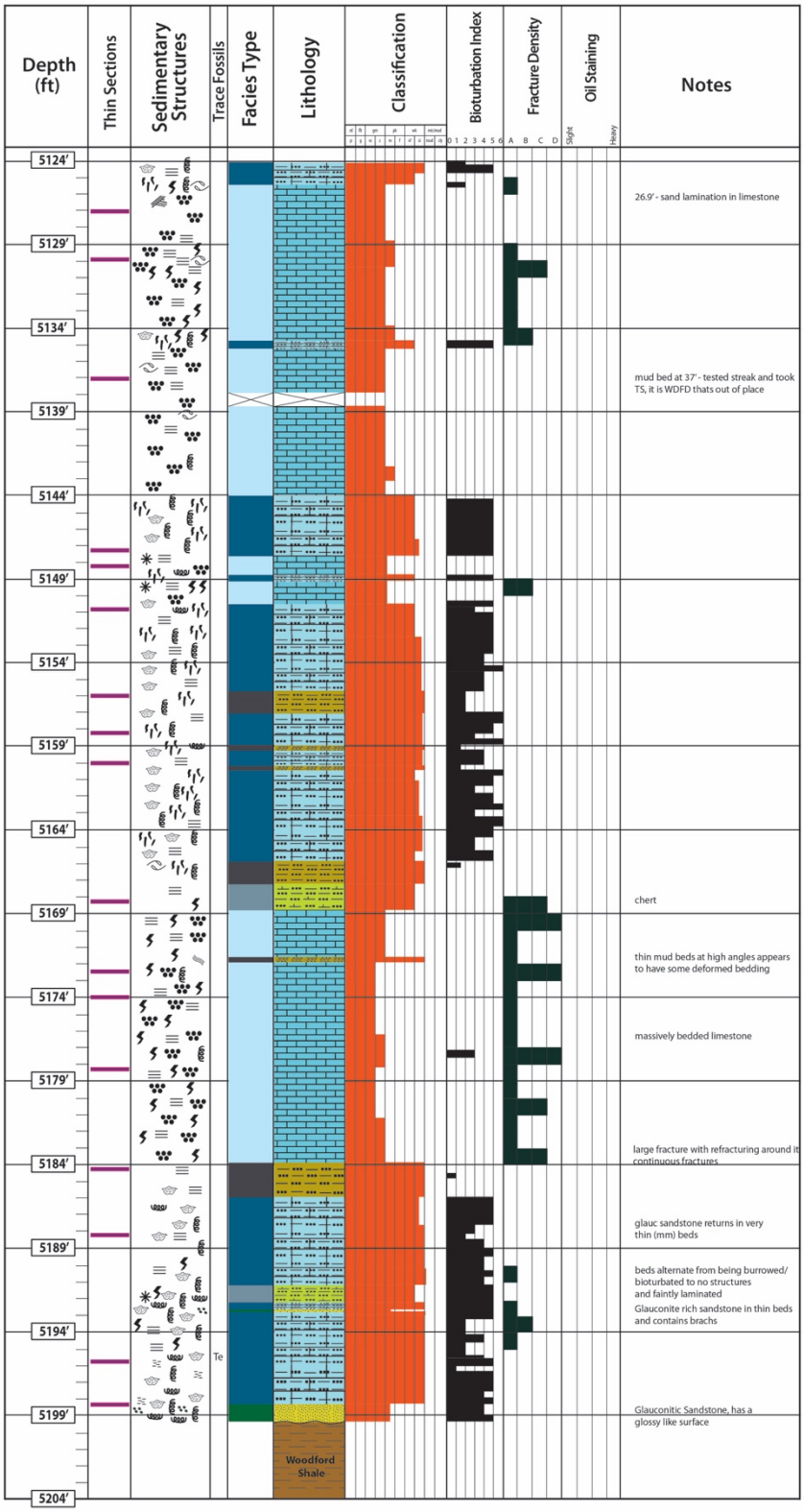

## Core to Wireline Log Correlation

**Devon Energy - Doberman 1-25 SWD, Lincoln County, OK**

Formation: "Mississippian Limestone"

Depth Interval: 4964' - 5114'

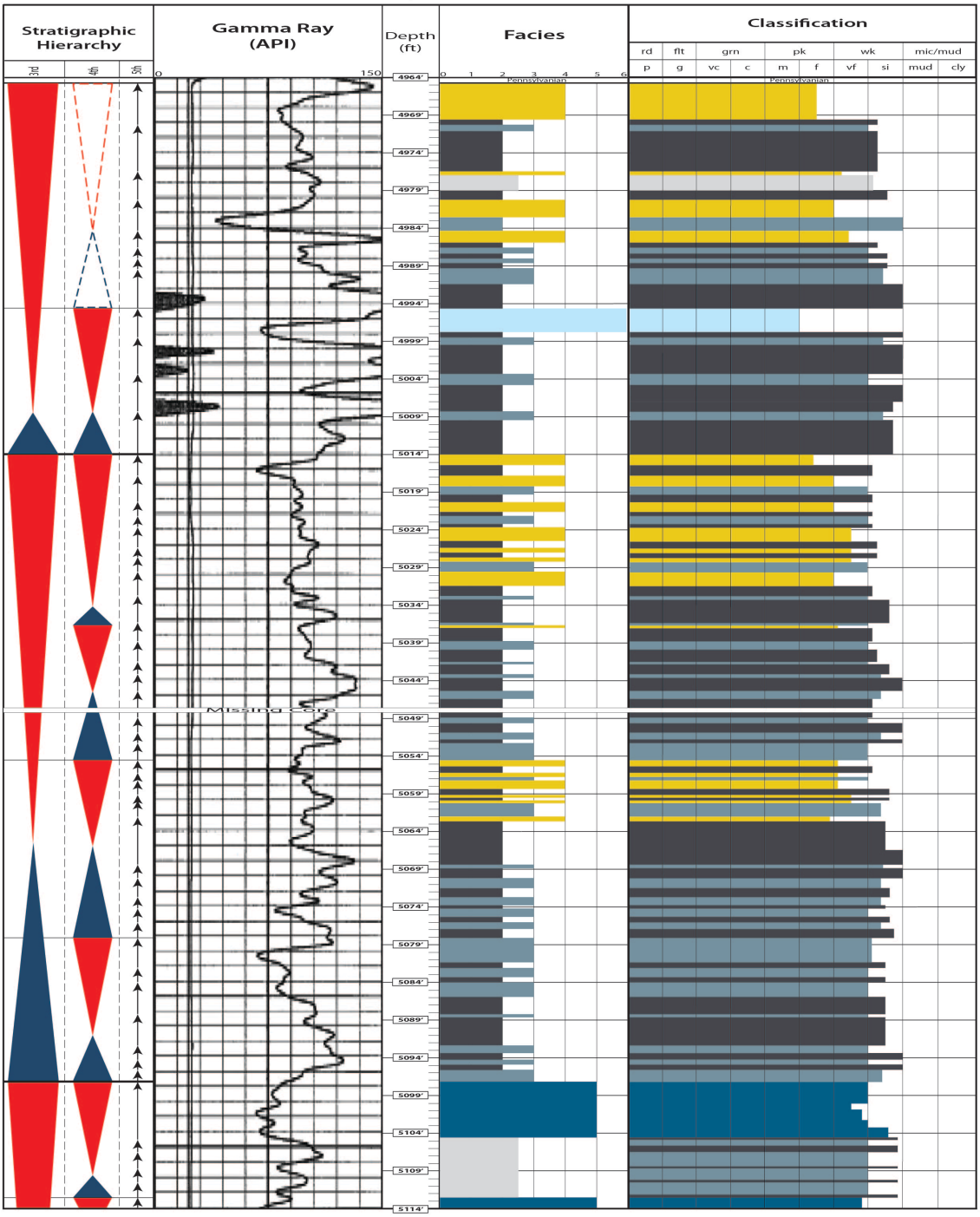

## Devon Energy - Doberman 1-25 SWD, Lincoln County, OK

Formation: "Mississippian Limestone"

Depth Interval: 5114' - 5204'

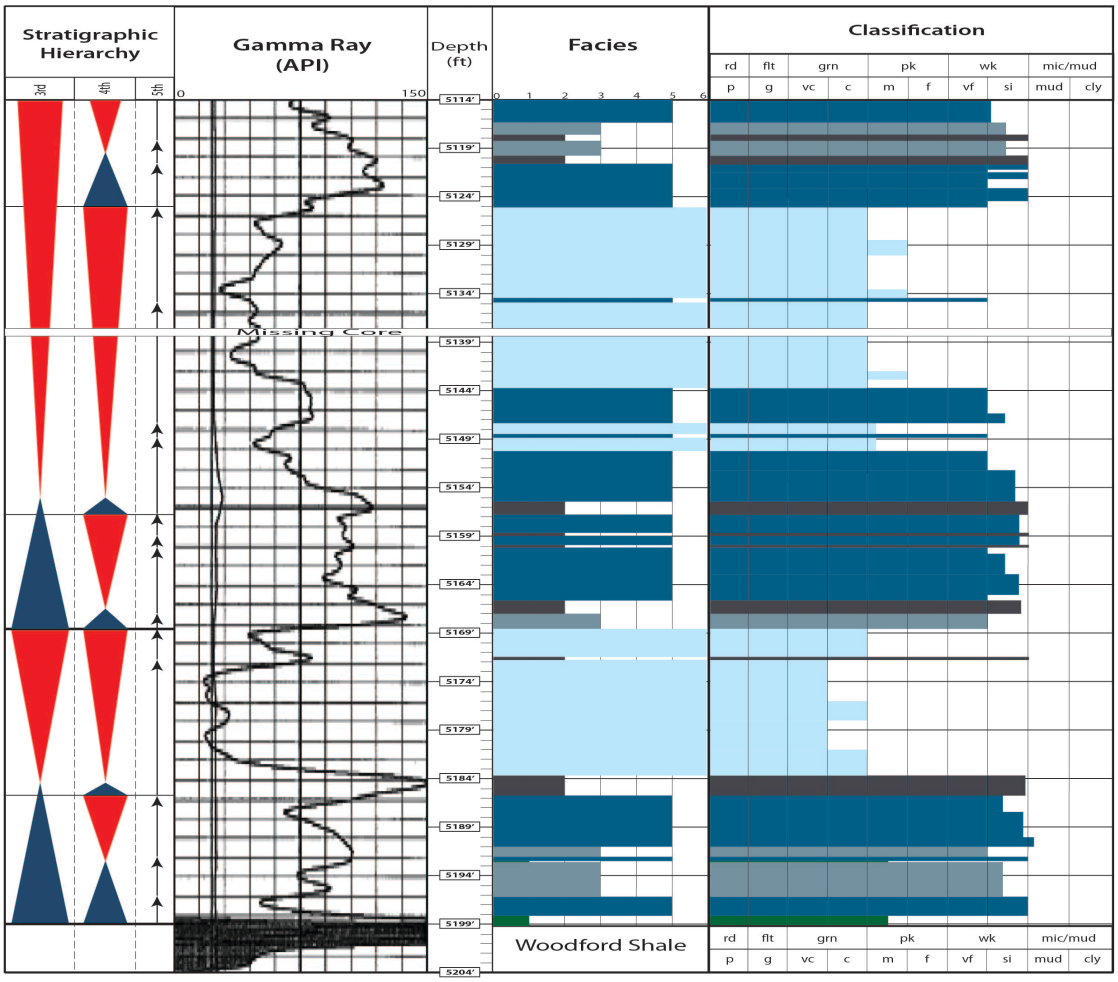


Facies 6 - Silty Peloidal Packstone - Grainstone

Facies 5 - Silty Burrowed Mudstone - Wackestone

Facies 4 - Silty Argillaceous Sandstone

Interbeded Facies 2&3

Facies 3 - Slightly Sandy Calcareous Siltstone

Facies 2 - Clay-rich Siltstone

Facies 1 - Glauconitic Sandstone

Missing Core

## III. Doberman #1-25 SWD Thin Section Photomicrographs

Thin section photomicrographs show enlarged views of samples that have been cut from the core. The samples and images shown are oriented as if looking at core, from shallower at the top of the image and deeper towards the base of the image. The images are formatted in order of facies (facies 1 - facies 6), and multiple images at magnifications of 2x and 5x are shown for each facies. All thin sections are blue epoxy impregnated, stained with alizarin red and potassium ferrocyanide on half of the slide. All photomicrographs are in plane polarized light (unless otherwise stated) and are labeled using the chart below.

| Doberman Thin Section Image Labels | | | |
|---|---|---|---|
| BR | brachiopod | ILL | illite/mica |
| BU | burrow | MG | micritized grain |
| CEM | calcite cement | MW | mud whisp |
| CG | calcite grain (indistinguishable) | OM | organic matter |
| CON | conodont | P | peloid |
| CR | crinoid | PH | phosphate |
| D | dolomite | PY | pyrite |
| FR | fracture | Q | quartz |
| G | glauconite | | |

Table 10. Abbreviations and their meanings used in labeling the thin sections for the Doberman #1-25 SWD core.

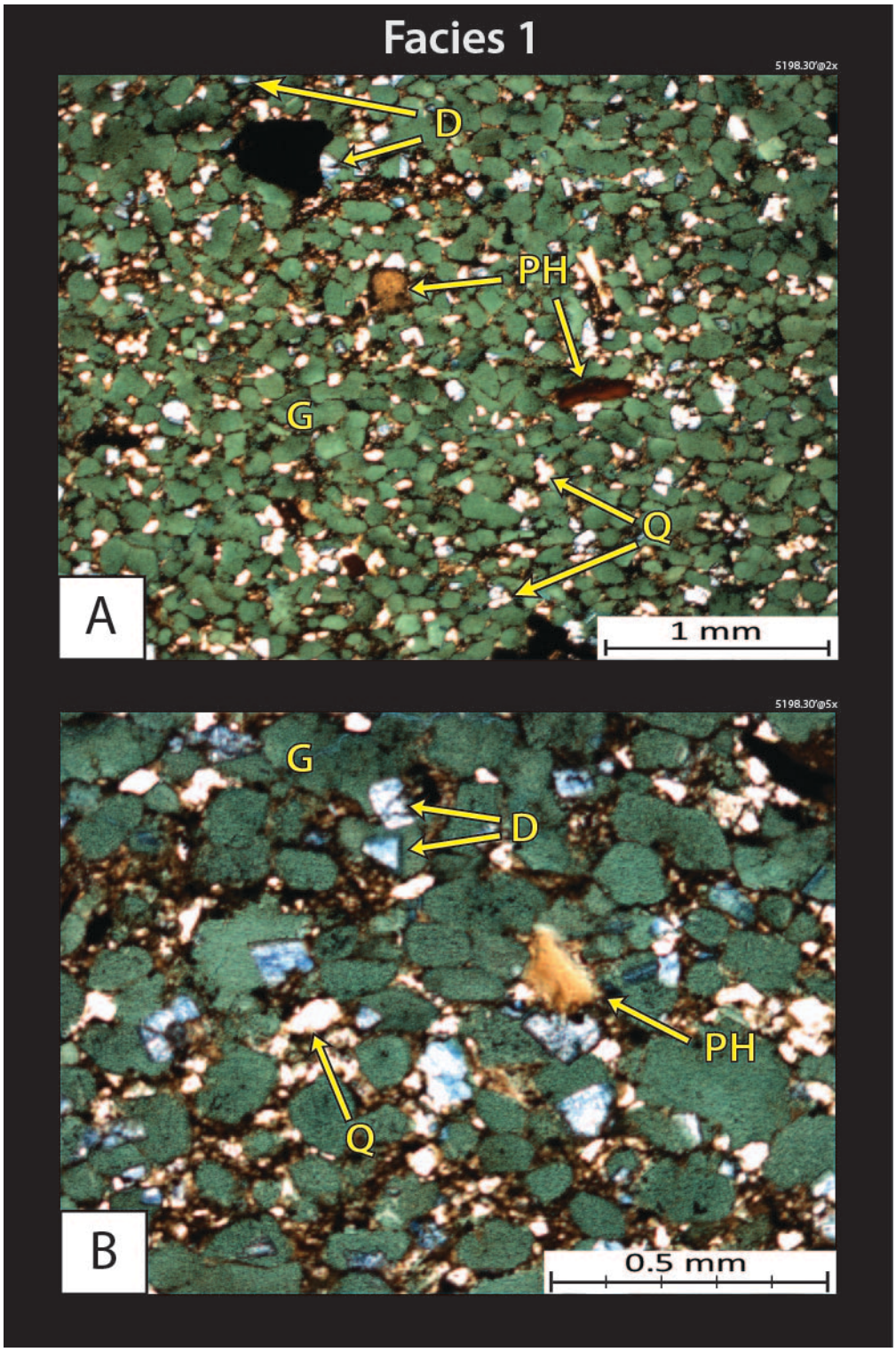


**5198.30' – Glauconitic sandstone.** Sample shows the sand sized glauconite (G) grains, silt to fine sand sized quartz (Q) grains, dolomite (D) grains and phosphate (PH) grains. XRD analysis: 45% quartz, 3% carbonates (3% dolomite), 37% clays (28% illite/mica, 9% mixed layer illite/smectite), and 15% other minerals (5% plagioclase feldspar, 4% potassium feldspar, 5% pyrite, and 1% marcasite).

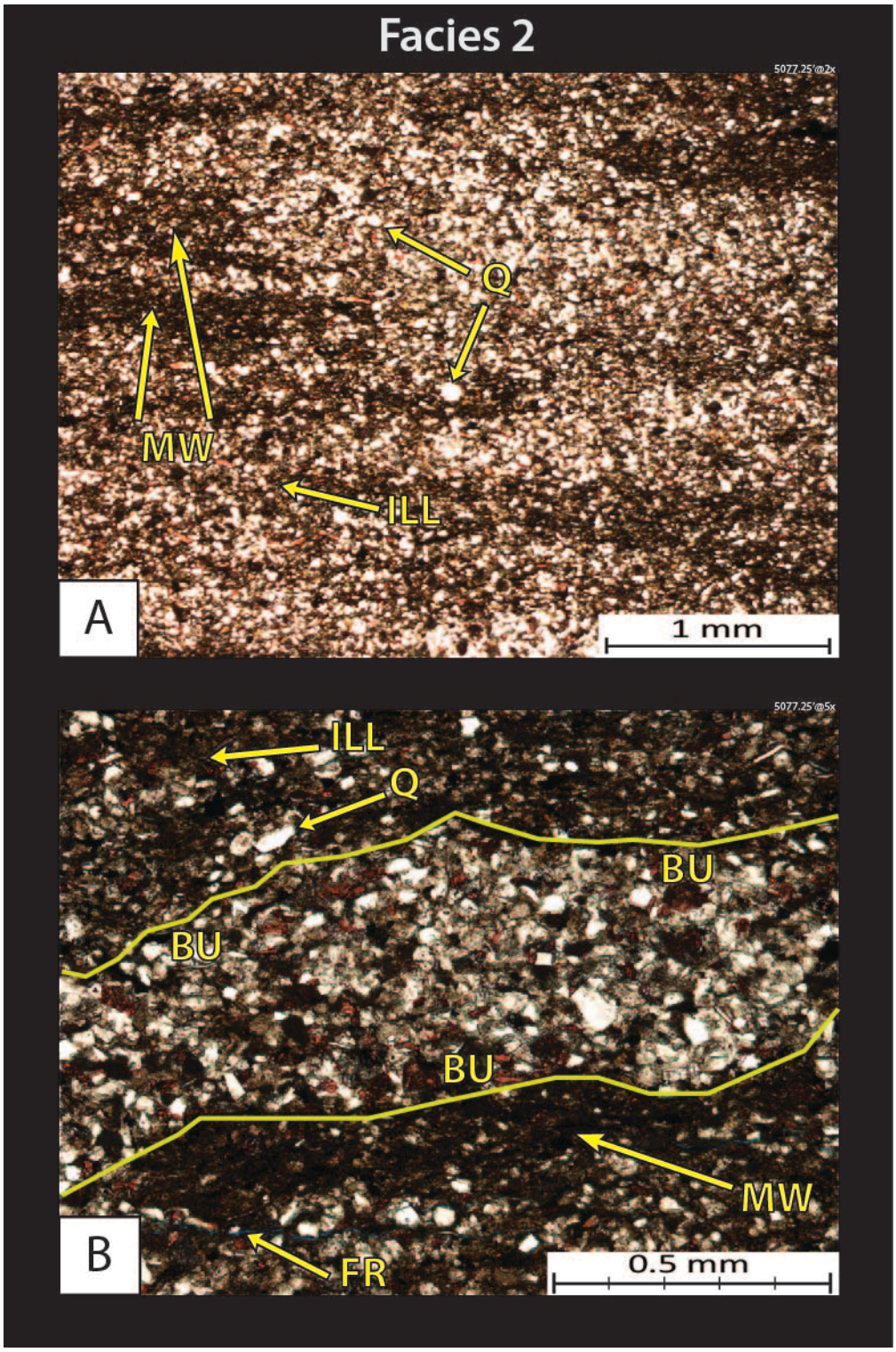


**5077.25' – Clay-rich siltstone.** Sample shows silt sized quartz grains (Q), clays-mainly illite (ILL), and displays burrowing (BU). XRD Analysis: 41% quartz, 14% carbonates (13% calcite, 1% dolomite), 26% clays (20% illite/mica, 4% mixed layer illite/smectite, and 2% chlorite), and 19% other minerals (10% plagioclase feldspar, 5% potassium feldspar, 4% pyrite).

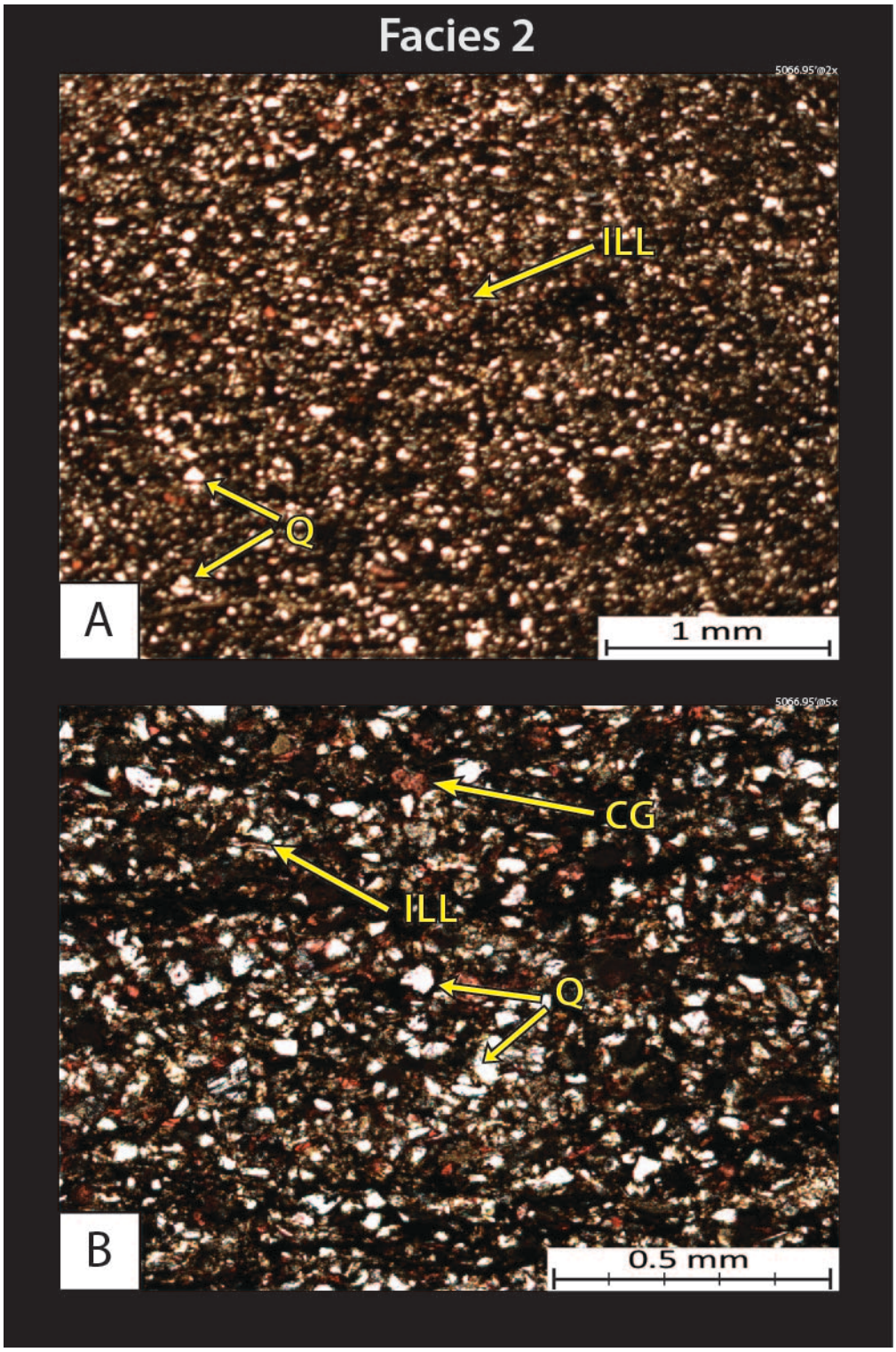


**5066.95' – Clay-rich siltstone.** Sample shows silt sized quartz grains (Q), indistinguishable calcite grains (CG), and clays-mainly illite (ILL). XRD Analysis: 42% quartz, 22% carbonates (20% calcite, 2% dolomite), 22% clays (16% illite/mica, 4% chlorite, and 2% mixed layer illite/smectite), and 14% other minerals (9% plagioclase feldspar, 2% potassium feldspar, 2% pyrite, and 1% apatite).

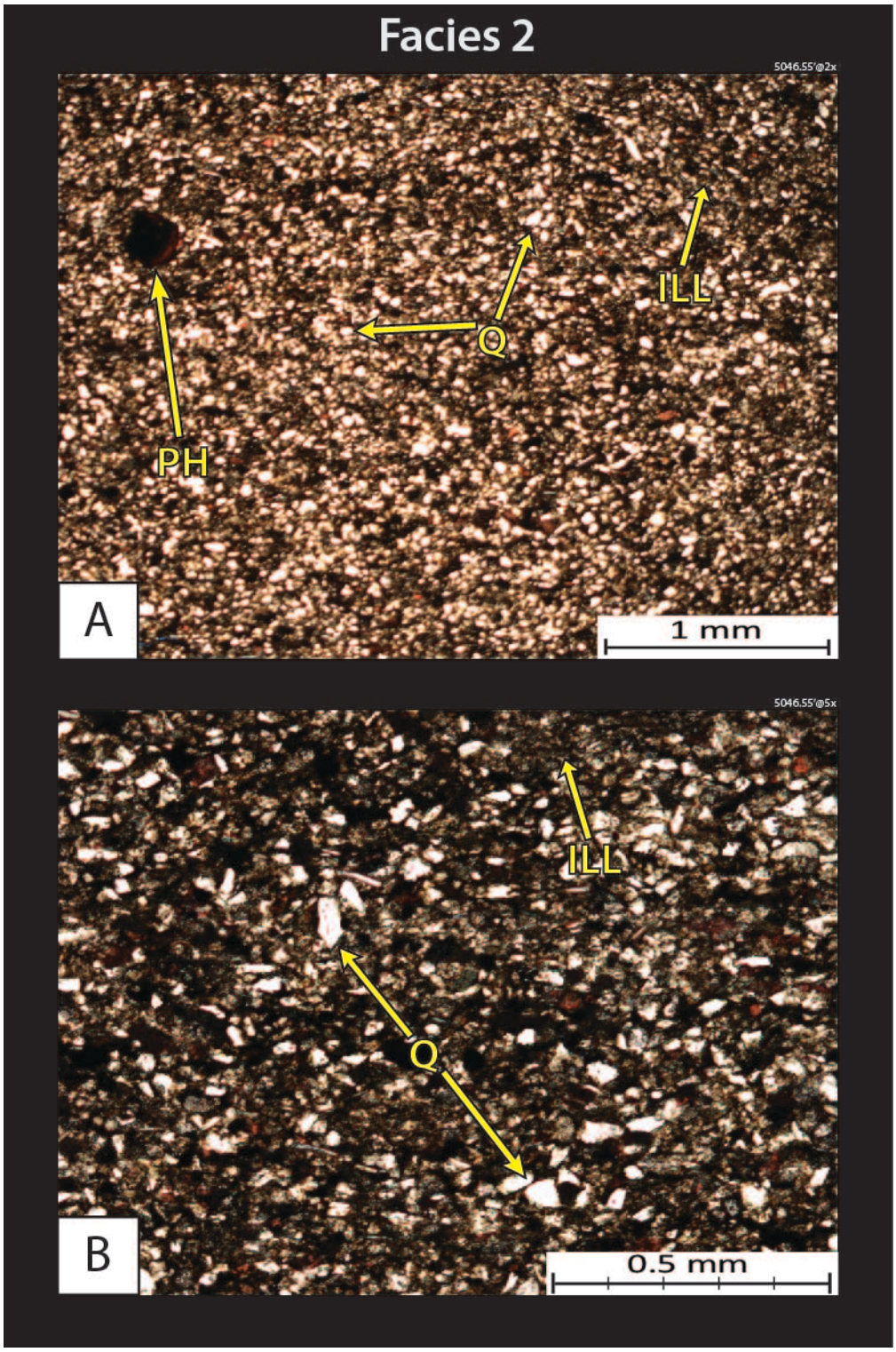


**5046.55' – Clay-rich siltstone.** Sample shows silt and VF sand sized quartz grains (Q), clays-mainly illite (ILL), and phosphate (PH). XRD Analysis: 50% quartz, 12% carbonates (10% calcite, 2% dolomite), 20% clays (15% illite/mica, 3% mixed layer illite/smectite, and 2% chlorite), and 18% other minerals (10% plagioclase feldspar, 4% potassium feldspar, 3% pyrite, and 1% apatite).

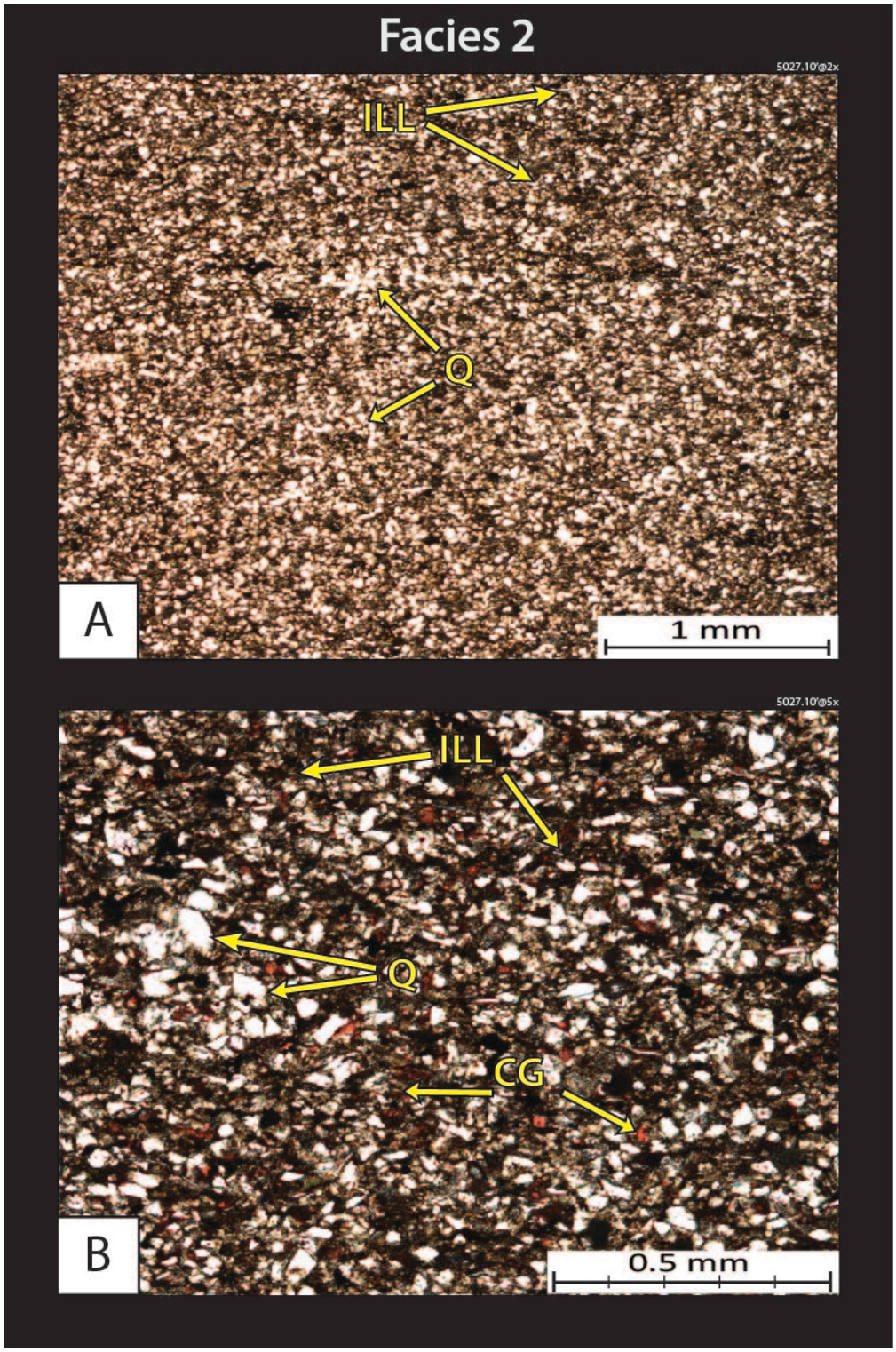


**5027.10' – Clay-rich siltstone.** Sample shows silt sized quartz grains (Q), indistinguishable calcite grains (CG), and clays-mainly illite (ILL). XRD Analysis: 44% quartz, 11% carbonates (10% calcite, 1% dolomite), 26% clays (19% illite/mica, 4% mixed layer illite/smectite, and 3% chlorite), and 19% other minerals (11% plagioclase feldspar, 4% potassium feldspar, 3% pyrite, and 1% apatite).

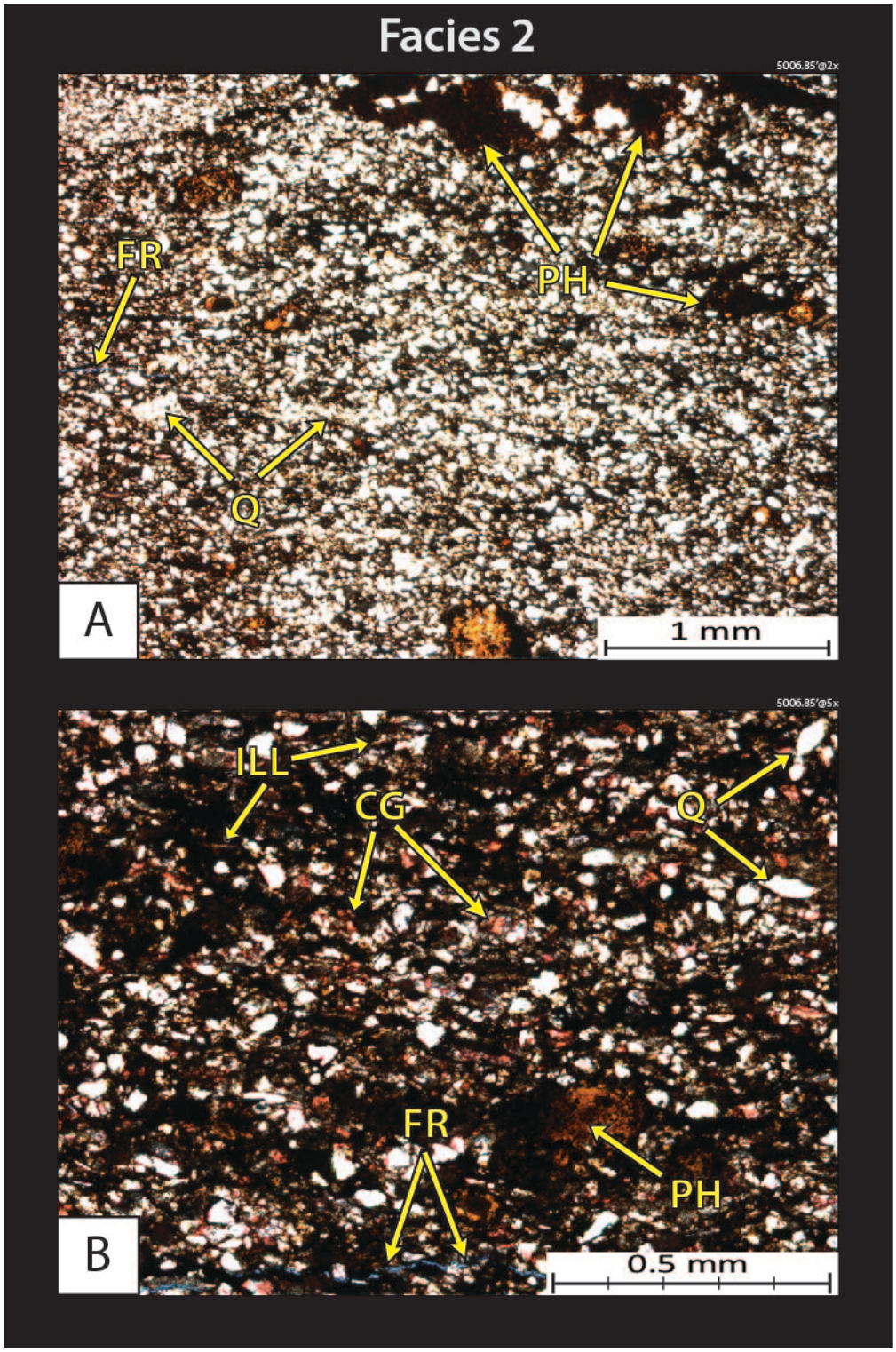


**5006.85' – Clay-rich siltstone.** Sample shows silt sized quartz grains (Q), indistinguishable calcite grains (CG), and clays-mainly illite (ILL), and phosphate (PH). XRD Analysis: 42% quartz, 17% carbonates (14% calcite, 3% dolomite), 20% clays (15% illite/mica, 3% mixed layer illite/smectite, and 2% chlorite), and 21% other minerals (10% plagioclase feldspar, 6% apatite, 3% potassium feldspar, and 2% pyrite).

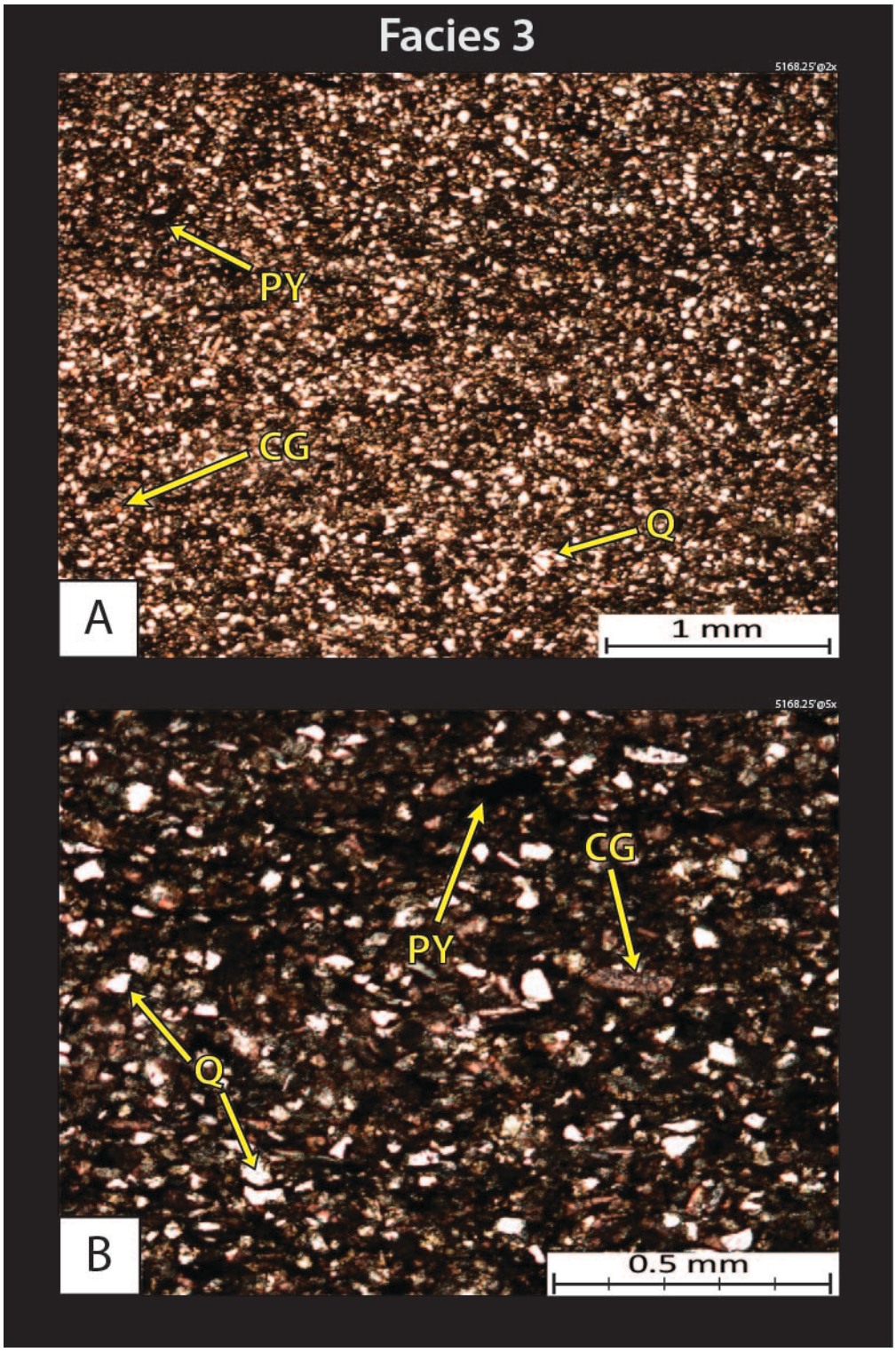


**5168.25' – Slightly sandy calcareous siltstone.** Sample shows silt to VF sand sized quartz grains (Q), calcite grains (indistinguishable), and pyrite (PY). Usually the calcite grains in this facies are indistinguishable bioclasts or micritized grains, when the grains are recognizable; they are generally brachiopod and crinoid fragments. XRD Analysis: 37% quartz, 35% carbonates (34% calcite, 1% dolomite), 15% clays (9% illite/mica, 4% mixed layer illite/smectite, and 2% chlorite), and 13% other minerals (8% plagioclase feldspar, 2% apatite, 2% potassium feldspar, and 1% pyrite).

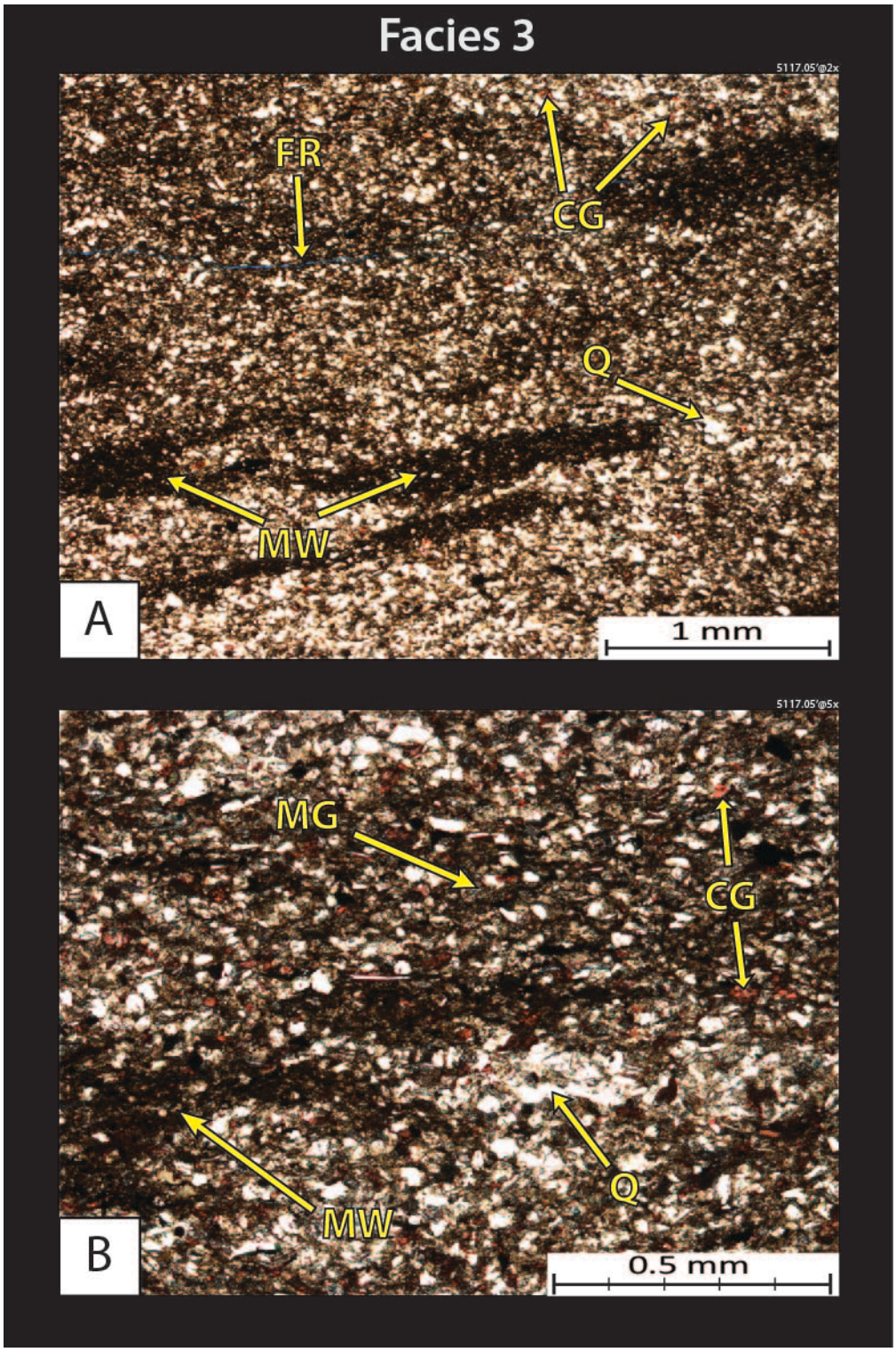


**5117.05' – Slightly sandy calcareous siltstone.** Sample shows silt to sand size quartz grains (Q), calcite grains- possibly crinoids (CG), and micritized grains (MG). XRD Analysis: 48% quartz, 21% carbonates (19% calcite, 2% dolomite), 17% clays (10% illite/mica, 5% mixed layer illite/smectite, and 2% chlorite), and 14% other minerals (9% plagioclase feldspar, 4% potassium feldspar, and 1% pyrite).

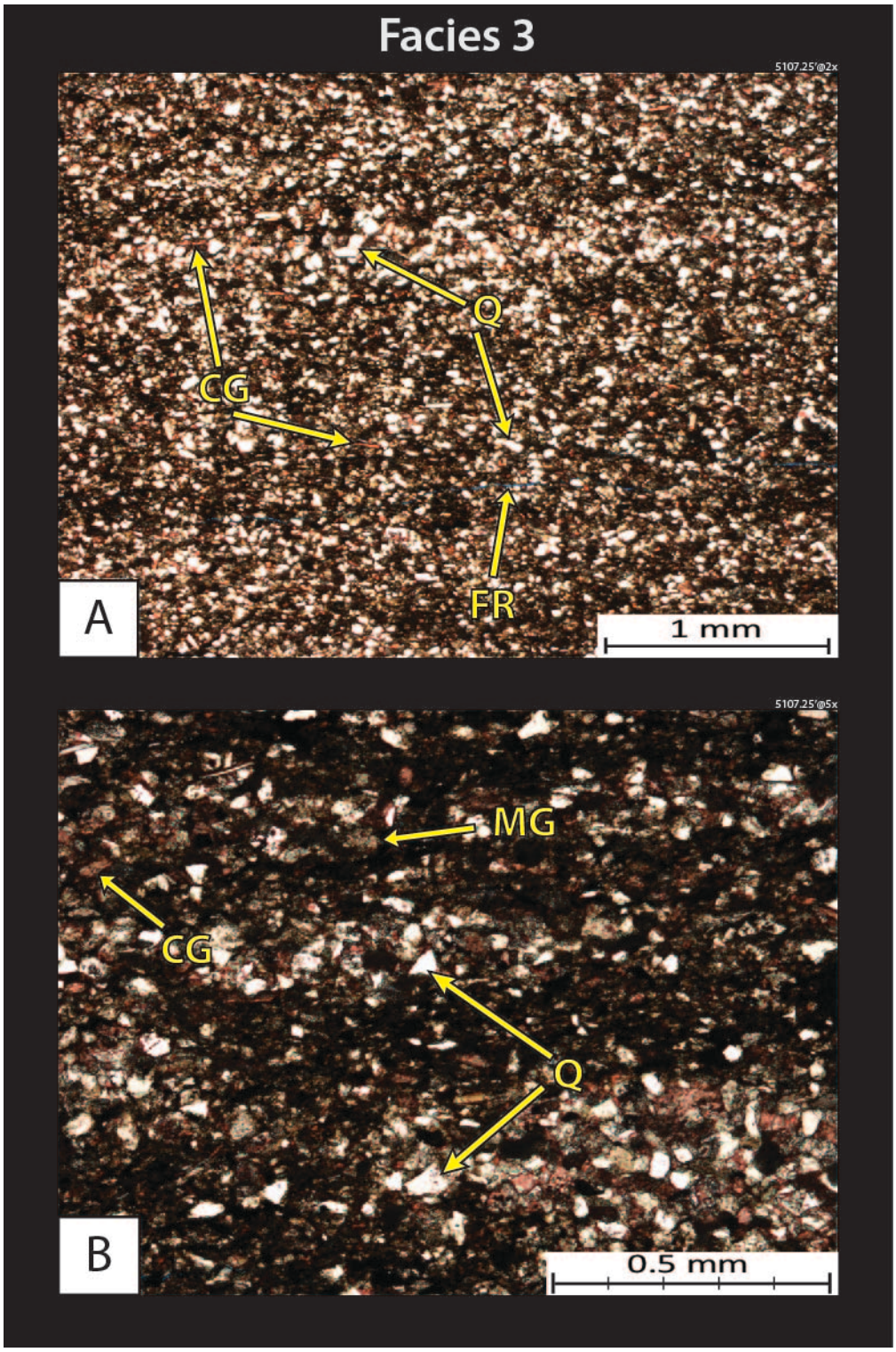


**5107.25' – Slightly sandy calcareous siltstone.** Sample is dominated by silt to very fine sand sized quartz (Q) grains, carbonate – mainly calcite (pink) grains, occasional clays – mainly illite, and a muddy organic-rich matrix. XRD analysis: 42% quartz, 25% carbonates (22% calcite and 3% dolomite), 18% clays (12% illite, 5% illite/smectite, and 1% chlorite), and 15% other minerals (9% plagioclase feldspar, 4% potassium feldspar, and 2% pyrite).

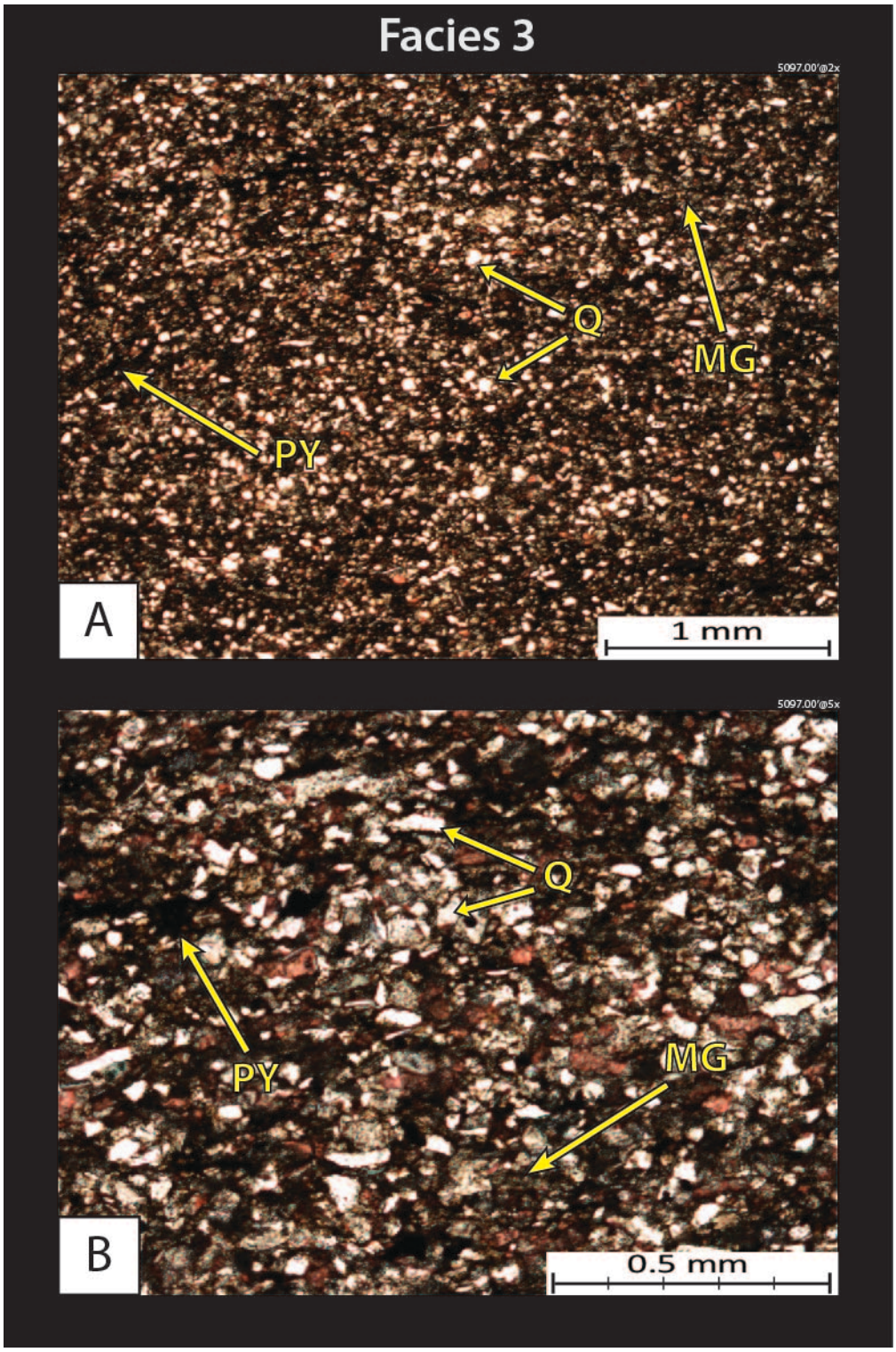


**5097.00' – Slightly sandy calcareous siltstone.** Sample is dominated by silt to VF sand sized quartz grains (Q), carbonate – mainly calcite (pink) grains, and occasional clays – mainly illite. XRD analysis: 46% quartz, 24% carbonates (19% calcite and 5% dolomite), 15% clays (11% illite, 2% illite/smectite, and 2% chlorite), and 15% other minerals (10% plagioclase feldspar, 3% potassium feldspar, and 2% pyrite).

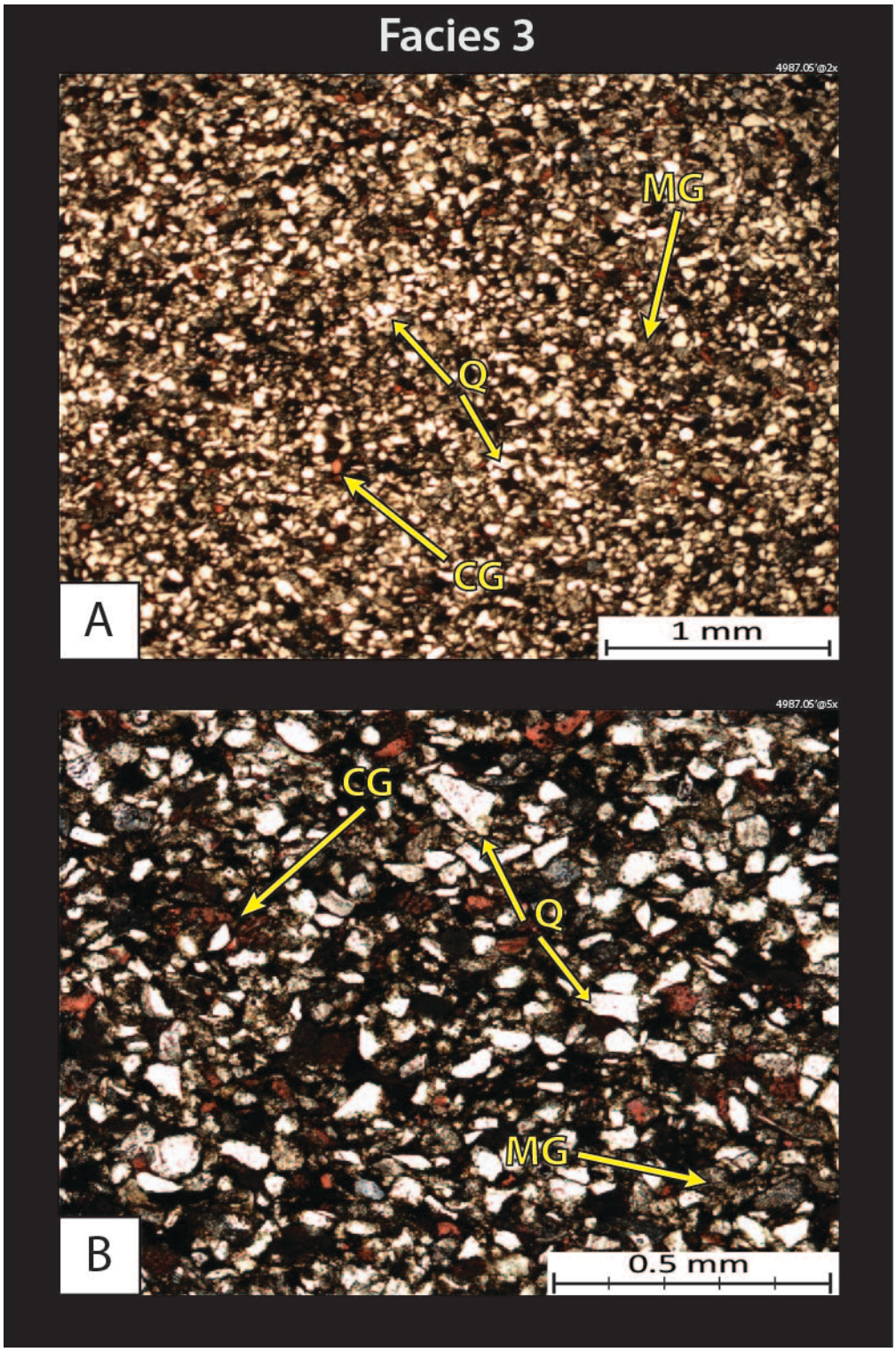


**4987.05' – Slightly sandy calcareous siltstone.** Sample is dominated by silt to very fine sand sized quartz (Q) grains, carbonate – mainly calcite (pink) grains and micritized grains, occasional clays – mainly illite, and a muddy organic-rich matrix. XRD analysis: 60% quartz, 13% carbonates (11% calcite and 2% dolomite), 12% clays (9% illite, 2% illite/smectite, and 1% chlorite), and 15% other minerals (9% plagioclase feldspar, 4% potassium feldspar, and 2% pyrite).

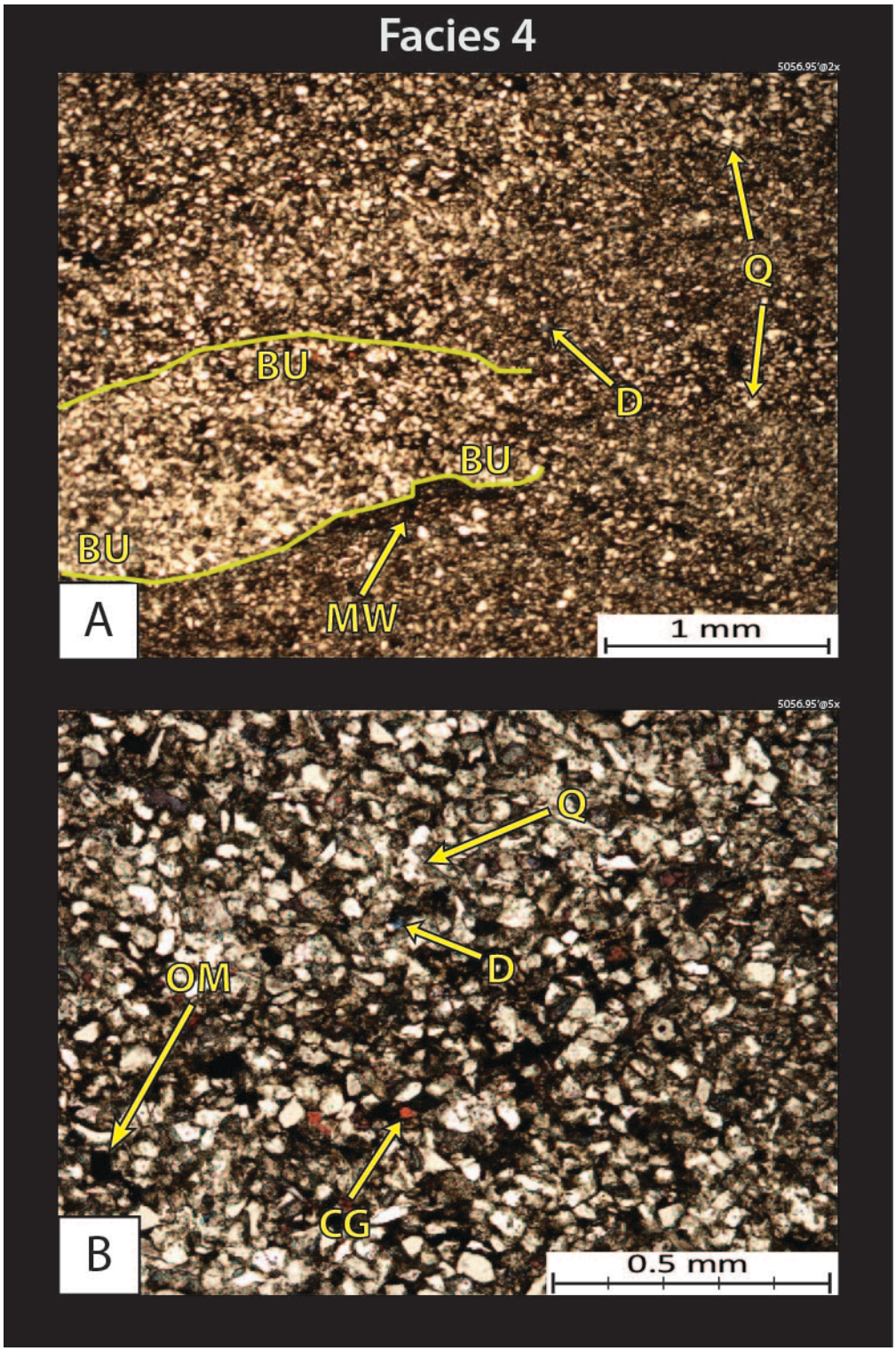


**5056.95' – Silty argillaceous sandstone.** This facies is dominated by very fine to fine sand sized quartz (Q) grains as well as silt sized quartz grains in areas, carbonate – mainly calcite (pink) grains, and clays. Calcite grains are commonly brachiopod fragments and indistinguishable bioclasts. XRD analysis: 60% quartz, 7% carbonates (5% calcite and 2% dolomite), 15% clays (11% illite, 2% illite/smectite, and 2% chlorite), and 18% other minerals (12% plagioclase feldspar, 4% potassium feldspar, 1% pyrite, and 1% apatite).

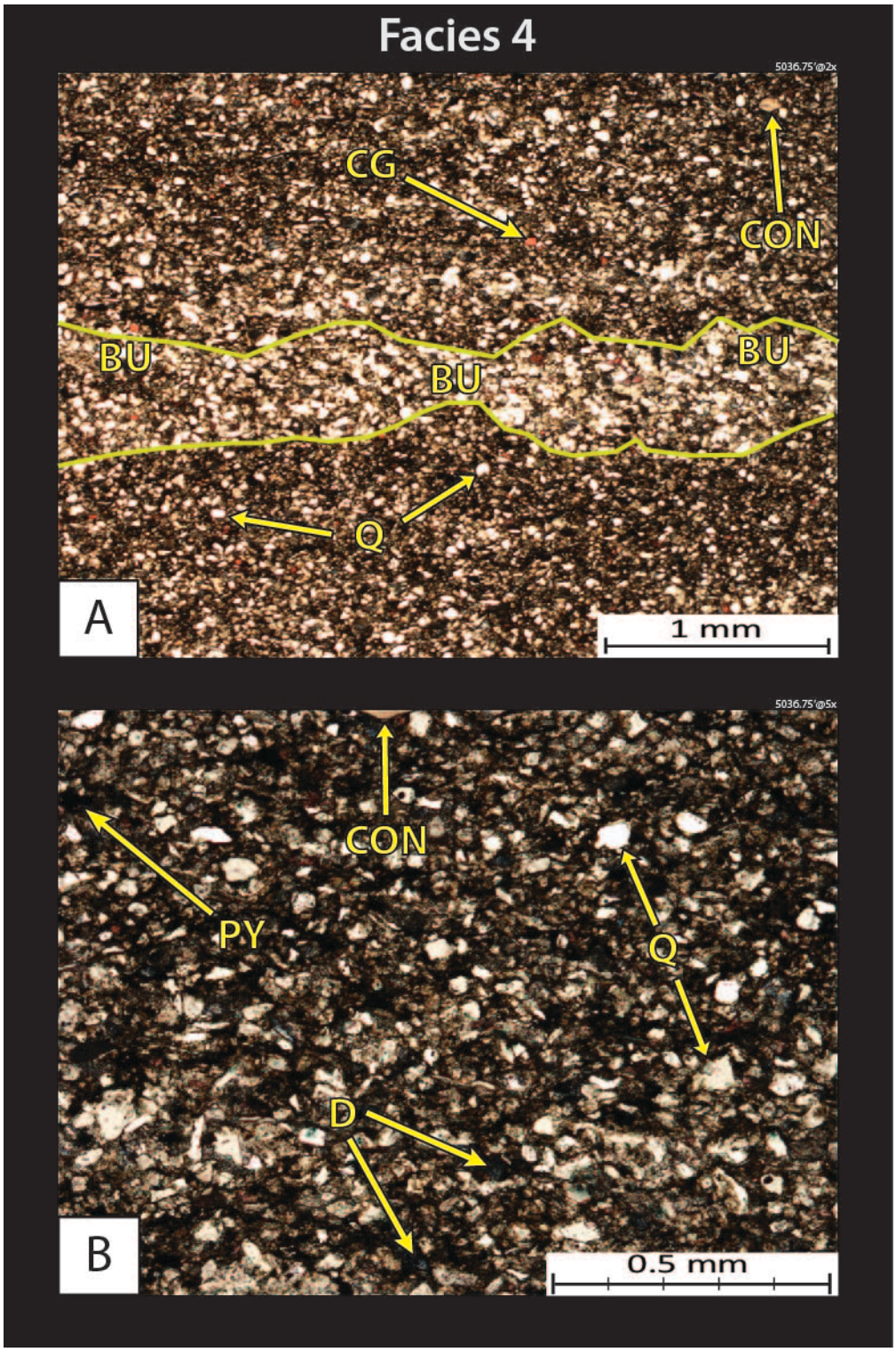


**5036.75' – Silty argillaceous sandstone.** Sample is dominated by very fine to fine sand sized quartz (Q) grains as well as silt sized quartz grains in areas, and clays-mainly illite. XRD Analysis: 54% quartz, 9% carbonates (5% dolomite, and 4% calcite), 18% clays (14% illite, 3% chlorite, and 1% illite/smectite), and 19% other minerals (12% plagioclase feldspar, 5% potassium feldspar, 2% pyrite, and Tr apatite).

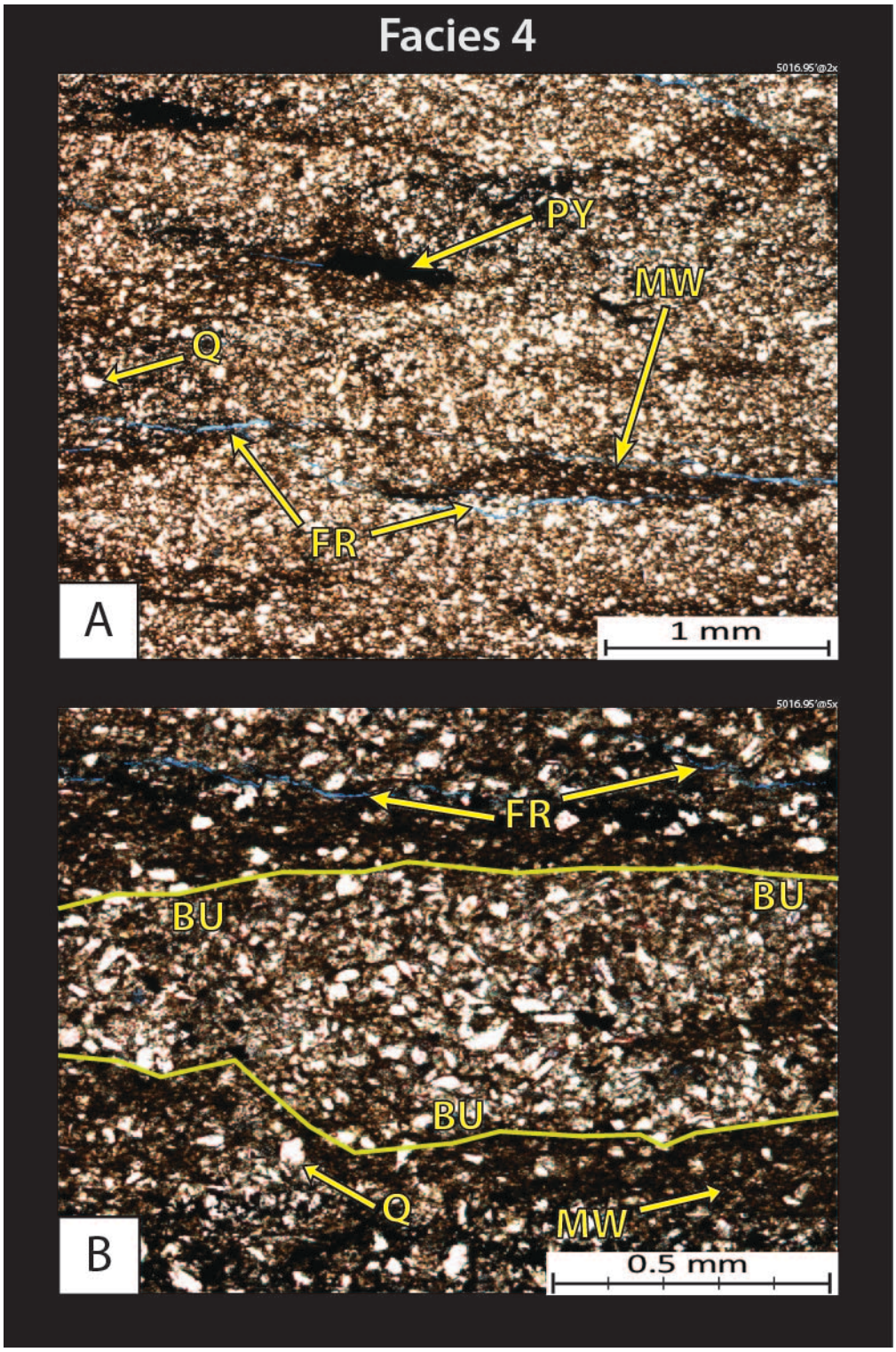


**5016.95' – Silty argillaceous sandstone.** Sample is dominated by very fine to fine sand sized quartz (Q) grains as well as silt sized quartz grains in areas, and clays. XRD Analysis: 50% quartz, 2% carbonates (1% dolomite, and 1% calcite), 27% clays (20% illite, 4% illite/smectite, and 3% chlorite), and 21% other minerals (12% plagioclase feldspar, 6% potassium feldspar, 2% pyrite, and 1% apatite).

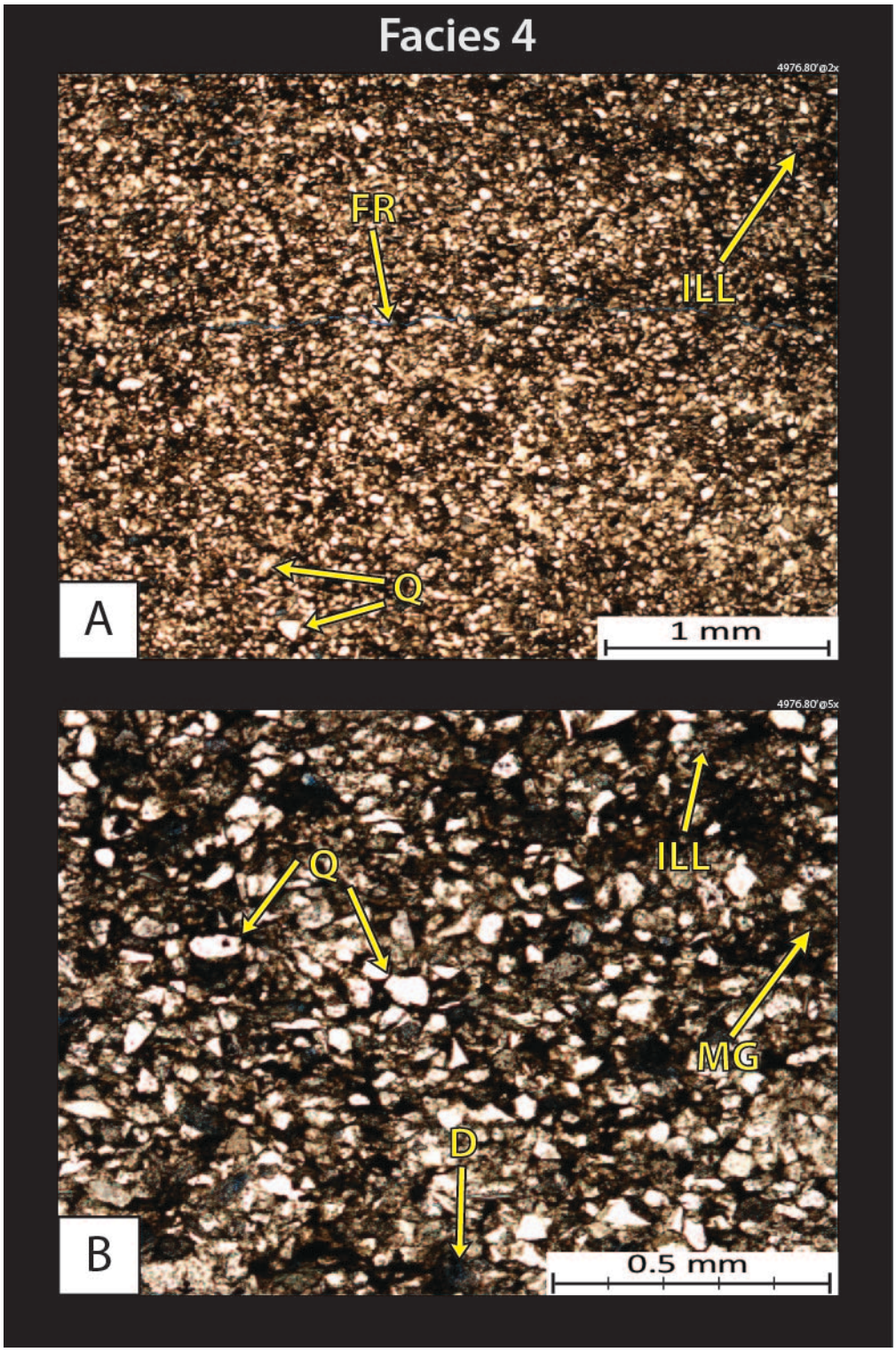


**4976.80' – Silty argillaceous sandstone.** Sample is dominated by very fine to fine sand sized quartz (Q) grains as well as silt sized quartz grains in areas, and clays. XRD Analysis: 64% quartz, 3% carbonates (2% dolomite, and 1% calcite), 17% clays (13% illite, 3% illite/smectite, and 1% chlorite), and 16% other minerals (10% plagioclase feldspar, 4% potassium feldspar, 1% pyrite, and 1% apatite).

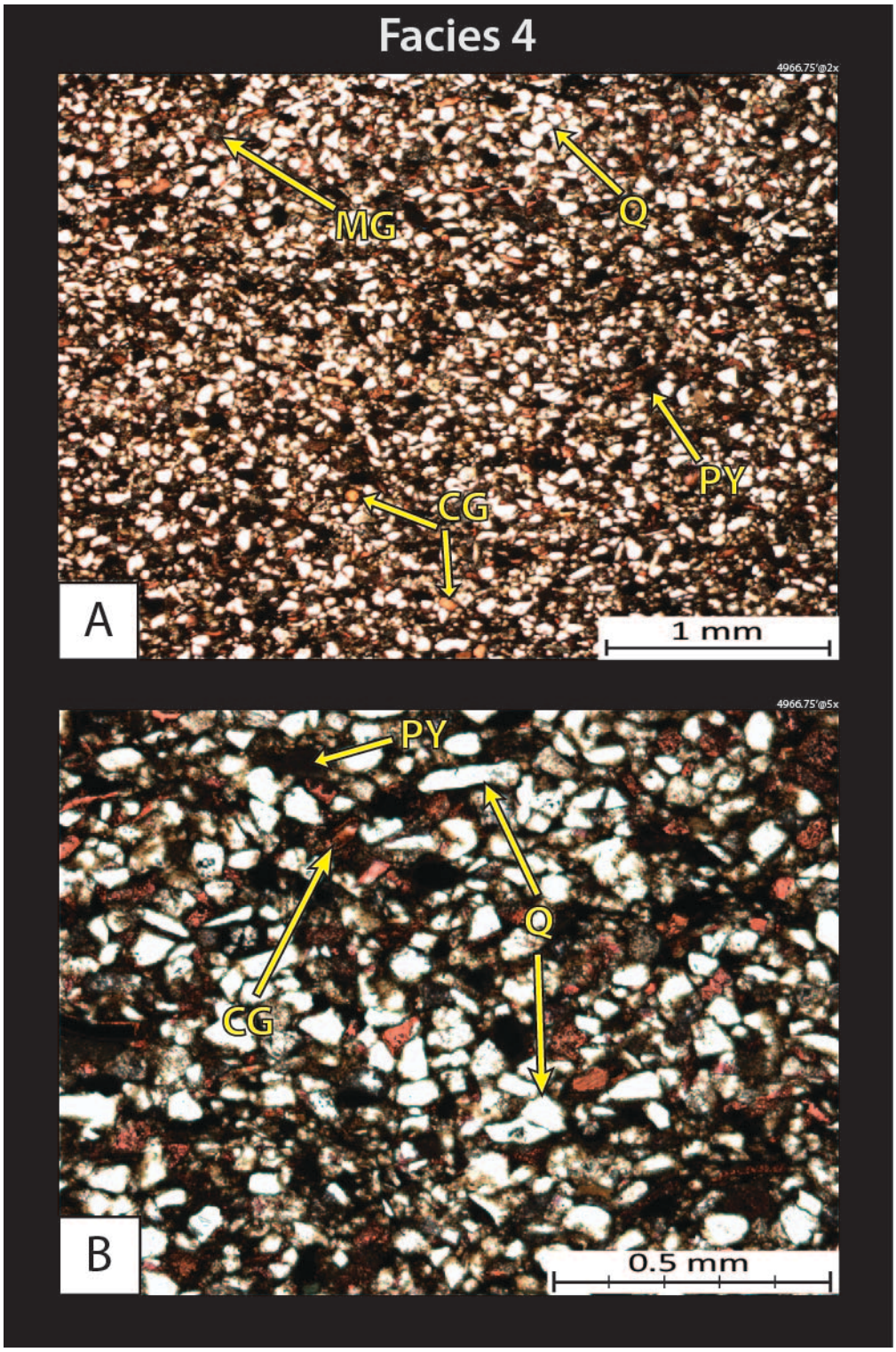


**4966.75' – Silty argillaceous sandstone.** The sample is dominated by very fine to fine sand sized quartz (Q) grains as well as silt sized quartz grains in areas, carbonate – mainly calcite (pink) grains, and some clays. Calcite grains are commonly brachiopod fragments and indistinguishable bioclasts. XRD analysis: 61% quartz, 12% carbonates (10% calcite and 2% dolomite), 12% clays (9% illite, 2% illite/smectite, and 1% chlorite), and 15% other minerals (9% plagioclase feldspar, 4% potassium feldspar, 2% pyrite, and trace amounts of apatite).

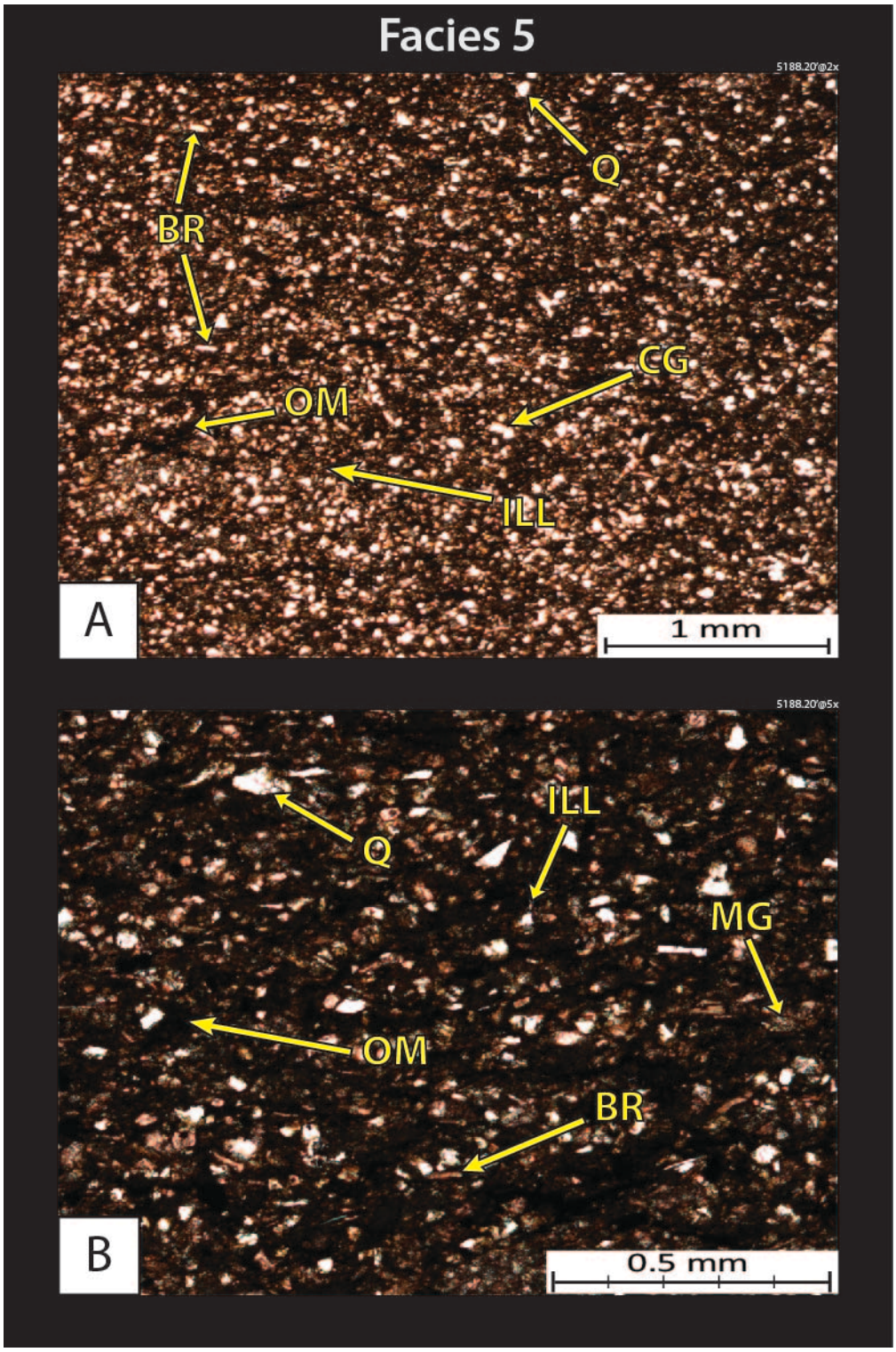


**5188.20' – Silty burrowed mudstone to wackestone.** This facies commonly contains abundant silt to very fine sand sized quartz (Q) grains, carbonate – calcite (pink) grains, brachiopods (BR), as well as clays (illite) in a muddy organic-rich matrix. XRD Analysis: 31% quartz, 46% carbonates (40% calcite and 6% dolomite), 15% clays (9% illite, 4% illite/smectite, and 2% chlorite), and 8% other minerals (5% plagioclase feldspar, 2% potassium feldspar, 1% pyrite, and trace amounts of apatite).

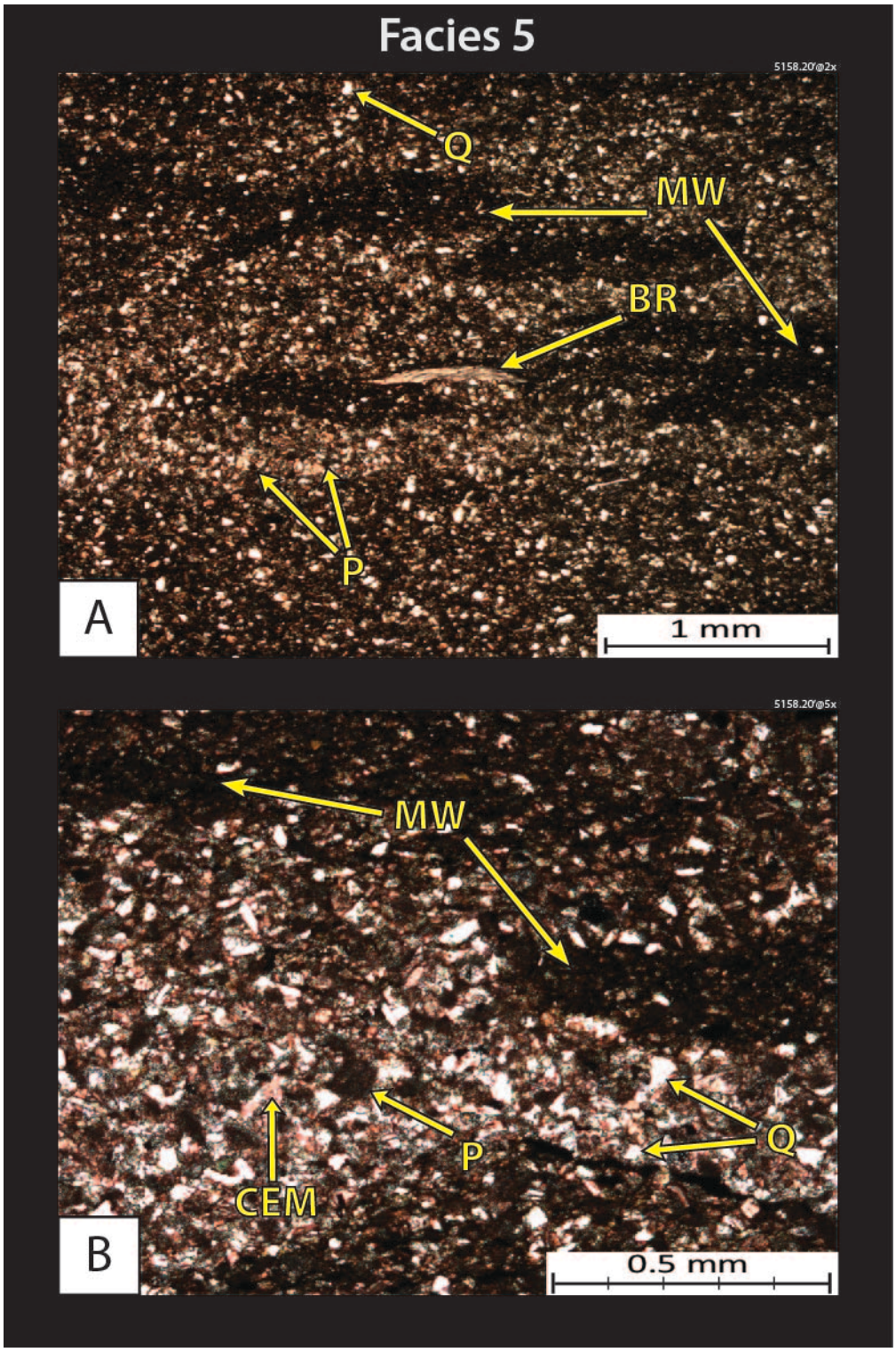


**5158.20' – Silty burrowed mudstone to wackestone.** The sample contains abundant silt to very fine sand sized quartz (Q) grains, carbonate – calcite (pink) grains, brachiopods (BR), as well as clays (illite) in a muddy organic-rich matrix. XRD analysis: 31% quartz, 46% carbonates (40% calcite, 6% dolomite), 15% clays (9% illite, 4% illite/smectite, 2% chlorite), and 8% other minerals (5% plagioclase feldspar, 2% potassium feldspar, 1% pyrite).

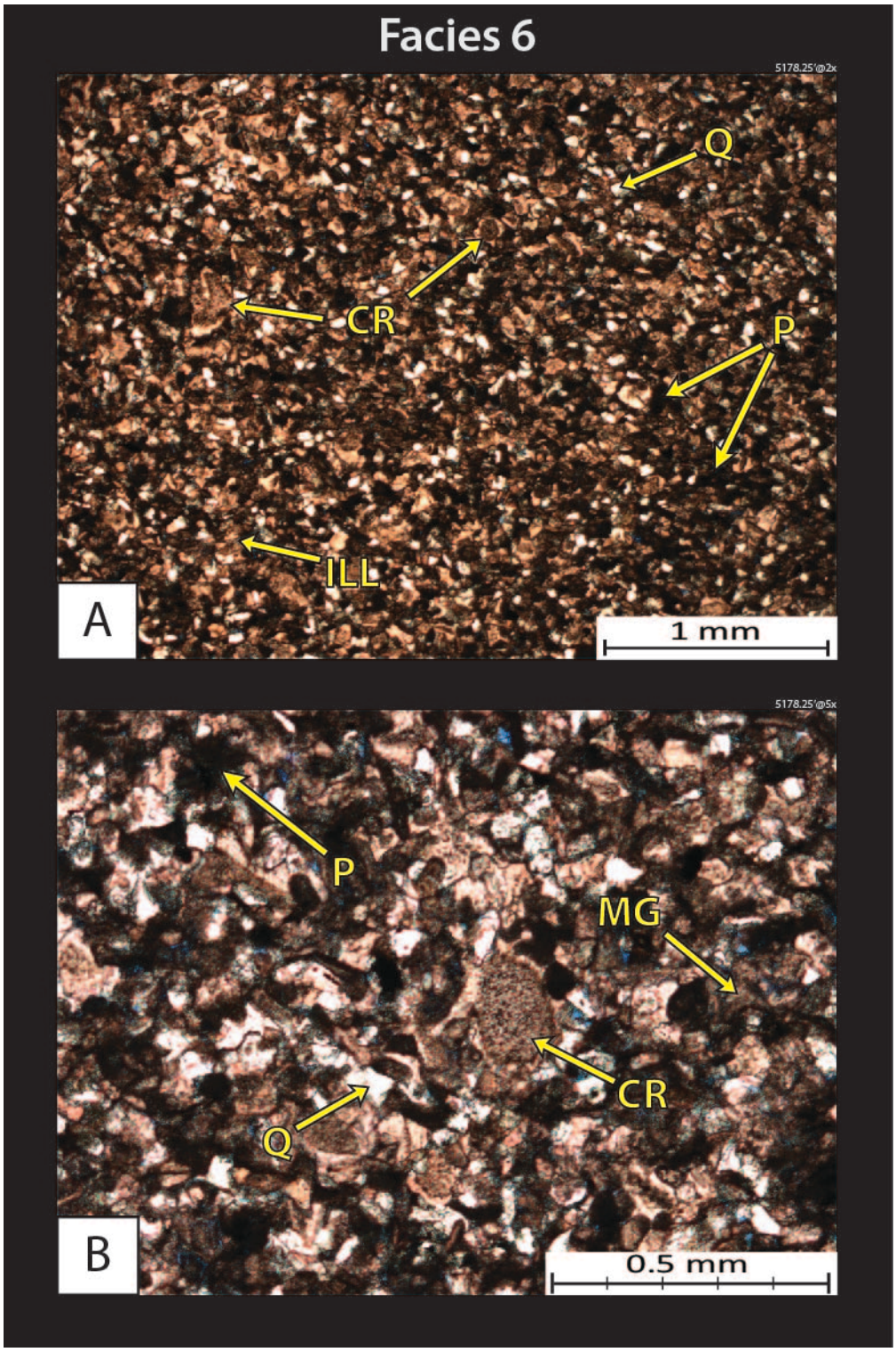


**5178.25' – Silty peloidal packstone to grainstone.** This facies is typically composed of silt to mostly sand sized peloid (P) grains, carbonate – mainly calcite (pink) grains, and silt to very fine sand sized quartz (Q) grains. It also contains skeletal debris such as, crinoids (CR) and brachiopods. XRD analysis: 22% quartz, 71% carbonates (65% calcite, 6% dolomite), 1% clay – illite, 6% other minerals (3% plagioclase feldspar, 1% potassium feldspar, 1% pyrite, 1% apatite).

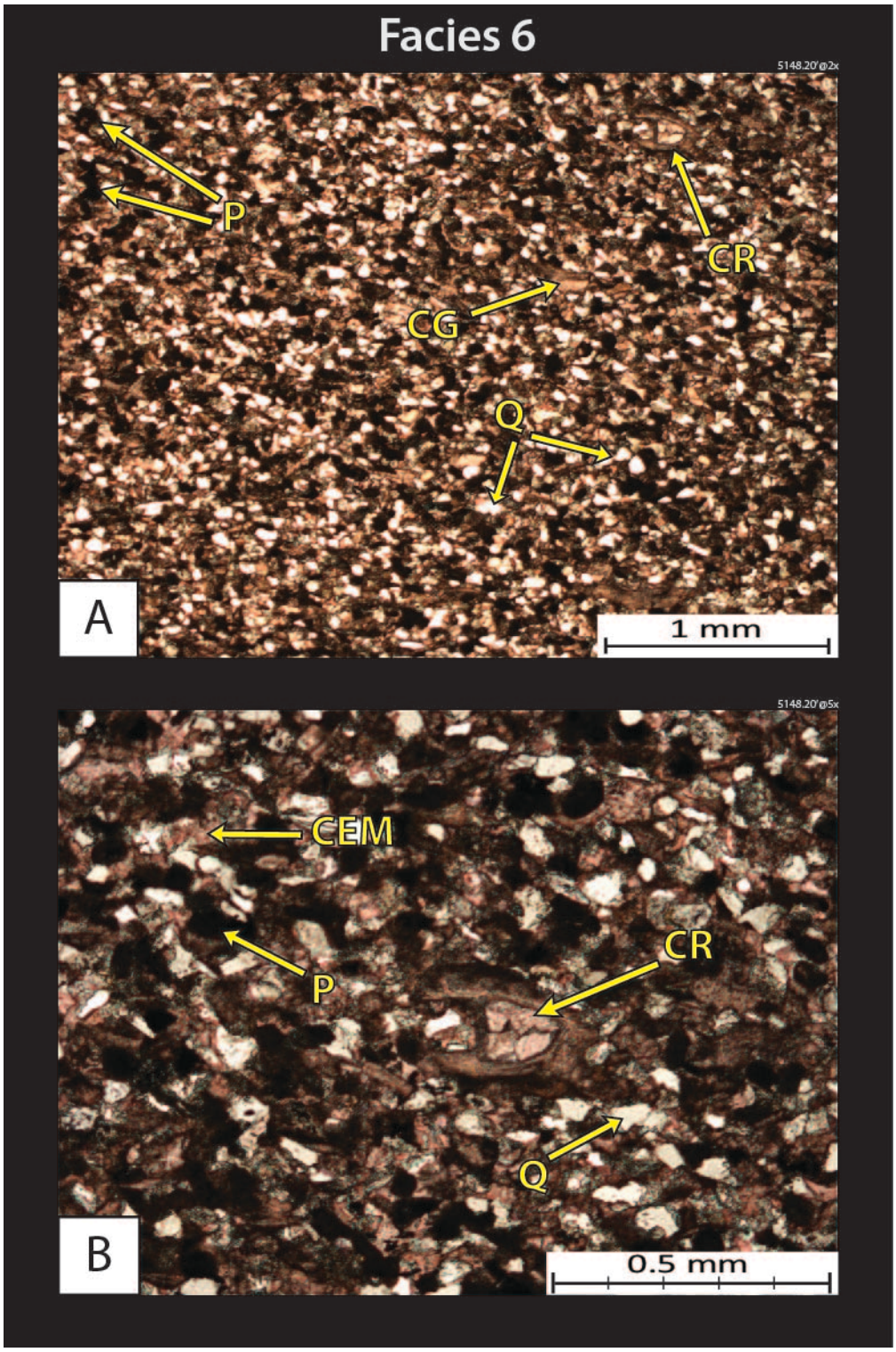


**5148.20' – Silty peloidal packstone to grainstone.** Sample is dominated by silt to mostly sand sized peloid (P) grains, carbonate – mainly calcite (pink) grains, and silt to very fine sand sized quartz (Q) grains. It also contains skeletal debris such as, crinoids (CR). XRD analysis: 35% quartz, 51% carbonates (48% calcite, 3% dolomite), 5% clays (3% illite, 1% illite/smectite, 1% chlorite), and 9% other minerals (5% plagioclase feldspar, 3% potassium feldspar, and 1% pyrite).

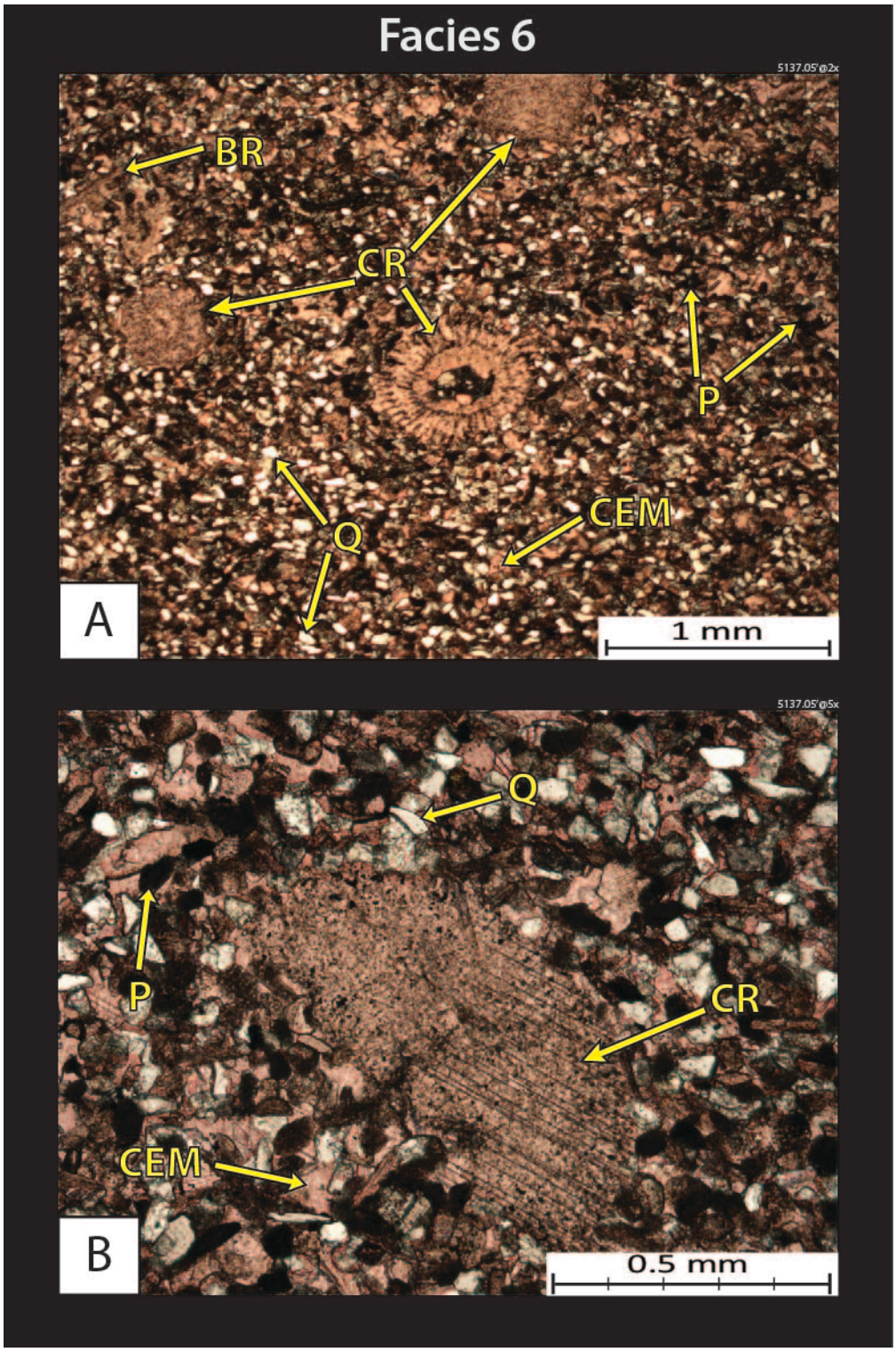


**5137.05' – Silty peloidal packstone to grainstone.** Sample is dominated by silt to sand sized peloids (P), skeletal debris such as crinoids (CR) and brachiopods (BR). XRD analysis: 23% quartz, 63% carbonates (59% calcite, 4% dolomite), 3% clays (2% illite, and 1% illite/smectite), and 11% other minerals (8% plagioclase feldspar, 3% potassium feldspar, and Tr pyrite).

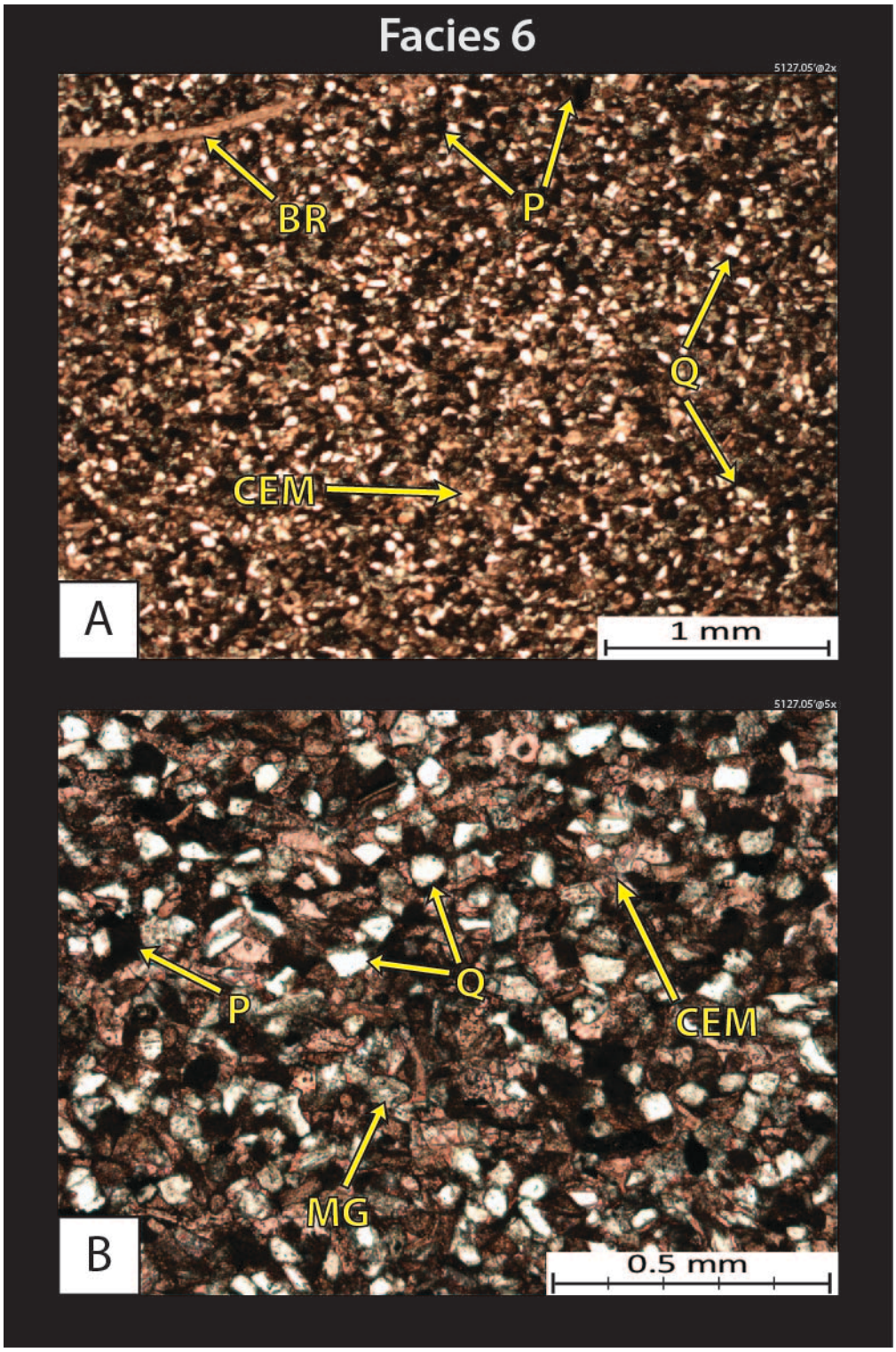


**5127.05' – Silty peloidal packstone to grainstone.** Sample is dominated by silt to sand sized peloids (P), calcite cement, and silt sized quartz grains (Q). XRD analysis: 33% quartz, 53% carbonates (49% calcite, 4% dolomite), 4% clays (2% illite, 1% illite/smectite, 1% chlorite), and 10% other minerals (7% plagioclase feldspar, 2% potassium feldspar, and 1% pyrite).

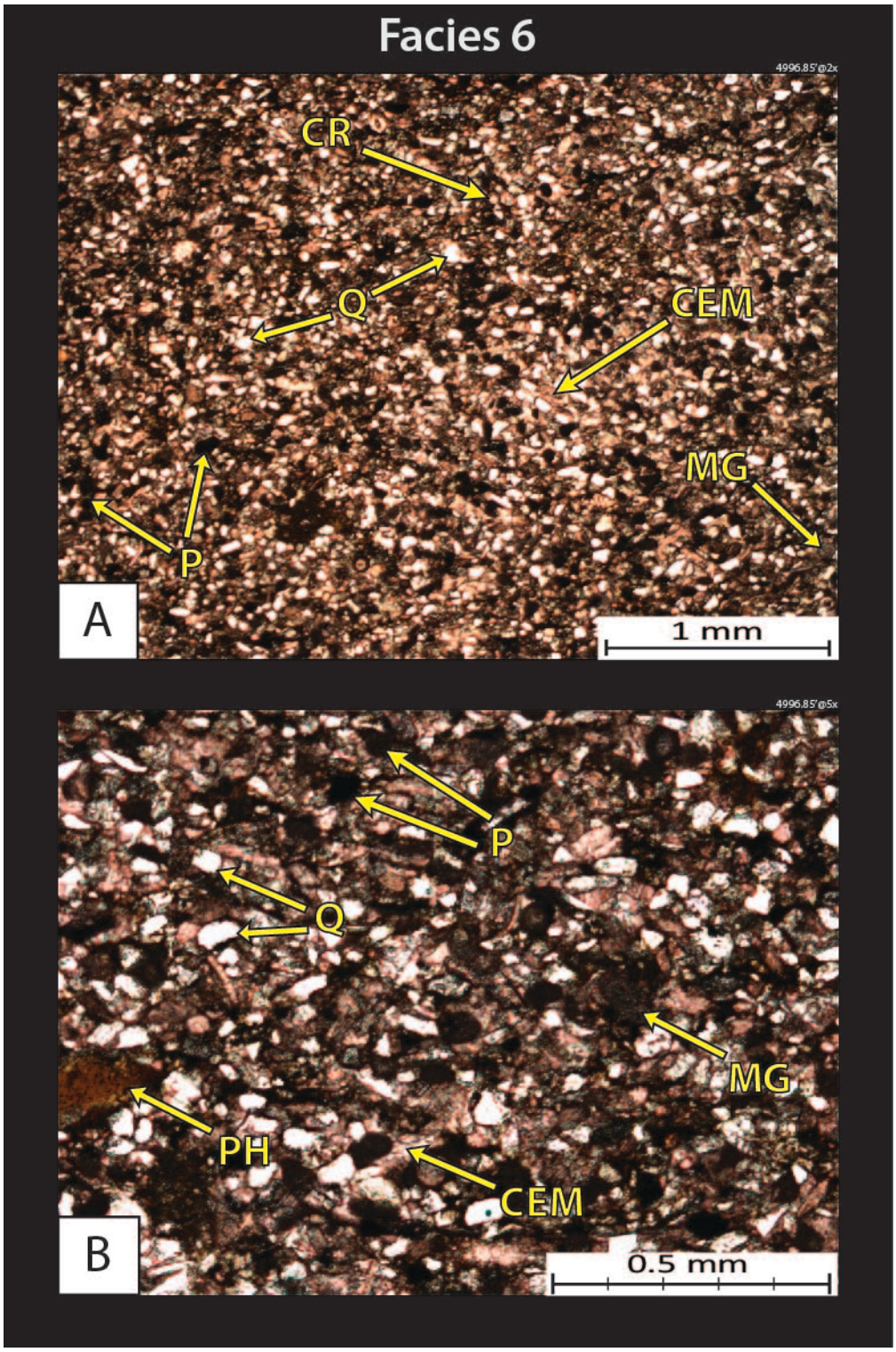


**4996.85' – Silty peloidal packstone to grainstone.** Sample is composed of silt to sand sized peloids (P), calcite grains and cement, silt sized quartz grains (Q), and phosphate (PH). XRD analysis: 34% quartz, 45% carbonates (44% calcite, 1% dolomite), 9% clays (7% illite, 1% illite/smectite, 1% chlorite), and 12% other minerals (7% plagioclase feldspar, 2% potassium feldspar, 2% pyrite, and 1% apatite).

## APPENDIX B:

Ihle #1-26

## I. Ihle #1-26 Whole Core Photographs

Whole core photographs of the Ihle core are shown under white light and are labeled with the abbreviations in the table shown below. The core slabs are placed in boxes containing 10 total feet of core (when full) and divided into 2 foot intervals. Where core is missing or has been removed, it is marked accordingly. The shallowest depths of the core are in the top left corner of the boxes, while the deepest depths of the core are in the bottom right corner. The scale positioned to the right of the core boxes is in tenths of feet. Next to each core slab, is a colored rectangle that corresponds to the facies stacking pattern colors. The contacts between the underlying Woodford Shale and overlying Pennsylvanian strata with the "Mississippian Limestone" are marked where present.

| Ihle Core Image Labels | | | |
|---|---|---|---|
| AMM | ammonite | LAM (Ca) | calcareous lamination |
| BR | brachiopod | PH | phosphate |
| BU | burrow | PSD | probable storm deposit |
| CC | clay clast | PY | pyrite |
| CR | crinoid | PY-BU | pyritized burrow |
| D | dolomite | RMC | rip-up mud clast |
| FB | fossil bed | IFD | indistinguishable fossil debris |
| FR | fracture | XB | cross-bedding |
| LAM | lamination | | |

Table 11. Abbreviations and their meanings used in labeling the whole box core photos for the Ihle #1-26 core.

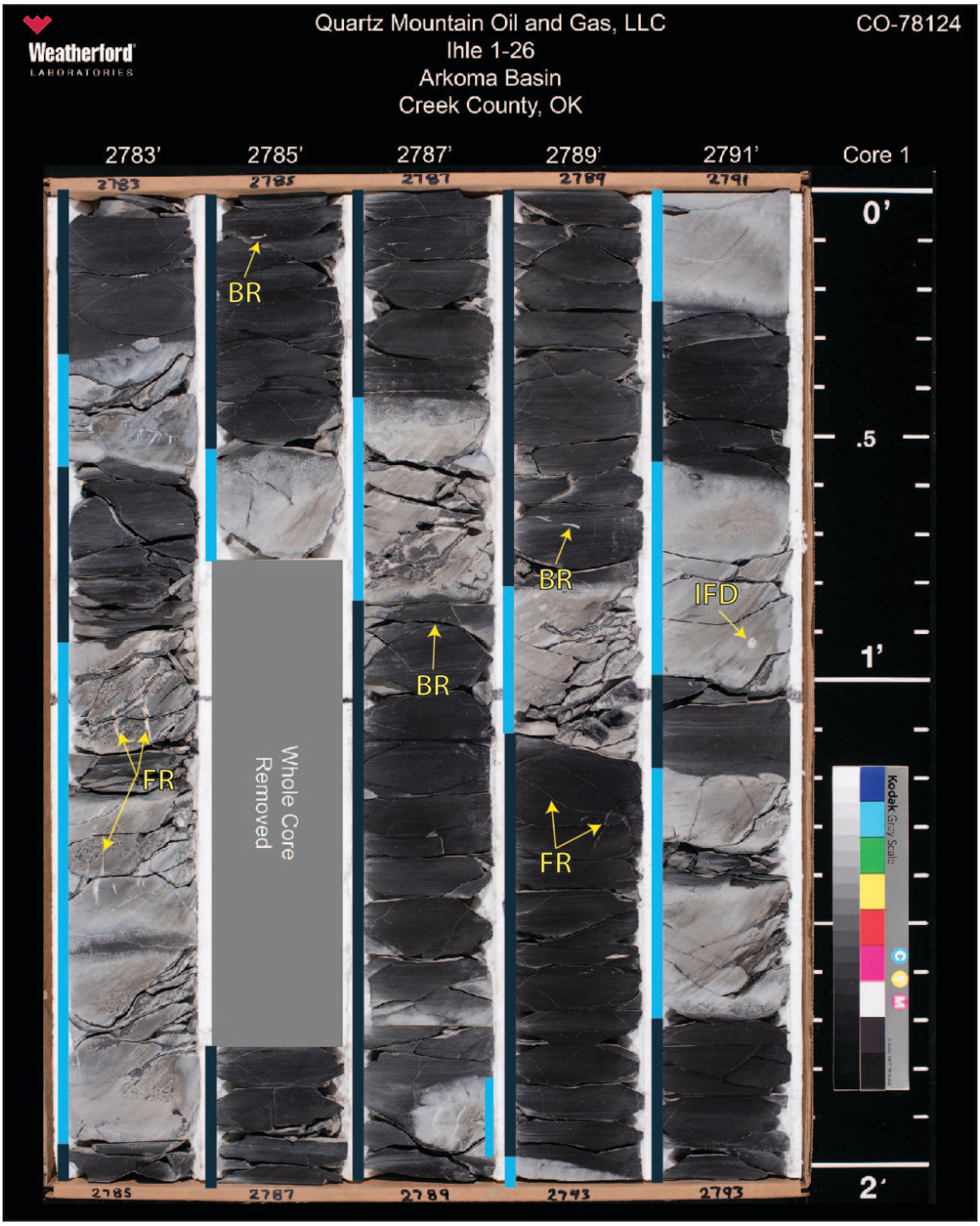
Weatherford
LABORATORIES
Quartz Mountain Oil and Gas, LLC
Ihle 1-26
Arkoma Basin
Creek County, OK
CO-78124
2783'
2785'
2787'
2789'
2791'
Core 1
0'
.5
1'
2'
BR
BR
BR
IFD
FR
FR
Whole Core
Removed
Kodak Gray Scale

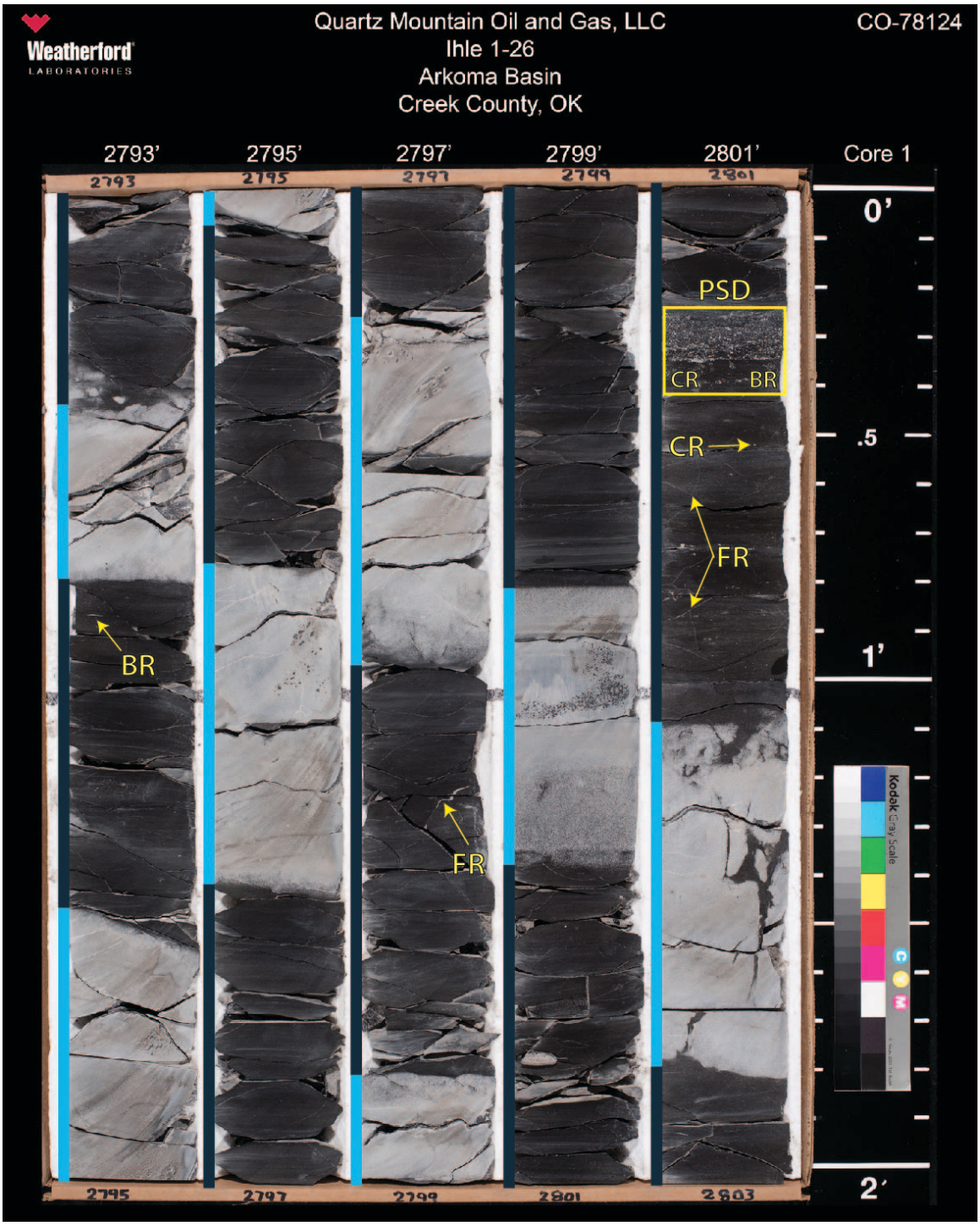
Weatherford
LABORATORIES
Quartz Mountain Oil and Gas, LLC
Ihle 1-26
Arkoma Basin
Creek County, OK
CO-78124
2793'
2795'
2797'
2799'
2801'
Core 1
0'
.5
1'
2'
PSD
CR
BR
CR
FR
BR
FR
Kodak Gray Scale

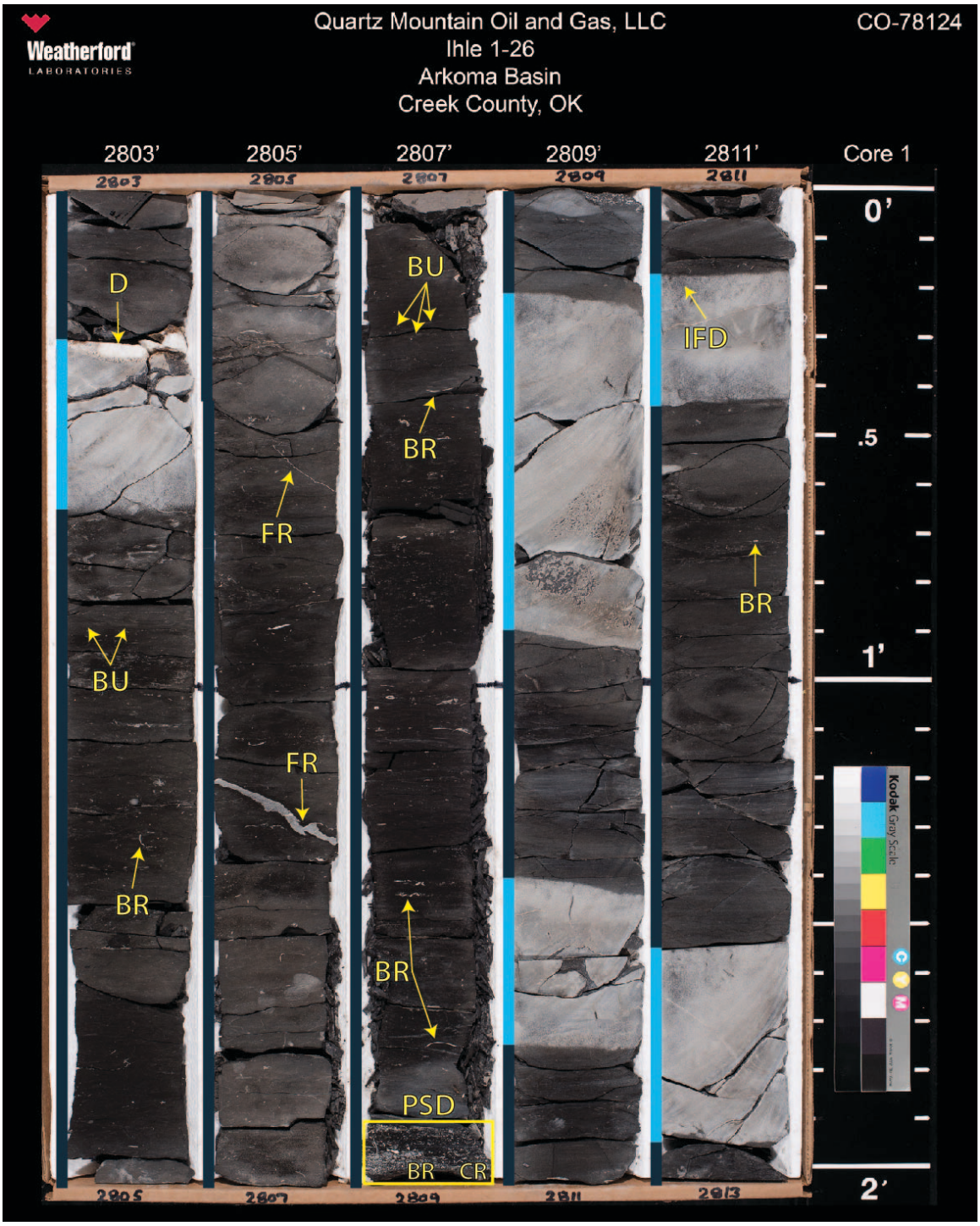
Weatherford
LABORATORIES
Quartz Mountain Oil and Gas, LLC
Ihle 1-26
Arkoma Basin
Creek County, OK
CO-78124
2803'
2805'
2807'
2809'
2811'
Core 1
0'
.5
1'
2'
D
BU
FR
FR
BU
BR
BR
BR
IFD
BR
PSD
BR CR
Kodak Gray Scale

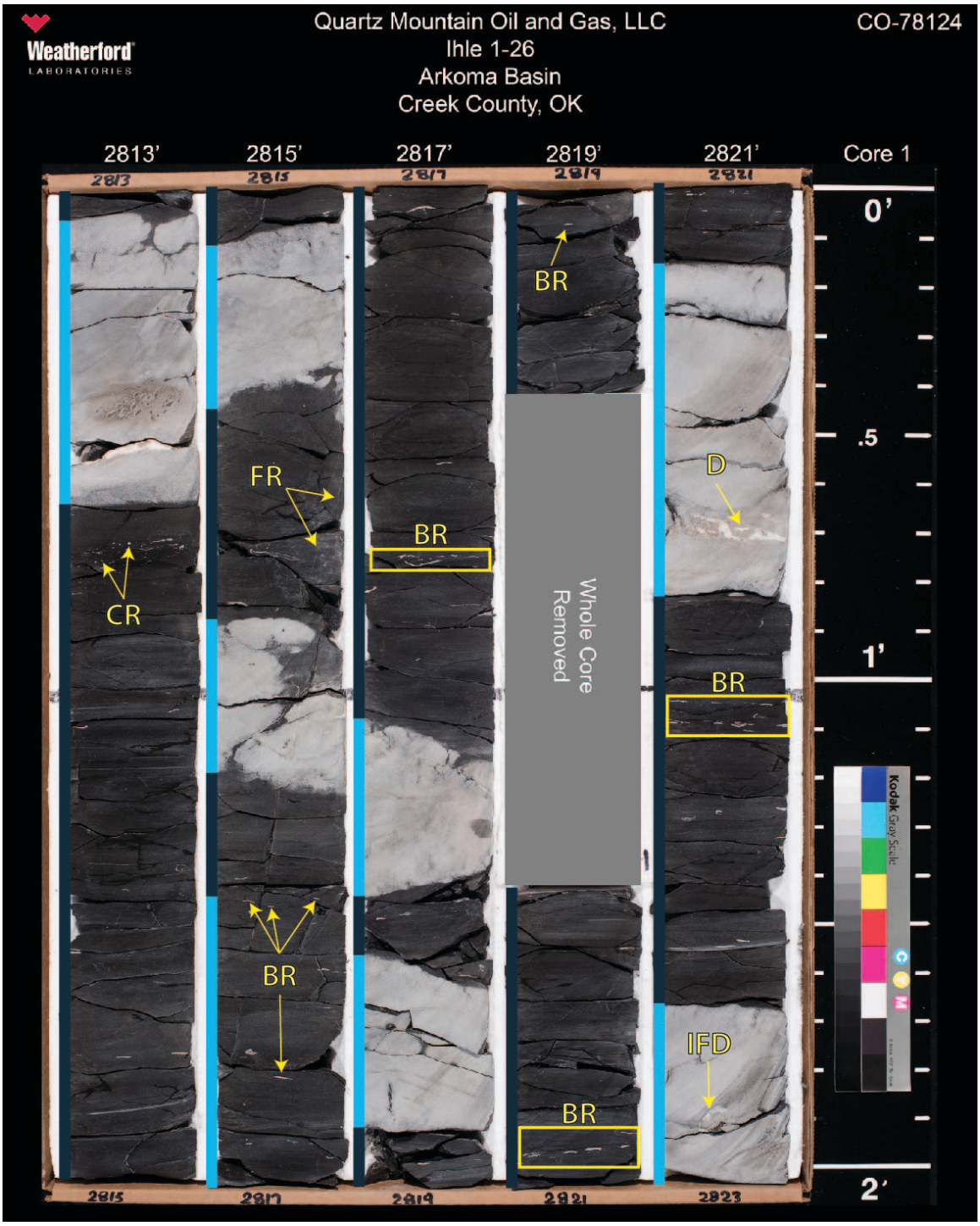
Weatherford
LABORATORIES
Quartz Mountain Oil and Gas, LLC
Ihle 1-26
Arkoma Basin
Creek County, OK
CO-78124
2813'
2815'
2817'
2819'
2821'
Core 1
0'
.5
1'
2'
BR
FR
BR
CR
Whole Core Removed
D
BR
BR
IFD
Kodak Gray Scale

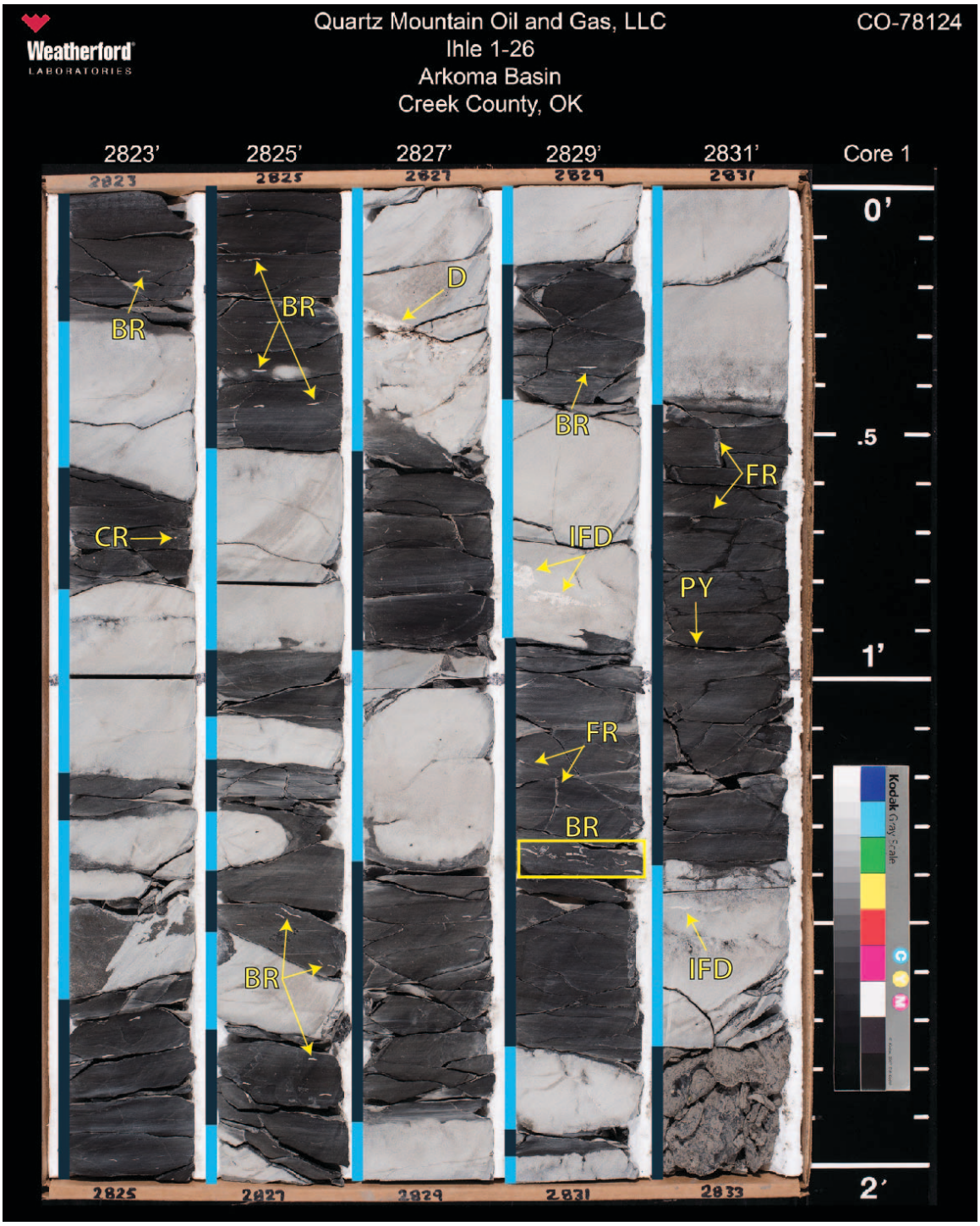
Weatherford
LABORATORIES
Quartz Mountain Oil and Gas, LLC
Ihle 1-26
Arkoma Basin
Creek County, OK
CO-78124
2823'
2825'
2827'
2829'
2831'
Core 1
0'
.5
1'
2'
BR
BR
D
BR
FR
CR
IFD
PY
FR
BR
BR
IFD
Kodak Gray Scale

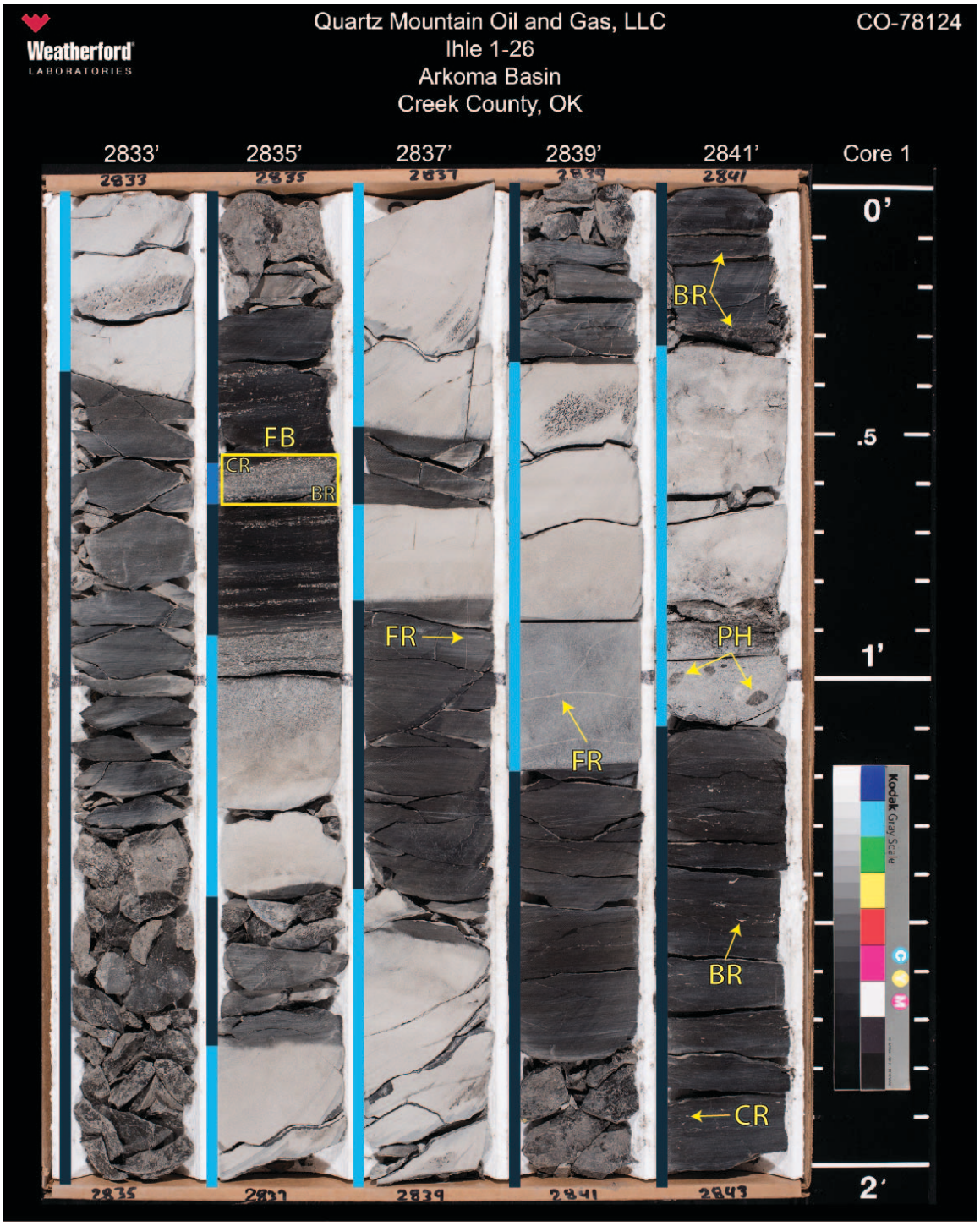
Weatherford
LABORATORIES
Quartz Mountain Oil and Gas, LLC
Ihle 1-26
Arkoma Basin
Creek County, OK
CO-78124
2833'
2835'
2837'
2839'
2841'
Core 1
0'
.5
1'
2'
FB
CR
BR
FR
FR
BR
PH
BR
CR
Kodak Gray Scale

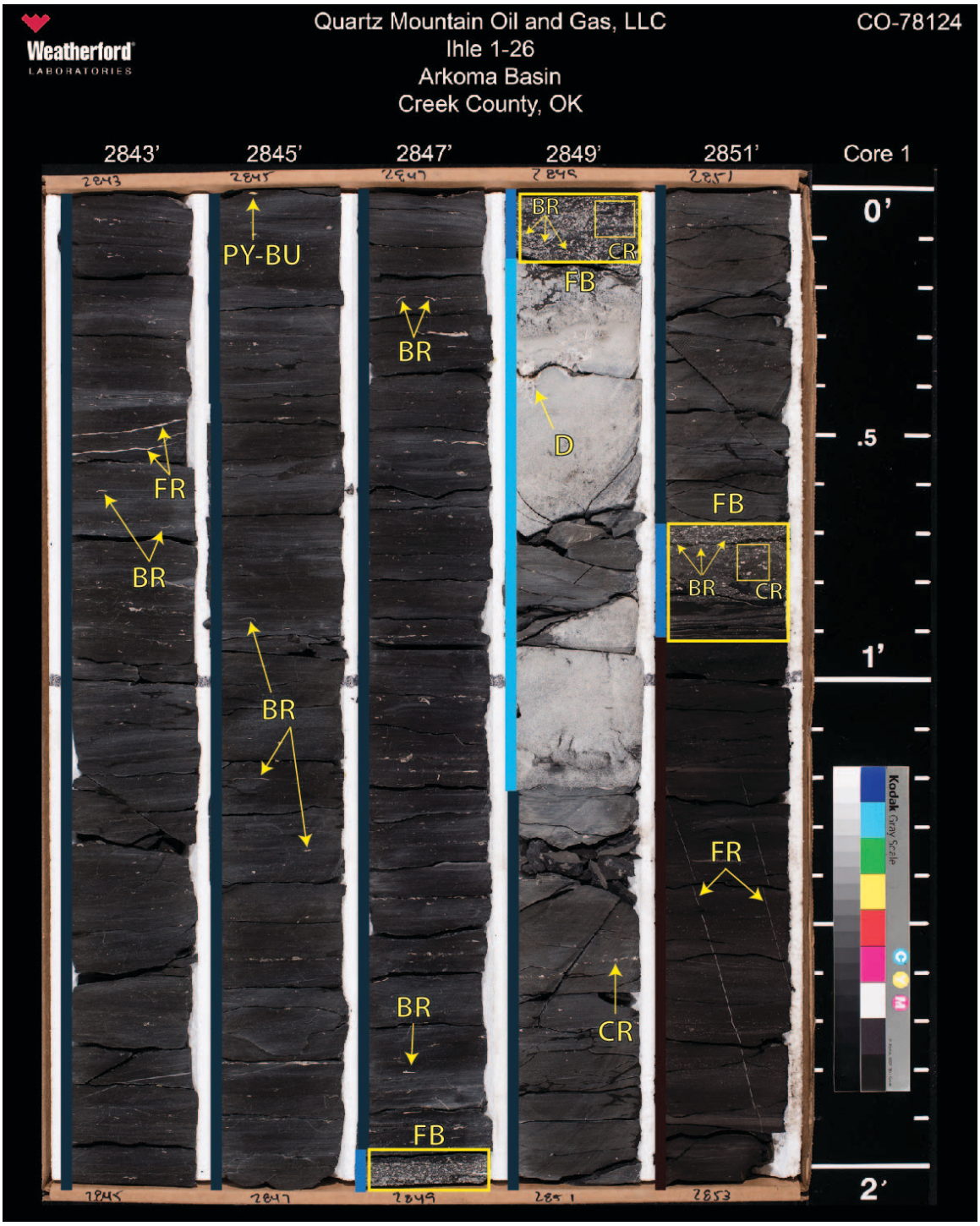
Weatherford
LABORATORIES
Quartz Mountain Oil and Gas, LLC
Ihle 1-26
Arkoma Basin
Creek County, OK
CO-78124
2843'
2845'
2847'
2849'
2851'
Core 1
0'
.5
1'
2'
PY-BU
BR
CR
FB
D
FR
BR
BR
FB
BR
CR
FR
BR
CR
FB
Kodak Gray Scale

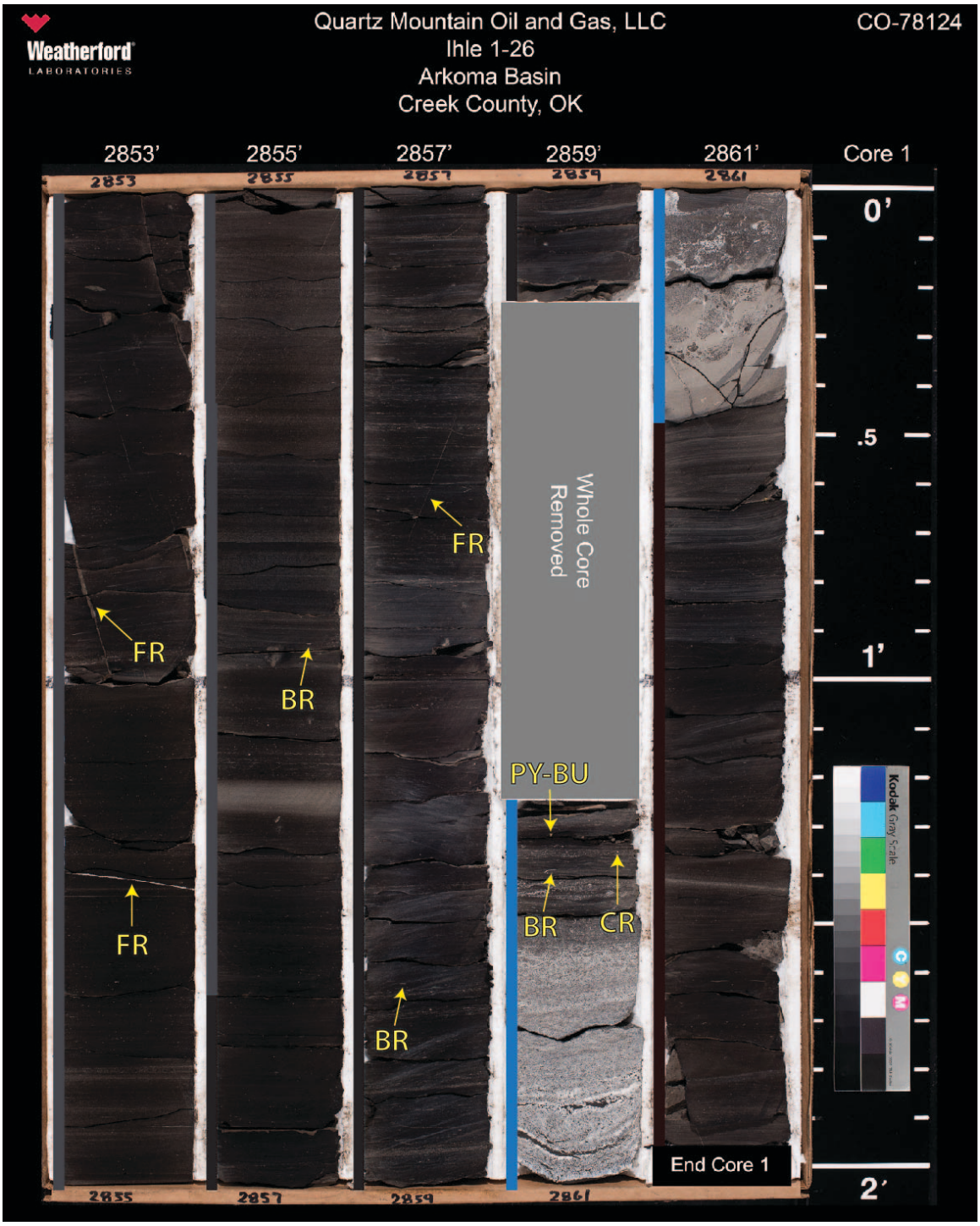


2863' – 2873' = missing core

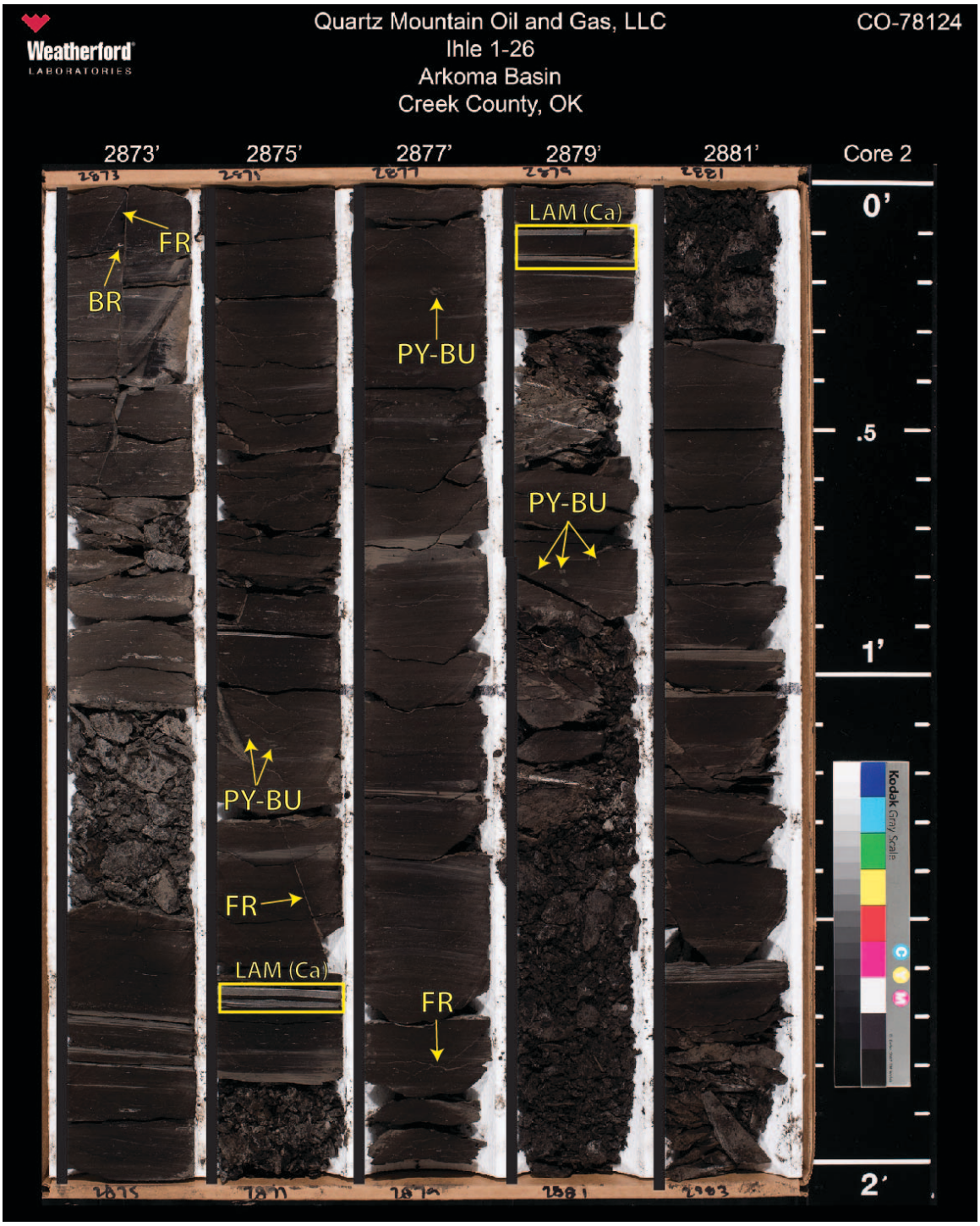
Weatherford
LABORATORIES
Quartz Mountain Oil and Gas, LLC
Ihle 1-26
Arkoma Basin
Creek County, OK
CO-78124
2873'
2875'
2877'
2879'
2881'
Core 2
0'
.5
1'
2'
FR
BR
PY-BU
LAM (Ca)
PY-BU
PY-BU
FR
LAM (Ca)
FR
Kodak Gray Scale

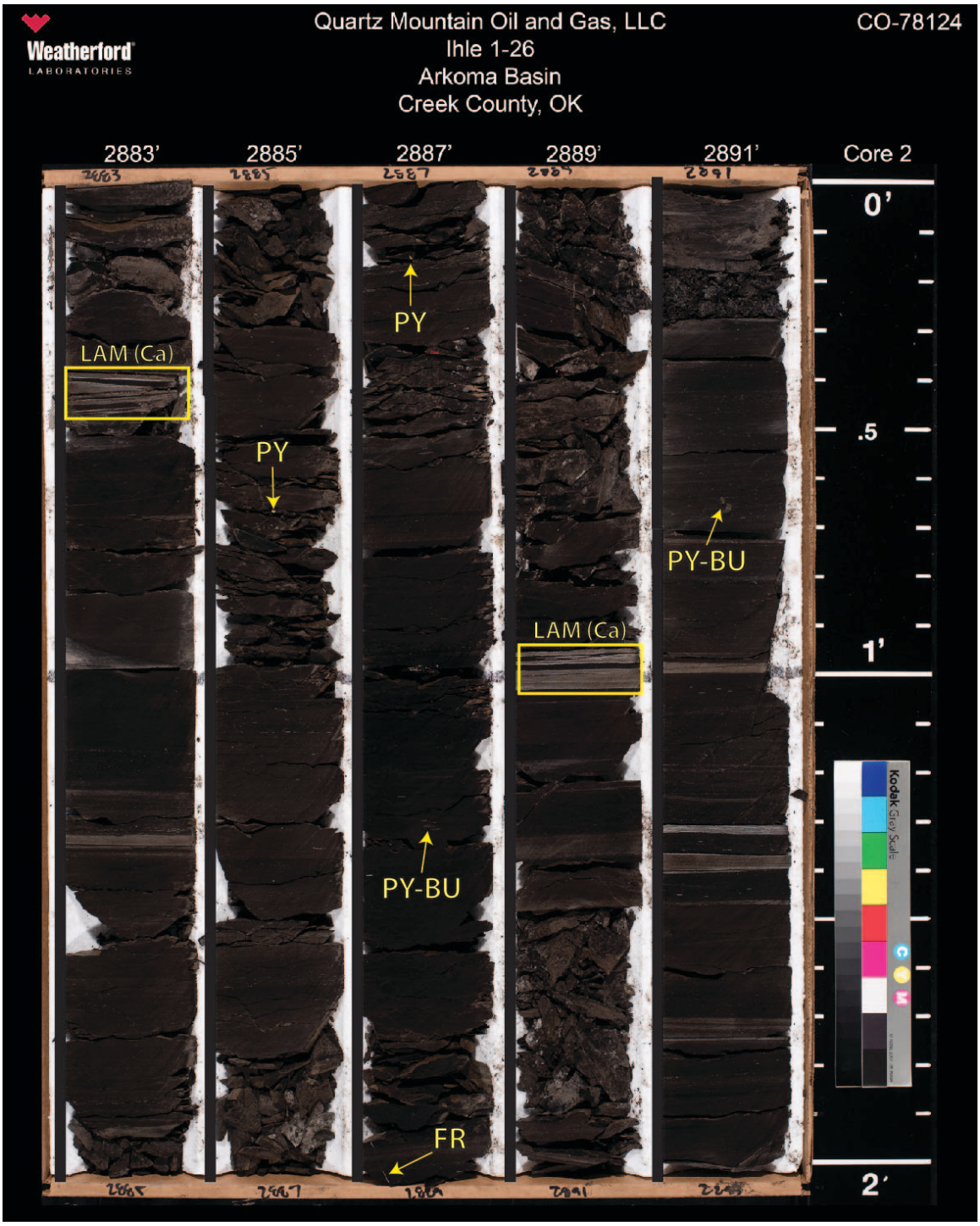
Weatherford
LABORATORIES
Quartz Mountain Oil and Gas, LLC
Ihle 1-26
Arkoma Basin
Creek County, OK
CO-78124
2883'
2885'
2887'
2889'
2891'
Core 2
0'
.5
1'
2'
LAM (Ca)
PY
PY
PY-BU
LAM (Ca)
PY-BU
FR
Kodak Gray Scale

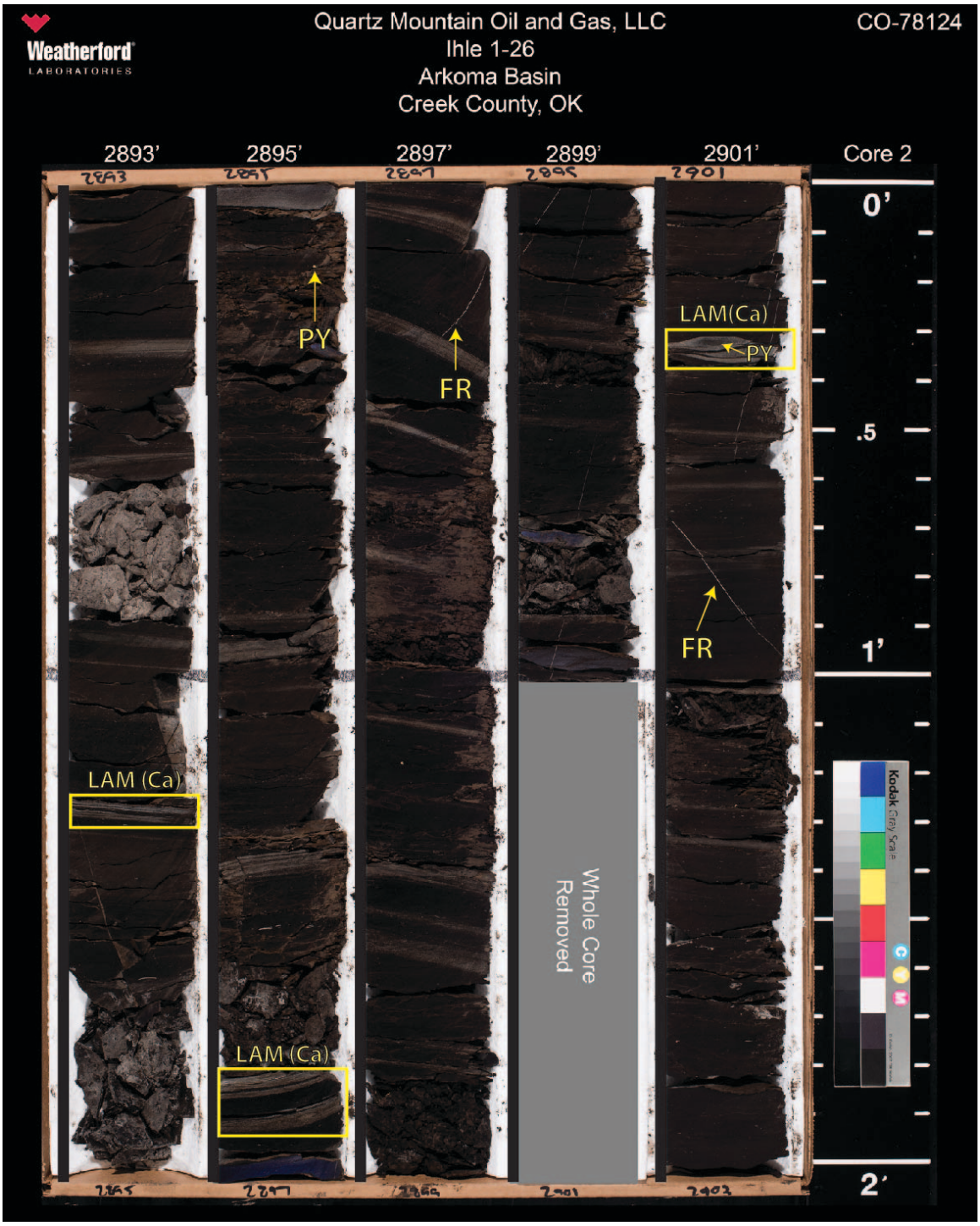
Weatherford
LABORATORIES
Quartz Mountain Oil and Gas, LLC
Ihle 1-26
Arkoma Basin
Creek County, OK
CO-78124
2893'
2895'
2897'
2899'
2901'
Core 2
0'
.5
1'
2'
PY
FR
LAM(Ca)
PY
FR
LAM (Ca)
LAM (Ca)
Whole Core
Removed

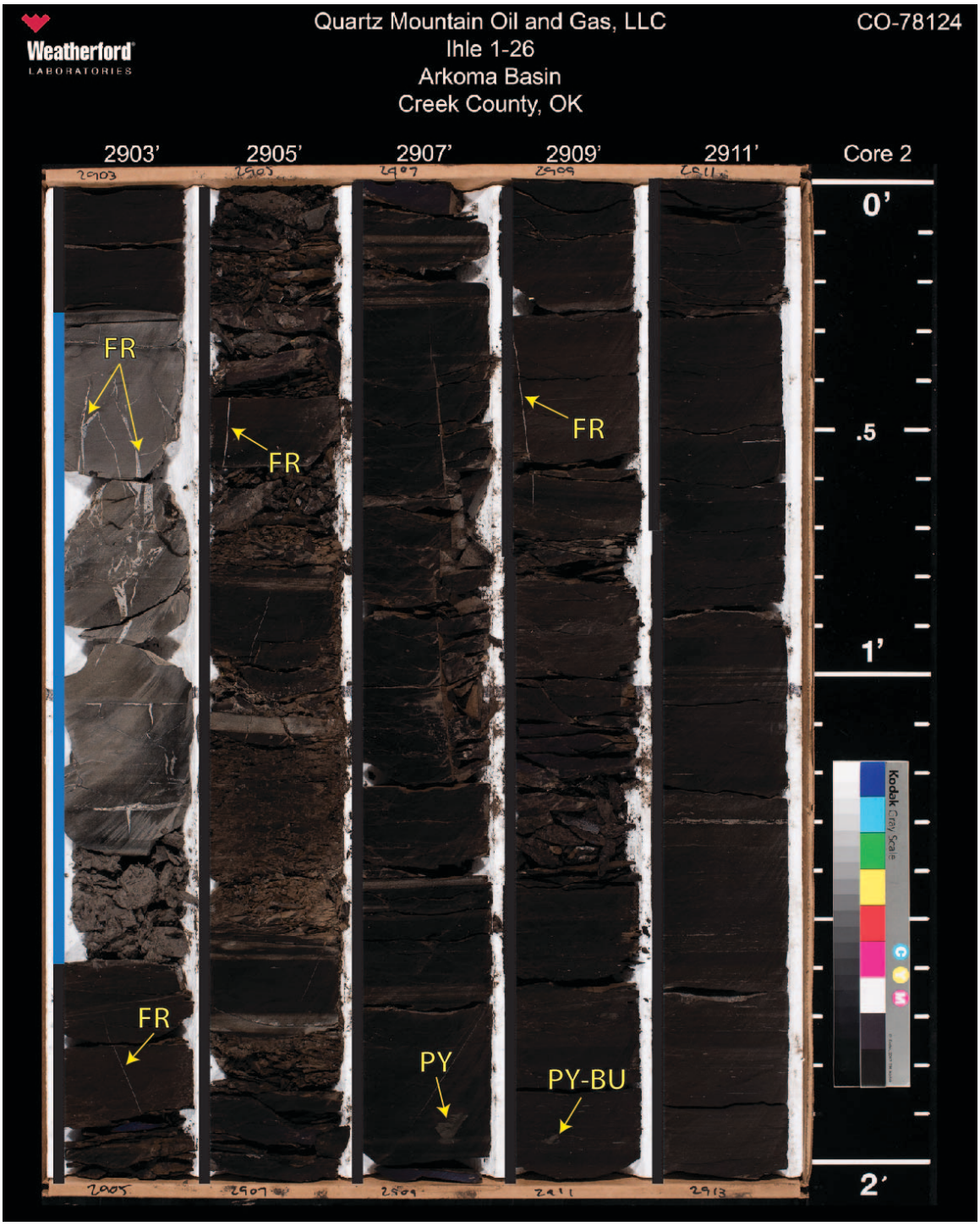
Weatherford
LABORATORIES
Quartz Mountain Oil and Gas, LLC
Ihle 1-26
Arkoma Basin
Creek County, OK
CO-78124
2903'
2905'
2907'
2909'
2911'
Core 2
0'
.5
1'
2'
FR
FR
FR
FR
PY
PY-BU

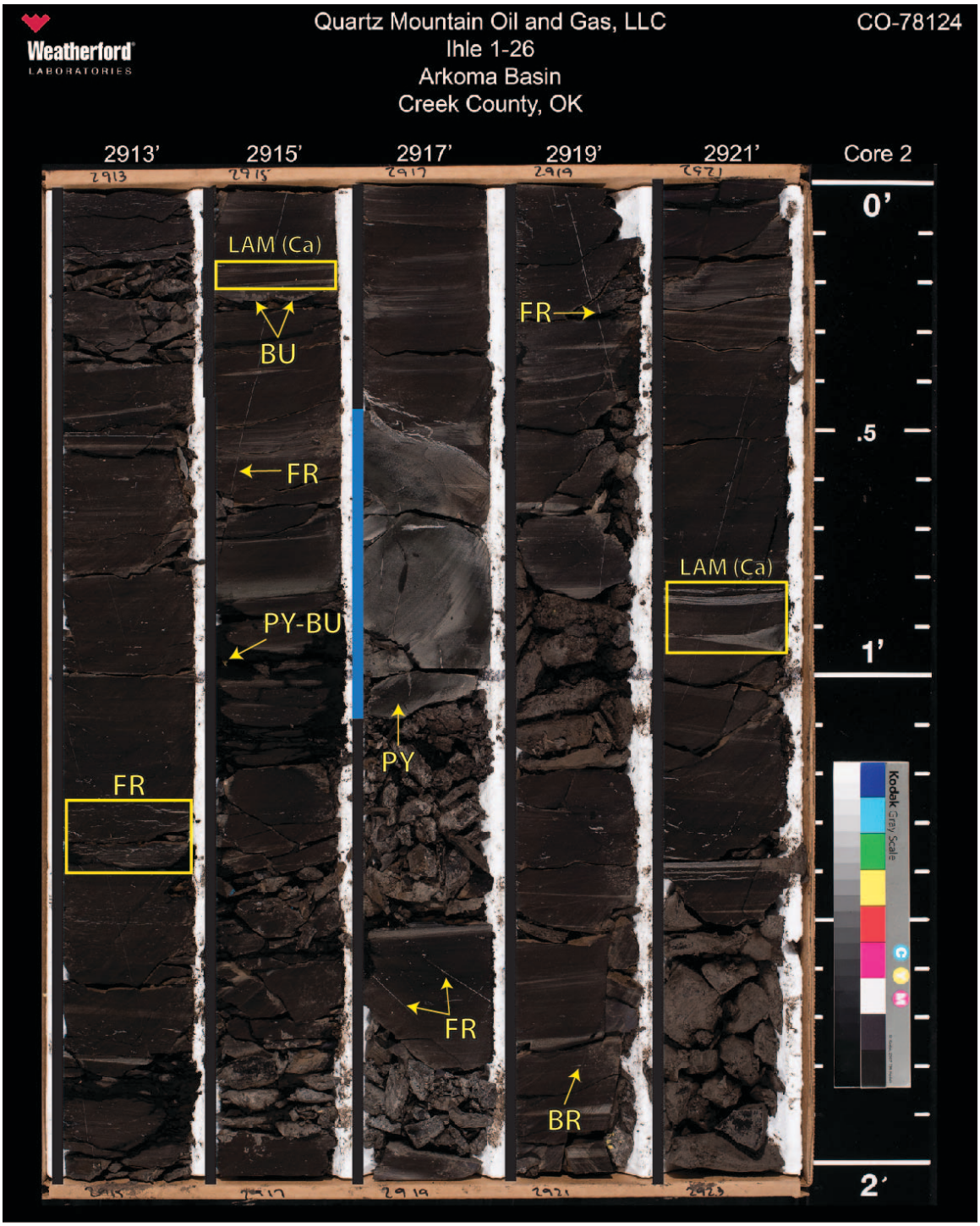
Weatherford
LABORATORIES
Quartz Mountain Oil and Gas, LLC
Ihle 1-26
Arkoma Basin
Creek County, OK
CO-78124
2913'
2915'
2917'
2919'
2921'
Core 2
0'
.5
1'
2'
LAM (Ca)
BU
FR
PY-BU
FR
PY
FR
FR
BR
LAM (Ca)
Kodak Gray Scale

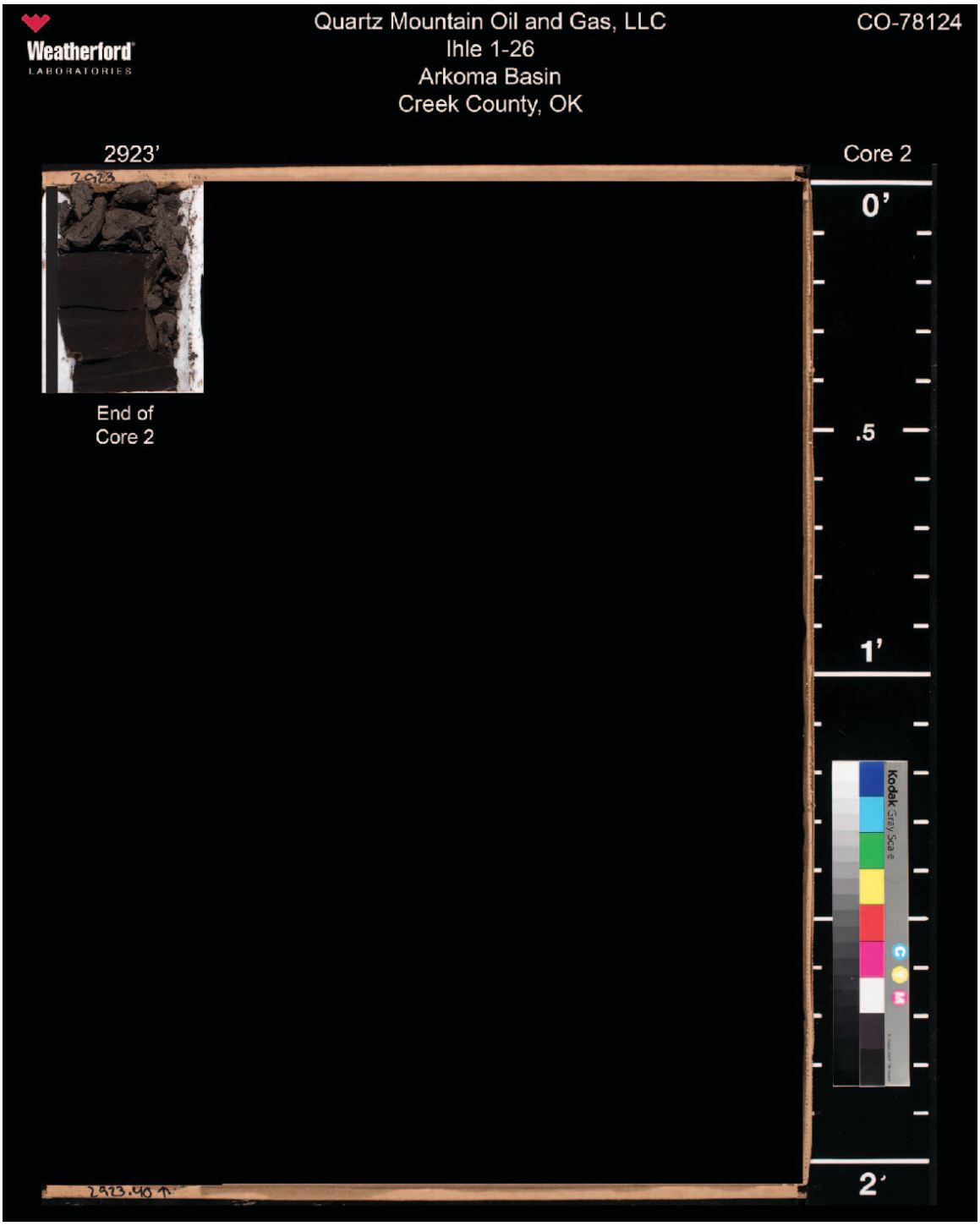


2923.40’ – 2924’ = missing

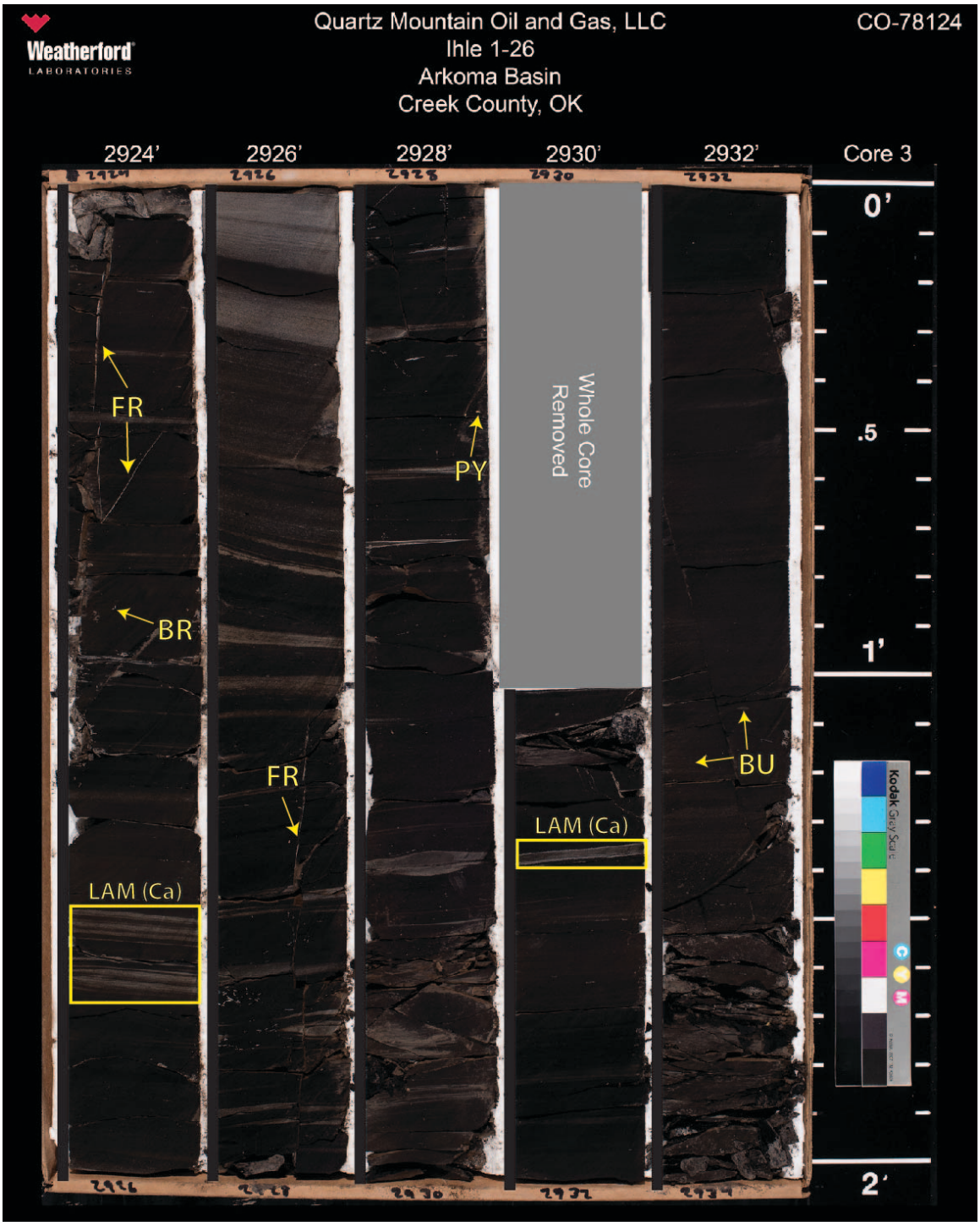
Weatherford
LABORATORIES
Quartz Mountain Oil and Gas, LLC
Ihle 1-26
Arkoma Basin
Creek County, OK
CO-78124
2924'
2926'
2928'
2930'
2932'
Core 3
0'
.5
1'
2'
FR
BR
FR
PY
Whole Core Removed
LAM (Ca)
LAM (Ca)
BU

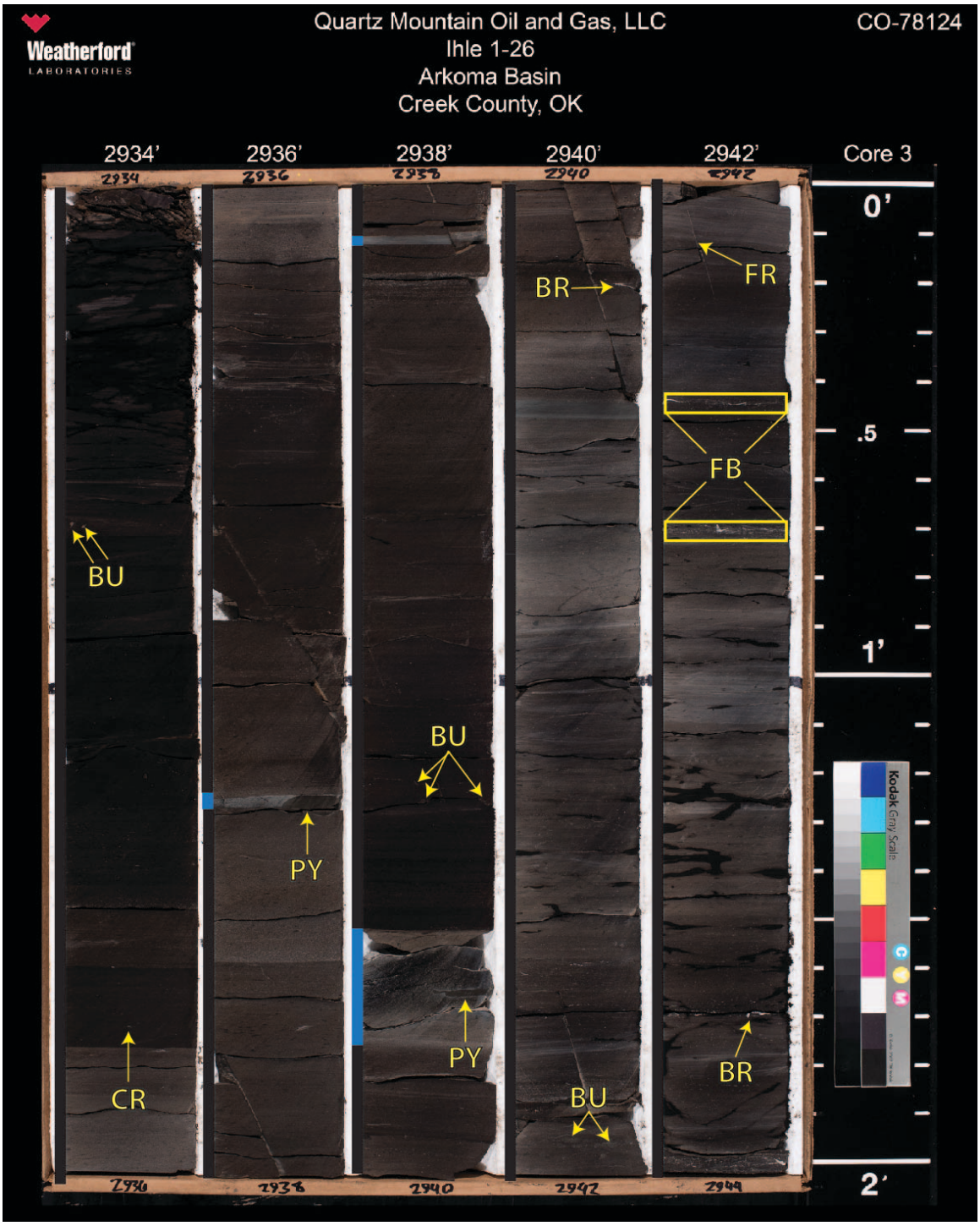
Weatherford
LABORATORIES
Quartz Mountain Oil and Gas, LLC
Ihle 1-26
Arkoma Basin
Creek County, OK
CO-78124
2934'
2936'
2938'
2940'
2942'
Core 3
0'
.5
1'
2'
BR
FR
FB
BU
BU
PY
PY
CR
BU
BR
Kodak Gray Scale

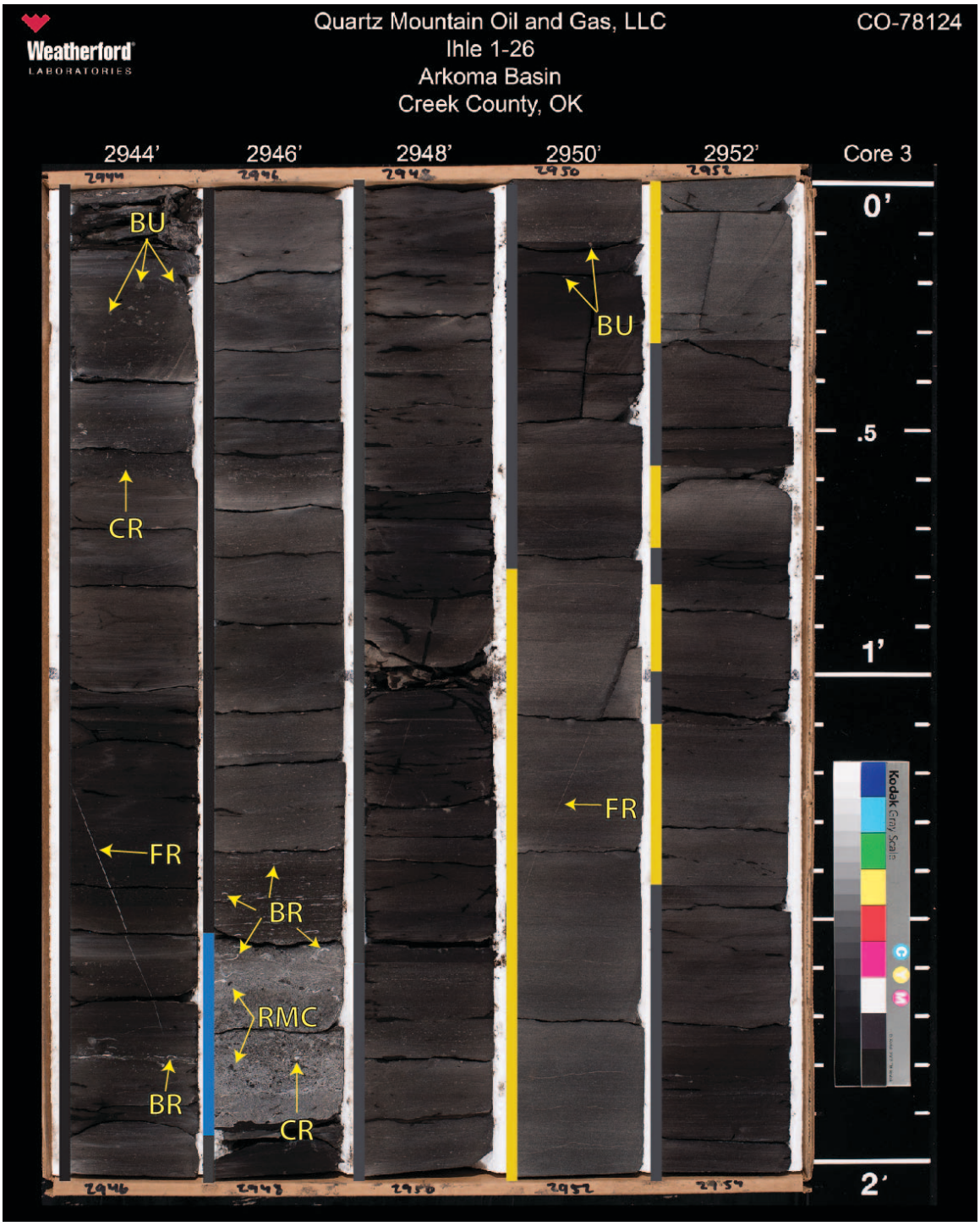
Weatherford
LABORATORIES
Quartz Mountain Oil and Gas, LLC
Ihle 1-26
Arkoma Basin
Creek County, OK
CO-78124
2944'
2946'
2948'
2950'
2952'
Core 3
0'
.5
1'
2'
BU
BU
CR
FR
FR
BR
RMC
BR
CR
Kodak Gray Scale

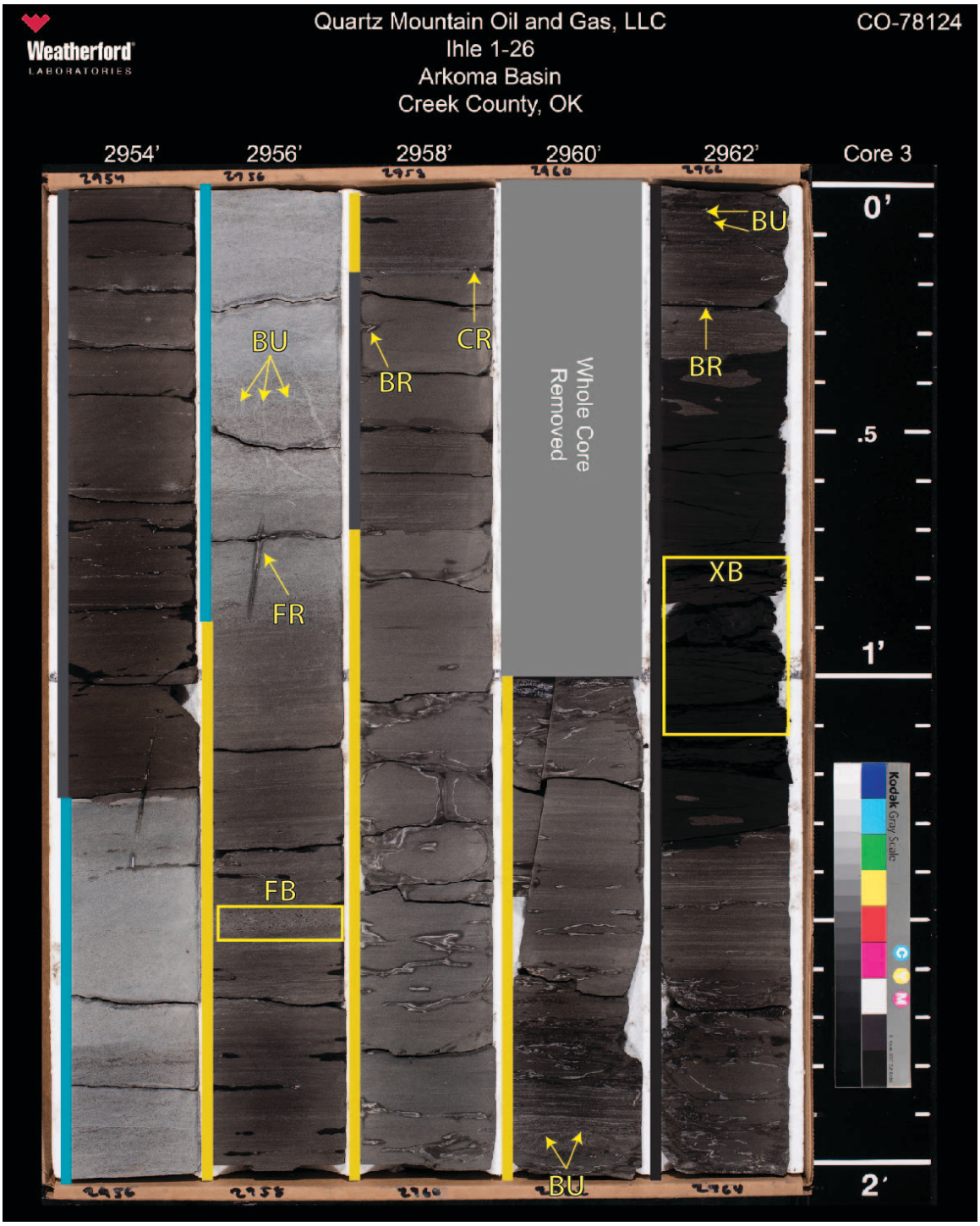
Weatherford
LABORATORIES
Quartz Mountain Oil and Gas, LLC
Ihle 1-26
Arkoma Basin
Creek County, OK
CO-78124
2954'
2956'
2958'
2960'
2962'
Core 3
0'
.5
1'
2'
BU
BR
CR
FR
FB
XB
Whole Core Removed
Kodak Gray Scale

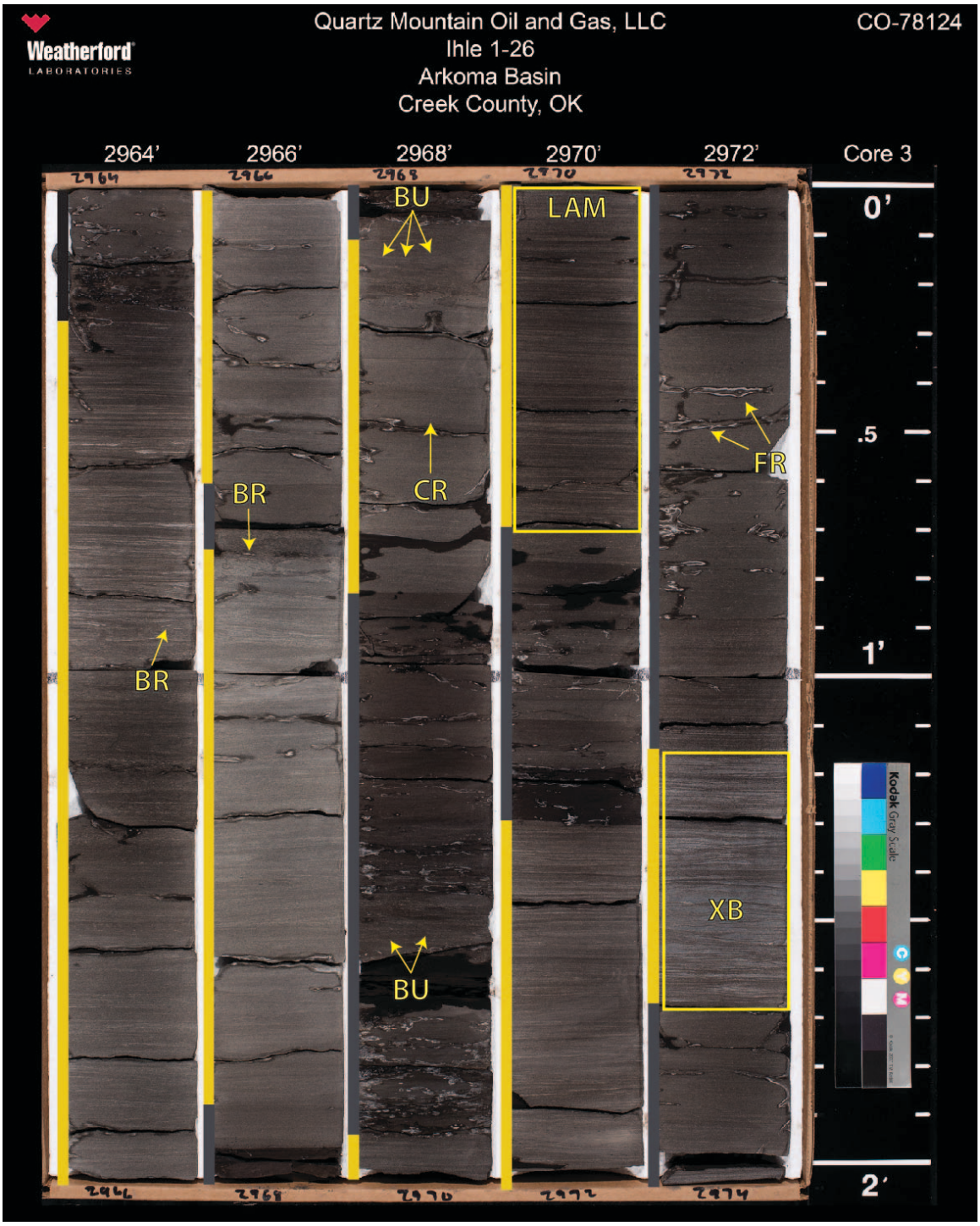
Weatherford
LABORATORIES
Quartz Mountain Oil and Gas, LLC
Ihle 1-26
Arkoma Basin
Creek County, OK
CO-78124
2964'
2966'
2968'
2970'
2972'
Core 3
0'
.5
1'
2'
BU
LAM
FR
CR
BR
BR
XB
BU

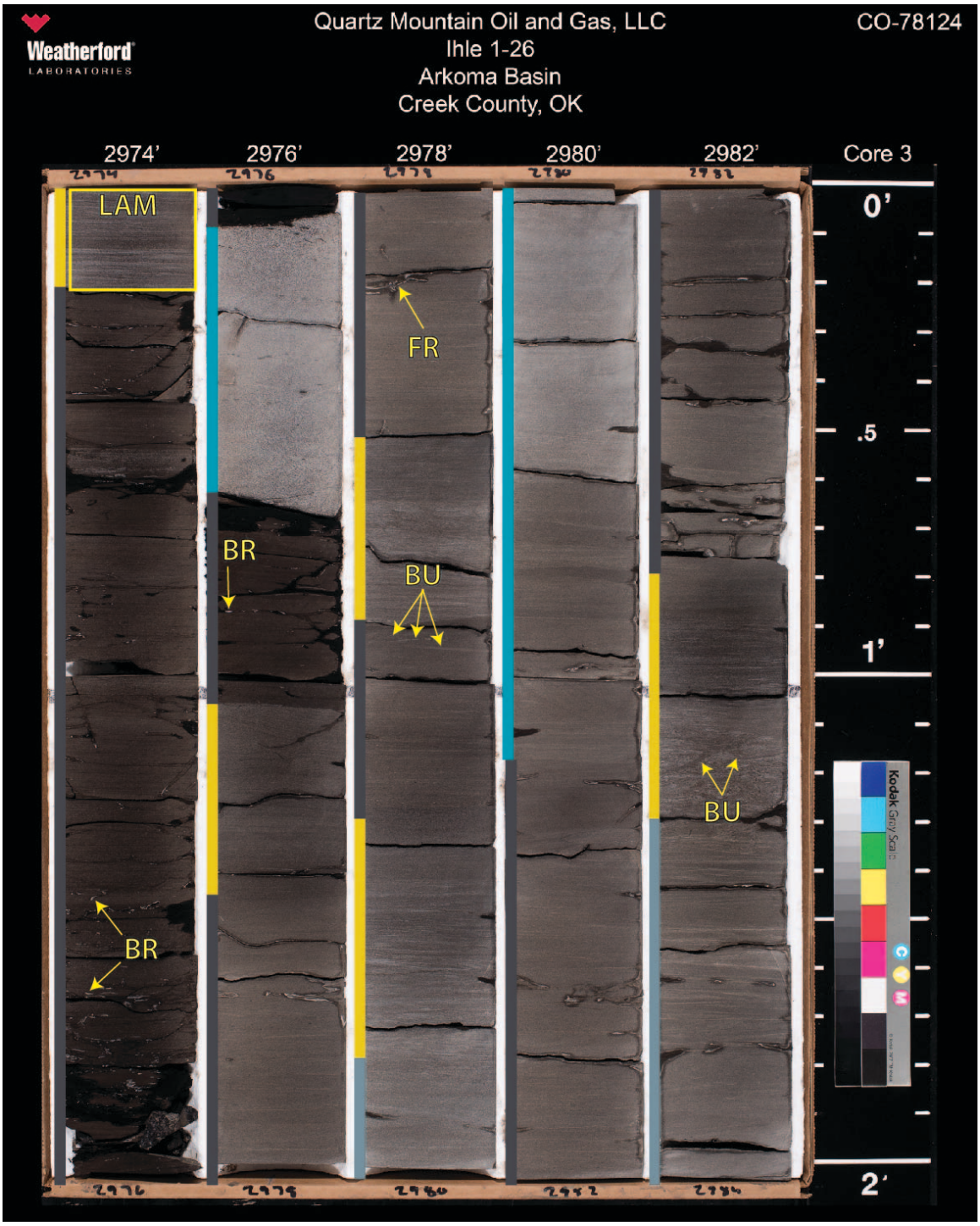
Weatherford
LABORATORIES
Quartz Mountain Oil and Gas, LLC
Ihle 1-26
Arkoma Basin
Creek County, OK
CO-78124
2974'
2976'
2978'
2980'
2982'
Core 3
0'
.5
1'
2'
LAM
FR
BR
BU
BU
BR

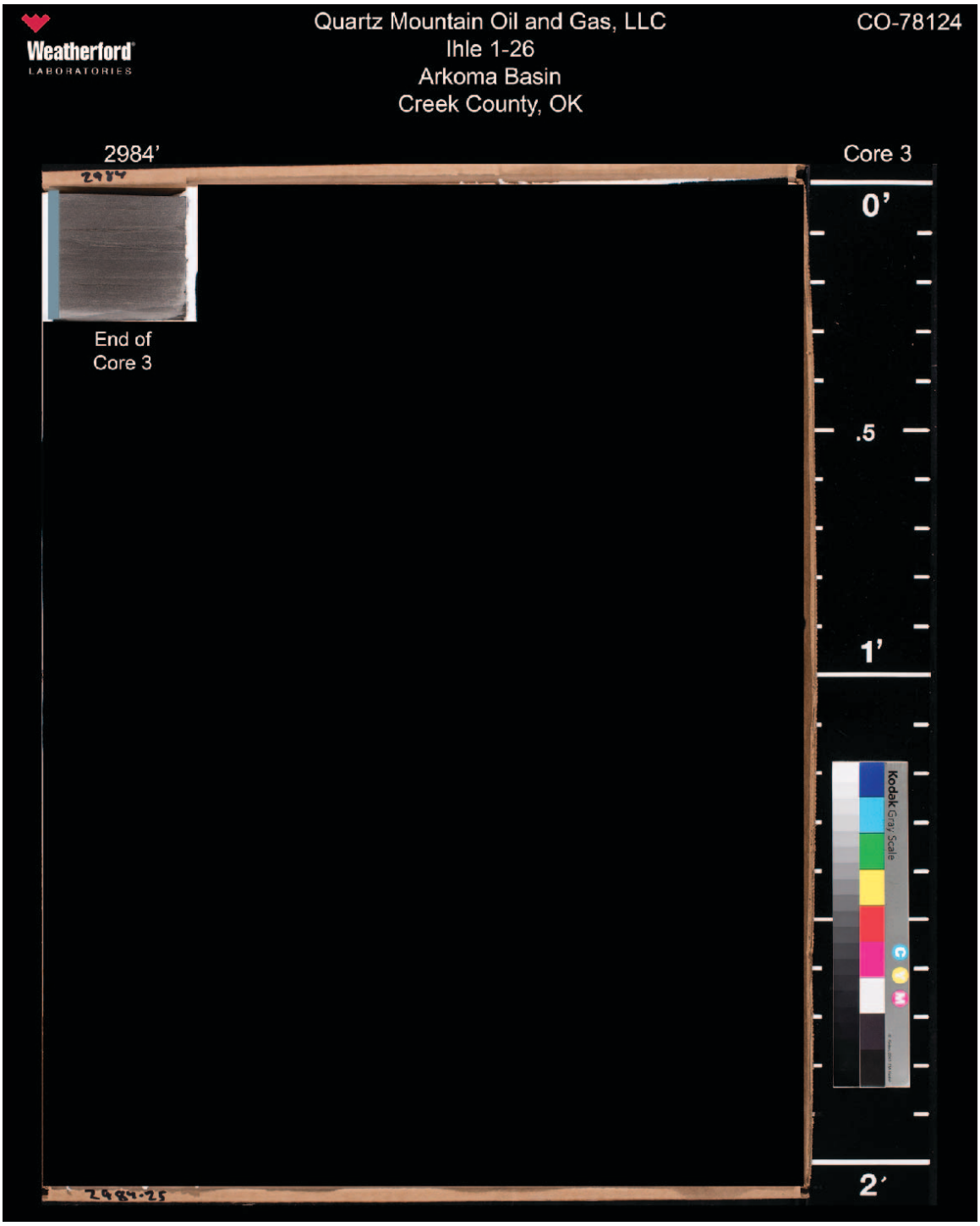


2984.25’ – 2985’ = missing

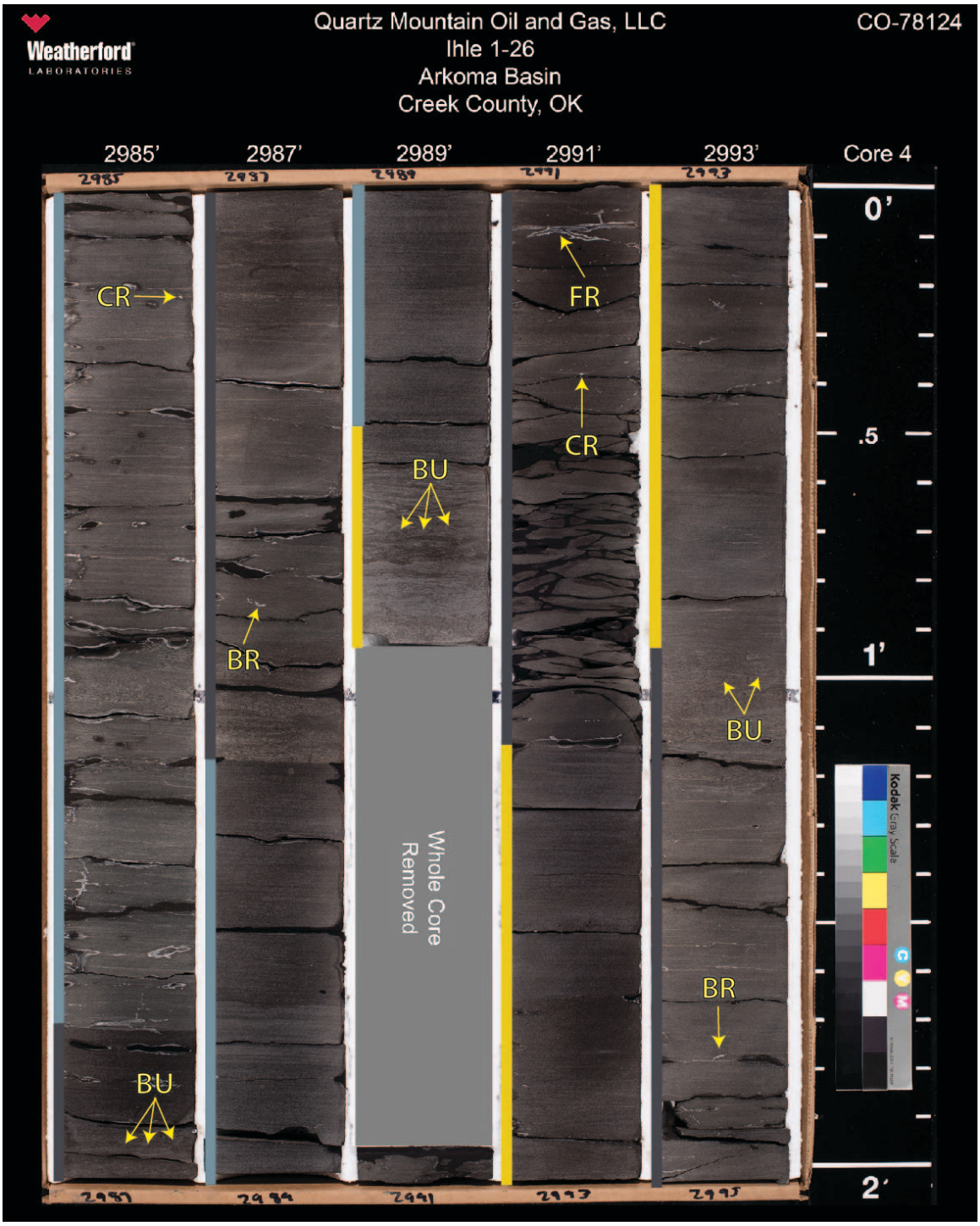
Weatherford
LABORATORIES
Quartz Mountain Oil and Gas, LLC
Ihle 1-26
Arkoma Basin
Creek County, OK
CO-78124
2985'
2987'
2989'
2991'
2993'
Core 4
0'
.5
1'
2'
CR
FR
CR
BU
BR
BU
Whole Core Removed
BR
BU
Kodak Gray Scale

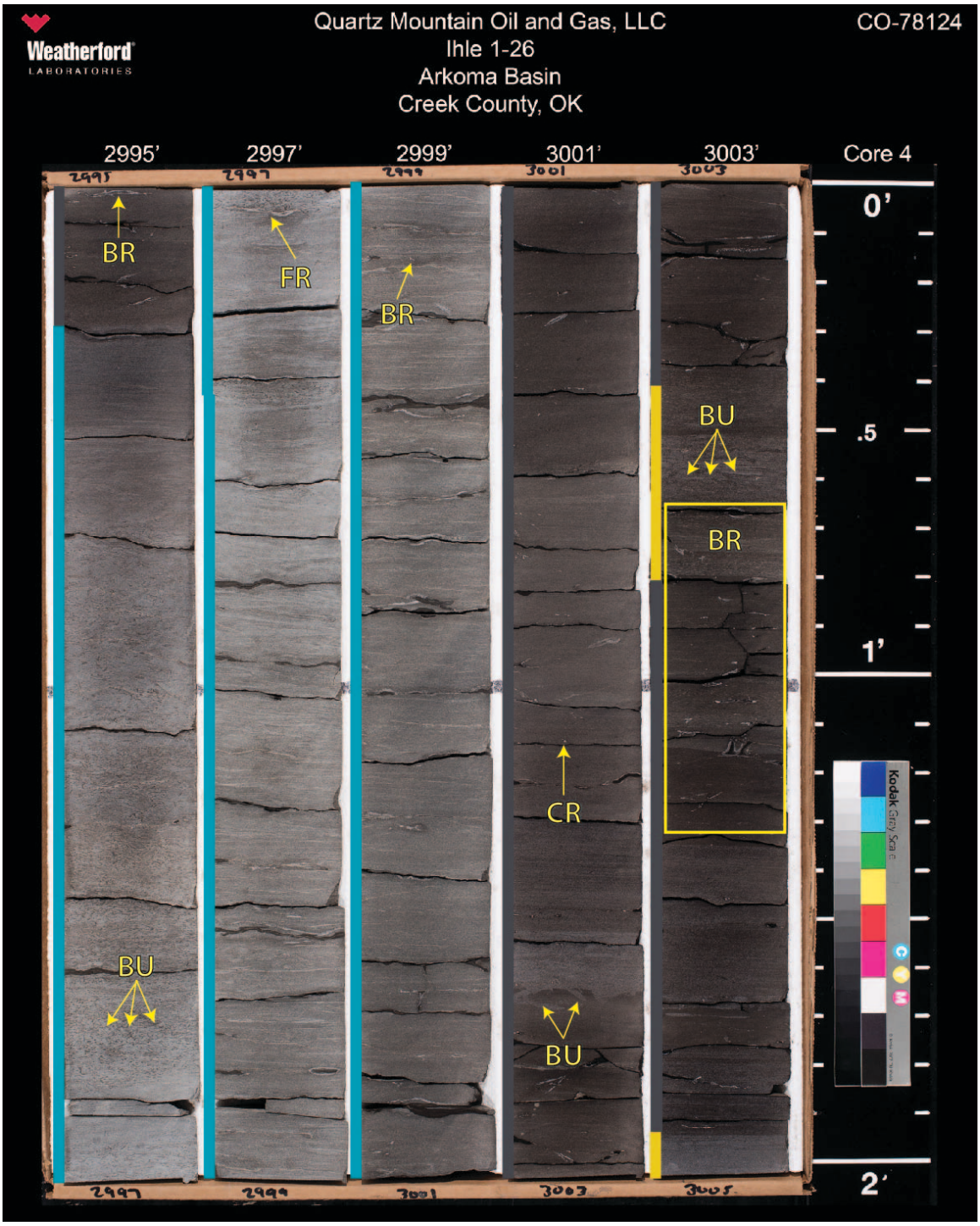
Weatherford
LABORATORIES
Quartz Mountain Oil and Gas, LLC
Ihle 1-26
Arkoma Basin
Creek County, OK
CO-78124
2995'
2997'
2999'
3001'
3003'
Core 4
0'
.5
1'
2'
BR
FR
BR
BU
BR
CR
BU
BU
Kodak Gray Scale

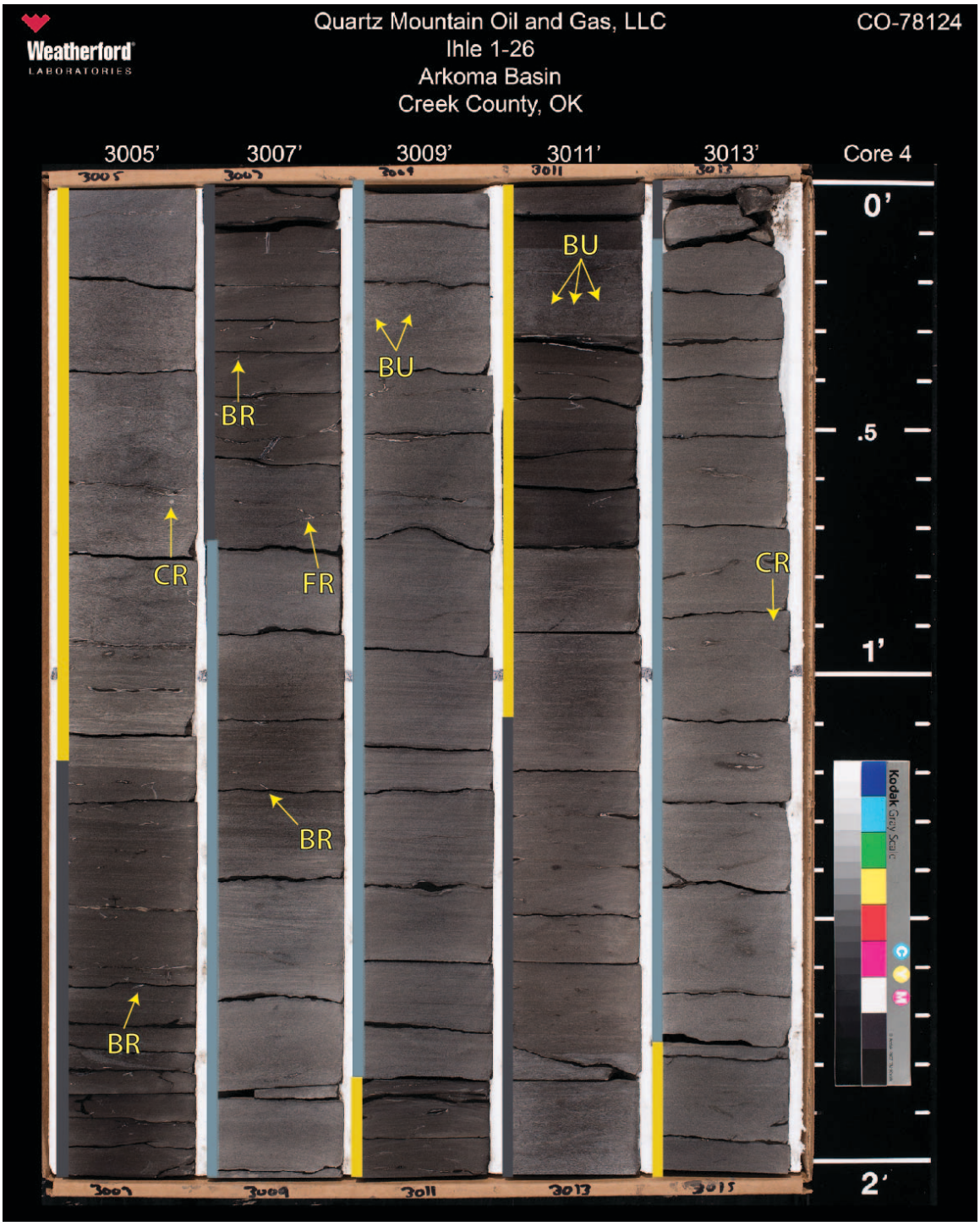
Weatherford
LABORATORIES
Quartz Mountain Oil and Gas, LLC
Ihle 1-26
Arkoma Basin
Creek County, OK
CO-78124
3005'
3007'
3009'
3011'
3013'
Core 4
0'
.5
1'
2'
BU
BU
BR
CR
FR
BR
CR
BR
Kodak Gray Scale

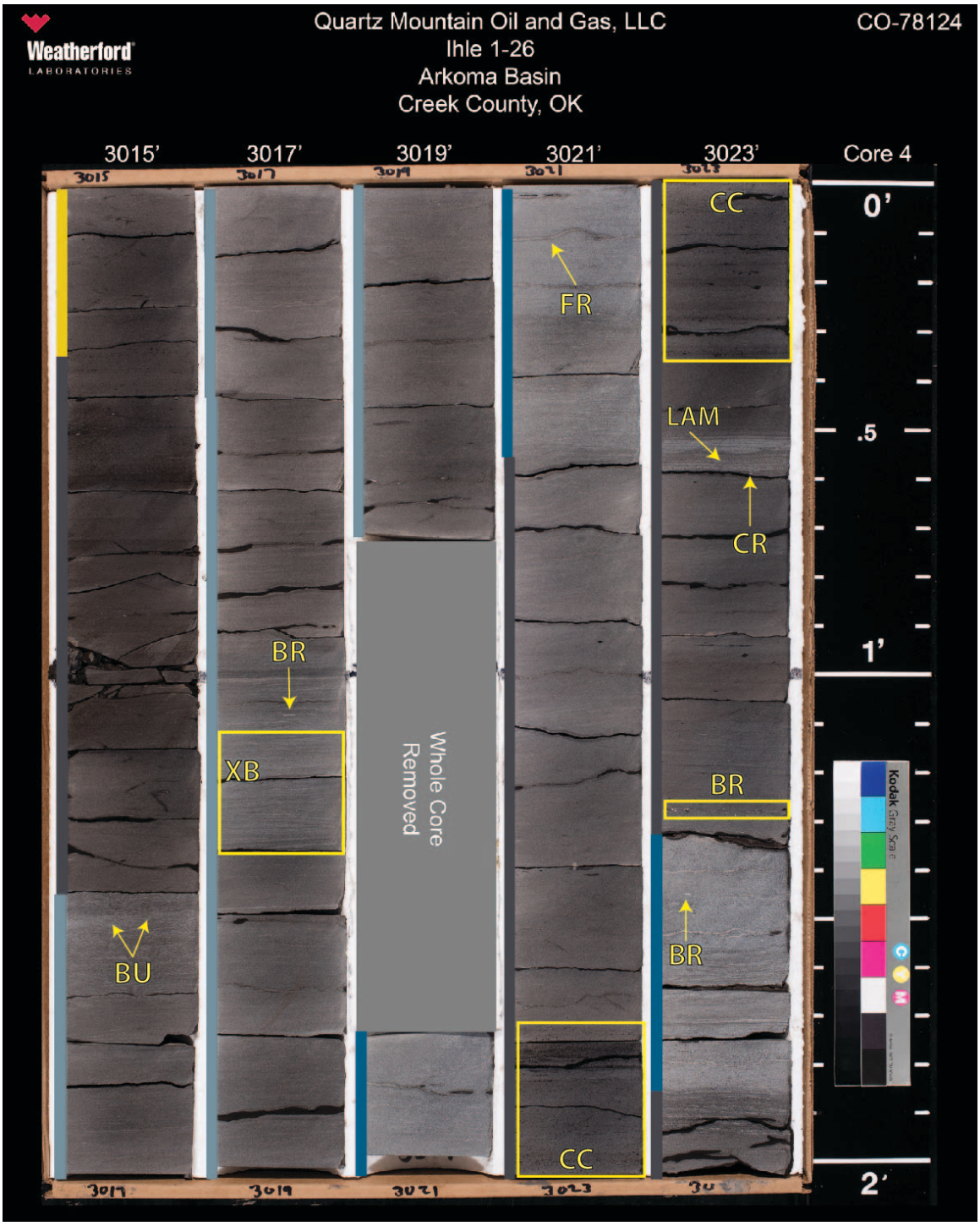
Weatherford
LABORATORIES
Quartz Mountain Oil and Gas, LLC
Ihle 1-26
Arkoma Basin
Creek County, OK
CO-78124
3015'
3017'
3019'
3021'
3023'
Core 4
0'
.5
1'
2'
CC
FR
LAM
CR
BR
XB
Whole Core
Removed
BR
BU
BR
CC

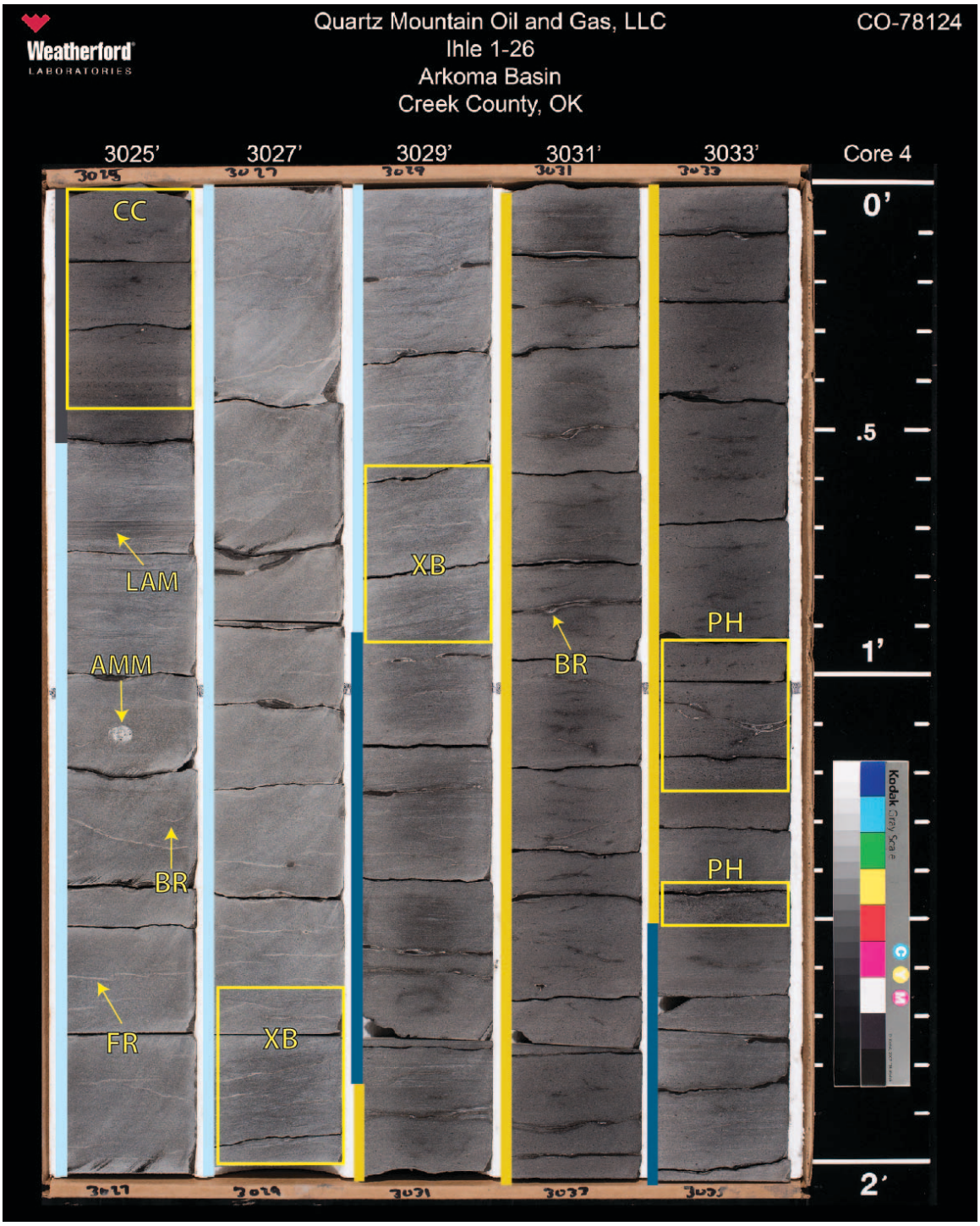
Weatherford
LABORATORIES
Quartz Mountain Oil and Gas, LLC
Ihle 1-26
Arkoma Basin
Creek County, OK
CO-78124
3025'
3027'
3029'
3031'
3033'
Core 4
0'
.5
1'
2'
CC
LAM
AMM
BR
FR
XB
XB
BR
PH
PH

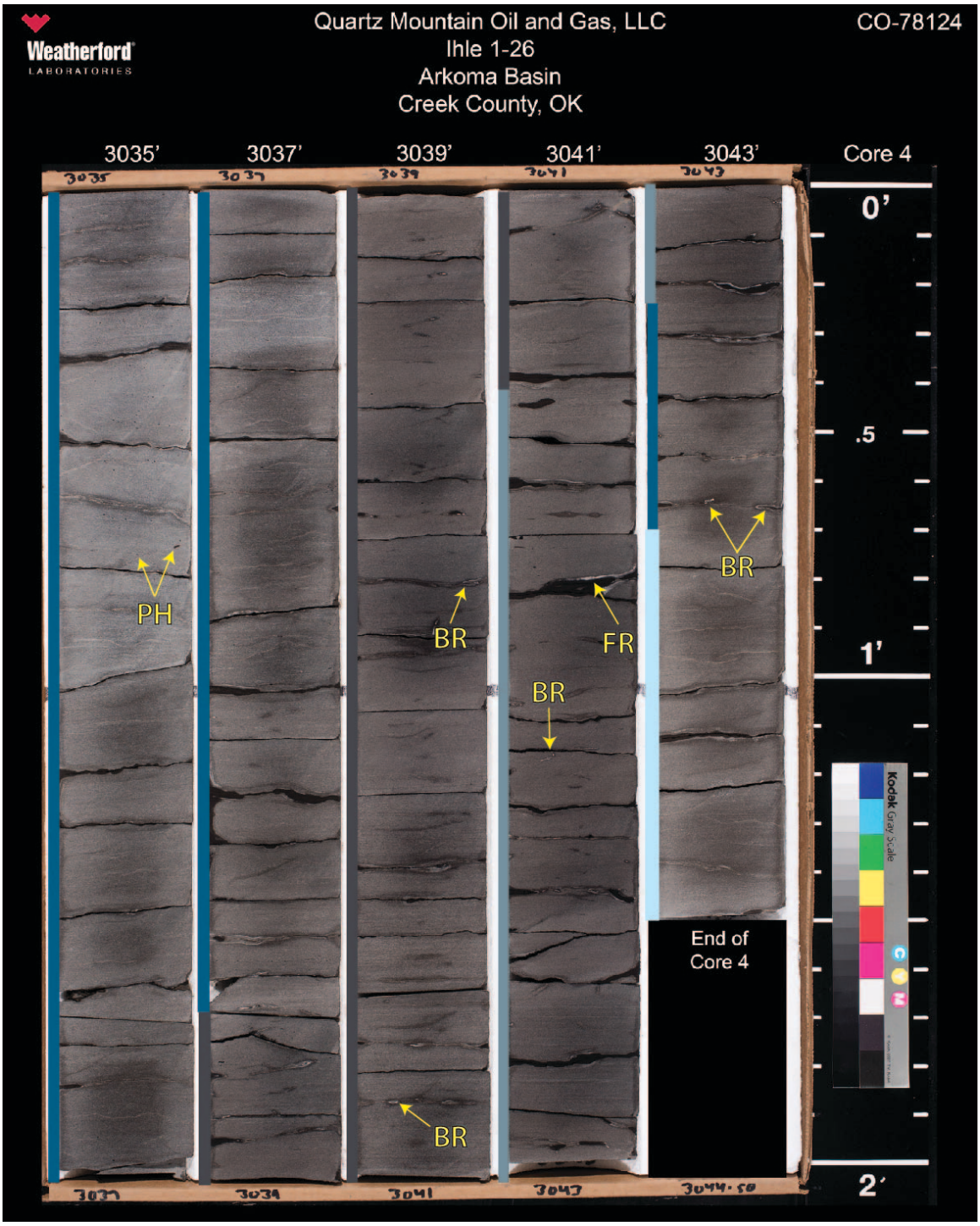


3044.50' – 3045' = missing

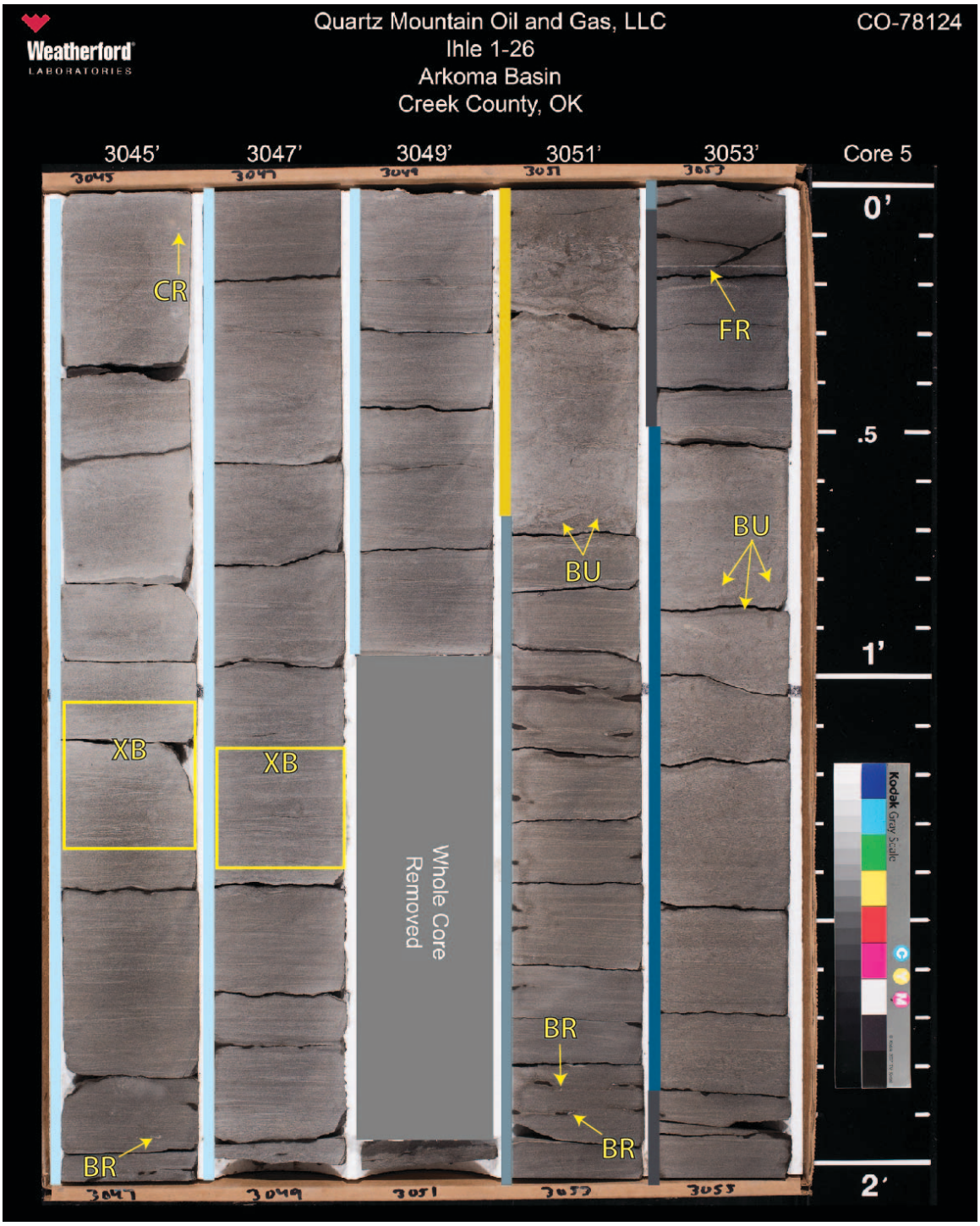
Weatherford
LABORATORIES
Quartz Mountain Oil and Gas, LLC
Ihle 1-26
Arkoma Basin
Creek County, OK
CO-78124
3045'
3047'
3049'
3051'
3053'
Core 5
0'
.5
1'
2'
CR
FR
BU
BU
XB
XB
Whole Core
Removed
BR
BR
BR
Kodak Gray Scale

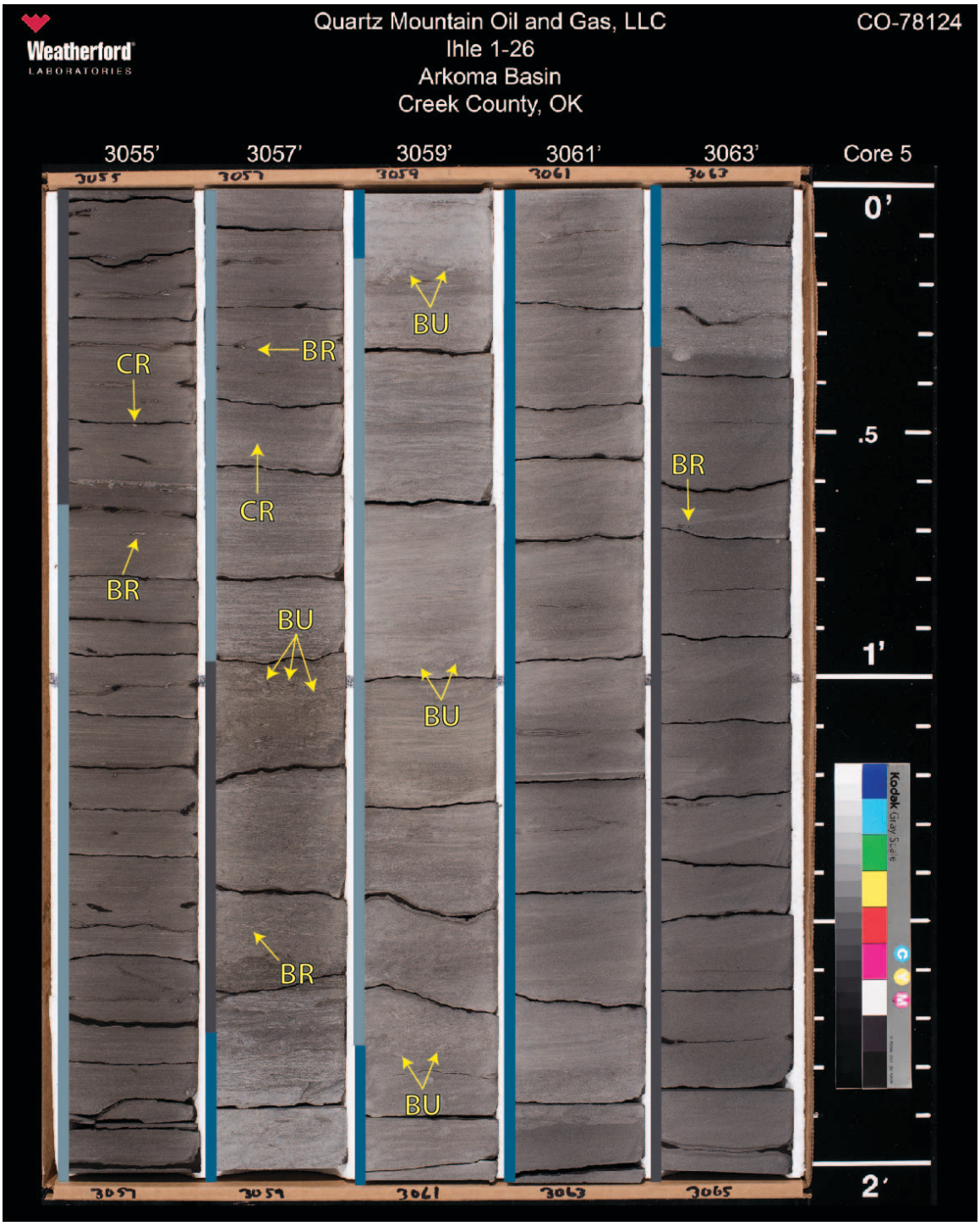
Weatherford
LABORATORIES
Quartz Mountain Oil and Gas, LLC
Ihle 1-26
Arkoma Basin
Creek County, OK
CO-78124
3055'
3057'
3059'
3061'
3063'
Core 5
0'
.5
1'
2'
CR
BR
CR
BR
BU
BU
BR
BU
BU
BR
3055
3057
3059
3061
3063
3057
3059
3061
3063
3065

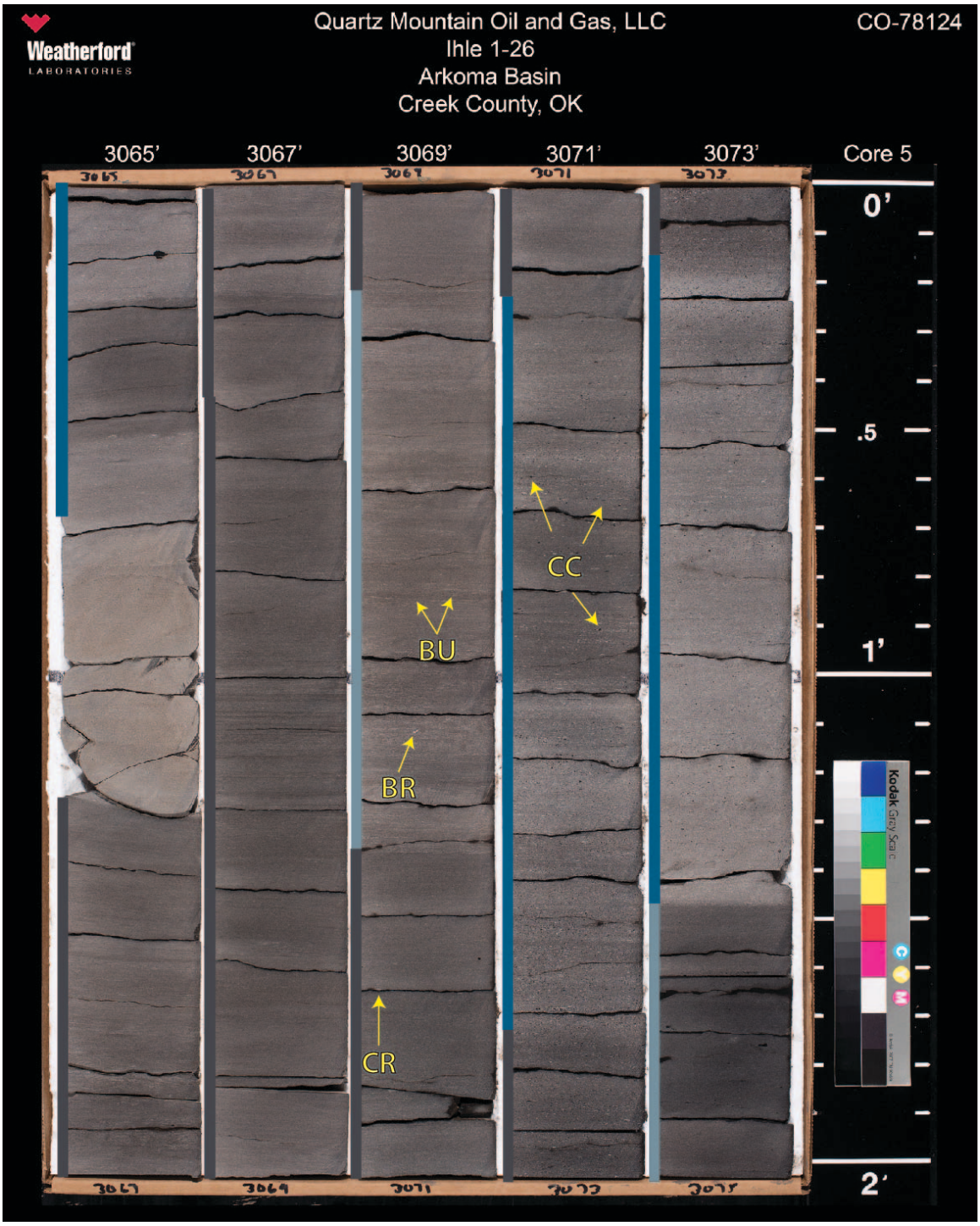
Weatherford
LABORATORIES
Quartz Mountain Oil and Gas, LLC
Ihle 1-26
Arkoma Basin
Creek County, OK
CO-78124
3065'
3067'
3069'
3071'
3073'
Core 5
0'
.5
1'
2'
CC
BU
BR
CR
Kodak Gray Scale

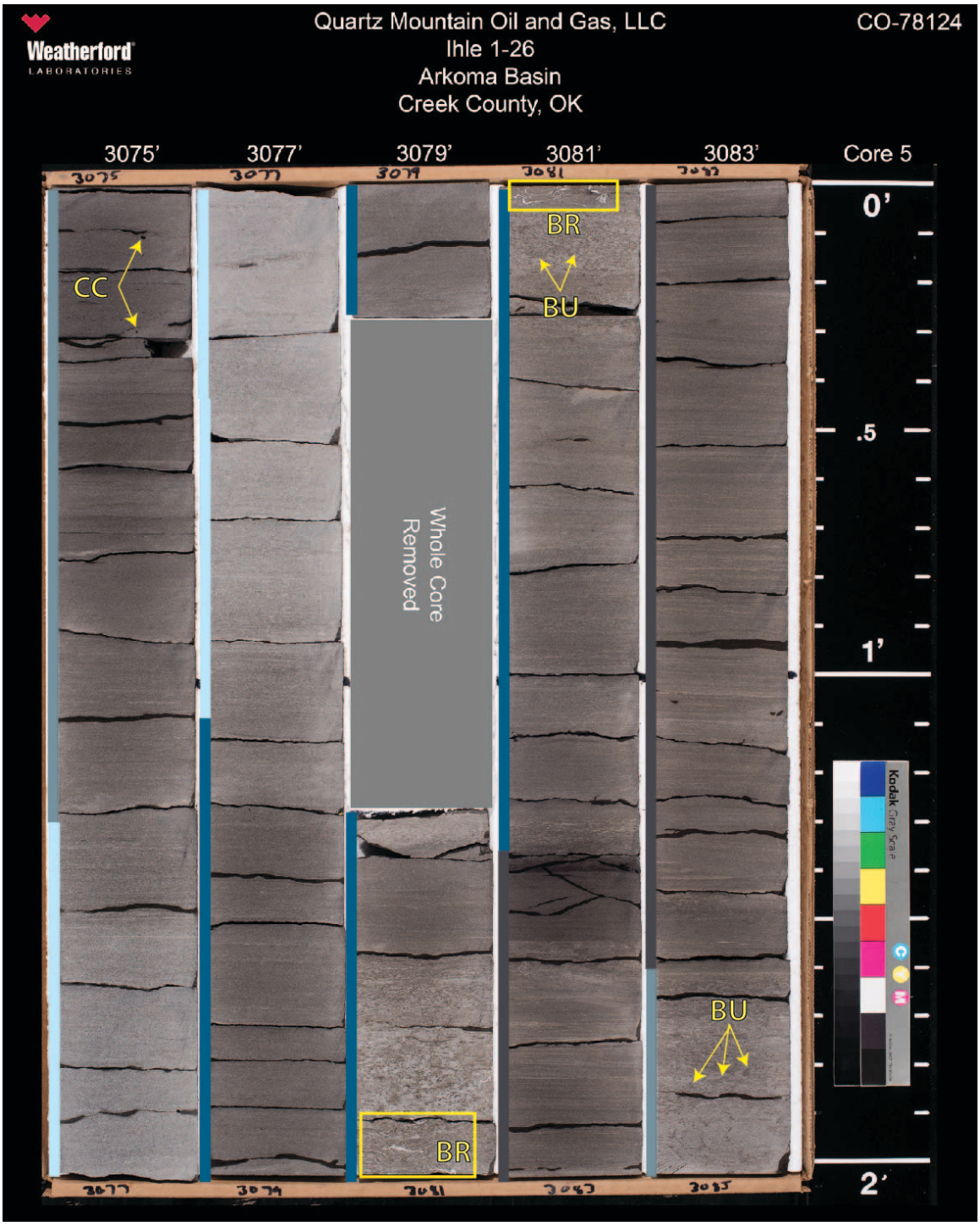
Weatherford
LABORATORIES
Quartz Mountain Oil and Gas, LLC
Ihle 1-26
Arkoma Basin
Creek County, OK
CO-78124
3075'
3077'
3079'
3081'
3083'
Core 5
0'
.5
1'
2'
CC
BR
BU
Whole Core
Removed
BU
BR

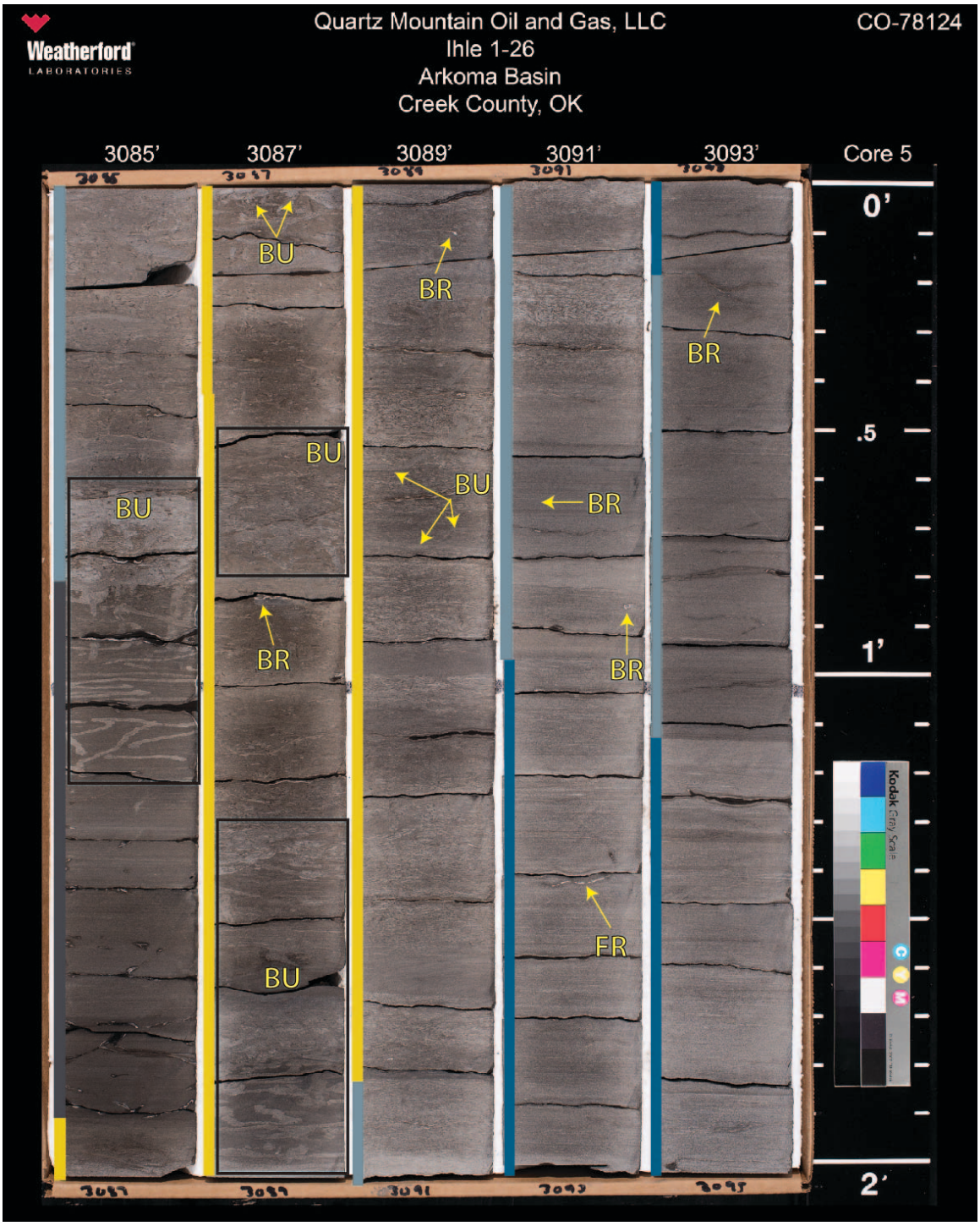
Weatherford
LABORATORIES
Quartz Mountain Oil and Gas, LLC
Ihle 1-26
Arkoma Basin
Creek County, OK
CO-78124
3085'
3087'
3089'
3091'
3093'
Core 5
0'
.5
1'
2'
BU
BU
BU
BU
BU
BR
BR
BR
BR
BR
FR

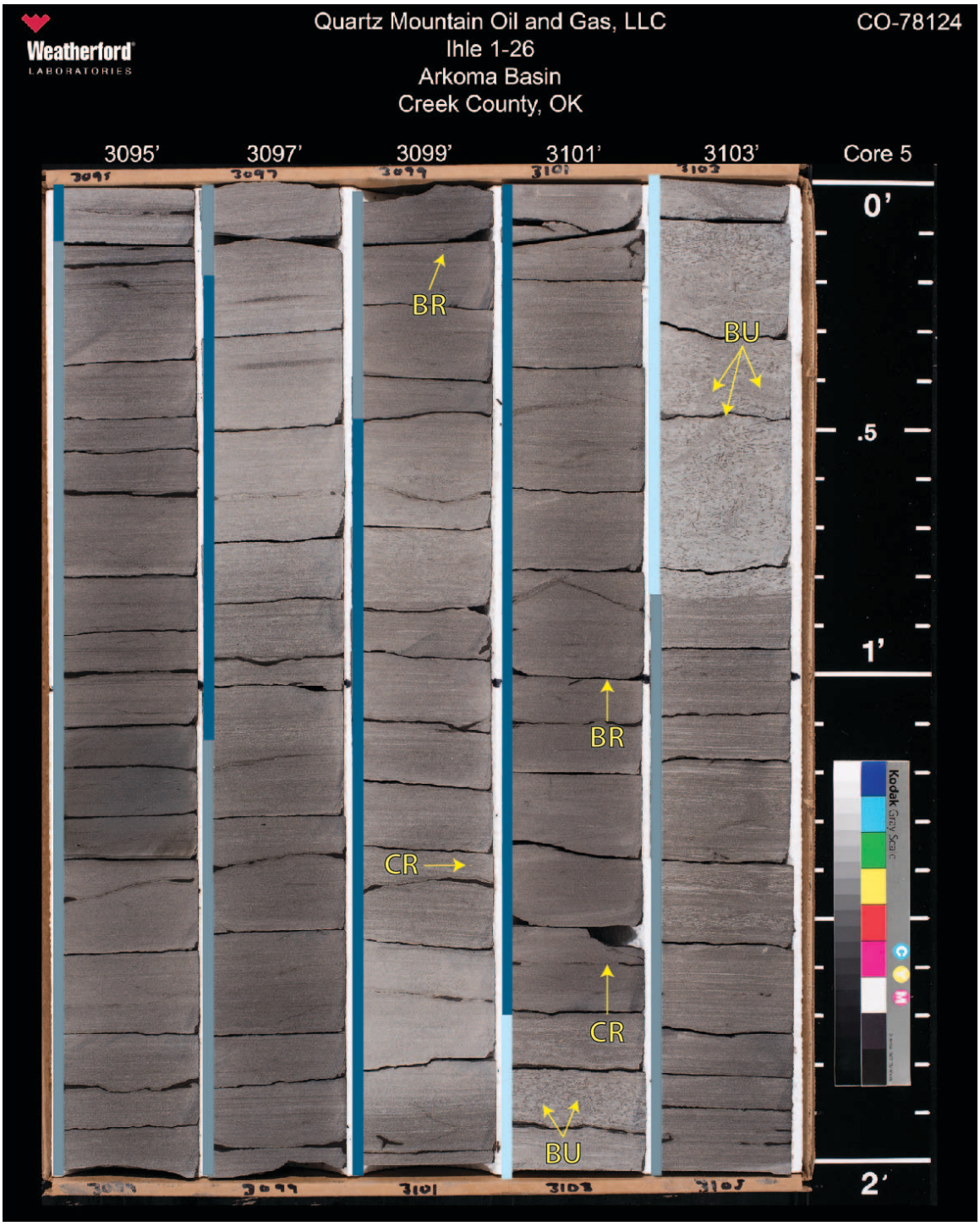
Weatherford
LABORATORIES
Quartz Mountain Oil and Gas, LLC
Ihle 1-26
Arkoma Basin
Creek County, OK
CO-78124
3095'
3097'
3099'
3101'
3103'
Core 5
0'
.5
1'
2'
BR
BU
BR
CR
CR
BU

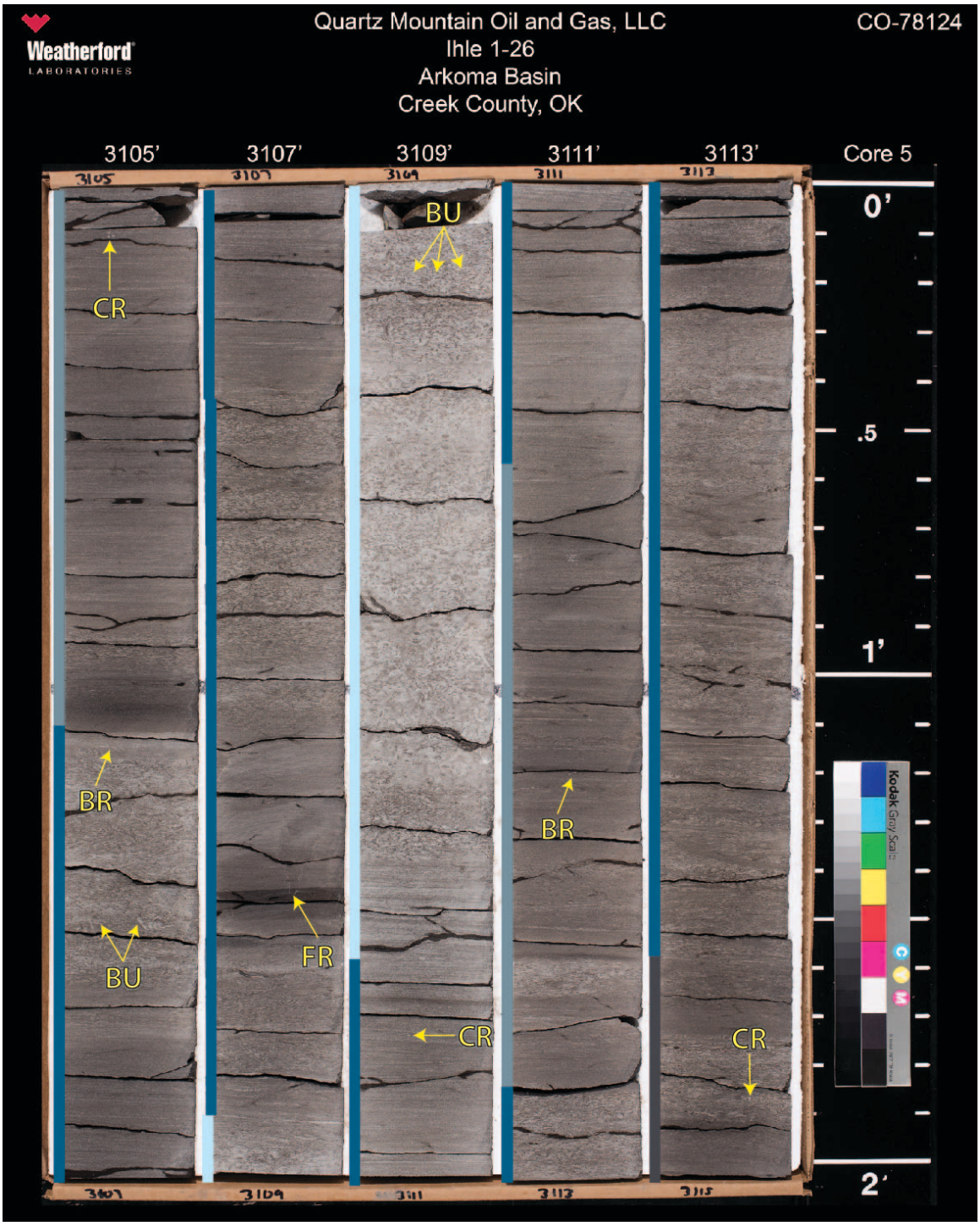
Weatherford
LABORATORIES
Quartz Mountain Oil and Gas, LLC
Ihle 1-26
Arkoma Basin
Creek County, OK
CO-78124
3105'
3107'
3109'
3111'
3113'
Core 5
0'
.5
1'
2'
CR
BU
BR
FR
BU
CR
BR
CR
Kodak Gray Scale

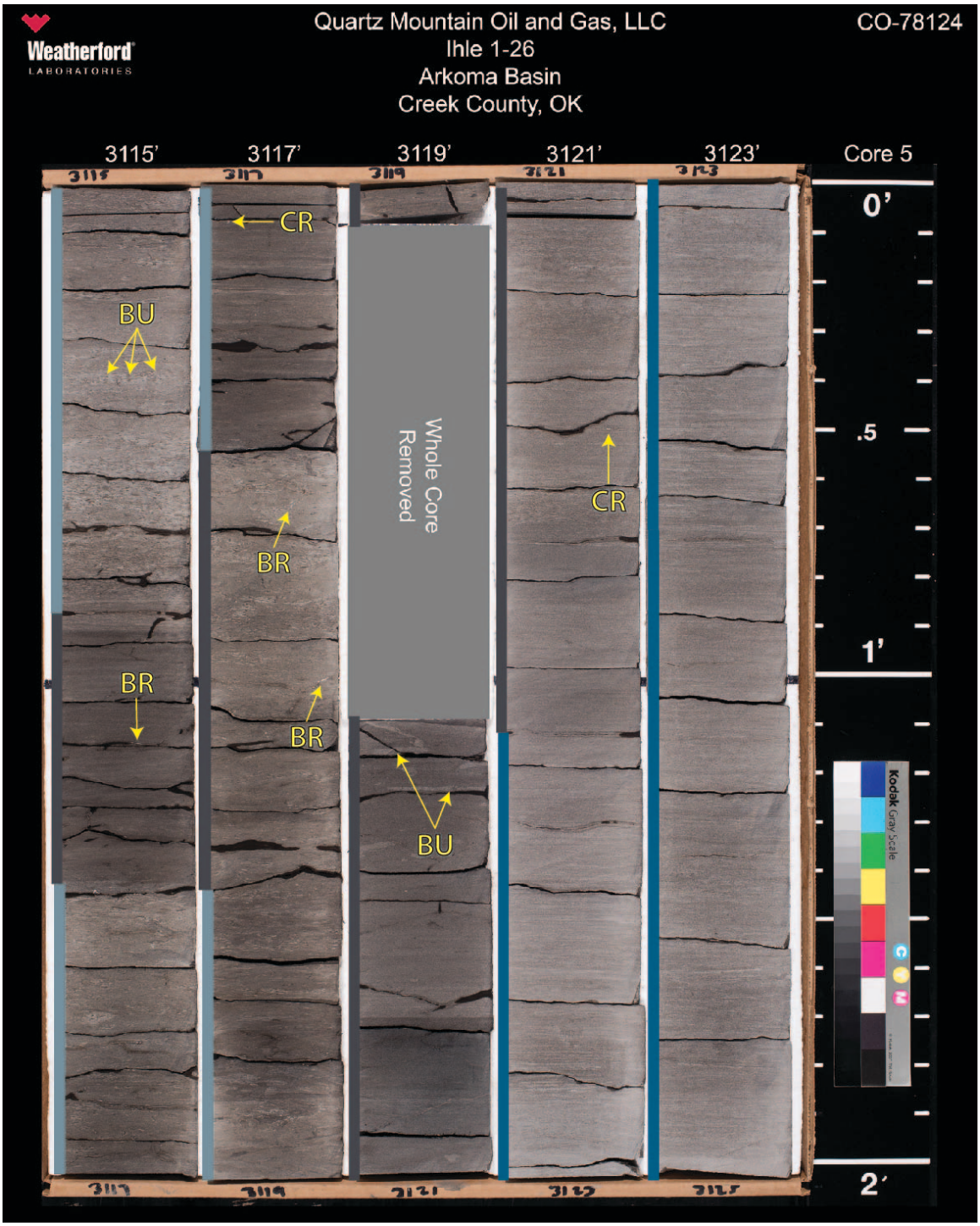
Weatherford
LABORATORIES
Quartz Mountain Oil and Gas, LLC
Ihle 1-26
Arkoma Basin
Creek County, OK
CO-78124
3115'
3117'
3119'
3121'
3123'
Core 5
0'
.5
1'
2'
CR
BU
BR
BR
BR
CR
BU
Whole Core
Removed
Kodak Gray Scale

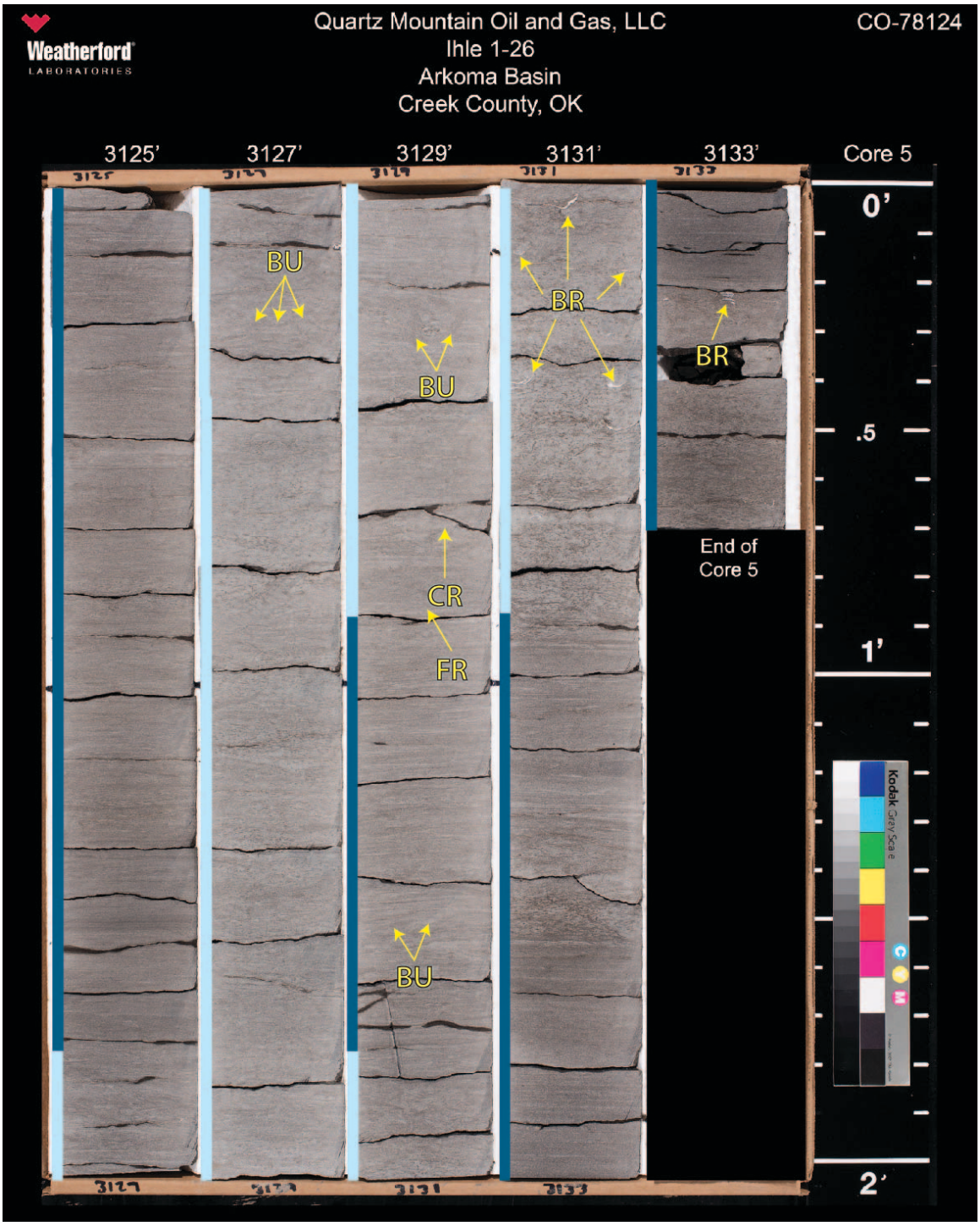


3133.60' – 3135' = missing

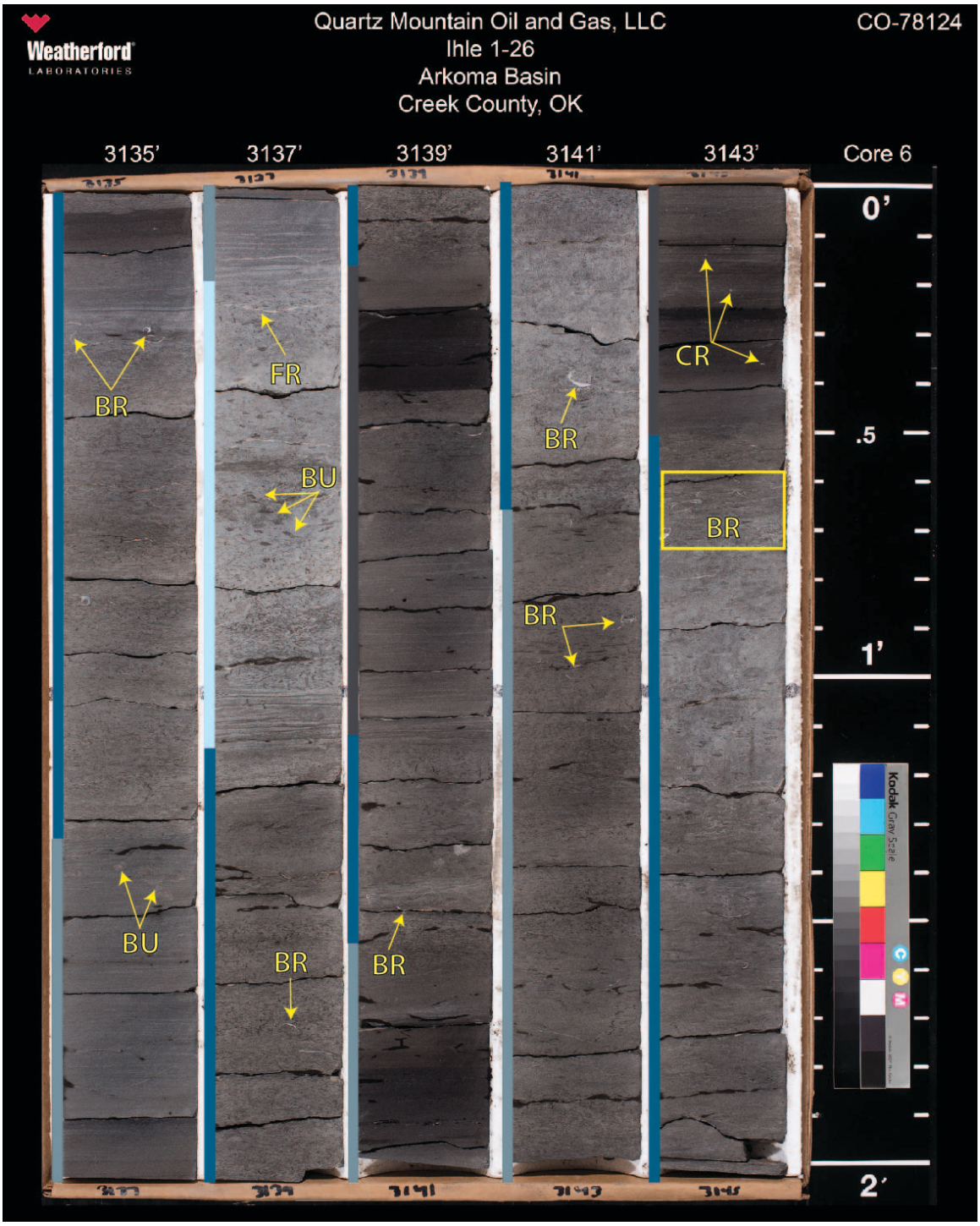
Weatherford
LABORATORIES
Quartz Mountain Oil and Gas, LLC
Ihle 1-26
Arkoma Basin
Creek County, OK
CO-78124
3135'
3137'
3139'
3141'
3143'
Core 6
0'
.5
1'
2'
BR
FR
BU
BR
CR
BR
BR
BU
BR
BR

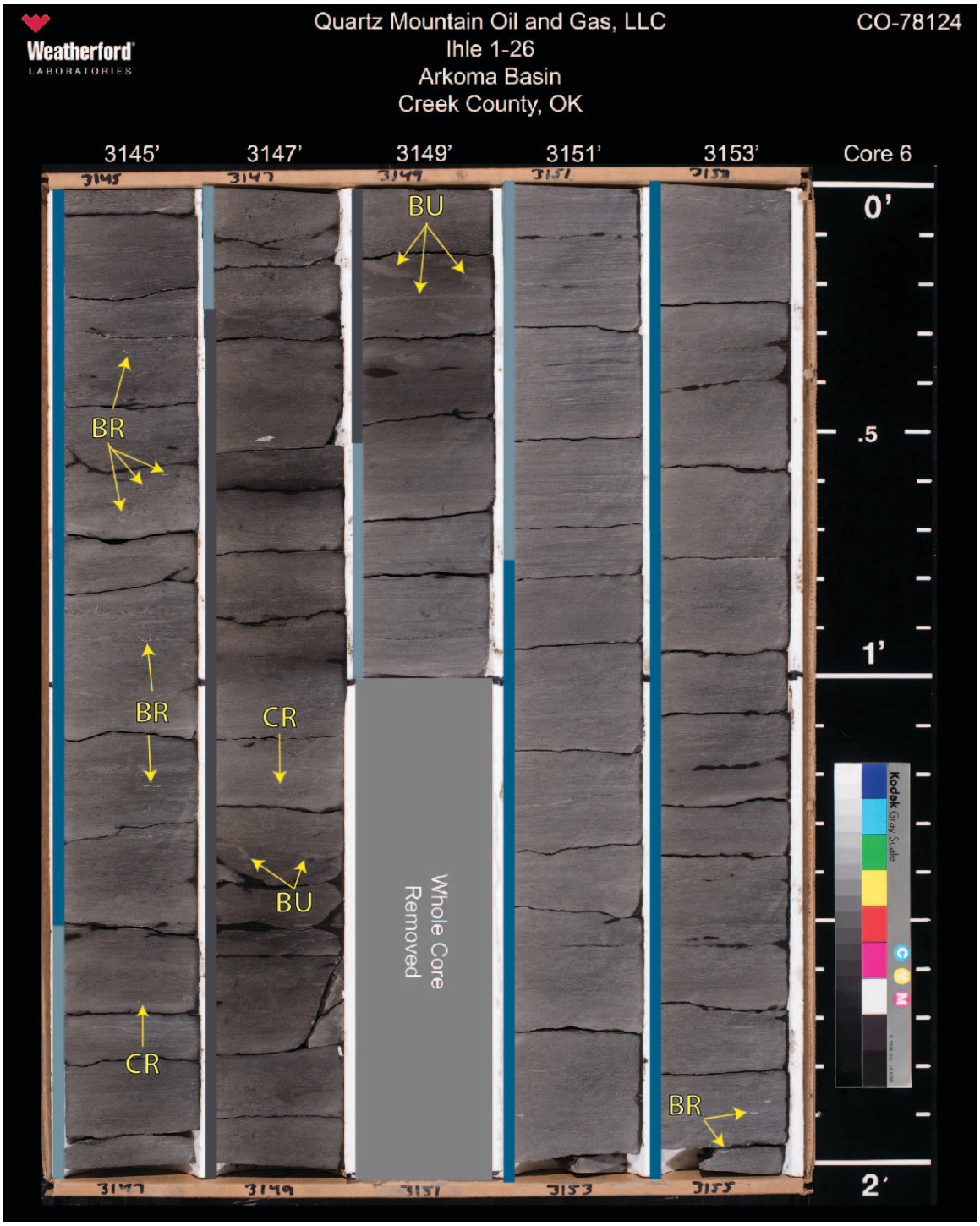
Weatherford
LABORATORIES
Quartz Mountain Oil and Gas, LLC
Ihle 1-26
Arkoma Basin
Creek County, OK
CO-78124
3145'
3147'
3149'
3151'
3153'
Core 6
0'
.5
1'
2'
BU
BR
BR
CR
BU
CR
BR
Whole Core
Removed
Kodak Gray Scale

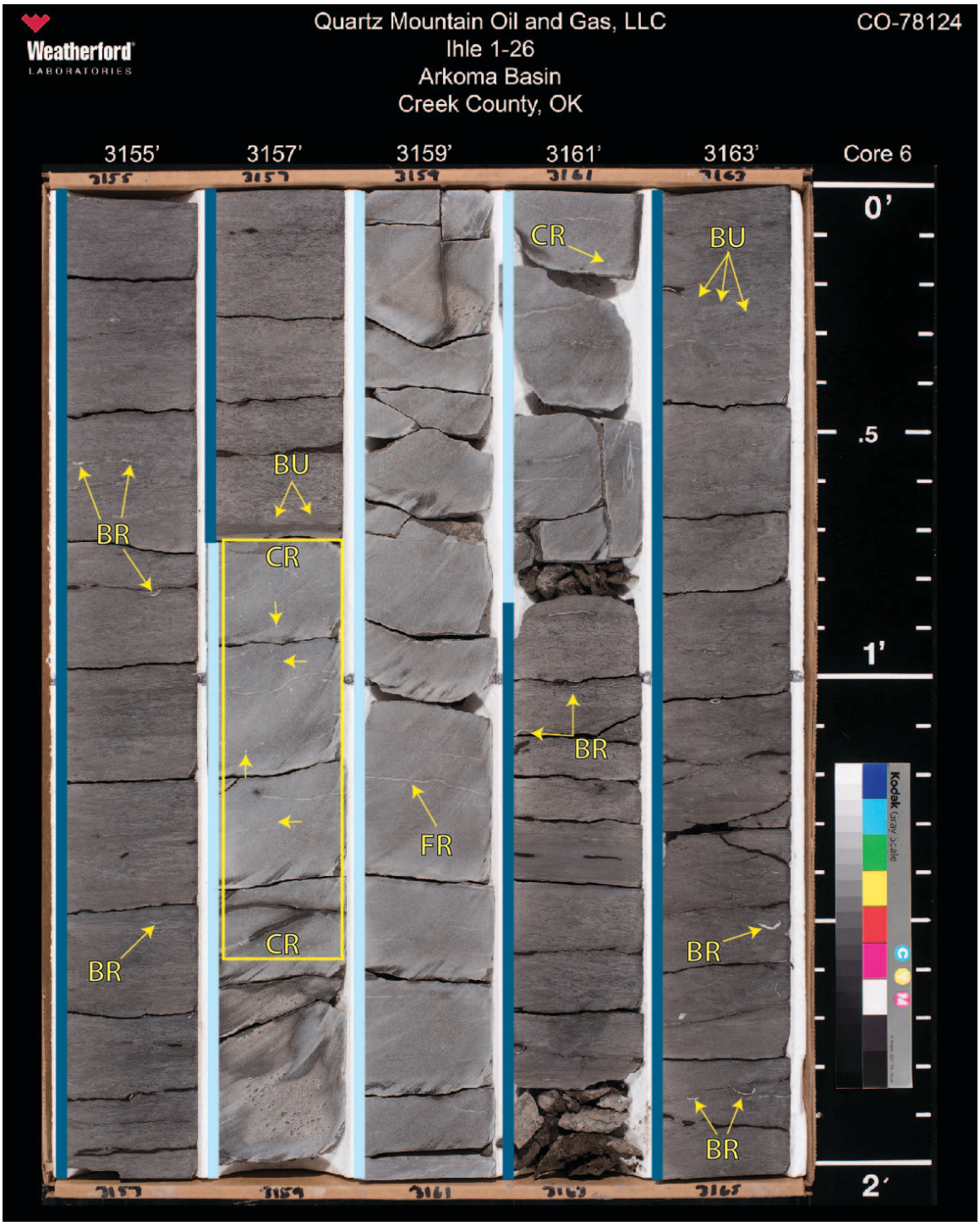
Weatherford
LABORATORIES
Quartz Mountain Oil and Gas, LLC
Ihle 1-26
Arkoma Basin
Creek County, OK
CO-78124
3155'
3157'
3159'
3161'
3163'
Core 6
0'
.5
1'
2'
BU
BR
CR
FR
Kodak Gray Scale

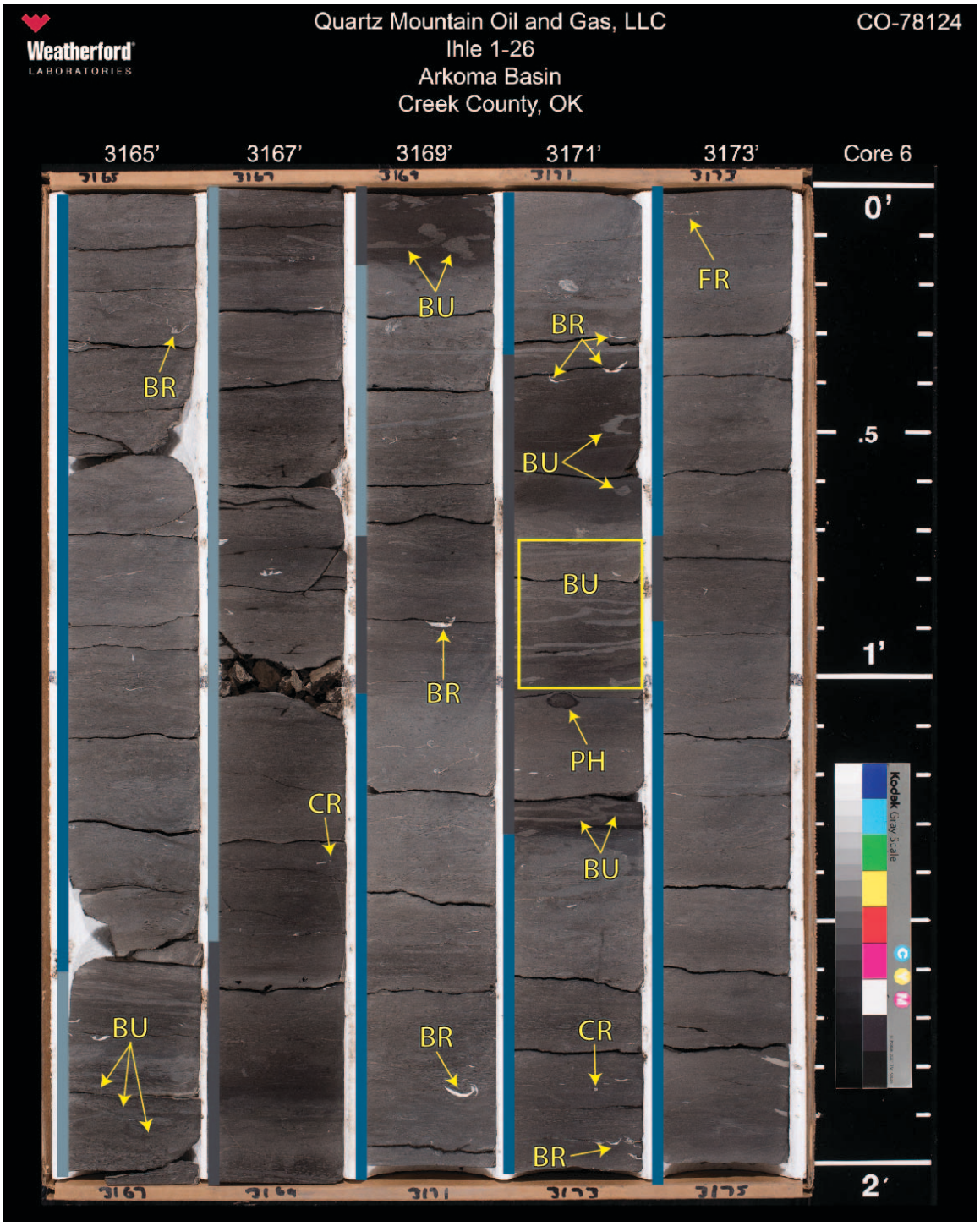
Weatherford
LABORATORIES
Quartz Mountain Oil and Gas, LLC
Ihle 1-26
Arkoma Basin
Creek County, OK
CO-78124
3165'
3167'
3169'
3171'
3173'
Core 6
0'
.5
1'
2'
BR
BU
BR
FR
BU
BU
BR
PH
CR
BU
BU
BR
CR
BR

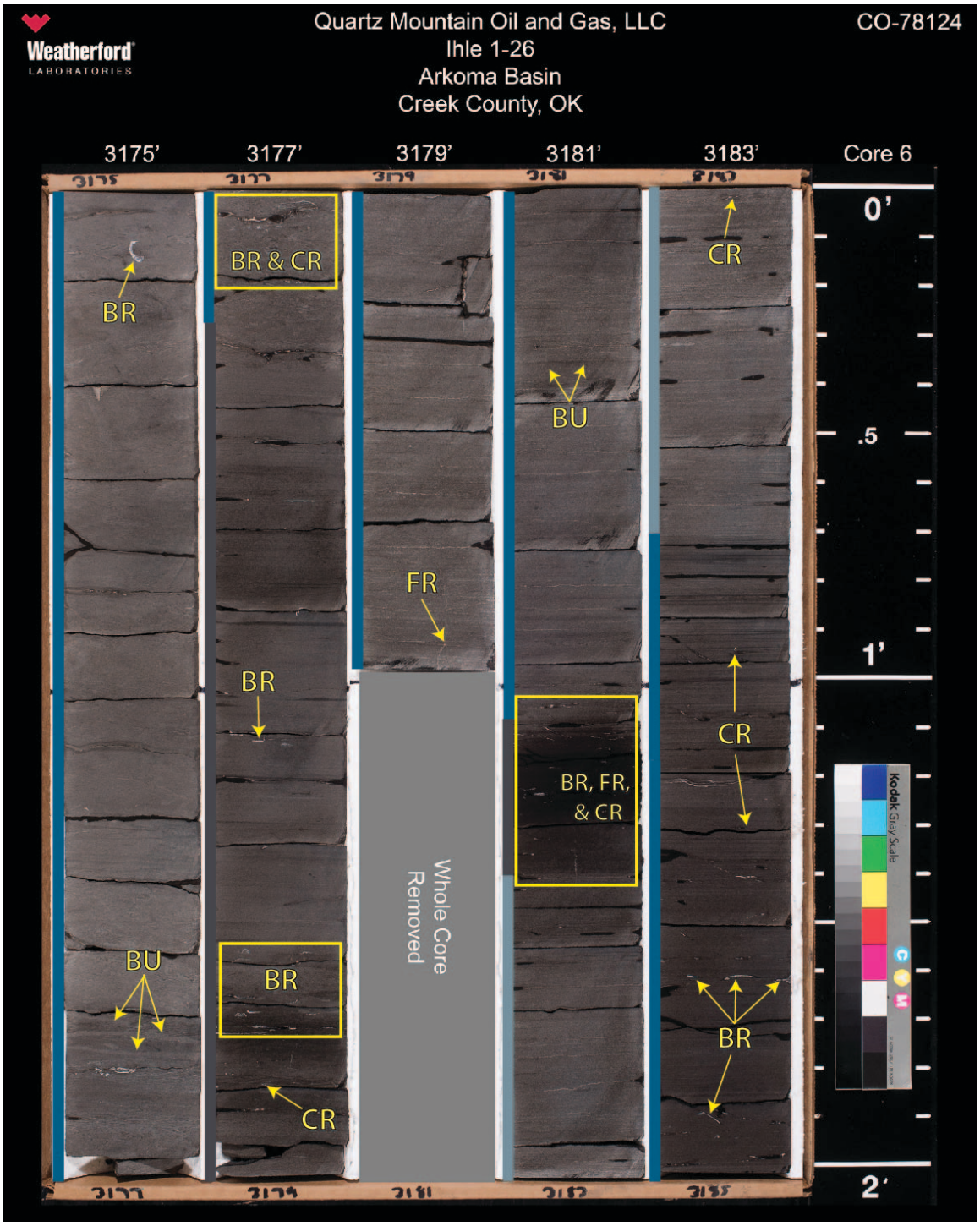
Weatherford
LABORATORIES
Quartz Mountain Oil and Gas, LLC
Ihle 1-26
Arkoma Basin
Creek County, OK
CO-78124
3175'
3177'
3179'
3181'
3183'
Core 6
0'
.5
1'
2'
BR
BR & CR
CR
BU
FR
BR
BR, FR, & CR
CR
Whole Core Removed
BU
BR
CR
BR
Kodak Gray Scale

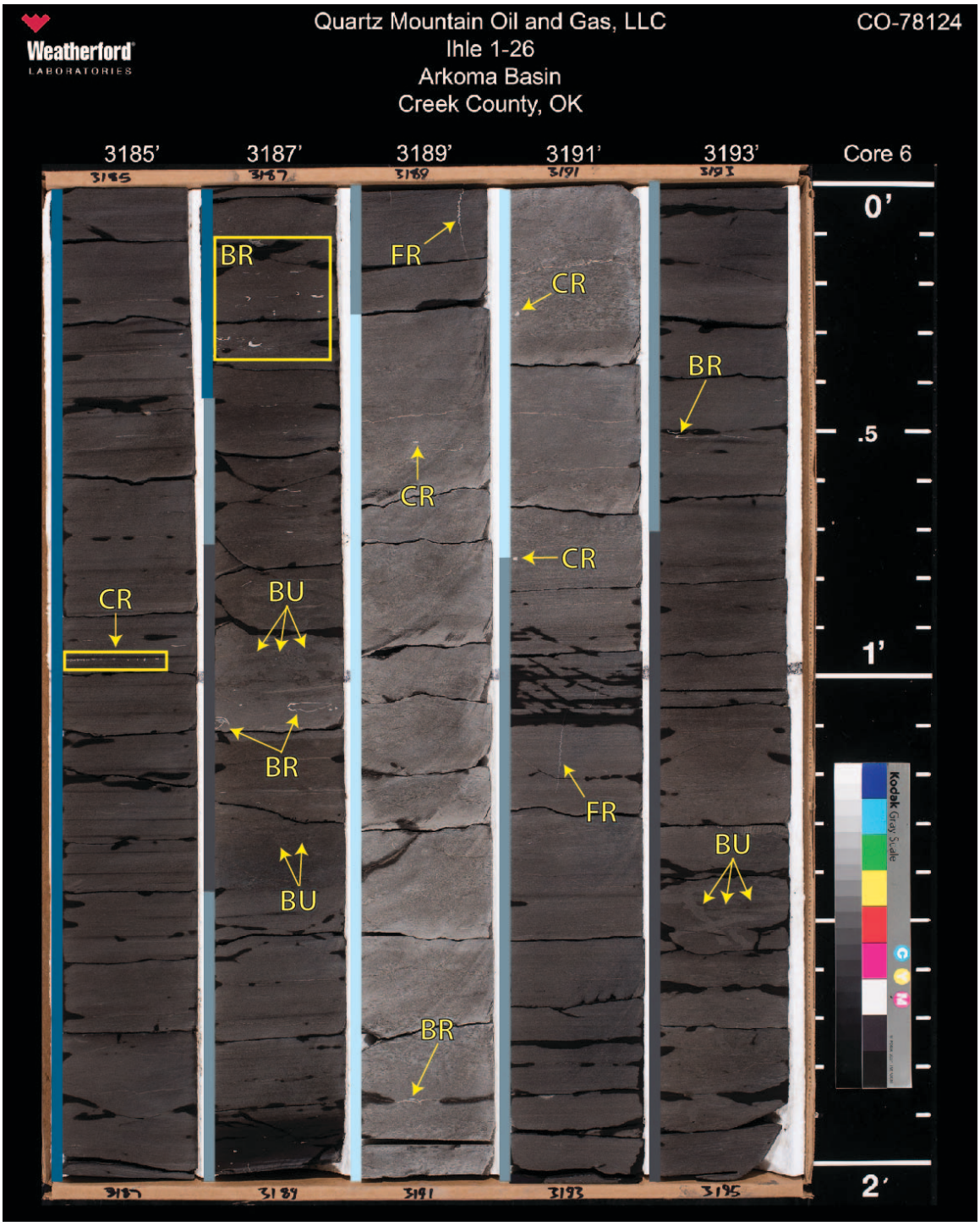
Weatherford
LABORATORIES
Quartz Mountain Oil and Gas, LLC
Ihle 1-26
Arkoma Basin
Creek County, OK
CO-78124
3185'
3187'
3189'
3191'
3193'
Core 6
0'
.5
1'
2'
BR
FR
CR
BR
CR
CR
CR
BU
BR
FR
BU
BU
BR
Kodak Gray Scale

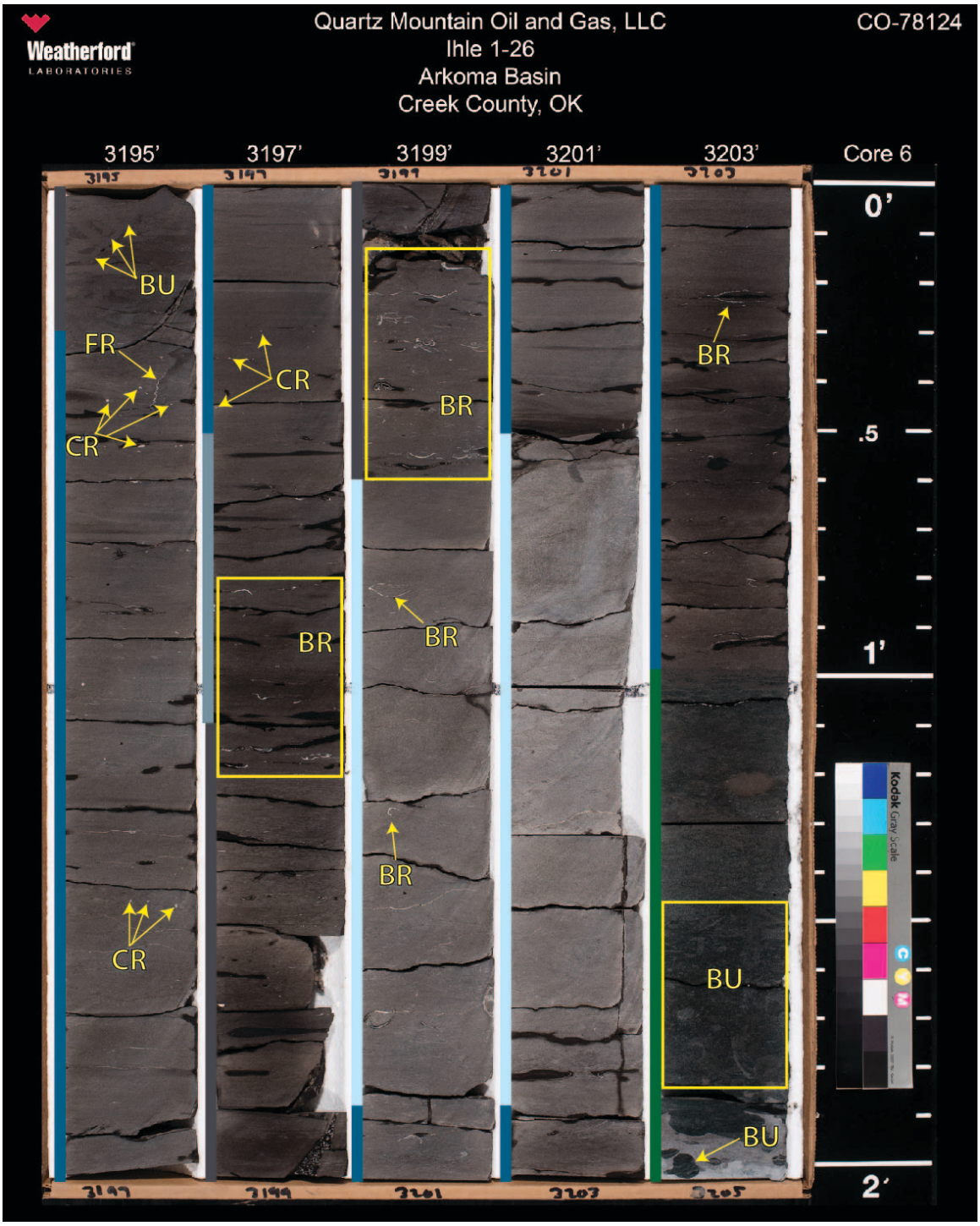
Weatherford
LABORATORIES
Quartz Mountain Oil and Gas, LLC
Ihle 1-26
Arkoma Basin
Creek County, OK
CO-78124
3195'
3197'
3199'
3201'
3203'
Core 6
0'
.5
1'
2'
BU
FR
CR
CR
CR
BR
BR
BR
BR
BR
BU
BU
Kodak Gray Scale

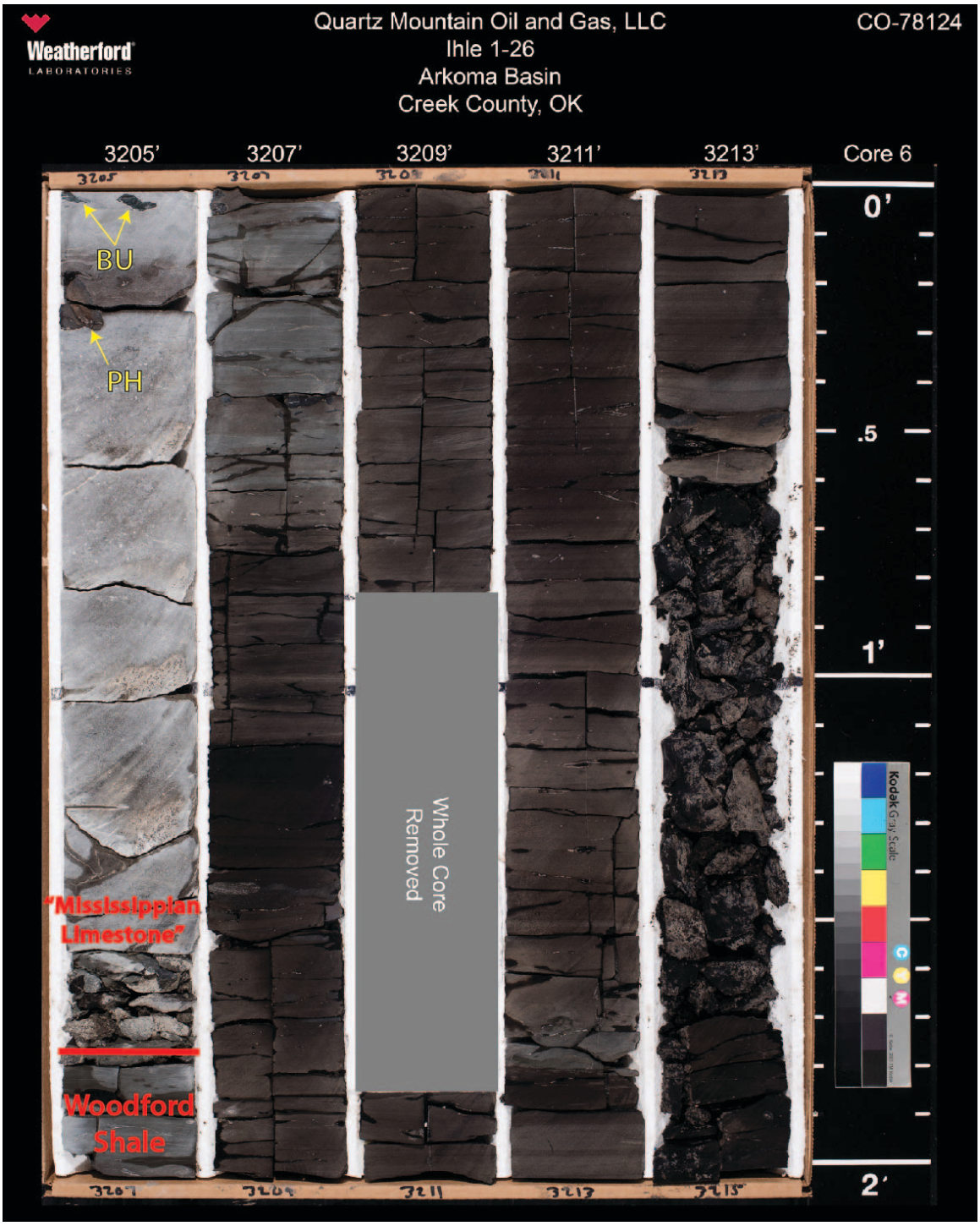
Weatherford
LABORATORIES
Quartz Mountain Oil and Gas, LLC
Ihle 1-26
Arkoma Basin
Creek County, OK
CO-78124
3205'
3207'
3209'
3211'
3213'
Core 6
0'
.5
1'
2'
BU
PH
"Mississippian Limestone"
Woodford Shale
Whole Core Removed
Kodak Gray Scale

## II. Ihle #1-26 Core Descriptions

The Ihle core was described using the Dunham (1962) classification scheme where applicable (i.e. – carbonate-rich intervals) whereas siliciclastic-rich intervals were classified based on abundant grain type and composition. The colors described from the core relate to the standardized color chart key (Table 12), which has been adapted from the revised rock-color chart developed by the rock-color chart committee (2009). The descriptions and degree of bioturbation uses a bioturbation index implemented from Bann et al., 2008 (refer to Table 8).

| Rock-Color Chart - Ihle #1-26 | | | |
|---|---|---|---|
| **Color Name** | **Numerical Designation** | **Color Name** | **Numerical Designation** |
| Black | N1 | Medium Light Gray | N6 |
| Brownish Black | 5YR 2/1 | Very Light Gray | N8 |
| Dusky Blue Green | 5BG 3/2 | White | N9 |
| Dusky Brown | 5YR 2/2 | | |
| Dusky Yellow Green | 5GY 5/2 | | |
| Grayish Black | N2 | | |
| Greenish Black | 5GY 2/1 | | |
| Greenish Gray | 5G 6/1 | | |
| Light Bluish Gray | 5B 7/1 | | |
| Light Gray | N7 | | |
| Medium Dark Gray | N4 | | |
| Medium Gray | N5 | | |

Table 12. Modified from the Rock-Color Chart prepared by the Rock-Color Chart Committee (representing the U.S.G.S., GSA, AAPG, SEG, and AASG) and distributed by The Geological Society of America. Revised and reprinted in 2009.

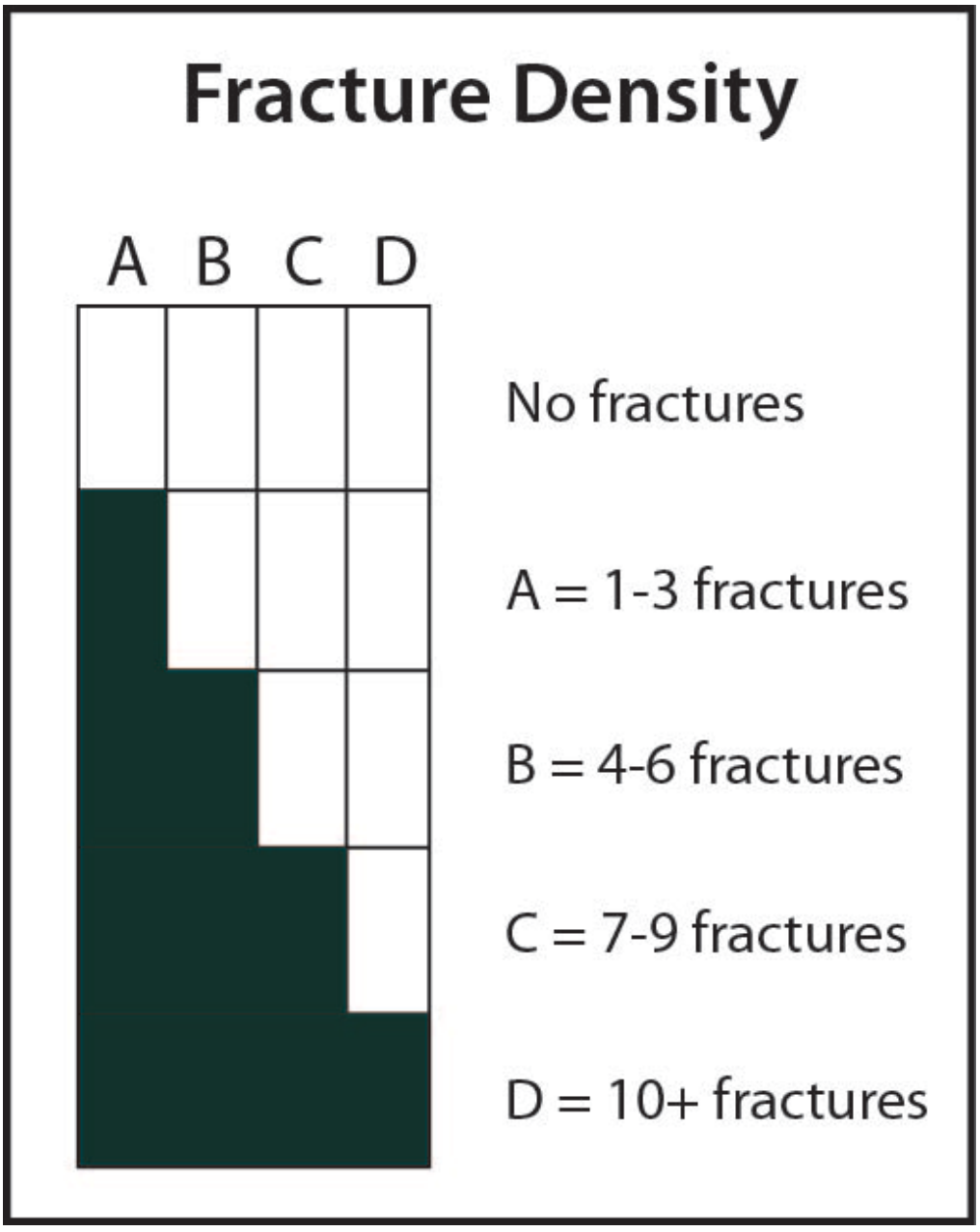


Table 13. Chart used for illustrating the fracture density within the core descriptions. The letters A through D relate to the number of fractures in one foot of core.

## LITHOLOGIC SYMBOLS

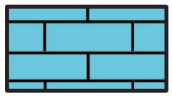
Limestone

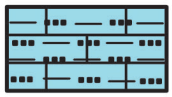
Silty Limestone

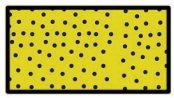
Sandstone

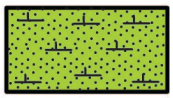
Calcareous Sandstone

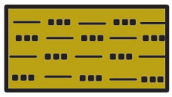
Siltstone

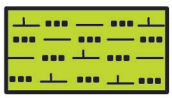
Calcareous Siltstone

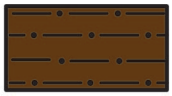
Silty Shale/Mudstone

Calcareous Silty Shale/Mudstone

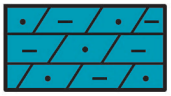
Silty Dolomite

Carbonate Concretion

## GRAIN TYPES, SEDIMENTARY STRUCTURES, & DIAGENETIC FEATURES

Bioturbated

Burrow

Brachiopod

Crinoid

Cross-Bedded

Unrecognizable Fossils

Filled Fracture

Horizontal Laminae

Argillaceous

Peloids

Glauconite

Pyrite

Nodule/Clast

## TRACE FOSSILS

| | | |
|---|---|---|
| Ch - Chondrites | He - Helminthopsis | Pl - Planolites |
| Cy - Cylindrichnus | Ph - Phycosiphon | Zo - Zoophycos |

# Devon Energy - Ihle #1-26, Lincoln County, OK

Formation: "Mississippian Limestone"

Depth Interval: 2783' - 2863'

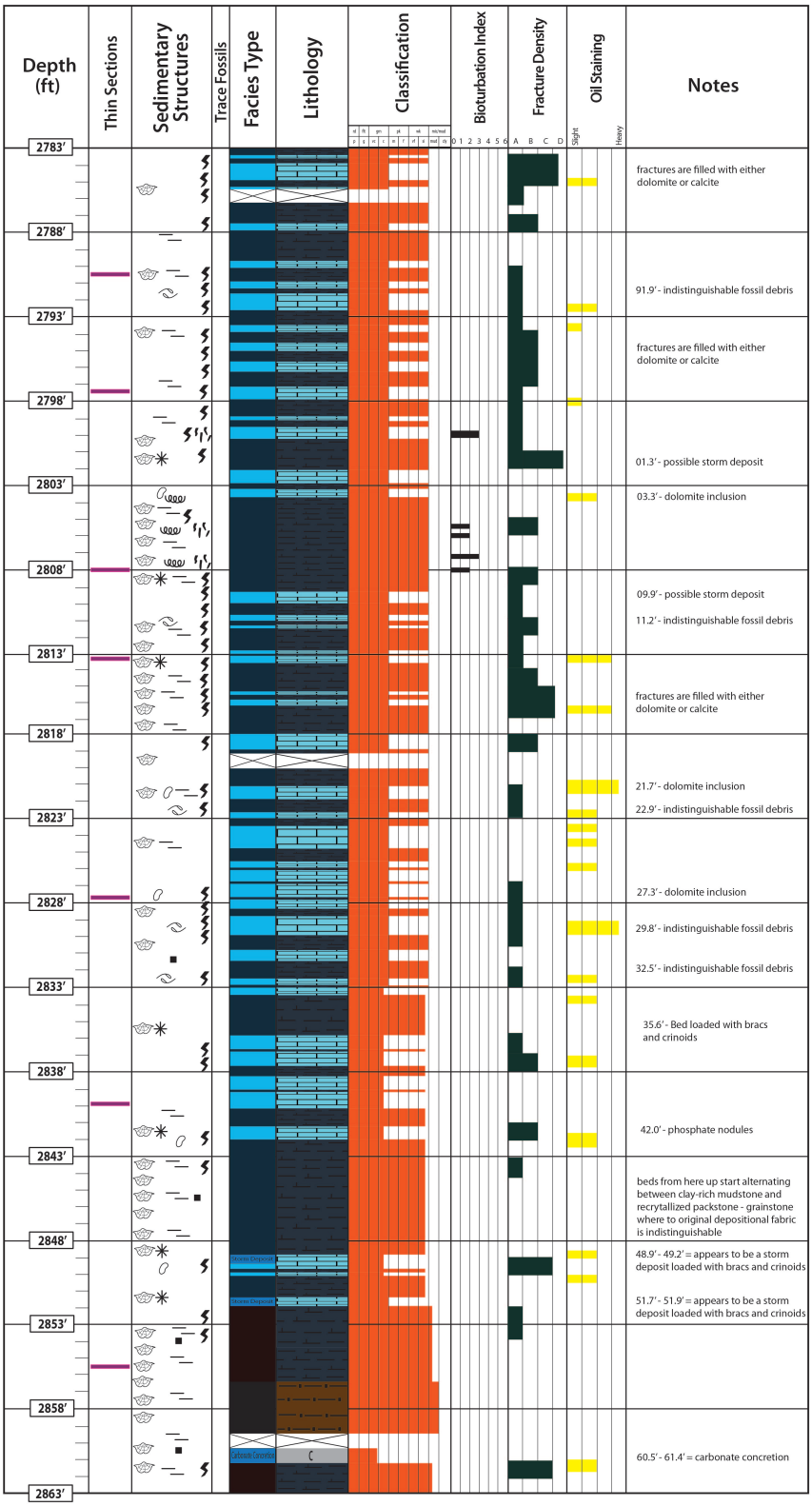

# Devon Energy - Ihle #1-26, Lincoln County, OK

Formation: "Mississippian Limestone"

Depth Interval: 2863' - 2943'

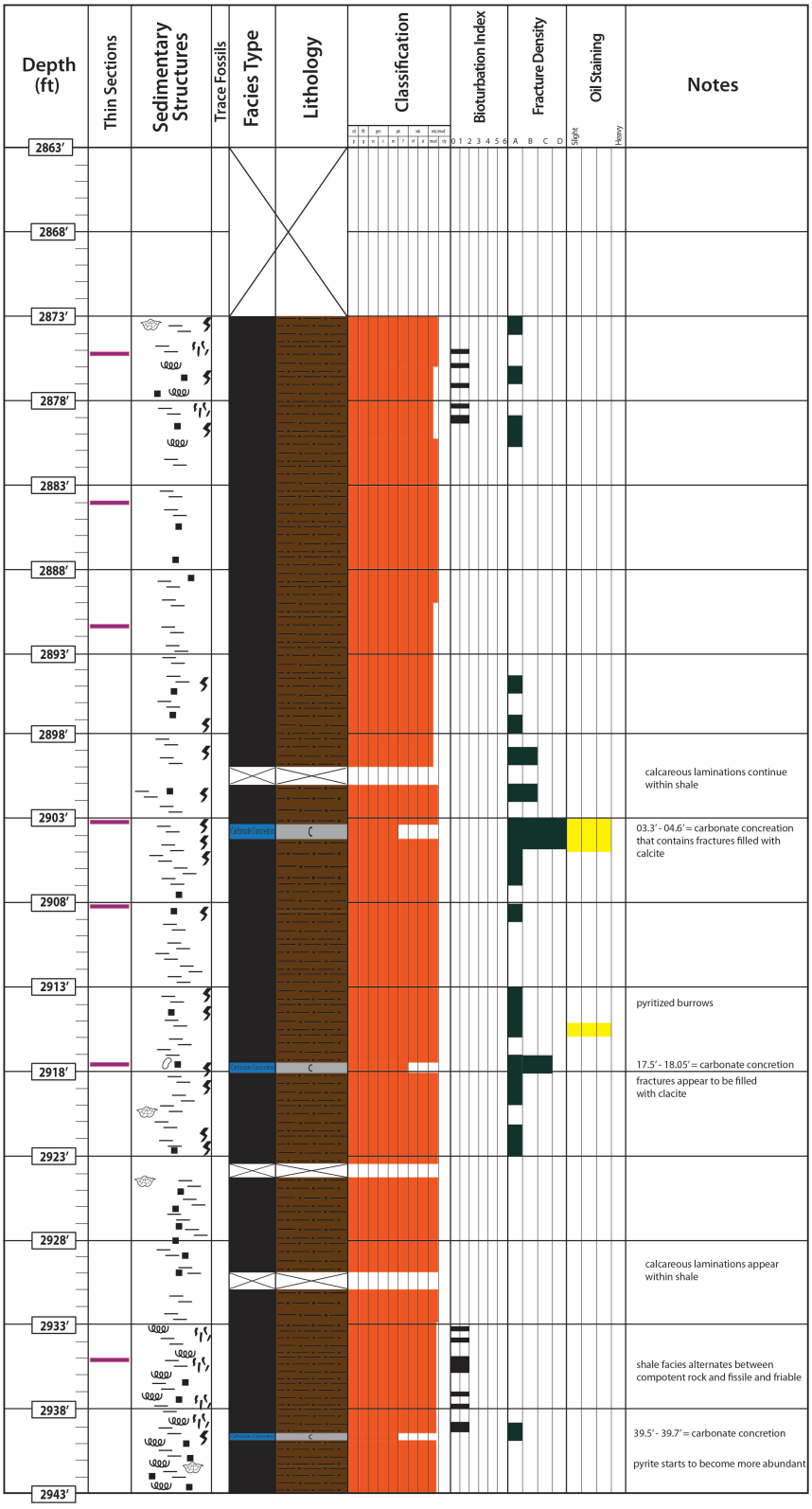

3

# Devon Energy - Ihle #1-26, Lincoln County, OK

Formation: "Mississippian Limestone"

Depth Interval: 2943' - 3023'

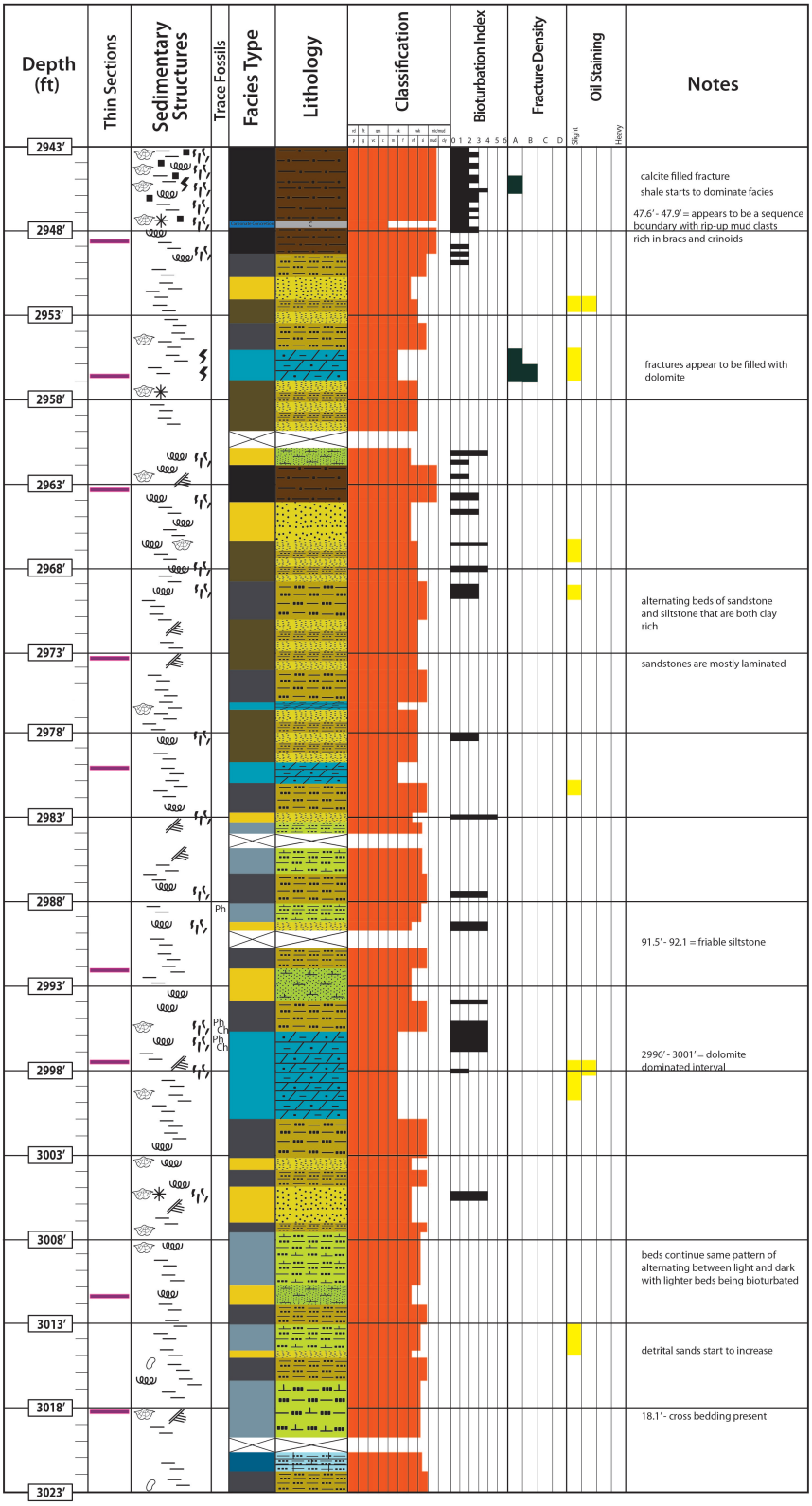

4

# Devon Energy - Ihle #1-26, Lincoln County, OK

Formation: "Mississippian Limestone"

Depth Interval: 3023' - 3103'

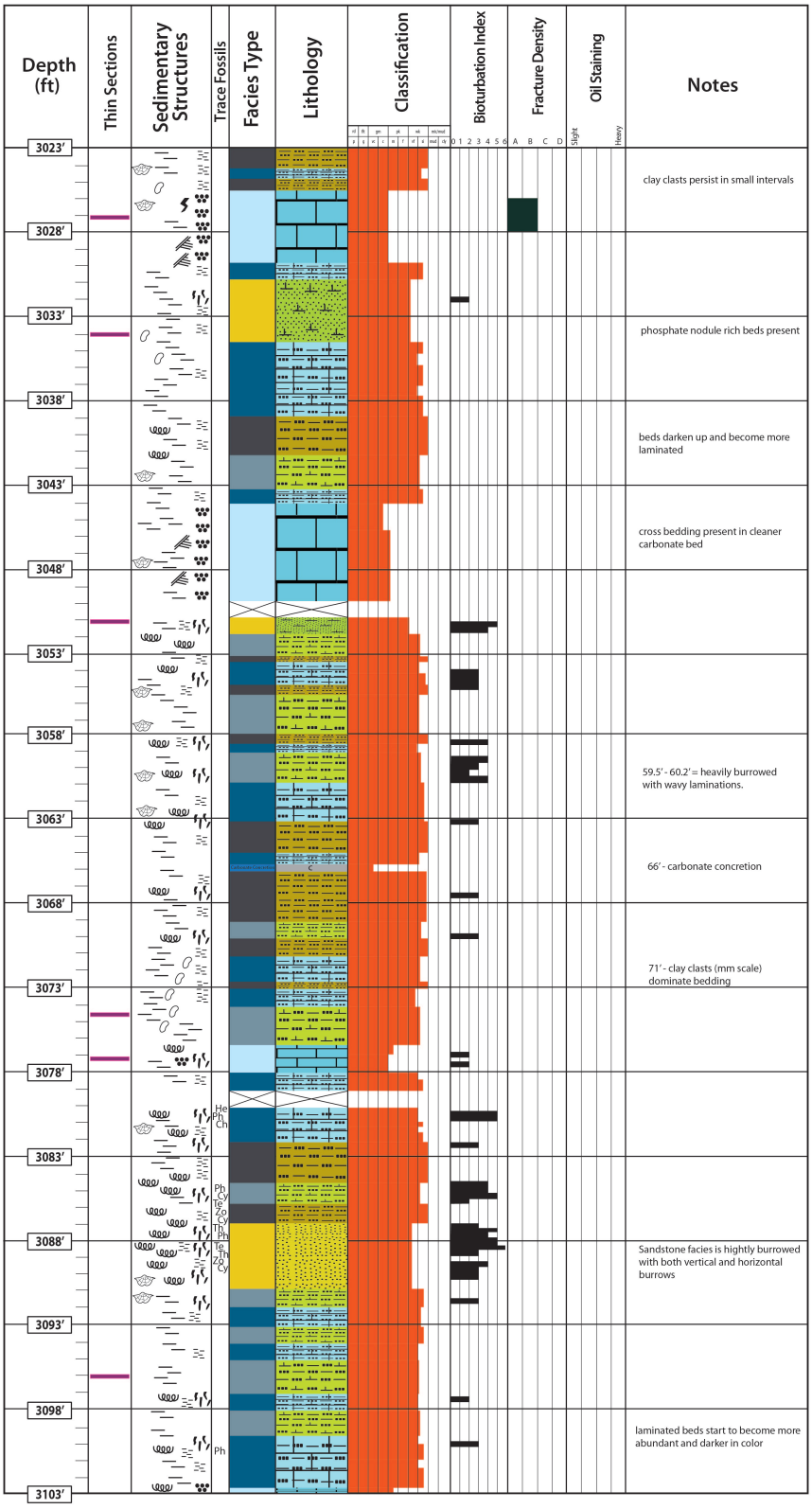

5

# Devon Energy - Ihle #1-26, Lincoln County, OK

Formation: "Mississippian Limestone"

Depth Interval: 3103' - 3183'

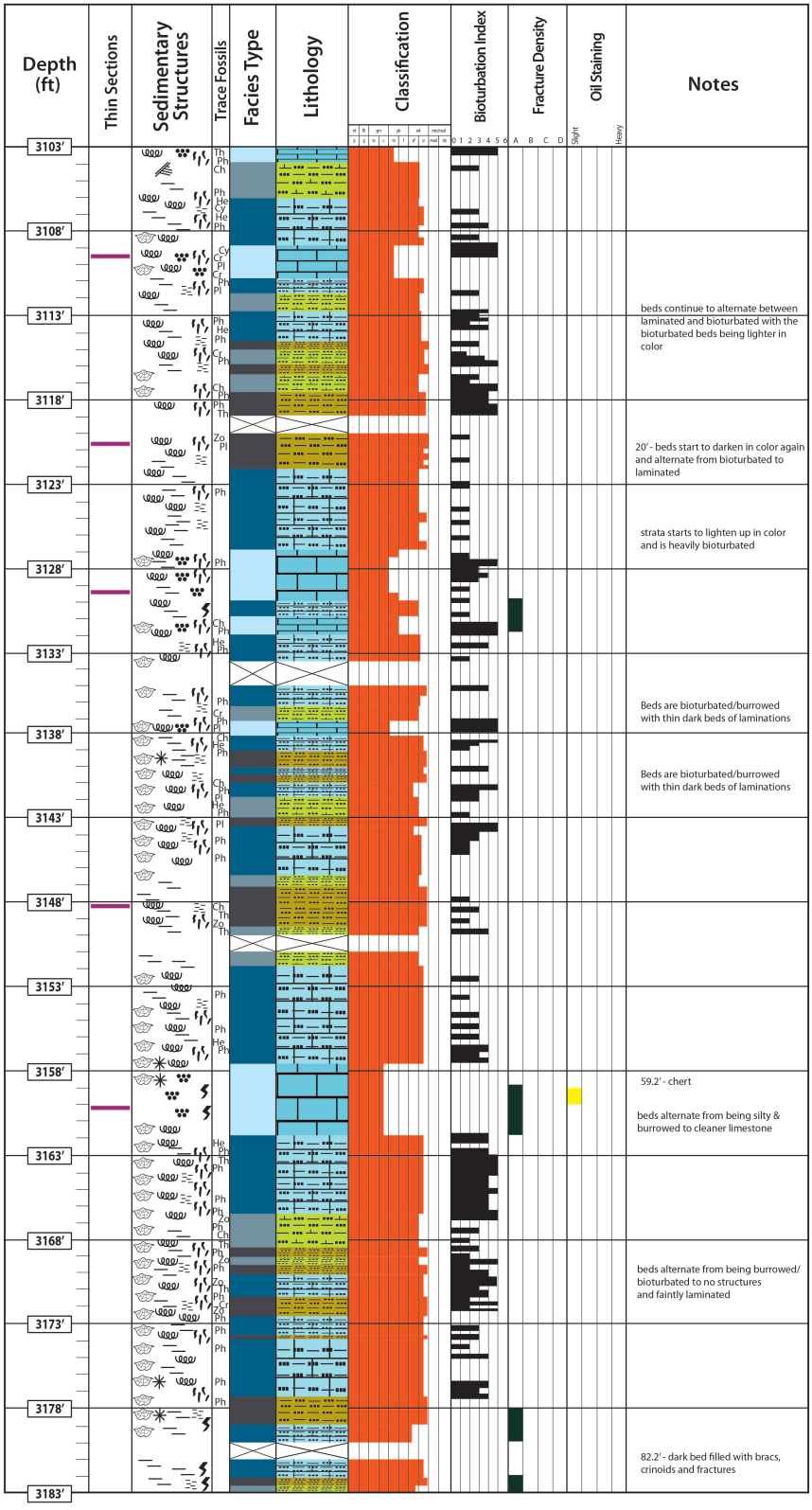

6

# Devon Energy - Ihle #1-26, Lincoln County, OK

Formation: "Mississippian Limestone"

Depth Interval: 3183' - 3213'

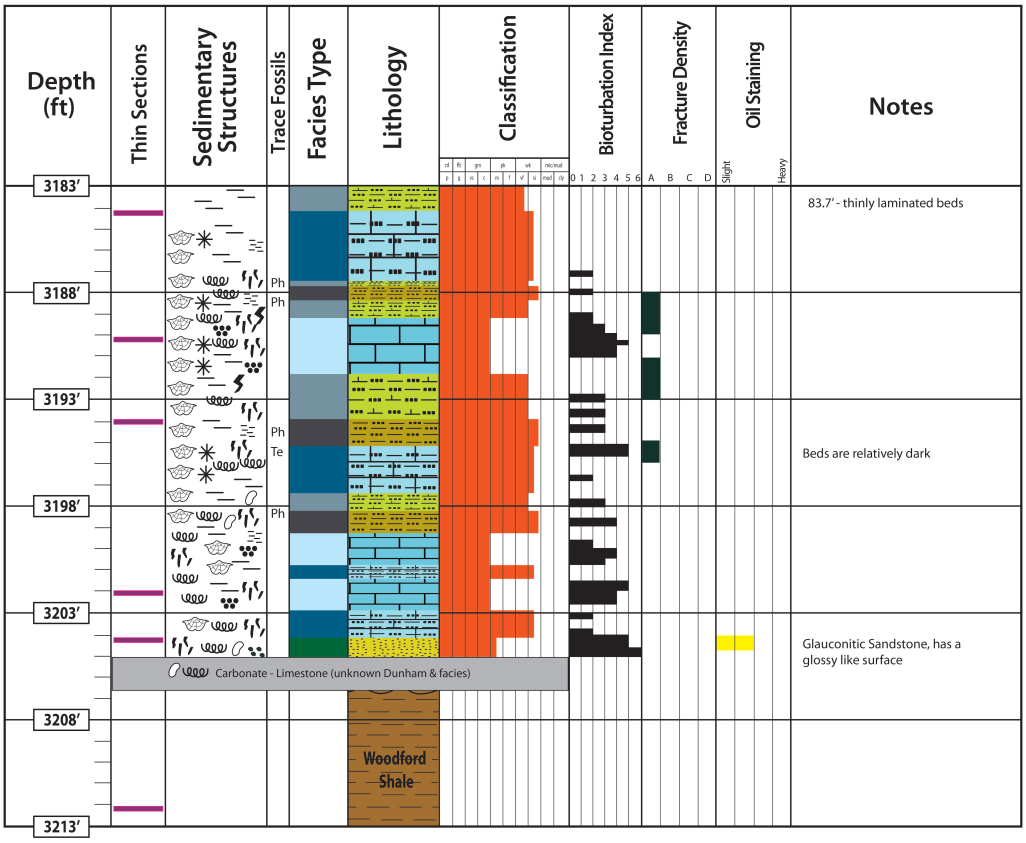

## Core to Wireline Log Correlation

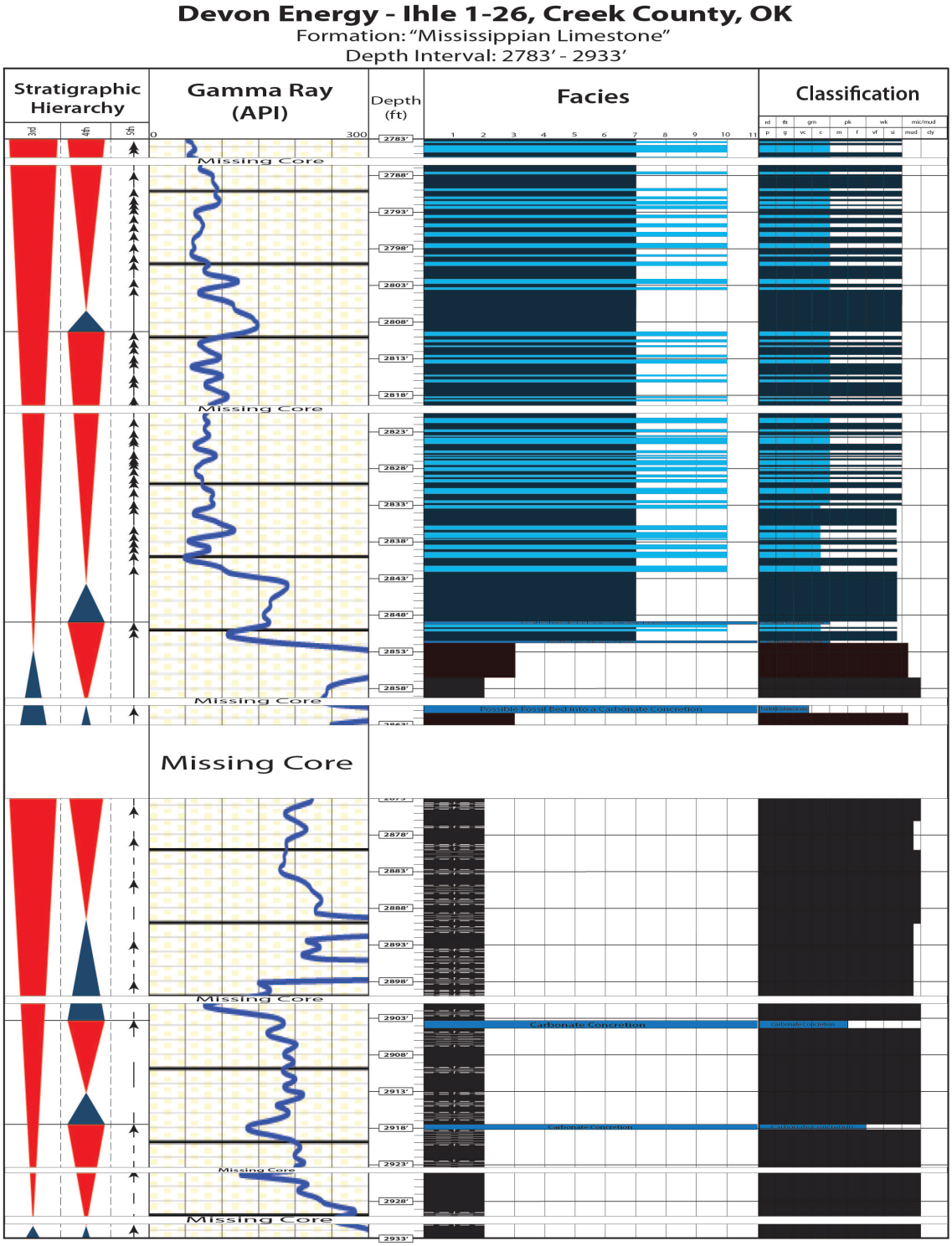

## Devon Energy - Ihle 1-26, Creek County, OK

Formation: "Mississippian Limestone"

Depth Interval: 2933' - 3083'

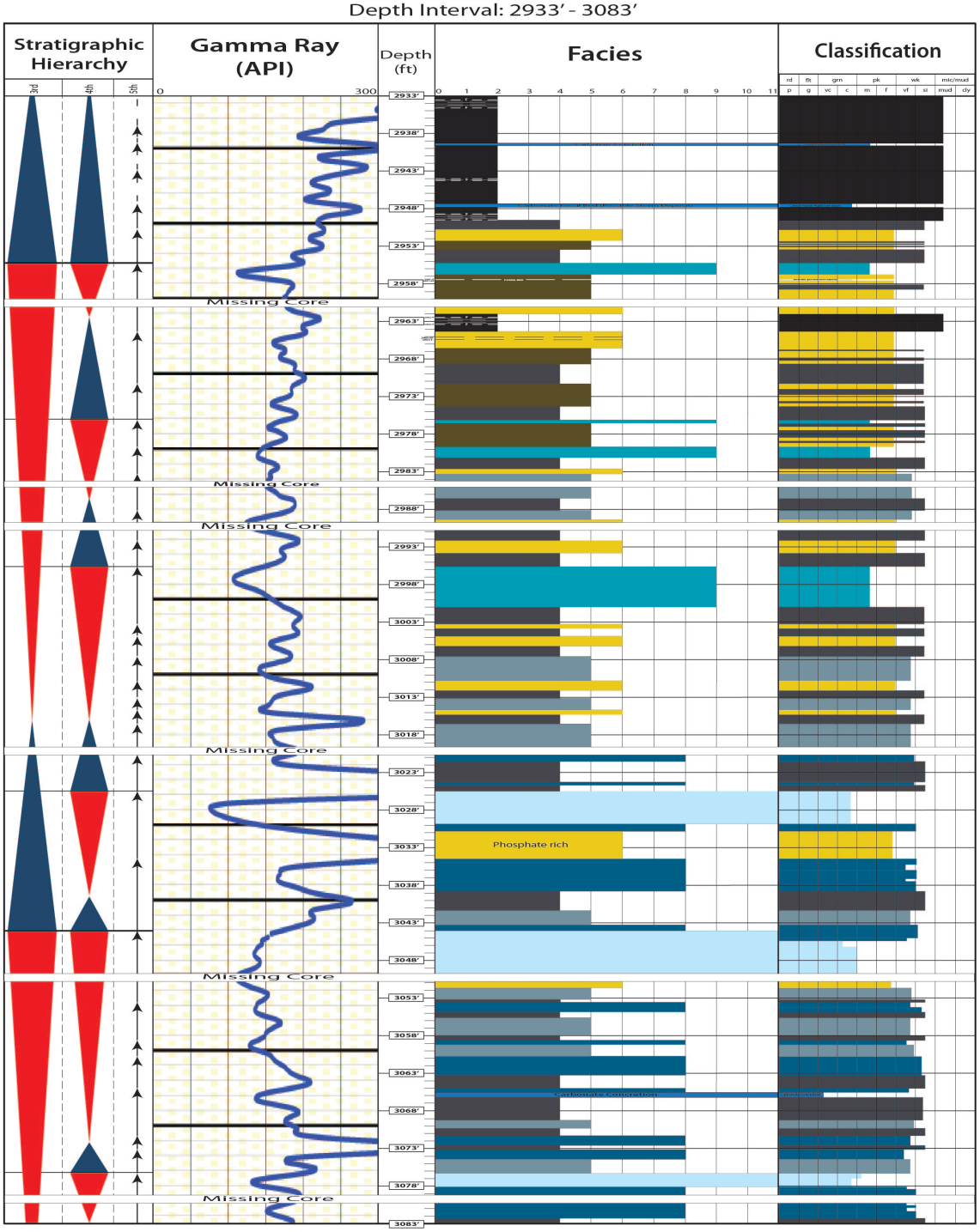

## Devon Energy - Ihle 1-26, Creek County, OK

Formation: "Mississippian Limestone"

Depth Interval: 3083' - 3213'

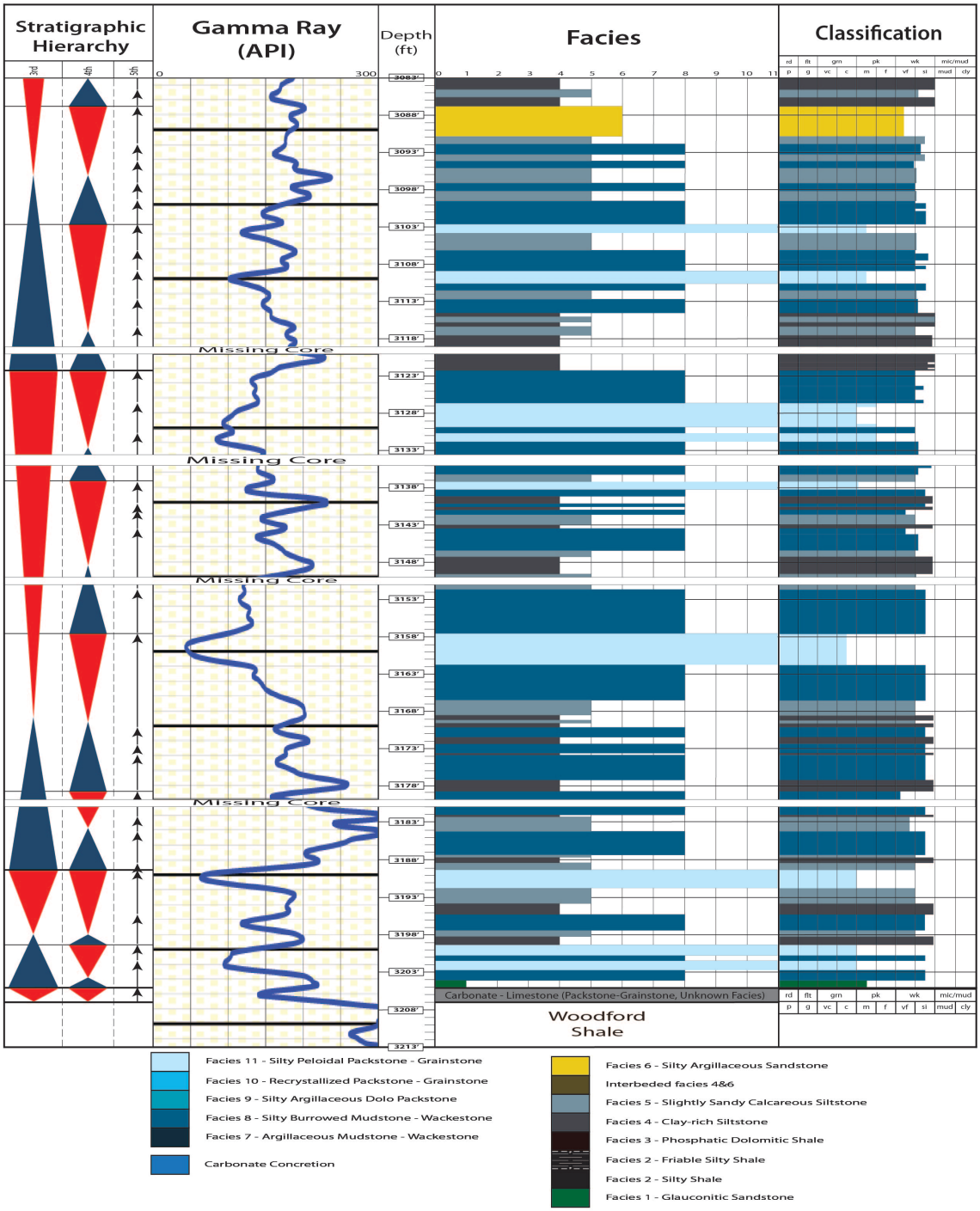

## III. Ihle #1-26 Thin Section Photomicrographs

Thin section photomicrographs show enlarged views of samples that have been cut from the core. The samples and images shown are oriented as if looking at core, from shallower at the top of the image and deeper towards the base of the image. The images are formatted in order of facies, starting with facies 1 (facies 1 – facies 11), and multiple images at magnifications of 2x and 5x are shown for each facies. All thin sections are blue epoxy impregnated, stained with alizarin red and potassium ferrocyanide on half of the slide. All photomicrographs are in plane polarized light (unless otherwise stated) and are labeled using the chart below.

| Ihle Thin Section Image Labels | | | | | |
|---|---|---|---|---|---|
| **AF** | agglutinated foram | **G** | glauconite | **P** | peloid |
| **BR** | brachiopod | **ILL** | illite/mica | **PH** | phosphate |
| **BU** | burrow | **LAM** | lamination | **PY** | pyrite |
| **CEM** | calcite cement | **M** | mud | **Q** | quartz |
| **CG** | calcite grain (indistinguishable) | **M&S** | mud & silt | **RCG** | recrystallized carbonate grain |
| **CH** | chert | **ME** | micritic envelope | **SK** | skeletal debris |
| **D** | dolomite | **MG** | micritized grain | **SP** | spicule |
| **FEL** | feldspar | **MW** | mud whisp | | |
| **FR** | fracture | **OM** | organic matter | | |

Table 14. Abbreviations and their meanings used in labeling the thin sections from Ihle #1-26.

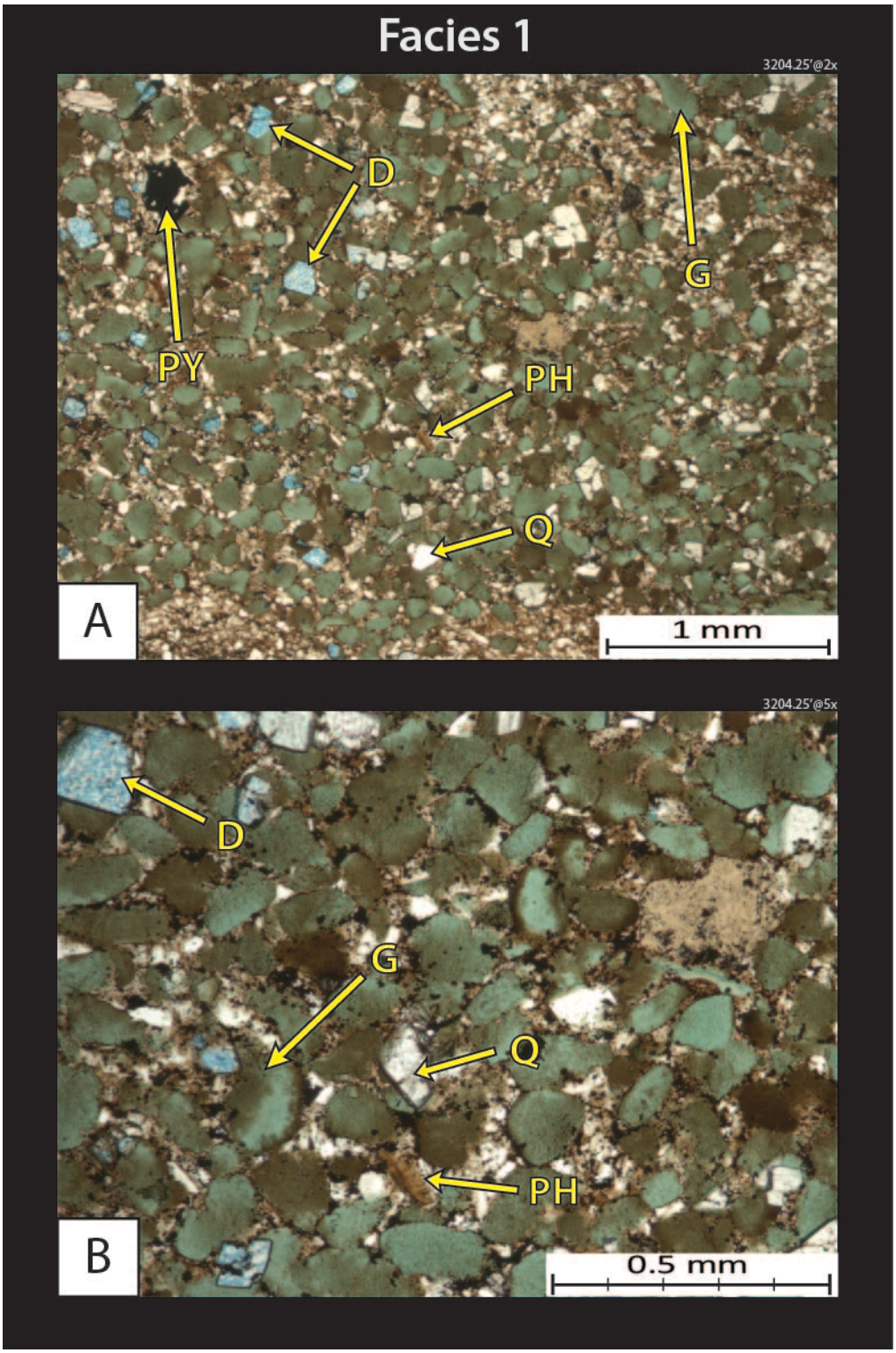


**3204.25' – Glauconitic sandstone.** This sample shows the sand sized glauconite (G) grains, silt to fine sand sized quartz (Q) grains, dolomite (D) grains and some phosphate grains. XRD analysis: 39% quartz, 7% carbonates (5% dolomite, and 2% calcite), 45% clays (inconclusive results on breakdown of clay types with XRD), and 9% other minerals (1% plagioclase feldspar, 2% potassium feldspar, and 6% pyrite).

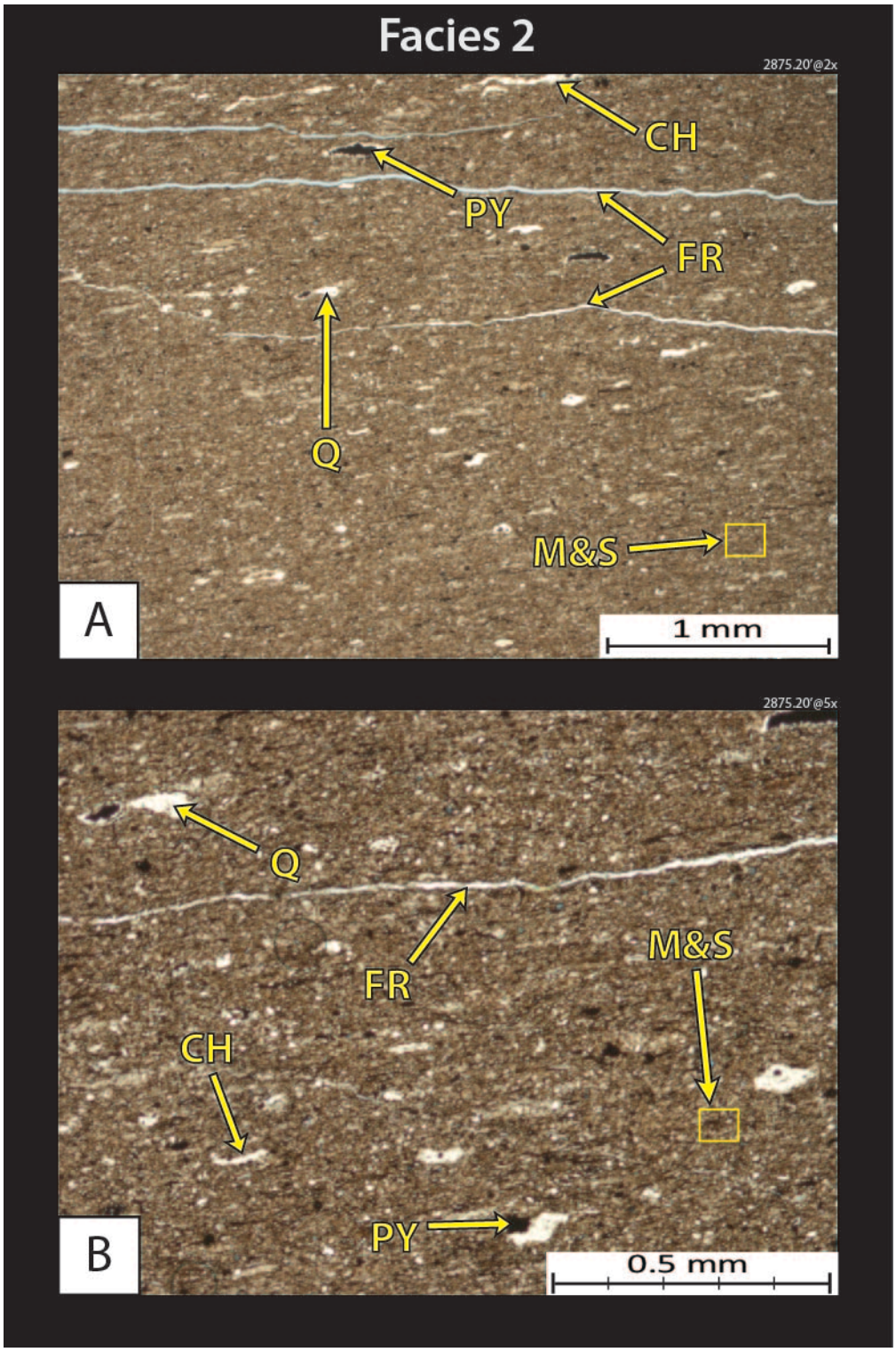


**2875.20' – Silty shale.** This facies is commonly composed of clays, silt & chert, and minor amounts of pyrite. XRD analysis: 22% quartz, 0% carbonates, 66% clays (33% mixed layer illite/smectite, 30% illite, 2% chlorite, and 1% kaolinite), and 12% other minerals (5% plagioclase feldspar, 4% potassium feldspar, and 2% pyrite).

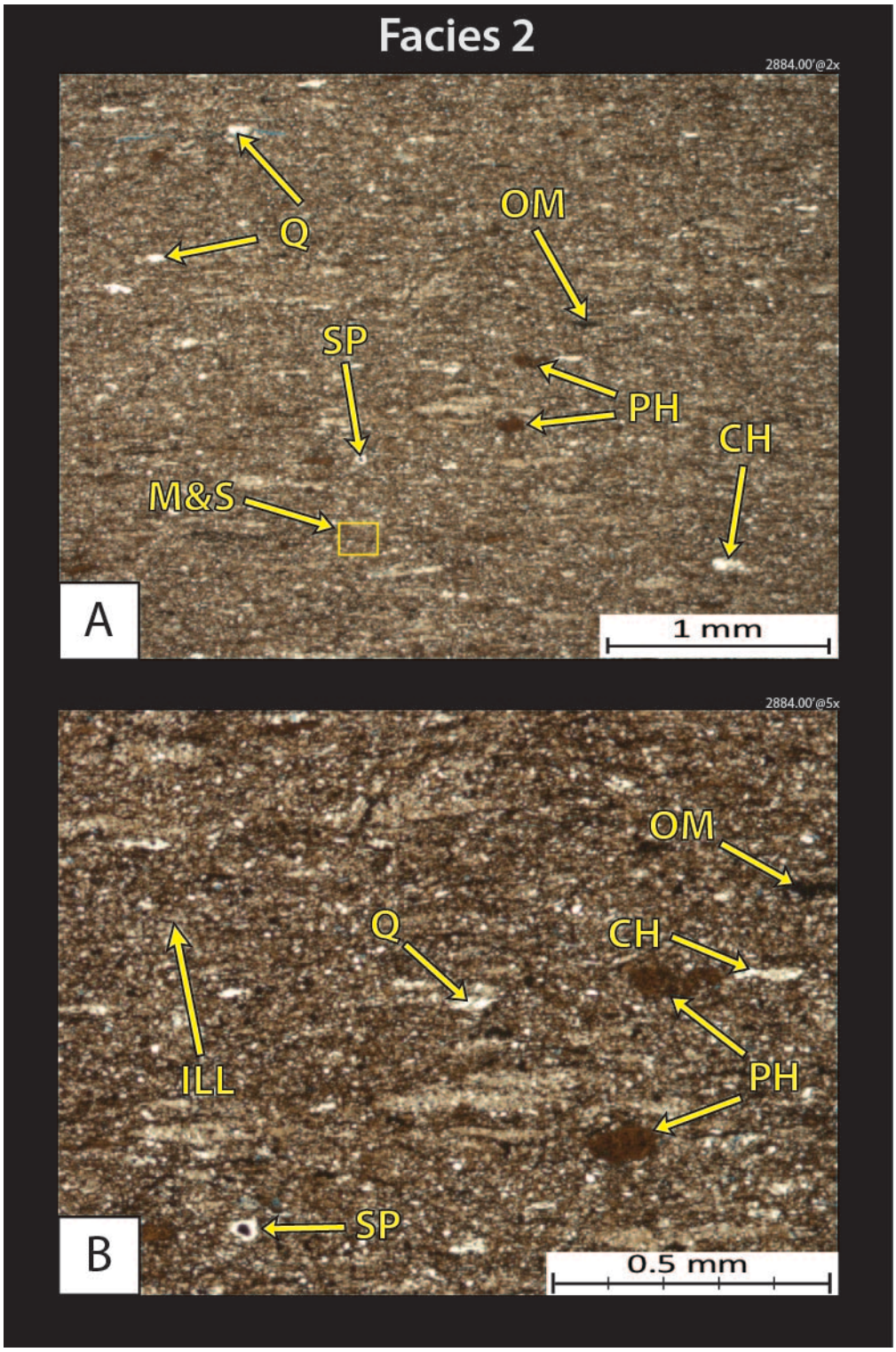


**2884.00' – Silty shale.** Sample is dominated by clays, silt & chert, and phosphate. XRD Analysis: 32% quartz, 3% carbonates (2% calcite, and 1% dolomite), 47% clays (36% illite , 8% mixed layer illite/smectite, 2% chlorite, and 1% kaolinite), and 18% other minerals (6% plagioclase feldspar, 4% potassium feldspar, 4% pyrite, and 4% apatite).

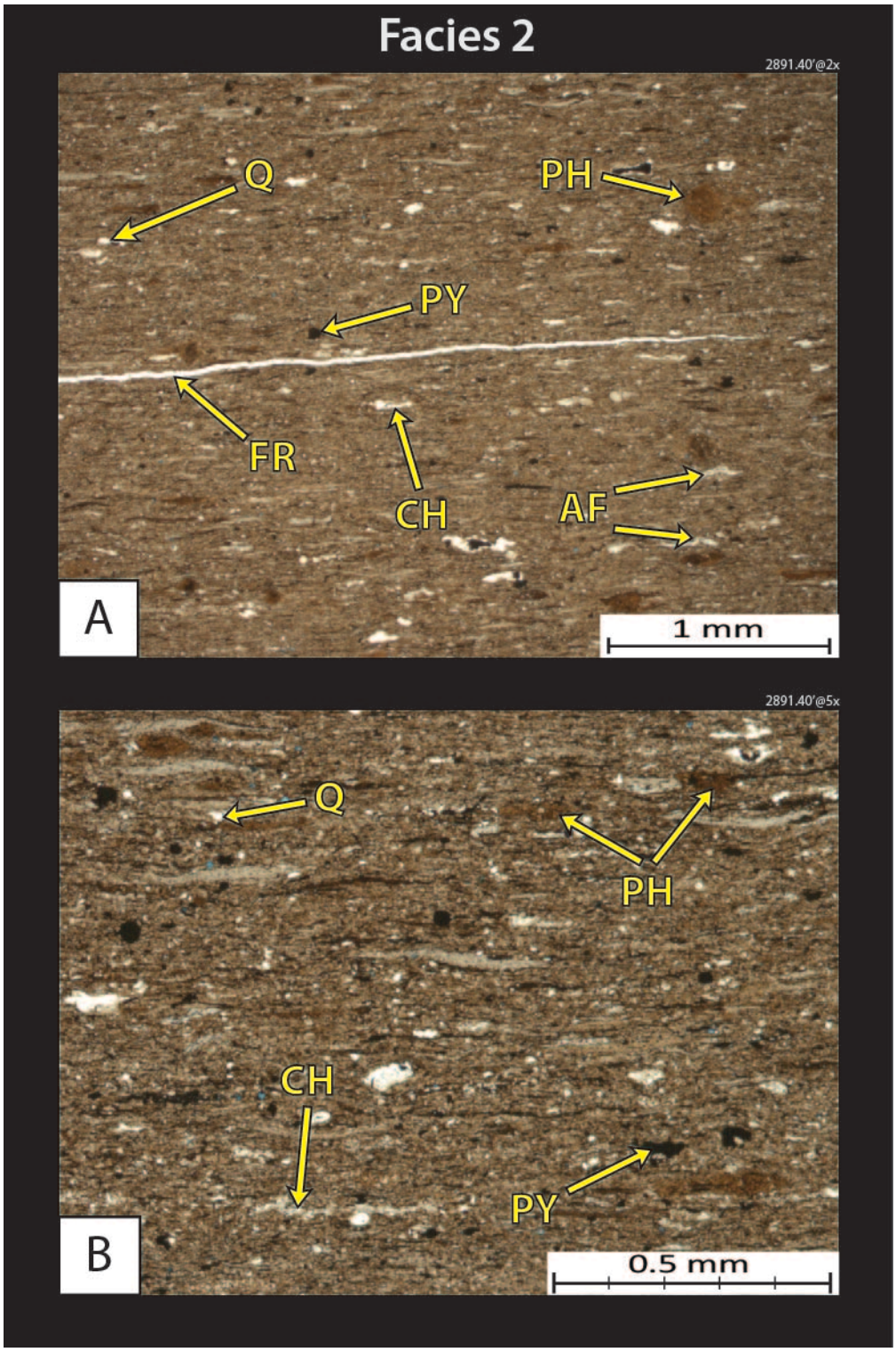


**2891.40' – Silty shale.** Sample is dominated by clays, silt & chert, and phosphate. XRD Analysis: 18% quartz, 0% carbonates, 70% clays (43% mixed layer illite/smectite, 25% illite , 1% chlorite, and 1% kaolinite), and 12% other minerals (4% potassium feldspar, 3% plagioclase feldspar, 3% pyrite, and 2% apatite).

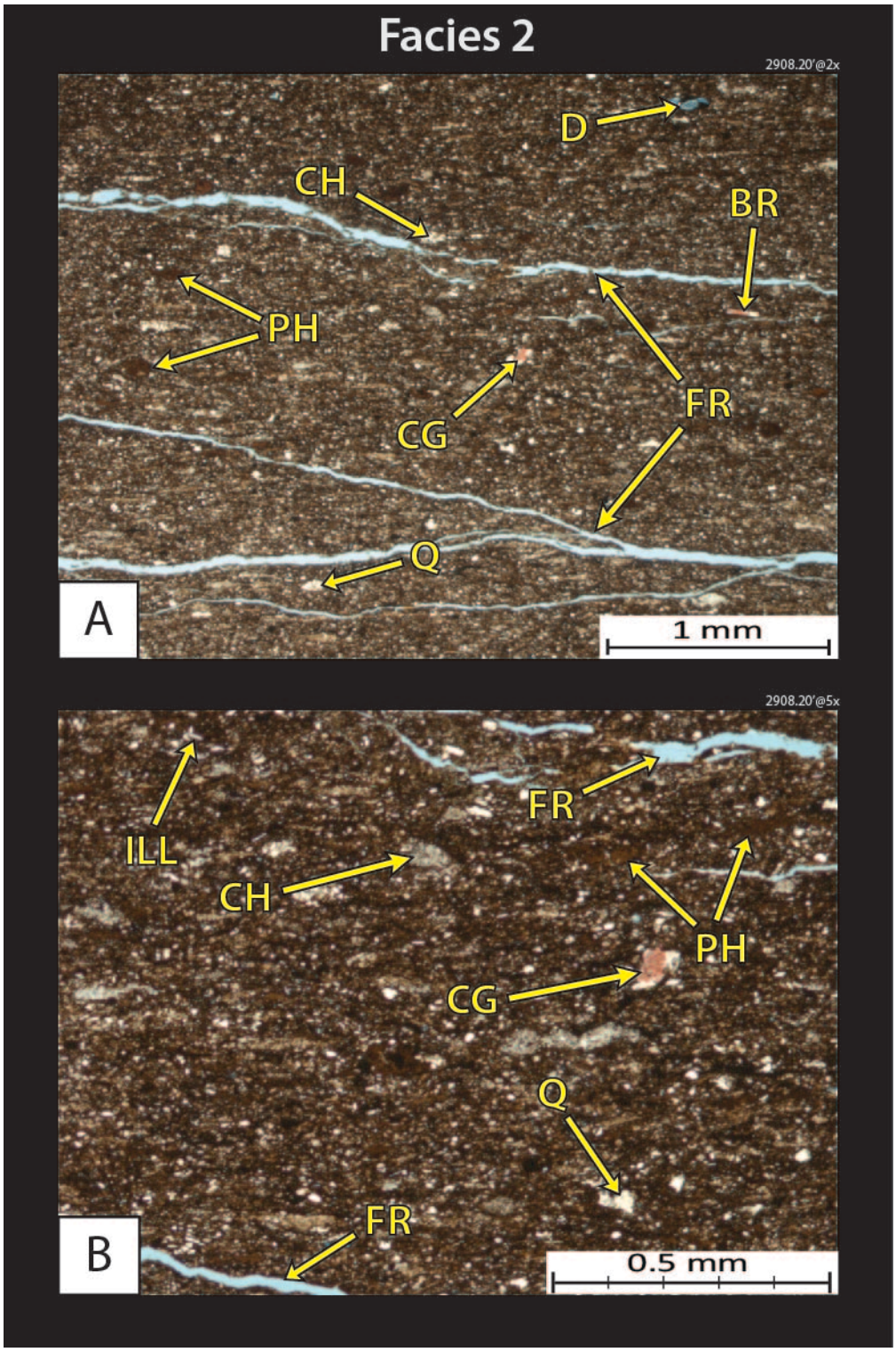


**2908.20' – Silty shale.** Sample is dominated by clays, silt & chert, and phosphate and is heavily fractured. XRD Analysis: 32% quartz, 7% carbonates – calcite, 46% clays (42% illite , 3% mixed layer illite/smectite, and 1% chlorite), and 15% other minerals (5% plagioclase feldspar, 5% apatite , 3% potassium feldspar, and 2% pyrite).

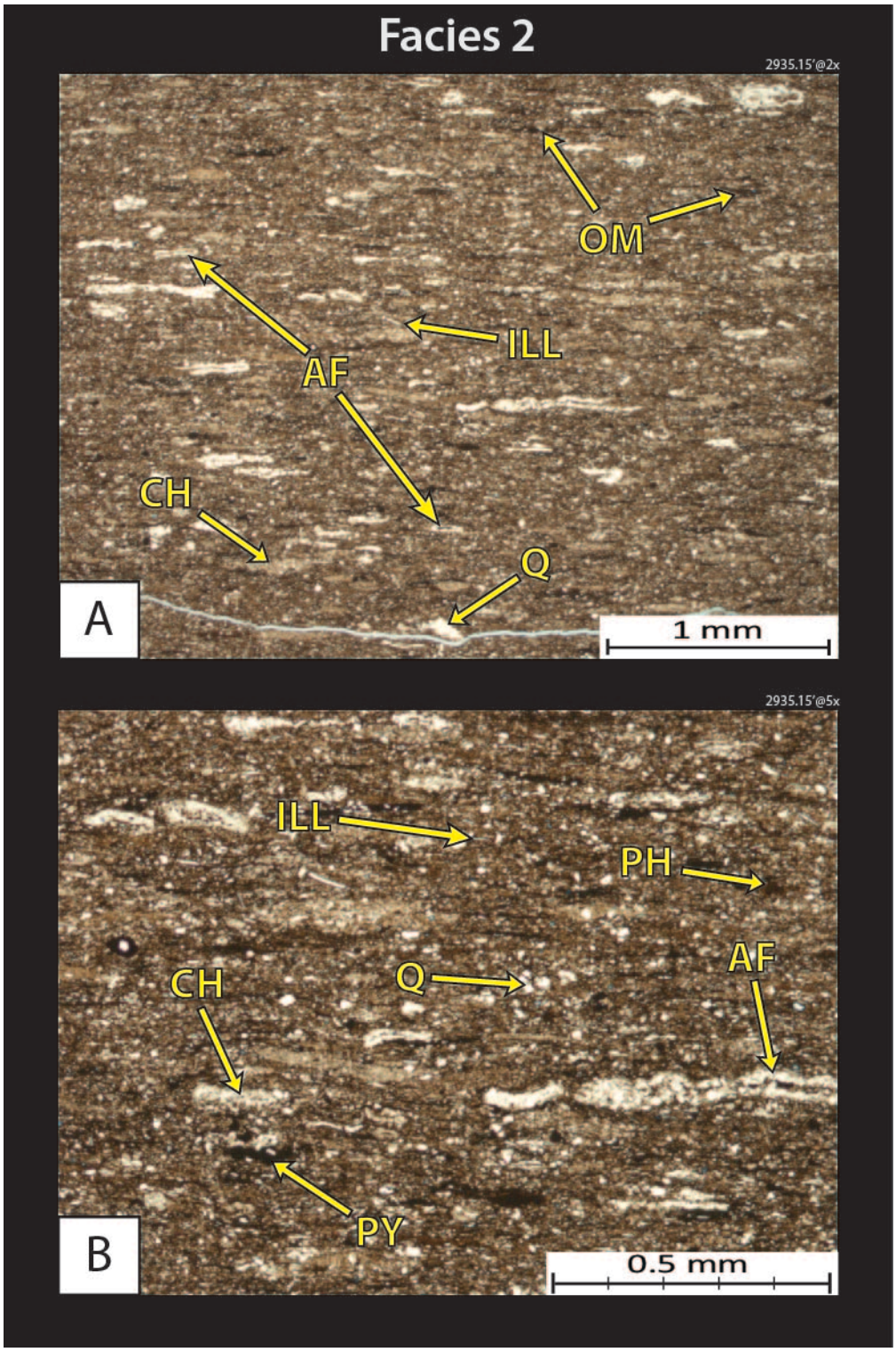


**2935.15' – Silty shale.** Sample shows silt to very fine sand sized quartz (Q) grains, clayey/muddy matrix, clusters of chert (CH), flattened (evidence of compaction) agglutinated foraminifera enclosed with microcrystalline quartz (AF), and some phosphate nodules/grains. XRD analysis: 22% quartz, 9% carbonates (9% calcite with trace amounts of dolomite), 58% clays (43% illite, 10% mixed layer illite/smectite, 3% kaolinite, and 2% chlorite), and 11% other minerals (3% plagioclase feldspar, 2% potassium feldspar, 4% pyrite, 1% marcasite, and 1% apatite).

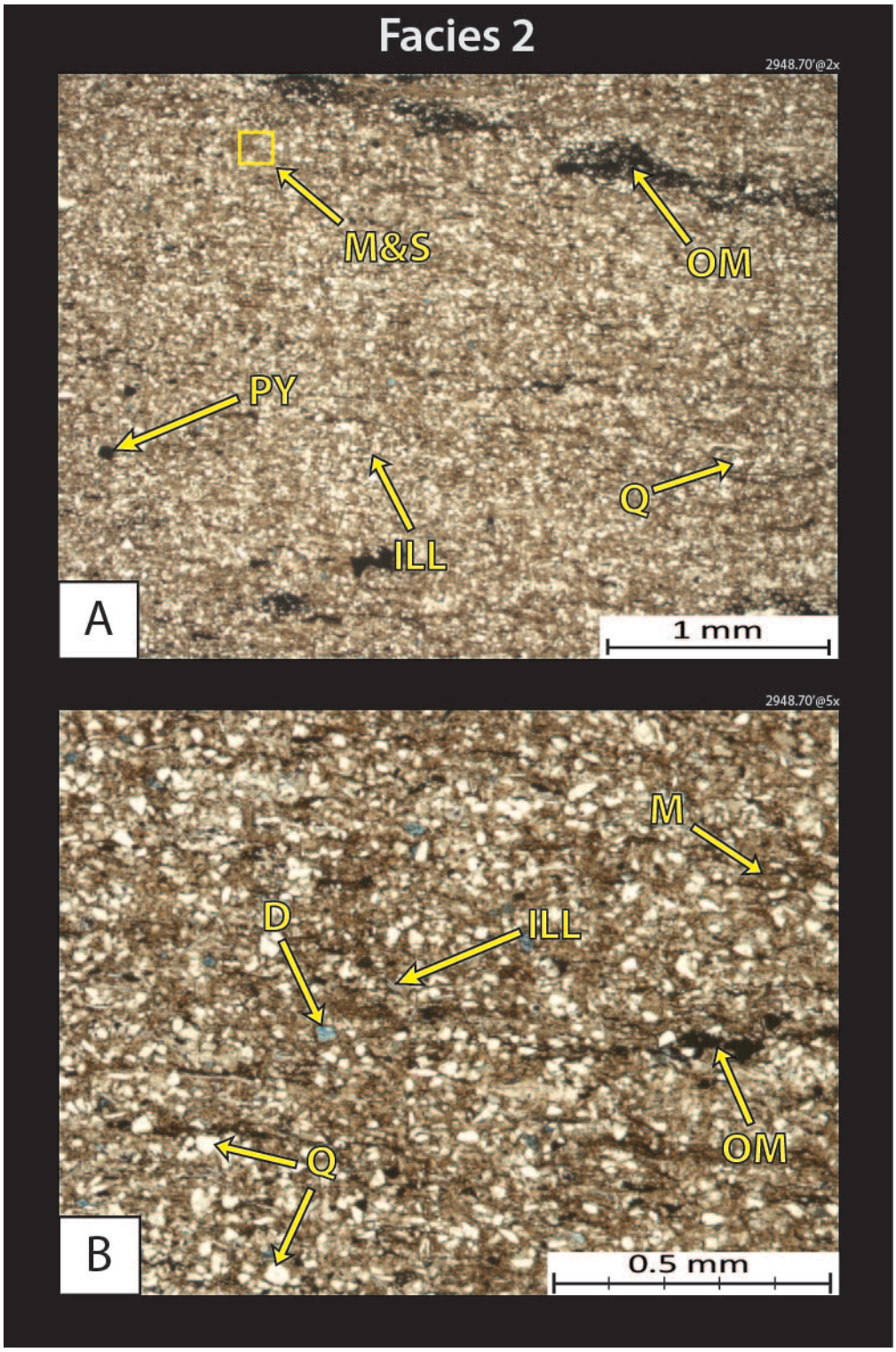


**2948.70' – Silty shale.** Sample shows abundant silt sized quartz grains (Q), and clays. XRD Analysis: 24% quartz, 6% carbonates (3% calcite, and 3% dolomite), 60% clays (31% mixed layer illite/smectite , 27% illite, and 2% chlorite), and 10% other minerals (3% plagioclase feldspar, 3% potassium feldspar, 3% pyrite, and 1% marcasite).

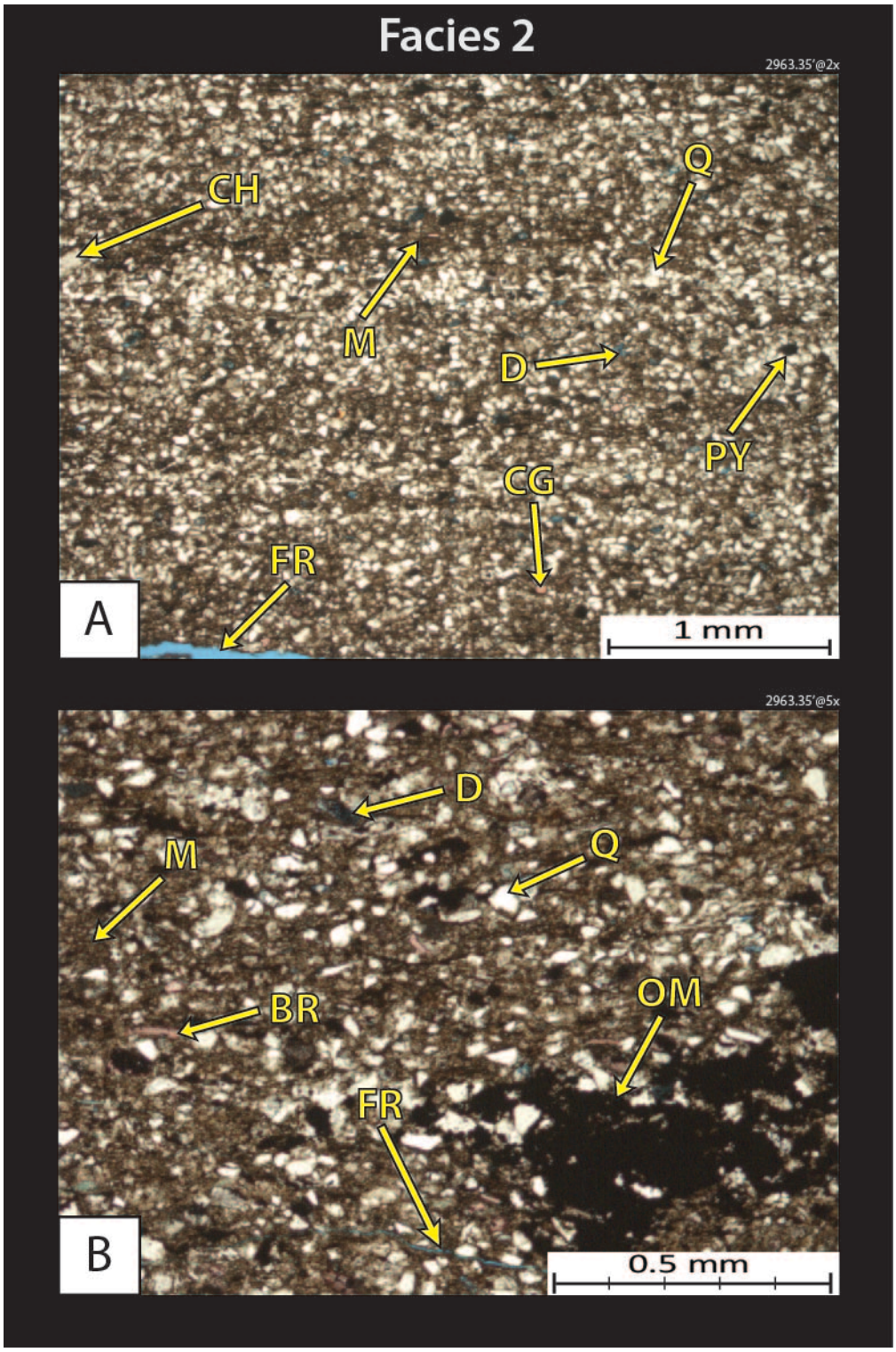


**2963.35' – Silty shale.** Sample is dominated by silt sized quartz grains (Q), clays/mud, and contains skeletal fragments – brachiopods (BR). XRD Analysis: 31% quartz, 4% carbonates (3% calcite, and 1% dolomite), 51% clays (32% mixed layer illite/smectite, 18% illite, and 1% chlorite), and 14% other minerals (6% potassium feldspar, 5% plagioclase feldspar, and 3% pyrite).

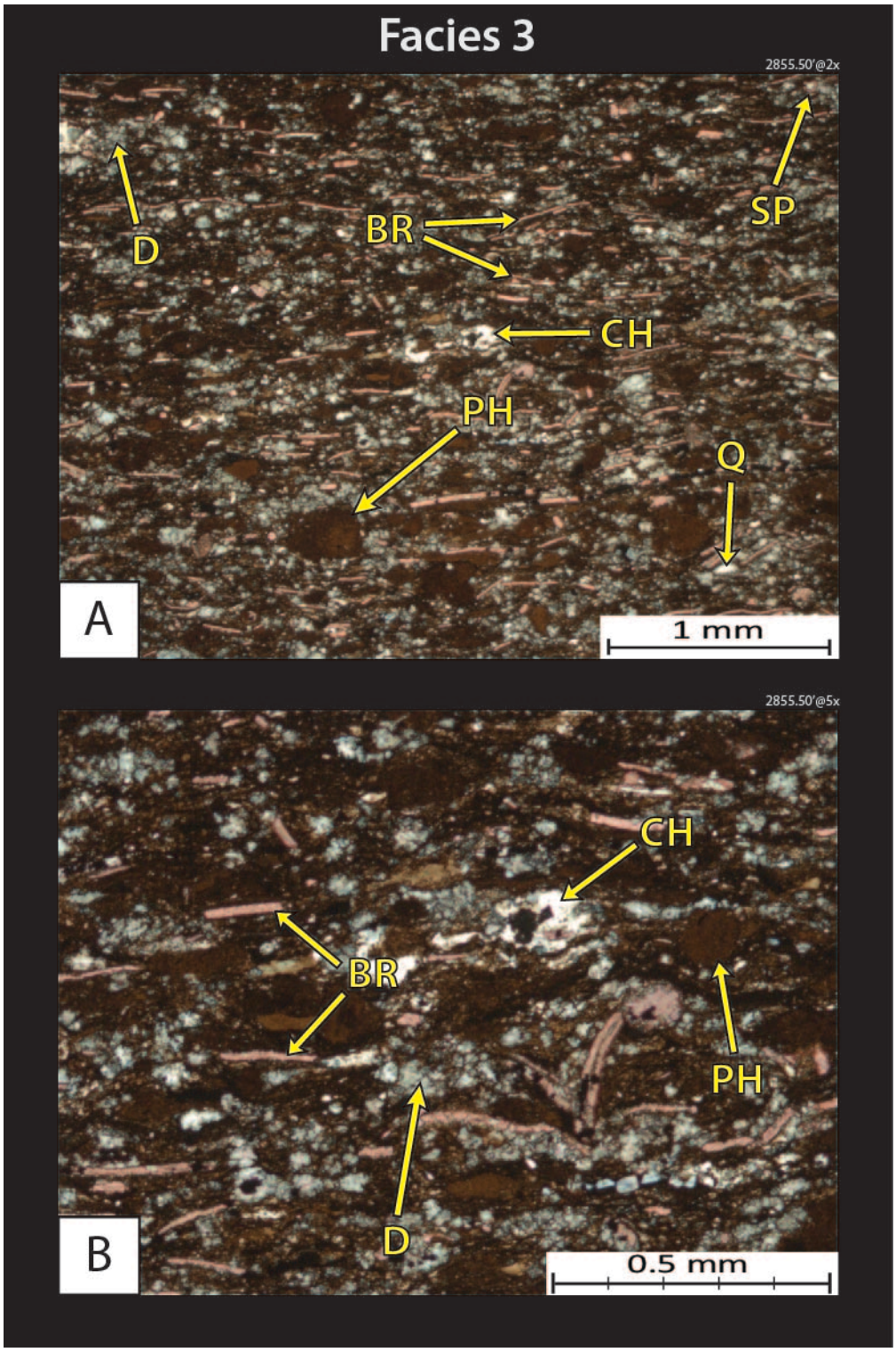


**2855.50' – Phosphatic dolomitic shale.** Sample shows silt sized quartz grains, an abundance of sand sized phosphate grains (PH), dolomite (D), and brachiopod fragments (BR). XRD analysis: 29% silt sized quartz grains, 29% clays (18% illite, 7% mixed layer illite/smectite, 2% kaolinite, and 2% chlorite), 25% carbonates (24% dolomite, 1% calcite – occurring as calcified brachiopod fragments), and 17% other minerals (9% apatite, 4% plagioclase feldspar, 2% potassium feldspar, and 2% pyrite).

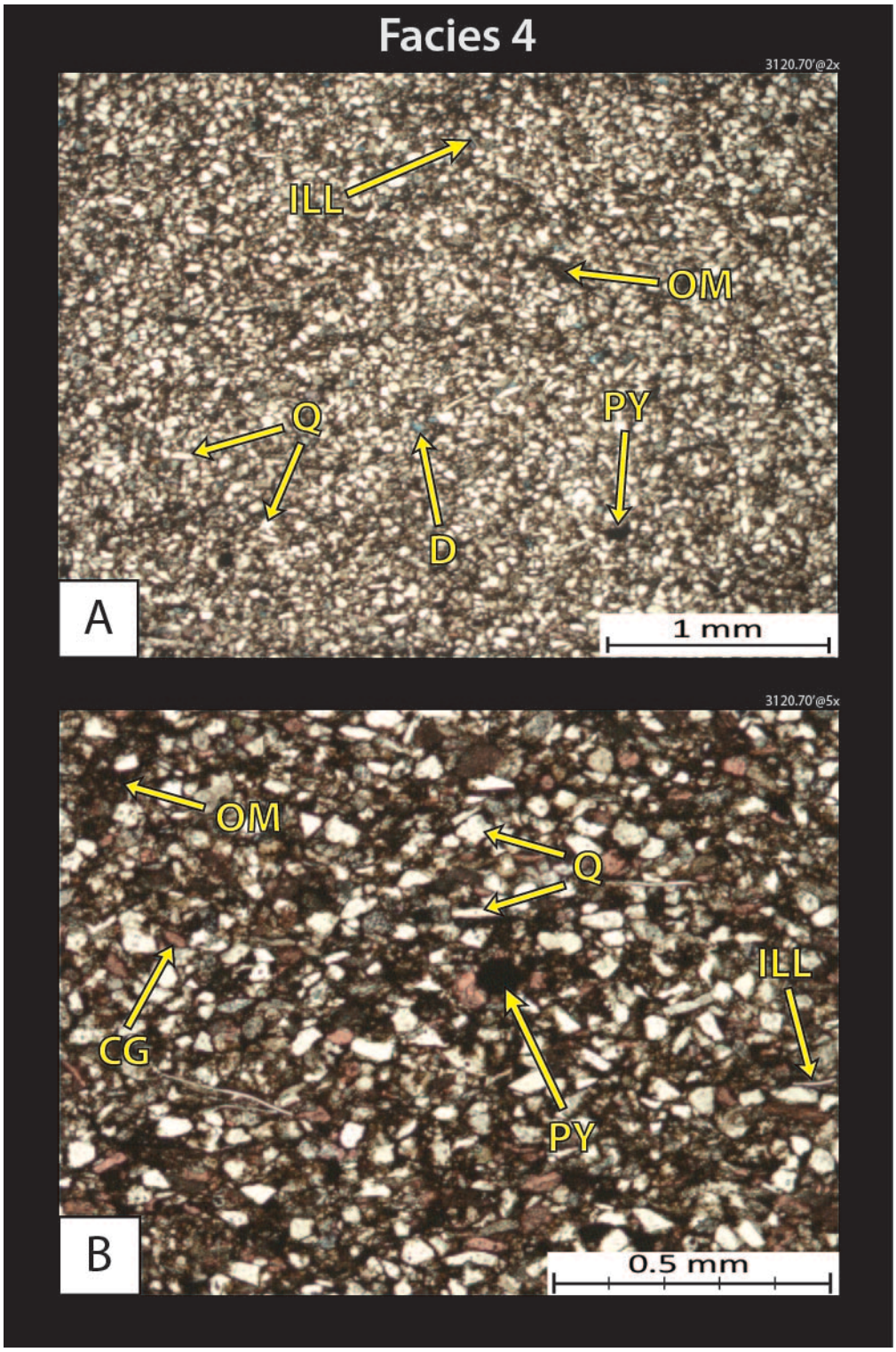


**3120.70' – Clay-rich siltstone.** This facies is typically dominated by silt to VF sand sized quartz grains (Q), clays, and lesser amounts of carbonates. XRD analysis: 47% quartz, 18% carbonates (13% calcite, and 5% dolomite), 20% clays (15% illite, 3% mixed layer illite/smectite, and 2% chlorite), and 15% other minerals (8% plagioclase feldspar, 5% potassium feldspar, and 2% pyrite).

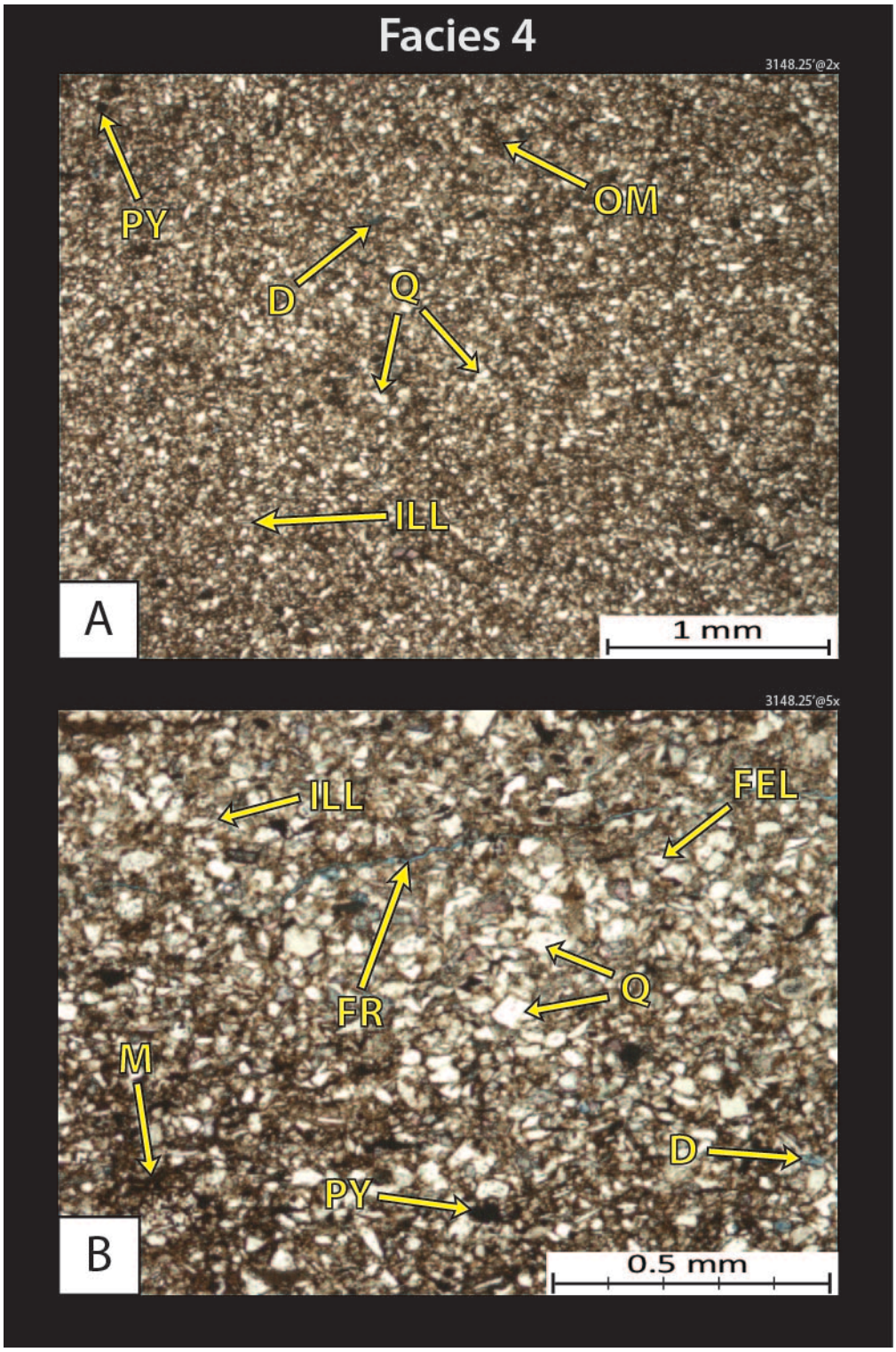


**3148.25' – Clay-rich siltstone.** The sample is dominated by silt sized quartz (Q) to very fine sand sized quartz grains in some areas, contains an abundance of clays along with some organic matter. This facies also contains sparse amounts of carbonates – mainly calcite grains (pink). The calcite grains are primarily indistinguishable bioclasts/fossils. XRD analysis: 46% quartz, 6% carbonates (4% calcite, and 2% dolomite), 31% clays (18% illite, 10% mixed layer illite/smectite, and 3% chlorite), and 17% other minerals (9% plagioclase feldspar, 5% potassium feldspar, 2% pyrite, and 1% apatite).

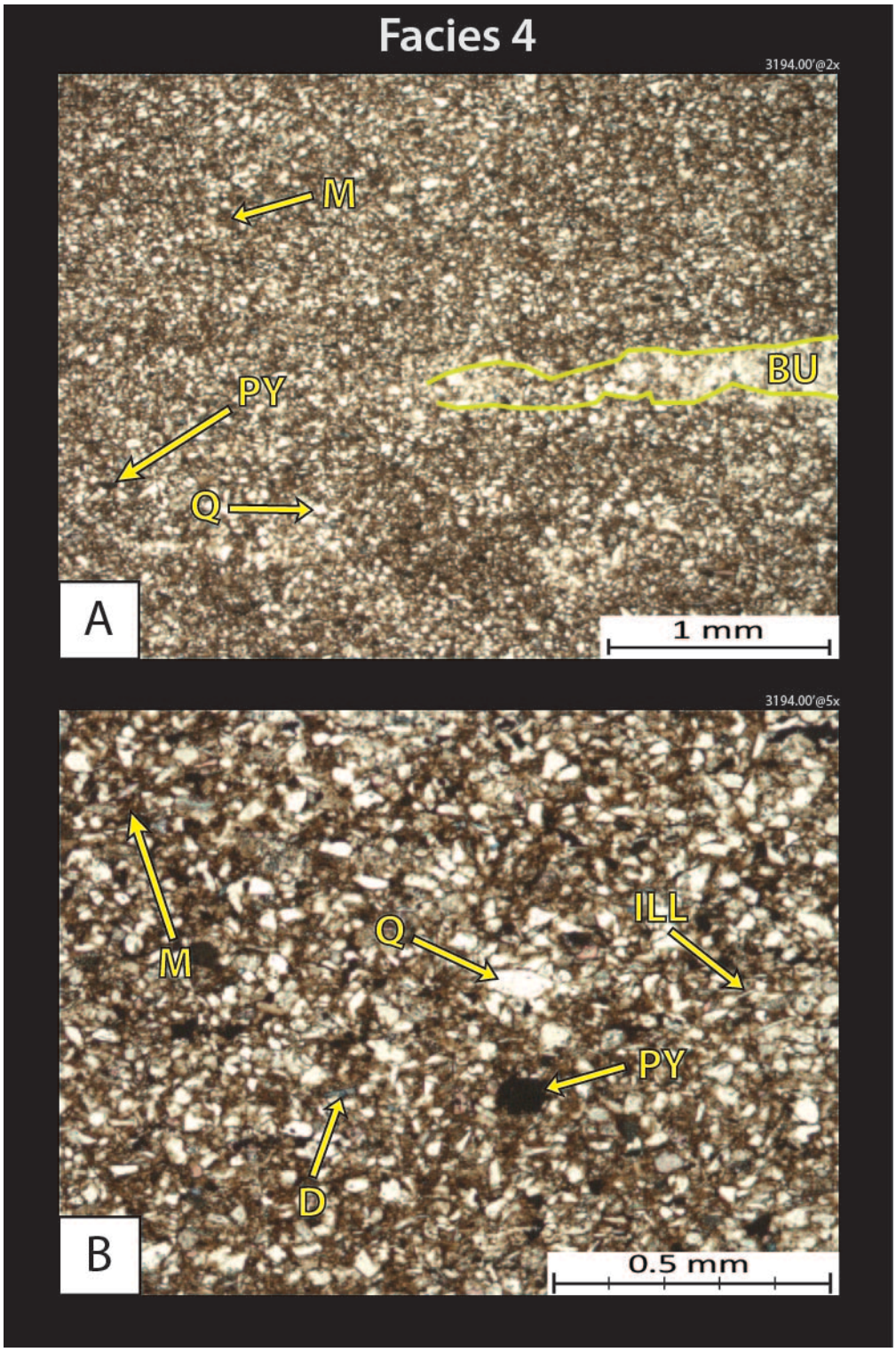


**3194.00' – Clay-rich siltstone.** The sample is dominated by silt sized quartz grains (Q), and clays, and also displays burrowing (BU). XRD analysis: 49% quartz, 7% carbonates (5% calcite, and 2% dolomite), 26% clays (16% illite, 8% mixed layer illite/smectite, and 2% chlorite), and 18% other minerals (8% plagioclase feldspar, 7% potassium feldspar, 2% pyrite, and 1% marcasite).

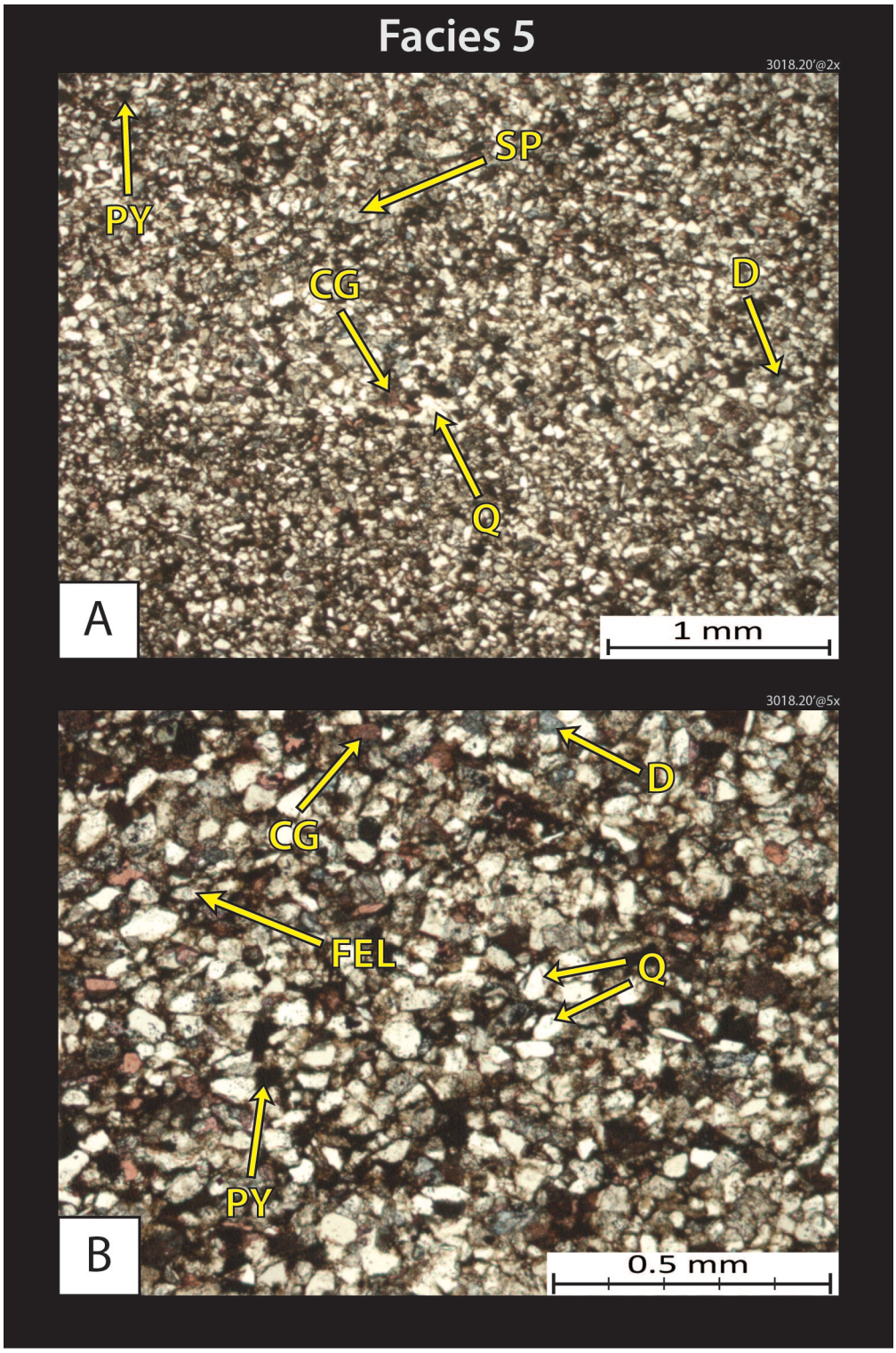


**3018.20' – Slightly sandy calcareous siltstone.** This facies is typically dominated by silt to very fine sand sized quartz (Q) grains, and carbonate debris. Usually the calcite grains in this facies are indistinguishable bioclasts or micritized grains, when the grains are recognizable; they are generally brachiopod and crinoid fragments. XRD Analysis: 51% quartz, 21% carbonates (14% calcite, and 7% dolomite), 14% clays (9% illite, 4% mixed layer illite/smectite, and 1% chlorite), and 14% other minerals (8% plagioclase feldspar, 4% potassium feldspar, and 2% pyrite).

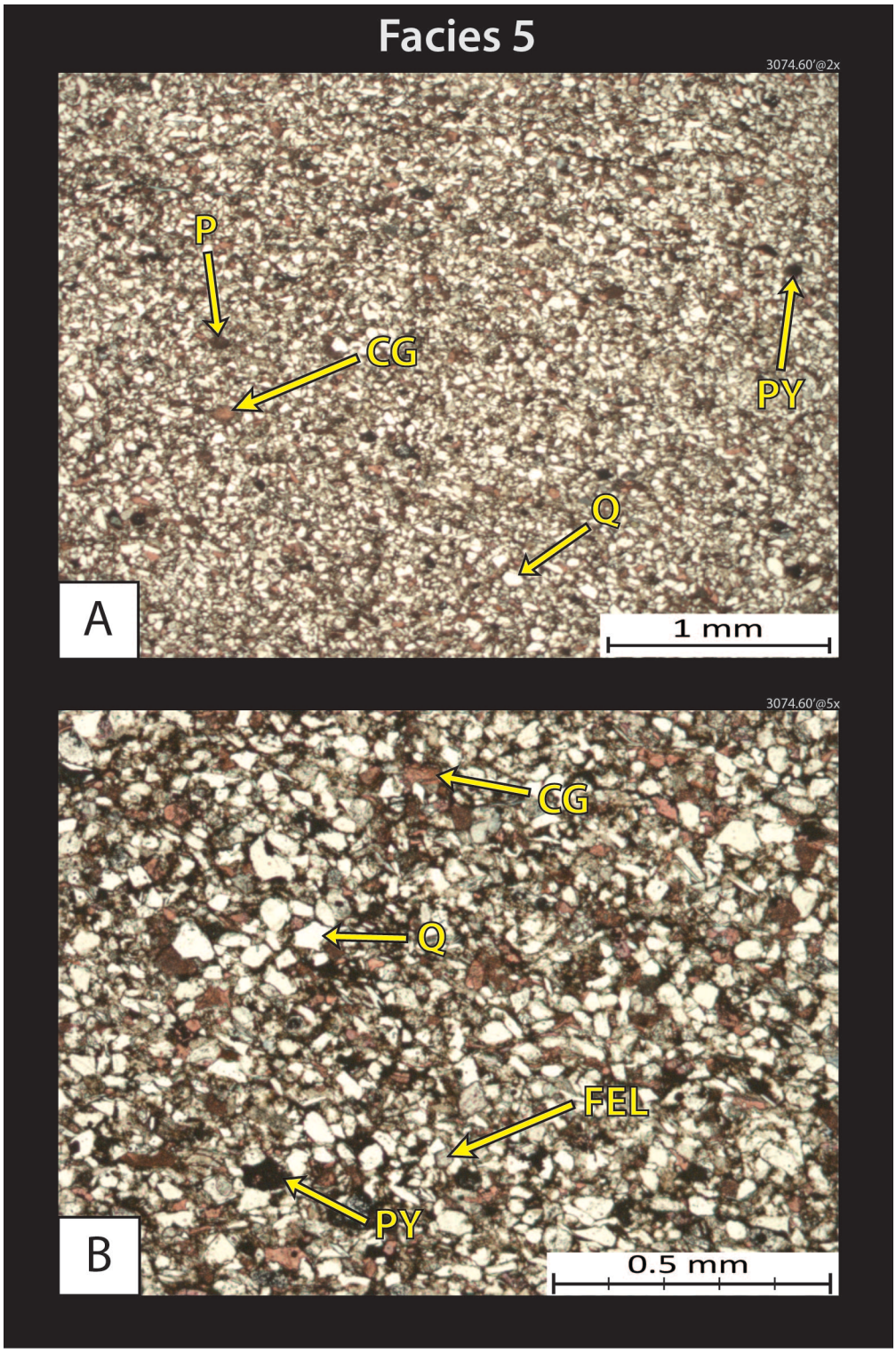


**3074.60' – Slightly sandy calcareous siltstone.** Sample dominated by silt to VF sand sized quartz grains (Q), carbonate grains – mainly calcite, and clays. XRD Analysis: 45% quartz, 16% carbonates (13% calcite, and 3% dolomite), 20% clays (12% illite, 7% mixed layer illite/smectite, and 1% chlorite), and 19% other minerals (10% plagioclase feldspar, 4% potassium feldspar, 4% pyrite, and 1% apatite).

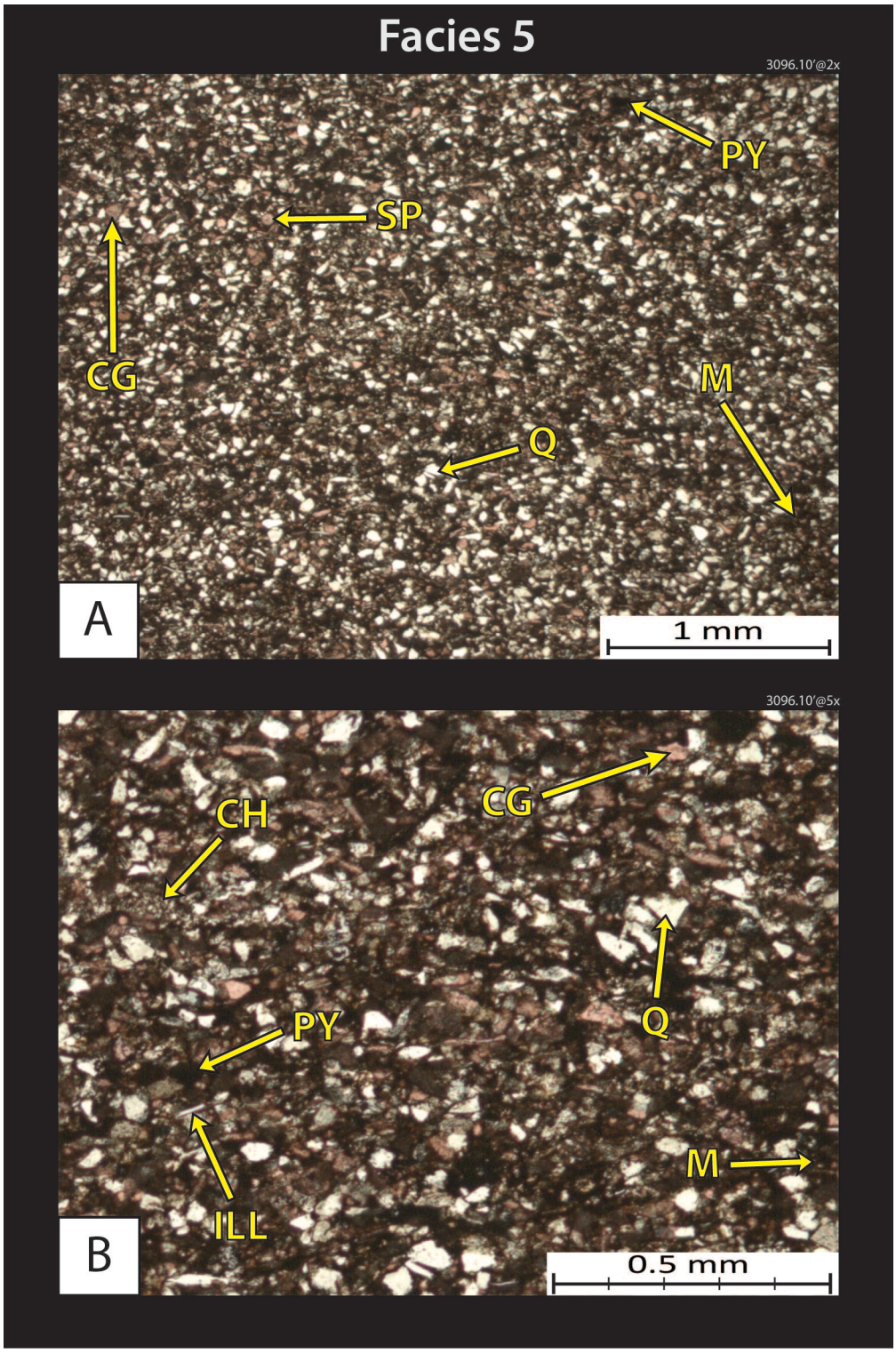


**3096.10' – Slightly sandy calcareous siltstone.** The sample is dominated by silt to very fine sand sized quartz grains (Q) that are sub-angular to sub-rounded and moderately sorted, carbonate – mainly calcite (pink) grains, sparse clays, and a muddy organic-rich matrix. XRD analysis: 38% quartz, 37% carbonates (33% calcite, and 4% dolomite), 16% clays (9% illite, 6% mixed layer illite/smectite, and 1% chlorite), and 9% other minerals (5% plagioclase feldspar, 2% potassium feldspar, and 2% pyrite).

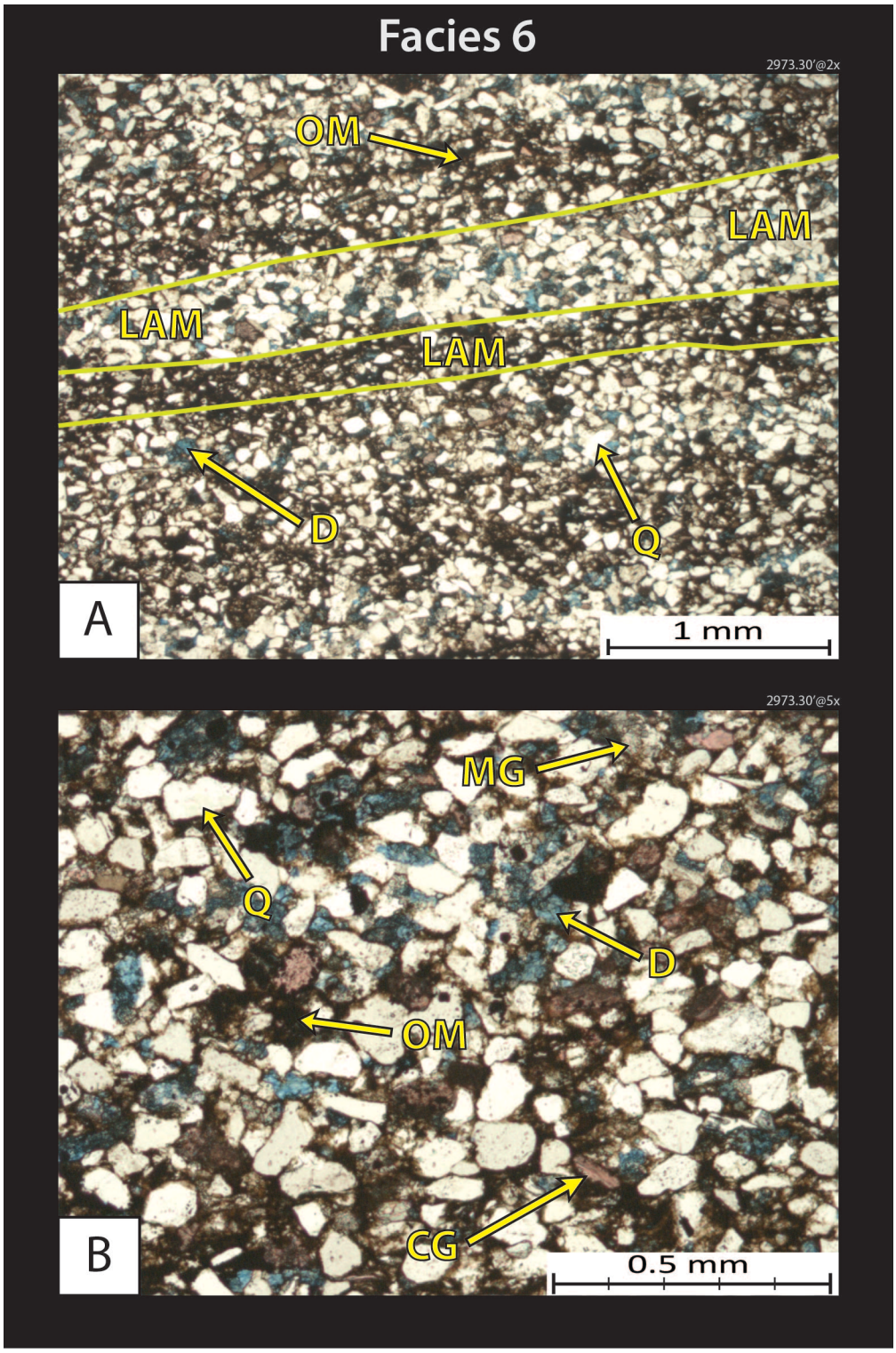


**2973.30' – Silty argillaceous sandstone.** The sample is dominated by very fine to fine sand sized quartz grains (Q), carbonates, and clays. XRD analysis: 57% quartz, 16% carbonates (8% calcite and 8% dolomite), 16% clays (inconclusive results on breakdown of clay types with XRD), and 11% other minerals (4% plagioclase feldspar, 4% potassium feldspar, 2% pyrite, and 1% apatite).

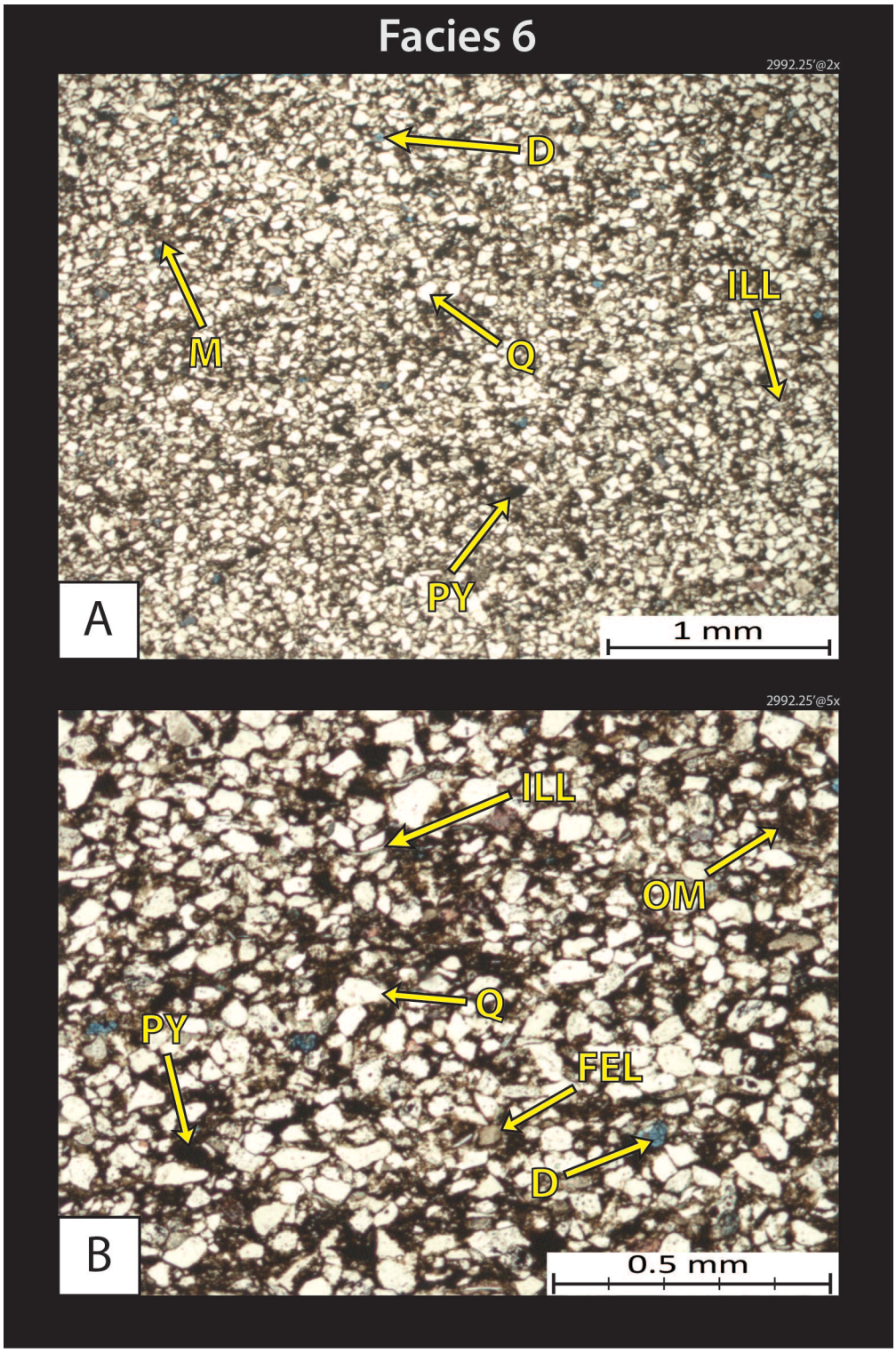


**2992.25' – Silty argillaceous sandstone.** Sample is dominated by very fine to fine sand sized quartz grains (Q), and clays with minor amounts of carbonates. XRD analysis: 59% quartz, 3% carbonates (2% calcite, and 1% dolomite), 23% clays (14% illite, 8% mixed layer illite/smectite, and 1% chlorite), and 15% other minerals (8% plagioclase feldspar, 5% potassium feldspar, and 2% pyrite).

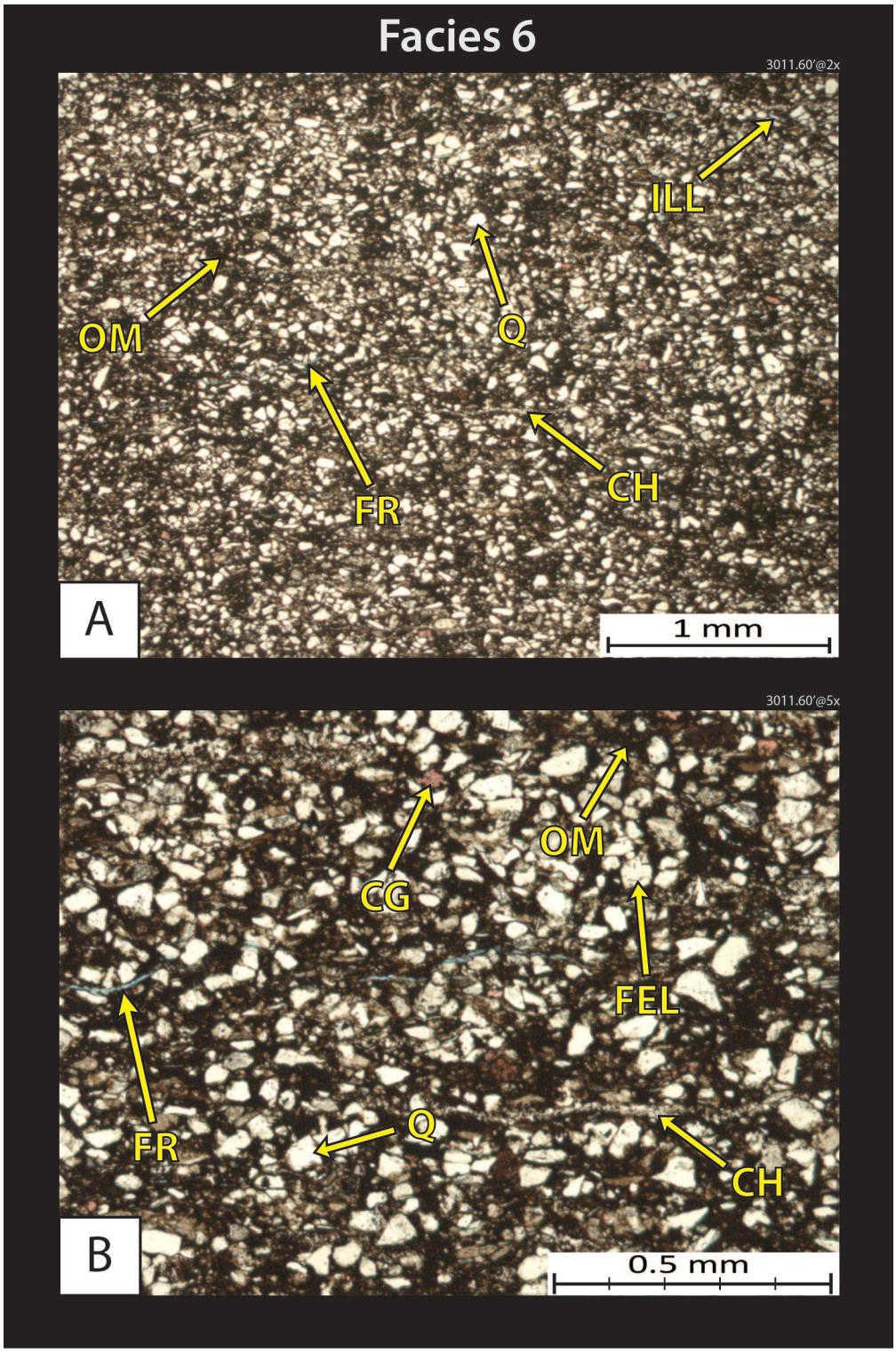


**3011.60' – Silty argillaceous sandstone.** Sample is dominated by very fine to fine sand size quartz grains (Q), and clays. XRD analysis: 40% quartz, 6% carbonates (5% calcite, and 1% dolomite), 37% clays (26% illite, 9% mixed layer illite/smectite, and 2% chlorite), and 17% other minerals (9% plagioclase feldspar, 5% potassium feldspar, and 3% pyrite).

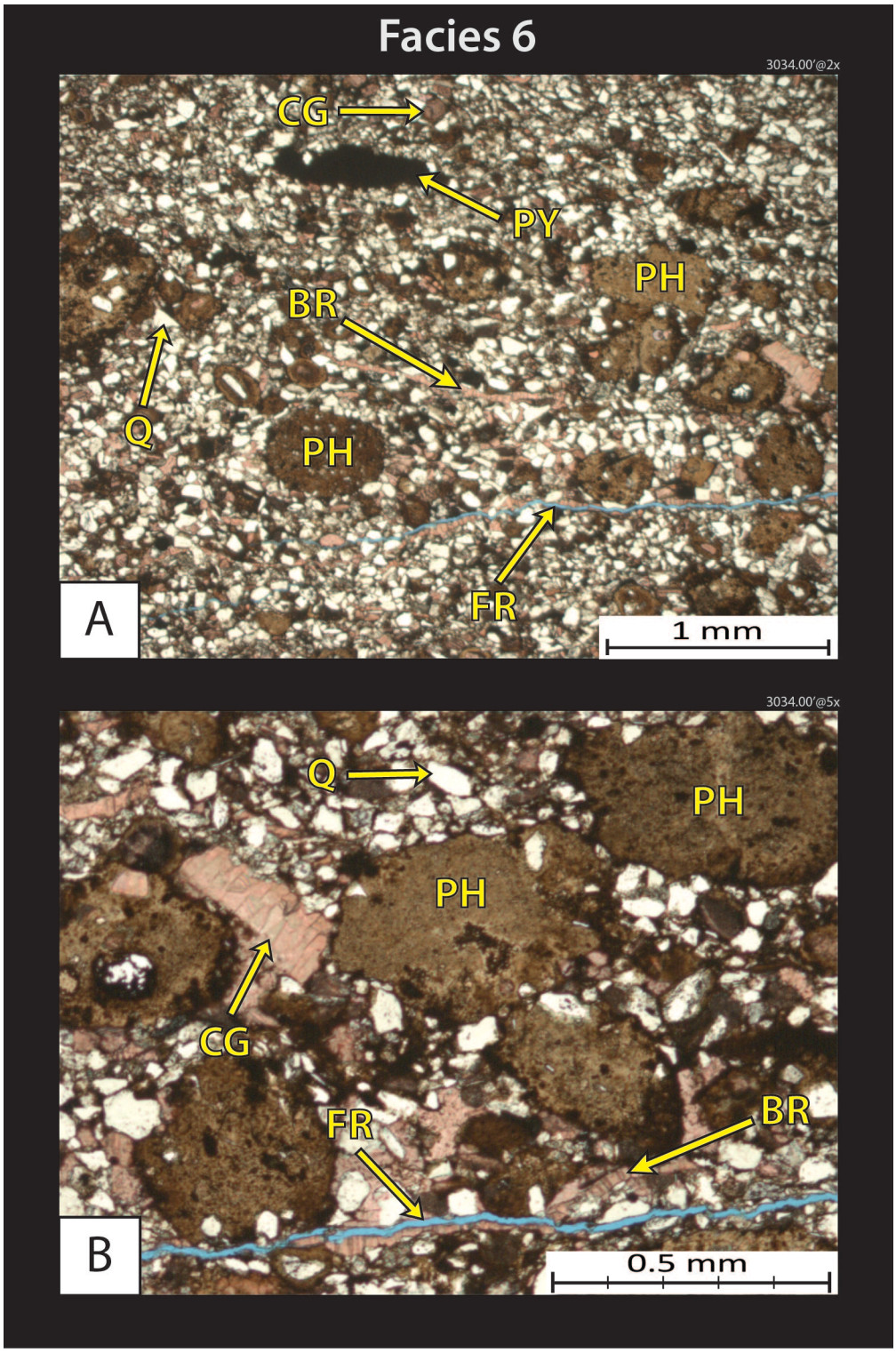


**3034.00' – Silty argillaceous sandstone.** Sample is dominated by very fine sand sized quartz grains (Q), phosphate grains (PH), and calcite skeletal debris – brachiopods (BR). XRD analysis: 39% quartz, 19% carbonates (16% calcite, and 3% dolomite), 20% clays (11% illite, 7% mixed layer illite/smectite, and 2% chlorite), and 22% other minerals (9% apatite, 7% plagioclase feldspar, 3% potassium feldspar, and 3% pyrite).

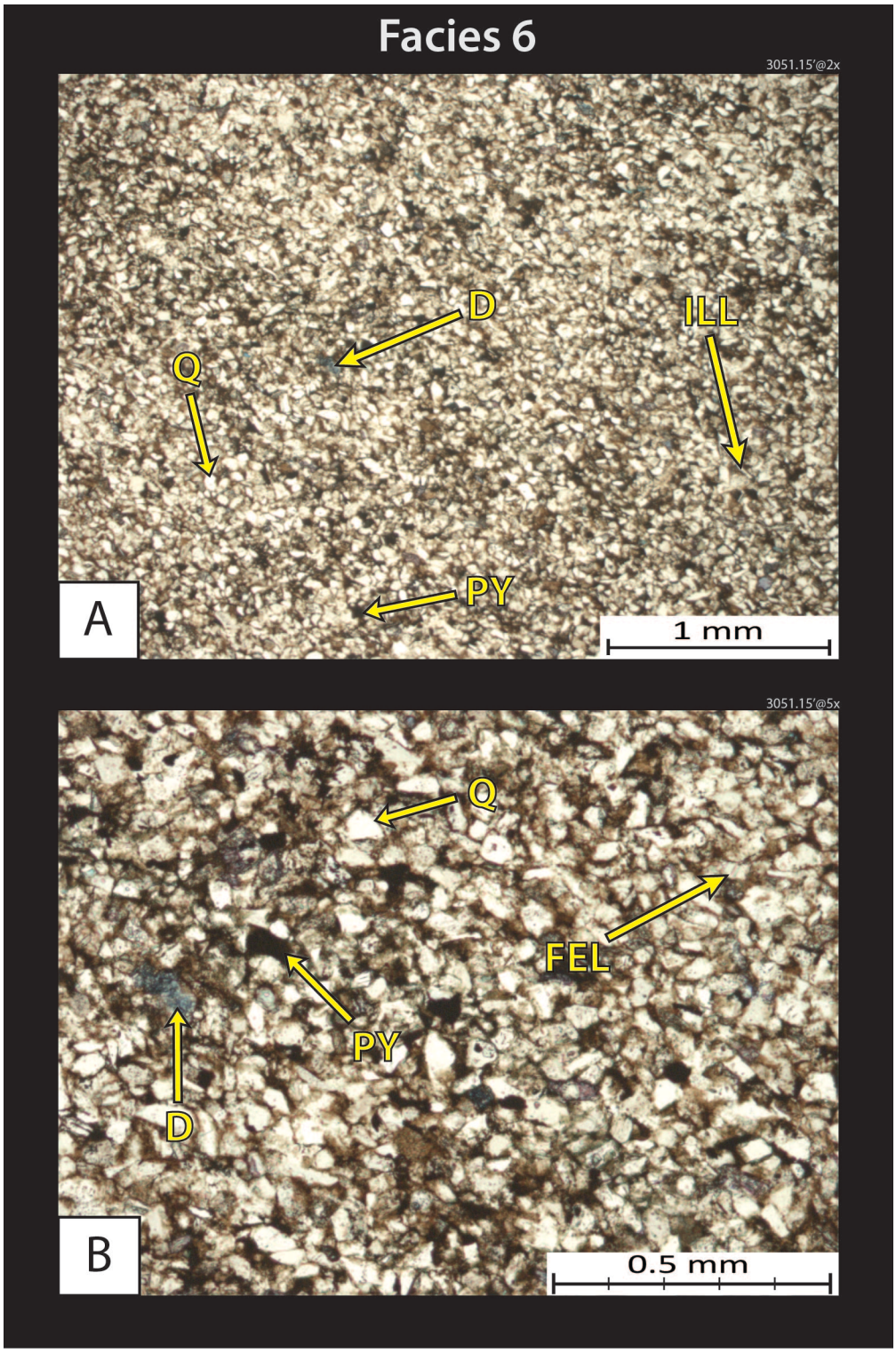


**3051.15' – Silty argillaceous sandstone.** The sample is dominated by very fine to fine sand sized quartz (Q) grains as well as silt sized quartz grains in some areas, carbonates – mainly calcite (pink) grains, and occasional clays – primarily illite. Calcite grains are commonly brachiopod and crinoid fragments along with indistinguishable bioclasts. XRD analysis: 61% quartz, 12% carbonates (10% calcite and 2% dolomite), 12% clays (9% illite, 2% mixed layer illite/smectite, and 1% chlorite), and 15% other minerals (9% plagioclase feldspar, 4% potassium feldspar, and 2% pyrite).

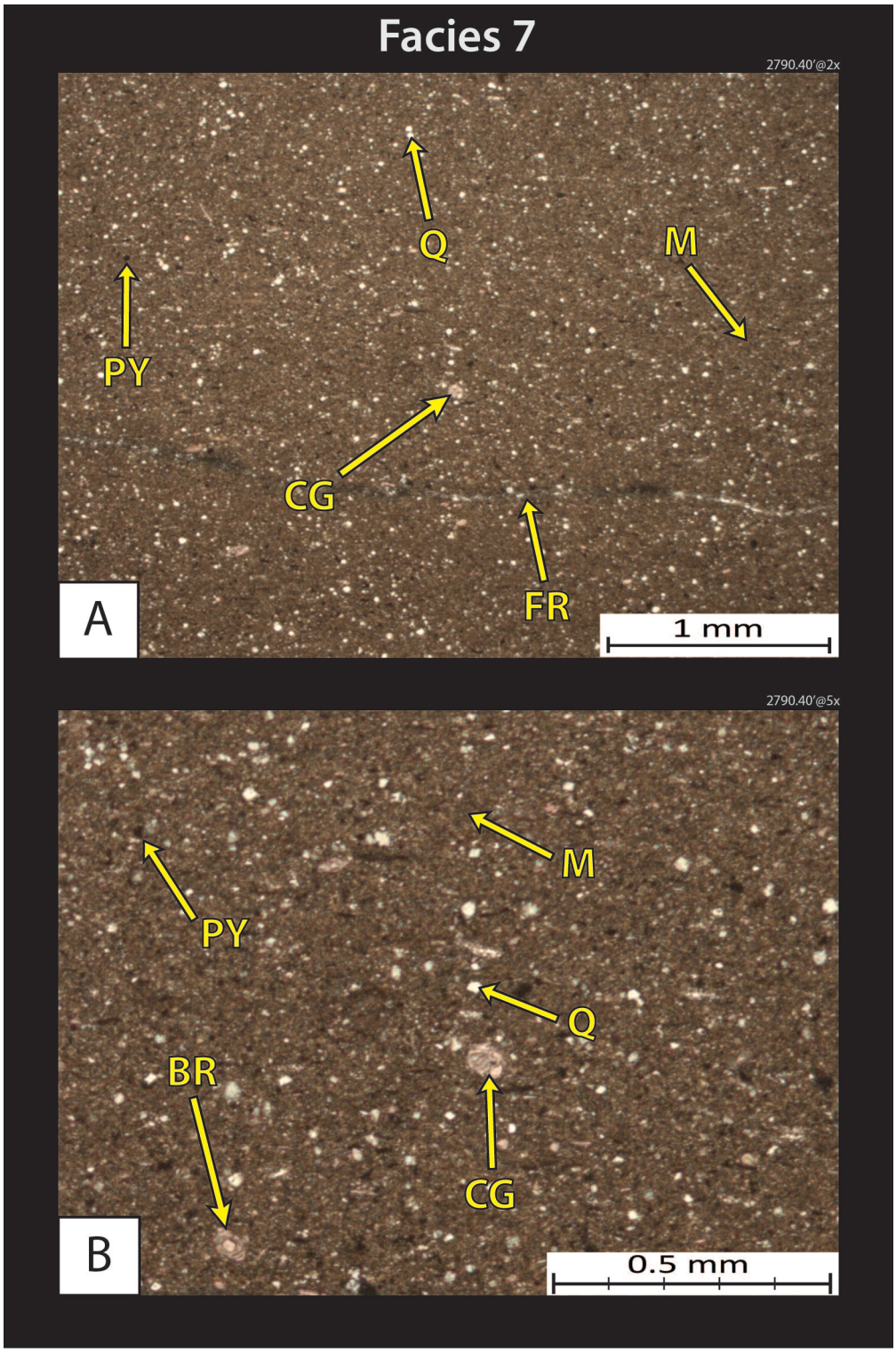


**2790.40' – Argillaceous mudstone-wackestone.** This facies is commonly dominated by carbonate mud and carbonate grains – mainly calcite (pink) grains, clays – mainly mixed layer illite/smectite, and minor silt sized quartz grains (Q). Calcite grains are commonly brachiopod and crinoid fragments and to a lesser degree indistinguishable bioclasts. XRD analysis: 8% quartz, 53% carbonates (49% calcite and 4% dolomite), 36% clays (23% mixed layer illite/smectite, 6% kaolinite, 4% chlorite, and 3% illite), and 3% other minerals (trace amounts of plagioclase feldspar, 1% potassium feldspar, and 2% pyrite).

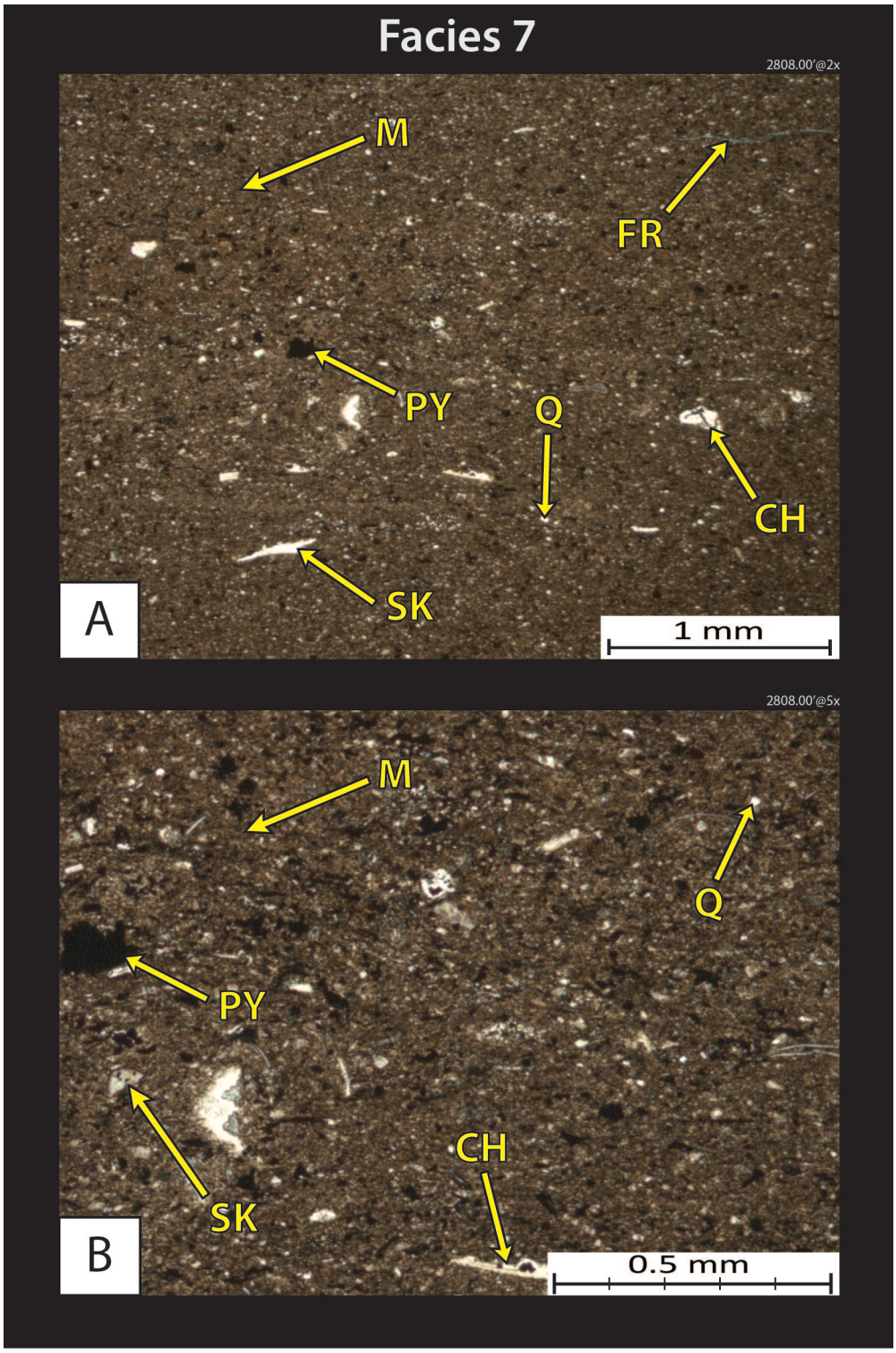


**2808.00' – Argillaceous mudstone-wackestone.** Sample is dominated by carbonate mud and carbonate grains – mainly calcite (pink) grains, clays – mainly mixed layer illite/smectite, and minor silt sized quartz grains (Q). XRD Analysis: 15% quartz, 27% carbonates – calcite, 50% clays (39% mixed layer illite/smectite, 6% kaolinite, 3% illite, and 2% chlorite), and 8% other minerals (3% potassium feldspar, 3% pyrite, and 2% plagioclase feldspar).

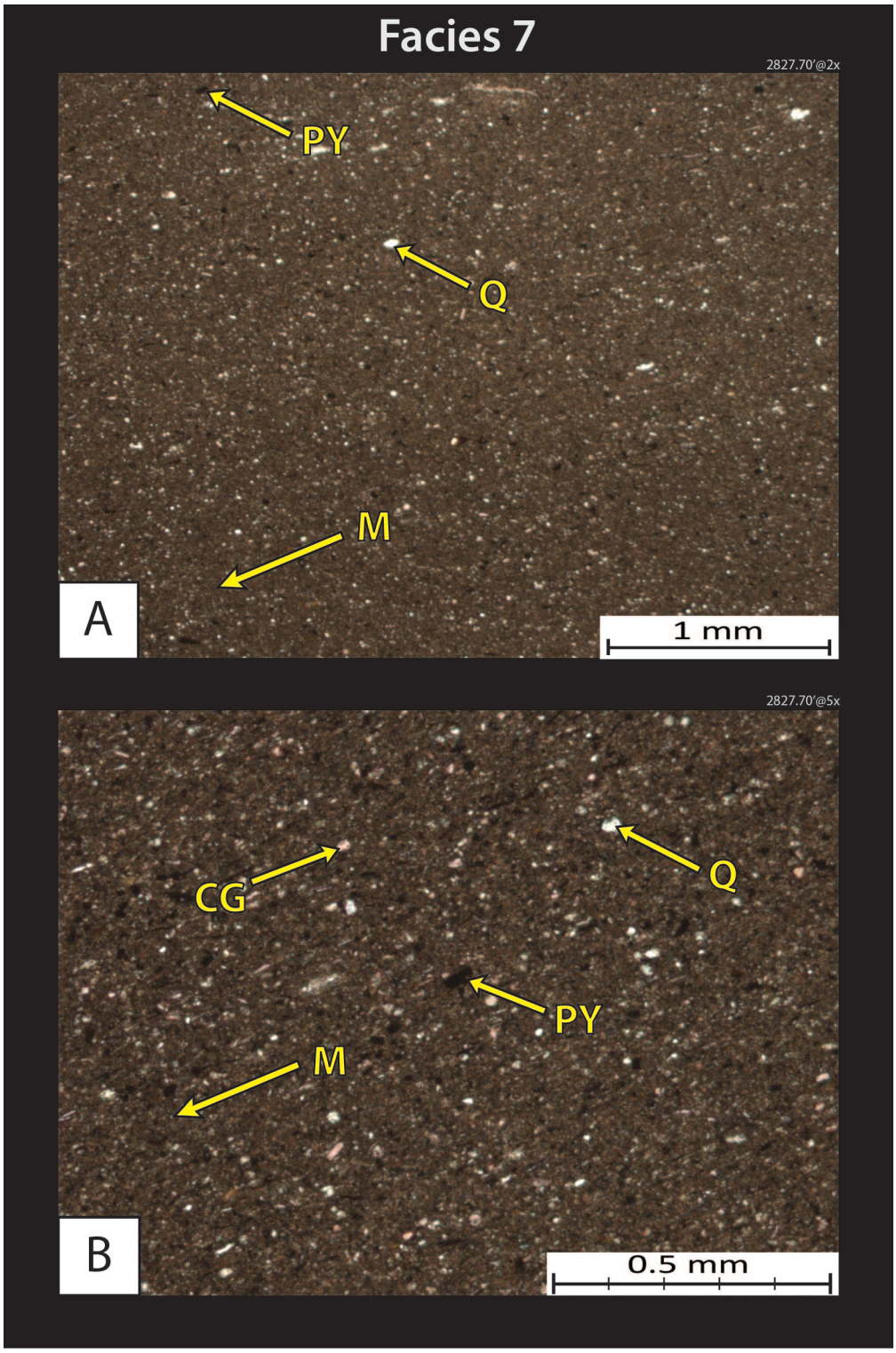


**2827.70' – Argillaceous mudstone-wackestone.** Sample is dominated by carbonate mud and carbonate grains – mainly calcite (pink) grains, clays – mainly mixed layer illite/smectite, and minor silt sized quartz grains (Q). XRD Analysis: 10% quartz, 52% carbonates (51% calcite and 1% dolomite), 36% clays (28% mixed layer illite/smectite, 4% kaolinite, 2% illite, and 2% chlorite), and 2% other minerals – pyrite.

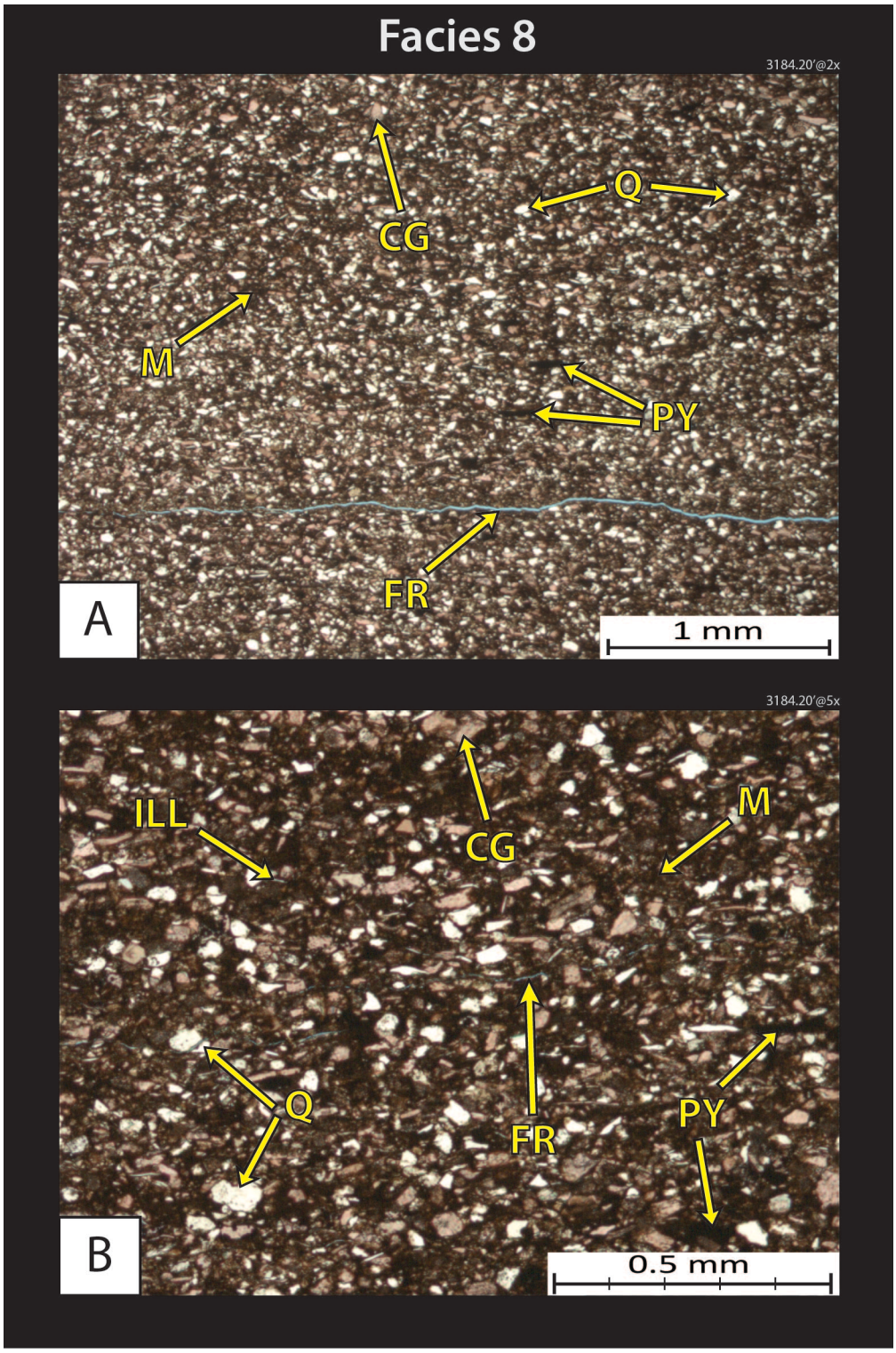


**3184.20' – Silty burrowed mudstone-wackestone.** This facies commonly contains abundant silt to very fine sand sized quartz grains (Q), carbonate – calcite (pink) grains, brachiopods (BR), as well as clays (illite) in a muddy organic-rich matrix. XRD analysis: 27% quartz, 46% carbonates (45% calcite and 1% dolomite), 14% clays (11% illite, 1% mixed layer illite/smectite, 1% kaolinite, and 1% chlorite), and 13% other minerals (5% plagioclase feldspar, 4% potassium feldspar, 2% pyrite, and 2% apatite).

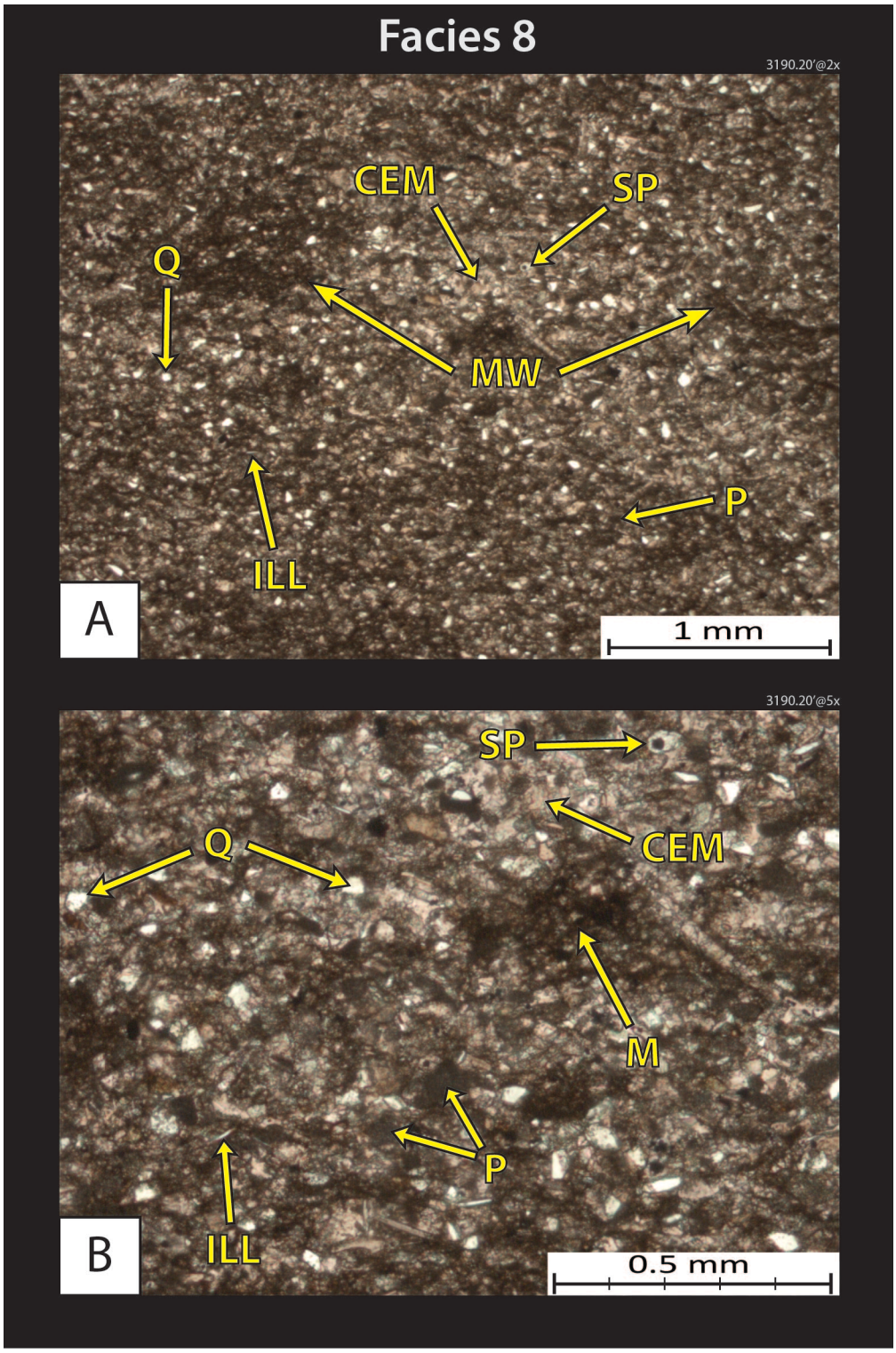


**3190.20' – Silty burrowed mudstone-wackestone.** Sample is dominated by calcite grains and calcite cement, with minor amounts of silt sized quartz grains (Q) and peloids (P). XRD analysis: 12% quartz, 71% carbonates (70% calcite and 1% dolomite), 12% clays (11% illite, and 1% mixed layer illite/smectite), and 5% other minerals (3% plagioclase feldspar, 1% potassium feldspar, and 1% pyrite).

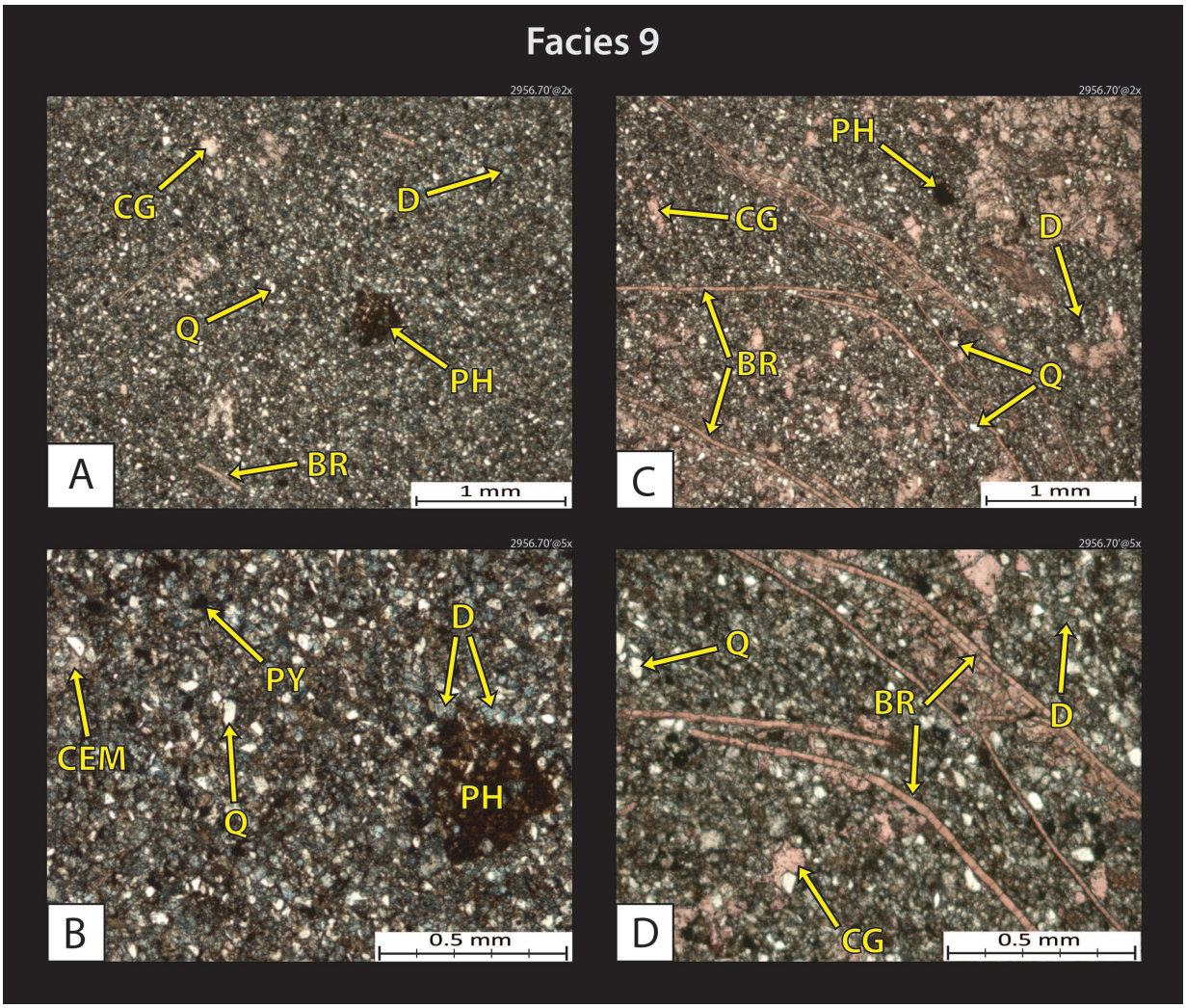


**2956.70' – Silty argillaceous dolomitic packstone.** The sample contains abundant silt sized quartz (Q) grains, carbonates – dolomite (D), and calcified brachiopods (BR), as well as clays. XRD analysis: 25% quartz, 37% carbonates (30% dolomite and 7% calcite), 29% clays (inconclusive results on breakdown of clay types with x-ray diffraction), and 9% other minerals (4% plagioclase feldspar, 2% potassium feldspar, and 3% pyrite).

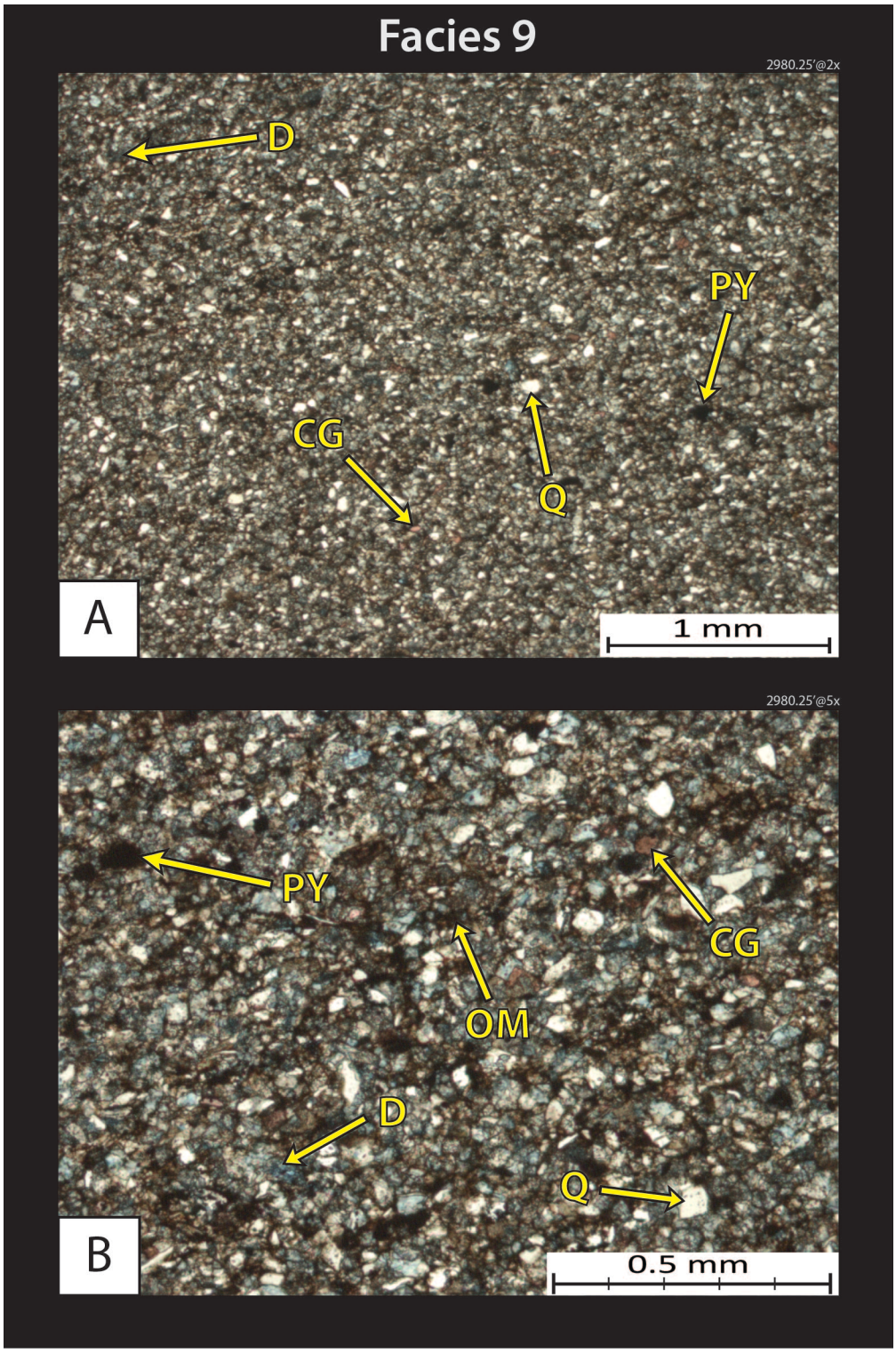


**2980.25' – Silty argillaceous dolomitic packstone.** Sample is dominated by silt sized quartz grains (Q), dolomite, and clays. XRD analysis: 30% quartz, 36% carbonates (29% dolomite and 7% calcite), 24% clays (inconclusive results on breakdown of clay types with x-ray diffraction), and 10% other minerals (5% plagioclase feldspar, 3% potassium feldspar, and 2% pyrite).

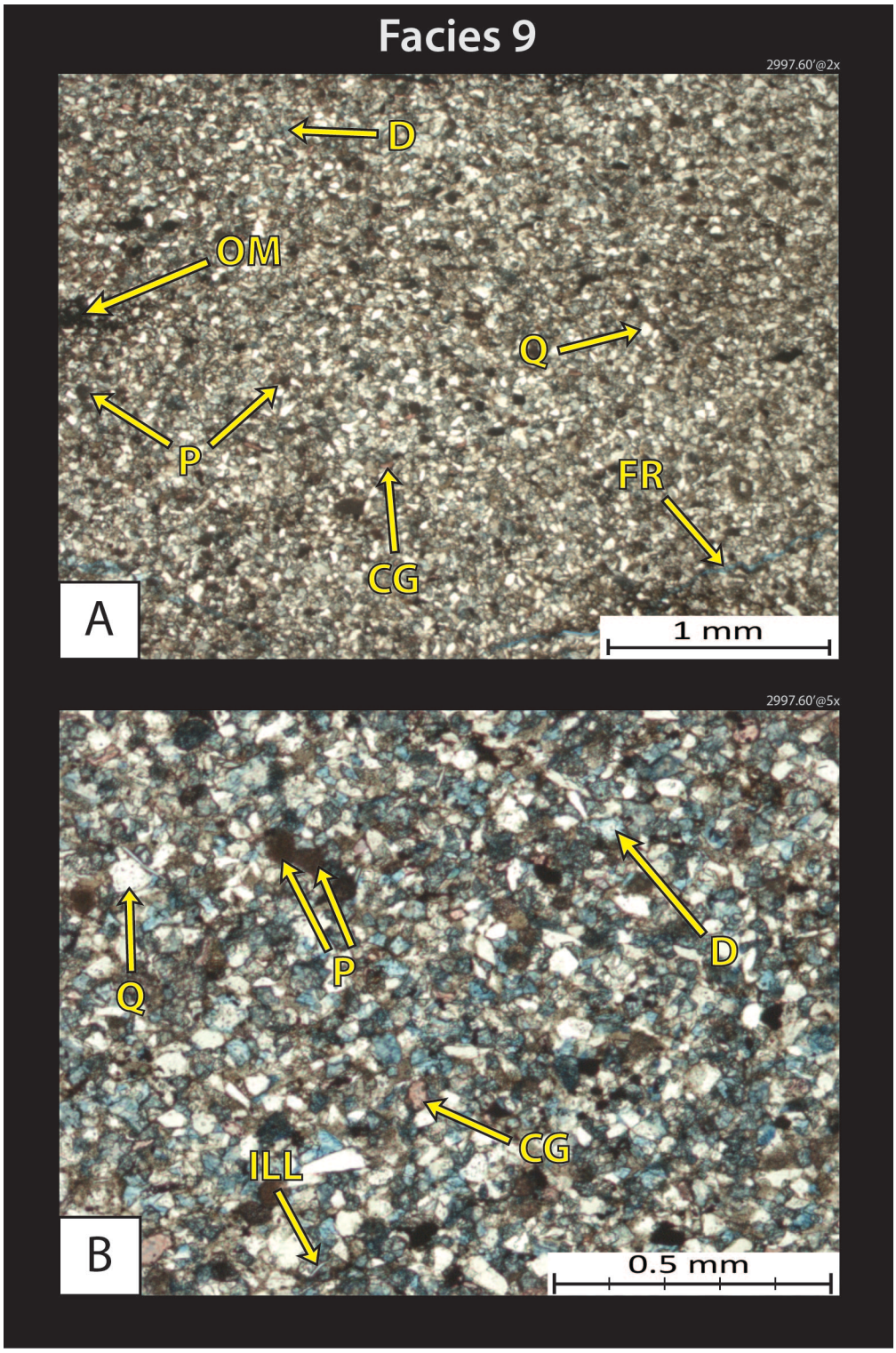


**2997.60' – Silty argillaceous dolomitic packstone.** Sample contains silt sized quartz grains (Q), dolomite, clays, and peloid grains (P). XRD analysis: 35% quartz, 34% carbonates (27% dolomite and 7% calcite), 22% clays (inconclusive results on breakdown of clay types with x-ray diffraction), and 9% other minerals (5% plagioclase feldspar, 2% potassium feldspar, and 2% pyrite).

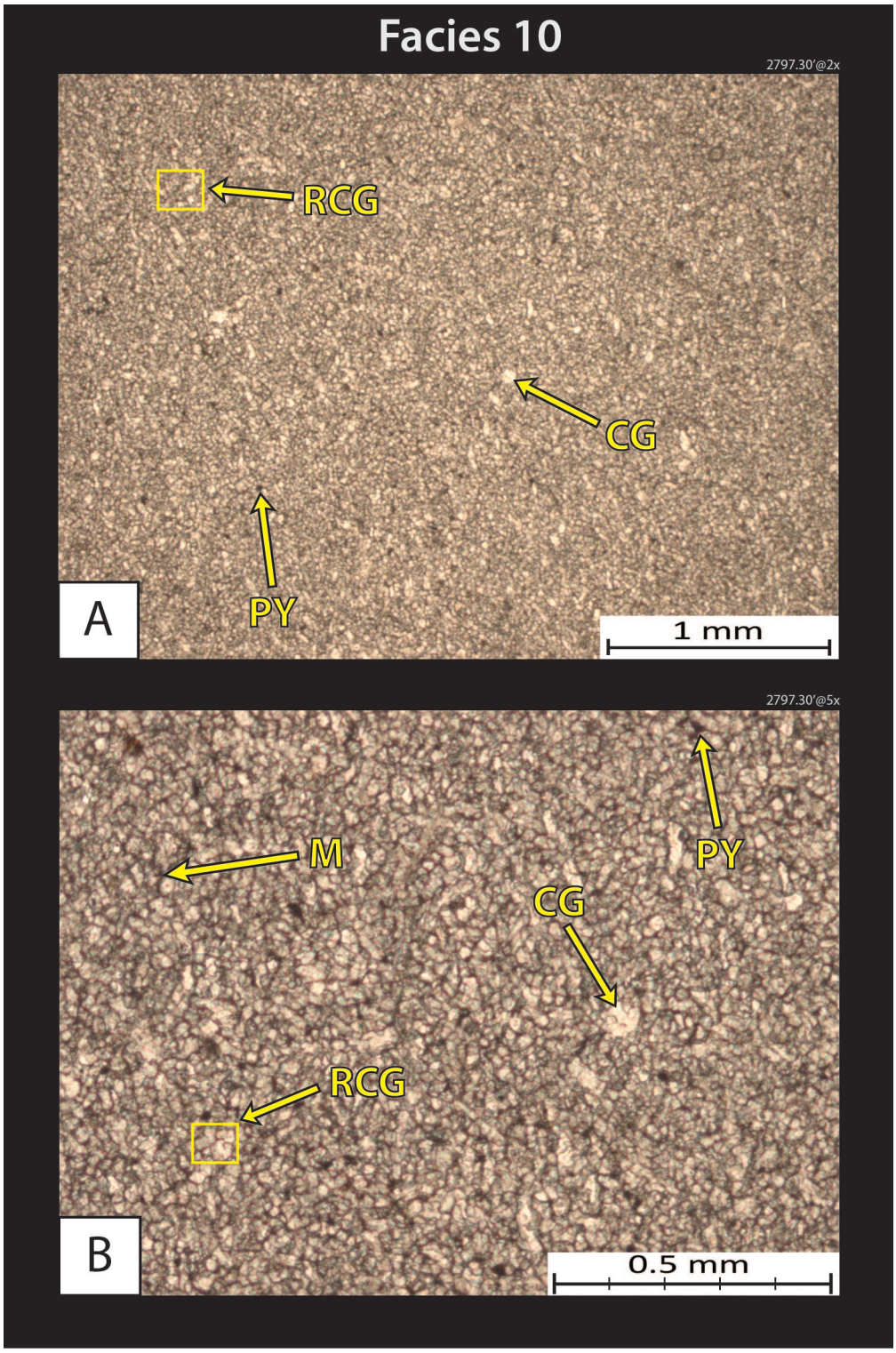


**2797.30' – Recrystallized packstone-grainstone.** This facies is dominated by indistinguishable calcite grains (due to heavy recrystallization) and contains minor amounts of clays and silt sized quartz grains. XRD analysis: 1% quartz, 92% carbonates (91% calcite and 1% dolomite), 6% clays (3% mixed layer illite/smectite, 1% illite, 1% kaolinite, and 1% chlorite), and 1% other minerals (1% pyrite).

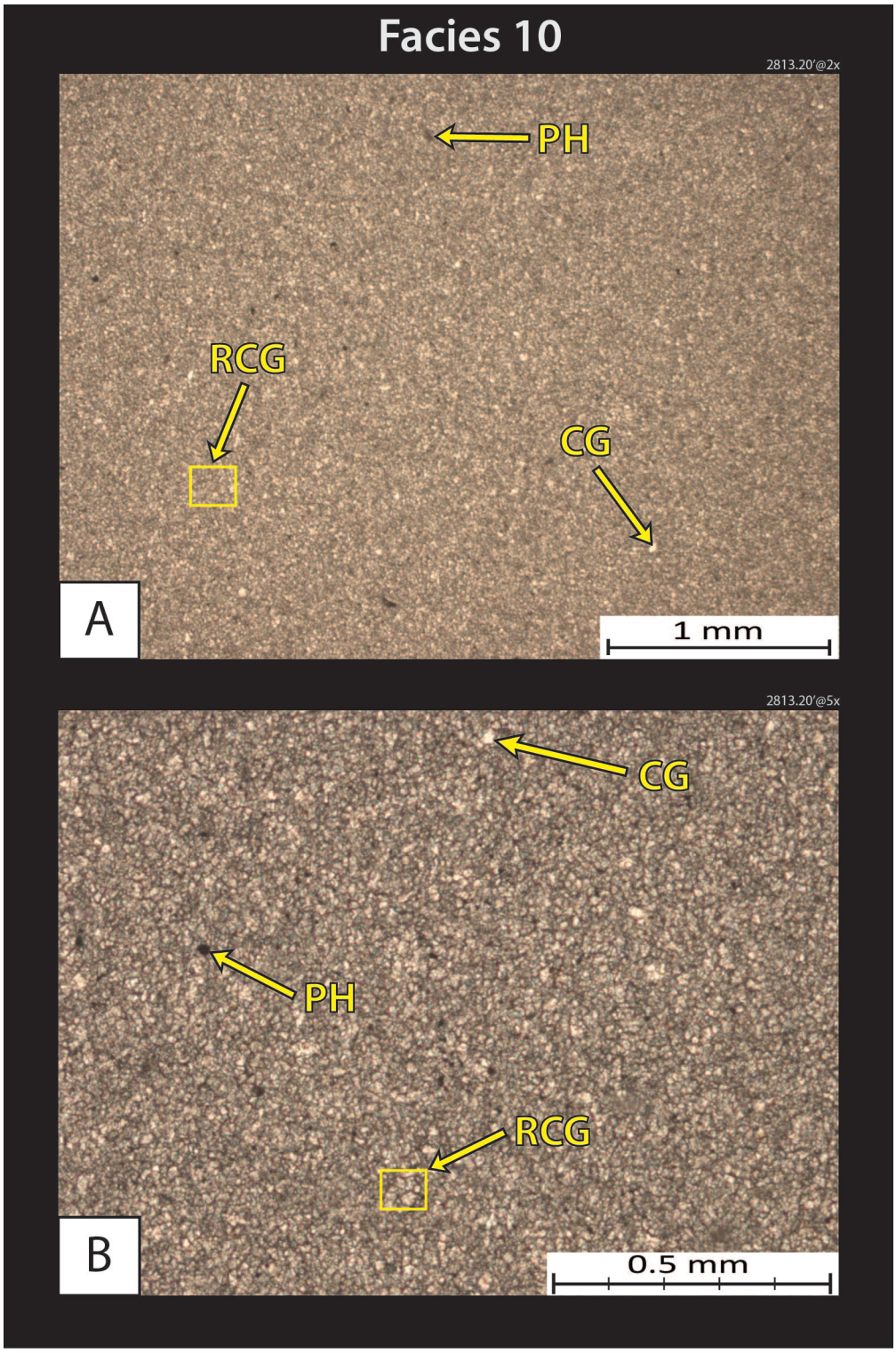


**2813.20' – Recrystallized packstone-grainstone.** The sample is dominated by indistinguishable calcite grains and contains minor amounts of clays and silt sized quartz grains. XRD analysis: 2% quartz, 92% carbonates (90% calcite and 2% dolomite), 6% clays (5% mixed layer illite/smectite, 1% illite), and 0% other minerals.

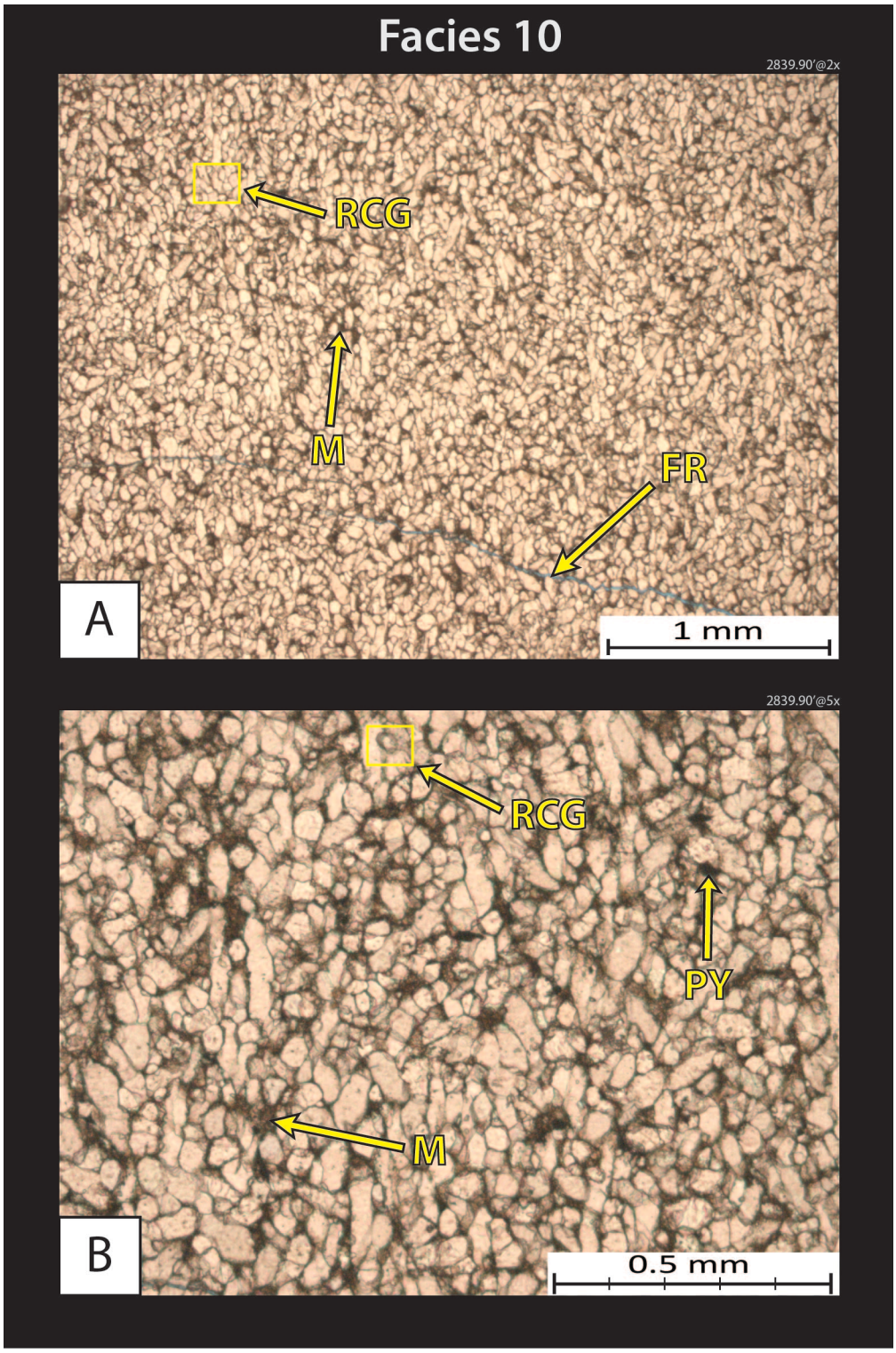


**2839.90' – Recrystallized packstone-grainstone.** The sample is dominated by indistinguishable calcite grains and contains minor amounts of clays and silt sized quartz grains. XRD analysis: 3% quartz, 88% carbonates (82% calcite and 6% dolomite), 8% clays (6% mixed layer illite/smectite, 1% illite, and 1% kaolinite), and 1% other minerals (1% pyrite).

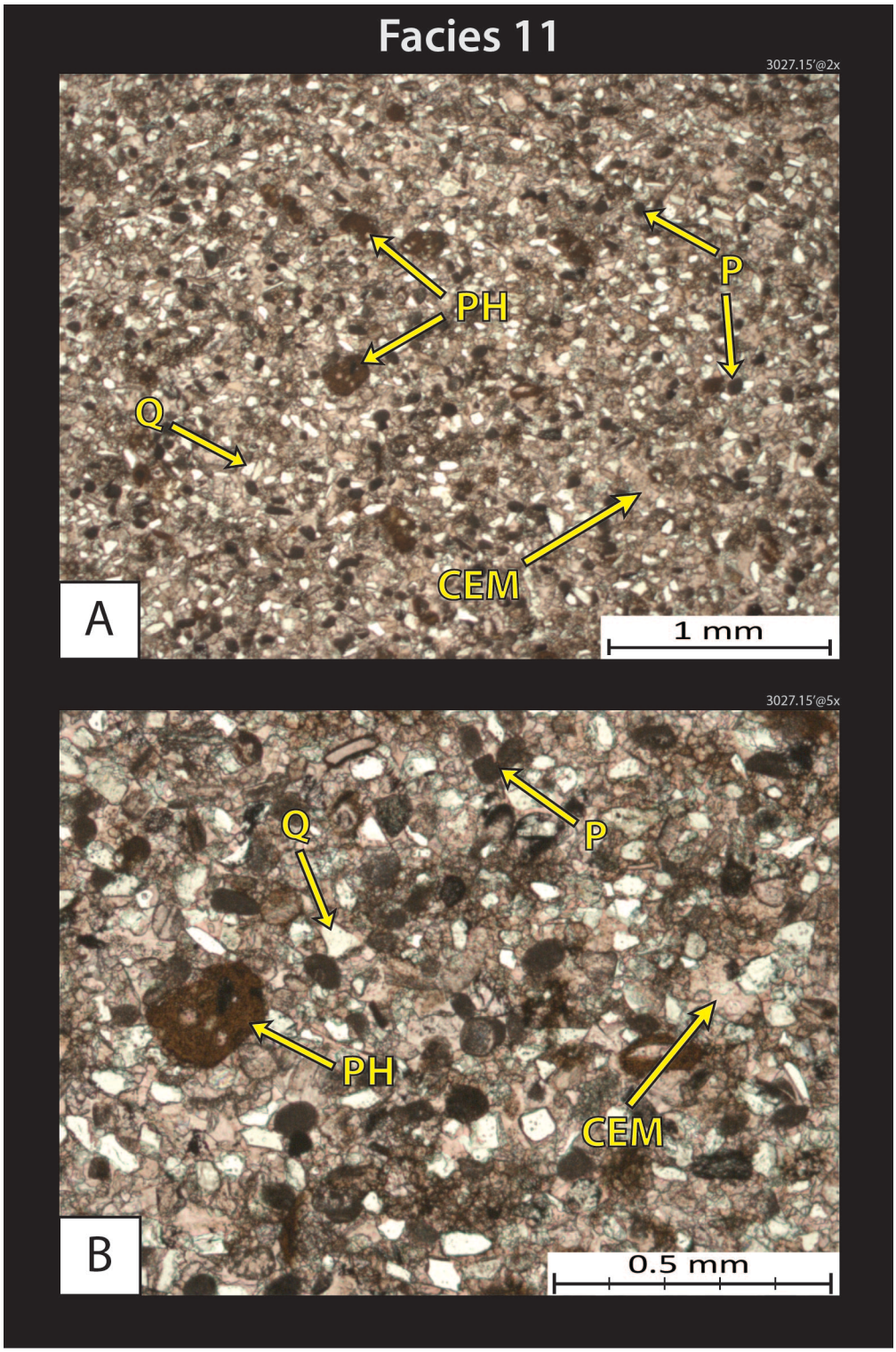


**3027.15' – Silty peloidal packstone-grainstone.** This facies is commonly composed of silt to mostly sand sized peloid (P) grains, carbonate – mainly calcite (pink) grains and cement, and silt to very fine sand sized quartz (Q) grains. It also contains skeletal debris such as, crinoids (CR) and brachiopods. XRD analysis: 19% quartz, 68% carbonates (67% calcite, 1% dolomite), 5% clays (inconclusive results on breakdown of clay types with x-ray diffraction), 8% other minerals (5% plagioclase feldspar, 1% potassium feldspar, 1% pyrite, and 1% apatite).

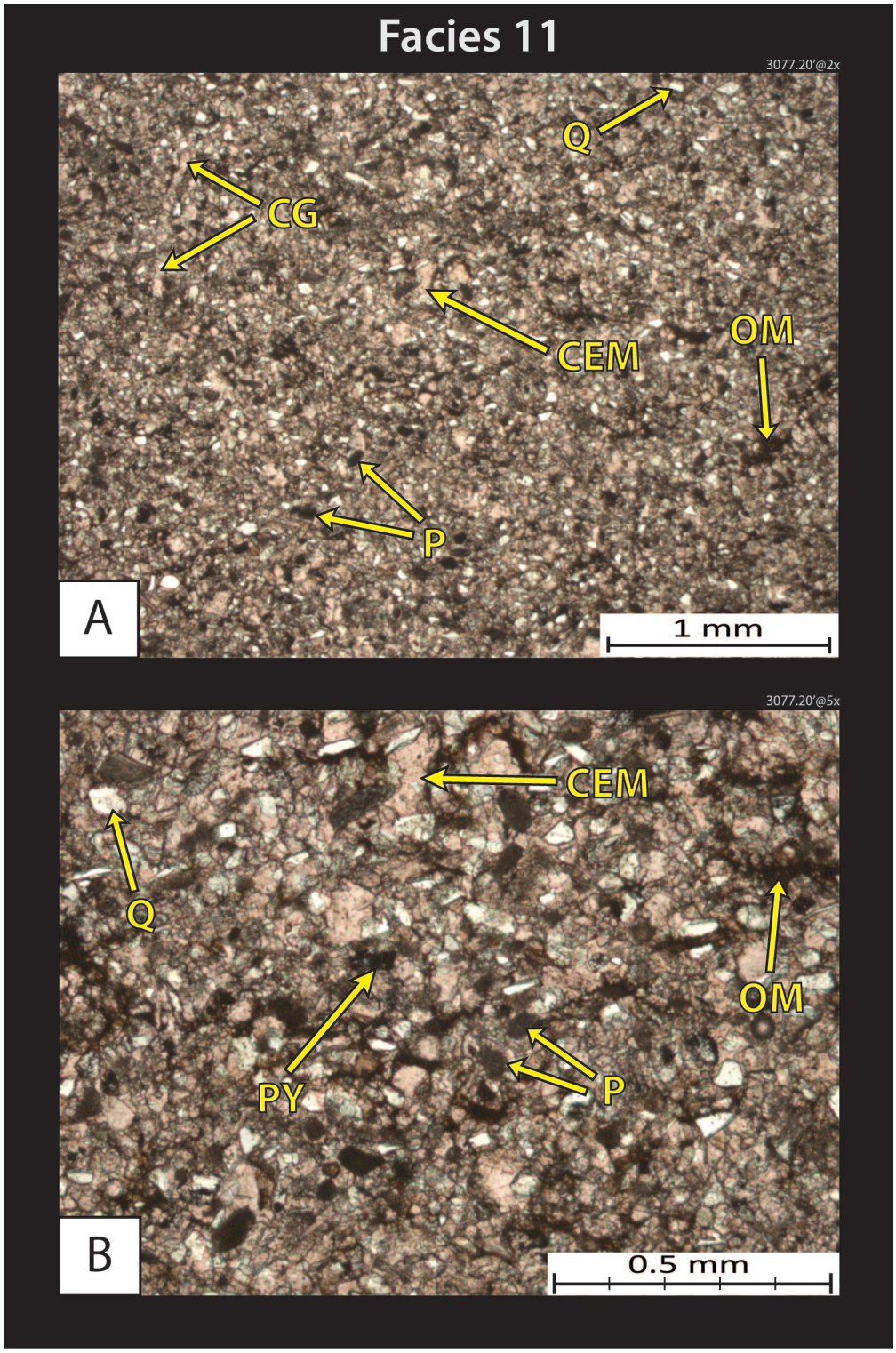


**3077.20' – Silty peloidal packstone-grainstone.** Sample is dominated by calcite grains & calcite cement, silt to sand sized peloid grains (P), and silt sized quartz grains (Q). XRD analysis: 20% quartz, 64% carbonates (63% calcite, 1% dolomite), 7% clays (inconclusive results on breakdown of clay types with x-ray diffraction), 9% other minerals (6% plagioclase feldspar, 2% potassium feldspar, and 1% pyrite).

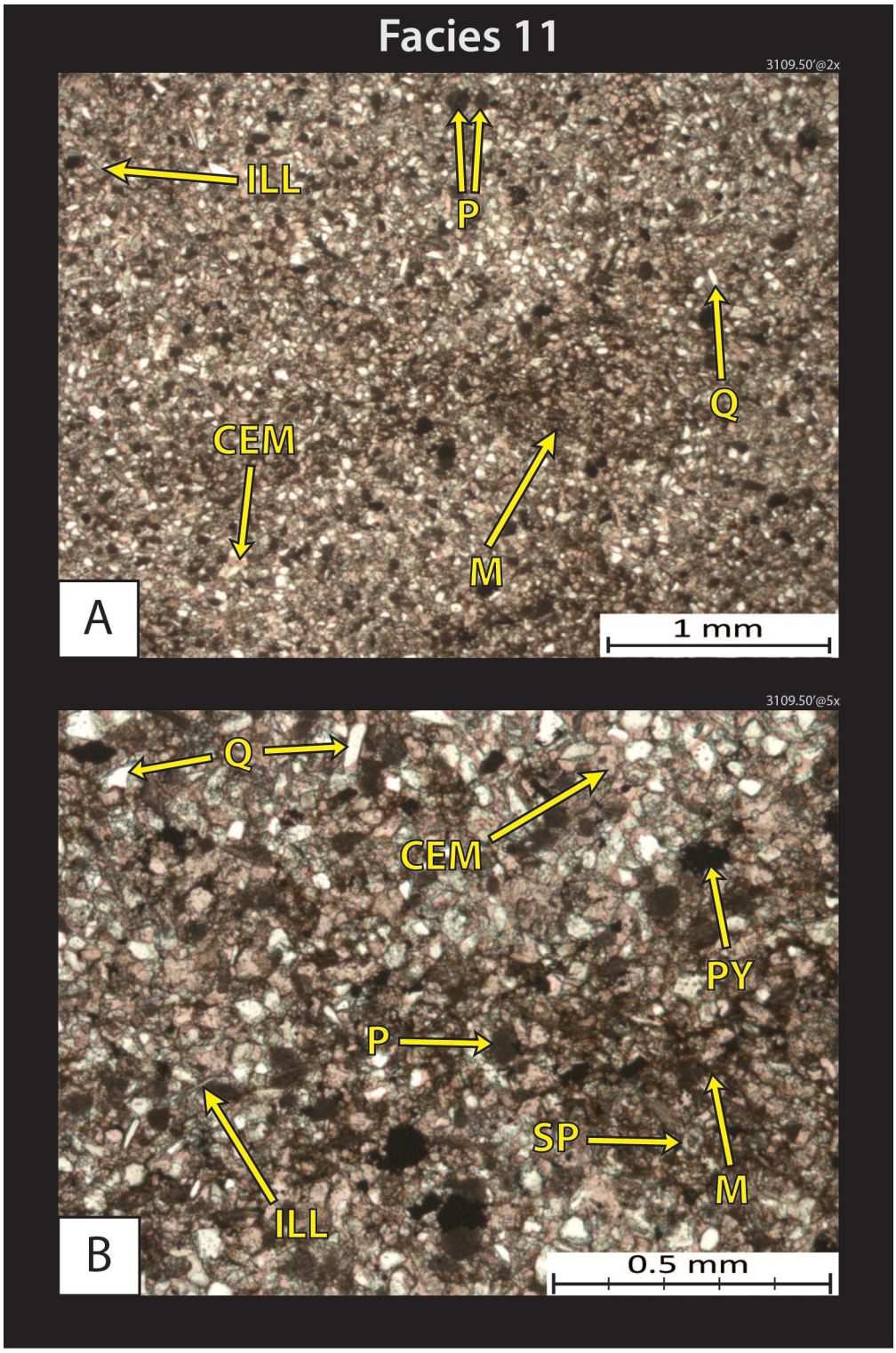


**3109.50' – Silty peloidal packstone-grainstone.** Sample is dominated by calcite grains & calcite cement, silt to sand sized peloid grains (P), and silt sized quartz grains (Q). XRD analysis: 22% quartz, 59% carbonates (55% calcite, 4% dolomite), 9% clays (inconclusive results on breakdown of clay types with x-ray diffraction), 10% other minerals (7% plagioclase feldspar, 2% potassium feldspar, and 1% pyrite).

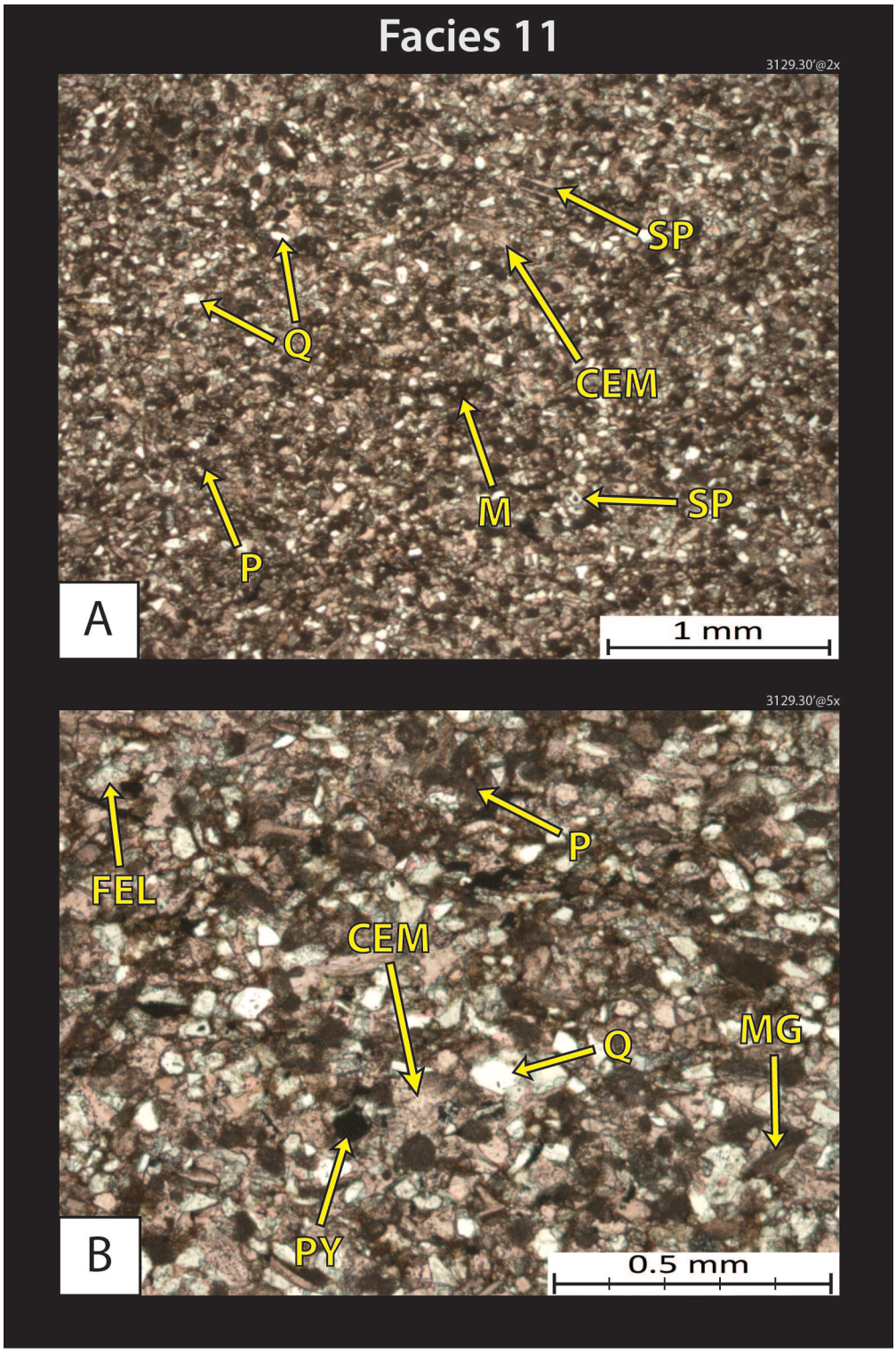


**3129.30' – Silty peloidal packstone-grainstone.** The sample is dominated by calcite grains & calcite cement, silt to sand sized peloid grains (P), silt sized quartz grains (Q), and occasional micritized grains. XRD analysis: 26% quartz, 57% carbonates (54% calcite, 3% dolomite), 8% clays (inconclusive results on breakdown of clay types with x-ray diffraction), 9% other minerals (5% plagioclase feldspar, 3% potassium feldspar, and 1% pyrite).

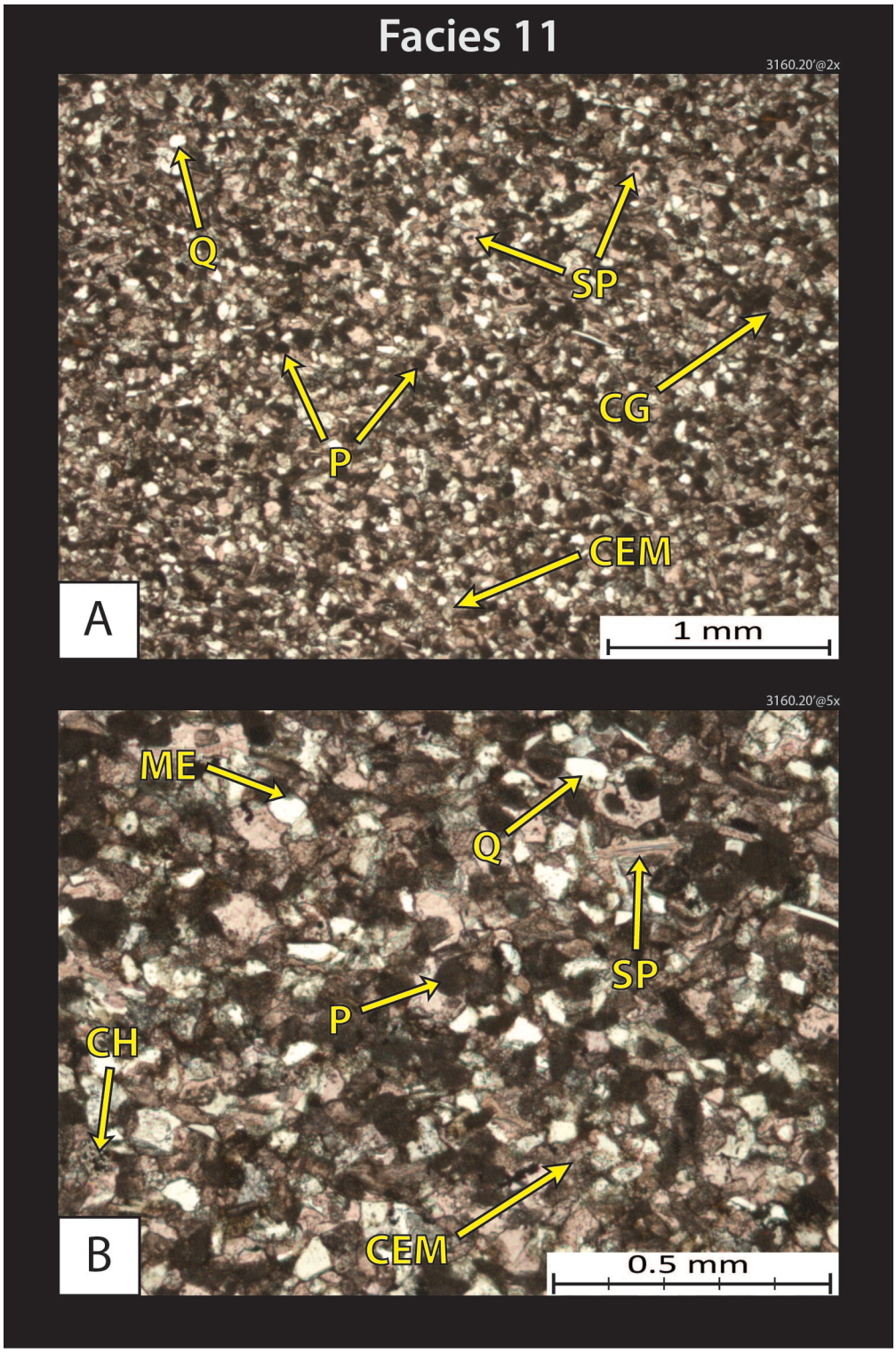


**3160.20' – Silty peloidal packstone-grainstone.** The sample is composed of silt to mostly sand sized peloid (P) grains, carbonate – mainly calcite (pink) grains, and silt to very fine sand sized quartz (Q) grains. It also contains skeletal debris such as, crinoids (CR) and brachiopods. XRD analysis: 24% quartz, 65% carbonates (61% calcite, 4% dolomite), 4% clays inconclusive results on breakdown of clay types with x-ray diffraction), 7% other minerals (4% plagioclase feldspar, 2% potassium feldspar, 1% pyrite).

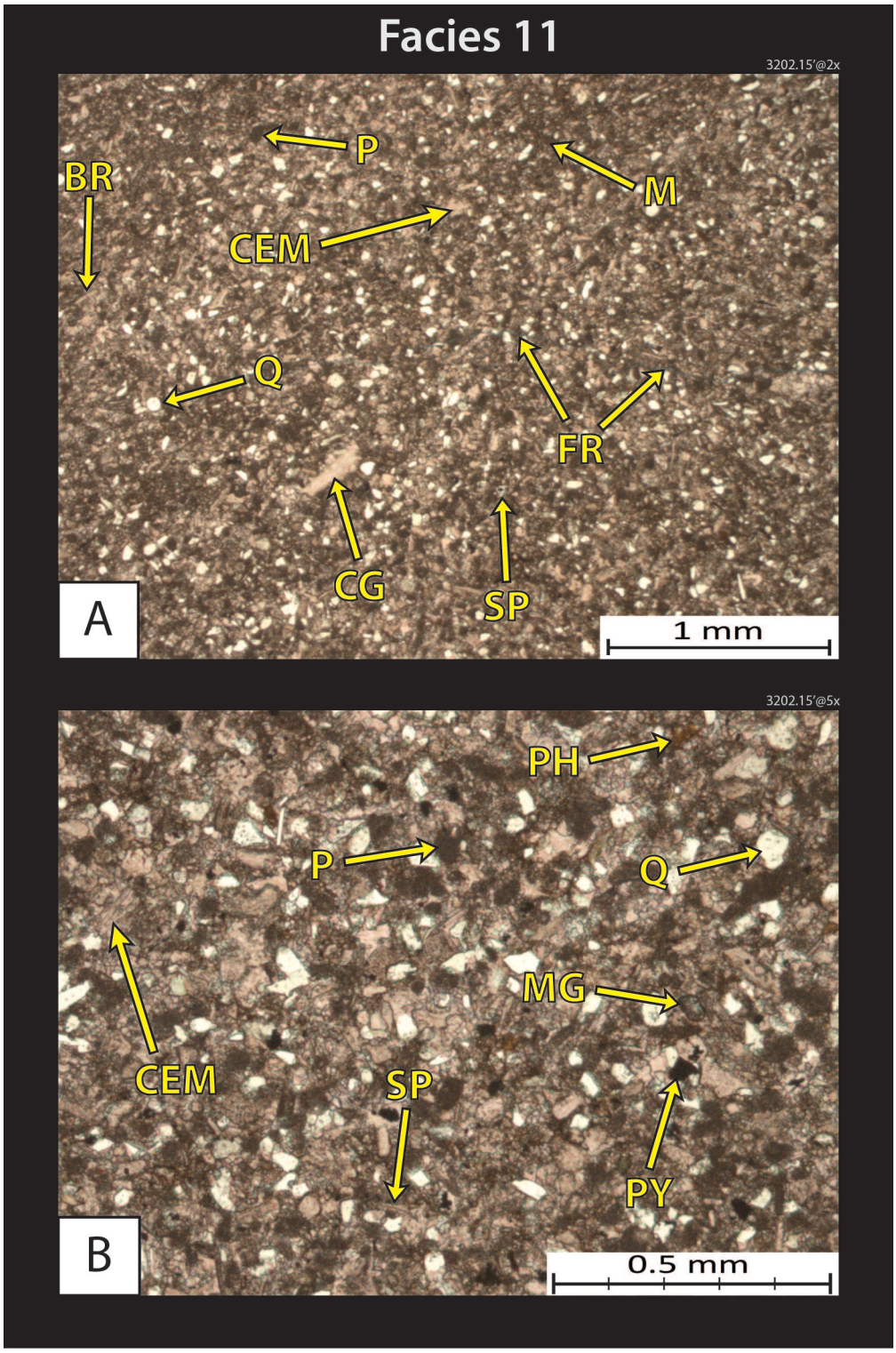


**3202.15' – Silty peloidal packstone-grainstone.** Sample is dominated by calcite grains & calcite cement, silt to sand sized peloid grains (P), silt sized quartz grains (Q), and minor amounts of phosphate. XRD analysis: 11% quartz, 81% carbonates (80% calcite, 1% dolomite), 4% clays (inconclusive results on breakdown of clay types with x-ray diffraction), 4% other minerals (3% plagioclase feldspar, and 1% potassium feldspar).

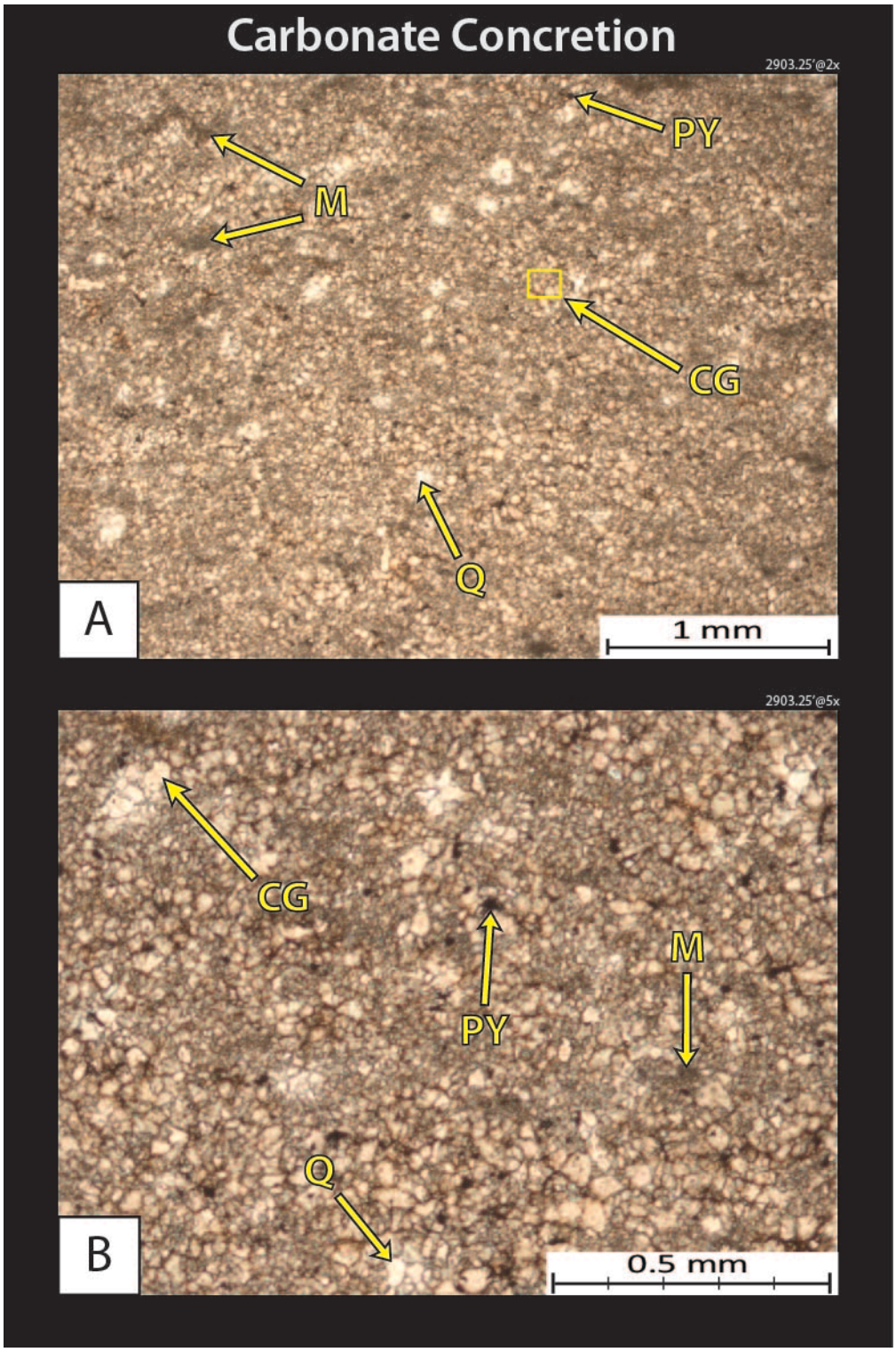


**2903.25' – Carbonate concretion.** These concretions are very infrequent but are typically dominated by indistinguishable calcite grains and calcite cement, with minor amounts of clays and silt sized quartz grains (Q). XRD analysis: 2% quartz, 85% carbonates (84% calcite, 1% dolomite), 4% clays (2% illite, and 2% mixed layer illite/smectite), 9% other minerals (5% pyrite, 3% marcasite, and 1% plagioclase feldspar).

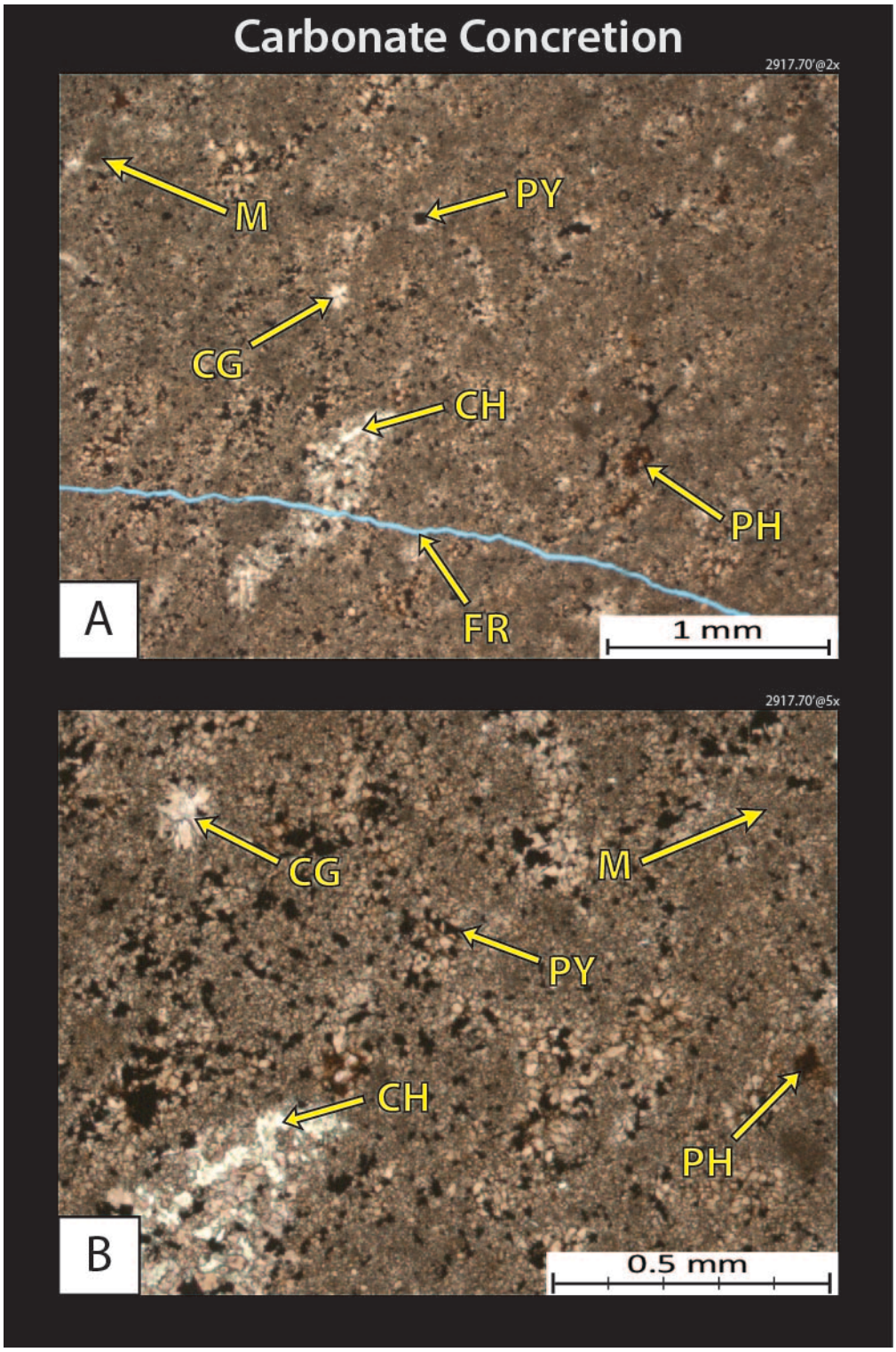


**2917.70' – Carbonate concretion.** Sample is dominated by indistinguishable calcite grains and calcite cement, with minor amounts of clays and silt sized quartz grains (Q). XRD analysis: 2% quartz, 90% carbonates (88% calcite, 2% dolomite), 5% clays (3% illite, and 2% mixed layer illite/smectite), 3% other minerals – pyrite.

# APPENDIX C:

Architecture of Mississippian Strata/Subsurface Mapping

Cross sections and subsurface maps were constructed using Petra geological software, an IHS product.

# I. Subsurface Cross Sections and Correlations

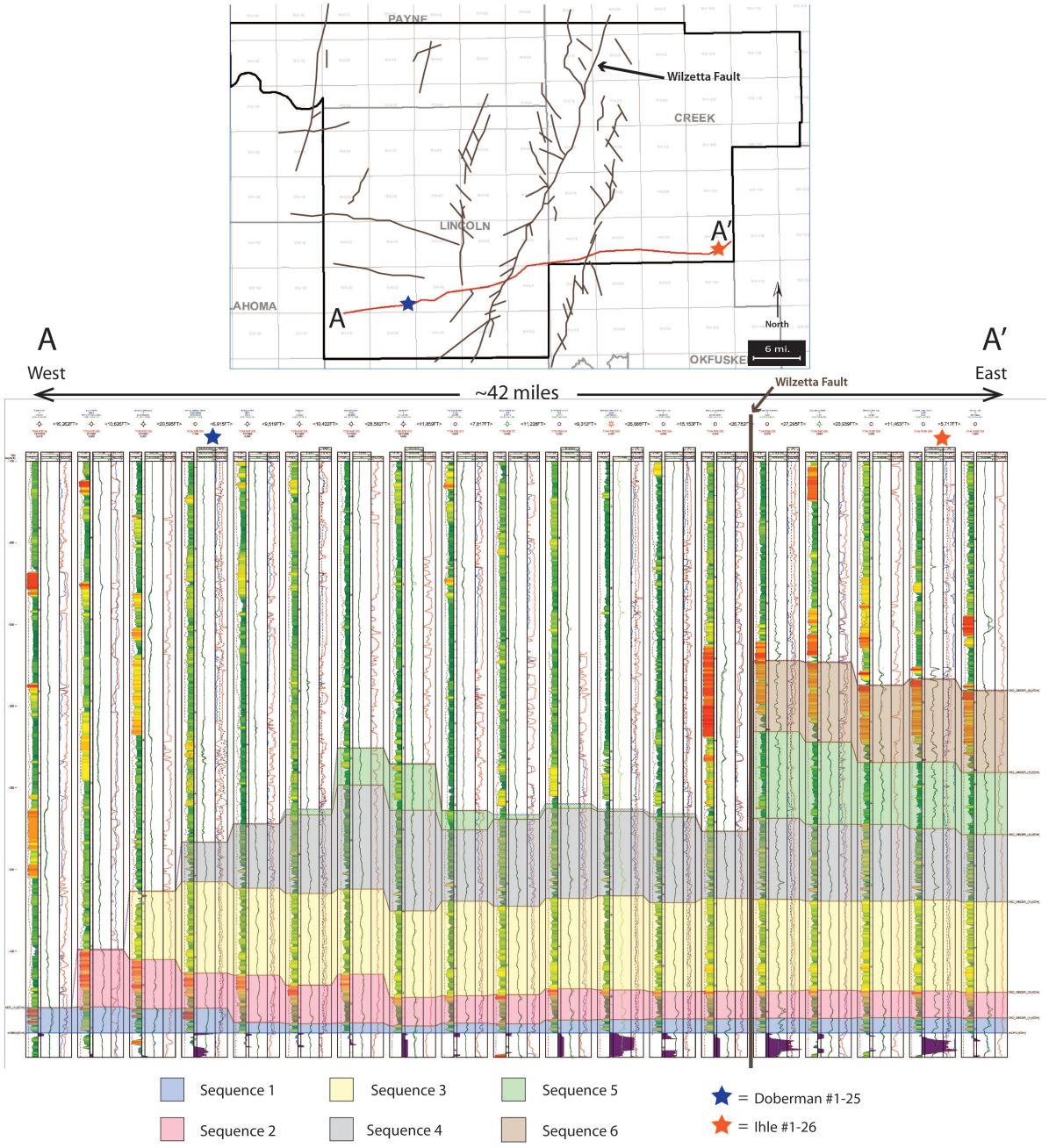


**C-I-a.** Top. Map of study area (outlined in black) showing the cross-section (red line). From west to east, the Doberman #1-25 well is indicated by the blue star and the Ihle #1-26 well is indicated by the orange star. Bottom. Strike oriented subsurface cross section from red line on map. Cross-section shows six probable 3rd order sequences. Vertical scale exaggerated 16x.

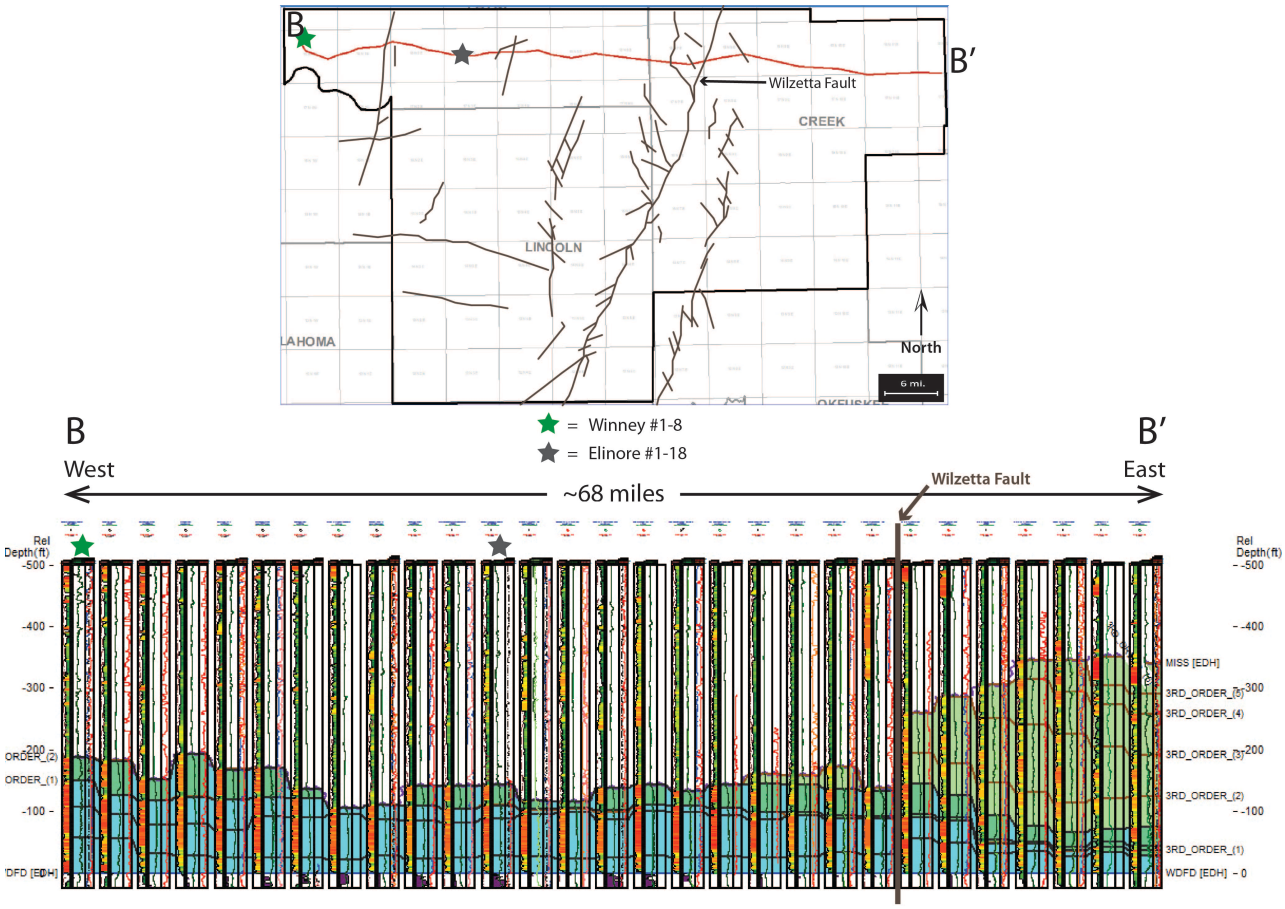


**C-I-b.** Top. Map of study area (outlined in black) showing the location of cross-section (red line). From west to east, the Winney #1-8 well is indicated by the green star and the Elinore #1-18 well is indicated by the gray star. Bottom. Strike oriented subsurface cross-section from red line on map. Cross-section displays the lateral continuity of these sequences moving along depositional strike. Vertical scale exaggerated 8x.

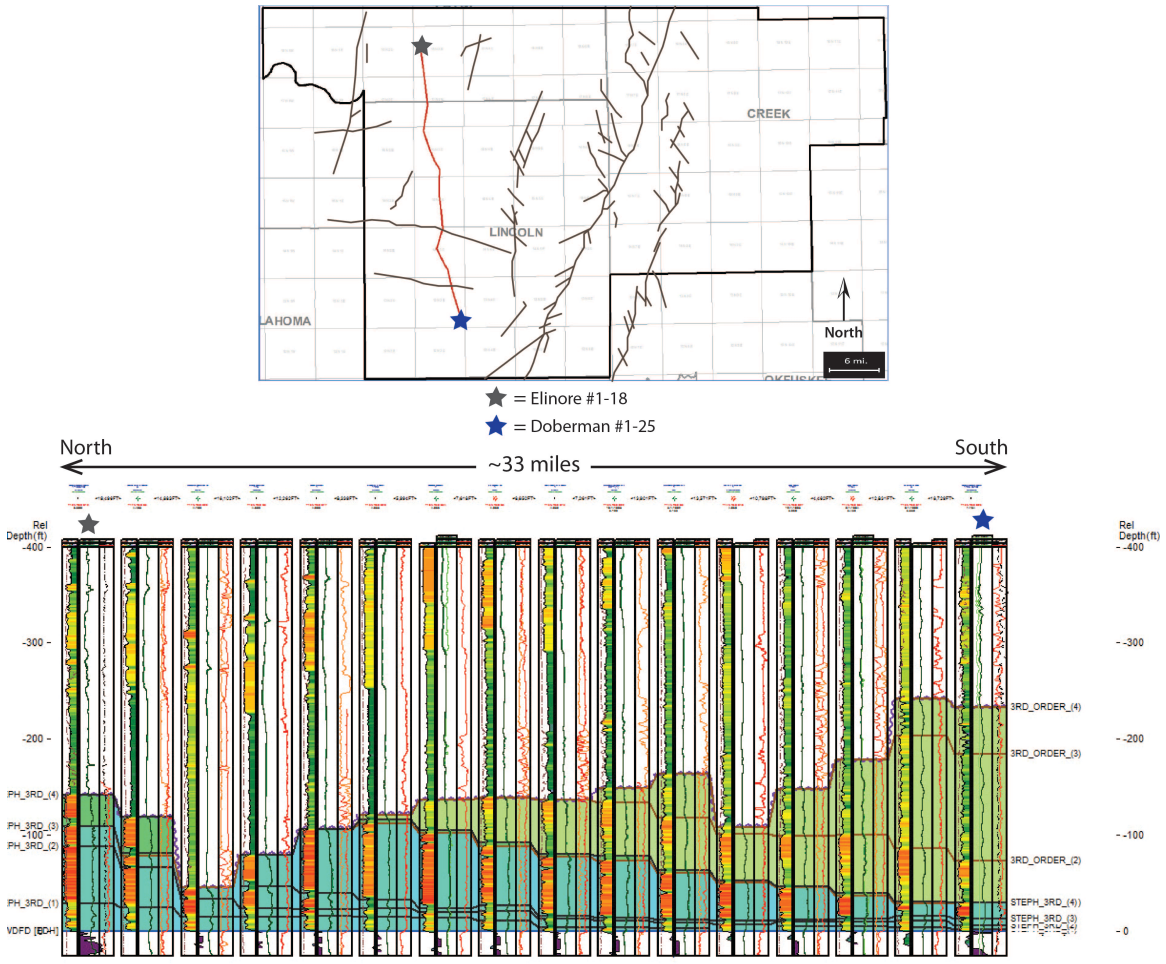


**C-I-c.** Top. Map of study area (outlined in black) showing location of the cross-section (red line). From north to south, the Elinore #1-18 well is indicated by the gray star and the Doberman #1-25 well is indicated by the blue star. Bottom. Dip oriented subsurface cross section of the red line in the above photo. Cross-section displays the geometry of these sequences moving along depositional dip. The correlations show these packages prograding in the dip direction. Correlations also reveal that prograding carbonate clinoforms are a logical interpretation for this system. Vertical scale exaggerated 8x.

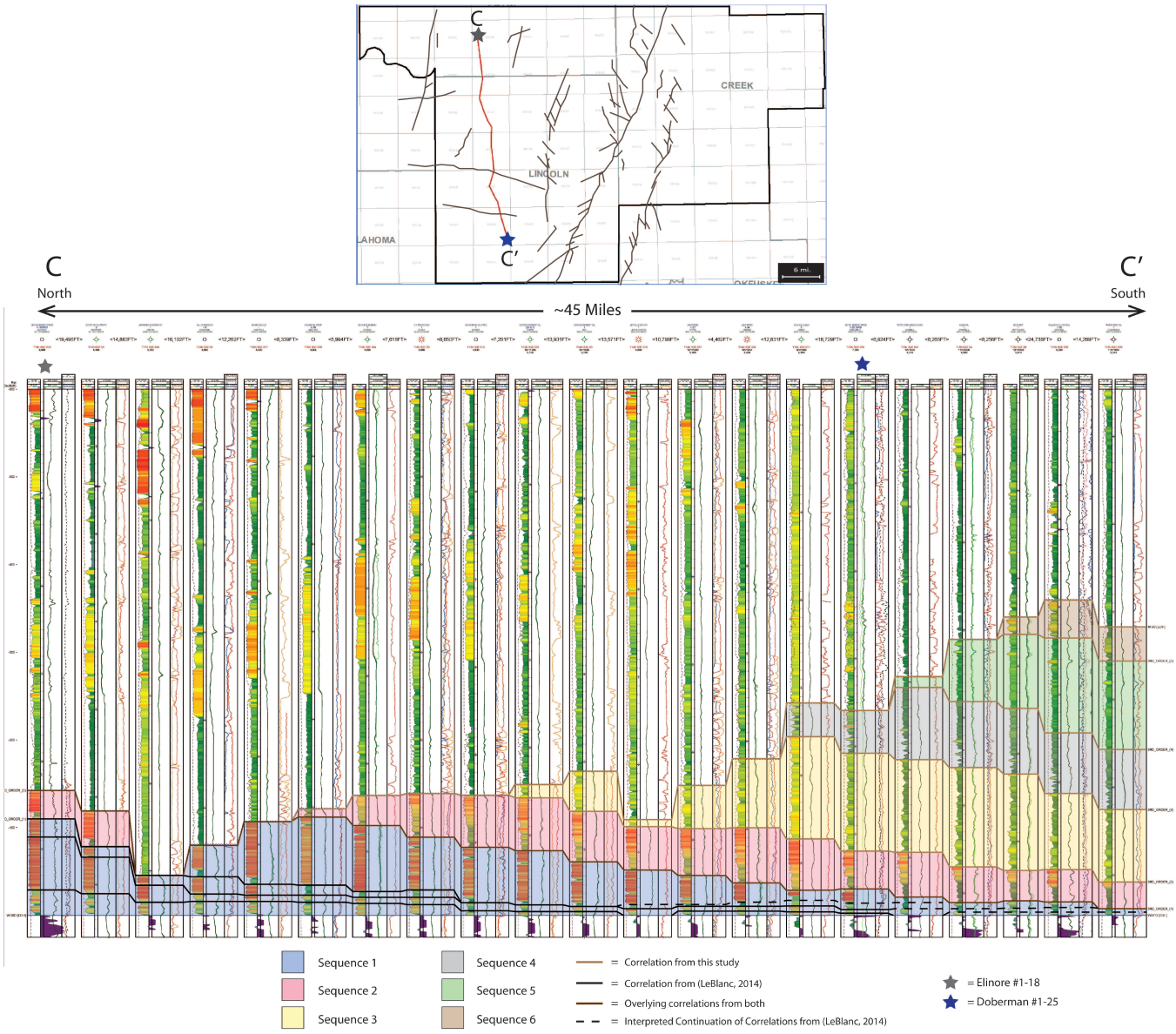


**C-I-d.** Top. Map of study area (outlined in black) showing the location of cross-section C – C' (red line). From north to south, the Elinore #1-18 well is indicated by the gray star and the Doberman #1-25 well is indicated by the blue star. Bottom. Dip oriented subsurface cross section of the red line in the above photo. Cross-section C – C' displays the geometry of these sequences moving along depositional dip. The correlations show these packages prograding in the dip direction. Correlations also reveal that prograding carbonate clinoforms are a logical interpretation for this system. Vertical scale exaggerated 16x.

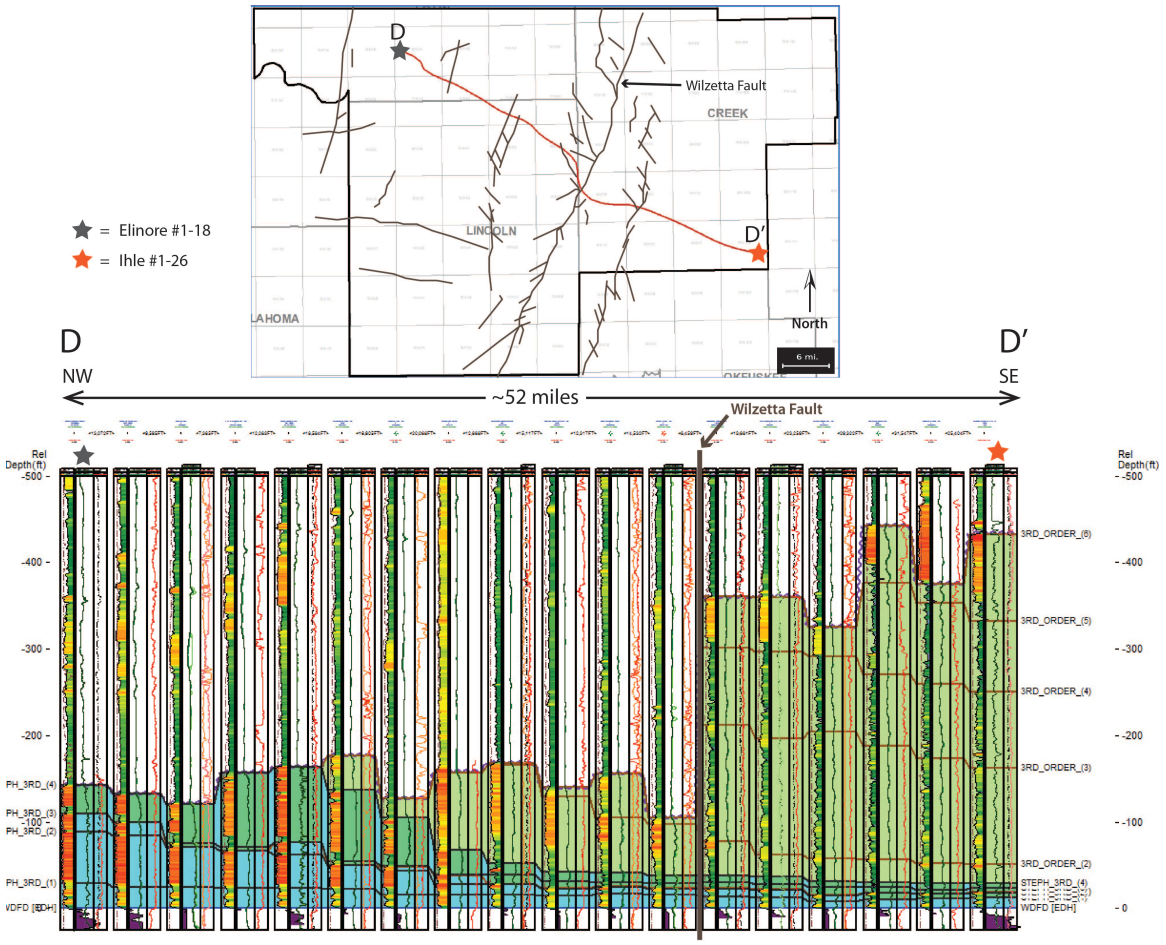


**C-I-e.** Top. Map of study area (outlined in black) showing the cross-section (red line). From northwest to southeast, the Elinore #1-18 well is indicated by the gray star and the Ihle #1-26 well is indicated by the orange star. Bottom. Dip oriented cross-section of the red line on map. Cross-section displays the geometry of these sequences moving along expected depositional dip. Correlations show these packages prograding towards the southeast. Correlations also reveal that prograding carbonate clinoforms are a logical interpretation for this system. Note the significant increase in the thickness of strata starting in the sixth well from the right to the end of the cross section. This thickness increase comes from cross the downthrown side of the Wilzetta Fault line. Vertical scale exaggerated 8x.

## II. Isopach Maps

The scale in the upper right corner of each isopach map represents thickness values in feet. Cooler (purple) colors indicate lower thickness values, whereas warmer (yellow and orange) colors indicate greater thickness values. The location of the Doberman is shown by the white star with the number 1, while the location of the Ihle is shown by the white star with the number 2. Brown lines represent cross-section transects throughout the study area (outlined in black).

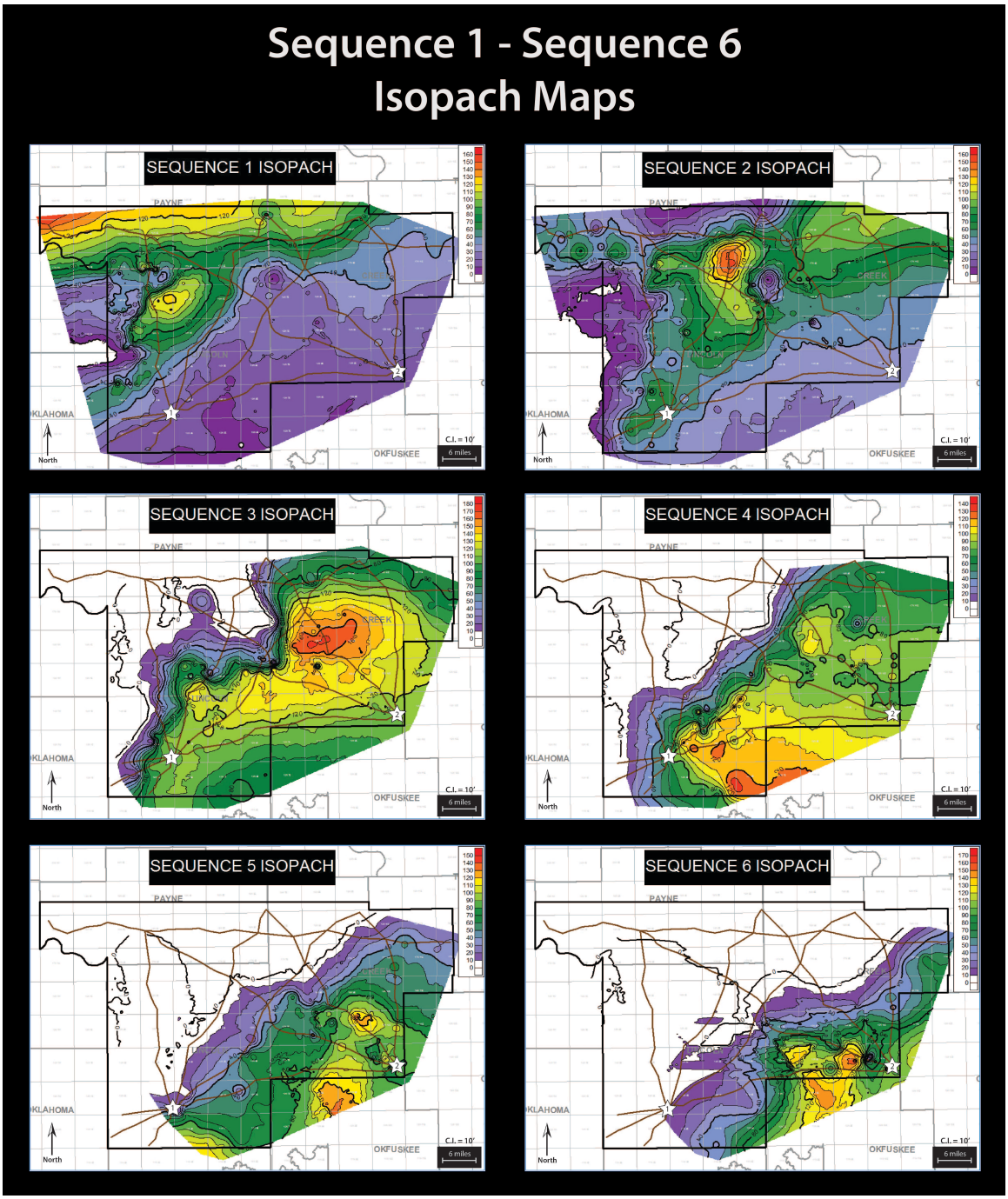


**C-II-a.** Combined figure of sequences 1 through 6. Starting in the top left corner with sequence 1 and moving left to right ending at sequence 6, the thickness maps of probable 3rd order sequences display progradation in a basinward direction (NW to SE). All maps have a contour interval of 10 feet.

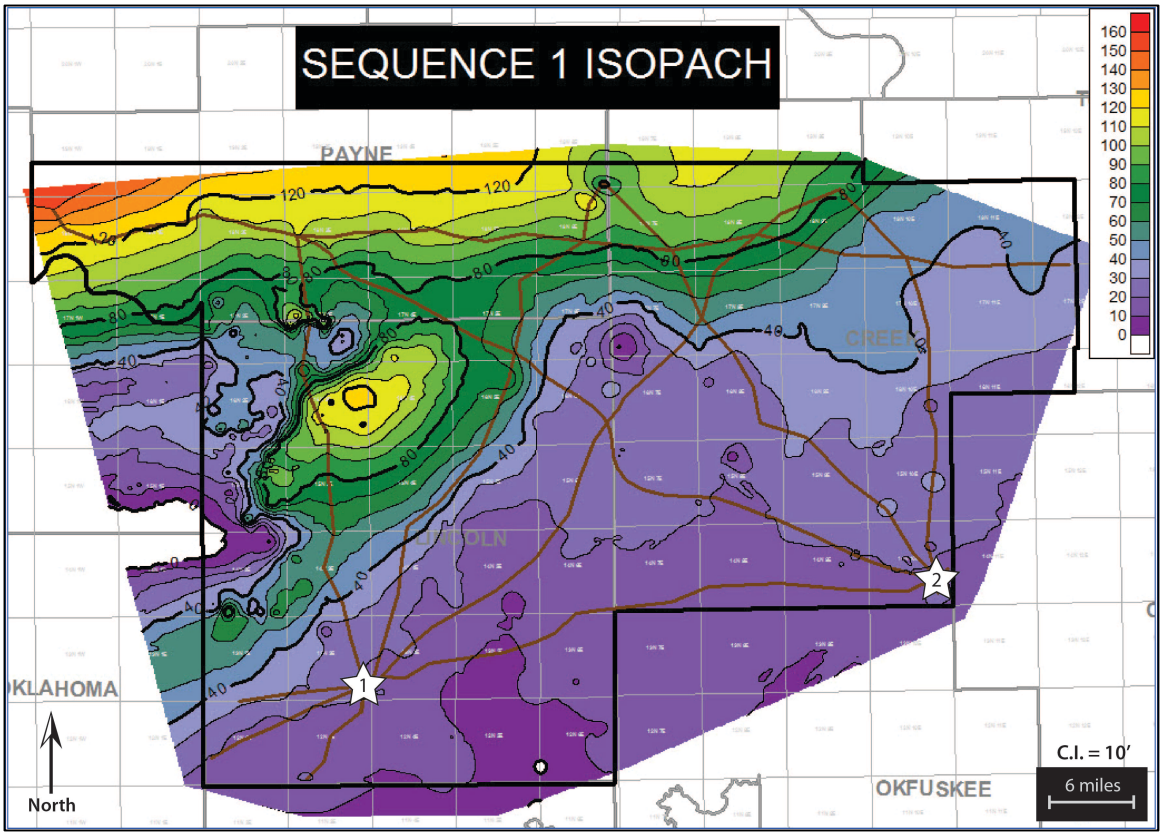


**C-II-b.** Thickness map of probable 3rd order sequence 1 (S1). Contour Interval = 10ft.

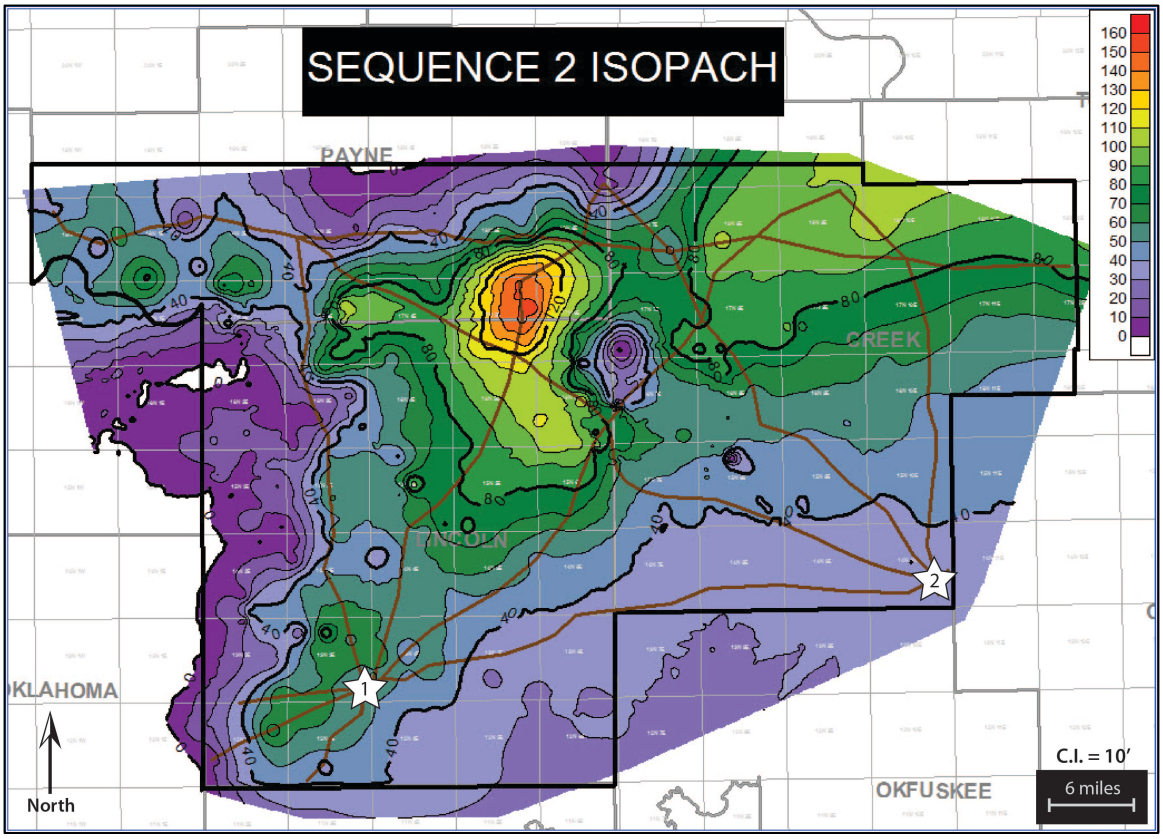


**C-II-c.** Thickness map of probable 3rd order sequence 2 (S2). Contour Interval = 10ft.

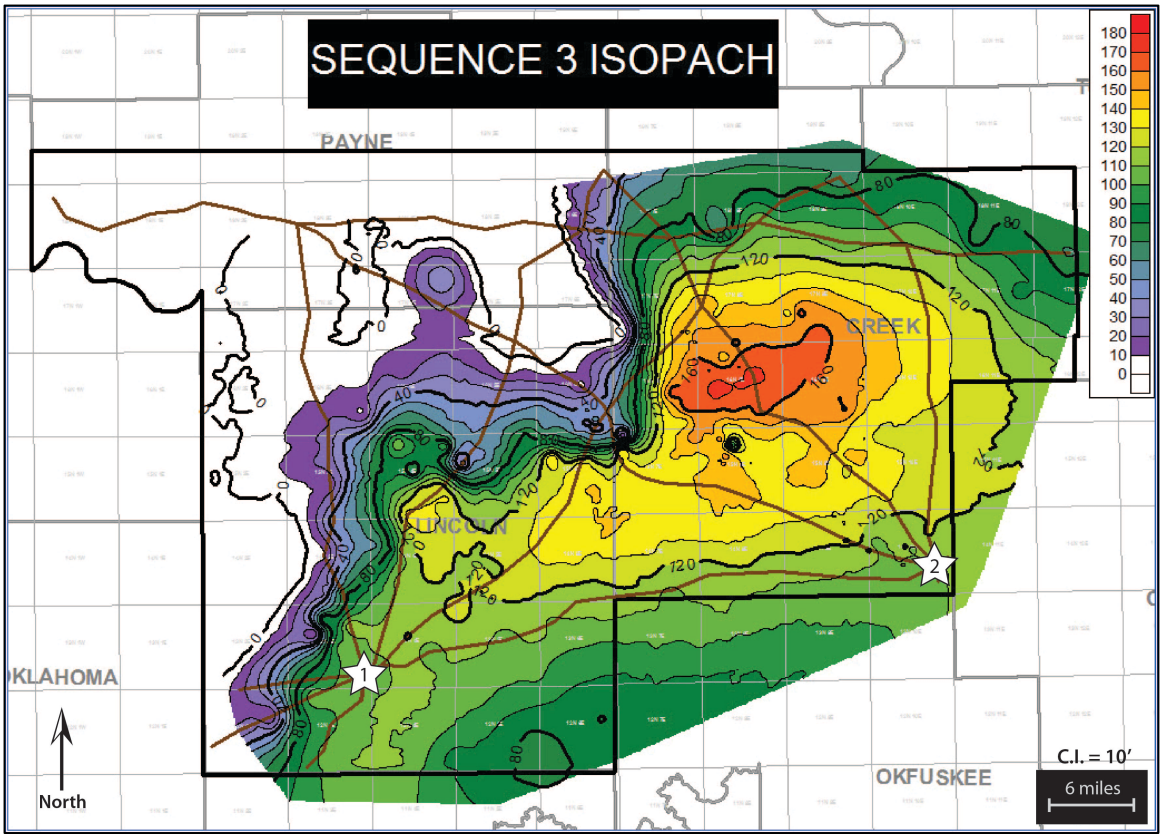


**C-II-d.** Thickness map of probable 3rd order sequence 3 (S3). Contour Interval = 10ft.

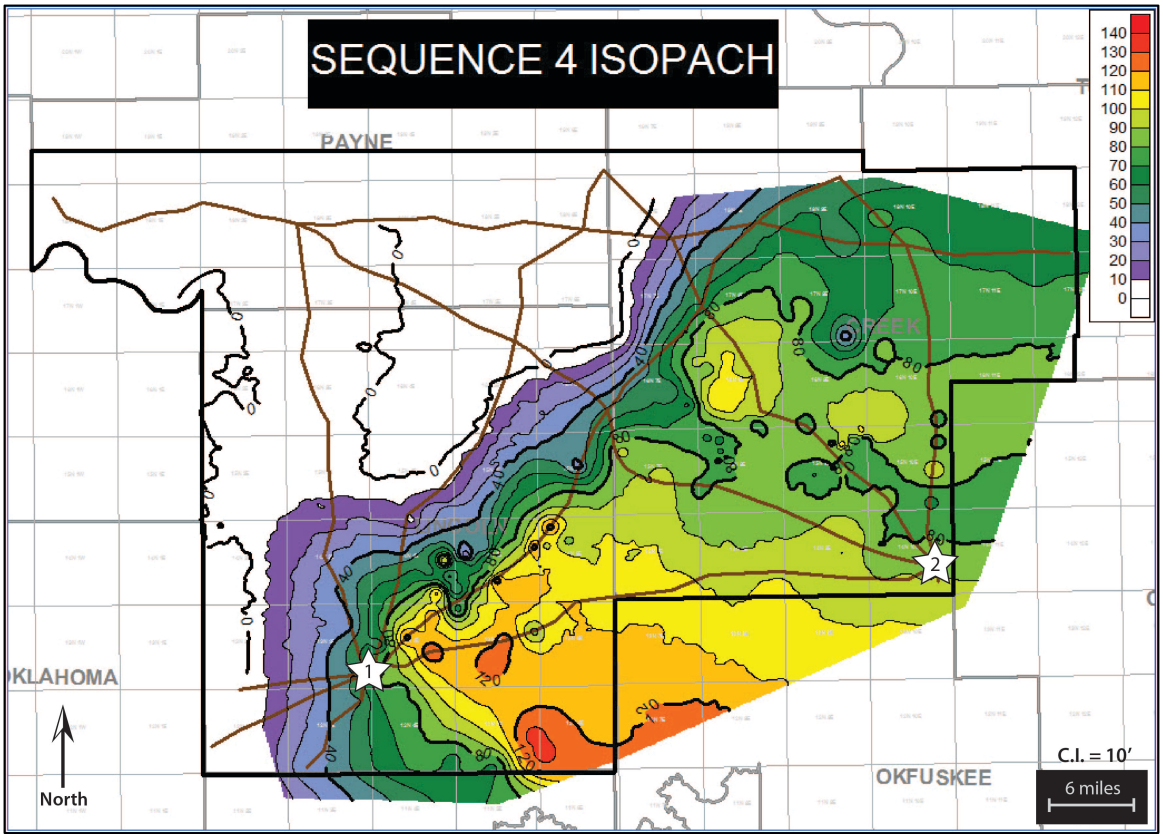


**C-II-e.** Thickness map of probable 3rd order sequence 4 (S4). Contour Interval = 10ft.

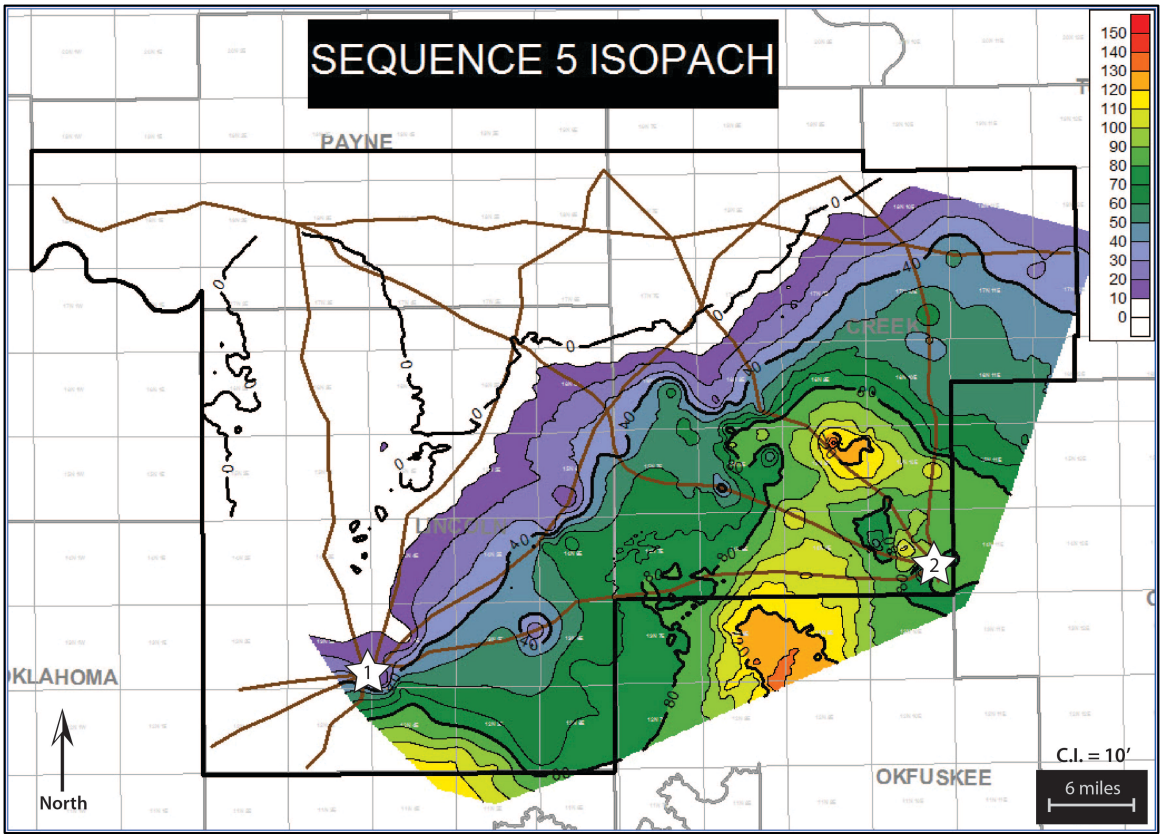


**C-II-f.** Thickness map of probable 3rd order sequence 5 (S5). Contour Interval = 10ft.

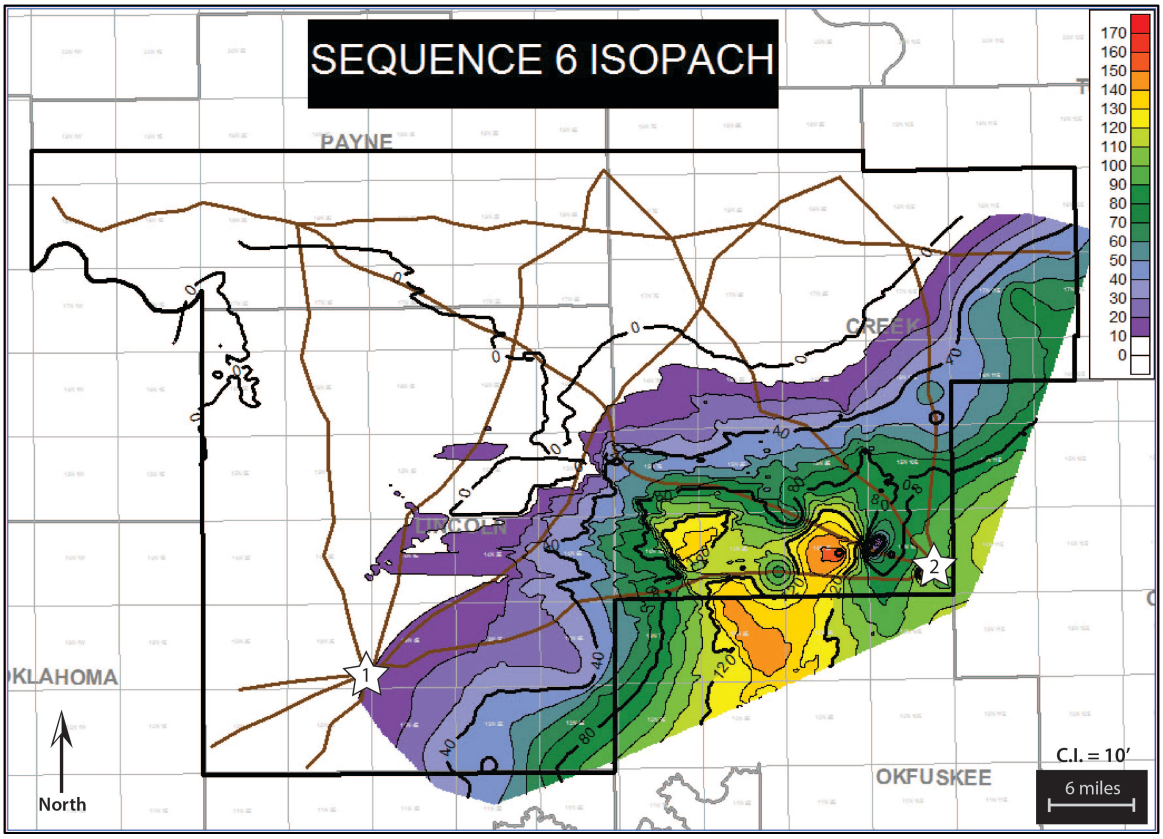


**C-II-g.** Thickness map of probable 3rd order sequence 6 (S6). Contour Interval = 10ft.

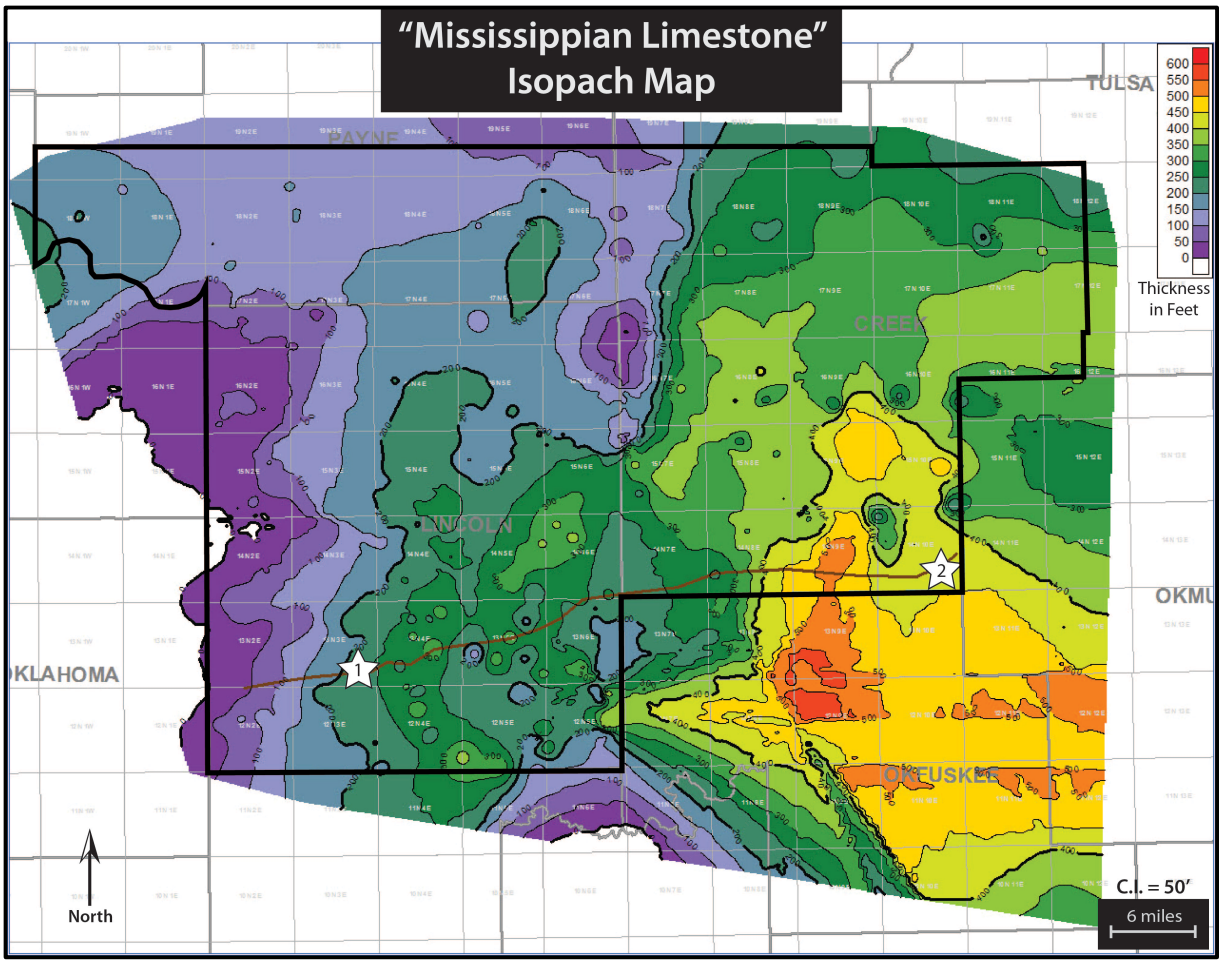


**C-II-h.** Thickness map of the "Mississippian Limestone" throughout the study area. Contour Interval = 50ft.

VITA

Ethan D. Hill

Candidate for the Degree of

Master of Science

Thesis: CORE AND WIRELINE LOG BASED, SHELF TO BASIN STRAIGRAPHIC FRAMEWORK OF MISSISSIPPIAN STRATA, EAST-CENTRAL OKLAHOMA

Major Field: Geology

Biographical:

Education:

Completed the requirements for the Master of Science in Geology at Oklahoma State University, Stillwater, Oklahoma in December, 2017.

Completed the requirements for the Bachelor of Science in Geology at Oklahoma State University, Stillwater, Oklahoma in 2014.

Experience:

Began full-time position as Wellsite Geologist / Geosteering Geologist for Hoss Geosciences in Oklahoma in 2017.

Contract Geophysical Data Technician at Devon Energy in Oklahoma City, OK in 2014 – 2016.

Roustabout at D&B Oilfield Construction in Ringwood, OK in 2012.

Professional Memberships:

American Association of Petroleum Geologists

Society for Sedimentary Geology